/VOLUME 75 SEPTEMBER 30, 1971 NUMBER 20

JPCHAx

THE JOURNAL OF PHYSICAL CHEMISTRY

PUBLISHED BIWEEKLY BY THE AMERICAN CHEMICAL SOCIETY

THE JOURNAL OF

PHYSICAL CHEMISTRY

BRYCE CRAWFORD, Jr., *Editor*
STEPHEN PRAGER, *Associate Editor*
ROBERT W. CARR, Jr., FREDERIC A. VAN-CATLEDGE, *Assistant Editors*

EDITORIAL BOARD: A. O. ALLEN (1970–1974), R. BERSOHN (1967–1971), J. R. BOLTON (1971–1975), S. BRUNAUER (1967–1971), M. FIXMAN (1970–1974), H. S. FRANK (1970–1974), J. R. HUIZENGA (1969–1973), M. KASHA (1967–1971), W. J. KAUZMANN (1969–1973), W. R. KRIGBAUM (1969–1973), R. A. MARCUS (1968–1972), W. J. MOORE (1969–1973), J. A. POPLE (1971–1975), B. S. RABINOVITCH (1971–1975), H. REISS (1970–1974), S. A. RICE (1969–1975), R. E. RICHARDS (1967–1971), F. S. ROWLAND (1968–1972), R. L. SCOTT (1968–1972), R. SEIFERT (1968–1972)

CHARLES R. BERTSCH, *Manager, Editorial Production*

AMERICAN CHEMICAL SOCIETY, *1155 Sixteenth St., N.W., Washington, D. C. 20036*
FREDERICK T. WALL, *Executive Director*

Books and Journals Division
JOHN K CRUM, *Director (Acting)*
JOSEPH H. KUNEY, *Head, Business Operations Department*
RUTH REYNARD, *Assistant to the Director*

©Copyright, 1971, by the American Chemical Society. Published biweekly by the American Chemical Society at 20th and Northampton Sts., Easton, Pa. 18042. Second-class postage paid at Washington, D. C., and at additional mailing offices.

All manuscripts should be sent to *The Journal of Physical Chemistry,* Department of Chemistry, University of Minnesota, Minneapolis, Minn. 55455.

Additions and Corrections are published once yearly in the final issue. See Volume 74, Number 26 for the proper form.

Extensive or unusual alterations in an article after it has been set in type are made at the author's expense, and it is understood that by requesting such alterations the author agrees to defray the cost thereof.

The American Chemical Society and the Editor of *The Journal of Physical Chemistry* assume no responsibility for the statements and opinions advanced by contributors.

Correspondence regarding accepted copy, proofs, and reprints should be directed to Editorial Production Office, American Chemical Society, 20th and Northampton Sts., Easton, Pa. 18042. Manager: CHARLES R. BERTSCH. Assistant Editor: EDWARD A. BORGER. Editorial Assistant: EVELYN J. UHLER.

Advertising Office: Century Communications Corporation, 142 East Avenue, Norwalk, Conn. 06851.

Business and Subscription Information

Remittances and orders for subscriptions and for single copies, notices of changes of address and new professional connections, and claims for missing numbers should be sent to the Subscription Service Department, American Chemical Society, 1155 Sixteenth St., N.W., Washington, D. C. 20036. Allow 4 weeks for changes of address. Please include an old address label with the notification.

Claims for missing numbers will not be allowed (1) if received more than sixty days from date of issue, (2) if loss was due to failure of notice of change of address to be received before the date specified in the preceding paragraph, or (3) if the reason for the claim is "missing from files."

Subscription rates (1971): members of the American Chemical Society, $20.00 for 1 year; to nonmembers, $40.00 for 1 year. Those interested in becoming members should write to the Admissions Department, American Chemical Society, 1155 Sixteenth St., N.W., Washington, D. C. 20036. Postage to Canada and countries in the Pan-American Union, $4.00; all other countries, $5.00. Single copies for current year: $2.00. Rates for back issues from Volume 56 to date are available from the Special Issues Sales Department, 1155 Sixteenth St., N.W., Washington, D. C. 20036.

This publication and the other ACS periodical publications are now available on microfilm. For information write to: MICROFILM, Special Issues Sales Department, 1155 Sixteenth St., N.W., Washington, D. C. 20036.

Notice to Authors last printed in the issue of June 10, 1971

THE JOURNAL OF
PHYSICAL CHEMISTRY

Volume 75, Number 20 September 30, 1971

NOTES

AUTHOR INDEX

In papers with more than one author the name of the author to whom inquiries about the paper should be addressed is marked with an asterisk in the by-line.

THE JOURNAL OF
PHYSICAL CHEMISTRY
Registered in U. S. Patent Office © Copyright, 1971, by the American Chemical Society

VOLUME 75, NUMBER 20 SEPTEMP

Energy Transfer in Thermal Isocyanide Isomerization. General Correlations in the C_2H_5NC System[1]

by S. P. Pavlou and B. S. Rabinovitch*

Department of Chemistry, University of Washington, Seattle, Washington 98105 *(Received May 6, 1971)*

Publication costs assisted by the National Science Foundation

Relative collisional activation–deactivation efficiencies, $\beta_0(\infty)$, for two dozen inert bath gases in the thermal unimolecular isomerization of ethyl isocyanide are summarized; data for seven new gases are included. Measurements were made in the lower region of falloff, just above the second-order region, at 231°. Good correlation of efficiency with static polarizability and boiling point is observed. For the latter correlation, three classes of bath molecules may be discerned and correspond to monatomic, diatomic and linear, and polyatomic molecules. Comparison is made with earlier results for the CH_3NC system, and the effect of several variables such as the complexity and nature of the substrate molecule, the effective number of transitional modes in the collision complex, and conservation of angular momentum restrictions on the process of intermolecular energy exchange is considered.

Introduction

The study of inert gas effects in the thermal isomerization of CH_3NC has provided information on some aspects of intermolecular energy transfer by molecules at high levels of vibrational excitation.[2,3] An extensive investigation has been made of the molecular parameters that affect the energy transfer process.[3] Evidence was presented that the strength of the intermolecular attraction is a contributing factor to the efficiency of collisional energy transfer, although factors related to conservation of angular momentum play a dominant role.

Extension of the experimental work on bath gas behavior to the C_2H_5NC isomerization system provides a second reaction system in which the complexity of the substrate molecule is changed significantly, with little concomitant alteration of the operational criteria for energy transfer efficiency.[4,5] From such a comparison, further information on the factors affecting collisional transition probabilities can be obtained.

This paper summarizes the results and conclusions derived from the experimental survey of two dozen bath gases in the C_2H_5NC system; of these, H_2, N_2, CO_2, HCN, C_2H_2, CH_3CN, and C_3H_7CN are newly described here.

Experimental Section

Materials. The preparation and purification of ethyl isocyanide has been described, and sources of some of the gases used have been given elsewhere.[4,5] Acetonitrile (J. T. Baker, reagent grade), *n*-butyronitrile (Matheson Coleman and Bell), and acetylene (J. T. Baker, 99.6%) showed no impurities on chromatographic analysis. Hydrogen cyanide had been prepared pre-

(1) (a) This work was supported by the National Science Foundation. (b) Abstracted in part from the Ph.D. Thesis, 1970, of S. P. Pavlou.

(2) F. J. Fletcher, B. S. Rabinovitch, K. W. Watkins, and D. J. Locker, *J. Phys. Chem.*, **70**, 2823 (1966).

(3) S. C. Chan, B. S. Rabinovitch, J. T. Bryant, L. D. Spicer, T. Fujimoto, Y. N. Lin, and S. P. Pavlou, *ibid.*, **74**, 3160 (1970).

(4) S. P. Pavlou and B. S. Rabinovitch, *ibid.*, **75**, 1366 (1971).

(5) S. P. Pavlou and B. S. Rabinovitch, *ibid.*, **75**, 2171 (1971). Table IV, last column: refers to 281°, while entries for $n = 4$, 5, and 6 for both alkanes and alkenes are based on best fit values with $\beta_0(\infty) = 1$ for $n = 4$.

Table I: Collision and Intermolecular Parameters for Various Gases[a]

	σ,[b] Å	ϵ/k,[b] °K	μ_{AM}[c]	σ_{AM},[d] Å	ϵ_{AM}/k,[e] °K	μ, D	$(\delta_{max})_{AM}$	$\Omega_{AM}^{(2,2)*}$ (T^*,δ_{max})	s_{AM}^2, Å^2	$(s_{AM}/s_{AA})^2$	$(\mu_{AA}/\mu_{AM})^{1/2}$
C_2H_5NC	5.00	400	27.50	5.00	400	3.93	1.12	1.65	41.25	1.00	1.00
C_3H_7CN	5.49	400	30.60	5.25	400	4.07	1.00	1.61	44.30	1.07	0.95
CH_3CN	4.47	380	23.51	4.73	390	3.83	1.32	1.75	39.20	0.95	1.08
HCN	3.93	320	18.13	4.47	358	2.95	1.31	1.67	33.40	0.81	1.23
C_2H_2	4.22	185	17.66	4.61	272			1.07	22.75	0.55	1.25
CO_2	4.00	190	24.45	4.50	276			1.22	24.65	0.60	1.06
N_2	3.68	92	18.58	4.34	192			1.07	20.15	0.49	1.22
H_2	2.92	38	1.87	3.96	123			0.96	15.02	0.36	3.84

[a] For all other gases listed in Table II, see ref 4 and 5. [b] All values as in ref 3 except for C_2H_5NC from K. M. Maloney and B. S. Rabinovitch, *J. Phys. Chem.*, **73**, 1652 (1969). [c] $\mu_{AM} = M_A M_M/(M_A + M_M)$. [d] $\sigma_{AM} = (\sigma_A + \sigma_M)/2$. [e] $\epsilon_{AM} = (\epsilon_A \epsilon_M)^{1/2}$.

viously;[3] it was purified by gas chromatography and was stored over P_2O_5. Hydrogen and nitrogen (Air Reduction Co., assayed reagent grade) and carbon dioxide (Ohio Chemical and Surgical Equipment Co., USP) were gas chromotographically clean and were used without further purification. All condensable gases were deoxygenated by the freeze–pump–melt technique.

Apparatus and Procedure. The experimental arrangement and procedure were the same as that described earlier.[4] The reaction vessel was a 229-l. Pyrex flask heated in a stirred air furnace controlled by a proportional controller. Temperature was measured by eight calibrated chromel–alumel thermocouples at various points of the reaction vessel. During a run the temperature was constant to ±0.3° and variation over the reaction vessel was ±0.2°.

A reaction mixture of C_2H_5NC containing ~6% of CH_3CN as an internal analytical standard was used for kinetic runs. Excess amounts of inert gases were added to a constant amount of C_2H_5NC (~3×10^{-4} Torr) such that the dilution, D, varied on a collision basis from around 20 to 320 throughout the series of runs, depending on the gas. The lower end of the range was used for the more efficient colliders so that, in practice, dilution was near-infinite in all cases. Isomerization was carried to between 10 and 40% reaction.

Analysis. The analytical technique was that of ref 4. All analyses were made by gas chromatography. A 12-ft 5% tricresyl phosphate on 60–80 mesh acid-washed Chromosorb G column was used. Rate constants for the isomerization were again calculated on both an "absolute" and "internal" standard basis.[4] When inert gas interference with the acetonitrile peak occurred, only absolute values were used.

Results and Discussion

In this section new results for H_2, N_2, CO_2, HCN, C_2H_2, CH_3CN, and C_3H_7CN are presented.

Treatment of the Data. The experimental data were corrected for temperature, dead space, and sample pump-out time in the same manner as described.[4] Rates of isomerization were obtained in a region of falloff, $0.13 \geq k/k_\infty \geq 0.02$, where wall effects were small. All rate data were standardized to a temperature of 231°. Time correction for sample removal averaged 5% for H_2 and N_2. For CO_2, C_2H_2, CH_3CN, and C_3H_7CN, the time correction was usually less than 2%, depending on total pressure and reaction time. The observed rate constants are summarized in the Appendix.

Collisional Efficiencies. The relative collisional efficiency quantities appropriate for these studies have been discussed in some detail;[4,5] their dependence on reaction order and dilution was characterized. Relative efficiencies on a pressure-to-pressure basis, $\bar{\beta}_p'(D)$ and $\bar{\beta}_p(D)$, and on a collision-per-collision basis, $\bar{\beta}_\omega'(D)$ and $\bar{\beta}_\omega(D)$, were obtained from relations derived previously,[4] and with use of the collisional diameter and intermolecular potential parameters given in Table I. The β quantities for each bath gas were averaged over the range of dilution (D) and falloff used; this procedure has been justified.

Values of $\bar{\beta}_p'(D)$, $\bar{\beta}_p(D)$, $\bar{\beta}_\omega'(D)$, and $\beta_\omega(D)$ are gathered in the Appendix. In practice D corresponds closely to infinity. Extrapolation of the average high dilution $\bar{\beta}_\omega'(\infty)$ and $\bar{\beta}_\omega(\infty)$ quantities to their second-order limit $\beta_0(\infty)$ was made for each bath gas, as in ref 4. The $\beta_0(\infty)$ values for all gases studied in the C_2H_5NC system are collected in Table II together with corresponding values obtained from energy transfer studies with the CH_3NC homolog;[3] the error in some values could be 10%. Some comparisons of the efficiency behavior of several series of inert bath gases (noble gases, *n*-alkanes, and *n*-alkenes) as between the CH_3NC and C_2H_5NC systems have already been made. The observed alterations in efficiencies were rationalized in terms of several counterbalancing factors that influence the process of energy transfer: these included the heat capacity of the substrate molecule, conservation of angular momentum restrictions, the effective number of transitional modes in the collision complex, and the chemical similarity of the substrate molecule with the inert deactivator.

Table II: Summary Values of $\beta_0(\infty)$ for Various Molecules in the C_2H_5NC and CH_3NC Systems

Molecule	C_2H_5NC,[a] 231°	CH_3NC[b] 231°	CH_3NC[b] 281°
1. He	0.27[c]	0.27	0.24
2. Ne	0.30[c]	0.31	0.28
3. Ar	0.39[c]	0.31	0.28
4. Kr	0.46[c]	0.27	0.24
5. Xe	0.44[c]	0.26	0.23
6. H_2	0.26[c]	0.28	0.25
7. N_2	0.45[c]	0.41	0.38
8. CO_2	0.70[c]	0.57	0.55
9. HCN	0.66[c]	0.62	0.60
10. CH_3CN	0.93[c]	0.91[f]	0.91
11. C_3H_7CN	1.10[c]	0.98	0.98
12 CH_4	$\leq$0.70[d]	0.63	0.61
13. C_2H_2	0.78,[e] 0.86	0.54	0.52
14. C_2H_4	1.00	0.62	0.60
15. C_2H_6	1.00	0.77	0.76
16. C_3H_6	1.06	0.81	0.80
17. C_3H_8	0.99	0.80	0.79
18. C_4H_8	0.99		1.00
19. C_4H_{10}	0.95		1.00
20. C_5H_{10}	1.00		0.99
21. C_5H_{12}	0.98		1.01
22. C_6H_{12}	1.03		1.01
23. C_6H_{14}	1.02		0.99
24. C_2H_5NC	(1.00)		

[a] For this system, $\beta_0(\infty)$ is the extrapolated second-order limit value; the value of unity is assigned for C_2H_5NC. [b] All values are abstracted from ref 3; values measured at 553.7°K for H_2 and noble gases may be brought to 504°K according to the measured temperature dependence of $\beta_0(\infty)$ for He [S. C. Chen, J. T. Bryant, and B. S. Rabinovitch, *J. Phys. Chem.*, **74**, 2055 (1970)], since all noble gases and H_2 have near-equal efficiencies for CH_3NC. More efficient gases were assumed to display proportionately lesser temperature dependence. [c] These values have been obtained with the use of cross sections, σ_M, as reported in the CH_3NC work, see ref 2 and 3, and are based on viscosity data, J. D. Hirschfelder, C. F. Curtiss, and R. B. Bird, "Molecular Theory of Gases and Liquids," Wiley, New York, N. Y., 1954; R. A. Svela, NASA Technical Report R-132, 1965. [d] This is the value obtained from the viscosity-based cross sections corrected by the same factor as that which converts the s_{AM_2} value for C_2H_6 from the viscosity basis to the self-consistent basis, as described in ref 5 (Table III, set I and II). [e] Based on s_{AM} derived from viscosity data; this quantity is reported on this basis here since the comparison made in Figure 2 with other linear molecules employs viscosity-based values for the latter; if s_{AM} is changed in the same proportion that the self-consistent value of s_{AM_2} for C_2H_4, measured in ref 5, was altered from the viscosity-based value, the higher value is obtained. [f] This is the value obtained for CD_3CN in the CH_3CN system.

Some further examination within small groups of molecules will be made now in order to assess further the effect of various factors on the efficiency of intermolecular energy exchange.

General Correlations. In the CH_3NC system several parameters of possible importance in the energy transfer process were examined. A general correlation was found between $\beta_0(\infty)$ and dispersion energy, $V_{dis} = -\frac{3}{2}[(I_A I_M)/(I_A + I_M)]\alpha_A\alpha_M/r^6$, where I is the ionization potential and the α are the static polarizabilities. Figure 1 shows a plot of $\beta_0(\infty)$ *vs.* α_M for the C_2H_5NC homolog. Almost all molecules congregate along a general curve. There are insufficient examples of polar gases to illustrate dipolar behavior.

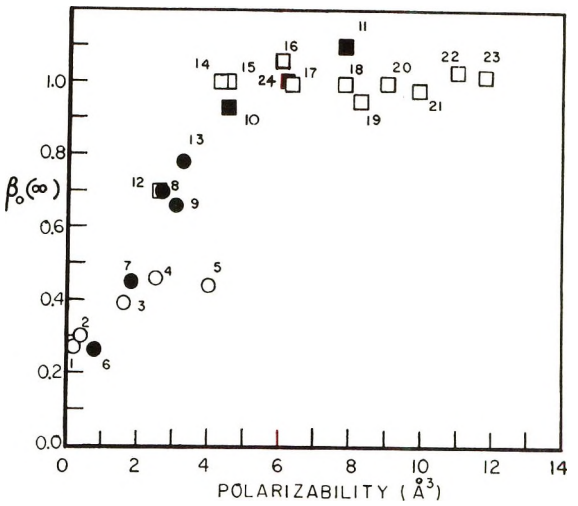

Figure 1. Plots of $\beta_0(\infty)$ *vs.* polarizability. Numbering of molecules follows Table II: ○, monatomic molecules; ●, diatomic and linear molecules; □, hydrocarbons; ■, alkyl nitriles, except C_2H_5NC.

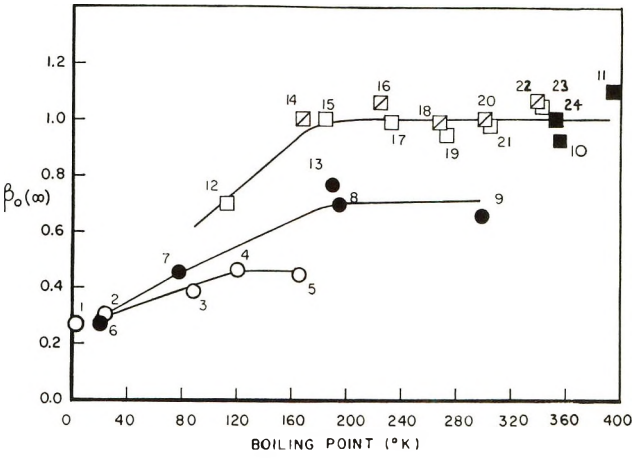

Figure 2. Plots of $\beta_0(\infty)$ *vs.* boiling point: ○, monatomic molecules; ●, diatomic and linear molecules; □, *n*-1-alkenes; □, *n*-alkanes; ■, alkyl nitriles, except C_2H_5NC.

Correlation of energy transfer efficiency with boiling point was suggested and observed by Volpe and Johnston for the NO_2Cl system.[6] A good correlation was also found in the CH_3NC system[3] for a large number of gases. Figure 2 shows a similar plot for the C_2H_5NC system; the correlation again is good, even though characteristically different behavior is discernible for monatomic gases, diatomic and small linear molecules and for polyatomics; so that although the number of

(6) M. Volpe and H. S. Johnston, *J. Amer. Chem. Soc.*, **78**, 3903 (1956).

Table III: Summary of Rate Data and Collisional Efficiencies

D[a]	ω_c,[a] 10^6 sec^{-1}	P(Mix), 10^{-2} mm	k(Mix),[b] 10^{-6} sec^{-1}	$\bar{\beta}_D'(D)$	$\bar{\beta}_D(D)$	$\bar{\beta}_\omega'(D)$	$\bar{\beta}_\omega(D)$
			N_2				
23	1.08	1.15	2.70	0.36	0.23	0.51	0.38
30	1.45	1.55	3.59	0.38	0.26	0.55	0.42
46	2.38	2.58	4.65 ± 0.15[c]	0.34	0.22	0.51	0.38
75	3.87	4.19	6.79 ± 0.30	0.35	0.24	0.51	0.39
115	5.23	5.66	7.71 ± 0.35	0.33	0.21	0.46	0.35
150	7.50	8.14	11.65 ± 0.10	0.39	0.26	0.55	0.42
			H_2[d]				
60	2.77	1.30	3.62	0.44	0.31	0.34	0.22
102	4.67	2.28	4.87	0.39	0.27	0.31	0.19
165	8.64	4.05	6.11	0.33	0.21	0.26	0.15
177	8.44	3.95	7.27	0.39	0.28	0.32	0.20
202	10.22	4.78	8.02	0.38	0.26	0.31	0.18
316	13.02	6.09	9.82	0.40	0.27	0.32	0.19
			CO_2				
18	0.84	0.84	3.27 ± 0.05	0.54	0.41	0.75	0.66
27	1.29	1.30	4.45 ± 0.15	0.54	0.42	0.76	0.67
42	2.08	2.11	6.24 ± 0.02	0.53	0.42	0.75	0.68
67	3.42	3.49	8.17 ± 0.20	0.49	0.37	0.69	0.60
108	5.48	5.58	12.44	0.54	0.41	0.74	0.67
			C_2H_2[d]				
15	0.71	0.66	3.46	0.68	0.58	0.84	0.78
27	1.15	1.09	4.70	0.65	0.54	0.86	0.83
50	2.30	2.17	7.87	0.66	0.58	0.75	0.69
69	3.16	2.99	8.73	0.57	0.48	0.87	0.83
175	7.50	7.13	15.87	0.59	0.45	0.74	0.64
			HCN[d]				
21	0.65	0.42	3.27	0.87	0.82	0.87	0.82
21	0.65	0.42	2.60	0.69	0.59	0.69	0.59
21	0.71	0.46	3.48	0.87	0.81	0.87	0.81
30	1.02	0.66	3.14	0.61	0.49	0.61	0.49
31	1.39	0.91	4.39	0.68	0.58	0.68	0.58
55	1.94	1.25	5.55	0.69	0.59	0.69	0.59
124	3.96	2.56	7.72	0.58	0.46	0.58	0.46
			CH_3CN				
6	0.18	0.11	1.82	1.24	1.36	1.23	1.34
8	0.66	0.41	4.02	1.12	1.14	1.10	1.13
9	0.85	0.53	3.74	0.86	0.80	0.87	0.80
11	0.44	0.27	2.45	0.89	0.85	0.89	0.84
13	0.50	0.31	2.74	0.91	0.88	0.90	0.87
14	0.53	0.33	3.46	1.10	1.14	1.10	1.11
16	0.48	0.30	2.70	0.92	0.89	0.92	0.88
17	0.81	0.50	4.78	1.14	1.20	1.12	1.19
20	1.03	0.64	5.04	1.02	1.02	1.00	1.00
23	2.01	1.24	7.04	0.89	0.85	0.92	0.83
25	1.27	0.79	5.47	0.95	0.94	0.95	0.93
28	0.83	0.52	4.81	1.12	1.18	1.12	1.18
37	1.27	0.19	5.86	1.02	1.02	1.01	1.01
41	2.20	1.34	7.33	0.87	0.84	0.87	0.83
48	2.24	1.38	6.81	0.79	0.73	0.80	0.72
56	2.77	1.71	8.69	0.87	0.82	0.88	0.82
67	3.42	2.11	9.39	0.80	0.74	0.78	0.72
75	4.21	2.61	10.07	0.74	0.66	0.72	0.64

Table III (*Continued*)

D[a]	ω,[a] 10^6 sec^{-1}	P(Mix), 10^{-2} mm	k(Mix),[b] 10^{-5} sec^{-1}	$\bar{\beta}_D'(D)$	$\bar{\beta}_D(D)$	$\bar{\beta}_\omega'(D)$	$\bar{\beta}_\omega(D)$
			C_3H_7CN				
2	0.23	0.44	1.80	1.01	1.02	1.01	1.02
50	0.20	0.13	1.92	1.18	1.27	1.18	1.28
10	0.29	0.19	1.97	0.93	0.90	0.94	0.92
3	0.35	0.22	2.30	0.98	0.94	0.96	0.94
16	0.31	0.20	2.76	1.26	1.40	1.26	1.40
12	0.47	0.30	3.17	1.10	1.10	1.09	1.11
22	0.89	0.51	4.46	0.97	0.97	1.01	1.01
30	1.11	0.70	5.14	0.97	0.96	1.01	1.01
30	0.89	0.57	5.36	1.18	1.23	1.18	1.27
11	1.29	0.83	5.43	0.91	0.88	0.92	0.89

[a] Dilution D is on a collision basis, where $\omega = \omega(A,D) + \omega(M,D) = 1.59 \times 10^7 P(A,D) + 1.97 \times 10^6[s_{AM}^2/\mu_{AM}^{1/2}]P(M,D)$; the average value of $P(A,D)$ was $3.1 \pm (0.2) \times 10^{-4}$ mm except for HCN where $P(A,D) = 2.2 \pm (0.2) \times 10^{-4}$ mm. [b] $k_\infty = 1.56 \times 10^{-3}$ sec^{-1}. [c] Average deviation of absolute and internal standard values from mean. [d] No internal standard was used in this series of runs.

molecules examined in this study is restricted relative to the CH_3NC system, good concordance with correlations made in the latter system is found here. Three classes of molecules are again found and point to the important role of conservation of angular momentum restrictions in the present system.

Internal Comparison among Small Groups of Molecules. H_2 and He are found to have near-equivalent efficiencies for both systems. For the CH_3CN system this was taken to indicate that the two extra transitional modes (five for a diatomic *vs.* three for a monatomic gas) in the collision complex that correlate with rotations of H_2 do not make a significant contribution to an increase in energy transfer; this was attributed pragmatically to the effect of restrictions on energy transfer imposed by conservation of angular momentum considerations. The same behavior is observed in the C_2H_5NC system.

The factors influencing the relative efficiency for He in the two isocyanide systems have been discussed previously.[4] They included the complexity (heat capacity) of the substrate molecule (higher for C_2H_5NC), conservation of angular momentum restrictions (which are roughly the same in severity in both systems), and the effective number of transitional modes in the collision complex (which is one more for C_2H_5NC). All of these appear to cancel in their net effect. The data for H_2 in this work lead to a similar conclusion.

The efficiency of N_2 is slightly higher for the C_2H_5NC homolog (0.45) than for CH_3NC (0.41). For this gas, the system angular momentum values (I_L) are 286 and 320 amu Å^2 for CH_3NC and C_2H_5NC, respectively. The disparity between the I_L value and the I_C^A value is considerably larger for CH_3NC.

The triad, C_2H_2, C_2H_4, and C_2H_6, has similar polarizabilities and boiling points. Their $\beta_0(\infty)$ values are 0.86 (see footnote *e*, Table II) 1.00 and 1.00 with C_2H_5NC and 0.55, 0.62, and 0.77 with CH_3NC, respectively. The trend is the same in both cases and may reflect the increase of the number of transitional modes (five for C_2H_2 and six for C_2H_4 and C_2H_6). The effect of the lowered torsional frequency for C_2H_6 on the magnitude of efficiency may be of importance in the CH_3NC system. The relative magnitudes of the $\beta_0(\infty)$ in the two isocyanide systems values have been discussed in some detail;[5] similar arguments hold for the enhanced efficiency of C_2H_2 in the C_2H_5NC system.

N_2, HCN, and C_2H_2 which are all isoelectronic and linear, and have roughly similar moments of inertia and display different trends in the two systems. Their efficiencies are 0.45, 0.66, and 0.78, relative to 0.41, 0.63, and 0.55, for the C_2H_5NC and CH_3NC systems, respectively. C_2H_2 and HCN are much more efficient than N_2 in both systems and this suggests that internal degrees of freedom of M may be active in the energy transfer process. All three molecules appear to have higher efficiencies in the C_2H_5NC system, especially in the case of C_2H_2. Attempts to refine the deductions further would be unwarranted.

Appendix

A summary of rate data and of relative collisional efficiencies is given in Table III.

The Temperature Dependence of Simple Hot Atom Reactions

by H. M. Chang[1] and Richard Wolfgang*

Department of Chemistry, Yale University, New Haven, Connecticut 06520 *(Received April 19, 1971)*

Publication costs assisted by the U. S. Atomic Energy Commission

The magnitude of temperature effects of hot atom reactions is evaluated. Simple theoretical calculations indicate that the effect of thermal translational motion on the apparent threshold is greatest for light substrate molecules and high true threshold processes. It is also apparent that hot reaction yields are very weakly dependent on such temperature effects, and that the latter would normally escape detection by the usual techniques. Temperature effects due to internal motion of substrate molecules are more difficult to estimate and may often be somewhat larger than those due to translation. Experimental studies fail to confirm a previous report of a large temperature effect on the yield of HT from reactions of recoil tritium with *n*-butane.

The term "hot atom" implies an entity having a translational energy which is very high compared with the thermal energy of the surrounding medium. One would therefore expect that the reactions of hot atoms would be determined primarily by their own energy, with the temperature of the environment having only a minor influence. Exceptions to the normal expectation are, however, possible. Such would be reactions which are extremely insensitive to translational energy, but are instead driven strongly by the internal vibrational or rotational energy of the molecular reagent which is at thermal equilibrium. Another class of possible exceptions would be hot atom reactions which proceed efficiently at energies so low that thermal motion is not a negligible factor.

Information testing these expectations in the case of hot hydrogen atom reactions is rather scarce. Much of it comes from the early work[2] in which it was established that recoil tritium did indeed react as a hot atom, and that with saturated hydrocarbons the most common processes were direct single-step reactions, the now familiar hot abstraction

$$T + RH \longrightarrow HT + R \qquad (1)$$

and substitution

$$T + RH \longrightarrow RT + H \qquad (2)$$

In these studies the absence of gross temperature effects was actually one of the tests used to establish that the observed products did indeed result from hot atom events. Quantitative theoretical studies have also suggested that yields of hot reactions in the electron volt range are little affected by thermal translational motion of the substrate of ordinary temperatures.[3,4]

More recently it has been reported[5] that the HT yield from the abstraction process of recoil tritium and *n*-butane increased 50% between 24 and 125°. This large effect was cited as evidence supporting the "energy cutoff model" of the mechanism of the abstraction reaction.[6,7]

Our study of these results indicated to us that they seemed quantitatively inconsistent with the large body of existing results on hot reactions, and with the mechanisms that we feel are indicated by these data.[8] However, this work did show the need to test experimentally with much better precision the fundamental and general assumption that hot atom reactions are only weakly sensitive to temperature.

Of critical importance in establishing the temperature dependence of hot reaction is the role of scavenger. This must be highly effective in suppressing all thermal (and hence temperature-dependent) reactions leading to products also formed by hot processes. Bromine was used in the above-cited work[5] on *n*-butane. In our own studies of recoil tritium with alkanes we have also used bromine—but only at room temperature and after carefully verifying (by means of scavenger curves) that it suppressed interfering thermal processes to a sufficient extent.[9] On the other hand, it is apparent that the proclivity of Br_2 to participate in chain reactions in

(1) On leave from Chung Chi College, Chinese University of Hong Kong.

(2) M. A. El Sayed, P. Estrup, and R. Wolfgang, *J. Phys. Chem.*, **62**, 1356 (1958).

(3) R. N. Porter, *J. Chem. Phys.*, **45**, 2284 (1966).

(4) R. N. Porter and Sinan Kunt, *ibid.*, **52**, 3240 (1970).

(5) N. Kushner, A. Hosaka, and F. S. Rowland, Abstracts, 158th National Meeting of the American Chemical Society, New York, N. Y., Sept 1969, physical chemistry, p. 109.

(6) E. Tachikawa and F. S. Rowland, *J. Amer. Chem. Soc.*, **90**, 4767 (1968).

(7) A small temperature dependence has also been found for certain reactions of hot tritium with alkenes [R. Kushner and F. S. Rowland, *ibid.*, **91**, 1539 (1969)]. These processes are known to proceed by a two-step mechanism of addition, *e.g.*, $T + CH_2 = CHCH_2CH_3 \rightarrow CH_2CHTCH_2CH_3^*$, followed by a unimolecular decomposition of the resulting excited radical, *e.g.*, $CH_2CHTCH_2CH_3^* \rightarrow CH_2CHT + CH_2CH_3$, which is competing with collisional deactivation, $CH_2CHTCH_2CH_2^* + M \rightarrow CH_2CHTCH_2CH_3 + M$. It is known that the latter processes are dependent on the energy of the radical and hence on the thermal temperature of the alkene reagent. Because of this and because the frequency of collisional deactivation was not kept constant in these experiments, it is impossible to draw conclusions as to the temperature dependence of the actual hot step involved, namely the initial addition.

(8) R. Wolfgang, *Progr. React. Kinet.*, **3**, 99 (1965).

Table I: Yields of T + n-C_4H_{10} + I_2 System at Two Temperatures

Temp of irradiation, °C	Total pressure at irradiation temp, Torr	Mole % in ampoule[a] I_2	Mole % in ampoule[a] n-C_4H_{10}	HT-C_4H_9T ratio	Fraction T reacting to form products P_{HT}	$P_{CH_3T+C_2H_5T}$	$P_{C_4H_9T}$	$P_{CH_2T+C_2H_4T}$[b]	P_{total}[b]
80	529	0.22	99.8	1.97	0.435	0.038	0.221	0.035	0.729
80	516	0.54	99.5	1.93	0.397	0.034	0.206	0.032	0.669
80	568	1.06	98.9	1.93	0.405	0.040	0.210	0.033	0.688
80	641	1.75	98.2	1.95	0.414	0.035	0.212	0.033	0.694
80	514	2.68	97.3	1.90	0.420	0.038	0.221	0.034	0.713
170	660	0.56	99.4	2.18	0.515	0.044	0.236	0.040	0.835
170	698	1.10	98.9	2.04	0.501	0.048	0.245	0.040	0.834
170	816	1.78	98.2	2.06	0.496	0.036	0.241	0.039	0.803
170	668	2.71	97.3	2.05	0.447	0.037	0.218	0.035	0.737
170	643	5.41	94.6	1.81	0.453	0.037	0.250	0.037	0.777

[a] Not including the about 2% ^3He present in all samples. [b] Calculated on basis that yields of CH_2T and C_2H_4T amount to 5% of those of other hot products.

hydrogenous materials (which could in the presence of T eventually lead to HT) renders it suspect, at least in the absence of data to the contrary. Thus in the hot T–H_2 system, we found that large amounts of HT were formed thermally even in the presence of a considerable Br_2.[10] We felt therefore that for high temperature studies, iodine would be a more promising scavenger. The weakness of the HI bond makes chain reactions much less likely. Of more direct relevance is the fact that I_2 has always been found effective as a scavenger when present in sufficient concentration.

Experimental Section

The basic techniques for the study of hot hydrogen reactions are described in detail elsewhere.[9,11] The major reagent, in this case n-butane, together with small amounts of ^3He and iodine scavenger, is contained in a quartz ampoule. Hot hydrogen in the form of recoil tritium is produced by reaction of slow neutrons with the ^3He. Tritium-labeled products formed by its reaction with n-butane are analyzed by radiogas chromatography.[12]

Sample Preparations. Quartz ampoules of 1 cm radius and 7 cm length were used. Known quantities of iodine were introduced into these, either as a solid, or in a solution in n-hexane (in which case this solvent was then pumped off at −40°). Phillips research grade n-butane (purified of any air by three freeze–pump cycles) and ^3He were introduced in the usual manner. Total pressures at the irradiation temperature were about 550 Torr for the 80° samples and 650 Torr for the 170° samples. Since secondary decomposition of hot products is not a dominant factor in the n-butane system,[9] control of pressure and hence the efficiency of collisional activations were not critical.

Irradiation. Samples were irradiated for 3 hr in the thermal neutron port of the Brookhaven Medical Reactor (flux $\sim 1 \times 10^{10}$ cm^{-2} sec^{-1}). A vessel heated to either 80 or 170° contained the ampoules, which were rotated to ensure identical integrated fluxes for each. With each batch of samples two monitor samples containing only ^3He and n-butane were irradiated.

Analysis. The following columns were used in the usual radiogas chromatographic analysis: 10 ft silicone oil, 40% on Chromosorb P, separated (H_2,CH_4,C_2H_6) C_3H_8, C_4H_{10}, 10 ft silica gel, separated, H_2, CH_4, C_2H_6; 10 ft uncoated Chromosorb P, separated (H_2, C_1 to C_4 hydrocarbons) CH_3I C_2H_5I; 1 ft silicone oil, 20% on Chromosorb P, separated (H_2, C_1 to C_4 hydrocarbons) CH_3I, C_2H_5I. (Compounds appearing in the same parentheses were not separated from each other.)

Monitoring and Recoil Loss. Absolute yields were calculated by reference to monitor samples, making appropriate correction for the relative amounts of ^3He in the ampoules.[9] The usual correction for loss of tritium by recoil into the ampoule walls amounting to 5–8% in this work were also applied.[9]

Errors. Analysis of similar aliquots on different columns gave agreement to about 5%. The precision of absolute yields is estimated to be about 10% (relative). The limit of error on the ratios of yields of major products, *i.e.*, HT–C_4H_9T, is much smaller and appears to be reproducible to within 3%.

Results

Several series of runs of different I_2 concentration were made at both 80 and 170°. Results of the final series are shown in Table I. The earlier runs provided similar and entirely consistent data. Results are given both in terms of P_i, the absolute fraction of available recoil tritium reacting to give product i, and in terms of HT–C_4H_9T ratio, which is of much higher precision,

(9) R. T. K. Baker, M. Silbert, and R. Wolfgang, *J. Chem. Phys.*, 52, 1120 (1970).

(10) D. Seewald, Ph.D. Thesis, Yale University, 1967.

(11) D. Seewald and R. Wolfgang, *J. Chem. Phys.*, 47, 143 (1967).

(12) R. Wolfgang and F. S. Rowland, *Anal. Chem.*, 30, 903 (1958).

since the latter is obtained directly from each gas chromatographic analysis and is independent of the uncertainty in the net amount of ^3He used in the samples and monitors.

The constancy of yields, within experimental error, as the I_2 mole fraction increases from 0.54 to 3% indicates that scavenging is adequate within that range. It also means that at these concentrations the iodine does not provide significant competition for the hot tritium. The fact that our results are very similar to earlier work at 25° in which Br_2 scavenger was used[8] is consistent with these conclusions.

It is immediately obvious that (in sharp contrast to the earlier findings[5]) a 90° increase in temperature does not have a large effect on any product. The absolute yield of the displacement product, $P_{C_4H_9T}$, is 0.212 ± 0.006 at 80° and 0.235 ± 0.012 at 170°. The uncertainty limits indicated here are standard deviations, calculated from the scatter of the data. Systematic errors are not included and as far as absolute yields are concerned, it is not unusual for these to be of the magnitude similar to the total range of the above results. The temperature effect indicated, 10% (or 0.1% per degree), is therefore too small for us to be confident that it is real. It should be regarded as an approximate limit.

The temperature effect on the abstraction product, HT, while not large does seem to be outside the limit of errors of analysis. This is clearly shown in Figure 1 which presents the yield ratios HT–C_4H_9T. They are far more precise than absolute yields. The indicated 6% increase of this ratio between 80 and 170° may therefore be taken more seriously.

There is a possibility that the apparent increase in the ratio HT–C_4H_9T between 80–170° is due to tritium that has recoiled into the walls of the ampoule. This amounts to 5–8% of the total activity in these experiments. It is conceivable that at 170° some of this tritium may have reentered the gas phase as HT, while it did not do so at 80°. If this is the origin of the temperature effect it should of course be regarded as "spurious" as far as gas phase reaction is concerned. (Richard Hall has found that for two samples irradiated at 80°, the change in the HT–C_4H_9T ratio upon subsequent heating to 160° for 3 hr (the length of the irradiations) was within the limit of experimental error. Unfortunately this limit of such error is not much smaller than from the magnitude of the apparent temperature effect.)

We conclude that the magnitude of the apparent temperature effect on yields is 0.1% or less per degree for C_4H_9T and 0.2% or less per degree for HT.

Discussion

The thermal motion of the substate can affect hot reaction in two ways. The translational motion of the substrate will broaden the range of energies of collisions undergone by hot atoms of a defined laboratory energy.

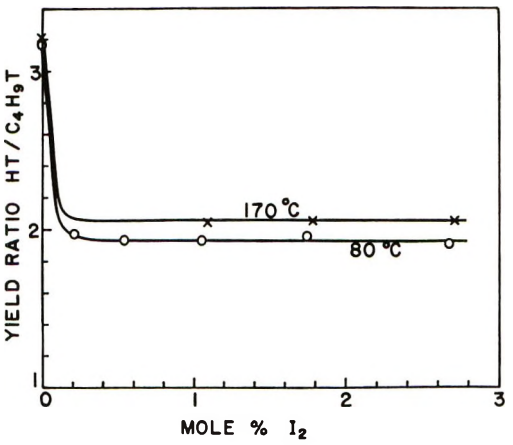

Figure 1. Ratio of yields of HT to C_4H_9T from reaction of hot T with n-C_4H_{10} as a function of scavenger concentration and temperature.

This causes a change in the effective probability of reaction when expressed as a function of the hot atom energy. Then the internal energy of the molecules as a function may directly affect the reaction cross section. Both these effects are very difficult to predict quantitatively, given our present ignorance of elementary reaction dynamics. However, we can make some rough estimates of the magnitudes likely to be involved.

Effect of Temperature-Dependent Translational Motion. We assume, first, that the internal energy of molecule does not affect the probability of reaction. Then the temperatures-dependent probability of reaction by a hot atom of energy E to give product i in a simple collision, $P_i(E,T)$ is rigorously given by

$$P_i(E,T) = \int_0^\infty \sigma_i(V)Vf(V,E,T)dV \Big/ \int_0^\infty \sigma_T(V)Vf(V,E,T)dV \quad (3)$$

Here V is the relative velocity of the collision partners, $\sigma_T(V)$ the total collision cross section, $\sigma_i(V)$ the cross section for forming product i. $f(V,E,T)$, the distribution of relative velocities, is obtained by vector addition of the laboratory velocity of the hot atom (corresponding to E) with the Maxwell distribution of laboratory velocities of the thermal molecule. The total probability of hot reaction at temperature T to give product i, is then obtained by summing over all collisions

$$P_i(T) = \sum P_i(E,T) \quad (4)$$

To evaluate this equation requires knowledge of the energy loss in nonreactive collision, information that is generally unavailable. The reaction cross section required for (3) is also unknown in most cases.

By making reasonable assumptions about excitation functions and energy loss parameters, eq 3 and 4 imply that for reactions such as those studied in this work the temperature dependence is almost negligible, compared

to the experimental precision available. However, the same conclusion can be reached with a similar degree of confidence by a much simpler argument.

The effect of temperature will be most pronounced in the threshold region. Here the excitation function is liable to be rising steeply, and the addition or subtraction of thermal velocity is most likely to make the difference between reaction and no reaction. (By contrast at energies where the excitation function is flat, *i.e.*, at maxima, temperature motion will have least influence.) We define a "shift" in energy of reaction as the increase in relative collision energy due to thermal motion of a substrate molecule with an energy arbitrarily chosen to be $(^3/_2)kT$, moving with a velocity vector opposed to that of the hot atom. This "shift" gives a measure of the displacement in reaction threshold when expressed in terms of the laboratory energy of the hot atom.[13] It is readily shown that this shift $\Delta E(T_2,T_1)$ in going from temperature T_1 to T_2 is given by

$$\Delta E(T_2, T_1) = (^1/_2)\frac{mM}{m+M}\left\{\left[\left(\frac{2E}{m}\right)^{1/2} + \left(\frac{3kT_2}{M}\right)^{1/2}\right]^2 - \left[\left(\frac{2E}{m}\right)^{1/2} + \left(\frac{3kT_1}{M}\right)^{1/2}\right]^2\right\} \quad (5)$$

Here m and M are the masses of the hot atom and the substrate, respectively.

Table II shows the magnitude of the shift between $T_1 = 300°K$ and $T_2 = 400°K$, for a light and a heavy substrate molecule. It is calculated at 0.3 eV, the approximate threshold for hot hydrogen abstraction from hydrocarbons,[14] and at 1.5 eV the approximate threshold for the corresponding displacement process.[15]

Table II: "Characteristic Shift" of Kinetic Energy of Collision as a Function of Temperature, $\Delta E(T_2, T_1)$ ($T_2 = 400°K$, $T_1 = 300°K$)

Molecular weight substrate, amu	Energy of hot atom, eV	
	0.3	1.5
2	0.024	0.045
58	0.008	0.017

Consideration of eq 5 and Table II leads to at least three generalizations. (1) Even for large temperature changes (100°K) the characteristic shift in the energies of collision is relatively small. The shifts shown in Table II are a good measure of the displacement to lower hot atom energies of the effective thresholds for reaction. It must be kept in mind, however, that corresponding to these collisions whose energies are enhanced by translation, there is an approximately equal number whose energies are similarly diminished. The net effect will depend principally on the shape of the excitation function (see eq 3), but it will in general be very small. Crude calculations based on the kinetic theory of hot reactions,[8] using assumed but plausible excitation functions and thresholds of the order of 0.3 eV, suggest that for a temperature change from 300 to 400°K an effect of 2% or more would be quite unlikely.

(2) Temperature increase will have more effect in shifting downward the minimum hot atom energy at which reaction occurs, if the threshold is high. In other words, when energy shifts are measured in absolute terms, the apparent threshold is reduced more for processes having a greater true threshold. This conclusion is perhaps unexpected. However, the increase in yield with temperature will tend to be greater for a low threshold reaction for two reasons. (a) Collision densities per unit energy interval are normally greater at low energies making a shift in threshold be more important in this region. (Note that the *relative* shift is larger for low threshold processes.) (b) The effect of thermal motion in decreasing energy loss on collision will usually be greater for lower energy hot atoms.

(3) Other things being equal, translational temperature effects will be less for reactions with heavier substrate molecules.

Effect of Temperature-Dependent Internal Energy. The effect of temperature in enhancing hot atom reaction through internal motion of a substrate cannot be estimated in the absence of information on the dependence of cross sections on vibrational and rotational energy. In general one would still expect this effect to be small simply because typical kinetic energies of reacting hot atoms (0.5–30 eV) greatly exceed internal energy changes with temperature increases of the order of 100°. Yet there are two reasons why temperature effects may be significantly larger when internal rather than translational thermal motion is considered. (a) For complex molecules, such as butane, thermal energy in vibration and rotation is greater by an order of magnitude or more than thermal translational energy. A 100° temperature rise may increase internal energy by tenths of an electron volt. However, because of the fast and localized nature of hot atom attack, particularly in the case of tritium, only a portion of this energy is likely to be available. (b) Some reactions are driven much more efficiently by internal rather than translational energy.[16,17]

Consequently if a true hot atom reaction (we define

(13) The choice of $^3/_2kT$ as the portion of substrate translational energy which contributes to a threshold shift is arbitrary since we do not know the shape of the excitation function. $^1/_2kT$ (corresponding to the line-of-centers model), or kT, could have been used with equal justification. The choice is however not important since we are only seeking an idea of the magnitude involved.

(14) R. G. Gann, W. M. Ollison, and J. Dubrin, *J. Chem. Phys.*, in press.

(15) M. Menzinger and R. Wolfgang, *ibid.*, **50**, 2991 (1969).

(16) K. G. Anlauf, *et al.*, *ibid.*, **51**, 5716 (1969).

(17) J. C. Polanyi and D. C. Tardy, *ibid.*, **51**, 5717 (1969).

this as a reaction having a threshold at least an order of magnitude greater than kT) does display a temperature dependence, it is likely to be due to internal motion of the substrate molecule.

Conclusions

In contrast to the indication provided by the earlier work[5] we find that the temperature effect on hot tritium reaction with butane is so small as to be comparable to experimental error. As discussed in the introduction, inadequate scavenging may have led to error in the previous result. To the extent that there is a temperature dependence it is much more likely to be due to the internal energy of the reactants rather than their translational motion.

Acknowledgments. This work was supported by the U. S. Atomic Energy Commission under contract AT-(30-1), 1957. One of us (H. M. Chang) acknowledges the support of a Yale-in-China Fellowship. We are grateful for the assistance and advice of Mr. Richard Hall and Dr. David Malcolme-Lawes.

Recombination of Bromine Atoms in a Laminar Hydrogen–Bromine Flame

by Osamu Horie and George C. Frazier, Jr.[1]*

The Johns Hopkins University, Baltimore, Maryland 21218 *(Received October 12, 1970)*

Publication costs borne completely by The Journal of Physical Chemistry

The rate of the recombination reaction of bromine atoms with HBr as third body was experimentally determined in the hot flame gases of a steady, laminar, low pressure, hydrogen–bromine flame. A Br atom detector was developed and combined with the microprobe sampling technique for measuring the Br atom concentration profile. The detector consisted of a pair of nickel wire coils which formed two adjacent arms of a Wheatstone bridge. A simple theory of Br atom conservation in the constant temperature hot flame gases was formulated in order to interpret the data in terms of the rate coefficient k_r of the recombination reaction: $Br + Br + HBr \xrightarrow{k_r} Br_2 + HBr^*$. The operating conditions of the flame were with an initial mixture of 45.6–45.8% Br_2, a burner pressure of 0.117–0.118 atm, and a total molar flow rate of 2.454×10^{-3} to 2.460×10^{-3} g mol/sec. At the flame temperature of 1417°K, the value for $k_r = 8.3 \pm 2.5 \times 10^{14}$ cc²/(mol² sec) was obtained.

Introduction

The kinetics of the reaction

$$Br_2 + M^* \underset{k_r}{\overset{k_d}{\rightleftharpoons}} Br + Br + M \qquad (1)$$

was studied experimentally at elevated temperature, where the third body, M, was HBr. The method used was the observation of the rate of approach of this reaction to final equilibrium in the hot gases of a hydrogen–bromine flame.

Reaction 1 is of interest to both those working in the area of rate processes of elementary reactions, and also to those interested in the behavior of flames considered as a complete physicochemical system. The connection between reaction 1 and the latter area of interest is mainly through the hydrogen–bromine flame, which is one of the simplest systems propagating by the chain mechanism characteristic of more complex flames.[2]

Reaction 1 has therefore received considerable attention during the last decade or so. The experimental work has centered primarily on two temperature regions. The first is a range of a few hundred degrees centigrade above room temperature,[3-5] and the second is the range of approximately 1000–2300°K.[6-11] The low temperature work has been conducted by the use of flash photolysis, while the shock tube mainly has been

(1) University of Tennessee, Department of Chemical and Metallurgical Engineering, Knoxville, Tenn. 37916.

(2) R. M. Fristrom and A. A. Westenberg, "Flame Structure," McGraw-Hill, New York, N. Y., 1965.

(3) (a) M. R. Basila and R. L. Strong, *J. Phys. Chem.*, **67**, 521 (1963); (b) W. G. Givens, Jr., and J. E. Willard, *J. Amer. Chem. Soc.*, **81**, 4773 (1959).

(4) J. K. K. Ip and G. Burns, *J. Chem. Phys.*, **51**, 3414 (1969).

(5) R. L. Strong, J. C. W. Chien, P. E. Graf, and J. E. Willard, *ibid.*, **26**, 1287 (1957).

(6) D. Britton, *J. Phys. Chem.*, **64**, 742 (1960).

(7) D. Britton and R. M. Cole, *ibid.*, **65**, 1302 (1961).

(8) D. Britton and N. Davidson, *J. Chem. Phys.*, **25**, 810 (1956).

(9) G. Burns and D. F. Hornig, *Can. J. Chem.*, **38**, 1702 (1960).

(10) C. D. Johnson and D. Britton, *J. Chem. Phys.*, **38**, 1455 (1963).

(11) H. B. Palmer and D. F. Hornig, *ibid.*, **26**, 98 (1957).

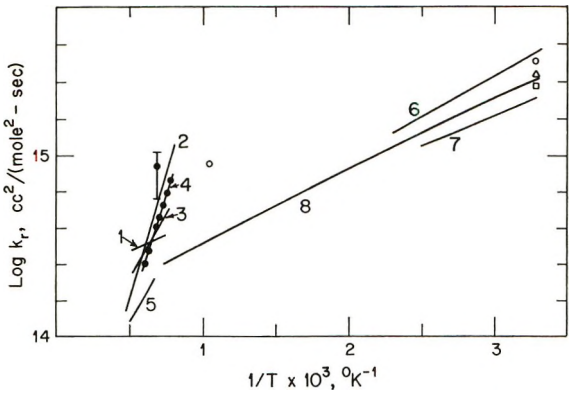

Figure 1. Recombination rate coefficients with argon and also HBr as third body: ●, present result; ○, Burns and Hornig (1960); △, Basila and Strong (1963); □, Rabinowitch and Wood (1936); 1, Britton and Davidson (1956); 2, Palmer and Hornig (1957); 3, Britton (1960); 4, Britton and Cole (1961), HBr as third body; 5, Johnson and Britton (1963); 6, Strong, *et al.*, (1957); 7, Givens and Willard (1959); 8, Ip and Burns (1969).

used to produce the high temperature in the latter range. Third bodies such as Ar, Br_2, HBr, N_2, O_2, and He have been used to effect the recombination of the bromine atoms in these experiments. However, most of the work has been conducted with Ar as the third body. The available data are shown in Figure 1 for Ar as third body along with the single data for HBr as third body.

The data of Figure 1 exhibit two shortcomings. The data of different investigators in the same temperature range are not in good agreement, and second, the data in the high temperature region do not extrapolate smoothly toward the low temperature data except for the data of Ip and Burns. This latter point suggests that the activation energy of the reaction for Ar as third body obtained from the shock tube data is questionable. This could be due to the method of interpretation of such data as well as to the question of the definition of such properties as temperature during shock tube experiments.[12,13]

The present study was therefore initiated in an attempt to provide an independent measurement of the bromine atom recombination rate coefficient k_r at relatively high temperature. Data from an independent measurement in principle can assist in resolving the apparent discrepancies among the existing data. An independent approach to this problem is that of observing the rate of change in position of the appropriate species in a steady flame, as discussed by Fristrom and Westenberg.[2] In particular, the spherical, laminar, premixed hydrogen–bromine flame is suitable for the present study where it has been observed that the flame gases provide a high temperature "thermostat" where the temperature remains constant to within a few degrees over a distance of approximately 1 cm.[14] It is mostly within this essentially uniform high temperature zone that the recombination of the Br atom takes place in this flame. This zone therefore provides both the atoms in a composition slightly removed from equilibrium, and also the high temperature medium, and thus serves as a basis of this study. As HBr is the only product in this reaction system, it acts as the third body for the atom recombination along with any unconsumed reactants.

An advantage of this approach over the shock tube is that the residence time of the gases in the observation zone is of the order of milliseconds in contrast to that of the order of microseconds in the shock tubes. The problems of time resolution and of relaxation of vibrational energy of the gases are therefore less severe than in shock tube experiments. A disadvantage of the present approach is that the temperature and composition ranges are restricted to those for which the hydrogen–bromine flame is stable.

The development of an experimental tool for measuring bromine atom concentration was required for this investigation. The basis chosen was a fine, quartz sampling probe[2] containing a nickel wire coil upon which the recombination of bromine atoms occurred. This probe provided an electrical signal proportional to the heat of recombination of the atoms, as was shown by calibration against a system containing known atom concentrations.

The measured bromine atom concentration profiles were interpreted in terms of a simple theory which was used to calculate the rate coefficient of the recombination reaction.

Experimental Procedure and Results

The apparatus consisted of a low pressure spherical burner, a temperature measuring device, and the bromine atom detector.

The burner was of the same basic design described previously[15] except for the bromine evaporator and Br_2 flow regulation. The evaporator used in this work was of the atmospheric pressure type which was continuously purged to prevent contamination of the bromine by air. The bromine flow was metered through a small orifice with the upstream pressure being monitored by use of an all-glass spiral manometer, as shown in Figure 2. Additional details are given in ref 16.

Temperature measurements were made with a small silica coated Pt—Pt–10% Rh thermocouple fabricated from 0.001 in. diameter wires and supported by 0.01

(12) J. N. Bradley, "Shock Waves in Chemistry and Physics," Wiley, New York, N. Y., 1962.

(13) E. F. Greene and J. P. Toennies, "Chemical Reactions in Shock Waves," Academic Press, New York, N. Y., 1964.

(14) G. C. Frazier, Jr., Ph.D. Dissertation, The Johns Hopkins University, 1962.

(15) G. C. Frazier, Jr., R. M. Fristrom, and J. F. Wehner, *AIChE J.*, 9, 689 (1963).

(16) O. Horie, Ph.D. Dissertation, The Johns Hopkins University, 1968.

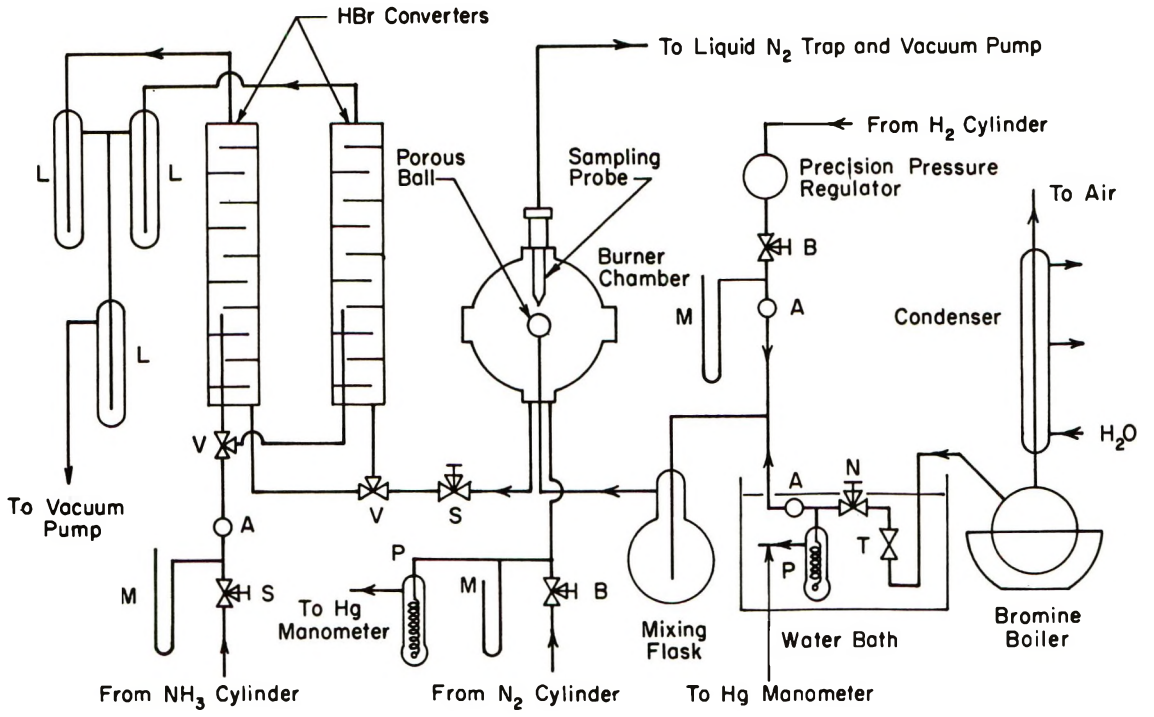

Figure 2. Flow system for the hydrogen–bromine flame.

in. diameter wires of the same materials. The junction was welded by the use of a natural gas–oxygen microflame under a microscope, and was coated with silica by passing it through the flame of a Meker burner containing a small stream of hexamethyldisiloxane.[2] Uncorrected thermocouple readings are shown in Table I for a typical run, and values corrected for radiation for the atom recombination zone of the flame are shown in Figure 3. The temperature corrections were made by the use of a simple heat balance[2] for the case of slow flow [$Re < \mathcal{O}(10^{-1})$] around the bead, which was essentially spherical

$$T_g - T_c \doteq \frac{e\sigma d T_c^4}{2\lambda_m} \qquad (I)$$

The diameter of the thermocouple d was determined under a microscope to be 0.009 cm. The emissivity of the bead, e, was not known precisely but was taken as 0.8, as the bead was darkened slightly during exposure to the hot gas. The thermal conductivity of the hot gas mixture, λ_m, was calculated by the relation of Mason and Saxena,[17] with the thermal conductivity of the individual species taken from Campbell and Fristrom.[18] Since the hot flame gas was essentially in equilibrium and consisted mainly of HBr and H_2, the equilibrium

Table I: Temperature Profile[a]

Position $r-R$, cm	Temperature T_c, °K	Position $r-R$, cm	Temperature T_c, °K
0.010	624	0.233	1278
0.025	686	0.252	1297
0.039	745	0.272	1309
0.052	806	0.292	1320
0.069	861	0.327	1326
0.084	915	0.390	1331
0.098	966	0.454	1331
0.114	1015	0.520	1331
0.129	1062	0.582	1329
0.143	1107	0.645	1328
0.160	1147	0.711	1327
0.177	1189	0.776	1325
0.195	1225	0.840	1325
0.214	1255		

[a] Experimental conditions: $x_{Br_2} = 0.456$, total molar flow rate = 2.46×10^{-3} g mol/sec, burner pressure = 89.6 mm.

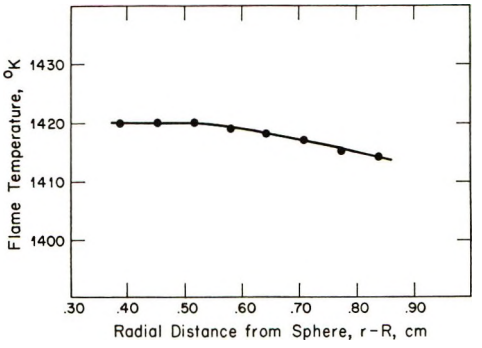

Figure 3. Temperature profile in atom recombination zone.

(17) E. A. Mason and S. C. Saxena, *Phys. Fluids*, **1**, 361 (1958).
(18) E. S. Campbell and R. M. Fristrom, *Chem. Rev.*, **58**, 173 (1958).

mole fractions of HBr and H_2 (they accounted for approximately 99% of the hot gas) were used in computing the mixture thermal conductivity λ_m. The equilibrium constants reported in ref 18 were used in computing the equilibrium composition, and these values agreed within experimental error with the measured HBr and H_2 values.[15,16]

The corrected temperatures in the recombination zone of the flame ($r-R \approx 0.4$–0.8 cm) vary from 1420 to 1414°K, as shown in Figure 3. Because this variation is only 6°K, the temperature in the experimental zone of interest is essentially constant, especially in view of the fact that the atom recombination rate coefficient is expected to be a relatively weak function of temperature. Therefore, an average temperature of 1417 ± 3°K is taken as the flame temperature of the atom recombination zone.

A new probe and atom detection system were developed for measuring the atom concentration. The approach of sampling the flame gases with a quartz microprobe was selected for this purpose because of the extensive background associated with this technique,[2] and a coil of fine nickel wire was included in the probe as a recombination surface for the Br atoms. Such a measuring device requires calibration against an atom-containing source of known concentration, as described subsequently.

A sketch of the sampling probe is shown in Figure 4. The sampling probe was made of quartz tubing 18 mm i.d. and about 300 mm long. One end was tapered to an orifice of about 110 μ. The orifice was fabricated by a procedure described in ref 2. The other end of the probe was fitted with a tapered joint to which the detector unit was attached. The detector coil was supported on a quartz tube of 12 mm o.d. Three ceramic supports were cemented on the detector tube to protect the coil from vibration and distortion by contact with the inner wall of the probe.

A 6 mm o.d. tube was inserted into the 12-mm tube, and the annular space between these tubes was used as a cooling jacket. A small flow of distilled water was introduced through a pair of stainless steel, 18-gauge, hypodermic needles.

The detector consisted of a pair of nickel wire coils having approximately the same resistance values. Nickel was used as the wire material because of its high temperature coefficient of resistivity and its resistance to corrosion. The coils were formed from 0.005-in. wire each 90 cm in length. The diameter of each coil was about 1.8 mm, so the annular space between the 12- and 16-mm tubes was almost completely occupied by the coils. This arrangement allowed essentially all of the gas sample to pass through the coil, thus providing maximum sensitivity, which was important in this application as the total atom flow rate was no greater than about 10^{-8} g atom/sec in the samples withdrawn from the flame.

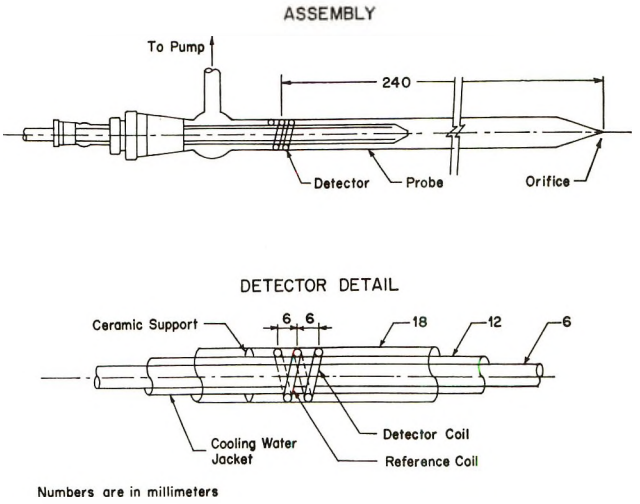

Figure 4. Schematic of the sampling probe and detector assembly.

The unique feature of this detector was the two coil arrangement, the two coils forming adjacent arms of a Wheatstone bridge. It was found with a single coil detector that the signal was extremely sensitive to temperature fluctuations in the reactor as well as the surroundings, to flow rate fluctuation, to aging of the nickel wire by corrosion, to deposit of carbon on the probe walls and detector, and to sampling pressure changes. With the two coil arrangement, the second coil being placed immediately downstream of the first, signals arising from extraneous sources were cancelled out, and a negligible potential difference developed between the coils in the absence of Br atoms. When the sample contained Br atoms, a fraction of the heat liberated on the first coil during atom recombination was carried to the second coil and its temperature also increased, though this was less than the temperature increase in the first coil. After a steady state was reached, the difference between the two coil temperatures was recorded as a potential difference. A marked increase in the stability of the signal was achieved by this arrangement, although it reduced the absolute sensitivity of the detector.

Positioning of the detector was achieved by moving the supporting tube axially along the probe. Several detector positions relative to the probe orifice were tried, but the measurements were made with the detector located just outside the reactor, and the distance between the center of the detector coil and the probe orifice was approximately 240 mm.

The probe and detector combination was calibrated against Br atoms sampled from the equilibrium system $Br_2 = 2Br$. By varying the temperature and partial pressure of Br_2 in a quartz reactor it was possible to generate Br atoms at concentration levels expected in the flame. Both HBr and N_2 were used as diluents. The equilibrium Br atom concentration could be computed from the measured temperature, pressure, and

the known equilibrium constants for this system. The microprobe was used to sample the equilibrium gas mixture. As the temperature and pressure within the probe were different from that of the equilibrium mixture, the sample equilibrium point was shifted, and the Br atoms were detected by measuring their heat of recombination on the nickel coil.

Bromine was ACS reagent grade supplied by J. T. Baker Chemical Co. After the bromine was transferred into a flask in the calibration system, it was partially flashed several times under vacuum to eliminate gaseous impurities. No further purification was made. Hydrogen bromide was supplied by The Matheson Co. and rated as 99.8% purity. HBr was used without purification.

The calibration system consisted of an electrically heated quartz tubular reservoir, four mixing flasks, an HBr cylinder, a Br_2 storage flask, two Pyrex glass spiral manometers, and the sampling probe and detector unit.

All the stopcocks upstream of the reactor were of greaseless, Teflon-stem, high vacuum type, and a needle valve for controlling the flow of the reactant mixture was made of Monel metal, in order to avoid any possible contamination of the reactant mixture with carbonaceous materials. Most of the connections were made with 10-mm Pyrex glass tubing. Pyrex-to-quartz graded seals were used to join the quartz reactor to the rest of the system.

The calibration reservoir was made of quartz tubing 30 mm i.d. and 300 mm long to which a set of semi-ball and socket ground joints were attached. One joint was connected to a thermocouple sheath, and the other was reserved for the sampling probe. No grease was used to connect these joints. A thin Teflon film was placed between the ground parts, and they were pressed against each other. An epoxy resin was applied around the joints to give mechanical strength and desired vacuum tightness.

The reservoir was packed with quartz chips to reduce temperature gradients in both the radial and axial directions. The system was heated by a main electric heater and two minor electric heaters placed near the two ends of the tube. These minor heaters were used to minimize the longitudinal temperature gradient. The reservoir temperature was measured by a 0.01-in. diameter Pt—Pt–10% Rh thermocouple. The junction was placed approximately at 4 mm away from the sampling orifice position, and the temperature profile was sufficiently flat that the temperature read was essentially that at the probe tip.

Standard gas mixtures for the calibration runs were prepared by introducing Br_2 and HBr to each of five 1-l. storage flasks. The composition of the mixture was determined by measuring the partial pressure of HBr and Br_2 with a Pyrex glass spiral manometer. The mixtures were stored at least for 48 hr to allow complete mixing before use.

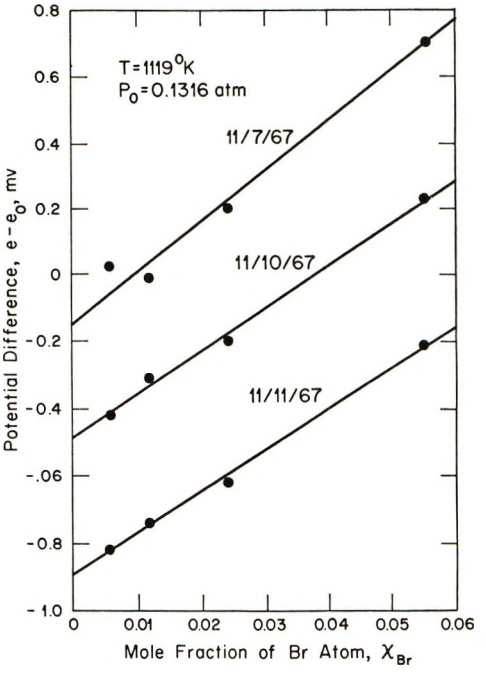

Figure 5. Calibration curves for the sampling probe and detector assembly.

The reservoir was heated to a desired temperature, while the entire system was evacuated. The constancy of the temperature was attained by regulating the input voltage by use of a 2 kVA Sörensen voltage stabilizer. The temperature was regulated to within ±3° during a run. When a steady state was reached, the signal from the detector was recorded and this was taken as a reference potential, e_0, for a run.

At this point a known gas mixture was introduced into the reservoir. The pressure was regulated by the Monel metal fine-controlling needle valve. This was necessary because as soon as the mixture began to flow into the reactor, a small fraction of the mixture was withdrawn from the reactor through the quartz sampling probe. The pressure was read by a Pyrex glass spiral manometer.

Change of the output from the detector was recorded, and a steady state was reached in about 30 min, and after 30 more minutes, the output was recorded as representing the equilibrium concentration of Br atoms under specified conditions, e.

Actual calibration runs were made under the following conditions: temperature 843–846°; pressure in the reservoir of 100 mm; pressure in the sampling probe 0.025 mm under vacuum and 0.25–0.3 mm under sampling condition; mole fractions of Br_2 in the reaction mixtures of 0.0129, 0.05, 0.20, and 1.0; temperature at the detector 30–35°.

The calibration results are plotted in Figure 5 which shows the potential difference ($e - e_0$) plotted against calculated (equilibrium) Br atom mole fractions in the reactor reservoir.[19]

These results show that the signal is essentially linear with atom fraction in the gas sample, that aging does occur, but that the aging does not affect the slope of the curves appreciably. The aging effect was not prohibitive, but it did require that the calibration be checked frequently against a reference value during application in the flame gases. The reference point used was the (asymptotic) equilibrium mole fraction value far from the flame holder, as discussed below.

The aging was attributed primarily to carbon deposition within the probe, which could be reduced by elimination of greased joints from the system, but the aging could not be entirely overcome.

Our original intent was to develop an atom detector of the scavenging probe type,[20] using titration by NOCl.[21] However, titration by NOCl did not appear quantitative under our experimental conditions which was probably due to the fact that NOCl decomposes at relatively low temperatures.[22,23] Incomplete mixing of the NOCl with the sample stream may have also been a factor.

Experimental runs in which atom measurements were made were in flames of 45.3–45.8 mol % bromine, total molar flow rate of 2.46×10^{-3} to 2.47×10^{-3} g mol/sec, and a burning pressure of 89.3–89.6 mm. The reproducibility of the inlet mixture composition and of flow rate from day to day were both within 0.5%. These burning conditions were essentially the same as those of previous investigations,[15] and the character of these flames was as observed previously.

The bromine atom concentration was measured in the uniform temperature region which lay between approximately 0.4 and 0.8 cm from the ball. The microprobe sampling technique combined with the Br atom detector described above was used for this purpose. The sampling probe was mounted on a 40 turn per inch micrometer screw mechanism for positioning purposes.

Prior to each run, the probe was removed from the burner and washed thoroughly with a dilute HF solution and with distilled water to remove impurities from the probe wall and the detector. The sampled gas was pumped out through a liquid nitrogen trap. A section of 80 cm long, 10 mm o.d. Pyrex glass tubing was used between the probe and the evacuating system to minimize the pressure drop in the line. The flexibility provided by this glass tubing was sufficient to render a smooth shift of the position of the sampling probe for a range of about 0.6 cm. Occasionally the sampled gas was collected into a 1-l. flask and analyzed for hydrogen in order to check the overall material balance.

After a flame was stabilized, it took approximately 2 hr for the signal from the detector to reach a steady state. The measurements were made by changing the position of the probe by the micrometer screw mechanism, and a steady signal was achieved 6–8 min after each repositioning and was recorded with a 1-mV range Brown recording potentiometer. By this procedure 12–15 measurements were made within a period of about 2 hr. A comparison of the probe calibration conditions with the flame conditions is shown in Table II. The calibration conditions were selected to approximate as nearly as possible the conditions anticipated during actual use in the flame. The one property that it was not possible to duplicate during calibration was that of the hydrogen content of the gases in the flame system. Therefore, the question arises of whether or not hydrogen influences the calibration. The effect of hydrogen is thought not to be significant for two reasons. First, hydrogen is only slightly adsorbed on nickel at the detector temperature of about 40°.[24] It may be adsorbed even less in the presence of HBr and Br_2. In any event, no detectable signal was noted for the case of a H_2–Br_2 mixture flowing past the detector at room temperature. It is therefore concluded that reactions of hydrogen on the detector were negligible.

Table II: Comparison of Probe Sampling Conditions

Property	Value or range during calibration	Value or range during use in flame
Temp at probe tip, °K	1120	~1400
Temp of detector, °C	30–35	40
Sample pressure, mm	100	89
Probe pressure, mm	0.25–0.3	0.2–0.5
x_{Br_2} in mixture	0.013–1.0	~0.01
x_{HBr} in mixture	0–0.987	0.89
x_{H_2} in mixture		0.10
Sampling rate, μmol/sec	2.2–2.3	2.0–2.1

Because of the aging and the contamination problem on exposure of the probe to atmospheric conditions, the calibration could not be considered a fixed quantity when the probe was transferred from the calibration reactor to the flame burner. However, the linearity of the probe signal with atom flux was considered reliable, as this property was shown to be essentially independent of aging and mixture composition. What was needed in the flame was a known reference composition that could serve as a fixed reference point for the calibration. The near-equilibrium conditions in the hot flame gases were selected as this point. Theoretically, the equilibrium is not reached in an adiabatic, spherical flame until the gases move through an infinite distance ($r \rightarrow \infty$).

(19) The negative potential differences are due to the fact that the flow would cool the wire below the reference potential to a greater extent than the heating effect raised the temperature when the atom fraction was small.

(20) R. M. Fristrom, *Science*, **140**, 297 (1963).

(21) E. A. Ogryzlo, *Can. J. Chem.*, **39**, 2556 (1961).

(22) T. Welinsky and H. A. Taylor, *J. Chem. Phys.*, **6**, 466 (1938).

(23) P. G. Ashmore and J. Chanmugam, *Trans. Faraday Soc.*, **49**, 254, 265 (1953).

(24) H. S. Taylor, "Advances in Catalysis," Vol. 1, Academic Press, New York, N. Y., 1948, p 19.

However, at some finite radial position the Br atom fraction will approach its equilibrium value x^e to within a small quantity which is negligible with respect to the experimental error. The equilibrium atom fraction can be computed from the known temperature, pressure, initial mixture composition, and the appropriate equilibrium constants.

The actual procedure was to (1) demonstrate that the signal tended toward an asymptotic value, e_0 mV, as the probe was moved downstream through the recombination zone (this asymptotic value corresponds to the equilibrium concentration of Br atoms in the hot gas), (2) calculate the equilibrium Br atom concentration in the region, (3) record the signal at each probe position, e mV, and subtract from it the value of the reference region, $e - e_0$ mV, (4) locate the equilibrium Br atom fraction on the calibration curve, and (5) determine the fraction of Br atoms x_{Br} at each position by correlating the change in the signal, $e - e_0$ mV, with the slope of the calibration curve.

The results of the measurements are shown in Figure 6, and the concentration data are provided in Table III.

Table III: Bromine Atom Concentration Profiles[a]

Run no. 1 (5/4)		Run no. 2 (7/26)		Run no. 3 (8/2)	
Position $r-R$, cm	Mole fraction of Br atoms	Position $r-R$, cm	Mole fraction of Br atoms	Position $r-R$, cm	Mole fraction of Br atoms
0.910		0.807	0.00771	0.806	
0.874	0.00771	0.777		0.775	0.00771
0.842		0.744	0.00837	0.738	
0.811		0.714	0.00851	0.713	0.00847
0.779	0.00779	0.680	0.00970	0.678	0.00922
0.744	0.00817	0.649	0.0104	0.647	0.0101
0.716	0.00856	0.617	0.0107	0.616	0.0111
0.680	0.00910	0.586	0.0116	0.583	0.0117
0.649	0.00971	0.551	0.0124	0.551	0.0123
0.620	0.0101			0.521	0.0128
0.588	0.0109			0.487	0.0138
0.555	0.0113			0.454	0.0143
0.524	0.0120				
0.490	0.0126				
0.461	0.0135				
0.424	0.0142				

[a] Experimental conditions: run no. 1, $x_{Br_2} = 0.456$, total molar flow rate = 2.454×10^{-3} mol/sec, burner pressure = 89.3 mm; run no. 2, $x_{Br_2} = 0.458$, total molar flow rate = 2.460×10^{-3} mol/sec, burner pressure = 89.0 mm; run no. 3, $x_{Br_2} = 0.458$, total molar flow rate = 2.460×10^{-3} mol/sec, burner pressure = 89.0 mm. Note: equilibrium Br atom mole fraction (0.00771) is determined by averaging over the distance of constant output signal.

The steadiness of the signal at a particular position was not strictly observed because gradual carbon deposition[25] tended to decrease the signal level. Therefore, during a run, the detector calibration was checked against the reference region and, if necessary, a correction was applied. The signal was sensitive to changes in flow rate of bromine and pressure of the burner. Adjusting these variables during a run was avoided as much as possible; nevertheless a few adjustments of bromine flow rate had to be made. The experimental conditions of the flame for which the concentration measurements were made are as follows: Br_2 mole fraction in the initial mixture 0.456–0.458, the total molar flow rate $2.454–2.460 \times 10^{-3}$ mol/sec, the burner pressure 89.0–89.3 mm, and the uncorrected maximum temperature 1331°K.

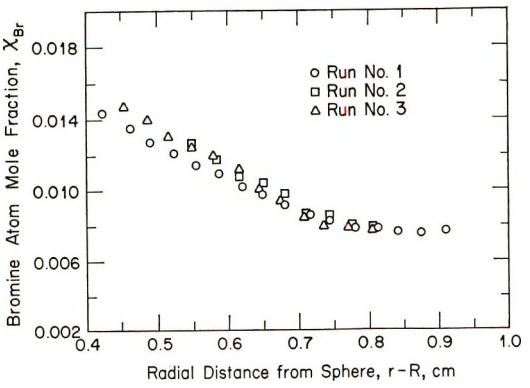

Figure 6. Bromine atom profiles.

There is roughly 20% difference in the observed concentration of Br atoms for the two series of runs, namely for a measurement taken on May 4th, and for those taken on July 26th and August 2nd. This difference may be due to slight modifications in the experimental conditions, particularly in the burner pressure. Although the difference in the burner pressures in the experimental runs was only 0.3%, it was estimated that this was one of the major factors affecting the reproducibility of the measurement.

An interpretation of these data in terms of the atom recombination rate coefficient k_r is given in the following section, but it is of interest to first comment on the question of departure of the internal degrees of freedom from equilibrium in the Br_2 and HBr molecules in the experimental zone.

As a means of estimating whether or not appreciable departure of the internal degrees of freedom from equilibrium occurs here, one can compare the residence time of the molecules in the first increment of the experimental recombination zone to the characteristic relaxation times for rotational and vibrational change of states. The residence time in the first 10%, say, of the experimental flame recombination zone can be computed from the flame velocity in the zone, which is approximately 65 cm/sec. This gives a residence time in a zone 0.05 cm thick of the order of 10^{-3} sec.

This characteristic residence time is to be compared with the slowest or controlling molecular relaxation

(25) The source of the carbon was probably the bromine, although this was not checked.

time. Of rotational and vibrational relaxation the latter is generally the slower process; for Br_2, the vibrational relaxation time appears to be of the order of 10^{-6} sec in the neighborhood of room temperature,[26] and is probably less at the higher temperatures of this experiment. There apparently are no data for vibrational relaxation of HBr. However, if it is assumed that the order of 10^4 collisions are required for its vibrational relaxation, as is the case with many diatomic molecules,[12,26] then under the pressure of 0.118 atm and temperature of 1417°K in the hot flame gases, the HBr collision frequency is of the order of 10^{10} sec^{-1}, which yields an estimated relaxation time of the order of 10^{-6} sec. As the residence time is several magnitudes greater than these estimated relaxation times, it would appear that the chemical species are relaxed in the hot flame gases of the present experiment.

Interpretation of Results

The data of Figure 6 may be interpreted in terms of the recombination coefficient k_r of reaction 1 by use of a special, restricted form of the atom conservation equation. The starting equation, for the constant temperature, atom recombination zone of the steady spherical flame, may be written

$$\frac{m_0}{4\pi\rho r^2}\frac{dx_1}{dr} = \frac{1}{r^2}\frac{d}{dr}\left(r^2\mathfrak{D}_1\frac{dx_1}{dr}\right) + 2C[k_d x_m x_2 - k_r C x_m x_1^2] \quad \text{(II)}$$

The unknown mole fractions are those for the atom, x_1, the bromine molecule, x_2, and the third body, x_m, so additional conservation equations are required, strictly speaking, in order to determine this system. For the present case, however, some approximations are suggested by the special form of the experimental results and by the magnitudes of the parameters, as discussed below.

The terms in brackets on the right in eq II for the disappearance of Br atoms by chemical reaction are consistent with the chemical steady-state approximation for the hydrogen atom,[27] which has been shown to be a good approximation in this flame.[28,29]

The first task is to identify the third body(s) for the recombination zone. There are five possibilities: the bromine and hydrogen atoms, and the bromine, hydrogen, and hydrogen bromide molecules. The first three are thought to contribute negligibly to recombination because of their low concentration (see Table IV). The hydrogen molecule is present in appreciable concentration, so a reaction such as

$$Br + Br + H_2 \longrightarrow Br_2 + H_2^* \quad (2)$$

must be considered. The low temperature data indicate that H_2 is roughly 1.7 times as effective as Ar as third body,[30] which makes it of the same order of effectiveness as HBr as third body, as determined by Britton and Cole at elevated temperature.[7]

Table IV: The Conditions in the Recombination Zone (Parameters for Use in Eq IX)[a]

Property	Value
Total mass flow rate, m_0, g/sec	0.182
Burner pressure, atm	0.118
Flame temperature, °K	1417
Average density, ρ, g/cm³	0.755×10^{-4}
Total molar concentration, C, mol/cc	1.016×10^{-6}
Initial Br_2 mole fraction	0.456
Equilibrium constant, K, mol/cc	2.96×10^{-7}
Equilibrium composition	
x_{Br_2}	0.205×10^{-3}
x_{Br}	0.771×10^{-2}
x_{H_2}	0.0889
x_H	0.516×10^{-5}
x_{HBr}	0.903
Diffusion coeff, $\mathfrak{D}_{HBr-Br}$, cm²/sec	9.69
Diffusion coeff, $\mathfrak{D}_{H_2-Br}$, cm²/sec	64.4
Effective diffusion coeff, $\mathfrak{D}_e$, cm²/sec	10.56

Note: $\mathfrak{D}_{HBr-Br}$ and $\mathfrak{D}_{H_2-Br}$ are computed from ref 18.

However, a competitor to reaction 2 develops as the temperature is raised

$$Br + H_2 \longrightarrow HBr + H \quad (3)$$

This reaction is competitive at high temperature because of its large activation energy (17.6 kcal/mol). Thus the ratio of the rate coefficient of reaction 3 at 1400°K to its value at 300°K is of the order of 10^{10}. The following mechanism is therefore suggested for the high temperature range

$$Br + H_2 \longrightarrow [BrH_2] + Br \xrightarrow{k_2} Br_2 + H_2^* \quad (4)$$
$$\qquad\qquad\quad \Big| \xrightarrow{k_3'} HBr + H$$

The dominant path in this mechanism can be estimated by comparing the known rate, R_3, with an estimate of the maximum possible rate of reaction 2. This maximum rate is made by assuming that every ternary collision results in reaction. The maximum frequency factor for reaction 2 at 1400°K is $\sim 10^{15}$ cc²/(mol² sec).[27] Thus, at 1400°K, the ratio R_3/R_2 is at least 5×10^2, which suggests that collision of Br atoms with H_2 in the temperature range of interest leads to HBr rather than to recombination of atoms.

The dominant mechanism by which Br atom recombination takes place in this flame is therefore expected to be with HBr as third body, and x_m in eq II is the mole fraction of HBr. Actually the H_2 concentration is only about 10% that of HBr, so its effectiveness as third

(26) A. W. Read, *Progr. React. Kinet.*, **3**, 203 (1965).

(27) S. W. Benson, "The Foundations of Chemical Kinetics," McGraw-Hill, New York, N. Y., 1960.

(28) E. S. Campbell, *Symp. (Int.) Combust. [Proc.], 6th*, 213 (1957).

(29) G. C. Frazier, Jr., and J. Wendt, *Chem. Eng. Sci.*, **24**, 95 (1969).

(30) E. Rabinowitch and W. C. Wood, *Trans. Faraday Soc.*, **32**, 907 (1936).

body would have to be appreciably greater than that of HBr in order to change the result significantly.

The diffusion coefficient $\mathfrak{D}_1$ for use in eq II can be approximated in terms of an effective diffusion coefficient of atoms diffusing in a mixture of H_2 and HBr, where the effective coefficient is defined by[2]

$$\mathfrak{D}_e = [x_{H_2}/\mathfrak{D}_{H_2-Br} + x_{HBr}/\mathfrak{D}_{HBr-Br}]^{-1} \quad \text{(III)}$$

This method of computing and effective diffusion coefficient has been demonstrated experimentally.[31,32] As the hydrogen and hydrogen bromide mole fractions as well as the temperature and pressure are essentially constant in the flame zone of interest, $\mathfrak{D}_e$, is also essentially constant, so that eq II can be written in the following nondimensional form

$$\frac{1}{\xi^2}\frac{dx_1}{d\xi} = \frac{1}{Pe\xi^2}\frac{d}{d\xi}\left(\xi^2\frac{dx_1}{d\xi}\right) + \alpha x_2 - \beta x_1^2 \quad \text{(IV)}$$

where $\xi \equiv r/R$, and the rate coefficient k_r we wish to evaluate by use of the experimental data is contained in the parameter β. Equation IV is a nonlinear, second-order differential equation with two unknowns and an irregular singular point at $\xi = 0$. A solution for the system formed by this and its companion equation for x_2 is not known, although it is likely that an (asymptotic) series solution could be developed. The form of such a solution, however, would probably be such that an interpretation of the data in terms of a rate coefficient would be difficult.

A simple model of this problem is suggested by the magnitude of the Peclet number Pe and also the shape of the experimental data. From the data in Table IV, Pe = 14.3, which suggests that convective transport is of the order of one magnitude greater than the diffusive transport of the atom in the hot flame gases. Secondly, the data of Figure 6 show a range, $r-R < 0.75$ cm, where the second derivative is small. The data are thus visualized in two parts: that range below $r-R \approx 0.75$ where the rate of approach to equilibrium is relatively rapid and where the second derivative is small, and that part beyond $r-R \approx 0.8$, where the equilibrium conditions have been essentially achieved. The approach is therefore taken of using the data in this second range to establish the probe reference calibration, as discussed above and to use the data in the first range in the evaluation of the rate coefficient.

With this in mind, we neglect the second derivative in eq IV, yielding

$$\left(\frac{2}{Pe\xi} - \frac{1}{\xi^2}\right)\frac{dx_1}{d\xi} + \alpha x_2 - \beta x_1^2 \doteq 0 \quad \text{(V)}$$

where the first term in the parentheses provides an approximate correction for diffusive transport in the experimental zone, $0.4 \leq r-R \leq 0.75$.

The relative small diffusive transport in the zone of interest also suggests an approximate expression for x_2 in terms of x_1. By making an overall Br atom balance between any point $r-R$ in the recombination zone and a point $r-R \rightarrow$ large, we get for negligible diffusion

$$(C_{Br} + 2C_{Br_2} + C_{HBr})v_r A|_r \doteq (C_{Br}^e + 2C_{Br_2}^e + C_{HBr}^e)v_r A|_{r\to\infty} \quad \text{(VI)}$$

As the pressure, temperature, total mass density, and HBr concentration are all essentially constant in this zone,[15] eq VI reduces to

$$x_{Br} + 2x_{Br_2} \doteq x_{Br}^e + 2x_{Br_2}^e \equiv a \quad \text{(VII)}$$

Replacing x_2 in eq V with its value from eq VII provides a result that can be readily integrated

$$\left[\frac{2}{Pe\xi} - \frac{1}{\xi^2}\right]\frac{dx_1}{d\xi} + \frac{\alpha}{2}(a - x_1) - \beta x_1^2 \doteq 0 \quad \text{(VIII)}$$

at $\xi = \xi_1$, $x_1 = x_1'$. The solution of eq VIII is

$$\ln\left[\left(\frac{x_1 - x_1^e}{x_1' - x_1^e}\right)\left(\frac{x_1' + x_1^e + K/(2C)}{x_1 + x_1^e + K/(2C)}\right)\right] = \frac{C_m(K + 4x_1^eC)k_r}{2\mathfrak{D}_e} f(\xi; Pe) \quad \text{(IX)}$$

where

$$f(\xi; Pe) = \left[\xi^2 - \xi_1^2 + Pe(\xi - \xi_1) + \frac{Pe^2}{2}\ln\left(\frac{\xi - Pe/2}{\xi_1 - Pe/2}\right)\right]R^2/2$$

A plot of the left-hand side of eq IX against $f(\xi; Pe)$ should yield a straight line of slope $C_m(K + 4x_1^eC)k_r/(2\mathfrak{D}_e)$. Hence, the rate coefficient k_r may be obtained from an experimentally determined Br atom concentration profile and the measured (or known) values of C_m, C, x_1^e, K, and $\mathfrak{D}_e$.

Actually we would not expect in this instance that all the data of Figure 6 would be correlated by eq IX because of the necessity of approximating the data in the range of $r-R \approx 0.8$–0.9 cm as the equilibrium value x_1^e for calibration purposes. The effect of this reference calibration technique is essentially to move the point at $r-R = \infty$ to the range of $r-R \approx 0.8$–0.9 cm, and because of the logarithm terms in eq IX, we would expect the data to depart from the straight line as $r-R \rightarrow$ large [$f(\xi; Pe) \rightarrow$ small]. That this is the case is illustrated by Figure 7, where the data of Figure 6 are plotted in accordance with eq IX. However, there is a region greater than $f(\xi; Pe) \approx -0.01$ cm^2 where the data essentially follow the straight line behavior predicted by eq IX, and it is this range that is used in the evaluation of the rate coefficient k_r. A least-squares analysis yields a slope of 11.8 cm^2, and with the use of the appropriate

(31) D. F. Fairbanks and C. R. Wilke, *Ind. Eng. Chem.*, **42**, 471 (1950).

(32) R. E. Walker, N. de Haas, and A. A. Westenberg, *J. Chem. Phys.*, **32**, 1314 (1960).

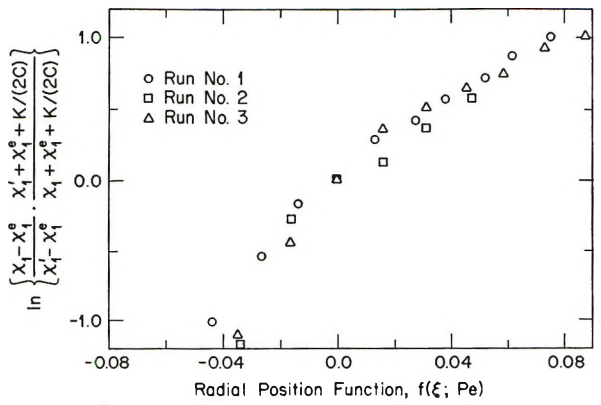

Figure 7. Bromine atom mole fractions interpreted in terms of eq IX.

parameters in Table IV, the value of the recombination rate coefficient with HBr as third body is computed to be k_r(HBr) = (8.3 ± 2.5) × 10^{14} cc²/(g mol² sec) at 1417°K.

This value is shown in Figure 1 along with the existing data of which only those by Britton and Cole[7] were with HBr as third body. Table V provides the values at 1417°K, the temperature of the present experiment.

Table V: Rate Coefficient k_r at 1417°K

Investigators	Third body	$k_r \times 10^{-14}$, cc²/(mol² sec)
This work	HBr	8.3 ± 2.5
Britton and Cole (1961)	HBr	4.67
Palmer and Hornig (1957)	Ar	5.66
Britton (1960)	Ar	4.17
Ip and Burns (1969)	Ar	2.3
Palmer and Hornig (1957)	Br_2	10.1
Britton and Cole (1961)	Br_2	27.3

The present result with HBr as a third body is about 78% greater than that of Britton and Cole, who used the shock tube approach. This agreement is fairly good, but we have been unable to obtain data over a sufficient temperature range to confirm the slope of the shock tube data. The shock tube data, Figure 1, do not extrapolate smoothly to the low temperature flash photolysis data, except for that of Britton and Davidson (1956). However, the high temperature, flash photolysis data of Ip and Burns (1969) do intersect the shock tube data, and a tentative conclusion is that HBr is from two to four times as effective as Ar for the recombination of Br atoms at 1417°K.

However, the present value of the rate coefficient, while in substantial agreement with previous work, does not provide strict confirmation, and it appears that additional work is needed in order to refine and perfect high temperature experimental techniques and their interpretation.

Acknowledgments. A grant from the National Science Foundation made this work possible. Additional financial support came from the Sloan Fellowship Fund, the General Electric Foundation, and the Shell Companies Foundation. Dr. Horie expresses his appreciation to the Fulbright Commission in Japan for a Travel Grant and for the David Sarnoff RCA Fellowship Award.

Notation

a = constant defined in eq VII
A = area of a spherical surface of radius r
C = total molar concentration
C_i = molar concentration of species i
C_i^e = equilibrium molar concentration of species i
d = thermocouple bead diameter
$\mathfrak{D}_i$ = diffusion coefficient of i
$\mathfrak{D}_e$ = effective diffusion coefficient
e = electric potential; emissivity
e_0 = reference electric potential
k_d = rate coefficient of the forward (dissociation) reaction
k_r = rate coefficient of the reverse (recombination) reaction
K = equilibrium constant of reaction 1
m_0 = total mass flow rate
M = third body in recombination reaction
Pe = Peclet number, $m_0/(4\pi R\rho\mathfrak{D}_e)$
r = radial coordinate position
R = radius of the porous, spherical burner (= 1.27 cm)
R_j = rate of reaction j
T_c = thermocouple temperature
T_g = gas temperature
v_r = mass average velocity in the radial direction
x_i = mole fraction of species i
x_i^e = equilibrium mole fraction of i
x_i' = value of x_1 at $\xi = \xi_1$
α = parameter in eq IV, $8\pi R^3\rho C x_m k_d/m_0$
β = parameter in eq IV, $8\pi R^3\rho C^2 x_m k_r/m_0$
λ_m = mixture thermal conductivity
ρ = total mass density
σ = Stefan–Maxwell constant
ξ = nondimensional radial position coordinate, r/R

Reaction of Oxygen Atoms with Cyclopentene[1a]

by R. J. Cvetanović,* D. F. Ring,[1b] and L. C. Doyle

Division of Chemistry, National Research Council of Canada, Ottawa, Ontario, Canada *(Received April 19, 1971)*

Publication costs assisted by the National Research Council of Canada

Molecular rearrangements and fragmentation subsequent to the primary addition of the ground-state oxygen atoms, O(^{3}P), at 25, 125, and 175° to the double bond in cyclopentene have been studied in some detail. The major products are cyclopentene oxide, cyclopentanone, cyclobutylcarboxaldehyde, ethylene, and acrolein. Dihydropyran, 4-pentenal, carbon monoxide, and two unidentified products (perhaps *cis*- and *trans*-2-pentenal) are formed in much smaller amounts. The type of products formed and the effect of pressure on their yields are fully consistent with a primary formation in the addition reaction of a triplet biradical intermediate.

Introduction

In an earlier report on the general features of the reactions of oxygen atoms with olefins, the results of several preliminary experiments with cyclopentene and cyclohexene were also briefly mentioned.[2] The products formed in the reaction of O(^{3}P) atoms with cycloolefins were found to be particularly interesting. Cyclohexene gave as the major products cyclohexene oxide, cyclohexanone, and cyclopentylcarboxaldehyde, a ring contraction product. In the case of cyclopentene, besides the analogous adducts (cyclopentene oxide, cyclopentanone, and cyclobutylcarboxaldehyde), equal amounts of ethylene and acrolein were also formed in substantial yields, corresponding to as much as about 25% of the overall reaction. At first glance these results may appear somewhat unusual and a more detailed study of these reactions could therefore contribute to the understanding of the finer features of the mechanism of addition of O(^{3}P) atoms to olefins. In view of this, the reaction of O(^{3}P) with cyclopentene has now been studied in greater detail, and the results are reported and discussed in the present paper.

Experimental Section

Ground-state oxygen atoms, O(^{3}P), were generated by the mercury-photosensitized decomposition of nitrous oxide, as described in a number of previous publications.[2-5] Nitrous oxide was present in large excess and mercury-photosensitized decomposition of cyclopentene was therefore generally negligible. On the other hand, O(^{3}P) atoms react extremely slowly with N_2O so that cyclopentene is solely responsible for their consumption even when it is present at very low partial pressures.

Reactions were carried out in a spherical quartz reaction vessel of total volume of 1106.7 ml, provided with a flat quartz window 50 mm in diameter, through which the reactants were irradiated by the mercury resonance light (253.7 nm) from a homemade low pressure mercury lamp. The reactor was contained in a thermostated box, and the experiments were carried out at 25, 125, and 175°. Before irradiation, the reactant gases (including mercury vapor) were thoroughly mixed by an all-glass paddle-wheel-type circulating pump. During the irradiation the circulating pump was effectively separated from the reactor by means of two ground, ball and socket type check valves, made of glass but containing iron cores for external operation by electromagnets.

Noncondensable gases, consisting of N_2 with very small amounts of CO and at best only traces of H_2 and CH_4, were collected in a Toepler pump-gas buret and measured manometrically before and after the removal of CO in a copper oxide furnace at about 240°. The residual N_2 was analyzed by mass spectrometry to determine any CH_4 present. The C_2 hydrocarbons, consisting essentially entirely of C_2H_4, were in some experiments measured manometrically after separation on a LeRoy still[6] and then analyzed by mass spectrometer. Alternatively, ethylene was determined gas chromatographically on an 18-ft 2% squalane "modified" alumina column with a hydrogen flame detector. Hydrogen flame detectors, insensitive to the excess N_2O present, were also used for the general analyses of condensable products on capillary columns. The capillary column mostly used was a 300-ft β,β'-thiodipropionitrile column. It had the great advantage of excellent resolution which permitted the observation and identification (by direct mass spectrometry of the eluents and by seeding with authentic samples when available) of the major products and of such minor products as dihydropyran and 4-pentenal. However, there was an appreciable scatter in the quantitative yields of cyclopentanone and cyclobutylcarboxaldehyde, perhaps because of some

(1) (a) Issued as N.R.C.C. No. 12173; (b) National Research Council of Canada Postdoctorate Fellow, 1968–1969.

(2) (a) R. J. Cvetanović, *Can. J. Chem.*, **36**, 623 (1958); (b) R. J. Cvetanović, *Advan. Photochem.*, **1**, 115 (1963).

(3) R. J. Cvetanović, *J. Chem. Phys.*, **23**, 1203, 1208, 1375 (1955).

(4) R. J. Cvetanović, *ibid.*, **25**, 376 (1956).

(5) R. J. Cvetanović, *Can. J. Chem.*, **38**, 1678 (1960).

(6) D. J. LeRoy, *Can. J. Res., Sect. B*, **28**, 492 (1950).

Table I: Effect of Irradiation Time on Product Yields (N_2O 190 Torr at 25°, Cyclopentene Close to 5 Torr at 25°, *i.e.*, *ca.* 300 μmol, Temp 25 ± 1°)

Irradiation, min	ΔN_2, μmol	Relative yields of products, r_{N_2} = 1										
		C_2H_4	Acr[a]	CPO[b]	CBA[c]	CNP[d]	DHP[e]	4-PA[f]	X_1[g]	X_2[h]	CO[i]	Σ O[j]
10	11.42	0.229	0.238	0.290	0.106	0.125	0.0057	0.0033	0.00072	0.00098	0.010	0.78
25	24.97	0.235	0.236	0.297	0.104	0.117	0.0069	0.0038	0.00071	0.00057	0.012	0.78
33	27.52	0.249	0.236	0.316	0.106	0.117	0.0072	0.0045	N.d.[k]	0.00045	0.014	0.80
35	37.06	0.242	0.229	0.289	0.103	0.108	0.0062	0.0040	N.d.	N.d.	0.014	0.75
60	65.49	0.243	0.225	0.274	0.096	0.110	0.0052	0.0033	N.d.	N.d.	0.014	0.73
75	78.40	0.243	0.257	0.299	0.108	0.117	0.0046	0.0026	N.d.	N.d.	0.012	0.80
90	104.0	0.238	0.241	0.283	0.098	0.113	0.0037	0.0020	N.d.	N.d.	0.012	0.75
90	84.51	0.240	0.246	0.311	0.101	0.109	0.0055	0.0039	N.d.	N.d.	0.013	0.79
115	104.5	0.242	0.242	0.313	0.100	0.119	0.0047	0.0039	N.d.	N.d.	0.021	0.80
120	98.69	0.245	0.247	0.302	0.092	0.105	0.0052	0.0039	N.d.	N.d.	0.020	0.78
	Mean	0.241	0.240	0.297	0.102	0.114	0.0055	0.0035	0.0007	0.0007	0.014	0.78

[a] Acrolein. [b] Cyclopentene oxide. [c] Cyclobutylcarboxaldehyde. [d] Cyclopentanone. [e] Dihydropyran. [f] 4-Pentenal. [g,h] Unidentified products (perhaps *trans*- and *cis*-2-pentenal). [i] Carbon monoxide. [j] Sum of the oxygen-containing products listed in the table. [k] N.d. = not determined.

spurious loss of these highly polar substances of low volatility on the (unavoidably) incompletely coated stainless steel column. The yields of these two compounds reported in the present work must therefore be regarded as only approximate.

Quantitative gas chromatographic evaluation of product yields was based on two internal standards, propane for the evaluation of C_2H_4, and benzene for all other products. The adopted relative molar hydrogen flame detector responses were: propane 300, benzene 614, ethylene 200, acrolein 197, cyclopentene oxide 386, dihydropyran 374, C_5 aldehydes 380, cyclopentanone 400. These choices were based on the related values and the overall trends reported in the literature[7,8] and on several calibrations with commercial samples of some of these compounds and their functionally related isomers (benzene, acrolein, propanal, cyclopentene oxide, dihydropyran, *n*-pentanal, 2-methylbutanal, pivalaldehyde, diethyl ketone, methyl propyl ketone).

Matheson Co. N_2O was used after thorough degassing and distillation from a trap at −78°. Phillips research grade cyclopentene was distilled on a Todd still to remove traces of some less volatile impurities (probably formed by the action of atmospheric oxygen). Matheson Co. SF_6 was used after degassing and bulb-to-bulb distillation. Oxygen was generated by heating analytical grade potassium permanganate.

Results

The observed products and the effect of irradiation time on their yields are shown in Table I for a series of experiments carried out at 25 ± 1°, using 190 Torr of N_2O and close to 5 Torr (300 μmol) of cyclopentene. Since in the mercury-photosensitized decomposition of N_2O[3]

$$N_2O + Hg6(^3P_1) \longrightarrow N_2 + O(^3P) + Hg6(^1S_0)$$

the rate of formation of N_2, r_{N_2}, serves as an "internal actinometer," the relative yields of products for r_{N_2} = 1 in Table I represent the yields of products per $O(^3P)$ atom consumed in the reaction. It is clear that up to quite large conversions (close to 35% of the initial cyclopentene) the yields of products remain constant, *i.e.*, there is no appreciable loss of $O(^3P)$ atoms in secondary reactions with the products. This result reflects the considerably greater specific rate of reaction of $O(^3P)$ atoms with cyclopentene than with the reaction products.

The main reaction products are cyclopentene oxide, cyclopentanone, cyclobutylcarboxaldehyde, ethylene, and acrolein. Equal formation of ethylene and acrolein indicates that these two compounds result from a direct split of the initial $O(^3P)$ adduct to cyclopentene. These observations are in agreement with the analogous observations and conclusions in the earlier work.[2a] Formation of dihydropyran as a reaction product is an interesting new observation, although its yield is very small. The same is true for 4-pentenal. Dihydropyran was confirmed by seeding with an authentic commercial sample and by mass spectrometry. Samples for identification of 4-pentenal were obtained in two ways: photolyzing cyclopentanone and by reacting $O(^3P)$ atoms with 1,4-pentadiene. Two additional products are eluted in the same general region as 4-pentenal and cyclobutylcarboxaldehyde; they are entered in Table I as X_1 and X_2 and are perhaps *trans*- and *cis*-2-pentenal. However, positive identification was not made. Their yields, calculated assuming a relative molar response of 380, *i.e.*, the same as adopted for 4-pentenal and cyclobutylcarboxaldehyde, are extremely small at 25°.

The sum of yields of the observed oxygen-containing

(7) W. A. Dietz, *J. Gas. Chromatogr.*, **5**, 68 (1967).
(8) R. G. Ackman, *ibid.*, **6**, 497 (1968).

Table II: Effect of Cyclopentene Pressure on Product Yields (N_2O 190 Torr at 25°, Irradiation 10 min, Temp 25 ± 1°)

Cyclopentene, μmol	ΔN_2, μmol	Relative yields of products, $r_{N_2} = 1$										
		C_2H_4	Acr[a]	CPO[b]	CBA[c]	CPN[d]	DHP[e]	4-PA[f]	X_1[g]	X_2[h]	CO[i]	ΣO[j]
137.9	9.98	0.235	0.234	0.308	0.106	0.125	0.0066	0.0038	N.d.	N.d.	0.012	0.80
306.1	11.42	0.229	0.238	0.290	0.106	0.125	0.0057	0.0033	0.0007	0.0010	0.010	0.78
438.3	9.26	0.231	0.230	N.d.	0.093	0.116	0.0047	0.0034	N.d.[k]	0.0015	0.010	N.d.
447.6	9.48	0.231	0.228	0.302	0.101	0.122	0.0066	0.0036	0.0025	0.0030	0.012	0.78
593.2	9.24	0.220	0.222	0.312	0.106	0.125	0.0068	0.0044	0.0035	0.0038	0.010	0.79
	Mean	0.229	0.230	0.303	0.103	0.122	0.0061	0.0037	(0.002)	(0.002)	0.011	0.79

[a] Acrolein. [b] Cyclopentene oxide. [c] Cyclobutylcarboxaldehyde. [d] Cyclopentanone. [e] Dihydropyran. [f] 4-Pentenal. [g,h] Unidentified products (perhaps *trans*- and *cis*-2-pentenal). [i] Carbon monoxide. [j] Sum of the oxygen-containing products listed in the table. [k] N.d. = not determined.

products, ΣO (last column of Table I), gives the oxygen atom material balance. The value of about 80% is somewhat low although this may be in part due to the uncertainties in the analyses for cyclopentanone and cyclobutylcarboxaldehyde mentioned in the Experimental Section, and to some difficulty with quantitative recovery of condensable products of lower volatility. Moreover, small amounts of ketenes which may be formed in the reaction would probably not be detected on the gc columns used. As will be shown later, the material balance tends to improve somewhat at higher overall pressures.

Table II shows that the yields of products are independent of a fourfold variation in the amount of cyclopentene initially taken. The experiments were carried out at 25 ± 1°, with 190 Torr of N_2O and constant irradiation of 10 min. The yield of N_2 is at best only slightly reduced in going from the smallest to the highest cyclopentene used, showing that the extent of the quenching of $Hg6(^3P_1)$ atoms by cyclopentene has been very small.

The results presented in Tables I and II were obtained at approximately constant pressure. The effect of pressure at 25 ± 1° is shown in Table IIIA and is presented graphically in Figure 1. In previous work with such simple olefins as C_2H_4, C_3H_6, 1-C_4H_8, 1,3-C_4H_6, it was observed that the yields of oxygen atom *addition* products increased with increasing pressure up to constant values. Such a behavior is readily explainable as a progressive increase in the fraction of the "hot" adduct molecules which are collisionally stabilized. A formally similar trend is shown in Figure 1 by cyclobutylcarboxaldehyde. However, the same trend is shown by ethylene and acrolein although they are obviously *fragmentation* rather than addition products. Evidently, this is a different type of pressure effect, as will be discussed in more detail in the next section. That the observed trends are indeed pressure effects is shown in Table IIIA and Figure 1 by the experiment with 100 Torr of SF_6 added to 25 Torr of N_2O and 1.2 Torr of cyclopentene. The product yields are similar

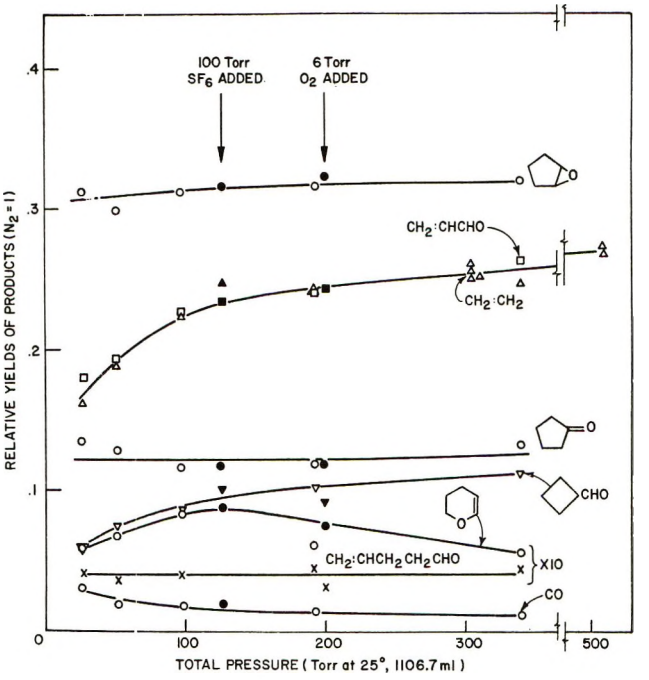

Figure 1. The effect of total pressure on the yields of the products of the reaction of $O(^3P)$ with cyclopentene at 25°.

to those obtained with N_2O and cyclopentene alone at comparable total pressure. The experiment with 5.8 Torr of O_2 added shows that the products originate from short-lived precursors and are not formed by intercombination of free radicals.

Table III also shows the yields of products at 125° (B) and 175° (C). The trends are qualitatively similar to those observed at 25°. There are some quantitative changes but, considering the large temperature increase of 150°, they are on the whole remarkably small. The most conspicuous change at higher temperature is a decrease in the yield of cyclopentene oxide and increase in the yields of the two unidentified products (X_1 and X_2).

Discussion

Reactions of $O(^3P)$ atoms with olefins are characterized by the magnitudes of the rate constants and the

Table III: Effect of Total Pressure on Product Yields in the Reaction of O(³P) Atoms with Cyclopentene

N_2O	c-C_5H_8	Total pressure	Irradiation,	ΔN_2,	Relative yields of products, $r_{N_2} = 1$										
Torr at 25°, 1106.7 ml			min	μmol	C_2H_4	Acr[a]	CPO[b]	CBA[c]	CPN[d]	DHP[e]	4-PA[f]	X_1[g]	X_2[h]	CO[i]	ΣO[j]
								A. 25°							
25.4	1.22	26.7	6.25	3.86	0.160	0.181	0.312	0.060	0.135	0.0059	0.0040	0.0055	0.0035	0.030	0.74
50.5	1.55	52.0	6	4.12	0.187	0.194	0.299	0.074	0.128	0.0067	0.0036	N.d.	N.d.	0.019	0.72
95.7	2.71	98.4	6.25	4.28	0.222	0.224	0.311	0.086	0.113	0.0083	0.0040	N.d.	N.d.	0.017	0.76
188.1	5.01	193.1	70	53.83	0.242	0.246	0.316	0.101	0.118	0.0061	0.0044	N.d.	N.d.	0.013	0.80
330.5	9.70	340.2	75	54.88	0.246	0.263	0.320	0.110	0.133	0.0055	0.0043	N.d.	N.d.	0.009	0.84
25.1	1.26	127.1[l]	11	3.71	0.247	0.234	0.316	0.099	0.116	0.0086	0.0038	0.0014	0.0011	0.019	0.80
188.9	5.07	199.8[m]	6.25	(4.2)[n]	N.d.[o]	0.242	0.324	0.090	0.117	0.0075	0.0030	N.d.	N.d.	N.d.	(0.78)
								B. 125°							
25.6	2.01	27.6	4.5	4.45	0.160	0.186	0.257	0.054	0.161	0.0050	0.0059	0.029	0.032	0.035	0.76
77.0	2.39	79.4	150	14.15	0.218	0.213	0.260	0.079	0.135	0.0089	0.0052	0.019	0.017	0.031	0.77
189.7	4.83	194.5	15	17.96	0.242	0.268	0.272	0.110	0.150	0.0100	0.0056	0.019	0.021	0.019	0.87
319.5	9.65	329.2	15	17.86	0.270	0.291	0.272	0.123	0.155	0.0086	0.0057	0.022	0.023	0.014	0.91
								C. 175°							
25.0	1.95	26.9	4.5	4.46	0.178	0.177	0.215	0.048	0.139	0.0040	0.0065	0.037	0.047	0.050	0.72
76.9	2.40	79.3	45	4.31	N.d.	0.208	0.228	0.089	N.d.	0.0098	0.0065	0.044	0.052	0.044	N.d.
100.2	2.43	102.6	45	3.95	N.d.	0.207	0.226	0.085	N.d.	0.0107	0.0048	0.032	0.033	0.039	N.d.
129.4	2.41	131.8	4	4.25	0.220	0.229	0.234	0.083	0.128	0.0106	0.0066	0.021	0.022	0.028	0.76
161.9	2.30	164.2	4	4.37	0.248	0.252	0.236	0.095	0.142	0.0106	0.0061	0.028	0.031	0.021	0.82
182.8	4.78	187.6	4	4.24	0.269	0.266	0.256	0.103	0.147	0.0110	0.0059	0.034	0.034	0.022	0.88
190.2	6.07	196.3	40	3.61	N.d.	0.254	0.230	0.130	0.163	0.0118	0.0059	0.059	0.063	0.044	0.96
270.5	7.36	277.9	4	4.21	0.255	0.292	0.259	0.131	0.150	0.0112	0.0065	0.035	0.043	0.019	0.95
321.2[k]	9.91[k]	331.1	135	12.80	0.279	0.260	0.237	0.134	0.139	0.0092	0.0062	0.053	0.061	0.040	0.94
330.8	10.72	341.5	45	4.36	N.d.	0.284	0.245	0.153	0.164	0.0092	0.0049	0.058	0.065	0.030	1.01

[a] Acrolein. [b] Cyclopentene oxide. [c] Cyclobutylcarboxaldehyde. [d] Cyclopentanone. [e] Dihydropyran. [f] 4-Pentenal. [g,h] Unidentified products (perhaps *trans*- and *cis*-2-pentenal). [i] Carbon monoxide. [j] Sum of the oxygen-containing products listed in the table. [k] Average of two experiments at equal reactant pressures and irradiation time. [l] 100.7 Torr of SF_6 added. [m] 5.8 Torr of O_2 added. [n] Estimated by analogy. [o] N.d. = not determined.

type of the reaction products formed. The two are largely dependent on different factors, as has been discussed in considerable detail in previous publications[2,9,10] from this laboratory. The present work is concerned only with the type of the reaction products formed, and this has been found to be always predictable by postulating that (1) O(³P) atom adds predominantly to the less substituted of the two doubly bonded carbon atoms, and (2) the initial adduct is a "triplet biradical" intermediate in which free rotation is possible and which rearranges to the final products by ring closure (to form epoxides) and by migration of an H atom or an alkyl group from the C atom to which O(³P) becomes attached to the other C atom of the original double bond (to form carbonyl compounds). At normal temperatures, the alkyl radical migrations are partly internal: the greater fraction of the migrating radicals become completely detached from the olefin. In this latter case the rearrangement is completed by recombination of the free radicals, *i.e.*, "external" migration predominates. Thus, for example, in the reaction of O(³P) with 2-butene at room and higher temperatures, isobutanal is largely formed in the reactions

$$CH_3\dot{C}HCH_3 \longrightarrow CH_3 + \underset{\displaystyle O}{\underset{|}{\dot{C}}}H_2CHO \longrightarrow (CH_3)_2CHCHO \quad (1)$$

although some internal migration occurs as well. (At cryogenic temperatures,[11,12] in condensed phase, on the other hand, the CH_3 migration is probably entirely internal.)

The variety of products formed and the pressure effects observed in the present work show that the reaction of O(³P) with cyclopentene is quite complex. This complexity, however, can be explained readily and logically in terms of the above general reaction mechanism. As has already been pointed out earlier,[2,10] the initial adduct is a "triplet biradical" intermediate (A)

(9) R. J. Cvetanović, *J. Chem. Phys.*, **30**, 19 (1959); **33**, 1063 (1960).

(10) R. J. Cvetanović, *J. Phys. Chem.*, **74**, 2730 (1970).

(11) M. D. Sheer and R. Klein, *ibid.*, **73**, 597 (1969).

(12) R. Klein and M. D. Scheer, *ibid.*, **73**, 1598 (1969).

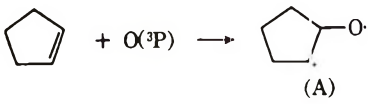

(A) (2)

This intermediate reacts further mainly by (a) ring closure to give cyclopentene oxide, (b) by 1,2 H atom shift to give cyclopentanone, (c) by 1,2 ring contraction to give cyclobutylcarboxaldehyde, and (d) by molecular fission into equal amounts of ethylene and acrolein.

Steps a, b, and c are entirely analogous to the rearrangements of the corresponding biradical intermediates of the simple acyclic olefins. By analogy with 2-butene (and higher internal olefins), step (c) in the case of cyclopentene probably proceeds largely by ring opening in the cyclic biradical A to give an acyclic biradical (B) which then partly recyclizes to form cyclobutylcarboxaldehyde

$$\underset{\text{(B)}}{\dot{C}H_2CH_2CH_2CHCHO} \longrightarrow \dot{C}H_2CH_2CH_2CHCHO \quad (3)$$

The biradical intermediate B undergoes simultaneously with reaction 3 a molecular fission into ethylene and acrolein (step d)

$$\dot{C}H_2CH_2CH_2\dot{C}HCHO \longrightarrow CH_2{=}CH_2 + CH_2{=}CHCHO \quad (4)$$

which does not require a prior or concurrent migration of H atoms and thus can occur readily in competition with the recyclization reaction 3. In the case of cyclohexene, an analogous molecular fission would have to be accompanied by migration of an H atom and has not been observed.[2a]

In the temperature range investigated in this work, 25–175°, the major reaction products are formed in the four steps a–d which follow reaction 2. This is evident from the data in Tables I–III and Figure 1. At the same time, the effect of pressure on the yields of these products requires an explanation. The "hot" products formed in the addition of $O(^3P)$ atoms to simple acyclic olefins (*e.g.*, C_2H_4, C_3H_6, C_4H_8, 1,3-C_4H_6) are well known[2] to undergo substantial fragmentation at low total pressures and the fragmentation tends to be suppressed as the pressure is increased, more readily so in those molecules which have a greater number of degrees of freedom and in which the bonds undergoing breakage are stronger. This is in agreement with the general postulates of the theory of unimolecular decomposition. In a similar manner, an appreciable fragmentation of the addition products is also observed in the case of cyclopentene at the lowest pressures used, as indicated by some formation of 1-butene (but not 2-butene nor cyclobutane) and a considerable number of unidentified other minor products (not shown in Table III and Figure 1) detected by gas chromatography. As the pressure is increased, this fragmentation is rapidly suppressed. Carbon monoxide, another minor fragmentation product, shows a similar behavior. The yields of cyclopentene oxide and cyclopentanone are affected relatively little by pressure, although this may be largely masked by analytical uncertainties in the case of cyclopentanone. At higher temperatures the decline in the yield of cyclopentene oxide at lower pressures is somewhat more pronounced although it is still quite small. This is not surprising in view of the relatively large number of degrees of freedom in this molecule and in comparison with the trends observed before.[1,2]

In sharp contrast to these trends, there is a large decline at lower pressures in the yields of the other three major products: cyclobutylcarboxaldehyde, ethylene, and acrolein. The yields of these three products show parallel trends and those of ethylene and acrolein are within the experimental error the same. All the three yields approach plateau values at higher total pressures. These observations indicate a common "hot" precursor and it is most logical to postulate that this is a vibrationally excited ("hot") biradical B. At low pressures, this "hot" intermediate undergoes preferential fragmentation and rearrangements (presumably leading to the production of butene-1, CO, and other unidentified products observed by gc in the low pressure experiments). At higher pressures its excess vibrational energy is removed in collisions and the deexcited radical undergoes then only reactions 3 and 4.

The aldehydic biradical B also undergoes a minor rearrangement to 4-pentenal

$$\dot{C}H_2CH_2CH_2\dot{C}HCHO \longrightarrow CH_2{=}CHCH_2CH_2CHO \quad (5)$$

and perhaps also to *cis*- and *trans*-2-pentenal

$$\dot{C}H_2CH_2CH_2\dot{C}HCHO \longrightarrow CH_3CH_2CH{=}CHCHO \quad (6)$$

These rearrangements require H migration in the biradical B and are somewhat favored by higher reaction temperatures, especially the latter.

As the temperature is increased from 25 to 175°, there appears to be some increase in the rearrangement of the biradical A to B at the expense of the cyclization of A to cyclopentene oxide. However, the increase is not very pronounced. On the other hand, in the condensed phase at −196°,[10] fission to ethylene and acrolein is completely suppressed but rearrangements to cyclopentene oxide, cyclopentanone, and cyclobutylcarboxaldehyde still occur. It is likely that at −196° these products are formed entirely by direct rearrangement from the biradical A in concerted reactions.

Although the yield of dihydropyran is quite small, at 25° less than and at 175° slightly more than 1% of the $O(^3P)$ atoms consumed in the reaction with cyclopentene, it is a reaction product of considerable interest from a mechanistic point of view. Its formation can be understood readily by assuming that although most of the biradicals A which rearrange by ring opening are

converted to the biradical B, a very small fraction is converted to another biradical (C), a less stable isomer of B, which then cyclizes to dihydropyran

$$\underset{(C)}{\dot{C}H_2CH_2CH_2CH{=}CHO\cdot} \longrightarrow \underbrace{CH_2CH_2CH_2CH{=}CH}_{O} \qquad (7)$$

It is evident that all the results of the present work are logically explainable in terms of the general mechanism of the reactions of O(^{3}P) atoms with olefins developed earlier in this laboratory. Moreover, the formation of such a variety of products and the fact that at increasing pressures the yields of the two molecular fission products, ethylene and acrolein, *increase* up to plateau values, require, in our opinion, the postulate that intermediates of finite lifetimes are involved. Occurrence of a process of such complexity in a concerted reaction would be extremely difficult to understand. The spin conservation rule also argues against a rapid concerted formation of the final reaction products. At the same time, the lack of an effect of 6 Torr O_2 on the yields of the products (Table IIIA Figure 1) shows that the three intermediates involved in the reaction are relatively short-lived. A similar conclusion has already been reached in earlier work[2,4] for the initial adducts, the "triplet biradicals" (A and its analogs), formed in the reactions of O(^{3}P) atoms with olefins.

Acknowledgment. The authors are grateful to Dr. R. F. Pottie for assistance with the determination and interpretation of the mass spectra of the gas chromatographic eluents.

Environmental Effects on the Deprotonation of Indole Derivatives in Alkaline Ices

by René Santus,*[1a,b] Thérèse Montenay-Garestier,[1a,c] Claude Helene,[1c] and Michel Aubailly[1a]

Muséum National d'Histoire Naturelle, Laboratoire de Biophysique, 75, Paris 5°, France, and Centre de Biophysique Moleculaire, C.N.R.S., La Source, 45, Orleans, France *(Received February 8, 1971)*

Publication costs assisted by Muséum National d'Histoire Naturelle

At 77°K, in alkaline frozen aqueous solutions (pH 13), tryptophan and various indole derivatives emit a fluorescence whose maximum is localized at about 380 nm. Additions of small amounts of alcohols before freezing produces the disappearance of this fluorescence band and the appearance of the well-known fluorescence of tryptophan molecules (λ_{max} 328 nm). As the temperature is raised from 77 to 200°K, the λ_{max} is shifted from 380 to 420 nm. Comparison with results obtained at room temperature in highly alkaline solutions (KOH concentration up to 2 *M*) makes it possible to attribute this emission to indole anion fluorescence. The deprotonation process might occur in the first excited singlet state of indole ring and is favored by the freezing of the aqueous solutions which form aggregates where both high local concentration of OH^- ions and tryptophan molecules are present.

Introduction

The knowledge of excited state properties of constituents of biological macromolecules is required to understand and eventually control their photochemical reactions. Many biomolecules have heterocyclic rings which often present unusual spectroscopic and photochemical behaviors. Indole derivatives such as tryptophan belong to this kind of molecules. During the last decade, a large number of studies dealing with the effect of temperature, solvent, and environment on the spectroscopic properties of free tryptophan or tryptophan incorporated into peptides or proteins, has been published.[2] At room temperature, in aqueous or ethanolic solutions, the fluorescence of indole derivatives is quenched in the pH range 11–14.[3,4] There is no modification of the absorption spectra in the same pH range. The quenching is not observed when the $N_{(1)}H$ group of the indole ring is substituted by methyl

(1) (a) Muséum National d'Histoire; (b) on leave at Illinois Institute of Technology, Biophysics Laboratory, Physics Department, Chicago, Ill. 60616; (c) Centre de Biophysique.

(2) See, for example, S. S. Lehrer and G. D. Fasman, *J. Biol. Chem.*, **242**, 4644 (1967), or J. W. Longworth, *Photochem. Photobiol.*, **7**, 587 (1968).

(3) (a) A. White, *Biochem. J.*, **71**, 217 (1959); (b) R. W. Cowgill, *Arch. Biochem. Biophys.*, **100**, 36 (1963).

(4) J. W. Bridges and R. T. Williams, *Biochem. J.*, **107**, 227 (1968).

groups. The pK which can be deduced from the fluorescence quenching is 12.3 for indole and changes only slightly in the presence of substituents in the 2 or 3 positions.[5] At 77°K, in a mixture of water and ethanol, no fluorescence quenching is observed in the same pH range.[4] Therefore, the quenching observed at room temperature can be ascribed to an excited-state deprotonation of the NH group of indole in a diffusion-controlled reaction with hydroxyl ions.[5] This excited state deprotonation is also postulated in 10 M alkaline glasses at 77°K.[6]

We wish to report here some results on the spectroscopic properties of tryptophan and various indole derivatives in alkaline frozen aqueous solutions. During the freezing of alkaline aqueous solutions, solute molecules can form aggregates in which tryptophan (or indole) molecules as well as hydroxyl ions can be found. This local increase in hydroxyl ion concentration facilitates indole ring deprotonation and the appearance of the fluorescence spectrum of indole anion.

Materials and Methods. Chemicals. The compounds investigated in this study, except 1-methyltryptophan, were purchased from Calbiochem, Mann Research, and J. T. Baker Co. 1-Methyltryptophan was synthesized according to the method described by Yamada, *et al.*[7] Identity and purity of the compounds were monitored through use of nmr, uv absorption, and visible-uv fluorescence spectroscopic techniques. Purification by crystallization was done when necessary.

Spectroscopic Measurements. Uncorrected luminescence spectra were obtained with Aminco Keirs and Jobin and Yvon spectrofluorophosphorimeters equipped with low temperature accessories. For low temperature measurements, samples were frozen in quartz tubes of 3 mm internal diameter. No significant differences were found in the luminescence spectra of degassed samples as compared with undegassed samples. Absorption spectra were recorded on Cary 15 spectrophotometer.

pH measurements were performed at room temperature using a Radiometer Type 25 pH meter for the pH range 5–12, and calculated outside this pH range using Hammett functions.[8]

Results

Luminescence Measurements at 77°K. At 77°K, the luminescence spectrum of a frozen aqueous solution (pH 5.5) of tryptophan (2.5×10^{-4} M) is composed of a fluorescence band (λ_{max} 340 nm) and a very weak structureless phosphorescence band (λ_{max} 500 nm) (Figure 1a). The fluorescence observed at 77°K is characteristic of tryptophan aggregates,[9] whereas the phosphorescence seems to be due to some impurities acting as energy traps for the excitation energy migrating in the aggregates.[10] When the pH is increased before freezing, a broadening and a red shift of the fluorescence spectrum are observed (Figure 1b). At pH 13, the

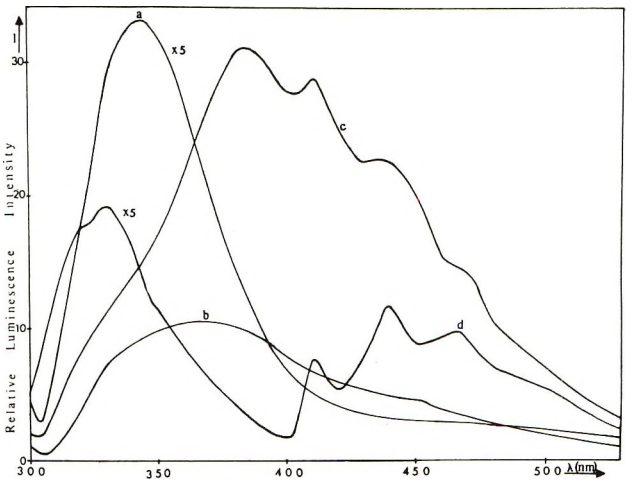

Figure 1. Luminescence spectra of tryptophan (5×10^{-4} M) at 77°K: excitation wavelength, 280 nm; (a) frozen aqueous solution pH 5.5 (gain × 5); (b) pH 12 (gain × 1); (c) pH 13.15 (gain × 1); (d) pH 13.4, the solution contains 20% of ethanol (in volume) (gain × 5) pH measured at room temperature.

fluorescence maximum is recorded at 380 nm (only a shoulder is observed around 340 nm), and the characteristic phosphorescence spectrum of tryptophan with vibronic peaks at 410, 445, and 475 nm appears (Figure 1c). This phosphorescence spectrum is easily resolved using a phosphoroscope. Excitation spectra are practically identical for these different emissions. The pH dependence of the intensity of the 380-nm band is shown in Figure 2A. Addition of small amounts of ethanol in these alkaline solutions before freezing leads to a disappearance of the 380-nm fluorescence band and the well-known fluorescence of dispersed tryptophan molecules is observed at 330 nm (Figure 1d). The intensity of the 380-nm band decreases with ethanol concentration as shown in Figure 2B. We had previously shown that addition of small amounts of alcohols or salts to an aqueous solution before freezing precludes the formation of aggregates and permits the observation of the fluorescence and phosphorescence spectra of dispersed molecules.[9] In an aqueous solution containing 10% ethanol, there is no pH dependence of the fluorescence characteristics (quantum yield and λ_{max}) in the pH range 5–14 (Figure 2A). All the results reported above are similar for various indole derivatives, namely indole, 3-methylindole, N^{α}-acetyltryptophan, N^{α}-methyltryptophan, tryptamine, in-

(5) E. Vander Donckt, *Progr. React. Kinet.*, 5, 5 (1970).

(6) S. V. Konev in "Fluorescence and Phosphorescence of Proteins and Nucleic Acids," Plenum Press, New York, N. Y., 1967.

(7) S. Yamada, T. Shioiri, T. Itaya, T. Hara, and R. Matsueda, *Chem. Pharm. Bull. (Tokyo)*, 13, 88 (1965).

(8) K. Bowden, *Chem. Rev.*, 66, 119 (1966).

(9) C. Helene, R. Santus, and M. Ptak, *C. R. Acad. Sci., Ser. C*, 262, 1349 (1966).

(10) M. E. McCarville and S. P. McGlynn, *Photochem. Photobiol.*, 10, 171 (1969).

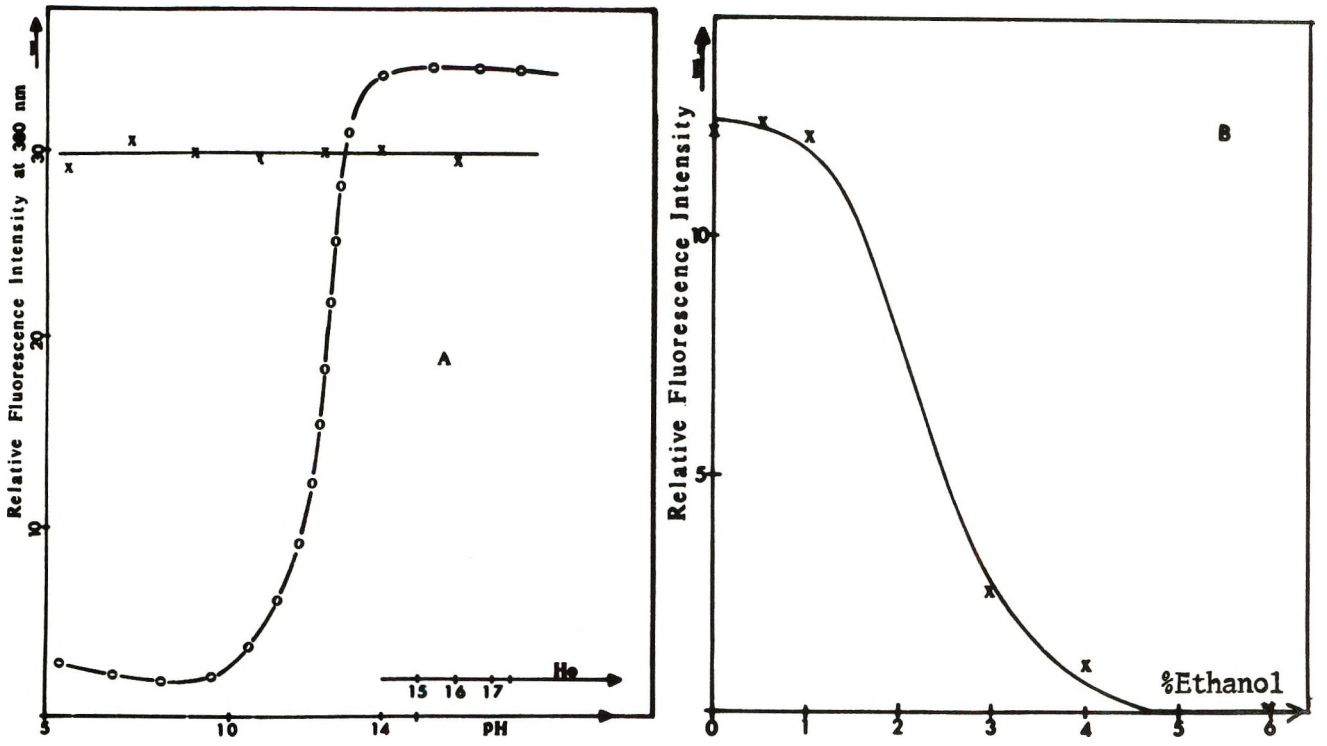

Figure 2. (a) Fluorescence intensity at 380 nm as a function of pH: excitation wavelength, 280 nm; tryptophan concentration 5×10^{-4} *M*; temperature, 77°K; O—O, frozen aqueous solutions of tryptophan; ×—×, frozen aqueous solutions of tryptophan containing 20% ethanol in volume. (b) Fluorescence intensity at 380 nm as a function of alcohol concentration (% in volume): temperature, 77°K; excitation wavelength, 250 nm; tryptophan concentration, 2.5×10^{-4} *M*; pH 13.

dole-3-acetic acid, indole-3-propionic acid, indole-3-butyric acid, and dipeptides such as tryptophyltyrosine, tryptophyltryptophan (see Figure 3a and b).

In order to determine the importance of the nitrogen proton of the indole ring, we have studied the spectroscopic behavior of 1-methyltryptophan. In the pH range 11–14, the fluorescence spectrum of 1-methyltryptophan is not modified. The fluorescence λ_{max} remains at about 340 nm (Figure 3c). The fluorescence at 380 nm which was observed with other derivatives (see above) cannot be seen in the case of 1-methyltryptophan (Figure 3c). Addition of 10% ethanol to an aqueous solution of 1-methyltryptophan at pH 13 produces only a blue shift from 340 to 328 nm characteristics of the destruction of aggregates.

Luminescence Studies as a Function of Temperature. Between 77 and 160°K, the phosphorescence intensity of frozen alkaline (pH 13) aqueous solution of tryptophan decreases and disappears at about 180°K in deaerated solutions and at about 160°K in aerated solutions. This disappearance of the phosphorescence is very likely due to oxygen diffusion in the aerated frozen solutions. Mossbauer[11] and proton magnetic resonance studies[12] of frozen aqueous salt solutions have shown that molecular motions could occur above about 150°K. In dilute aqueous solutions (2.5×10^{-4} *M*) at pH 13, between 77 and 170°K, the fluorescence spectrum of tryptophan is not greatly modified. Above 170°K, the fluorescence band (whose λ_{max} 380 nm up to 170°K) is

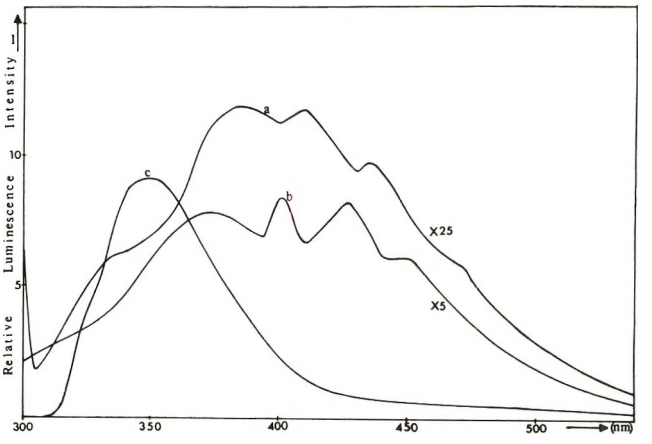

Figure 3. Luminescence spectra of indole derivatives in alkaline ices (pH 13) at 77°K: excitation wavelength, 280 nm; (a) indole-3-butyric acid (1.7×10^{-5} *M*) (gain × 25); (b) indole (5×10^{-5} *M*) (gain × 5); (c) 1-methyltryptophan (5×10^{-4} *M*) (gain × 1).

shifted to the red (Figure 4), whereas its intensity remains approximately constant. At 200°K, the fluorescence λ_{max} is about 420 nm and, then, does not appreciably change when the temperature is further raised until the ice melts. Only a decrease in the intensity is observed above 200°K. In the liquid phase, the well-

(11) A. J. Nozik and M. Kaplan, *J. Chem. Phys.*, **47**, 2960 (1967).
(12) A. Janossy, G. Gruner, and K. Tompa, *ibid.*, **51**, 5189 (1969).

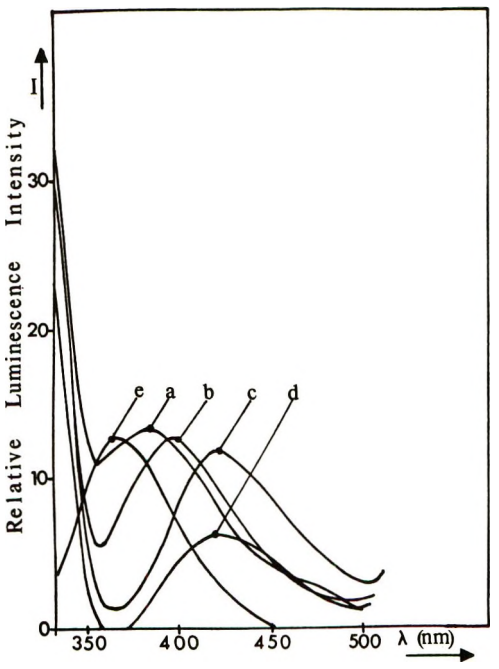

Figure 4. Luminescence spectra of a frozen aqueous solution of tryptophan (5×10^{-4} M) as a function of temperature: excitation wavelength, 280 nm; pH 13; (a) 77°K; (b) 173°K; (c) 200°K; (d) 240°K; (e) 273°K (liquid solution). Scattered light does not allow to record luminescence spectra at wavelength shorter than 340 nm.

known fluorescence spectrum of tryptophan in alkaline medium (λ_{max} 360 nm) is obtained (Figure 4e). Also, the solution recovers its original absorption spectrum. Between 77°K and the melting temperature there is no change in the fluorescence characteristics of 1-methyltryptophan in alkaline aqueous solutions, or with tryptophan in alkaline aqueous solutions containing 10% ethanol.

If a concentrated tryptophan solution (5×10^{-3} M), in alkaline conditions (pH 13), is frozen to 77°K and then heated to 240°K and maintained at this temperature, the fluorescence spectrum changes with time as indicated in Figure 5A. The intensity at 340 nm decreases while that at 420 nm increases (Figure 5A). An isoemissive point is observed at about 400 nm suggesting that only two species are involved. This is not observed in dilute solution of tryptophan but is observable with dilute solution of tryptamine (Figure 5B) whose solubility is lower than that of tryptophan.

At room temperature, in highly alkaline solutions (KOH 10 M), it is possible to observe a fluorescence of tryptophan whose λ_{max} is 420 nm. This fluorescence has been ascribed to tryptophan dianion[4,6] in which the NH group of the indole ring is deprotonated. Its excitation spectrum has a maximum at about 290 nm (uncorrected) and is not very different from the excitation spectrum of the tryptophan fluorescence at 330 nm in neutral conditions. By cooling the sample, the fluorescence intensity at 420 nm experiences a 30-fold increase until the medium becomes rigid (vitreous solidification). The luminescence spectrum obtained at 77°K is similar to that obtained at the same temperature with a 0.1 M KOH frozen aqueous solution of tryptophan (λ_{max} 380 nm). Nevertheless, the maximum emission wavelength shifts to the red in the glassy medium (10 M KOH) at lower temperatures (140°K) than in polycrystalline samples (obtained with low concentration of KOH such as 0.1 M). This point emphasizes the role of ice structure in the observed red shift and will be discussed in the forthcoming paragraph.

Discussion

The comparison of the results obtained with various indole derivatives (including 1-methyltryptophan) shows that the NH group of the indole ring is involved in the fluorescence behavior of tryptophan and similar compounds, in polycrystalline alkaline ices. During the freezing of the aqueous solution, solute molecules are excluded from the ice crystals and form aggregates. This has been demonstrated by dipolar broadening of esr spectra of manganous ions,[13] photodimerization of thymine in ice,[14] the increase in the rate of some chemical reactions upon freezing,[15] luminescence studies,[9] and solute redistribution in some multicomponent aqueous systems on freezing.[16]

In the case of alkaline hydroxides (NaOH or KOH) thermal analysis have shown that two phases are formed:[17] one of them is pure ice crystals and the other one is an eutectic phase containing ice crystals and alkaline hydrate crystals ($NaOH \cdot 7H_2O$; $KOH \cdot 4H_2O$). When these solutions contain solute molecules such as tryptophan at a low concentration (10^{-3} M), we can assume that the same phases form. Tryptophan molecules will be included in aggregates in the ice crystals (as observed in the absence of alkaline hydroxide in pure ice) and will occur as dispersed molecules in the hydrate crystals. In these alkaline hydrate crystals, the local concentration of OH^- ions is greatly increased. Hence, tryptophan molecules which are surrounded by this high concentration of OH^- ions may lose a proton. These molecules give rise to the indole anion fluorescence, the maximum of which is located at 380 nm while tryptophan aggregates emit their fluorescence (λ_{max} 340 nm). Some deprotonation may occur in the ground state in strong alkaline environment, although no new absorption band is detected at room temperature. Also at 77°K, the excitation spectrum of the indole anion fluorescence is similar to that of neutral indole while the phosphorescence characteristics (spectrum, lifetime)

(13) R. T. Ross, *J. Chem. Phys.*, **42**, 3919 (1965).

(14) S. Y. Wang, *Fed. Proc., Fed. Amer. Soc. Exp. Biol.*, **24**, S-71 (1965).

(15) T. C. Bruice and A. R. Butler, *ibid.*, **24**, S-45 (1965).

(16) G. Taborsky, *J. Biol. Chem.*, **245**, 1063 (1970).

(17) A. Rollet, "Nouveau traité de Chimie Minérale," Paul Pascal, Ed., Masson et Cie, Paris, 1963, Vol. 2, no. 1, p 254, and Vol. 2, no. 2, p 50.

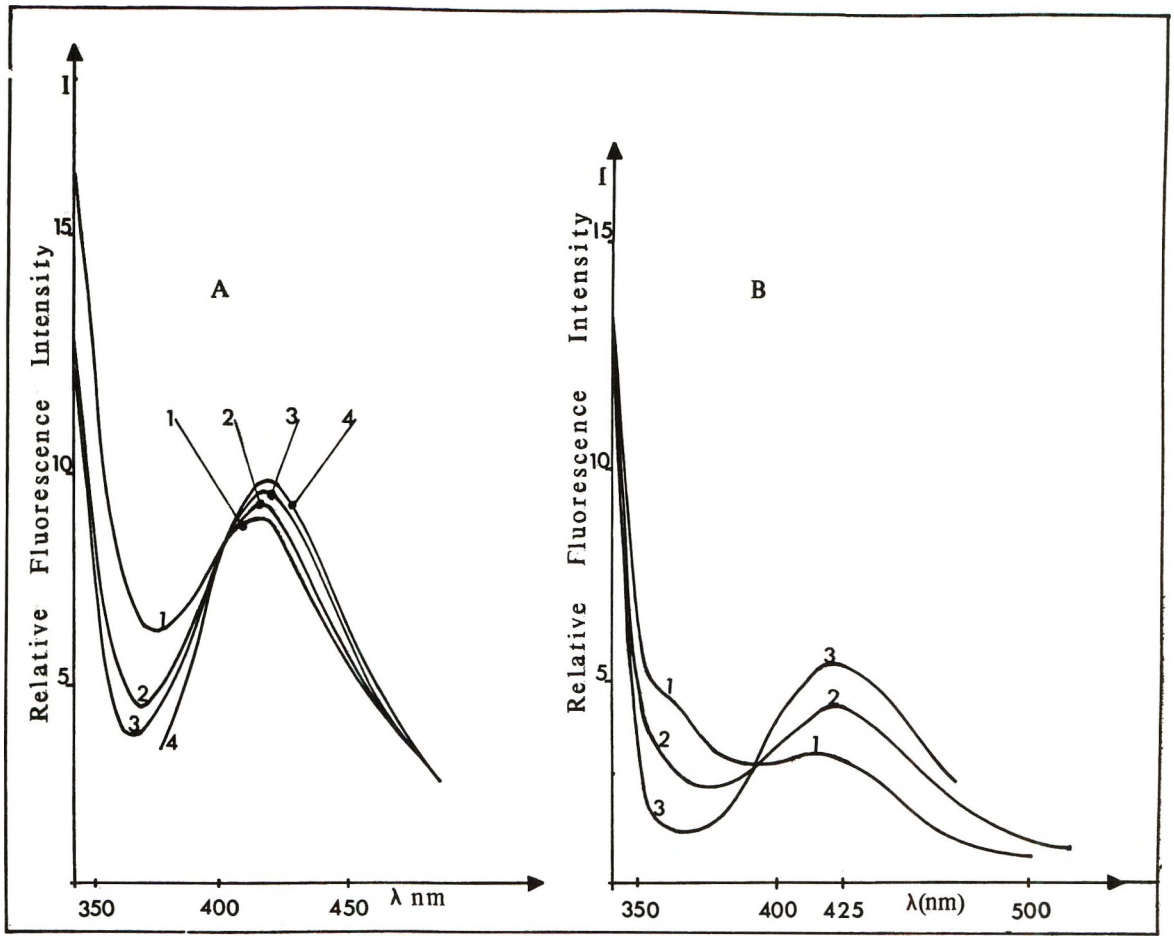

Figure 5. Fluorescence spectra obtained at 240° K as a function of time: time between emission scans, 1 min; excitation wavelength, 290 nm; (a) frozen aqueous solutions of tryptophan (5×10^{-3} *M*) at pH 13; (b) frozen aqueous solutions of tryptophan (5×10^{-4} *M*) at pH 13; increasing time from spectrum 1 to 4 in 5A and from 1 to 3 in 5B. Scattered light does not allow to record fluorescence spectra at wavelength shorter than 340 nm.

are that of the neutral molecule. We can suggest the possibility of excited-state deprotonation at the single level, according to the scheme[6]

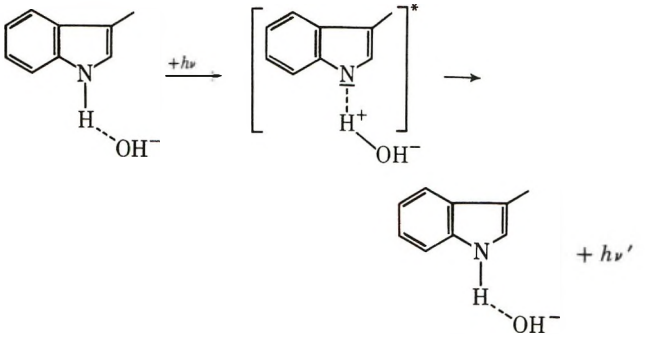

The modification of ice structure which occurs by increasing the concentration of Na^+ or K^+ ions produces a redistribution of the tryptophan molecules in the medium[9] thus preventing a rough estimation of the pK_a for the species responsible of the 380-nm fluorescence band. Addition of ethanol prevents the formation of the different phases previously described. The OH^- concentration is not sufficient in the neighborhood of tryptophan molecules to produce ionization.

When increasing the temperature, oxygen diffusion occurs at about 150°K since we notice a quenching of the phosphorescence. At higher temperatures, namely 170°K, motion of water molecules occurs.[11,12] Interaction of water molecules with an indole anion leads to a shift of the spectrum from 380 to 420 nm. This shift is similar to that observed with tryptophan from 320 to 350 nm. This has been mainly explained by exciplex formation[18] or more likely by solvation of the excited species.[19] At about 240°K the eutectic phase begins to melt;[17] thus, aggregated tryptophan molecules are solubilized and dispersed molecules can now migrate in liquid clusters where OH^- ion concentration is quite high. This explains the increase of tryptophan dianion fluorescence in concentrated tryptophan solutions at this temperature (Figure 5A and B). Then, in fluid medium, with tryptophan solutions containing low concentration of alkaline hydroxide, the OH^- ion concentration is homogeneous and not sufficient to observe

(18) M. S. Walker, T. W. Bednar, and R. Lumry, *J. Chem. Phys.*, **47**, 1020 (1967).

(19) J. Eisinger and G. Navon, *ibid.*, **50**, 2069 (1968).

the dianion fluorescence which is observed only in highly alkaline solution.

Conclusion

The above results indicate that indole ring deprotonation of many indole derivatives occurs in alkaline ices even at relatively low OH^- concentrations. This is explained by formation of clusters in ices, produced by the rapid cooling of water. These clusters may be of two types, one where tryptophan aggregates are present while others may contain dispersed tryptophan molecules and high local concentration of OH^- ions. Such a phenomenon may be important in proteins where the nature of local environment has been shown to be of great importance both in enzymic and spectroscopic properties[20] and where microenvironments can be quite different from the outer solvent. Furthermore, the implication of such phenomena, in the primary processes of the photoionization of indole derivatives is obvious. At low temperatures in neutral, acid, or basic frozen aqueous solutions tryptophan can be photoionized by uv light (see, for example, ref 21 and 22) and the photoejected electrons are trapped in the solvent matrix. The stimulation of the recombination of trapped electrons by ir or visible light induces the appearance of tryptophan fluorescence and phosphorescence.[22] In basic frozen aqueous solutions of tryptophan, the fluorescence spectrum obtained by the stimulated recombination is that of the indole anion.[23]

Acknowledgments. We wish to thank Professor C. Sadron for this continued interest in this work. It is a pleasure to thank Drs. P. Douzou and C. Balny for making it possible to use their variable temperature accessory and Dr. M. Bazin for synthesizing 1-methyltryptophan.

(20) I. Weinryb and R. F. Steiner, *Biochemistry*, **9**, 135 (1969).

(21) R. Santus, C. Helene, and M. Ptak, *Photochem. Photobiol.*, **7**, 341 (1968).

(22) Y. A. Vladimirov, D. I. Roshchupkin, and E. E. Fesenko, *ibid.*, **11**, 227 (1970).

(23) R. Santus, M. Aubailly, and C. Helene, *C. R. Acad. Sci., Ser. C*, **272**, 2008 (1971).

Photopolymerization Mechanisms. I. Dye-Triplet Reactions with para-Substituted Benzenesulfinate Ions

by J. D. Margerum,* A. M. Lackner, M. J. Little, and C. T. Petrusis

Hughes Research Laboratories, Malibu, California 90265 *(Received January 28, 1971)*

Publication costs assisted by Hughes Research Laboratories

Methylene blue sensitized reactions with benzenesulfinate ions are studied in regard to the photopolymerization mechanism of aqueous acrylamide solutions. Flash bleaching, fluorescence quenching, and quantum yields of photopolymerization and bleaching are compared using a series of para-substituted benzenesulfinates. A detailed reaction mechanism is proposed. The excited singlet state of the dye is quenched by the sulfinate ions, without reaction. A triplet state of the dye undergoes a redox reaction with the sulfinates, but the products rapidly revert back to the starting materials when monomer is absent. Efficient photobleaching and photopolymerization occur in deaerated acrylamide solutions. The Hammett equation correlates the substituent effects on the benzenesulfinates with the rate of the dye-triplet redox reaction. These results and other evidence indicate that in these systems the sulfonyl radicals probably are the polymerization initiators rather than semimethylene blue radicals. A weak complex may exist between the dye and acrylamide.

Introduction

The photopolymerization of acrylic monomer solutions initiated by dye-sensitized reactions with benzenesulfinate ions[1] is of interest in rapid-access imaging processes[2,3] for displays[4] and holography.[4-6] Photopolymer images of very high resolution can be obtained instantaneously from aqueous solutions of barium acrylate and acrylamide, using photoredox reactions of phenothiazine dyes with benzenesulfinate ions to initiate free-radical polymerization. We are studying basic

(1) J. B. Rust, L. J. Miller, and J. D. Margerum, *Polym. Eng. Sci.*, **9**, 40 (1969).

(2) J. D. Margerum, L. J. Miller, and J. B. Rust, *Photogr. Sci. Eng.*, **12**, 177 (1968).

(3) L. J. Miller, J. D. Margerum, and J. B. Rust, *J. SMPTE*, **77**, 1177 (1968).

aspects of these photochemical reaction processes in order to understand and improve the operation of such systems. In this paper we examine the reaction mechanisms by observing the substituent effect on the reactivity of a series of para-substituted benzenesulfinate ions with photoactivated methylene blue

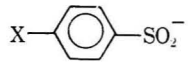

where X = CH_3, H, CH_3CONH, Cl, Br, or NO_2. Acrylamide is used as the monomer in these studies, because of its reactivity and the convenience of analyzing polyacrylamide. Several experimental techniques are used, including flash photolysis (without monomer), fluorescence quenching, and analysis of the quantum yields for bleaching and polymerization under steady illumination. The Hammett equation is used to correlate substituent effects on the reactivity of the benzenesulfinates with the dye triplet state, which is shown to be the photochemically reactive species.

There have been many related dye-sensitized photopolymerization studies carried out, as indicated by Oster and Yang[7] in their general survey on the photopolymerization of vinyl monomers. Among the studies most pertinent to our work are papers by Oster, *et al.*,[8-10] Chaberek, *et al.*,[11,12] and Chen.[13] Each of these groups has studied the photopolymerization of acrylamide by photolysis of methylene blue in the presence of a reducing agent. One area of discussion has been the identity of the free-radical species initiating polymerization, and whether or not a trace of oxygen is required. (It is generally agreed that oxygen acts as an inhibitor if more than a trace is present.) Chaberek, Shepp, and Allen[12] argue that oxygen is not required and that semimethylene blue is the free-radical initiator. Yang and Oster[10] say that a trace of oxygen is required and that it reacts with a reduced form of the dye to produce fite-radical initiators. In both cases these authors tend to ignore the role of other free radicals formed by the photochemical redox reactions. Benzenesulfinic acids are well known thermal polymerization initiators for methyl methacrylate,[14,15] and we previously assumed that the photoredox reaction between dye and sulfinate ions produces sulfonyl radicals which initiate polymerization.[1,2] This mechanism and the role of semimethylene blue and oxygen are also examined in the present studies.

Experimental Section

Materials. Zinc-free methylene blue CI 52015 (Matheson Coleman and Bell) has a high absorption coefficient and is used without additional purification. Acrylamide (J. T. Baker) is recrystallized three times from methanol. Sodium benzenesulfinate (Eastman), sodium *p*-toluenesulfinate (Aldrich), and *p*-acetamidobenzenesulfinic acid (Aldrich) are each recrystallized from water. The sodium salts of *p*-chloro-, *p*-bromo-, and *p*-nitrobenzenesulfinic acids are synthesized from the sulfonyl chlorides (Eastman) by reduction with sodium sulfite.[16] They are purified by precipitation as ferric sulfinates[15] and conversion into aqueous sodium sulfinate solutions. These solutions are analyzed by potentiometric titrations.[17] Commerical sources of sodium formaldehydesulfoxalate (Aldrich), ferrous sulfate (MCB), and buffer compositions (Beckman) were used. All studies are of pH 7 except those indicated in Table II. The volume per cent of standard buffer solutions is 10% for flash studies and 20% for all other studies.

Flash Photolysis. The microsecond flash system is similar to one described previously.[18] The xenon flash is filtered with a CS 3-69 glass filter. The monitoring light passes through two grating monochromators (Bausch and Lomb high intensity), one before and one after the sample cell, 6.66-cm path length. Evacuated or N_2-bubbled solutions at pH 7 are used with 1×10^{-6} M methylene blue. The 665-nm absorbance recovery rate after photolysis of the dye alone gives a linear first-order plot for log $(A_\infty - A)$ *vs.* time over a 35-μsec time period. Photolyses of the dye with 1.5×10^{-3} M sulfinate ions show a linear second-order plot for the function $(A_\infty' - A)^{-1}$ *vs.* time over the first 3.5 msec after the flash, where A_∞' is the absorbance after 3 sec. The slope of these lines is used to calculate apparent second-order rate constants of the back reaction, where $k_{app} = \epsilon l(\text{slope}) = 5.8 \times 10^5(\text{slope})$.

Long Period Dye–Sulfinate Photolysis. An N_2-bubbled, pH 7 solution with 7.6×10^{-6} M methylene blue and 1.3×10^{-3} M sodium *p*-toluenesulfinate is exposed to 3.6×10^{14} photons cm^{-2} sec^{-1} at 666 nm for 22 hr in a 1-cm cell. The dye concentration decreased to 3.2×10^{-6} M, but returned to 6.4×10^{-6} M after O_2 was added. Ultraviolet analysis of the sulfinate at 265 nm showed no change in absorbance. The exposed

(4) R. G. Brault, J. A. Jenney, J. D. Margerum, L. J. Miller, and J. B. Rust, *Image Technol.*, **13**, 13 (1971); *cf.* "Applications of Photopolymers," R. J. Povinelli, Ed., SPSE, Washington, D. C., 1970, pp 113-132.

(5) D. H. Close, A. D. Jacobson, J. D. Margerum, R. G. Brault, and F. G. McClung, *Appl. Phys. Lett.*, **14**, 159 (1969).

(6) J. A. Jenney, *J. Opt. Soc. Amer.*, **60**, 1155 (1970).

(7) G. Oster and N. L. Yang, *Chem. Rev.*, **68**, 125 (1968).

(8) G. Oster, *Nature*, **173**, 300 (1954).

(9) G. K. Oster, G. Oster, and G. Prati, *J. Amer. Chem. Soc.*, **79**, 595 (1957).

(10) N. L. Yang and G. Oster, *J. Phys. Chem.*, **74**, 856 (1970).

(11) A. Shepp, S. Chaberek, and R. MacNeil, *ibid.*, **66**, 2563 (1962).

(12) S. Chaberek, A. Shepp, and R. J. Allen, *ibid.*, **69**, 641, 647, 2834, 2842 (1965).

(13) C. S. H. Chen, *J. Polym. Sci., Part A*, **3**, 1107, 1127, 1137, 1155 (1965).

(14) G. M. Brauer and F. R. Burns, *ibid.*, **19**, 311 (1956).

(15) C. G. Overberger and J. J. Godfrey, *ibid.*, **40**, 179 (1959).

(16) S. Smiles and C. M. Bere, *Org. Syn.*, **I**, 7 (1958).

(17) B. Lindberg, *Acta Chem. Scand.*, **17**, 383 (1963).

(18) J. D. Margerum and C. T. Petrusis, *J. Amer. Chem. Soc.*, **91**, 2467 (1969).

solution showed the same photopolymerization initiation rate in 1 M acrylamide as the initial dye–sulfinate solution.

Photopolymerizations. Acrylamide solutions at pH 7 with 8×10^{-6} M methylene blue and various sulfinate ion concentrations are exposed in 1-cm path length cells with long necks and small apertures. Prepurified N_2 is bubbled through the solution for 10 min prior to exposure and then over the top of the solution during the exposure. A 100-W Zr arc lamp, lens, and interference filter are used to expose the entire solution to a narrow spectral bandwidth of approximately parallel light. The light intensity is measured by replacing the cell with an Eppley thermopile. The incident intensity at the face of the cell is about 5×10^{14} photons cm^{-2} sec^{-1}. The beam passing through the cell is used to monitor its transmission. This beam passes through a 0.25-m Ebert Jarrell-Ash monochromator and neutral density filters onto an RCA 7326 photomultiplier and the signal is read out on a Sanborn 7701 recorder. The absorbancies are in good agreement with those obtained on a Cary 14R spectrophotometer. Initial experiments (such as the data in Figure 2) are with a 656-nm interference filter, but most of the data are obtained with a 666-nm filter. Exposures are made for about 100 sec, and then the 4.0-ml sample is dumped into 200 ml of methanol to precipitate the polyacrylamide. It is separated on a fine sintered glass filter and is weighed after drying 3 hr at 80°. Molecular weights are measured by viscosity measurements at 30° in 1 N NaCl using the following relationship:[19] $\eta = 3.73 \times 10^{-4}(M_w)^{0.66}$.

Fluorescence Measurements. Relative fluorescence intensities are obtained at 680 nm from 8×10^{-6} M methylene blue solutions at pH 7 and room temperature, using an Aminco-Keirs fluorimeter, with an RCA 7102 photomultiplier cooled to −80°. Photopolymerization is avoided by not removing oxygen, which appears to have no effect on the fluorescence intensities.

Results

Dye–Sulfinate Reactions (without Monomer). Methylene blue is used as the light-sensitive component in these studies. It has a short-lived excited single state, which in dilute solutions gives a high yield of triplet state. The triplet lifetime has been estimated by Parker[20] to be about 15–20 μsec in 0.01 N H_2SO_4. Earlier, Oster and Wotherspoon[21] had calculated that its lifetime was about 87 μsec or more in the pH 4.8 to 11 range. With our microsecond flash system we have made an indirect measurement of the triplet lifetime in evacuated aqueous solution of 10^{-6} M dye at pH 7. The rate of absorbance recovery after flashing is followed at the dye's visible absorption maximum. The absorbance recovery rate closely follows first-order kinetics and shows a rate constant of 8.9×10^4 sec^{-1}. This corresponds to a triplet lifetime ($\tau = k^{-1}$) of about 11 μsec.

We have previously assumed[1,2,4] that it is the dye triplet state that reacts with sulfinate ions to form the free radicals which initiate polymerization. In the absence of monomer, which captures free radicals, the photosensitized reaction between methylene blue and the benzenesulfinates is reversible. No bleaching is observed with several minutes of steady illumination under the same conditions used for photopolymerizations. Even long period (22 hr) illumination bleaches only part of the dye and causes no measurable decrease in the sulfinate concentration. The bleaching rate of the same methylene blue–*p*-toluenesulfinate system is about 10^3 times faster in the presence of 1 M acrylamide.

Flash photolysis of N_2-bubbled dye–sulfinate solutions show that appreciable bleaching occurs at high intensities, but most of the dye is recovered in a few milliseconds and the rest returns in several minutes. The flash photolysis of the dye is compared in solutions containing a series of five para-substituted benzenesulfinate ions. The rate of the fast back reaction follows second-order kinetics in each case. A short extrapolation back to "zero time" indicates the amount of bleaching due to the microsecond flash. Each sample has the same pH and sulfinate ion concentration and approximately the same initial dye absorbance (A_i). The flash intensity is fairly reproducible, so that the "zero-time" absorbance (A_0) should indicate the reactivity of the dye triplet state with the sulfinate ion. Figure 1a shows the per cent of flash bleaching, $100(A_i - A_0)/A_i$, plotted as a Hammett equation. The points are the average of several values, each extrapolated from the first flash of a stock solution. Samples of a given sulfinate each show about the same per cent of flash bleaching, but their rates of dye recovery are not very reproducible. The apparent second-order rate constants for the fast back reaction are quite large. The following average values of k_{app} (in l. mol^{-1} sec^{-1}) are given here for X-$C_6H_4SO_2^-$ ions with various para substituents to indicate their approximate magnitude: CH_3 (4×10^9), H (4×10^9), CH_3COHN (5×10^9), Cl (1×10^{10}), Br (3×10^9). The experimental errors in measuring these k_{app} values may be due to traces of oxygen, since the concentration of the flash intermediates is only about 10^{-7} or less.

Dye-Sensitized Photopolymerization. Solutions of methylene blue in 1 M acrylamide are used to study the effect of sulfinate ion structure and concentration on photopolymerization. The exposure light is also utilized to monitor the transmission of the sample as

(19) New Product Bulletin No. 34, American Cyanimid Co., New York, N. Y., June 1955.

(20) C. A. Parker, *J. Phys. Chem.*, **63**, 26 (1959).

(21) G. Oster and N. Wotherspoon, *J. Amer. Chem. Soc.*, **79**, 4836 (1957).

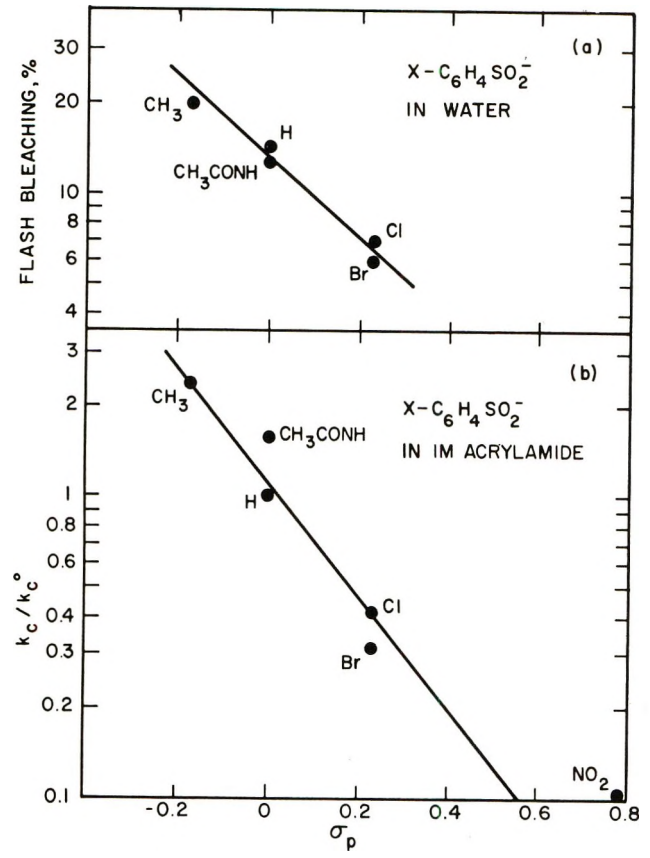

Figure 1. Hammett equation correlations for dye-triplet reaction with para-substituted benzenesulfinate ions: (a) flash photolysis bleaching yields with 1.5×10^{-3} *M* sulfinate ions in water (no monomer); (b) photopolymerization bleaching reaction rate constant ratios in 1 *M* acrylamide.

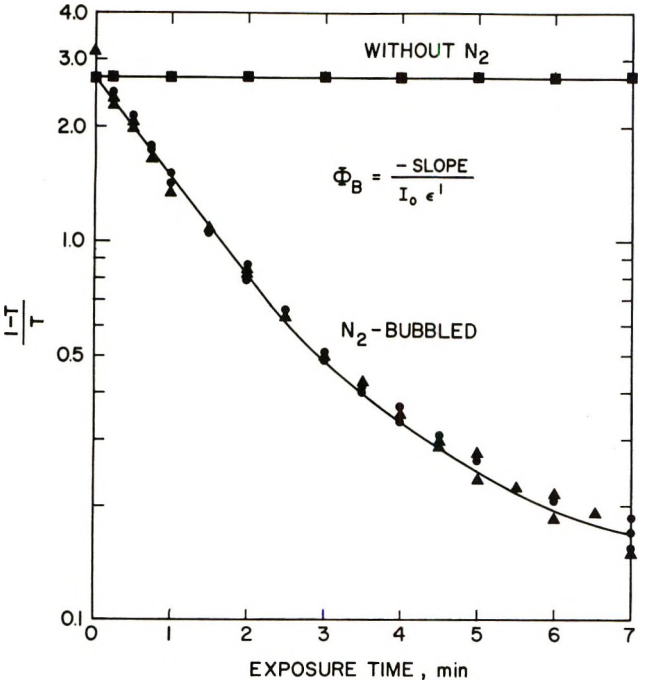

Figure 2. Bleaching function at 656 nm from photopolymerization of 1 *M* acrylamide with 8×10^{-6} *M* methylene blue and 1.5×10^{-3} *M* *p*-toluenesulfinate ions.

the dye bleaches during each run. If we assume that the reaction products have no effect on the photochemical step, then the rate of bleaching of the dye (D^+) is given by eq 1

$$\frac{-d[D^+]}{dt} = I_0 f_a \Phi_B = I_0(1 - T)\Phi_B \qquad (1)$$

where I_0 = incident intensity, f_a = fraction of light absorbed, Φ_B = effective quantum yield of bleaching, T = transmission, and $[D^+] = A/\epsilon l = -\log T/\epsilon l$. Substitution, rearrangement, integration, and using l = 1 cm gives

$$\log\left(\frac{1 - T}{T}\right) = -\epsilon I_0 \Phi_B t + C \qquad (2)$$

A plot of eq 2 should give a straight line with slope = $-\epsilon I_0 \Phi_B$, as shown in Figure 2. Each value for the quantum yield of dye bleaching is determined in this manner, but using exposure periods of only 1 to 2 min. The effect of oxygen and the reproducibility of three separate N_2-bubbled runs are shown in Figure 2. With exposure intensities of about 5×10^{14} photons cm^{-2} sec^{-1} no polymerization occurs in the presence of oxygen. If the oxygen is partially removed, there is an induction period in which the oxygen is used up prior to the photobleaching and polymerization. Ten minutes of bubbling prepurified nitrogen through the small cells is sufficient to eliminate any induction period.

Quantum yields of dye bleaching and of monomer polymerization, Φ_M, are shown in Figures 3a and b, respectively, for the six different benzenesulfinate ion derivatives over a wide range of concentrations. The total light absorbed during a run is determined by graphical intergration from the transmission data and is used in calculating the quantum yield of polymerization. Thus, Φ_B = initial quantum yield of bleaching, while Φ_M = average quantum yield of monomer polymerized during a run. The weight-average molecular weight of the polyacrylamide is typically about 10^6, *e.g.*, from runs using 10^{-2} *M* benzenesulfinate.

The quantum yield comparisons are all made with 1 *M* acrylamide solutions. As the acrylamide concentration is increased above 1 *M*, there is an approximately linear increase in Φ_M. It exceeds 10^4 molecules of monomer polymerized per photon absorbed in 4 *M* acrylamide solutions of benzenesulfinate and *p*-toluenesulfinate ions. The bleaching yields, Φ_B, increase very rapidly with the acrylamide concentration below 1 *M* and then increase gradually in the 1–4 *M* range.

The relative values of Φ_B in Figure 3a for photopolymerizations with different sulfinates at 1.5×10^{-3} *M* closely parallel the relative flash bleaching yields (Figure 1) at this concentration without monomer. However, at higher concentrations the relative values of Φ_B deviate from the Hammett equation correlation. In general, Φ_B and Φ_M follow similar behavior patterns

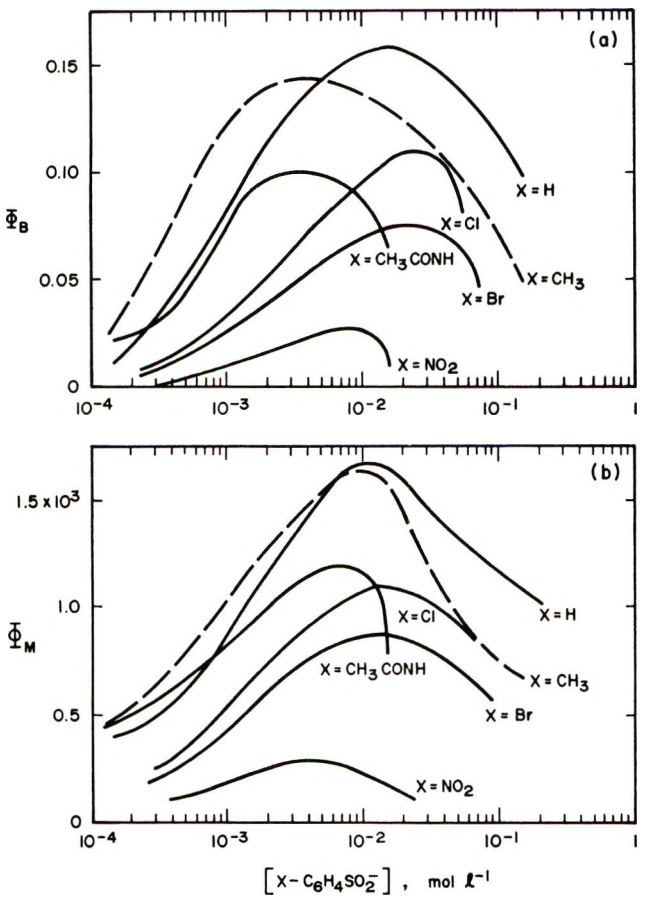

Figure 3. Effect of concentration of para-substituted benzenesulfinate ions on photopolymerization of 1 M acrylamide: (a) initial quantum yield of bleaching; (b) quantum yield of monomer polymerized.

for the various sulfinate ion structures. The most striking feature in Figure 3 is that at higher sulfinate ion concentrations the yields do not level off to a constant value. Instead, they go through a maximum in the 10^{-3} to 10^{-2} M region and decrease rapidly at higher concentrations. We have found no evidence for inhibitor impurities which account for this behavior, nor is it due to the ionic dark reaction[22,23] of the sulfinates with acrylamide to form sulfones. The presence of these sulfones does not inhibit photopolymerization. Several days of ageing acrylamide solutions of high sulfinate concentration (0.2 N) does convert some of the sulfinate into the corresponding sulfone, and the solutions then become more reactive to photopolymerization (after readjusting the pH). This suggests that at high concentrations the sulfinate ions themselves have a quenching effect on the photopolymerization.

Fluorescence Quenching of the Dye. Methylene blue has a weak fluorescence maximum at 680 nm from its first excited singlet state. Although it is relatively unaffected at low concentrations of quenching agents (*e.g.*, oxygen has no effect), fluorescence quenching has been reported at high concentrations of other ions such as potassium iodide.[24] We find that high concentrations

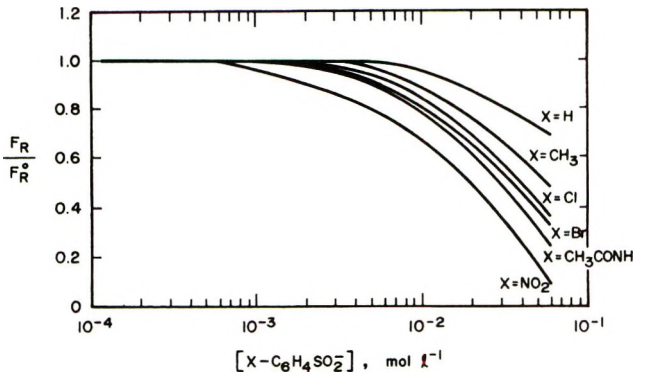

Figure 4. Effect of sulfinate ion concentration on relative fluorescence yields of 8×10^{-6} M methylene blue in 1 M acrylamide.

of sulfinate ions also quench the excited singlet state of methylene blue, as shown in Figure 4. The relative fluorescence yield (F_R) is compared to the fluorescence yield in the absence of sulfinate (F_R°). At low concentrations the sulfinates have no effect, but quenching begins in the 10^{-3} to 10^{-2} M range and the fluorescence yields drop sharply as the concentrations increase. The Stern–Volmer quenching equation (eq 3) provides an excellent linear correlation for the data in Figure 4. The slopes of the lines from eq 3 give the quenching

$$(F_R^\circ - F_R)/F_R = K_Q[RSO_2^-] \qquad (3)$$

constants, K_Q, which are listed in Table I.

Table I: Fluorescence Quenching Constants of Methylene Blue by Sulfinate Ions[a]

p-X-C$_6$H$_4$SO$_2^-$	K_Q[b]
X = H	8
CH_3	16
Cl	26
Br	31
CH_3CONH	42
NO_2	56

[a] 8×10^{-6} M dye in 1 M acrylamide at pH 7. [b] Quenching constant from Stern–Volmer plots.

Free-Radical Initiators. Approximately one-half of the methylene blue bleached from photopolymerization is present as a leuco dye that is readily reoxidized upon the admission of oxygen. The polyacrylamide formed by photolysis contains chemically bonded groups from both the dye and the sulfinates, as indicated by spectral analysis of polymer twice precipitated in methanol and

(22) O. Achmatowicz and J. Michalski, *Rocz. Chem.*, **30**, 243 (1956); *Chem. Abstr.*, **51**, 1064*b* (1957).

(23) R. G. Brault, J. D. Margerum, and L. J. Miller, paper in preparation.

(24) H. Merkelo, S. R. Hartman, T. Mar, and G. S. Govindjee, *Science*, **164**, 301 (1969).

redissolved in water. Methylene blue is observed as a colored form, attached to the polymer, with absorption maxima at 657 and 293 nm. A substantial part of the dye is not recovered in a colored form either in the filtrates or in the polymer, or else its absorption coefficient is much lower when it is part of the polymer. Apparently some of the dye is either decomposed or is present as a colorless form in the polymer. The formation of a sulfone in the photopolymer is observed when using *p*-acetamidobenzenesulfinate ions with the dye in 1 *M* acrylamide. Its photopolymer has a strong ultraviolet absorption band at 260 nm due to the *p*-acetamidobenzenesulfone structure. The sulfones from benzenesulfinate and *p*-toluenesulfinate have weaker sets of absorption bands (272, 265, 258 nm and 273, 264, 262 nm, respectively) in this region,[23] but these bands are observed in photopolymers made from 0.5 *M* acrylamide solutions. The presence of the dye and sulfone structures in the polymer could be due either to initiation or to termination of the free-radical chains. However, we have found other evidence indicating that semimethylene blue radicals do not initiate polymerization in some cases. This is illustrated by the following results, which are compared quantitatively in Table II.

Table II: Comparison of Photopolymerization Yields with Different Electron Donating Reagents

Electron donor			Photopolymerizations[b]	
Compd	Concn, *M*	pH[a]	Φ_B	Φ_M
p-$CH_3C_6H_4SO_2Na$	4×10^{-3}	7	0.17	1740
$C_6H_5SO_2Na$	4×10^{-3}	7	0.15	1670
$HOCH_2OSONa$	4×10^{-3}	7	0.27	0
$C_6H_5SO_2Na$	1×10^{-2}	4.6	0.34	1920
$FeSO_4$	1×10^{-2}	4.6	0[c]	0[c]
$FeSO_4$	1×10^{-4}	4.6	0[c]	0[c]

[a] Phosphate buffer at pH 7 and acetate buffer at pH 4.6. [b] Using 1 *M* acrylamide and 8×10^{-6} *M* methylene blue with intensity $\sim 4 \times 10^{14}$ photons cm^{-2} sec^{-1}. [c] Photostationary state bleaching, without polymerization, is observed at higher light intensities.

Sodium formaldehydesulfoxalate ($HOCH_2OSONa$) is an excellent reducing agent for the excited dye, but no polymerization occurs when acrylamide is present. All of the bleached dye is in a leuco form that is completely regenerated to the dye upon exposure to oxygen. The same reaction occurs in the absence of monomer, and flash photolysis shows that the dye initially bleached by the flash is rapidly converted into the colored dye and a leuco dye. This is consistent with the behavior expected of semimethylene blue, which is probably the intermediate in this bleaching reaction.

Methylene blue is known to undergo reversible photobleaching in the presence of ferrous ions.[20,25] A rapid back reaction occurs between the redox products: ferric ions and leucomethylene blue. Parker[20] has shown that the dye triplet initially reacts with the ferrous species to form semimethylene blue which undergoes a disproportionation reaction to form leucomethylene blue. At low light intensities the back reaction is fast enough so that no bleaching occurs, but at higher intensities we observe photostationary state bleaching in acrylamide solutions. In either case no polymerization occurs. On the other hand, Table II shows that under the same conditions benzenesulfinate ions cause both dye bleaching and considerable polymerization.

Effect of Monomer of the Dye. The presence of acrylamide has an effect on the spectrum, fluorescence efficiency, and photobleaching efficiency of methylene blue. Spectral absorption effects are summarized in Table III. The values in water are in good agreement with the highest absorption coefficients reported.[26] Acrylamide shifts the visible absorption maximum of the dye to a slightly longer wavelength, increases the peak to shoulder intensity ratio, and increases the absorption coefficient of the peak. The coefficients are the highest observed for methylene blue. Acrylamide increases the relative fluorescence intensity of methylene blue, as indicated in Table IV. It also decreases fluorescence quenching of the dye by the sulfinates. We have also noted that quantum yield of photobleaching with sodium formaldehydesulfoxalate is higher in the presence of acrylamide. Plots of the type shown in Figure 2 for the photobleaching of 8×10^{-6} *M* methylene blue at pH 7 with 1.5×10^{-3} *M* $HOCH_2OSONa$ give $\Phi_B = 0.13$ in the abesence of acrylamide and $\Phi_B = 0.24$ in the presence of 1.0 *M* acrylamide.

Table III: Effect of Acrylamide on Methylene Blue Absorption Spectrum

10^6[dye], *M*	Monomer[e]	λ_{max}, nm	$10^{-4}\epsilon$	$\frac{A_{max}}{A_{620}}$[f]
81.3[a]	None	664	6.52	1.30[g]
81.3[a]	1 *M*	667	8.99	1.95
81.3[a]	3 *M*	668	9.70	2.24
8.13[b]	None	664	8.58	1.94
8.13[b]	1 *M*	667	9.46	2.20
8.13[b]	3 *M*	668	9.71	2.28
2.03[c]	None	665	8.85	2.04
2.03[c]	1 *M*	668	9.57	2.22
2.03[c]	3 *M*	669	9.66	2.29
1.02[d]	None	665	9.01	2.10
1.02[d]	1 *M*	668	9.83	2.22

[a] 1-mm cell. [b] 1-cm cell. [c] 5-cm cell. [d] 10-cm cell. [e] Acrylamide in pH 7 buffered aqueous solution. [f] Ratio of peak to shoulder absorbancies. [g] Ratio of peak to second peak at 613 nm.

(25) R. Havemann and H. Pietsch, *Z. Phys. Chem. (Leipzig)*, **208**, 210 (1958).

(26) K. Bergmann and C. T. O'Konski, *J. Phys. Chem.*, **67**, 2169 (1963).

Table IV: Effect of Acrylamide on Relative Fluorescence Intensity of Methylene Blue

Acrylamide concn, M	Relative fluorescence yield[a] (F_R) No sulfinate	Low sulfinate[b]	High sulfinate[c]
0	1.00	0.92	0.43
0.5	1.12	1.06	0.65
1.0	1.18	1.11	0.78
2.0	1.23	1.26	1.01
3.0	1.35	1.28	1.13
4.0	1.41	1.34	1.21

[a] 8×10^{-6} M methylene blue at pH 7. [b] With 1.5×10^{-3} M p-toluenesulfinate. [c] With 5×10^{-2} M p-toluenesulfinate ion.

Discussion

Reaction Mechanism. At higher concentrations the sulfinate ions quench the fluorescence of methylene blue (Figure 4) and also give decreased quantum yields of bleaching and polymerization (Figure 3). This indicates that the excited singlet state of the dye ($^1D^+$) is quenched by the sulfinates without much, if any, redox reaction or polymerization occurring. On the other hand, small concentrations of triplet state quenchers such as oxygen and β-carotene decrease the bleaching and polymerization yields without affecting the fluorescence yield of the dye. These observations are consistent with a mechanism in which a dye-triplet ($^3D^+$) is the reactive species, as indicated in the general schematic diagram shown in Figure 5. The free radicals formed from the dye-triplet reaction with a sulfinate ion (RSO_2^-) back react rapidly in the absence of monomer, but initiate polymerization in the presence of acrylamide, if inhibitors do not interfere. We assume that sulfonyl radicals ($RSO_2\cdot$) are formed and are rapidly captured by acrylamide to initiate polymerization. The monomer successfully competes with the fast back reaction of $RSO_2\cdot$ with semimethylene blue ($D\cdot$). The observation that sulfonyl groups are found attached to the polyacrylamide is consistent with this mechanism.

Although it is possible that $D\cdot$ also acts as an initiator, our results show that this is unlikely to be important under the conditions of our experiments. About half of the bleached dye is leucomethylene blue, presumably from the disproportionation of $D\cdot$, indicating that $D\cdot$ is not readily captured by acrylamide. This is confirmed by the results given in Table II showing that with some other electron donors $D\cdot$ can be formed as an intermediate in N_2-bubbled acrylamide solutions without causing polymerization. In our photopolymerizations some of the dye becomes bonded to the polymer, but this could be due to chain transfer or termination reactions—especially when the colored form of the dye becomes attached to the polymer.

Only inhibition effects are observed in the presence of oxygen, but we cannot exclude the possibility that trace amounts of oxygen may have a beneficial effect as

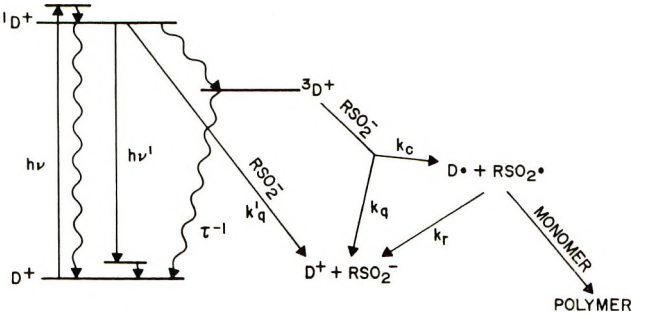

Figure 5. Schematic diagram for reaction mechanisms in dye-sensitized photopolymerization with sulfinate ions.

is claimed by Yang and Oster.[10] However, it should be noted that we observe polymer yields (using 10^{-2} M benzenesulfinate) which are more than an order of magnitude greater than those reported by Yang and Oster, so that the significance of traces of oxygen may be much less in our system than in theirs. Also it seems likely that any initial traces of oxygen would be removed rapidly by the leuco dye which is formed during the exposure.

We assume that the following equations are consistent with the major reactions involved in these dye-sensitized polymerizations.

$$D^+ + h\nu \xrightarrow{I_a} {}^1D^+ \quad (4)$$

$$^1D^+ \xrightarrow{\phi} {}^3D^+ \quad (5)$$

$$^1D^+ + RSO_2^- \xrightarrow{k_q'} D^+ + RSO_2^- \quad (6)$$

$$^3D^+ \xrightarrow{\tau^{-1}} D^+ \quad (7)$$

$$^3D^+ + RSO_2^- \xrightarrow{k_c} D\cdot + RSO_2\cdot \quad (8)$$

$$^3D^+ + RSO_2^- \xrightarrow{k_q} D^+ + RSO_2^- \quad (9)$$

$$D\cdot + RSO_2\cdot \xrightarrow{k_r} D^+ + RSO_2^- \quad (10)$$

$$2D\cdot + H_2O \xrightarrow{k_d} D^+ + DH + OH^- \quad (11)$$

$$RSO_2\cdot + M \xrightarrow{k_i} M\cdot \quad (12)$$

$$M\cdot + M \xrightarrow{k_p} P\cdot \quad (13)$$

$$2P\cdot \xrightarrow{k_t} PP \quad (14)$$

$$P\cdot + D\cdot \xrightarrow{k_t'} PD \quad (15)$$

If most of the sulfonyl radicals are captured by acrylamide (eq 12), then the free-radical back reaction (eq 10) can be ignored. Otherwise eq 10 introduces an inefficiency in the utilization of the free radicals. Semimethylene blue is assumed to undergo disproportionation (eq 11) to form *leuco*-methylene blue (DH) or else act as a chain terminating agent (eq 15). In this simplified mechanism we have deferred the ques-

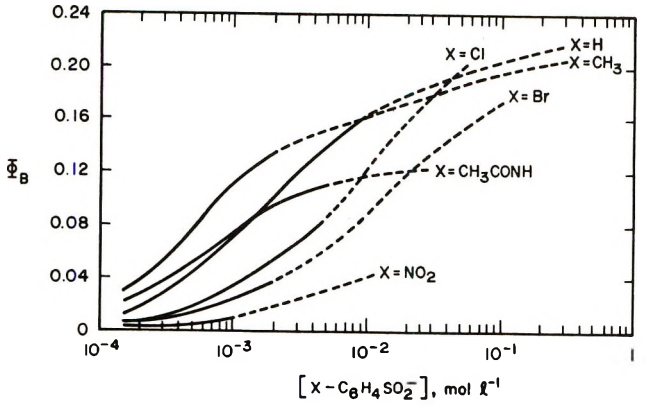

Figure 6. Effect of sulfinate ion concentration on the quantum yield of bleaching after correcting for excited singlet state dye quenching. Dashed lines indicate corrected values.

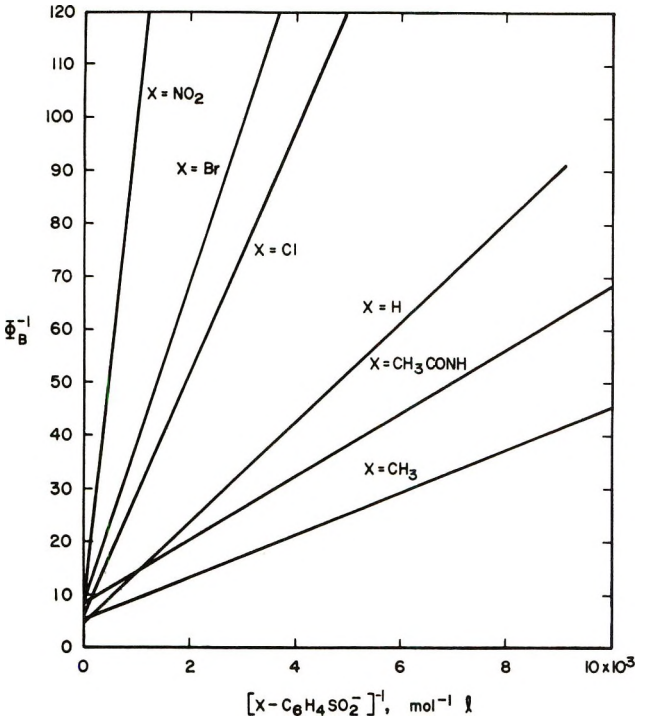

Figure 7. Sulfinate ion substituent effect on kinetic equation plot for bleaching of methylene blue in acrylamide.

tion of how part of the dye in a colored form becomes chemically bonded to the polymer. Studies of these reactions are in progress.

When the data in Figure 3a for the quantum yield of bleaching is corrected for the excited singlet state quenching (eq 6), the corrected Φ_B values level off at high sulfinate concentrations. The corrected curves are shown in Figure 6, where the broken lines indicate that the actual Φ_B is corrected by multiplying it times the F_R°/R_R fluorescence yield factor appropriate for the concentration and particular sulfinate ion. These corrected values of Φ_B give good straight line reciprocal plots of Φ_B^{-1} *vs.* $[RSO_2^-]^{-1}$, as indicated by the least-squares plots in Figure 7. Because the straight lines in Figure 7 do not have a common intercept, we have introduced the triplet quenching term (eq 9) in the reaction mechanism. The triplet quenching could actually be a local cage two-step reaction in which the redox reaction (eq 8) occurs and if followed by a rapid back reaction (eq 10) before the radicals separate or are captured.

A kinetic analysis of the corrected yields of bleaching can be made with the above mechanism by assuming photostationary state conditions for $[^3D^+]$, $[D\cdot]$, $[RSO_2\cdot]$, and $[P]\cdot$ and the following simplifications: (a) that corrections are made for eq 6 and it can be ignored; (b) that all of the $RSO_2\cdot$ radicals are captured by the monomer and eq 10 can be ignored; (c) that all of the $M\cdot$ radicals yield polymer radicals, $P\cdot$, which can be considered as one species. Then a photostationary state assumption for $[^3D^+]$ gives eq 16, where I_a = intensity of light absorbed and ϕ = intersystem crossing to the dye-triplet.

$$[^3D^+] = \frac{I_a\phi}{\tau^{-1} + (k_c + k_q)[RSO_2^-]} \quad (16)$$

Stationary state assumptions for $[D\cdot]$, $[RSO_2\cdot]$, and $[P\cdot]$ give eq 17, 18, and 19, respectively. The quantum yield of bleaching is given by eq 20. These five equations can be combined to give eq 21, where $C = (2 + A)/(1 + A)$ and $A = k_t'(k_dk_t)^{-1/2}$.

$$k_c[^3D^+][RSO_2^-] - 2k_d[D\cdot]^2 - k_t'[D\cdot][P\cdot] = 0 \quad (17)$$

$$k_c[^3D^+][RSO_2^-] - k_i[RSO_2\cdot][M] = 0 \quad (18)$$

$$k_i[RSO_2\cdot][M] - 2k_t[P\cdot]^2 - k_t'[D\cdot][P\cdot] = 0 \quad (19)$$

$$\Phi_B = \frac{k_d[D\cdot]^2 + k_t'[D\cdot][P\cdot]}{I_a} \quad (20)$$

$$\Phi_B^{-1} = \frac{C}{\phi}\left(1 + \frac{k_q}{k_c}\right) + \frac{C}{\tau k_c\phi}[RSO_2^-]^{-1} \quad (21)$$

Dye-Triplet Reactions. Equation 21 indicates that the reciprocal plots in Figure 7 should be straight lines whose slopes are inversely proportional to k_c, the rate constant for the dye-triplet reaction with each sulfinate ion. Ratios of these slopes compared to that of the benzenesulfinate ion give the k_c/k_c° values which are plotted as a Hammett equation correlation in Figure 1b. This correlation from the photopolymerizations is similar to that shown in Figure 1a for the flash photolysis bleaching of methylene blue in the absence of monomer. The somewhat larger ρ value (slope) in Figure 1b may be due to the presence of acrylamide and its effect on the dye. In both cases there is good agreement that the dye-triplet reaction rate (eq 8) becomes appreciably slower as electron withdrawing groups are substituted in the para position of the benzenesulfinate ions.

If there was no triplet quenching reaction (eq 9), the lines in Figure 7 should have a common intercept. The observed intercepts indicate that the k_q of the sulfinates follows the order $NO_2 > Br > CH_3CONH > Cl > CH_3 > H$. This triplet quenching order is similar to that shown in Table I for the excited singlet state quenching of the dye. The intercept value for the benzenesulfinate plot in Figure 7 corresponds to $\Phi_B = 0.23$. This falls in the same range as the values of 0.21 to 0.24 reported[21,27] for similar extrapolations of the bleaching of methylene blue in EDTA solutions without monomer. By choosing an approximate value for the constant C in eq 21 the intercept can be used to estimate a minimum value of the intersystem crossing quantum yield (ϕ) of methylene blue triplet formation. The polymer termination rate constant for acrylamide is reported[28] to be $k_t = 1.45 \times 10^7$ l. mol^{-1} sec^{-1}. The semimethylene blue disproportionation rate constant in acid solutions is reported[20] to be $k_d = 1.5 \times 10^9$ l. mol^{-1} sec^{-1}. Thus k_t' is probably between these two values, so that $1.1 < C < 1.9$. If we assume a mid-range value and let $k_t' \cong 1.5 \times 10^8$ l. mol^{-1} sec^{-1}, then $C \cong 1.5$. Then using the intercept and slope from the benzenesulfinate plot in Figure 7 gives the following approximate values.

$$\phi \cong \frac{1.5(1 + k_q/k_c^\circ)}{\text{intercept}} \geq 0.34$$

$$k_c^\circ \cong \frac{1.5}{(\tau\phi)\ \text{slope}} \leq 4 \times 10^7 \text{ l. mol}^{-1} \text{ sec}^{-1}$$

Dye–Acrylamide Complex. Acrylamide changes the characteristics and reactivity of aqueous methylene blue solutions sufficiently to indicate that a solvation effect occurs, which may be a weak complex beween the monomer and the dye. Our observations of increased absorption coefficients and increased fluorescence intensities suggest that acrylamide solvates and helps isolate individual dye ions from each other, decreasing dye-dimer effects. It tends to stabilize the dye's excited states by decreasing the quenching effects. The enhanced photobleaching of sodium formaldehydesulfoxalate indicates that acrylamide solvation may increase the dye-triplet yield or perhaps increase its effective lifetime.

Conclusions

We conclude that benzenesulfinate ions undergo an oxidation–reduction reaction with a triplet state of methylene blue to form sulfonyl and semimethylene blue free radicals. In the absence of monomer, these back react very rapidly to reform the starting materials. In the presence of monomer, free radicals are captured and polymerization and dye-bleaching occurs. The first excited singlet state of the dye does not react in this manner. It is quenched at higher concentrations of benzenesulfinate ions, but this does not produce a significant yield of redox products or polymerization. In a series of para-substituted benzenesulfinates the excited singlet state quenching constants follow the order: $NO_2 > CH_3CONH > Br > Cl > CH_3 > H$. There is also some triplet state quenching observed, which follows approximately in this same order for the various substituents. The reaction rate constants for the dye-triplet redox reaction with the para-substituted benzenesulfinates fit a Hammett equation correlation, using σ_p. The reaction rates with the triplet are decreased by electron-withdrawing substituents, so that $CH_3 > CH_3CONH > H > Cl > Br > NO_2$. The photopolymer yields and end groups are consistent with a mechanism in which the sulfonyl radicals initiate the polymerization, and semimethylene blue radicals either undergo disproportionation reactions or act as chain termination agents. This mechanism is supported by observations that the formation of semimethylene blue radicals in two other photoredox systems does not cause polymerization to occur. Acrylamide appears to solvate or form a weak complex with methylene blue. At high acrylamide concentrations the dye shows a longer wavelength absorption maximum with a higher absorption coefficient, less dimer formation, more fluorescence, and less quenching of fluorescence than in aqueous solutions without the monomer.

Acknowledgment. We are indebted to Dr. L. J. Miller for the synthesis of three substituted benzenesulfinate salts and to the Directorate of Chemical Sciences, Air Force Office of Scientific Research, Contract No. F44620-68-C-0043, for partial support of these studies.

(27) N. Kosai, K. Uchida, and M. Koizumi, *Bull. Chem. Soc. Jap.*, **38**, 1958 (1965).

(28) F. S. Dainton and M. Tordoff, *Trans. Faraday Soc.*, **53**, 499 (1957).

The Ultraviolet Photochemistry of Ruthenium(III) Ammine Complexes[1]

by W. L. Wells and John F. Endicott*

Department of Chemistry, Wayne State University, Detroit, Michigan 48202 *(Received March 22, 1971)*

Publication costs assisted by the National Science Foundation

It has been demonstrated that $Ru(NH_3)_6^{3+}$ and $Ru(NH_3)_5Cl^{2+}$ are largely unreactive when their ultraviolet absorption bands are irradiated. The single reaction which can be unequivocally established for each complex is a low yield ($\phi < 0.1$) photoinduced aquation of an ammine ligand. Flash and continuous photolysis studies have demonstrated that irradiation of charge transfer to metal (CTTM) absorption bands does not result in detectable photoredox processes ($\phi < 0.001$). The relative photochemical inertness of these ruthenium(III) complexes can be related to the relatively small distortion expected of the CTTM excited states, with a t_{2g}^6 electronic configuration, and to the expectation that the CTTM states are lower in energy than the d–d excited states in the $Ru^{III}(NH_3)_5X$ complexes.

Introduction

Despite the recent increase of interest in the photochemistry of coordination complexes,[2] most of the systematic investigations of substitution inert complexes have been confined to cobalt(III) and chromium(III)[2] with a few studies of platinum metal complexes.[2,3] Owing to their varied photochemical behavior, complexes of the $M^{III}(NH_3)_5X$ type have been of particular interest to us.[3,4] Previous photochemical studies of this class of compounds have been confined to central metals with nd^3 (chromium(III)) or nd^6 (cobalt(III), rhodium(III), platinum(IV), etc.) electronic structures.[2-4] The present report is of the first systematic photochemical study of $Ru^{III}(NH_3)_5X$ complexes. Ruthenium(III) complexes of this type are substitution inert,[5-7] exhibit about the same thermodynamic potential for reduction as the $Co^{III}(NH_3)_5X$ complexes,[6-9] and their principal absorption bands have been characterized and assigned.[10,11] These ruthenium(III) complexes provide an interesting contrast with the spin-paired nd^6 systems since the metal acceptor orbital in CTTM transitions is nonbonding (t_{2g}) in the former and antibonding ($^*e_g$) in the latter complexes. As a result of this electronic difference and since ruthenium(II) is reasonably inert to substitution[6-8,12] while cobalt(II) is labile,[13] one might expect some striking contrasts between the behavior of charge transfer to metal (CTTM) excited states of ruthenium(III) and those of the nd^6 complexes.

It should also be observed that the $Ru^{II}(NH_3)_5X$ complexes are themselves low spin $4d^6$ in their central metal electronic configuration, but their photochemistry seems to involve oxidation of the metal center as well as a variety of ligand exchange processes.[14,15]

Experimental Section

A. Preparations. All compounds studied in this investigation were prepared from hexaammineruthenium(III) chloride purchased from Matthey-Bishop. The perchlorate salt $[Ru(NH_3)_6](ClO_4)_3$ was prepared by adding a few drops of concentrated perchloric acid to an ice-cold solution of the starting material dissolved in a minimum amount of water. The white precipitate was dried on an evaporating dish in a desiccator. Usually about 0.5 g or less of the hexaammine perchlorate was prepared at any one time. The purity of the perchlorate salt was verified from the solution absorbance ($\epsilon_{275} = 475 \pm 10\ M^{-1}\ cm^{-1}$).[5-7,16]

$[Ru(NH_3)_5Cl]Cl_2$. This complex was prepared photolytically, a procedure which appears to be more efficient than the classical method.[17] In a typical preparation

(1) (a) Partial support of this research by the National Science Foundation is gratefully acknowledged. (b) Presented in part before the 161st National Meeting of the American Chemical Society, Los Angeles, Calif., Mar 1971.

(2) V. Balzani and V. Carassiti, "Photochemistry of Coordination Coupounds," Academic Press, New York, N. Y., 1970.

(3) (a) T. L. Kelly and J. F. Endicott, *J. Amer. Chem. Soc.*, **92**, 5733 (1970); (b) T. L. Kelly and J. F. Endicott, unpublished observations.

(4) (a) J. F. Endicott and M. Z. Hoffman, *J. Amer. Chem. Soc.*, **87**, 3348 (1965); (b) G. Caspari, R. G. Hughes, J. F. Endicott, and M. Z. Hoffman, *ibid.*, **92**, 6801 (1970); (c) J. F. Endicott, M. Z. Hoffman, and L. S. Beres, *J. Phys. Chem.*, **74**, 1021 (1970); (d) J. F. Endicott, *Israel J. Chem.*, **8**, 209 (1970).

(5) J. A. Broomhead, F. Basolo, and R. G. Pearson, *Inorg. Chem.*, **3**, 826 (1964).

(6) (a) J. F. Endicott and H. Taube, *ibid.*, **4**, 437 (1965); (b) *J. Amer. Chem. Soc.*, **84**, 4985 (1962).

(7) J. F. Endicott and H. Taube, *ibid.*, **86**, 1686 (1964).

(8) T. J. Meyer and H. Taube, *Inorg. Chem.*, **7**, 2369 (1968).

(9) W. Latimer, "Oxidation Potentials," Prentice-Hall, Englewood Cliffs, N. J., 1952.

(10) H. Hartman and C. Bushbeck, *Z. Phys. Chem. (Frankfurt am Main)*, **11**, 120 (1957).

(11) C. K. Jorgensen, "Orbitals in Atoms and Molecules," Academic Press, New York, N. Y., 1962, pp 107–110.

(12) P. Ford, *Coord. Chem. Rev.*, **5**, 75 (1970).

(13) R. Wilkins and M. Eigen, *Advan. Chem. Ser.*, **No. 49**, 55 (1965).

(14) C. Sigwart and J. Spence, *J. Amer. Chem. Soc.*, **91**, 3992 (1969).

(15) P. C. Ford, D. H. Stuermer, and D. P. McDonald, *ibid.*, **91**, 6209 (1969).

(16) J. A. Stritar and H. Taube, *Inorg. Chem.*, **8**, 2281 (1969).

(17) K. Gleu and K. Rehm, *Z. Anorg. Allg. Chem.*, **227**, 237 (1936).

about 5 g of $Ru(NH_3)_6Cl_3$, 8 ml of concentrated HCl, 6 ml of methanol, and 30 ml of water were added to a Vycor 791 tube, around which were placed low-pressure (254 nm) mercury arc lamps of high intensity (approximately 10^{-3} einstein $l.^{-1}$ min^{-1}). After several hours of photolysis in the presence of argon, the vessel was noted to contain a bluish colored solution and a yellow-green residue. Isolation of this solid and recrystallization gave the light yellow chloropentaammineruthenium(III) chloride with yields up to about 70%. The purity here was also determined spectrophotometrically (ϵ_{328} = 1930[10] and 1890 M^{-1} cm^{-1} [16]). The chloride salt was converted into perchlorate as above.

$[Ru(NH_3)_5Br]Br_2$. A small amount of the bromo salt was prepared in an identical fashion to the chloro complex, except that HBr was used in place of HCl. The compound was characterized by its 398-mm band.[10]

$[Ru(NH_3)_5I]^{2+}$. This species was never isolated. A solution containing 10^{-4} M $[Ru(NH_3)_5Cl]^{2+}$ and 10^{-1} M I^- was observed to turn purple in color on standing several hours in the laboratory. A visible spectrum confirmed the presence of the iodopentaammineruthenium(III) moiety (λ_{max} 540 nm[6,10]).

B. Photolysis Procedures. All 254-nm irradiations were carried out as described earlier.[4] The design of the apparatus allowed both good deaeration with argon gas and good mixing *via* a Teflon-coated stirring bar in the bottom of the cell. The cell was placed in a water bath which allowed accurate control of temperature (25 ± 1°). Aliquots of photolyte were extracted with a Teflon syringe needle and injected as rapidly as possible into serum-capped flasks continuously flushed with argon. All argon used in this work was passed through a Cr^{2+} scrubbing tower before use. Connections of tubing, needles, serum caps, etc., were sealed with copper wire, parafilm, etc., to exclude air.

Photolyses at wavelengths other than 254 nm were made using a Xenon Corp. Model 727 spectral irradiator. The desired wavelength region was selected using a grating spectrometer (Bausch and Lomb). The intensity profile was determined with a RDR-F2 thermopile from Charles M. Reeder and Co., Detroit, Mich. The bandwidth at half-maximum intensity was about 60 Å for the wavelengths used in this study. A regular 1-cm path length quartz cell of about 4-ml capacity held the photolyte during irradiation. Air was excluded by use of a parafilm-wrapped wire sealed serum cap and argon flushing to both deareate and agitate the solution.

Flash photolyses were performed with the Xenon Corp. Model 270 as described previously.[4b] Sample solutions were deaerated before each flash experiment with Cr^{2+}-scrubbed argon. The sample cell for flash photolysis was surrounded by a concentric quartz jacket into which various filter solutions were placed.

C. Actinometry and Other Analytic Procedures. For the 254-nm irradiations, ferrioxalate actinometry was performed[18,19] as described elsewhere.[4] This procedure provides values of I_a in units of einsteins $l.^{-1}$ min^{-1} as listed in Table I. Actinometry determinations, with ferrioxalate, of I_a at other wavelengths (using the spectral irradiator) have been recorded in the same units by taking account of the fact that an area of 0.9 cm^2 (adjusted with slits) of a 1-cm quartz cell was irradiated when the irradiator was used. We experienced considerable variations in the output of one of the low-pressure mercury lamps used in this study and therefore have used chemical actinometers to check the lamp output for every series of determinations. We often found it convenient to perform these intensity checks using $Co(NH_3)_5Cl^{2+}$ (ϕ = 0.17 at pH 1)[4a,b] or $Co(NH_3)_5OH_2^{3+}$ (ϕ = 0.19)[4a] as the actinometric reference compounds. The quantum yields used in these cases were independently checked by reference to the primary ferrioxalate actinometry. To obtain a value for I_a at 230 nm we have assumed a quantum yield of 1.25 for ferrioxalate decomposition; this of course assumes that the wavelength independence of the quantum yield for ferrioxalate decomposition continues this far into the uv. Output intensity of the irradiator was checked before and after each irradiation using the RDR thermopile.

Cobalt(II) determinations were made using a thiocyanate method previously described.[4b,20] Care was taken to expose both blank and sample solutions to minimum contact with stainless steel needles, as these introduce iron easily into the solution. Later analyses in this work used platinum needles and metal-free syringes.

Ion-exchange chromatography was carried out using AG 50W-X4, 200–400 mesh, analytical grade H^+ ion exchange resin from Bio-Rad Laboratories.

Reducing solutions (Cr^{2+} and Ru(II)) were prepared under an argon atmosphere by addition of Cr^{3+} and Ru(III) solutions to zinc amalgam in a serum-capped flask. Generally, 0.5–1 hr was allowed for reduction to occur.

Measurements of pH and potentiometric determinations of Cl^- were made using a Delta-matic Model 145 pH meter–millivoltmeter from Instrumentation Laboratories, Inc., Boston, Mass. The electrodes were calomel and silver metal, with a $NaNO_3$ salt bridge connecting the solutions surrounding the two electrodes. The Ag electrode was placed into a solution made up of a 5-ml aliquot of photolyte, a 10-ml portion of an acetone–HNO_3 solution, and a few milligrams of Alconox. The acetone–HNO_3 solution (1 qt of acetone plus 25 ml of concentrated HNO_3) was added to enhance sensitivity

(18) C. A. Parker and G. C. Hatchard, *Proc. Roy. Soc., Ser. A*, **235**, 518 (1956).

(19) J. G. Calvert and J. N. Pitts, Jr., "Photochemistry," Wiley, New York, N. Y., 1967.

(20) R. E. Kitson, *Anal. Chem.*, **22**, 664 (1950).

Table I: Product Yields from the Continuous Photolysis of Ruthenium(III) Ammines

Radiation λ, nm	Band irradiated[a]	Medium[b]	$10^4 I_a$, einsteins $l.^{-1}$ min^{-1}	10^3-$[Ru(III)]_{init}$, M	Product yields[c] $\Sigma Ru^{III}(NH_3)_5Y$[d]	NH_4^+[e]	Cl^-[f]
		A. $Ru(NH_3)_6^{3+}$					
254	CTTM[g]		1.2	1.0	0.087	0.072	
		0.5 M CH_3OH	1.2	1.0	0.080		
		5.0 M CH_3OH	1.2	1.0	0.086		
		0.5 M C_3H_7OH	1.2	1.0	0.084		
		pH 5.8	1.2	1.0	0.082		
		0.1 M $HClO_4$	1.6	1.0	0.077		
		0.1 M NaCl	1.6	1.0	0.070	0.05	
		(O_2)[g]	4.0	1.0	0.075		
		0.1 M NaCl, (O_2)[h]	4.0	1.0	0.075	0.087	
		HX, NaX[i] with 0.1 $M \geq [X^-] \geq 10^{-3}$ M	3.3	1.0	0.012 ± 0.009[i]		
		HX, NaX[i] with 1 $M \geq [X^-] \geq 10^{-3}$ M and $[CH_3OH] = 0.5$ M	3.3	1.0	0.04 ± 0.03[i]	0.09 ± 0.04	
		0.1 M NaI	6.0	1.0	0.04 ± 0.01[j]		
321	d–d	0.1 M NaBr	1.9	1.0	0.01		
		B. $Ru(NH_3)_5Cl^{2+}$					
230	CTTM		0.45	2.0		0.017	
		0.5 M C_3H_7OH	0.45	2.0	~1[k]	0.1	
254	CTTM;		4.0	2.2	0.05[k]		
	d–d(?)		3.3	2.2	0.06 ± 0.01[k]	0.032 ± 0.002	0.029
		0.1 M NaCl	3.3	2.2	~0.006[k,l]	0.032	
		0.01 M NaCl, 0.5 M C_3H_7OH	3.3	2.2	~0[k,l]	0.042	
			2.9	2.2		0.041	0.04
321	CTTM ($Cl^- \rightarrow Ru$)		5.3	1.0	0.0023[k]		
		0.5 M C_3H_7OH	5.3	1.0	0.04 ± 0.01[k]		
		0.1 M NaCl, 0.5 M C_3H_7OH	5.3	1.0	0.008[k]	0.020	
		5 M C_3H_7OH	5.3	1.0	0.03[k]	0.027	
		10^{-2} M NaI	5.3	1.0	0.01[k]; 0.004[m]		

[a] Absorption bands assigned per ref 10 and 11. [b] 25°; pH 3 except as indicated. [c] Quantum yields for the various products as indicated. [d] Based on the rate of appearance of all $Ru^{III}(NH_3)_5Y$ (Y = halide, X^-, or H_2O) products from the irradiation of $Ru(NH_3)_6^{3+}$ or the disappearance of the absorbance of $Ru^{III}(NH_3)_5X$ when $Ru^{III}(NH_3)_5X$ was irradiated. In the latter cases yields are based on total absorbance decreases since quantitative separations of the tetramine and pentamine and pentaammine species present in the photolyte was not achieved. Solutions were equilibrated catalytically with $Ru(NH_3)_5OH_2^{2+}$, except as indicated. The $Ru^{III}(NH_3)_5Y$ product yields are based on the sum of measured halopentaammine absorbances and calculated aquopentaammine concentrations. [e] Based on increases in measured pH. [f] Based on potentiometric titration with $AgNO_3$. [g] This assignment has been made using Jørgensen's optical electronegativities and by comparison of CTTM energies at band maxima for $Ru^{III}(NH_3)_5X$ and $Co^{III}(NH_3)_5X$ complexes. [h] O_2 bubbled through solution during irradiation. All other photolyses were performed under argon. [i] These solutions were not equilibrated with respect to $Ru^{III}(NH_3)_5X$ and $Ru(NH_3)_5OH_2^{3+}$ following photolysis. The yields in these cases represent the sum of the $[Ru^{III}(NH_3)_5X]$ observed to result from irradiation and the $[Ru(NH_3)_5OH_2^{3+}]$ which would have been present at equilibrium with that $[Ru(NH_3)_5X]$. For these studies X = Cl^- or Br^-. [j] Under these conditions I^- is the absorbing species. Product yield is based on e_{aq}^- yield of 0.25 from I^- [G. Stein, *Advan. Chem. Ser.*, **No. 50**, 230 (1965); J. F. Endicott and M. Z. Hoffman, *J. Phys. Chem.*, **70**, 3389 (1966)] and 100% scavenging of e_{aq}^- by $Ru(NH_3)_6^{3+}$; I_3^- was not a photolysis product. [k] Estimated from the decrease in absorbance at 328 nm assuming only $Ru(NH_3)_5Cl^{2+}$ absorbs at this wavelength. [l] Solution equilibrated with respect to (1) before irradiation. [m] Estimated from $\sim 7 \times 10^{-7}$ M $Ru(NH_3)_5I^{2+}$ which was formed in this experiment. No $Ru(NH_3)_5I^{2+}$ was found in an unirradiated sample of this solution which was allowed to stand in the room while the irradiation was performed.

while the Alconox prevented coagulation of the colloidal silver chloride.[4b]

Results

A. Continuous Photolysis. Our identifications of products and yields are summarized in Table I. In general the photolysis of ruthenium(III) ammines was observed to result in an increase in pH; we have associated these pH changes with the release of coordinated ammonia into the solution. We have used changes in pH over the region $3 \leq pH \leq 4$ as the basis of our estimates of ammonia photoaquated (the pK_a of $Ru(NH_3)_5OH_2^{3+}$ is 4.2).

In column 6 of Table I we have listed two different

kinds of observations: (1) entries listed for the irradiation of $Ru(NH_3)_6^{3+}$ correspond to our best estimate of the amount of $Ru^{III}(NH_3)_5Y$ (Y = halide or H_2O) produced based on spectral measurements; and (2) entries listed for the irradiation of $Ru(NH_3)_5Cl^{2+}$ correspond to the change of absorbance observed at 328 nm divided by the 328-nm molar absorptivity of $Ru(NH_3)_5Cl^{2+}$. In estimating the total $[Ru^{III}(NH_3)_5Y]$ species produced from the irradiation of $Ru(NH_3)_6^{3+}$, we have taken account of (1) using stability constants from ref 6 at ionic strengths of 0.1 and determining

$$Ru(NH_3)_5OH_2^{3+} + X^- \rightleftharpoons Ru(NH_3)_5X^{2+} \quad (1)$$

the concentration of the halopentaammine complex, $Ru^{III}(NH_3)_5X$, from its near-uv absorbance; at low ionic strengths ($\leq 10^{-3}$) or in solutions with [alcohol] ≥ 0.5 M we have found that K_1 is sufficiently large (>500 M^{-1}) that $[Ru^{III}(NH_3)_4X] + [Ru(NH_3)_5OH_2^{3+}] \simeq [Ru^{III}(NH_3)_5X]$. Since we have estimated the total pentaammineruthenium(III) yield assuming (1) is at equilibrium, the only quantitatively useful yields are those for which we introduced a reducing agent (Cr^{2+} or $Ru(NH_3)_5OH_2^{2+}$) to catalyze the equilibration.[6] We have included in Table I a summary of a large number of determinations of the apparent pentaammineruthenium(III) yield under conditions that equilibration was not catalytically induced after irradiation. These low apparent yields are of considerable qualitative significance in that they imply: (1) that neither $Ru(NH_3)_5OH_2^{2+}$ or $Ru(NH_3)_6^{2+}$ is a significant photochemical product and (2) that the primary product from irradiation of $Ru(NH_3)_6^{3+}$ is $Ru(NH_3)_5OH_2^{3+}$. Spectral changes deep in the uv are consistent with the latter deduction, but quantitative interpretation is unreliable as $Ru(NH_3)_6^{3+}$ (λ_{max} 275; ϵ = 475),[12] $Ru(NH_3)_5OH_2^{3+}$ (λ_{max} 268 mn; ϵ = 757),[6b] and $Ru(NH_3)_6^{2+}$ (λ_{max} 275; ϵ = 670).[12] All absorb in the same spectral region, and we only irradiated to $\leq 20\%$ conversion into products in the quantitative determinations. The catalyzed equilibrations were generally carried out in excess Cl^-, thus providing a sensitive means of detecting pentaammineruthenium(III) species.

The photochemical behavior of $Ru(NH_3)_5Cl^{2+}$ proved to be relatively difficult to elucidate. This difficulty arose because the complex is relatively photoinsensitive and because the substrate and some of the photolysis products have similar absorption spectra. The system is further complicated by the fact that the production of very small amounts of ruthenium(II) can catalyze the hydrolysis of $Ru(NH_3)_5Cl^{2+}$ (*i.e.*, the reverse of (1)). Thus the irradiation of $Ru(NH_3)_5Cl^{2+}$ in perchlorate media (or at least under conditions such that equilibrium 1 was not achieved prior to photolysis) produced relatively large spectral changes at 328 nm and some free Cl^-. However, the apparent yields based on these changes (either in $[Cl^-]$ or absorbance at 328 nm) are neither very reproducible or strictly constant with increasing periods of irradiation. Furthermore, solutions which were catalytically equilibrated with respect to (1) before irradiation showed only very small change in the 328-nm absorbance. These observations do not rule out the production of $Ru(NH_3)_5OH_2^{3+}$, but they do require that if the aquo complex is a primary product some $Ru(NH_3)_5OH_2^{2+}$ (in amounts we have been unable to detect) must also be produced to catalyze the equilibrium (1). It may be significant that on irradiation of $Ru(NH_3)_5Cl^{2+}$ the system does tend toward the equilibrium ratio of $[Ru(NH_3)_5Cl^{2+}]$ and $[Ru(NH_3)_5OH_2^{3+}]$ and that $Ru(NH_3)_5OH_2^{3+}$ is never produced in excess of its equilibrium concentration. Furthermore, in a more sensitive experiment, when $Ru(NH_3)_5Cl^{2+}$ was irradiated in 0.01 M NaI the $[Ru(NH_3)_5I^{2+}]$ produced was less than 2% of its equilibrium value, indicating that very little ruthenium(II) can be produced.

It is relevant to observe that irradiation (to less than 10% reaction based on the NH_4^+ yield) or $Ru(NH_3)_5Cl^{2+}$ did result in slight shifts of the 328-nm absorption maximum to longer wavelengths. Separations of the components of the photolyte, by precipitation of $[Ru(NH_3)_5Cl]Cl_2$ and/or ion-exchange chromotography, gave evidence of several species in solution. Early fractions of eluent (eluted with HCl) exhibited intense absorption maxima at 350 and 310 nm consistent with *cis*-$Ru(NH_3)_4Cl_2^+$ (with some of the trans complex possibly present). In one particularly instructive experiment, 2×10^{-3} M $Ru(NH_3)_5Cl^{2+}$ was irradiated at 321 nm ($I_a = 5.3 \times 10^{-4}$ einstein $l.^{-1}$ min^{-1}) in 10^{-3} M HCl and 5 M 2-propanol. Addition of concentrated HCl to the photolyte after irradiation precipitated $Ru(NH_3)_5Cl_3$ nearly quantitatively leaving a supernatant solution which exhibited a new absorption band at 350 nm (A = 0.90) and a shoulder at 310 nm (A = 0.70) with more intense absorbances at much shorter wavelength. Using the appropriate extinction coefficients[21] these absorptions in the supernatant imply ϕ(*cis*-$Ru(NH_3)_4Cl_2^+$) = 0.01 which can be compared with $\phi(NH_3) \simeq 0.025$ (Table I).

A final pertinent observation is that for none of these ruthenium(III) complexes did we observe significant differences in photolysis of areated and deareated solutions.

B. Flash Photolysis Studies. The results of our flash photolysis studies are summarized in Table II. In general we have searched for transients at several wavelengths in the range 250 nm $< \lambda <$ 550 nm. As expected, the only transients observed were the dihalide radical anions, which absorb strongly in the 340–380-nm wavelength region.[22] Although weakly absorbing

(21) According to P. Ford (private communication to J. F. E.) these are (for *trans*-$Ru(NH_3)_4Cl_2^+$); λ_{max} 331 nm ($\epsilon = 4.95 \times 10^3$); 255 (sh, $\epsilon = 7 \times 10^2$); and (*cis*-$Ru(NH_3)_4Cl_2^+$): λ_{max} = 352 nm ($\epsilon = 1.46 \times 10^3$) and 311 ($\epsilon = 1.23 \times 10^3$).

(22) A. Treinin, "Radical Ions," E. T. Kaiser and L. Kevan, Ed., Interscience, New York, N. Y., 1968, Chapter 12, pp 544–551.

transients were observed in several cases when the ruthenium(III) complexes were flashed in the deep uv regions (*i.e.*, using filters which cut off all $\lambda \leq 230$ nm) in the presence of free halide ions, in each of these cases the generation of a transient can be attributed to ion-pair (or outer sphere) charge transfer absorptions. In no case do we have evidence for formation of a radical from photooxidation of a ligand coordinated to ruthenium(III).

Table II: Flash Photolysis of Ruthenium(III) Ammine Complexes

Complex flashed	Solvent medium	Wavelength, λ, region flashed, nm	Observations[a]
$Ru(NH_3)_6^{3+}$	10^{-3} *M* $HClO_4$	≥ 215[b]	No transient
	0.1 *M* NaCl	≥ 215[b]	Cl_2^-
	0.1 *M* NaBr	≥ 215[b]	Br_2^-
	0.1 *M* KBr	≥ 270[c]	No transient
$Ru(NH_3)_5Cl^{2+}$	10^{-2} *M* $HClO_4$	≥ 200[d]	No transient
	10^{-4} *M* HCl	≥ 215[b]	No transient
	0.1 *M* NaCl	≥ 215[b]	No transient
	0.1 *M* NaBr	≥ 320[e]	No transient
$Ru(NH_3)_5I^{2+}$	0.1 *M* NaI	≥ 200[d]	I_2^-
	0.1 *M* NaI	≥ 455[f]	No transient

[a] Transient identification is consistent with spectral characteristics, decay lifetimes, and medium composition (see ref 22). [b] 1 *M* NaBr filter used. [c] Acetic anhydride filter solution used. [d] Water used as filter. [e] Naphthalene in methanol used as filter. [f] Filter solution was composed of $FeCl_3$ and 5,7,7,12,14,-14-hexamethyl-1,4,8,11-tetrazacyclotetradeca-4,11-dienenickel·(II) with concentrations adjusted so the solution absorbance >2 at all wavelengths λ <455 nm.

Discussion

At a very naive level it might be expected that CTTM irradiation of Ru(III) would not produce much photoreaction as the CTTM "excited state" can be formally described as a ruthenium(II) complex with a coordinated radical as ligand. Such a species is not expected to dissociate on a microsecond time scale but would be expected to undergo facile internal redox to regenerate the original ruthenium(III) species. In accord with such expectations it is to be noted that upon irradiation of $Ru(NH_3)_6^{3+}$ and of $Ru(NH_3)_5Cl^{2+}$ less than 10% of the excitations produce any kind of photochemical product.

In addition to the limited photochemical reactivity noted above, we have evidence that there is virtually no ($\phi < 10^{-3}$) net photoredox of $Ru^{III}(NH_3)_5X$ complexes. Certainly the lower energy $X^- \rightarrow$ Ru(III) CTTM bands do not produce any detectable X· radicals. Most impressive in this regard is the absence of Br_2^- when $Ru(NH_3)_5Cl^{2+}$ is flashed at $\lambda \geq 300$ nm in the presence of 0.1 *M* Br^-; apparently the CTTM excited state is too short-lived to oxidize Br^-, and no Cl· is released into solution.

Of the apparent photolabilization reactions[23,24] only ammine aquation (2 and 3) can be confidently regarded to be the result of a primary photochemical reaction

$$Ru(NH_3)_6^{3+} + h\nu + H^+ \xrightarrow{\phi_2 I_a} Ru(NH_3)_5OH_2^{3+} + NH_4^+ \quad (2)$$

(see Table III). The aquation of Cl^- from $Ru(NH_3)_5Cl^{2+}$ (4) can be catalyzed by trace amounts of $Ru(NH_3)_5OH_2^{2+}$[6] and therefore may not occur as a primary process ($\phi_4 \leq 0.035 \pm 0.006$ at 254 nm). Similarly it seems evident, *e.g.*, from data in Table I, that the

$$Ru(NH_3)_5Cl^{2+} + H^+ + h\nu \begin{cases} \xrightarrow{\phi_3 I_a} Ru(NH_3)_4OH_2Cl^{2+} + NH_4^+ & (3) \\ \xrightarrow{\phi_4 I_a} Ru(NH_3)_5OH_2^{3+} + Cl^- & (4) \end{cases}$$

formation of $Ru(NH_3)_5Cl^{2+}$ from irradiation of $Ru(NH_3)_6^{3+}$ and the formation of $Ru(NH_3)_4Cl_2^+$ from irradiation of $Ru(NH_3)_5Cl^{2+}$ occur in secondary thermal reactions. Whether the primary tetraammine product from photolabilization of $Ru(NH_3)_5Cl^{2+}$ is cis or trans is ambiguous since at present no information is available concerning the relative stabilities or the isomerization rates of these complexes.

The photochemical behavior of the $Ru(NH_3)_5Cl^{2+}$ complex is on the whole not very dependent on wavelength (Table III). The relatively high yields observed at 230 nm in 0.5 *M* 2-propanol (conditions favoring formation of $Ru(NH_3)_5OH_2^{2+}$ and catalytic aquation of $Ru(NH_3)_5Cl^{2+}$) can be regarded as suggestive of population of a CTTM excited state with a different electronic configuration from that produced by 254- or

(23) An interesting modification of some mechanistic details might be suggested by our observation that the sequence of reactions (for Ru(III) = $Ru(NH_3)_6^{3+}$)

$$I^- + h \longrightarrow I + e^- \quad (a)$$

$$Ru(III) + e^- \longrightarrow Ru(II) \quad (b)$$

$$Ru(II) + I \text{ (or } I_2^- \text{ or } I_3^-) \longrightarrow Ru(III) + I^- \quad (c)$$

results in the formation of $Ru(NH_3)_5I^{2+}$ from about 4% of the cycles (a–c). This might imply that ammonia aquation normally accompanies a small percentage of reductions (b) of ruthenium(III). Such a hypothesis would relate the thermal and photochemical behavior of $Ru(NH_3)_6^{3+}$ but provides no useful insight into the detailed mechanism of such a process. We do not consider this a useful approach to the photochemistry partly because a likely explanation of this particular observation is that the $Ru(NH_3)_5I^{2+}$ results from the combination of (a) with (d).

$$Ru(NH_3)_6^{3+} + I_2^- \xrightarrow{H^+} Ru(NH_3)_5OH^{2+} + I_2 + NH_4^+ \quad (d)$$

Note that the irreversibility of (e), a redox disproportionation, implies that I_2^- should be a reasonable reducing agent and that ruthenium(III) can apparently expand its coordination sphere.[24]

$$2I_2^- \longrightarrow 2I^- + I_2 \quad (e)$$

(24) J. N. Armor, H. A. Scheideger, and H. Taube, *J. Amer. Chem. Soc.*, **90**, 5928 (1968).

Table III: Probable Primary Product Yields in the Photochemistry of Ruthenium(III) Ammines

Complex irradiated	λ, nm	ϕ_2 or ϕ_3
$Ru(NH_3)_6^{3+}$	254	0.079 ± 0.004
	321	0.01
$Ru(NH_3)_5Cl^{2+}$	230	0.02[a]
	254	0.037 ± 0.005
	321	0.025 ± 0.006

[a] In the absence of alcohol.

321-nm irradiation (*e.g.*, $t_{2g}^5e_g$ as opposed to t_{2g}^6, respectively). With this one possible exception it can be postulated that the photochemistry of $Ru(NH_3)_5Cl^{2+}$ is the result of the eventual population of some common excited state regardless of the nature of the initial excited state.

It is instructive to compare the photochemistry of these substitutions inert $4d^5$ (low spin) ruthenium(III) complexes to the nd^6 cobalt(III) and rhodium(III) analogs. Characteristically the cobalt(III) and rhodium(III) complexes generate oxidized ligand species when CTTM bands are irradiated and ligand labilization on irradiating d–d absorption bands. Although the cobalt(III) analogs exhibit little d–d photochemistry, the $Rh^{III}(NH_3)_5X$ complexes seem to have very photosensitive d–d absorption bands with quantum yields of products varying from 0.2 to 1.[3,25] One might expect the d–d excited states of ruthenium(III) to be more similar in reactivity to those of rhodium(III) than cobalt(III).

In the halopentaammineruthenium(III) complexes, the halide-to-ruthenium CTTM absorption bands occur at lower energy than the d–d absorption bands, and it seems reasonable to postulate that in these cases the lowest energy excited state is CTTM and is the state eventually populated (by nonradiative internal conversions to the lowest state of appropriate multiplicity) following absorption of radiation. The wavelength independence of product yields suggests that the observed limited photoreactivity most likely comes from ligand exchange in this lowest energy excited state or in a nonspectroscopic state generated from it. Thus a qualitative comparison of their photochemical behavior suggests that d–d ↔ CTTM internal conversions are facile among ruthenium(III) excited states but not among rhodium(III) excited states. This is no doubt because the metal center can achieve a relatively undistorted t_{2g}^6 excited-state electronic configuration in the former case while the rhodium(III) (and probably also cobalt(III)) CTTM excited states must be significantly distorted due to their electronic configuration ($t_{2g}^6e_g$) and charge density at the metal center. Such variations in excited-state distortions would be expected to result in different relative rates of internal conversion between CTTM and d–d excited-state compared to deactivation of the CTTM excited states directly to the ground state.

(25) L. Moggi, *Gazz. Chim. Ital.*, **97**, 1089 (1967).

Electronic Processes in the Pulse Radiolysis of Aqueous Solutions of Halide Ions

by Shamsher Khorana and William H. Hamill*

Department of Chemistry and the Radiation Laboratory,[1] University of Notre Dame, Notre Dame, Indiana 46556
(Received January 25, 1971)

Publication costs assisted by the U. S. Atomic Energy Commission

Formation of Cl_2^- in radiolytic systems at high $[Cl^-]$ and pH ~7 does not involve OH in the acid spur because $G(Cl_2^-)$ is not markedly decreased by concentrated bases. $G(Cl_2^-)$ in air-free solutions increased only from 2.80 to 3.06 as H^+ increased from 10^{-2} to 1 *M*. The results indicate $G_{OH} = 2.80$ is almost equal to $G^\circ(OH)$. The results are consistent with $Cl_{aq}^- + H_2O^+ \rightarrow Cl + H_2O$. High concentrations of F^- increase $G(e_{aq}^-)$ and OH^- increases $G(OH)$, both attributed to charge transfer to H_2O^+. At high $[I^-]$, $G(I_3^-)$ approaches a limiting value of 6.0 equiv, while $G(I_2^-)$ first increases to ~3, then decreases to ~1.8. The mechanism may involve $I_{aq}^- + H_2O^+ \rightarrow I + H + OH$, since somewhat more energy is available with I_{aq}^- than with Cl_{aq}^-. Measuring $G(OH)$ as $G(I_2^-)$ in 10^{-2} to 10^{-1} *M* I^- at 0–2 *M* $C_2H_3O_2^-$, $-\Delta G(I_2^-)$ approaches a limiting value ~3 after correcting for competition of I^- and $C_2H_3O_2^-$ for OH. The effect is attributed to electron transfer from $C_2H_3O_2^-$ to H_2O^+. For 1 *M* Cd^{2+}, $G(Cd^+)$ decreased from 3.76 to 3.55 as $[H^+]$ increased from 0 to 1 *M*. The results indicate that $G_{e_{aq}^-} \cong G^\circ(e_{aq}^-)$.

Introduction

The radiation chemistry of water begins at $\sim 10^{-11}$ sec, and Schwartz has shown that it can be described thereafter in considerable detail by the spur diffusion model.[2] The nature of the principal transient species (*i.e.*, H, OH, and e_{aq}^-), their yields, and their chemistry have been thoroughly investigated from 10^{-9} sec to the steady state. The work of Hunt and his group[3] is extending the range of direct measurement to 10^{-11} sec which is the threshold of diffusion and chemical kinetics.

The chemical regime is preceded by a physical regime, during which molecular motions can be ignored and electronic processes set the stage for the chemistry to follow. These very early events are not susceptible to direct observation, but they can be inferred to some extent through chemistry. As an example, Cl^- is not oxidized by OH in neutral solution, and the formation of Cl_2^- by pulse radiolysis of concentrated solutions of Cl^- implies electron transfer to dry H_2O^+.[4] If this is correct, molecular diffusion is not involved, and the primary mechanism is purely electronic. This requires the presence of Cl^- as a near-neighbor of a given H_2O prior to its ionization. As a consequence, to trap appreciable yields of such a very transient electronic species as H_2O^+ requires rather concentrated solutions of reagents.

Electron transfer from halide ions is particularly well suited to the investigation of some electronic processes in water. Halide ions, X_{aq}^-, have low electron detachment energies (~5 eV for I_{aq}^-) which facilitates field ionization by the positive hole. The halogen atom produced by electron transfer forms a relatively stable species, X_2^-, which has an intense optical absorption band in a convenient spectral region ($\epsilon \cong 10^4$ M^{-1} cm^{-1}, λ_{max} 350–400 nm). If a halide ion reacts with H_2O^+, there are two possibilities

$$H_2O^+ + X_{aq}^- \longrightarrow H_2O + X \qquad (1a)$$

$$H_2O^+ + X_{aq}^- \longrightarrow H + OH + X \qquad (1b)$$

For Cl^-, one positive hole yields one Cl_2^- by either mechanism in neutral solution. In acid solution, one Cl_2^- is produced by reaction 1a, but two Cl_2^- are produced by (1b). For Br_2^- and I_2^- the yields of X_2^- are 1 and 2, respectively, at either high or low pH. If halide ions react with dry H_3O^+, then (H_3O^+, OH) can yield up to two X_2^- (or one X_3^-) for each charge pair and this could not be distinguished from mechanism 1b.

If Cl_{aq}^- cannot transfer an electron to either H_2O^+ or H_3O^+, then formation of Cl_2^- in neutral solutions may be attributed to the conventional reaction 2. In acid solutions

$$(H_3O_{aq}^+, OH) + Cl_{aq}^- \longrightarrow Cl + 2H_2O \qquad (2)$$

and $G(Cl_2^-)$ should approach or exceed $G_{OH} + 2G_{H_2O_2} \geq 4.3$. At high concentrations of base (*e.g.*, NH_3) $G(Cl_2^-)$ should approach zero according to this mechanism.

(1) The Radiation Laboratory of the University of Notre Dame is operated under contract with the U. S. Atomic Energy Commission. This is AEC document No. COO-38-770.

(2) H. A. Schwarz, *J. Phys. Chem.*, **73**, 1928 (1969).

(3) R. K. Wolff, M. J. Bronskill, and J. W. Hunt, *J. Chem. Phys.*, **53**, 4211 (1970).

(4) T. Sawai and W. H. Hamill, *J. Phys. Chem.*, **74**, 3914 (1970).

Annihilation of the hole by an anion can be expected to increase the yield of e_{aq}^-[5] and may provide a means to measure the primary 100-eV yield of dry electrons, $G^\circ(e^-)$. The yield of trapped holes can be measured, by hypothesis, using neutral Cl^-, as $G(Cl_2^-)$. If holes are trapped as H_2O^+ by reaction 1a, then $G(OH)$ should diminish and this component of the primary yield can be measured.

The aqueous halide ions have fairly low-lying optically allowed transitions, commonly described as charge transfer to solvent, which lead to ionization and the formation of X_2^-. The halide ions may therefore prove to be useful for counting $H_2O(^1B_1)$ at 6.6 eV. In addition, halide ions with $^1S_0$ ground states should have low-lying $^3P^0_{2,1,0}$ states which may act as energy acceptors for $H_2O(^3B_1)$.[6] There is evidence from photochemistry that excited states of X_{aq}^- can be produced by heavy atom perturbation and detected by their ability to transfer electrons to weak electron acceptors, such as N_2O.[7]

The work reported here describes an attempt to interrupt the normal course of electronic events in the radiolysis of aqueous systems, in a more or less predictable manner, using halide ions as the principal probes.

The dependence of product yields on the concentrations of scavengers S will be presented in terms of eq A whenever this is appropriate.

$$G(\text{product}) = G_1^\circ \pm \frac{G_2^\circ \sigma_I [S]}{\sigma_I [S] + \sigma_{II}} \qquad (A)$$

The parameters G_1° and G_2° refer to a product or to its precursor, according to convenience. For e_{aq}^-, $G_1^\circ \cong 2.7$ and G_2° is the additional yield of e^- and e_{aq}^- susceptible to scavenging, *e.g.*, as Cd^+. For Cl_2^-, $G_1^\circ = 0$ in neutral solution and G_2° is the total yield of oxidant capable of producing Cl_2^- from Cl^-, *e.g.*, H_2O^+. σ_I/σ_{II} measures the probability for a precursor to react with S, at $[S] = 1\ M$, relative to some alternative fate, *e.g.*, recombination of H_2O^+ and e^-. Equation A is an arbitrary trial function for electronic processes, and it becomes the Stern–Volmer equation for slow, competing first- and second-order processes.

Experimental Section

All chemicals were Baker's Analyzed reagent grade except potassium iodide, Matheson Coleman and Bell reagent grade, and cadmium sulfate, Fisher Certified reagent grade. Water was triply distilled. Irradiations were performed with 1-μsec pulses of 2-MeV electrons from a Van de Graaf accelerator, unless otherwise stated, when 5-nsec, 5-MeV Linac pulses were used. All solutions were purged with nitrogen unless otherwise stated.

Results

All yields are relative to limiting yields at low scavenger concentrations. For reactions which are nearly diffusion controlled, such products as Cd^+ and I_2^- are measurable at the end of 1-μsec pulses and can be obtained by very short extrapolations for 5-nsec pulses, using $\sim 10^{-2}\ M$ reagent. Consequently, neither separate dosimetry nor extinction coefficients are required.

The principal uncertainty in the present work arises from the necessity of assuming that extinction coefficients of all measured transients are invariant over the range of solute concentrations. The effect of additives on the shape and position of a spectrum can provide limited support for this assumption. The spectrum of Cd^+ is the same (*i.e.*, can be normalized for intensity by a single parameter) for $10^{-2}\ M$ $CdSO_4$, for $10^{-2}\ M$ $CdSO_4$ with 1 M KF, and for 1 M $CdSO_4$. This indicates that the extinction coefficient of Cd^+ is also unchanged. The spectrum of I_2^- for $10^{-2}\ M$ KI is unchanged by adding 1 M Na_2SO_4, but the optical density is decreased by 3%. It will be assumed hereafter that the extinction coefficients of Cd^+ and X_2^- are the same in dilute and in concentrated solutions of the reagents used.

It is known from earlier work[4] that high concentrations of Cl^- considerably increase $G(e_{aq}^-)$. It is also desirable to identify anions which do not trap holes and SO_4^{2-} was tested for this purpose. The yield of e_{aq}^- was measured at λ 305 nm in deaerated solutions as $G(Cd^+)$ using $10^{-2}\ M$ Cd^{2+}. Assuming the extinction coefficients to be constant, there was only a small increase in $G(e_{aq}^-)$ at $\gtrsim 0.5\ M$ Na_2SO_4. The results appear in Table I as nominal yields.

Table I: The Effect of SO_4^{2-} and of ClO_4^- on $G(Cd^+)$

$[Na_2SO_4]$, M	$G(Cd^+)^a$	$[KClO_4]$, M	$G(Cd^+)^a$
0	(2.70)	0	(2.70)
0.12	2.70		
0.25	2.70		
0.50	2.85	0.50	2.76
1.00	2.77	1.00	2.80
1.50	2.90	1.50	2.85
2.00	2.90	2.00	2.85

[a] The OD was measured at 305 nm with $10^{-2}\ M$ $CdSO_4$.

For many purposes the use of HCl to control pH is quite unsuitable because of hole trapping and interference by Cl_2^-, as well as another effect to be described later. The use of $HClO_4$ is preferred to H_2SO_4 and $KClO_4$ was tested for possible effects of ClO_4^- on $G(Cd^+)$. There is only a rather weak dependence, as

(5) It has been noted by J. J. Weiss, *Nature*, 215, 150 (1967), that reaction of the hole with a suitable scavenger would free the electron.

(6) D. Lewis and W. H. Hamill, *J. Chem. Phys.*, 52, 6348 (1970).

(7) S. Khorana and W. H. Hamill, unpublished results.

shown in Table I. ClO_4^- induced no new absorption bands in the region of interest; SO_4^- absorbs negligibly.

Radiolysis of F^- and OH^-. High concentrations of Cl^- increase $G(e_{aq}^-)$, either as a consequence of hole trapping or of conventional oxidation by OH in the acid spur.[4] For F^- there are two possible mechanisms

$$(H_2O^+, e^-) + F_{aq}^- \longrightarrow H_2O + F + e_{aq}^- \quad (3a)$$

$$H_2O + F \longrightarrow HF + OH \quad (3b)$$

$$(H_3O^+, OH, e^-) + F_{aq}^- \longrightarrow H_2O + HF + OH + e_{aq}^- \quad (4)$$

In solutions of F^- there was no evidence for absorption attributable to F_2^- which absorbs at λ_{max} 348 nm in LiF crystals.[8] Using 0.125 *M* F^- and varying $[Cd^{2+}]$, $G(Cd^+)$ was consistently higher than it was when no fluoride was present, as shown in Table II. This provides evidence for hole trapping, but it does not distinguish between mechanisms 3 and 4 since the same geminate entities are present. Other evidence, to be presented, indicates that mechanism 1 is responsible. In the conventional model, $H_3O_{aq}^+$ in the spur is replaced by HF which reacts very slowly with e_{aq}^-, thus increasing $G(e_{aq}^-)$.

Table II: Dependence of $G(Cd^+)$ on $[F^-]$ and of $G(Cl_2^-)$ on $[Cd^{2+}]$ in Neutral, Air-Free Solutions

$[Cd^{2+}]$,[a] *M*	$G(Cd^+)$[b] ($[F^-]$ = 0.25 *M*)	$G(Cd^+)$[c] ($[F^-]$ = 0)	$[Cd^{2+}]$, *M*	$G(Cd^+)$[b,d] ($[Cl^-]$ = 1 *M*)	$G(Cl_2^-)$[b,e] ($[Cl^-]$ = 1 *M*)
			0.00		1.17
0.007	3.06	2.70	0.05	3.40	1.24
0.015	3.08	2.74	0.10	3.40	1.28
0.030	3.16	2.78	0.20	3.40	1.30
0.060	3.32	2.83	0.40	3.52	1.32
0.080	3.38	2.86	0.60	3.76	1.34
0.100	3.43	2.89	0.80	4.16	1.35
0.125	3.50	2.99	1.00	4.42	1.36
			1.50	4.68	1.36
			2.00	4.80	1.37

[a] Concentration of F^- was limited by the solubility of CdF_2. [b] From OD measurements at 305 nm. [c] From ref 14, interpolated. [d] Corrected for Cl_2^- absorption. [e] From OD measurements at λ 345 nm, corrected for Cd^+ absorption.

For solutions containing 10^{-2} *M* Cd^{2+} with increasing $[F^-]$, the results in Figure 1 show $G_2°(Cd^+) = 1.6$ and $\sigma_I/\sigma_{II} = 1.6$ on the basis that $G_1° = 2.70$.

The dependence of $G(OH)$ on $[F^-]$ was tested in deaerated solutions with 10^{-2} *M* I^-, assuming $G(I_2^-) = G_{OH} = 2.80$ for $[F^-] = 0$. At 1 *M* F^-, $G(I_2^-) = 2.98$ and at 2 *M* F^-, $G(I_2^-) = 3.1$ provided that the extinction coefficient of I_2^- remains constant. Some increase in G_{OH} is to be expected by either mechanism.

The system OH^- with 10^{-2} *M* I^- in deaerated solutions is analogous to the preceding and hole trapping

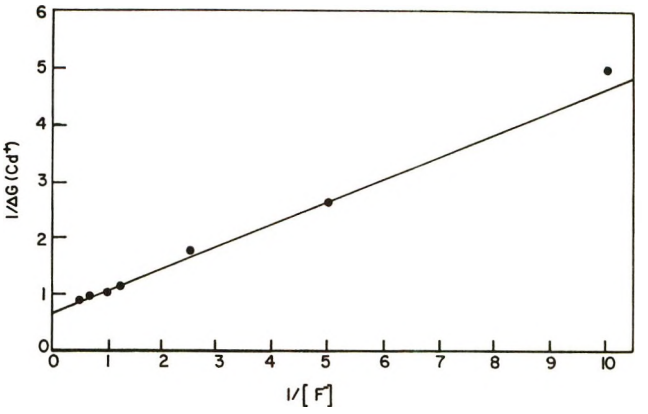

Figure 1. The effect of $[F^-]$, used as a hole trap, on the yield of e_{aq}^- with 10^{-2} *M* $CdSO_4$ in terms of $G(Cd^+)$.

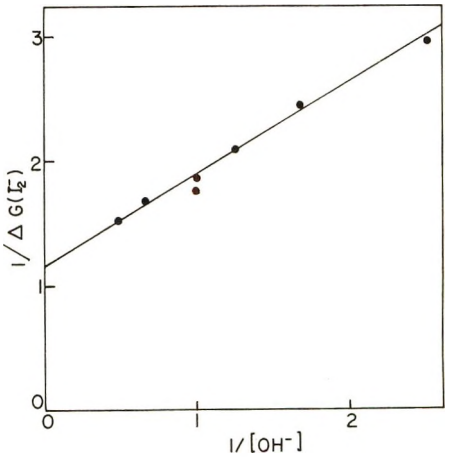

Figure 2. The effect of $[OH^-]$, used as a hole trap, on the yield of OH with 10^{-2} *M* KI in terms of $G(I_2^-)$.

by OH^- may proceed either by electron transfer or by proton transfer. From the results in Figure 2 one obtains $G_1°(I_2^-) = 2.70$ (from a best fit), $G_2°(I_2^-) = 0.87$ and $\sigma_I/\sigma_{II} = 1.5$.

Radiolysis of Cl^-. If Cl^- is oxidized in the spur, whether by the hole or by OH, the oxidized species may then be partially reduced by electrons. A measure of this effect is provided by adding an electron scavenger at high concentrations. In a series of measurements using neutral, air-free solutions of 1 *M* Cl^-, addition of Cd^{2+} increased $G(Cl_2^-)$ from 1.17 at $[Cd^{2+}] = 0$ to 1.37 at $[Cd^{2+}] = 2$ *M*. These results are included in Table II.

Hole trapping by Cl^- is expected to increase the yield of e_{aq}^-. Solutions containing high concentrations of KCl unavoidably contain sufficient amounts of electron scavengers to affect measurements in the microsecond range. All solutions in one series of experiments therefore contained 10^{-2} *M* Cd^{2+}, and the optical densities of Cd^+ and Cl_2^- were measured at 305 and 345 nm.

(8) C. J. Delbeq, W. Hayes, and P. H. Yuster, *Phys. Rev.*, **121**, 1043 (1961).

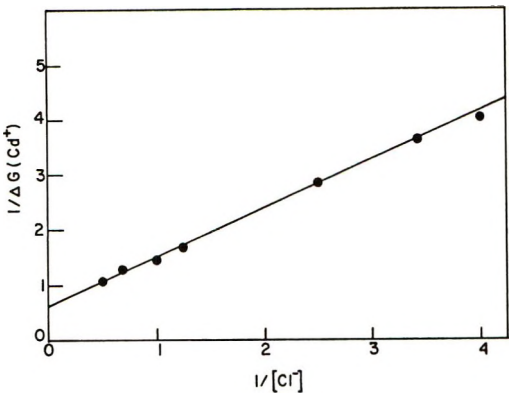

Figure 3. The dependence of $G(Cd^+)$ on $[Cl^-]$ with 10^{-2} M Cd^{2+} at neutral pH.

A small correction was applied to $OD(Cd^+)$ for overlapping absorption by Cl_2^-. These results appear in Figure 3, where all values of $G(Cd^+)$ are relative to the assumed value 2.70 at $[Cl^-] = 0$ and $G_2^\circ(Cd^+) = 1.56$, $\sigma_I/\sigma_{II} = 0.72$.

In one attempt to measure the complete early yield of oxidizing species, aerated mixtures of HCl and KCl were examined for $G(Cl_2^-)$ at 350 nm with 1 M Cl^-. The results in Table III show that $G(Cl_2^-)$ increased only from 2.80 to 2.98 as $[H^+]$ increased from 10^{-2} to 1 M. In another series of experiments with air-free solutions of KCl and HCl at $[Cl^-] = 1$ M, the OD of Cl_2^- at 350 nm was constant within 1% from 10^{-2} to 1 M H^+. These results, and others, indicate a small effect of oxygen which has not been reported previously.

Table III: The Yield of Cl_2^- from the OD at 350 nm in Aerated Mixtures of HCl and KCl at $[Cl^-] = 1$ M

$[H^+]$, M	OD	$G(Cl_2^-)$
0	0.200	1.16
10^{-3}	0.337	2.06
3.3×10^{-3}	0.398	2.44
6.7×10^{-3}	0.436	2.68
10^{-2}	0.456	(2.80)[a]
5×10^{-2}	0.478	2.92
1	0.482	2.98

[a] All yields of Cl_2^- are relative to this value, which is assumed.

In a related series of observations, $[Cl^-]$ was varied in aerated solutions containing 0.05 M $HClO_4$ and the OD of Cl_2^- was measured at 350 nm. The results appear in Figure 4 which includes the results of Anbar and Thomas[9] for neutral, aerated, chloride ion solutions. In acid solutions, $\Delta G(Cl_2^-) = 0.13[Cl^-] \pm 0.014$, and this weak dependence suggests a direct effect of radiation on Cl^-.

The dependence of $G(Cl_2^-)$ on $[Cl^-]$ in 0.05 M $HClO_4$ can be entirely accounted for, however, in terms

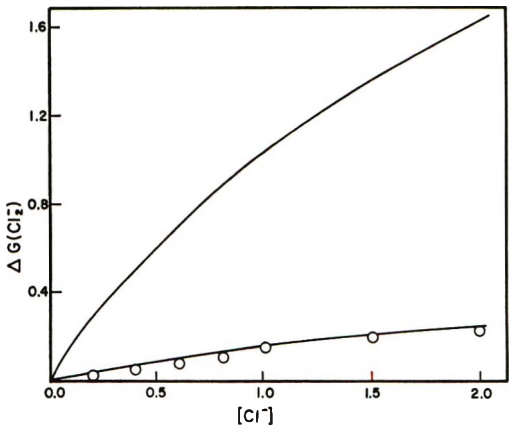

Figure 4. The dependence of $G(Cl_2^-)$ on $[Cl^-]$ in aerated solutions at $[HClO_4] = 0.05$ M (lower curve). The curve is calculated from eq A using $G_2^\circ = 0.6$ and $\sigma_I/\sigma_{II} = 0.38$. The results of Anbar and Thomas (ref 9) in neutral solutions are included for comparison in the upper curve.

of eq A, as shown in Figure 4. The combined primary yield of OH is $G_1^\circ + G_2^\circ \cong 3.8$.[4] Since $\Delta G_{OH} \cong 0.40$ as pH decreases from ~7 to ~1.3,[10] the residual primary yield is $G_2^\circ \cong 3.8 - (2.8 + 0.4) \cong 0.6$. The calculated increments in $\Delta G(Cl_2^-)$ as $[Cl^-]$ increases from 0 to 1 and 2 M are 0.17 and 0.26 for $\sigma_I/\sigma_{II} = 0.38$.[4] The observed values of $\Delta G(Cl_2^-)$ were 0.15 and 0.23. The much stronger increase of $G(Cl_2^-)$ in neutral solution is also described by eq A with $G_1^\circ = 0$, $G_2^\circ = 3.8$, and $\sigma_I/\sigma_{II} = 0.38$.[4] It appears that any direct ionization of Cl^- is fortuitously canceled by a decreased formation of H_2O^+.

The effect of N_2O on $G(Cl_2^-)$ at various concentrations of Cl^- has already been described.[7,11]

Radiolysis of I^- and Br^-. The preceding results bear upon the nature of the spur and even raise questions concerning its existence. To probe this problem further the yields of I_2^- and of I_3^- have been measured at 390 and at 290 nm, respectively, in aerated solutions with corrections for spectral overlap. Yields are based on an assumed value $G(I_2^-) = 2.80$ at 10^{-3} M I^-. The results, which are summarized in Table IV and Figure 5, show a marked decrease in $G(I_2^-)$ at higher concentrations of I^-. Neither $G(I_2^-)$ nor the combined yields obey eq A, while $1/G(I_3^-)$ is linear in $1/[I^-]$ over the entire range with $G(0.5I_2) = 6.0$ and $\sigma_I/\sigma_{II} = 1.15$. Equation A has been rearranged to

$$1/G - 1/G_2^\circ = \sigma_2/G_{II}^\circ\sigma_I[I^-]$$

and the corresponding log–log plot has been used in

(9) M. Anbar and J. K. Thomas, *J. Phys. Chem.*, 68, 3829 (1964).

(10) A. O. Allen, "The Radiation Chemistry of Water and Aqueous Solutions," Van Nostrand, Princeton, N. J., 1961.

(11) At high concentrations of Cl^- the OD of Cl_2^- is high at the end of the pulse and decays slowly, whether in aerated or deaerated solutions. When such solutions are saturated with N_2O, the OD of Cl_2^- is unchanged at the end of the pulse by comparison with N_2-purged neutral solutions, but increases steadily for hundreds of nanoseconds before slowly decaying.

Table IV: Yields of I_2^- and I_3^-, and of Br_2^- and Br_3^-, in Aerated Neutral Solutions of I^- and of Br^-

$[X^-]$	$G(I_3^-)$	$G(I_2^-)$	$\Sigma G(I)$	$G(Br_3^-)$	$G(Br_2^-)$	$\Sigma G(Br)$
0.001	<0.003	(2.80)	(2.80)	<0.003	(2.80)	(2.80)
0.012	0.006	2.98	2.99	<0.003		
0.025	0.054	3.04	3.15	<0.003	2.96	2.96
0.05	0.110	3.19	3.41	0.11	3.04	3.26
0.10	0.284	2.96	3.53		3.22	
0.20	0.580	2.64	3.80	0.41	3.43	4.25
0.40	0.925	2.30	4.15	0.56	3.60	4.72
0.50				0.71		
0.60				0.76		
0.80	1.430	1.93	4.79	0.89	3.95	5.73
1.00	1.75	1.82	5.32	0.93	3.85	5.71
1.50	2.00	1.84	5.84	1.02	3.98	6.02
2.0	2.11					

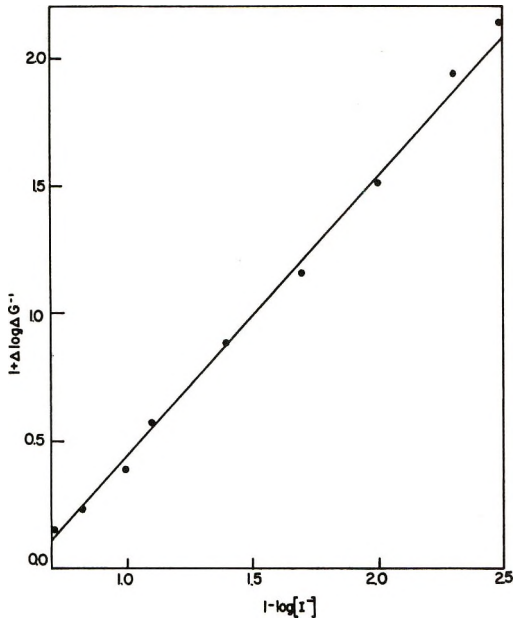

Figure 5. The dependence of $G(I_3^-)$ on $[I^-]$ is expressed in terms of the rearranged form of eq A, $1/G - 1/G_2^\circ = \sigma_{II}/G_2^\circ\sigma_I[I^-]$ in log–log form.

Figure 5 to display the entire range of measurement. It will be observed that $G(I_3^-)$ increased from approximately zero in dilute solution to 2.1 at 2 M I^-. At 1.5 M I^-, $2G(I_3^-) + G(I_2^-) = 5.84$, which is a rather large value. Since $OD(I_3^-)$ was measured immediately following the pulse, and since formation of I_3^- from I_2^- is fairly slow under the experimental conditions, it can be concluded that two or more oxidations of I^- to I occurred geminately. The effect observed is to be expected on the basis of the spur-diffusion model. An alternative mechanism involves (H_2O^+, H_2O^*) as an isolated entity formed by energy transfer from the excited, dry molecular ion, H_2O^{*+}.[12] This entity could generate (H_3O^+, H_2O^*, OH), capable of oxidizing two or three iodide ions.

Comparable results for bromide ion solutions are included in Table IV. Except at low halide ion concentrations, $G(Br_3^-) > G(I_3^-)$ when $[Br^-] = [I^-]$. Also $G(Br_2^-)$ increased with $[Br^-]$.

Radiolysis of Acetate Ion. Evidence has been presented that formation of Cl_2^- at high concentrations of Cl^- and pH ~7 corresponds to a primary yield of $G_2^\circ \cong 3.8$ precursors.[4] It is considered to be unlikely that any appreciable part of this product arises from oxidation of Cl^- by OH in the acid spur and the formation of Cl_2^- has been attributed to electron transfer from Cl^- to H_2O^+ or dry H_3O^+.[12] Nevertheless confirmation is desirable.

One approach toward resolving this problem is to neutralize the acid in the spur. Using aerated solutions of 1 M KCl and measuring $OD(Cl_2^-)$ at 350 nm, the following additives were tested: 1 M $NaC_2H_3O_2$, 0.1 M NH_4OH, 1 M K_2CO_3, 1 M $NaHCO_3$, and saturated $Na_2C_2O_4$. In all of these systems the OD of Cl_2^- approximated zero at the end of 1-μsec pulses. Subsequent tests with 5-nsec pulses for 1 M KCl showed that the OD of Cl_2^- decreased at the end of the pulse by ~20% with addition of 1 N NH_3. For addition of 1 M Na_2HPO_4 the decrease amounted to 13%. There is an uncertainty in the effect of such high solute concentrations on the extinction coefficients, but if OH oxidizes Cl^- in the acid spur of neutral solutions, the effect must be small.

As an alternative approach, G_{OH} was measured as $G(I_2^-)$ with high concentrations of acetate ion. Because $k_A(OH + C_2H_3O_2^-) \cong 5 \times 10^7\ M^{-1}\ sec^{-1}$, and $k_I(OH + I^-) \cong 10^{10}\ M^{-1}\ sec^{-1}$,[13] acetate ion not only may decrease G_{OH} by electron transfer to H_2O^+ prior to the reaction $H_2O^+ + H_2O \rightarrow H_3O^+ + OH$, but it also reacts slowly with homogeneously distributed OH. Consequently, for the homogeneous reaction alone

$$G(I_2^-) = G_{OH}\{k_I[I^-]/(k_I[I^-] + k_A[C_2H_3O_2^-])\} \equiv G_{OH}\kappa \quad (B)$$

(12) W. H. Hamill, *J. Phys. Chem.*, **73**, 1341 (1969).

(13) M. Anbar and P. Neta, *Int. J. Appl. Radiat. Isotopes*, **18**, 493 (1967).

Table V: The Effect of Acetate Ion on $G(OH)$, Measured as $G(I_2^-)$, in Aerated Solutions

Acetate, M	$G(I_2^-)$	0.01 M I^- $G(OH)^a$	$G(I_2^-)$	0.05 M I^- $G(OH)^a$	$G(I_3^-)$	0.10 M I^- $G(OH)^a$
0	3.00	3.00	3.00	3.00	3.00	3.00
0.01	3.00	3.00				
0.10	2.56	2.69				
0.20	2.27	2.50			2.92	2.92
0.30	2.02	2.32				
0.40	1.86	2.23	2.55	2.60	2.80	2.86
0.50	1.67	2.09				
0.60	1.50	1.95			2.74	2.82
0.80	1.23	1.72	2.02	2.10		
1.00	0.98	1.47	1.55	1.70	2.30	2.41
1.20			1.36	1.50		
2.00	0.48	0.96	0.97	1.15	1.50	1.65

[a] Corrected for competition between I^- and acetate ion for OH.

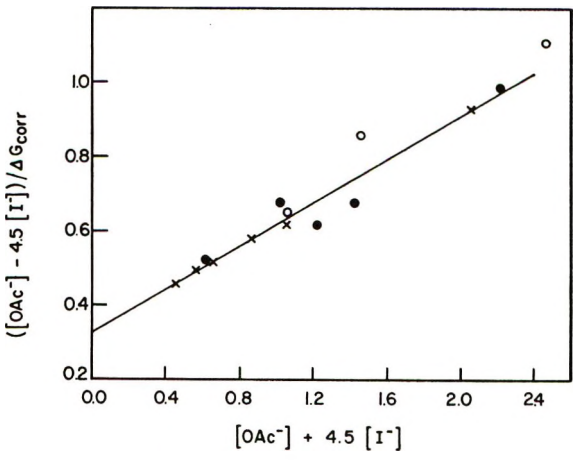

Figure 6. The corrected ΔG_{OH}, allowing for competition by I^- and $C_2H_3O_2^-$ for OH, is expressed as a function of $[OAc^-]$, the acetate ion concentration, according to eq D. Fitted values of ΔG_1 are 3.00 for 10^{-2} M I^- (×), 2.95 for 0.05 M I^- (●), and 3.05 for 0.1 M I^- (○).

For three series of measurements with $[C_2H_3O_2^-]$ varied from 0 to 2 M, $[I^-]$ was held constant at 10^{-2}, 5×10^{-2}, and 10^{-1} M. The results are summarized in Table V. If acetate ion engages in no reaction but the inefficient competition with iodide ion for OH, then G_{OH} must be constant after correcting for this competition. A plot of ΔG_{OH}^{-1} *vs.* $[C_2H_3O_2^-]$, which should describe such simple competition, is strongly nonlinear, however. Moreover, the OD of I_2^- at 390 nm increased from 0.18 for 2 M $C_2H_3O_2^-$ and 5×10^{-2} M I^- to 0.46 following tenfold dilution. For simple competition, there should be no change. If acetate ion can also engage in electron transfer to the positive hole, then both eq A and B are required to describe the combined effects by eq C.

$$\Delta G_{OH,cor} = G_{OH}^\circ - \kappa^{-1}G(I_2^-) = G_2^\circ(\sigma_A[C_2H_3O_2^-] - \sigma_I[I^-])/(\sigma_A[C_2H_3O_2^-] + \sigma_I[I^-] + \sigma_{II}) \quad (C)$$

The k's (in κ) refer to conventional rate constants, the σ's to cross sections for electronic processes, and G_2° to the precursor of OH, *e.g.*, H_2O^+. Representing σ_I/σ_A by n, then

$$\frac{[C_2H_3O_2^-] - n[I^-]}{\Delta G_{OH,cor}} = \frac{\sigma_A([C_2H_3O_2^-] + n[I^-]) + \sigma_{II}}{G_2^\circ \sigma_A} \quad (D)$$

Values of the parameters adopted by trial are $k_I/k_A = 200$, $n = 4.5$, and $G_{OH} \cong 3.0$ for evaluating $G(I_2^-)$. The results for Table V appear in Figure 6, plotted according to eq D, but omitting data for small acetate ion concentrations because of large uncertainties in small values of ΔG. It should be noted that G_2° from Figure 6 is 3.0, approximately the same as $G(I_2^-)$ for the range of iodide ion concentrations used when no competing solute is present. That is, substantially all precursor of uniformly distributed OH is scavengeable by acetate ion. If two or more species are involved, *e.g.*, H_2O^+ and H_2O^*, they must be scavenged with comparable efficiencies. Since acetate ion can only diminish $G(I_2^-)$ in these experiments, G_2° cannot measure the total yield of precursor, but only that component which contributes to measured yields of OH. From the slope and intercept of Figure 6, $\sigma_A/\sigma_{II} = 1.0$, from which it follows that $\sigma_I/\sigma_{II} = 4.5$. This value does not compare with the corresponding result from $G(I_3^-)$, but the very large value of G_2° from the latter data indicates that processes other than hole scavenging are involved.

It is a consequence of the dry electron model that hole scavenging interrupts prompt recombination of dry charge pairs, and annihilation of the local field due to the hole increases $G_{e_{aq}^-}$. In nitrogen purged solutions of 10^{-2} M Cd^{2+}, the OD of Cd^+ at λ 305 nm increased from 0.23 to 0.41 when $[C_2H_3O_2^-]$ increased from 0 to 1 M.

Competition by Cd^{2+}, H^+ for Electrons. The primary yield of electrons in the spur was investigated first in

air-free solutions with 1 M $HClO_4$ in terms of $G(Cd^+)$. The results in Table VI show that if $G(Cd^+) = 2.70$ at 10^{-2} M Cd^{2+}, then $G(Cd^+) = 3.55$ at 1 M Cd^{2+}. In neutral 1 M Cd^{2+}, $G(Cd^+) = 3.76$. It is quite clear that 1 M H^+ does not compete appreciably with 1 M Cd^{2+}. Alternatively, keeping $[Cd^{2+}] = 1$ M and $[ClO_4^-] = 1$ M, $G(Cd^+)$ decreased weakly and linearly as $[H^+]$ increased from 0 to 1 M, as shown in Table VI. The weak change may be a direct effect due to replacing K^+ by H^+.

Table VI: The Dependence of $G(Cd^+)$ on $[HClO_4]$ and on $[CdSO_4]$ in Deaerated Solutions

$[Cd^{2+}]$, M	$G(Cd^+)$[a,b]	$[^+H]$, M	$G(Cd^+)$[a,c]
0.2	1.33	0.0	3.76
0.3	1.56	0.2	3.72
0.4	1.85	0.4	3.70
0.5	2.20	0.6	3.64
0.6	2.59	0.8	3.60
0.8	3.23	1.0	3.55
1.0	3.55		

[a] Yields are relative to an assumed $G(Cd^+) = 2.70$ at $[H^+] = 0$, $[Cd^{2+}] = 10^{-2}$ M. [b] At 1 M $HClO_4$. [c] At 1 M Cd^{2+}, OD measured at 305 nm.

Discussion

The rather small and nearly linear effects of appreciable concentrations of SO_4^{2-} and ClO_4^- on the yields of e_{aq}^-, measured as $G(Cd^+)$, make it possible to measure separately and semiquantitatively the effects of hole traps and electron traps. Moorthy and Weiss[14] have deduced from esr spectra of frozen aqueous solids that high concentrations of $HClO_4$ and H_2SO_4 produce ClO_4 and SO_4^- by hole trapping. In aqueous solutions the results in Table I indicate that the combined effect of hole trapping and change in the extinction coefficient of Cd^+ is small. The small decreases produced by 1 M Na_2SO_4 on $OD(I_2^-)$ and by Na_2HPO_4 on Cl_2^- may also include contributions from hole trapping.

The ability of high concentrations of Cl^- to increase $G_{e_{aq}^-}$, to scavenge all precursor(s) of molecular H_2O_2 in neutral solutions, and to form large yields of Cl_2^- even in strongly basic solutions, can be accounted for by electron transfer to H_2O^+ by mechanism 1a. A small contribution by mechanism 2 cannot be excluded. For solutions of $CdSO_4$, $G_1^\circ(Cd^+) + G_2^\circ(Cd^+)$ is 4.0,[15] in fair agreement with $G^\circ(Cl_2^-)$ for solutions of Cl^-. In this work for dilute Cd^{2+} and concentrated F^- or Cl^-, $G_1^\circ(Cd^+) + G_2^\circ(Cd^+)$ was found to be 4.3.[16] The somewhat smaller value for Cl_2^- may be due to some formation of Cl_2 and Cl_3^-. There do not appear to be large errors from uncertainties in the extinction coefficients, and $G^\circ(H_2O^+, e^-)$ is tentatively ~4.1.

The decrease in $G_{H_2O_2}$ at high concentrations of OH^- observed by Hayon[17] is consistent with the increase in $G(OH)$ shown in Figure 2. Both effects are attributed to electron transfer from OH^- to H_2O^+.

Figure 4 shows that all precursors of homogeneously distributed OH are susceptible to scavenging by acetate ion in competition with iodide ion. According to the dry electron model, this requires scavenging H_2O^+ by electron transfer since appreciable scavenging of OH by acetate ion is not consistent with the results and no other conventional mechanism is evident. Electron transfer is completely consistent with the electrolytic decomposition of acetate ion, but the expected large yields of CH_4 at high concentrations of acetate ion were not found in a recent investigation.[4] These facts can be reconciled if the acetoxy radical is stabilized as $(C_2H_3O_2)_2^-$, by analogy with X_2^-, until radical dimerization or H abstraction confers ultimate stability.[18] The relative scavenging efficiency is $\sigma_I/\sigma_{II} = 1.0$ for acetate ion, quite comparable to values of 0.7–1.6 for halide and hydroxide ions.

The very large primary yield, $2G^\circ(I_3^-) = 6.0$ equiv, is a remarkable result. The combined primary yield for all oxidizing species may be even greater since $G(I_2^-) = 1.84$ in 1.5 M I^- and it is not decreasing rapidly. The primary yield of ionization is $G(H_2O^+) = G(e^-) \cong 4$ on the basis of this and earlier work.[4,15] An indeterminate contribution from direct excitation is involved, but it should be noted that the total yield for oxidation of Br^- exceeds that for I^- over the range of high halide ion concentrations. This indicates a rather small net change from direct effects. Energy transfer from H_2O may also contribute, but this problem has not yet been examined experimentally for Br^- and I^- in a radiolytic system.

No considerable part of so large a yield of I_3^- can be attributed to geminate OH radicals. A possible mechanism involves the reaction

$$H_2O^+ + I_{aq}^- \longrightarrow H + OH + I$$

The combined electron affinity (3.1 eV), hydration energy of I^- (~2.2 eV), and unknown coulombic energy may not suffice to stabilize H_2O following charge neutralization, although a nondissociative process was required to account for results using Cl^-. For I^- the electron affinity is less by 0.55 eV, and the hydration energy is less by ~0.75 eV. The barrier being smaller,

(14) P. N. Moorthy and J. J. Weiss, *Advan. Chem. Ser.*, **No. 50**, 180 (1965).

(15) P. L. T. Bevan and W. H. Hamill, *Trans. Faraday Soc.*, **66**, 2533 (1970).

(16) For concentrated solutions of KF, $G_1^\circ(e_{aq}^-) + G_2^\circ(e_{aq}^-) = 4.1$.

(17) E. Hayon, *Trans. Faraday Soc.*, **61**, 723 (1965).

(18) In 1 M $C_2H_3O_2^-$ and 0.02 M N_2O (to remove electrons) an intense absorption band is present at the end of a 5-nsec pulse, with λ_{max} 330 nm. Its half-life is >1 μsec. The transient may be $(C_2H_3O_2)_2^-$ which can disproportionate to biacetyl peroxide and acetate ion.

field ionization of I_{aq}^- will occur at greater distances with higher coulombic energy than for Cl_{aq}^- so that the recombination energy will again be higher for I_{aq}^- than for Cl_{aq}^-. Qualitatively similar arguments apply to Br^-. Also, for Br^- the second oxidation step (by OH) is appreciably slower than diffusion controlled, and this may account for a larger ratio of $G(X_2^-)/G(X_3^-)$ than was observed for I^-, while the combined yields are comparable.

The preceding mechanism predicts an upper limit for the yield of oxidation at $\sim 2\ G^\circ(H_2O^+)$, or ~ 8, apart from contributions due to direct effects. If $G(I_2^-) = 1.8$ for $[I^-] > 1\ M$ represents a limiting value, as it appears to do, then $G^\circ(\text{oxidation}) \cong (1.8 + 2 \times 3.0)$ or ~ 7.8 equiv. This mechanism does not require spurs. The spur-diffusion model cannot account for an observed $G(\text{oxidation}) = 5.8$, much less the higher extrapolated value. To attribute the entire discrepancy to direct effect creates a severe problem to explain an already weak dependence of $G(Cl_2^-)$ on $[Cl^-]$ at pH 1.3. The large values of $G(I_2^-) + 2G(I_3^-) = \Sigma G(I)$ in Table IV are consistent with earlier measurements by Anbar, *et al.*,[19] for solutions of KI saturated with N_2O. For 1 M I^-, $\Sigma G(I) = 5.32$ from Table IV, and with N_2O the expected yield is

$$\Sigma G(I) = 5.32 + (G_e + \Delta G_e) - G_H - 2G_{H_2O_2}$$

where ΔG_e is the extra yield of electrons from hole trapping. From data for 1 M Cl^- in Table II, $G_e + \Delta G_e = 3.40$. If $G_H = 0.60$ and $G_{H_2O_2} = 0.4$ in 1 M I^-,[19] then $\Sigma G(I) = 5.32 + 3.40 - 0.40 - 0.80 = 7.32$. Anbar, *et al.*,[19] reported $\Sigma G(I)_{cor} = 7.30$.

A final point concerning the spur is the effect of H^+ on $G(Cd^+)$. At the high concentrations of electrolytes employed (*cf.* Table V) the relative rate constants of H^+ and Cd^{2+} with e_{aq}^- are not precisely known, but the ratio may be $k_{H^+}/k_{Cd^{2+}} \sim 0.5$–$2$.[13] Since acid exerted a negligible effect on $G(Cd^+)$, the results are consistent with the assumption that 1 M Cd^{2+} traps most of the electrons prior to hydration, that H^+ does not compete for dry electrons, and that $G(e_{aq}^-)_{spur}$ is very small.

The large values of $G(Cd^+)$ at large concentrations of Cd^{2+} and Cl^- include only a small component from direct electron transfer between these solutes. The increase in $G(Cd^+)$ between 0.05–2.0 M Cd^{2+} considerably exceeds that for $[Cl^-] = 0$, while high concentrations of Na_2SO_4 have only a small effect. Since $CdSO_4$ alone at high concentrations gives $G_2^\circ(Cd^+) = 1.26$, energy absorption by Cd^{2+} is not responsible. Possibly single charge scavenging (*viz.* H_2O^+ or e^-) is effective only for spurs with a single charge pair, including primary regions of multiple ionization which decay rapidly to the single charge pair. If so, diminishing the positive core of the spur from n to $n - 1$ charges by Cl^- would considerably enhance the range of e^-, and so increase $G(Cd^+)$. On the other hand, decreasing the number of e^- by one would not be likely to alter the fate of H_2O^+, which usually degrades to H_3O^+. Consequently $G(Cl_2^-)$ would not be greatly affected by $[Cl^-]$.

Acknowledgment. The authors are indebted to Professor J. K. Thomas for helpful discussions and for practical advice. They are also grateful to Mr. Dale W. Schutt and Mr. Terrence Deal for technical assistance.

(19) M. Anbar, D. Meyerstein, and P. Neta, *J. Phys. Chem.*, **68**, 2967 (1964).

Electron Spin Resonance Studies on Zinc Peroxide and on Zinc Oxide Obtained from a Decomposition of Zinc Peroxide

by R. D. Iyengar*[1] and V. V. Subba Rao

Center for Surface and Coatings Research, Lehigh University, Bethlehem, Pennsylvania 18015 *(Received February 4, 1971)*

Publication costs borne completely by The Journal of Physical Chemistry

Zinc peroxide prepared by the interaction of H_2O_2 on zinc oxide has been found to be esr active. Apparently the activity arises from the H_2O_2 used which can give rise to species such as O_2^- or HO_2. Evidence is presented to indicate a reaction between diamagnetic peroxide ions (O_2^{2-}) and water vapor, leading to the formation of superoxide ions (O_2^-). Zinc oxide formed on decomposition of the peroxide shows greater thermal stability compared to other preparations and does not readily lead to the formation of O_2^- species at the surface.

Zinc peroxide (ZnO_2) is looked upon in many ways as a transition between ionic and covalent peroxides[2] and a consideration of its electronic structure (Figure 1) leads to the belief it is a diamagnetic oxide. However, during the course of an investigation, it was found that ZnO_2 prepared by the interaction of ZnO and concentrated H_2O_2 was paramagnetic and esr active. Experiments were, therefore, carried out on the ZnO_2 to trace the origin of the esr activity and identify the species responsible. Also, properties of ZnO formed from the decomposition of ZnO_2 were investigated. The present notes describes some unexpected but interesting observations made during the course of such a study.

Experimental Section

Materials. Two ZnO_2 samples were used in the investigation. One of them, furnished by the New Jersey Zinc Co., was prepared by the reaction of a $ZnSO_4$ solution with an ammoniacal solution of H_2O_2 followed by drying at 90° and at 140°. The second sample was prepared by the interaction of ZnO (in the form of a paste) with 30% H_2O_2 over a period of 2 weeks. The material obtained was filtered and dried at 140° for 2 hr. While a majority of experiments were done with the second sample, both samples showed very similar, if not identical, behavior.

Apparatus. The vacuum outgassing of samples was carried out in a conventional vacuum system provided with a mercury diffusion pump and a liquid nitrogen trap. Esr studies were made with a Varian spectrometer (V-4500) with TE-104 mode dual cavity operating at about 9.5 kMHz. The exact frequency could be measured using a Hewlett-Packard wavemeter. 1,1-Diphenylpicrylhydrazyl (dpph) was used as a standard for g measurements. Except where mentioned, all spectra were recorded at liquid nitrogen temperature.

Results

The esr spectrum of an "as is" sample of zinc peroxide is shown in Figure 2a. For comparison the spectrum O_2^- species, obtained by adding oxygen at 10^{-3} Torr at 25° to a sample of pure ZnO (SP-500; N. J. Zinc Co.) vacuum outgassed for 2 hr at 500°, is shown in Figure 2b. On outgassing ZnO_2 for 2 hr at 150°, the intensity of the spectrum increased (Figure 3a). However, additional increase in the outgassing temperature (Figures 3b and c) lowered the intensity of the spectrum. Vacuum treatment at 200° for 2 hr eliminated the signal altogether.

Since zinc peroxide decomposes completely around 200°, its behavior, following outgassing at temperatures above 300°, should be similar to that of ZnO. Contrary to expectations, ZnO_2 vacuum treated at 400° (Figure 3d) indicated the total absence of any esr signal around $g = 1.96$ (characteristic of Zn and/or oxygen vacancies). At still higher temperatures for the vacuum treatment (500°, 2 hr), the esr spectrum revealed the formation of a new, intense, symmetric signal (ΔH(peak to peak) = 2.5 G) at $g = 2.002$ (*cf.* g_e(free electron) = 2.0023) besides a much smaller signal at $g = 1.96$ (Figure 3e). Exposure at room temperature of this sample to oxygen (5 to 100 Torr) produced approximately a 10% decrease in the intensity of the $g = 2.002$ signal and no changes in the $g = 1.96$ signal. Further increase in oxygen pressure produced no further changes. Outgassing at 25° of the sample exposed to oxygen produced no new signals.

On heating the peroxide sample at 500° for 3 hr in a flowing stream of oxygen, the esr spectrum showed only

(1) To whom correspondence should be addressed at Sherwin-Williams Chemicals, Research Center, 10909 Cottage Grove Avenue, Chicago, Ill. 60628.

(2) N. G. Vannerberg in "Progress in Inorganic Chemistry," Vol. 4, F. A. Cotton, Ed., Interscience, New York, N. Y., p 125.

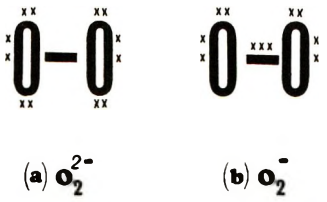

Figure 1. Electronic structure of (a) peroxide ion and (b) superoxide ion.

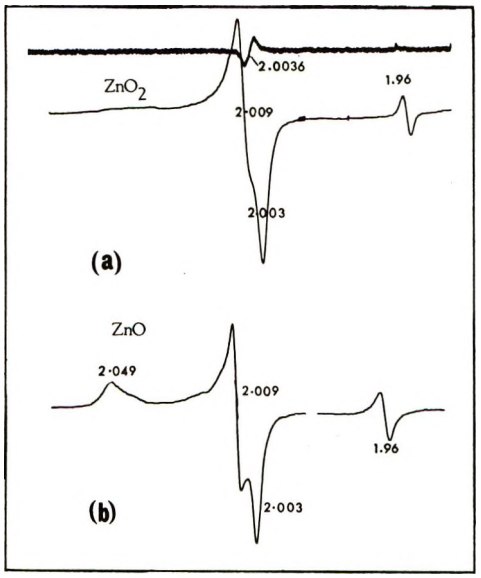

Figure 2. Esr (x-band) spectra of (a) zinc peroxide "as is" (not outgassed), and (b) O_2 on zinc oxide obtained following exposure of vacuum-treated ZnO (prepared by vapor phase oxidation of Zn) to oxygen at 10^{-3} Torr. Both spectra at $-196°$; signal level 25; 70 mW.

a minor signal at $g \cong 1.96$ (Figure 4a). Removal of excess oxygen (by outgassing for 5 min at 25°) increased slightly the intensity of this signal. Additional vacuum outgassing at 500° for 2 hr enhanced the intensity of the ($g \cong 1.96$) signal by more than 100% (Figure 4b). However, addition of oxygen (10^{-3} Torr) to this sample left the spectrum essentially unchanged (Figure 4c) and did not lead to the formation of the triplet characteristic of O_2^- on ZnO (*cf.* Figure 2b).

On exposing ZnO_2, outgassed under vacuum for 2 hr at 150°, to water vapor (5 Torr), the esr spectrum showed an increase in the intensity of the triplet by about 50% (Figure 5b). No new signals were observed. Room temperature outgassing to remove the water vapor restored more or less the original intensity (Figure 5c). Addition of a second dose of water vapor again produced an increase in intensity but only by about 25%. Soaking an "as is" sample of ZnO_2 in water for over 12 hr followed by drying at 100° for 48 hr also showed an increase in the intensity but not to the extent earlier observed (Figure 5d). However, exposure of a sample of ZnO_2, previously vacuum heated at 200° for more than 2 hr, to water vapor at 25°, did not produce the triplet.

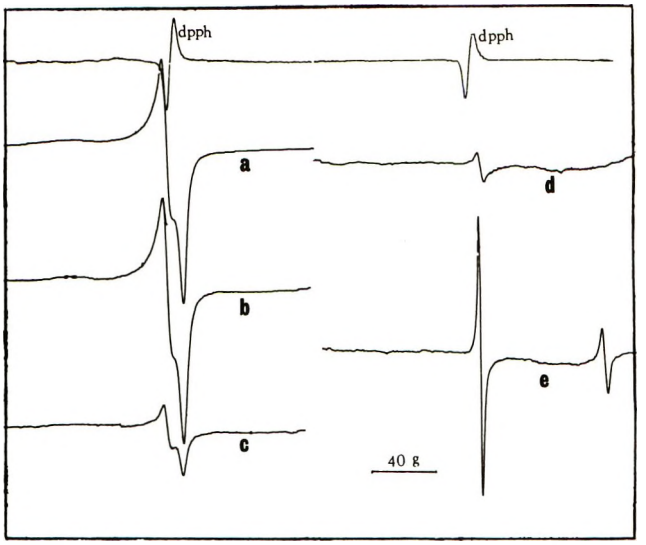

Figure 3. Esr (x-band) spectra of zinc peroxide following vacuum treatment: (a) at 150° for 2 hr, signal level 10, 70 mW; (b) at 200° for 5 min, signal level 50, 70 mW; (c) at 200° for 30 min, signal level 50, 70 mW; (d) at 400° for 2 hr, signal level 100, 70 mW; and (e) at 500° for 2 hr, signal level 100, 70 mW. All spectra recorded at $-196°$.

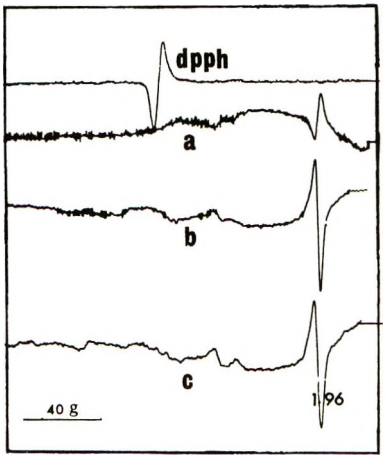

Figure 4. Esr (x-band) spectra of zinc peroxide. (a) heated in a stream of oxygen at 500° (3 hr), cooled in oxygen to 25°, sample sealed with oxygen in tube, signal level 200, 70 mW; (b) sample from (a) vacuum treated at 500° for 2 hr, signal level 200, 70 mW; (c) oxygen added (10^{-3} Torr) and re-outgassed at 25° for 5 min, signal level 200, 70 mW. All spectra recorded at $-196°$.

Discussion

If the superoxide ions (O_2^-), formed during the preparation, occupy regular lattice positions in the pyrite type of lattice reported for ZnO_2,[2,3] the esr spectra obtained should be similar to those published for alkali metal superoxides[4,5] where O_2^- ions occupy regular

(3) R. D. Iyengar, V. V. Subba Rao, and A. C. Zettlemoyer, *Surface Sci.*, 13, 251 (1969).

(4) J. E. Bennett, D. J. E. Ingram, and D. Schonland, *Proc. Phys. Soc. London, Ser. A*, 69, 556 (1956).

(5) J. E. Bennett, B. Mile, and A. Thomas, *Trans. Faraday Soc.*, 64, 3200 (1968).

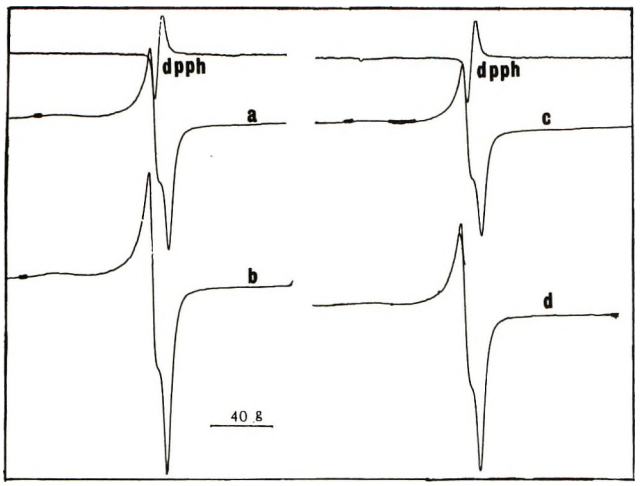

Figure 5. Esr (x-band) spectra of zinc peroxide: (a) vacuum treated at 150° (2 hr); (b) sample from (a) following addition of water vapor (5 Torr); (c) sample b outgassed at 25° for 30 min; (d) soaked in water for 12 hr and dried at 100° for 48 hr. All spectra recorded at −196° at the same signal level and microwave power.

lattice positions[6-9] and are located in an environment of axial symmetry. Thus, for NaO_2 the reported[4] g values are $g_x = g_y = (g_\perp) = 2.002$ and $g_z(= g_{||}) = 2.175$. A comparison of these values with the g values obtained from spectra in the present study shows no similarities whatever, indicating no regular arrangement for O_2^- ions. On the other hand, the triplet observed with ZnO_2 is quite similar to that observed for O_2^- on ZnO except for the fact that the g component on the low-field side (g_1) is broader than observed for the latter. This broadening, associated with the absorption on the low-field side, is probably caused by the existence of an array of sites where the crystal field environments for the paramagnetic species are different and can cause a spread of g values and consequently broaden the peak. The effect of such broadening should be greatest for the peak observed at the lowest magnetic field where the deviation from the free spin value ($g_e = 2.0023$) is the largest. This is also in accordance with our observations.

It seems that the observed triplet in the esr spectrum of ZnO_2 could very well arise from an excess of hydrogen peroxide used in the preparation which can yield species such as O_2^- or HO_2. The adsorption of such species on small particles of ZnO_2 resulting during the preparation is quite possible; however, the observation that oxygen added to the sample (maintained at liquid nitrogen or room temperature) causes no broadening or a reduction in the intensity of the esr signals argues in favor of the paramagnetic species (arising from H_2O_2) being trapped within the bulk or present in the form of an addition compound. Such addition compounds have been known to exist.[10,11]

The increase in intensity observed on soaking in water or exposure to water vapor is suggestive of a reaction, between the peroxide ions, present close to the surface, and water, such as

$$3O_2^{2-} + 2H_2O \rightleftharpoons 2O_2^- + 4OH^- \quad (1)$$

wherein superoxide ions are formed. Removal of water from the hydroxyl ions by vacuum treatment at 150° can lead to reformation of O_2^{2-} and can account for the observed decrease in intensity. Heating the sample of ZnO_2 under vacuum at 200° or above can be expected to bring about the decomposition of not only the H_2O_2 associated with the sample but of the ZnO_2 as well. The triplet in the esr spectrum is thus eliminated. Exposure of the sample following the heat treatment at or above 200° to water vapor does not lead to the formation of the triplet since there is no ZnO_2 and as such O_2^- formation cannot occur as suggested in eq 1.

Previous studies[3,12-15] have shown that ZnO, following vacuum treatment at temperatures above 350°, yields an intense and broad signal ($g \cong 1.96$) which has been variously attributed in the past to conduction electrons,[12] Zn^+ ions in shallow donor bands,[16] and oxygen ion vacancies with trapped electrons.[17] Iyengar and coworkers[15] observed that the broad signal at $g = 1.96$ was resolved into two components under certain conditions such as in the presence of an adsorbed layer of *tert*-butyl hydroperoxide. The two components with g values of 1.961 and 1.965 were attributed by these authors to the formation of interstitial Zn^+ ions and oxygen vacancies with trapped electrons, respectively. These observations have been generally confirmed by the recent work of Setaka, *et al.*[18] However, according to Sancier,[19] both the components of the $g = 1.96$ signal in the esr spectrum of ZnO probably arise from conduction electrons, and the two slightly different g values are indicative of the presence in ZnO of two different environments for these electrons. Admittedly, while there are differences in the expressed views pertaining to the identity of the species responsible for the two components, it is clear that the initial formation of

(6) V. Kassatochkin and V. Kotov, *J. Chem. Phys.*, **4**, 458 (1936).
(7) V. Kassatochkin and V. Kotov, *Zh. Tekn. Fiz.*, **7**, 1468 (1937).
(8) V. Kassatochkin, *Dokl. Akad. Nauk SSSR*, **47**, 199 (1945).
(9) I. A. Kazaranovskii, *Zh. Fiz. Khim.*, **14**, 320 (1940).
(10) S. Z. Makarov and L. V. Ladeinova, *Zh. Neorg. Khim.*, **1**, 2708 (1956).
(11) S. Z. Makarov and L. V. Ladeinova, *Izv. Akad. Nauk SSSR Otd. Khim. Nauk*, 139 (1957).
(12) R. J. Kokes, *J. Phys. Chem.*, **66**, 99 (1962).
(13) J. Schneider and R. Rauber, *Z. Naturforsch. A*, **16**, 712 (1961).
(14) K. M. Sancier, *J. Catal.*, **5**, 314 (1966).
(15) M. Codell, J. Weisberg, H. Gisser, and R. D. Iyengar, *J. Phys. Chem.*, **72**, 2460 (1968).
(16) K. A. Muller and J. Schneider, *Phys. Lett.*, **4**, 2288 (1965).
(17) P. H. Kasai, *Phys. Rev.*, **130**, 989 (1963).
(18) M. Setaka, S. Fujieda, and T. Kwar, *Bull. Chem. Soc. Jap.* **43**, 2377 (1970).
(19) K. M. Sancier, *Surface Sci.*, **21**, 1 (1970).

the $g \cong 1.96$ signal of the two components therein begins with the loss of oxygen from the sample either by a thermal or photochemical means. Since ZnO_2 decomposes to ZnO completely around 200°, its behavior following outgassing at temperatures above 200° should be similar to that of ZnO. However, the total absence of formation of the $g \cong 1.96$ signal in samples outgassed under vacuum at 400°, and the difficulty in inducing such a signal even after vacuum treatment at higher temperatures, suggests that the oxygen loss from the sample does not readily occur. It is possible that incorporation of certain cationic impurities into the lattice structure of ZnO can bring about a change in its surface properties and render the removal of oxygen from it more difficult. However, the method of preparation of ZnO_2 revealed no specific impurity likely to be incorporated into the lattice. The reasons, if any, for the need for more drastic outgassing conditions to regenerate the donor defects (possibly) oxidized and destroyed by the H_2O_2 used in the preparation, are therefore not clear.

The symmetric signal formed at $g = 2.002$ when ZnO_2 is vacuum treated at 500° for 2 hr is irreversibly reduced in intensity (10%) by the added oxygen. The signal is not observed in ZnO_2 samples subjected to oxygen treatment at 500° for 3 hr. In the past, such signals on ZnO in the vicinity of $g = 2.002$ have been attributed to (a) O^- ions,[20] (b) bulk defects,[3] (c) an electron trapped is an ensemble of oxygen atoms,[21] (d) a species such as $(ZnO_2)^{-\nu-1}$ where ν is an integer,[22] and (e) electrons in mechanically induced shallow traps.[19] A positive identification of this signal from observations made in the present study has not been possible.

Acknowledgment. This research was supported by the Advanced Research Projects Agency, Department of Defense, monitored by the Naval Research Laboratory under Contract No. NONR 610(09).

(20) M. Sedaka and T. Kwan, *Bull. Chem. Soc. Jap.*, **38**, 1414 (1965).

(21) Y. Fujita and J. Turkevich, *Discuss. Faraday Soc.*, **4**, 407 (1966).

(22) H. Ueda, *Can. J. Chem.*, **46**, 891 (1968).

Metal–Ethylenediamine Solutions. Extinction Coefficients and Equilibria[1]

by Marc G. DeBacker and James L. Dye*

Department of Chemistry, Michigan State University, East Lansing, Michigan 48823 *(Received March 15, 1971)*

Publication costs assisted by the U. S. Atomic Energy Commission

The V band, characteristic of the optical absorbance of solutions of sodium metal in ethylenediamine, was produced by the reaction of cesium metal solutions with solutions of sodium salts. By keeping the cesium concentration in excess and using flow techniques, problems caused by decomposition were minimized. The absorbance of the V band was a linear function of the initial concentration of the sodium salt and yielded an oscillator strength of 1.9 ± 0.2 and an extinction coefficient of $8.2 \pm 0.3 \times 10^4\ M^{-1}\ cm^{-1}$ based upon the stoichiometry Na^-. Combination of these results with pulse-radiolysis studies yielded an oscillator strength of 0.88 ± 0.12 and an extinction coefficient of $2.0 \pm 0.3 \times 10^4\ M^{-1}\ cm^{-1}$ for the solvated electron in ethylenediamine. Other equilibria involving M^+ and e^- were examined.

Introduction

The spectra of metal solutions in amines and ethers have been studied extensively[2-11] but these studies have failed to provide quantitative values of the molar extinction coefficients. The major obstacle has been the instability of solutions, especially in spectral cells of large surface-to-volume ratio. Catalysis of the decomposition by the container walls seems to be a major limiting factor.[10] Another source of difficulty has been the confusion over band assignments which was ultimately traced to the ease of contamination by sodium from the Pyrex container.[6]

There has been general agreement that the broad absorption band in the infrared is characteristic of the

(1) This work was supported by the U. S. Atomic Energy Commission.

(2) R. R. Dewald and J. L. Dye, *J. Phys. Chem.*, **68**, 121 (1964). (See this paper for earlier references.)

(3) M. Ottolenghi, K. Bar-Eli, H. Linschitz, and T. R. Tuttle, Jr., *J. Chem. Phys.*, **40**, 3729 (1964).

(4) M. Ottolenghi, K. Bar-Eli, and H. Linschitz, *ibid.*, **43**, 206 (1965).

(5) L. R. Dalton, J. D. Rynbrandt, E. M. Hansen, and J. L. Dye, *ibid.*, **44**, 3969 (1966).

(6) I. Hurley, T. R. Tuttle, Jr., and S. Golden, *ibid.*, **48**, 2918 (1968).

solvated electron, either alone or in ion pairs or higher aggregates.[12] Recent pulse-radiolysis studies have confirmed the similarity in band shape between the infrared band of metals in ethylenediamine and that of the solvated electron at high dilution in the same solvent.[13] After the realization that the V band at 650–700 nm requires that sodium be present[6] it became apparent that this band is the sodium analog of the R bands at about 850, 900, and 1020 nm for K, Rb, and Cs respectively.[2] Matalon, Golden, and Ottolenghi,[7] by analogy with the spectrum of iodide ion in amine solvents, assigned the metal-dependent band to a charge-to-transfer-solvent (ctts) transition of the alkali anion, M^-. This assignment was also used in several photochemical studies[14,15] of the bleaching and reformation of the sodium V band.

With the observation that sodium ions react rapidly and quantitatively with the solvated electron in ethylenediamine,[16] we decided to take advantage of this property to measure the extinction coefficient of the sodium V band at 650 nm. Several other properties of these solutions were measured as well.

Experimental Section

Ethylenediamine was first dried *in vacuo* over calcium hydride or barium oxide. It was then subjected to a freeze-purification procedure[17] involving at least five cycles. Solvent prepared in this way could be distilled onto a potassium film to form stable blue solutions. However, it could not be mixed with a very dilute metal solution without causing decomposition. Therefore, the freeze purification was followed by a degassing and distillation procedure. The ethylenediamine was distilled from a blue solution of potassium and/or sodium immediately prior to use. The salts used were AR grade. They were dried under vacuum and washed with anhydrous ammonia prior to use. The metals (Na and K; J. T. Baker Co., 99.99%; Cs; a gift from the Dow Chemical Co.) were distilled under high vacuum through several constrictions. Solutions of cesium in ethylenediamine of *ca.* 2×10^{-4} *M* concentration, when prepared in this way and stored in 1-l. vessels, usually had half-lives of 12 hr or more at room temperature. Sodium solutions were much more stable.

Analyses for sodium and potassium were made by both emission and absorption flame photometry by using a Beckman DB flame photometer and/or a Jarrel-Ash atomic absorption flame photometer. These metals were introduced into dilute aqueous HCl and analyzed by comparison with standard solutions.

Optical spectra were measured in a flow system (path length 1.0 mm) which has been described elsewhere.[18] This utilizes a Perkin-Elmer Model 108 rapid-scan monochromator. The signal and a reference signal were detected by two RCA 7102 multiplier phototubes, (which limited the spectral range covered to 600–1000 nm) converted to absorbance by a logarithmic operational amplifier, and recorded on an Ampex SP-300 FM tape recorder. Absorbance calibrations were made by using neutral density filters (Oriel Optical Corp.) which were checked with a Cary Model 14 spectrophotometer. Wavelength calibration was done by using neodymium glass filters. The data were transferred to punched cards *via* a Varian C-1024 computer of average transients and a C-1001 CAT-to-Card coupler. All corrections were made and all spectra were fitted to equations by using a CDC-6500 digital computer and the appropriate least-squares programs.[19]

Results

Contamination by Sodium from Pyrex. We verified the observations of Hurley, Tuttle, and Golden[6] which indicated that Pyrex can easily be a source of sodium contamination. Distillation of potassium through Pyrex with an oxy–gas flame always resulted in sodium contamination of the distillate. However, distillation with a "cool flame" did not give detectable contamination. Potassium solutions, when prepared in Pyrex vessels, always showed a V band. Analysis showed that these solutions contained enough sodium to have been responsible for the absorption. Solutions prepared in a quartz apparatus did not show a V band and contained no detectable sodium contamination. However, contact of such solutions with Pyrex for as little as 10 sec resulted in the formation of a V band, and sodium could be detected by analysis. These observations are in complete agreement with the earlier work.[6] It should be noted, however, that fresh solutions of rubidium and cesium in ethylenediamine do not show a V band, even in a Pyrex cell.

Extinction Coefficients. In order to minimize the effects of decomposition, the V band (maximum absorbance at 650 nm) was produced by the reaction of dilute cesium solutions with sodium bromide or sodium

(7) S. Matalon, S. Golden, and M. Ottolenghi, *J. Phys. Chem.*, **73**, 3098 (1969).

(8) J. L. Dye, M. G. DeBacker, and V. A. Nicely, *J. Amer. Chem. Soc.*, **92**, 5226 (1970).

(9) I. Hurley, T. R. Tuttle, Jr., and S. Golden, *Pure Appl. Chem.*, 449 (1970).

(10) G. Gabor and K. Bar-Eli, *J. Phys. Chem.*, **75**, 286 (1971).

(11) V. A. Nicely and J. L. Dye, *J. Chem. Phys.*, **53**, 119 (1970).

(12) J. L. Dye and R. R. Dewald, *J. Phys. Chem.*, **68**, 135 (1964).

(13) J. L. Dye, M. G. DeBacker, and L. M. Dorfman, *J. Chem. Phys.*, **52**, 6251 (1970).

(14) D. Huppert and K. Bar-Eli, *J. Phys. Chem.*, **74**, 3285 (1970).

(15) S. H. Glarum and J. H. Marshall, *J. Chem. Phys.*, **52**, 5555 (1970).

(16) J. L. Dye, ref 9, p 483.

(17) L. H. Feldman, R. R. Dewald, and J. L. Dye, *Advan. Chem. Ser.*, **No. 50**, 163 (1964).

(18) J. L. Dye and L. H. Feldman, *Rev. Sci. Instrum.*, **37**, 154 (1966).

(19) V. A. Nicely and J. L. Dye, *J. Chem. Educ.*, **48**, 443 (1971).

iodide in the stopped-flow system. The cesium solutions showed only the ir band (maximum absorbance at 1280 nm) of the solvated electron.[2,13] Growth of the V band was complete within the mixing time (*ca.* 1 msec) and the spectra did not change with time after mixing over a period of at least several minutes. When the sodium ion concentration was even in slight excess, no infrared absorbance (detection limit 1050 nm) was detected, in agreement with the results for pure sodium solutions.[2] When the ratio [Cs]/[Na^+] was high enough to give a residual infrared absorption, the absorbance of the V band was a linear function of the concentration of Na^+ as shown in Figure 1. Either NaBr or NaI could be used with identical results. In order to subtract the contribution of the infrared band to the total absorbance, the spectrum was fitted by least-squares to a linear combination of the spectra of pure cesium solutions and of pure sodium solutions in ethylenediamine.[2] A typical fit is shown in Figure 2. The results and a statistical estimate of the standard deviation for each fit are given in Table I. The variation of absorbance of the V band with concentration shown in Figure 1 yields a least-squares value of the molar extinction coefficient of $8.2 \pm 0.3 \times 10^4\ M^{-1}\ cm^{-1}$ based upon 1 mol of sodium ions per mole of absorbing species. (All of the uncertainties given in this paper represent statistical estimates of the standard deviation). If two sodium ions were required, the molar extinction coefficient would be $1.64 \pm 0.06 \times 10^5\ M^{-1}\ cm^{-1}$.

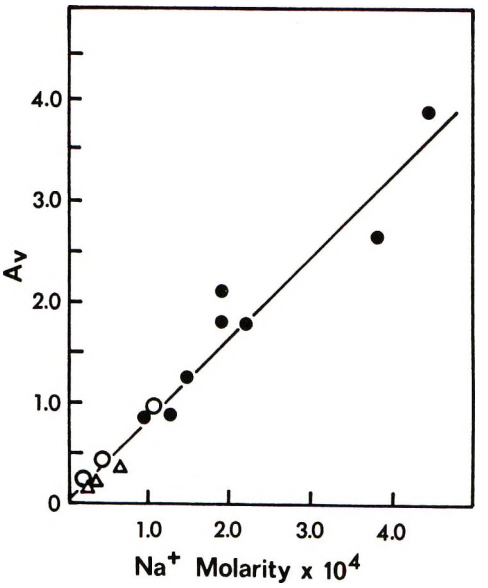

Figure 1. Contribution of the V band to the absorbance of solutions formed by mixing a solution of cesium in ethylenediamine with a solution of either sodium bromide or sodium iodide in ethylenediamine. The different symbols refer to different runs.

Table I: Absorbance of the V Band at 15,200 cm^{-1} Produced by the Addition of Sodium Ions to a Cesium Solution (Path Length: 1.0 mm. Individual Entries Represent the Average of Three to Five Replications)

$[Na^+]$, $M \times 10^6$	A	Standard deviation
2.15	0.23	0.02
2.50	0.195	0.02
3.15	0.22	0.02
4.30	0.41	0.04
6.30	0.356	0.07
9.45	0.85	0.07
10.75	0.94	0.07
12.60	0.89	0.03
14.60	1.25	0.08
18.90	1.82	0.10
18.90	2.11	0.05
22.00	1.79	0.12
37.85	2.65	0.15
44.00	3.86	0.40

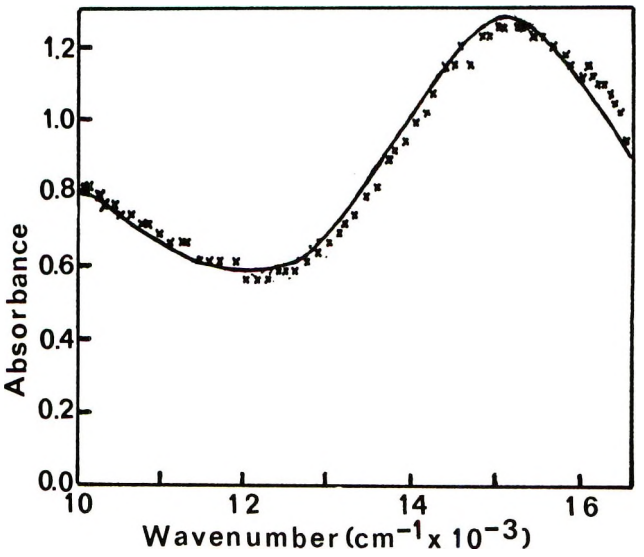

Figure 2. A typical spectrum of a solution formed by mixing a solution of cesium metal in ethylenediamine with a $1.26 \times 10^{-4}\ M$ solution of sodium iodide in ethylenediamine. The solid line was obtained by the least-squares fit of a linear combination of the spectra of pure Cs (ir band) and pure Na(V band).

Pulse-radiolysis studies of the reaction between Na^+ and e_{solv}^- in ethylenediamine[16,20] show that the growth of the V band and the decay of the ir band occur simultaneously and are both second order in [e^-]. Either NaBr or NaI could be used with identical results. The spectrum at "infinite time" is that of the V band only and shows little or no ir band. By comparing the absorbance of the V band at the end of the reaction with the absorbance of the solvated electron at the beginning of the reaction, the ratio of extinction coefficients of the two species per mole of electrons could

(20) J. L. Dye, M. G. DeBacker, J. Eyre, and L. M. Dorfman, unpublished work.

be obtained. This ratio was independent of the concentration of sodium bromide (or sodium iodide) over the range of concentration $10^{-2}\ M < [Na^+] < 0.5\ M$. These experiments yield $A_V^{\infty}/A_{ir}^{0} = 2.1 \pm 0.3$. The ratio given refers to absorbances at the wavelengths of maximum absorbance of the V band and the ir band respectively. Other details of these pulse radiolysis studies will be reported elsewhere.[20]

Equilibrium Studies. The addition of potassium salts ($C = 4 \times 10^{-4}$ to $6 \times 10^{-3}\ M$) to a solution of cesium in ethylenediamine resulted in the appearance of the potassium R band at 850 nm. Since even pure potassium solutions contain both the R band and the ir band,[2] complete conversion of the ir band to the R band was not expected, nor was it found. The contribution of each band was determined by using the spectra of the separate bands[2] and a least-squares fit of the absorbance over the entire wavelength region studied (600–1050 nm). The results are displayed in Figure 3. The absorbances of the two bands are the computed values at the respective maxima.

Solutions containing KI at relatively high concentrations were mixed with solutions of sodium in ethylenediamine in the expectation that the V band of sodium might be converted into the R band of potassium. Surprisingly, the change in absorption corresponded to a contribution from the ir band rather than the R band. To verify the presence of a common-ion effect, solutions which contained both KI and NaI were mixed with sodium solutions. No change in the spectrum occurred in these cases. The results of these experiments are given in Table II and the spectra are shown in Figure 4. Once again, Table II gives the computed absorbances at the respective maxima of the ir, R, and V bands which would be required to fit the observed spectra. The values given for A_R should be considered as upper limits only.

Table II: Equilibrium Studies: K^+ + V Band (Contributions to the Total Absorbance by Three Species.[a] Path Length: 1.0 mm)

Run number	$[K^+]$, M	A_{ir}	A_R	A_V
3.3	0.125	0.108	0.036	0.253
3.4		0.143	0.030	0.379
3.5		0.129	0.031	0.292
3.6		0.136	0.030	0.373
3.7		0.146	0.019	0.348
5.2	0.125	0.0	0.020	0.297
5.3	$[Na^+]$ added	0.0	0.013	0.334
5.4		0.012	0.010	0.324
6.3	0.1875	0.044	0.00	0.610
6.4		0.042		0.641
6.5		0.042		0.646
7.3	0.375	0.139	0.00	0.431
7.4		0.165	0.00	0.554
7.5		0.149	0.01	0.374
8.7	0.375 $[Na^+]$ added	0.026	0.00	0.481

[a] See text for a description of the method of data treatment and the meaning of the A values.

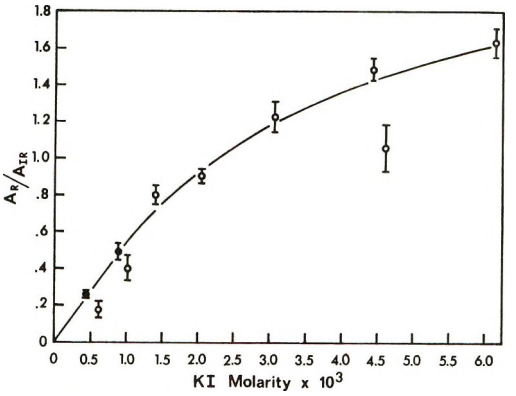

Figure 3. The ratio of the absorbance contribution of the R band of K to the ir band of Cs in solutions formed by mixing a solution of cesium metal in ethylenediamine with a solution of potassium iodide in ethylenediamine. The uncertainties represent statistical estimates of the standard deviation for repeated determinations (normally three replications). The estimated initial absorbance of Cs is 4.0 for points represented by open circles and 0.6 for points represented by solid circles.

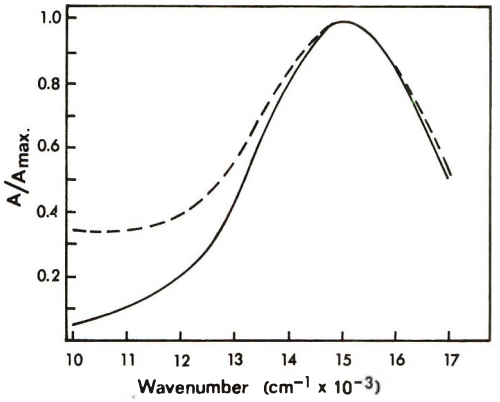

Figure 4. Comparison of the spectra of a solution of sodium in ethylenediamine in the presence (dashed line) and absence (solid line) of added potassium iodide.

Discussion

In order to determine the stoichiometry of the species responsible for the V band, oscillator strengths were calculated from the data on the basis of one and two sodium nuclei per units. Because of the characteristic asymmetry of the absorption bands it seems inappropriate to attempt to fit the bands with symmetrical functions or to calculate the oscillator strengths from half-widths. As shown by Dye, DeBacker, and Dorf-

man,[13] the absorption band shapes of solvated electrons in water–ammonia and water–ethylenediamine mixtures are conveniently and accurately described by a combination of gaussian and lorentzian functions. Such a procedure fits the entire band, including the high-energy "tail." When the oscillator strengths are computed from these functions, the values are appreciably higher for the solvated electron in water and in ammonia than had been previously assumed. Instead of the value of 0.71 for the hydrated electron[21] we obtain an oscillator strength of 0.81 while the value of 0.64 for the ammoniated electron[22] becomes 0.92 ± 0.10.

When the spectra obtained by the addition of Na^+ to cesium solutions are treated in this way, an oscillator strength of 1.9 ± 0.2 is obtained for the V band, based upon one sodium nucleus per absorbing unit. This would become 3.8 ± 0.4 if two sodium nuclei were required. According to the f sum rule[23,24] we would expect that an oscillator strength of about 2 would require at least two equivalent electrons involved in the transition. The species Na^- fulfills this requirement. As an added comparison, it should be noted that the oscillator strength for the $3^1P \leftarrow 3^1S$ transition of the gaseous magnesium atom is 1.745.[25] This gives strong evidence that the species responsible for the V band contains two electrons per sodium nucleus. It should be noted that because of the requirements of charge balance, studies on pure sodium solutions would be expected to yield an extinction coefficient and oscillator strength per sodium nucleus which is only $^1/_2$ that found in these studies.

A further verification of the stoichiometry is obtained from the pulse-radiolysis studies.[20] The assumed stoichiometry

$$2e^- + Na^+ \longrightarrow Na^-$$

and the ratio $A_V^\infty/A_{ir}^0 = 2.1 \pm 0.3$ yield an extinction coefficient for the solvated electron in ethylenediamine of $2.0 \pm 0.3 \times 10^4$ and an oscillator strength of 0.88 ± 0.12. The agreement of this value with those for the hydrated and ammoniated electron adds further strength to the assigned stoichiometry.

Similarity of the V and R bands strongly suggests that the latter also result from absorption by M^-. Since the peak positions are strongly dependent upon the metal used, it seems likely that the alkali metal interaction with the pair of electrons is not the result of weak interactions such as would be expected for the ion pair $M^+e_2^{2-}$. Indeed, the simultaneous existence in solution of bands attributable to Na^- and K^- and the complete absence of peaks at intermediate wavelengths[26] suggests that the species might well be the spherically symmetrical alkali anion with both electrons in s orbitals. The existence of such a species in metal–ammonia solutions has been suggested.[27] However, in this case, no metal-dependent absorption bands have been observed.

The results obtained by mixing KI with cesium solutions indicate the presence of the equilibrium

$$K^+ + 2e^- \rightleftharpoons K^-$$

At the salt concentrations used, we would expect most of the ions to be paired so that the equilibrium might better be written as

$$K^+\cdot I^- + 2M^+\cdot e^- \rightleftharpoons M^+\cdot K^- + M^+\cdot I^-$$

in which M^+ represents either Cs^+ or K^+. This would be further complicated by the tendency for solvated electrons to form spin-paired species.[28] Therefore, correct analysis of the equilibrium data is virtually impossible. We can note from Figure 3, however, that the intensity of the R band relative to the ir band increases with increasing concentration of KI.

We expected that the addition of KI to a sodium solution would yield the R band of K^- according to

$$Na^- + K^+\cdot I^- \rightleftharpoons K^- + Na^+\cdot I$$

However, this was not the case. Instead, the addition of KI caused the growth of an infrared absorption, presumably caused by the solvated electron. This effect has also recently been observed in pulse-radiolysis studies.[20] It seems that the presence of KI shifts the equilibrium

$$2e^- + Na^+ \rightleftharpoons Na^-$$

to the left. We have no explanation for this phenomenon.

Acknowledgments. We wish to acknowledge support of this research by the U. S. Atomic Energy Commission under Contract AT-11-1-853. We thank Drs. V. A. Nicely and E. R. Minnich, who provided valuable assistance with the experiments and with the data analysis and also Mssrs. M. T. Lok and F. J. Tehan, who checked some of the results. We are also grateful to Professor Leon Dorfman of the Ohio State University for many helpful discussions and for the opportunity to use the OSU LINAC.

(21) E. J. Hart and M. Anbar, in "The Hydrated Electron," Wiley-Interscience, New York, N. Y., 1970, p 40.

(22) R. K. Quinn and J. J. Lagowski, *J. Phys. Chem.*, **73**, 2326 (1969).

(23) W. Kuhn, *Z. Phys.*, **33**, 408 (1925).

(24) W. Thomas, *Naturwissenschaften*, **13**, 627 (1925).

(25) L. Bierman and E. Trefftz, *Z. Astrophys.*, **26**, 213 (1949).

(26) See, however, ref 10 for evidence of additional bands in solutions which contain a high concentration of a single metal.

(27) S. Golden, C. Guttman, and T. R. Tuttle, Jr., *J. Chem. Phys.*, **44**, 3791 (1966).

(28) J. L. Dye, ref 10, p 1.

The Effect of Varied Excitation on the Fluorescence Spectra of 2-Phenylnaphthalene and Biphenyl: Photoselection of Conformers

by Elvin Hughes, Jr., James H. Wharton, and Robert V. Nauman*

Department of Chemistry, Louisiana State University, Baton Rouge, Louisiana 70803 *(Received December 21, 1970)*

Publication costs borne completely by The Journal of Physical Chemistry

Narrow band or atomic line excitation in the very low extinction, low energy region of the lowest energy singlet–singlet absorptive electronic transition causes the fluorescences of 2-phenylnaphthalene and biphenyl to exhibit a structure and a contour significantly different from those found when the molecules are excited at higher energies with broader bands of ultraviolet radiation. The change in the structure of the observed fluorescence spectra is interpreted to be the result of the excitation of and the resulting emission of a different, narrower distribution of conformers; there results a more structured fluorescence more nearly characteristic of the low energy, relatively planar excited molecules.

Introduction

Previous experimental[1] and theoretical[2,3] work showed that both biphenyl and 2-phenylnaphthalene exist as a distribution of ground state conformers centered around a conformation that has a 30° angle between the planes of the two joined cyclic systems. The fluorescence of both molecular systems arises from a distribution centered around the planar conformation. An analysis of the potential function of the ground state, which has a small maximum at 0°, suggested that, even at 77°K, there should exist a small but experimentally accessible fraction of the molecules that have planar or near planar conformations. The planar conformation should have a lower first singlet–singlet transition energy than that of any other conformation; consequently, excitation with a line or a narrow band of the minimal transition energy should select for excitation only those molecules with conformations narrowly distributed around 0°. Since the first excited singlet state potential function has a minimum at 0°, the selected excited sample is produced in a minimal energy excited state. If thermal equilibration of excited state conformers were obtained before emission occurs, the same fluorescence spectrum would be obtained regardless of the nature of the excitation. When excitation is done with higher energy radiation than that required to excite the planar conformers, molecules with many different conformations are excited. Since our experiments were done with molecules embedded in a rigid glassy matrix at 77°K, there may or may not have been sufficient local heating to permit the molecular rotation necessary for the thermal equilibration of conformers when the higher energy excitations were used; but in any case there was sufficient electronic energy to excite many possible conformers which could then fluoresce. When excitation is done with the minimal electronic excitation energy, only the low energy conformers are excited. These low energy conformers can certainly fluoresce; higher energy conformers can fluoresce only if thermal energy is added to the excited low energy conformer to rotate the molecule to a new higher energy conformation; since there is little or no excess electronic energy in the low energy excitation with which to warm the sample locally, the normal mobility of the rigid matrix would have to permit the rotation required for thermal equilibration to a higher energy conformation. Since the fluorescence spectrum changes significantly upon low energy excitation, we assume that at least in this case thermal equilibration of the conformers has not occurred. Although the authors initially thought that equilibration of excited state conformers might occur and cause the experiment to be unsuccessful, the selected excitation experiment was planned and performed successfully.

Although excitation effects on the emissions of other systems[4] in which different conformations may exist have been observed, those systems were not as well characterized experimentally and theoretically as are the systems used in this work. The previous work[4] was concerned primarily with the effects of rotatable small auxochromes; however, there is a consistency between the two studies that indicates that the distribution of conformers may affect the fluorescence spectrum considerably.

Experimental Section

Solvent. Phillips Petroleum Co. technical grade 3-methylpentane was purified by the method previously

(1) H. E. Holloway, R. V. Nauman, and J. H. Wharton, *J. Phys. Chem.*, **72**, 4468 (1968).

(2) H. E. Holloway, R. V. Nauman, and J. H. Wharton, *ibid.*, **72**, 4474 (1968).

(3) A. Imamura and R. Hoffman, *J. Amer. Chem. Soc.*, **90**, 5379 (1968).

(4) A. N. Fletcher, *J. Phys. Chem.*, **72**, 2742 (1968).

reported.[1] The purified product contained 20% 2-methylpentane and had no observable emission or absorption in the spectral region pertinent to this investigation.

All solutions were in the concentration range 1×10^{-5} M to a maximum of 2×10^{-3} M.

Preparation and/or Purification of the Compounds. 2-Phenylnaphthalene was prepared by the method of Hey and Walker;[5] the adaptations and purification were described previously.[1] In view of a reviewer's belief that a small quantity of impurity could account for our observations, attempts to make impurity analyses were made. The results of these experiments and other earlier results will be summarized.

Before synthesis of 2-phenylnaphthalene was undertaken, experiments were performed with commercial 2-phenylnaphthalene which had undergone various degrees of purification. Two fluorescences and two phosphorescences were observed to be emitted by the commercial sample even after it had been subjected to many purification procedures such as zone refining, recrystallization, vacuum sublimation, and column chromatography. By means of analysis of the emission and absorption spectra, it was concluded that the persistent impurity was an alkylanthracene that existed in a very low steady-state concentration that could not be reduced to a sufficiently low level by reasonable application of the techniques available to us. The emissions of the alkylanthracene persisted even after the absorption could not be found in nearly saturated solutions contained in 10-cm cells. No attempt was made at that time to identify the alkylanthracene, but from knowledge of the extinction coefficient of 2-phenylnaphthalene and the order of magnitude of the extinction coefficient of any alkylanthracene, the concentration of the alkylanthracene was estimated to be no more than 2 mol % in the original commercial sample and appreciably less than 0.1 mol % in the highly purified sample that still gave the spurious alkylanthracene emissions.

Our inability to remove the impurity and eliminate the spurious emissions led to the synthesis of the 2-phenylnaphthalene. In the case of the purified synthesized 2-phenylnaphthalene, no second fluorescence or phosphorescence was found with normal excitation conditions that produce emissions from impurities. The changed emission that resulted from low energy excitation in no way resembled that of the impurity previously identified in the commerial sample. In addition, the observed phenomenon was not consistent with the behavior that has been found in other cases of impurity emission. For example, impurities that have absorptions at lower energies than does the primary compound usually emit when excited somewhere in the higher energy regions; in this case, the changed emission occurred only with very low energy excitation. In addition, any impurity that would be expected to exist should have an identifiable phosphorescence unless the quantum yield of phosphorescence were very low; the low energy excitation changed the nature of the fluorescence but did not change the phosphorescence spectrum.

In spite of the spectral evidence that an impurity was not involved, our analytical colleagues were consulted in attempts to learn methods by means of which the impurity analysis requested by the reviewer could be made. Mass spectroscopy and capillary column gas chromatography were suggested.

Mass spectra of both the commerical and the synthesized 2-phenylnaphthalenes were obtained. In the case of the commerical sample, parent ion peaks of both the 2-phenylnaphthalene and the alkylanthracene were found, and the alkylanthracene was found to be a methylanthracene. The methylanthracene parent ion peaks could be found barely above the noise level, even in the case of purified commercial samples that gave little absorption but considerable fluorescence and phosphorescence from the methylanthracene. The mass spectra of the synthesized 2-phenylnaphthalene gave parent ion peaks of 2-phenylnaphthalene identical with those found in the commercial sample, but there were no peaks characteristic of methylanthracene, no peaks at higher mass numbers where an impurity with the observed spectroscopic properties would be expected to occur, and no peaks anywhere that had not been observed in the mass spectra of the commercial sample. This evidence does not rule out the existence of very small quantities of impurities, but it does set a rather low level of contamination by anything other than an unexpectedly nonvolatile component that should be easily separable by the purification procedures. In spectroscopy, the presence of very small quantities of impurities that act as energy sinks for impurity emissions can rarely, if ever, be ruled out completely.

Our analytical services laboratory performed capillary column gas chromatographic experiments. The methylanthracene impurity in the commercial sample of 2-phenylnaphthalene was detected. The capillary gas chromatographic experiments on the synthesized 2-phenylnaphthalene gives no evidence of an impurity even though five kinds of columns, several of which were selected for their ability to separate aromatics, were used. Again, the absence of positive results does not prove that a minute impurity is not present.

Thermogravimetric analyses and differential thermal analyses were also performed, and, expectedly, added little to our knowledge. No evidence of an impurity was found.

It seems certain that the concentration of an impurity, if present, is considerably less than the 0.1 mol % suggested as the lower limit by the reviewer.

(5) D. H. Hey and W. E. Walker, *J. Chem. Soc.*, 2217 (1940).

Biphenyl was an Eastman Kodak Co. product that was recrystallized four times from 95% ethanol. The last recrystallization produce was vacuum sublimed twice. The second sublimate was used in the spectroscopic studies; the absorption and emission spectra remained unchanged during the final purification stages. The purification was done by King.[6] Attempts to find impurities in the biphenyl sample similar to the ones described above in the case of 2-phenylnaphthalene were equally unsuccessful.

2′-Methyl-2-phenylnaphthalene was prepared and purified by Holloway by the methods previously described.[1]

1,2-Benzofluorene was a K & K product that was purified by the fractional sublimation technique developed by Berg[7] and commonly used in these laboratories. The impurities, shown to be present by the multiple fluorescences detected, were removed. The product is believed to be spectroscopically pure, but there is a small doubt, and the sample size did not permit further purification attempts.

Fluorene was an Eastman Kodak Co. product that was recrystallized many times from different solvents, was vacuum sublimed many times, and was chromatographed several times. The exact history of the sample that was used in this work is unknown; it was passed from student to student and repurified repeatedly; finally, it was shown to be spectroscopically free from contamination by the common impurities carbazole, dibenzofuran, and dibenzothiophene.

Apparatus. The emissions were excited on the emitting surface by either bands of radiation from a 450-W xenon lamp selected by means of a Cary Model 15 monochromator or by the lines of zinc or mercury from an Osram lamp that were isolated either by filters or the excitation monochromator.

The monochromator detection system for broad band excitation studies was initially a Cary Model 14 spectrophotometer operated in the reference mode and previously described.[1] In the cases of atomic line or very narrow band excitation, the initial detection system was a Baucsh and Lomb medium quartz spectrograph with which Kodak F-103a photographic plates were used. Finally, in case of either very narrow or wide band excitation, a unique monochromator–detection system, designed by Professor Wharton and built by Dr. Hughes from a Jarrell-Ash 0.5-m Ebert monochromator and Princeton Applied Research Co. electronic components, was used. This apparatus is capable of detecting extremely low light levels by several procedures including photon counting. The apparatus is described in detail elsewhere.[8]

Results and Discussion

The fluorescence spectra of 2-phenylnaphthalene and biphenyl have been obtained by many investigators. The resolution of the solution spectra has varied, but

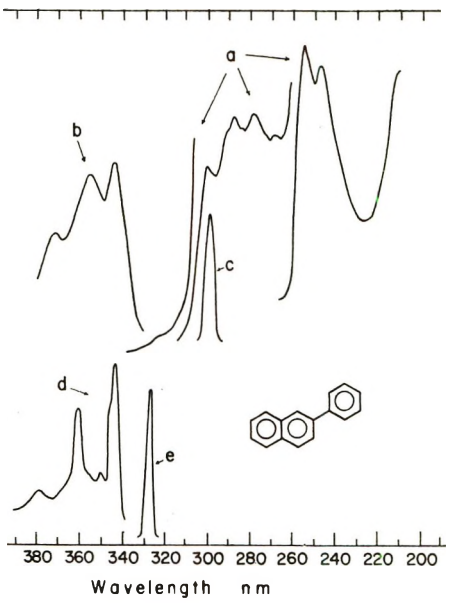

Figure 1. Spectra of 2-phenylnaphthalene in 3-methylpentane at 77°K: a, absorption spectrum; b, fluorescence spectrum resulting from narrow or wide band excitation in the region 220–320 nm; c, one example of excitation of spectrum b; d, fluorescence spectrum resulting from narrow band excitation e. Spectra b and d were recorded with Wharton–Hughes detection system with identical operating conditions, and essentially identical spectra were recorded with the Cary 14 detection system with wider slits and greater gain for d than those for b.

examples of the better resolved have been reported for 2-phenylnaphthalene by Holloway, Nauman, and Wharton[1] and for biphenyl by Berlman.[9]

An analysis[1,2] of the absorption and fluorescence spectra of 2-phenylnaphthalene and its derivatives led to the conclusion that the absorption of 2-phenylnaphthalene is that of a distribution of mainly nonplanar molecules and that the fluorescence is that of a distribution of near-planar molecules. The difference between the absorbing and emitting species rationalizes the rather large Stokes shift that is observed. The usual fluorescence and absorption spectra are shown in Figures 1a and 1b; this same fluorescence spectrum is obtained when broad or narrow band excitation is done in any region of the two electronic transitions found between 220 and 300 nm or in the 300–320-nm region of the lowest energy transition. Figure 1c gives an example of the excitation that produces Figure 1b. In accord with the rationale given in the Introduction, the fluorescence of 2-phenylnaphthalene was excited by the radiation of the 328.2-nm zinc line (Figure 1e) and

(6) J. R. King, Ph.D. Dissertation, Louisiana State University, Baton Rouge, La., Jan 1969.

(7) K. P. Reed and E. W. Berg, *Anal. Chim. Acta*, **37**, 472 (1967).

(8) E. Hughes, Jr., Ph.D. Dissertation, Louisiana State University, Baton Rouge, La., Jan 1971.

(9) J. B. Berlman, "Handbook of Fluorescence Spectra of Aromatic Molecules," Academic Press, New York, N. Y., 1965, p 92.

was detected by means of the Cary 14 operating with wider slits and greater gain than those used to record Figure 1b. The spectrum of Figure 1d resulted. The excitation occurs in the very low energy region of the lowest energy singlet–singlet electronic transition; in 3-methylpentane at 77°K the maximum of the lowest energy observable vibronic peak occurs at 322.5 nm. The new fluorescence spectrum was easily observed in spite of excitation in a spectral region of very low extinction by means of a narrow line of radiation from a weak source. The same well-resolved fluorescence spectrum (Figure 1d) was later obtained with narrow band excitation selected by the monochromator in the 330-nm region and photoelectric detection with the Wharton–Hughes detection system. The appearance of the fluorescence spectrum is considerably different from that previously found. The positions of the peaks in the old and new fluorescence spectra are given in Table I. The new fluorescence spectrum is reminiscent

Table I: Fluorescence Bands of 2-Phenylnaphthalene in 3-Methylpentane at 77°K

Low energy excitation			High energy excitation	
λ, nm		$\bar{\nu}$, kK	λ, nm	$\bar{\nu}$, kK
343.6		29.10	342.0	29.24
350		28.6	354.5	28.21
357	(?)	28.0	368.0	27.17
361.0		27.70	382.5	26.14
369	(?)	27.1		
380		26.3		
399	(?)	25.1		

of that of 2′-fluoro-2-phenylnaphthalene in which case only a very small Stokes shift was found and a very narrow distribution of essentially planar molecules was deduced to be present in both the ground and first excited singlet states. The new fluorescence spectrum is obviously better resolved and more structured than the other one, in spite of its being observed through wider slits of the same detection system. In addition, the short wavelength tail of the spectrum drops more precipitously and occurs at longer wavelengths than does that of the broader spectrum; the position of the highest energy fluorescence maximum appears at lower energy than does the highest energy peak of the original spectrum. The new high energy fluorescence peak matches well the position of the well-resolved lowest energy absorption maximum of 1,2-benzofluorene, which is a bridged 2-phenylnaphthalene that is restricted to an essentially planar conformation. The band separations and the spectral contour of the better resolved 2-phenylnaphthalene fluorescence spectrum are very similar to those of the presumed planar 2′-fluoro-2-phenylnaphthalene. The new fluorescence spectrum of 2-phenylnaphthalene shows a band-for-band correspondence in position and relative intensity with the more prominent bands of the better resolved fluorescence of planar 1,2-benzofluorene.

As stated in the Experimental Section, the solvent did not emit in the 280–400-mm region of the spectrum when the same very high detection sensitivities used for detection of the change in fluorescence were used for detection of a possible solvent emission. The fluorescence intensity of the phenylnaphthalene and the biphenyl to be discussed later does not change during the time required for making and repeating the sequence of fluorescence measurements that show the effect of excitation on the structure of the fluorescence. There is no evidence for photochemical reaction; no intensity change greater than experimental error was observed. Very long periods of irradiation do cause a very gradual decrease in the intensity of the emissions, but no change in the effect of excitation energy occurs; this gradual intensity decrease is observed in all cases that have been observed for long periods.

The sharpening of the fluorescence spectrum, the disappearance of the higher energy tail of the old spectrum, the similarity of the contour of the new fluorescence with those of 2′-fluoro-2-phenylnaphthalene and 1,2-benzofluorene, and the position of the highest energy fluorescence band in near coincidence with the position of the lowest energy absorption band of planar 2-phenylnaphthalene species all suggest that the previous[1] assignment of the fluorescence to a planar excited state was only approximately correct and that the new fluorescence spectrum is that of molecules much more narrowly distributed around the planar configuration.

To test this conclusion, the spectra of two control molecules were investigated. The temperature dependence of the absorption spectrum of 2′-methyl-2-phenylnaphthalene, for which nonplanar ground and first excited singlet states were deduced previously,[1] has recently been investigated[10] experimentally and theoretically. 1,2-Benzofluorene is restricted geometrically to a near-planar conformation or a narrow distribution of conformations. These were the two molecules chosen for control studies of excitation effects.

2′-Methyl-2-phenylnaphthalene has fluorescence and absorption spectra that exhibit a small Stokes shift and occur at higher energies than do the comparable spectra of planar molecules. This molecule is sterically prohibited from obtaining a planar configuration. The minima in the ground and first excited state potential functions are deeper than those of 2-phenylnaphthalene, and at 77°K molecular distributions narrow relative to those of 2-phenylnaphthalene are expected. In addition, the shapes of the two potential functions are rather similar; consequently, all accessible conforma-

(10) A. Maresco, G. Traverso, J. H. Wharton, and R. V. Nauman, in preparation for publication.

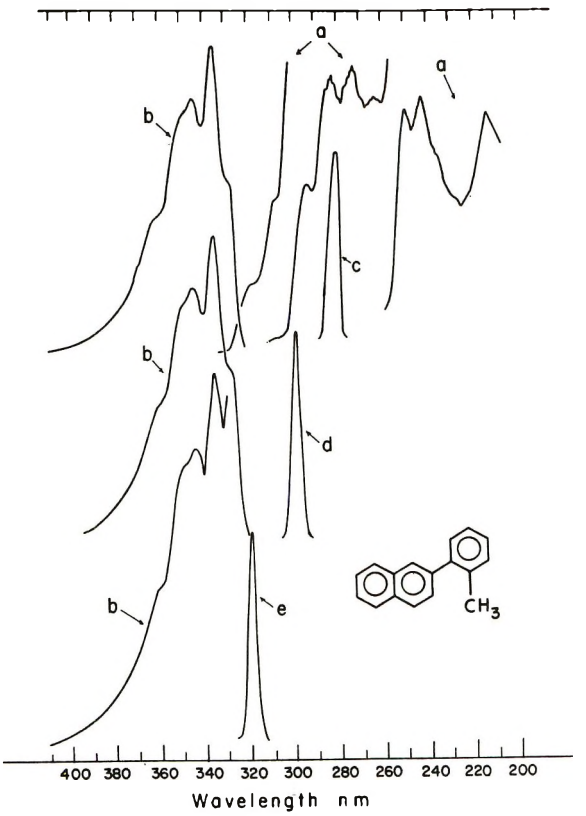

Figure 2. Spectra of 2′-methyl-2-phenylnaphthalene in 3-methylpentane at 77°K: a, absorption spectrum; b, fluorescence spectra resulting from excitations c, d, and e.

tions give spectra that are energetically similar. While selective excitation might cause some change, no major change in the fluorescence spectrum would be expected. In Figure 2 are shown the absorption and fluorescence spectra of 2′-methyl-2-phenylnaphthalene. There are only very minor changes in the contour of the fluorescence and no change in band positions or relative intensities as the excitation, either broad or very narrow band, is varied between 230 and 330 nm. In the case of narrow band excitation at 330 nm, the excitation overlaps the highest energy fluorescence band, but the remaining observable part of the fluorescence remains unchanged. Again, the experiment and the interpretation based on a distribution of conformations are in agreement.

1,2-Benzofluorene is a 2-phenylnaphthalene maintained in a near-planar conformation by a methylene bridge. It gives absorption and fluorescence spectra that are much more structured than those of 2-phenylnaphthalenes in which considerable interannular rotation is expected. Little, if any, change in the fluorescence spectrum as a result of changed excitation would be expected. When the excitation is changed throughout the first three or more electronic transitions in the 230–355-nm range, no change in band position or the general shape of any band is found. Two different groups of fluorescence bands do change in relative intensity when narrow band excitation is moved through the lowest energy absorptive transition. A similar change in relative intensity of pairs of bands in the absorption spectrum in the 240–270-nm region was found when the temperature dependence of that transition was studied; the temperature dependence of the third electronic transition of rotatable 2-phenylnaphthalenes was predicted and found and is the subject of another investigation.[10] These changes in relative intensities of groups of bands in both absorption and fluorescence may indicate the presence of two-preferred conformations in 1,2-benzofluorene; however, it was previously stated that there is some doubt about the purity of the 1,2-benzofluorene, and, consequently, the spectra are not given here and the interpretation is not defended at this time.

Since the potential functions of biphenyl were shown[3] to be similar to those of 2-phenylnaphthalene, the fluorescence spectra of some biphenyls were investigated by means of selected excitation. The calculations of Imamura and Hoffman[3] do not account for the lowest energy excited singlet state of biphenyl suggested by Berlman and Steingraber[11] on the bases of fluorescence lifetime data and calculations, found in biphenyl derivatives by many people, for example, Beaven, *et al.*,[12] and reinvestigated[6] recently along with the fluorescences in this laboratory. By analogy with the 2-phenylnaphthalene calculations, we believe the general shape of the first excited state potential function to be similar to that published[3] for the second excited state.

The results of the low energy selected excitation of biphenyl are shown in Figure 3 along with the conventional fluorescence and absorption spectra. The narrow band excitation at 290 nm gives a fluorescence that is much more structured than the one produced by 270-nm broad band excitation. The change was first observed by means of photographic detection but was later routinely and quickly redetermined by photoelectric detection which shows at least six distinct vibrational structures and several additional inflections. The new band contour is very similar to that of fluorene shown in Figure 4. While the peak of the highest energy fluorescence band observed in the usual biphenyl spectrum appears to move to higher energies as the excitation energy is lowered, this apparent movement is easily seen to be an artifact of the much better resolution of the new spectrum. The high energy tail of the usual fluorescence becomes sharper and moves to lower energies as the excitation energy is lowered and more structure develops in the fluorescence spectrum. The arguments applied to the 2-phenylnaphthalene case are again applicable, and a narrower distribution of molecules with near-planar conformations is believed

(11) I. B. Berlman and O. J. Steingraber, *J. Chem. Phys.*, **43**, 2140 (1965).

(12) G. H. Beaven, D. M. Hall, M. S. Lesslie, and E. E. Turner, *J. Chem. Soc.*, 854 (1952).

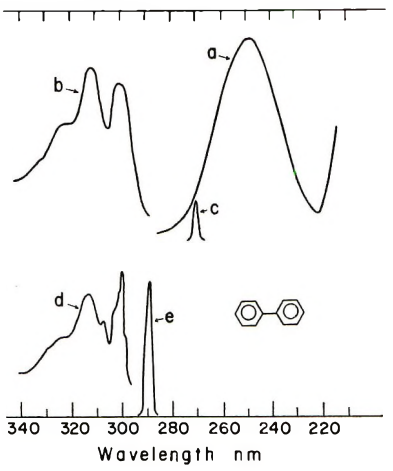

Figure 3. Spectra of biphenyl in 3-methylpentane at 77°K: a, absorption spectrum; b, usual fluorescence spectrum; c, one excitation of spectrum b; d, fluorescence spectrum excited with band e; e, excitation band for spectrum d. Spectrum b is produced by any excitation between 220 and 280 nm.

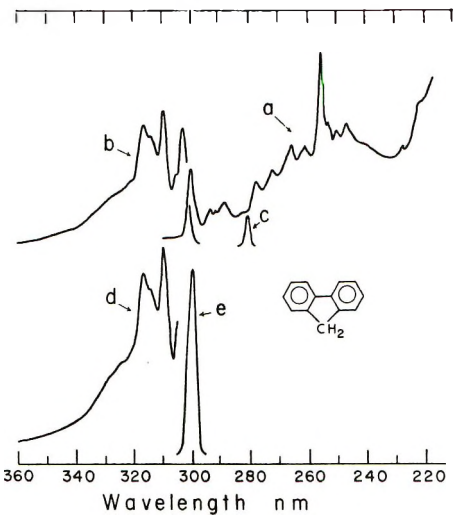

Figure 4. Spectra of fluorene in 3-methylpentane at 77°K: a, absorption spectrum; b, usual fluorescence spectrum; c, one excitation of spectrum b; d, part of usual fluorescence spectrum excited with band e; e, excitation band for spectrum d.

to be responsible for the new sharper spectrum. Again experimental conditions, such as slit widths, electronic amplification, etc., favor higher resolution in the usual spectrum; consequently, the newer, more structured fluorescence is not an experimental artifact.

Again in the case of biphenyl, a control experiment was done. Fluorene is a methylene-bridged biphenyl which gives absorption and fluorescence spectra that are considerably better resolved than those of biphenyl. No excitation effect due to changes in conformation of fluorene would be expected, and none was found. Selected narrow band and wide band excitations from 230 to 300 nm gave fluorescence spectra that are identical band for band. Even when a narrow excitation band at 300 nm is used and the first vibrational band is not observable, the remaining bands retain their shape, position, and relative intensities. The positions of the biphenyl and fluorene bands are given in Table II.

Table II: Bands of Electronic Transitions of Biphenyl and Fluorene in 3-Methylpentane at 77°K

Biphenyl fluorescence, —low energy excitation—			Fluorene absorption, ——first transition——	
λ, nm		ν̄, kK	λ, nm	ν̄, kK
299.9		33.34	288.5	34.66
301.5		33.16	291.4	34.32
303.5		32.94	293.2	34.10
306.5		32.62	299.8	33.36
314		31.8		
324	(?)	30.9		
—High energy excitation—			Fluorene fluorescence, ——all excitations——	
301.5		33.16	301.7	33.15
312.5		32.00	304	32.9
323.4		30.92	307.7	32.49
			313	32.0
			315.1	31.73
			322.0	31.05

At first it might seem peculiar that the vibrational progressions observed in the 2-phenylnaphthalene and biphenyl spectra excited at lower energy are different from those observed with high energy excitation. Reflection quickly indicates that the apparent progressions in the spectra excited with high energy radiation are probably artifacts that result from the overlapping of a distribution of spectra from many conformations. Each conformation probably gives a spectrum that is sharper and better defined than any spectrum shown herein and has progressions similar to those found in the spectra resulting from low energy excitation. When emission occurs simultaneously from a broad distribution of conformations, each of which has a slightly different energy, the result is a combination of many spectra with a resulting loss of structure, the disappearance of some bands completely, and a change in position of the bands that remain. The progressions and band positions in the fluorescences excited at the higher energies are probably, therefore, to a great extent artifacts of the overlap.

Investigators inclined to believe in dual fluorescences from two nearly isoenergetic singlet states might at first think that the change in fluorescence observed in this work is an example of the presumed dual emission phenomenon. We believe that our analysis in terms of a change in distribution of rotational conformers better fits the evidence. If a dual emission phenomenon existed, the 2′-methyl-2-phenylnaphthalene case should be ideal for its observation because the lowest energy absorptive transition severely overlaps the second transi-

tion and yet gives a rather well-isolated first vibronic band. Yet in this case, favorable for possible emissions from two nearly degenerate states, no significant fluorescence spectral change was observed, and none was expected on the basis of our interpretation.

In summary, both 2-phenylnaphthalene and biphenyl have fluorescences that change to sharper, better resolved, lower energy spectra when the excitation is changed from higher energies to the very low energy edge of the first absorptive transition. Similar changes are not observed in the case of similar molecules that cannot rotate around the interannular bond. The sharper new fluorescences are assigned to a narrow distribution of near-planar excited molecules excited by a narrow band of radiation. Since this narrow distribution cannot be obtained when there is excitation at higher energies, radiationless relaxation must lead to an inhomogeneously broadened distribution of molecules in the lowest excited state. To observe the emission from a narrow distribution of excited molecules, one must excite only those ground state molecules that have the same conformation as that of the lowest energy excited state and at the same time not produce any vibrational excitation. When it is possible to obtain this photoselection from the inhomogeneously broadened ground state distribution, it will be obtained by means of narrow beam excitation in the longest wavelength region of the broad absorption to produce a narrow distribution of excited state molecules that cannot be easily broadened inhomogeneously.

Low-Lying Electronic States of the Scandium Oxide, Yttrium Oxide, and Lanthanum Oxide Molecules

by David W. Green

Laboratory of Molecular Structure and Spectra, Department of Physics, University of Chicago, Chicago, Illinois 60637
(Received November 13, 1970)

Publication costs assisted by the Office of Naval Research

Evidence is presented that the low-lying electronic states of ScO, YO, and LaO can be interpreted in terms of molecular orbitals which are closely approximated as metal-centered atomic orbitals. Quantitative predictions are made of the excitation energies of the unobserved $A'^2\Delta$ states of ScO and YO. It is concluded that these two $^2\Delta$ states are not of importance to the partition function in the temperature range of interest and that spectroscopic transitions involving these states will be difficult to observe.

Introduction

Application of the "third-law method" to obtain heats of reaction and dissociation energies from vapor pressure measurements requires an accurate partition function. For high-temperature diatomic molecules, such as transition metal oxides and halides, a number of electronic states can make appreciable contributions to the partition function at the temperatures of interest. Complete spectroscopic studies of high-temperature molecules are rarely available.[1] Only in a few favorable cases can the molecular electronic structures be interpreted in a manner that leaves no large uncertainties in the partition function due to unobserved electronic states. In those cases the third-law method is generally more reliable than the second-law method.[2]

There is a general interest in diatomic scandium compounds as model systems for understanding the role of d electrons in chemical bonding. Because scandium is the lightest element with occupied d orbitals in its ground state, it could provide a suitable starting point for interpreting other transition metal compounds.

It has been pointed out that the ScO, YO, and LaO molecules have similar electronic spectra.[3] This is a consequence of the identical ground-state atomic orbital configurations, ns^2 $(n - 1)$d, of the metal atoms. It is convenient to use this similarity as a basis for in-

(1) See, for example, C. J. Cheetham and R. F. Barrow in "Advances in High Temperature Chemistry," Vol. 1, L. Eyring, Ed., Academic Press, New York, N. Y., 1967.

(2) See, for example, P. W. Gilles in "The Characterization of High-Temperature Vapors," J. Margrave, Ed., Wiley, New York, N. Y., 1967.

(3) D. W. Green, *J. Mol. Spectrosc.*, **38**, 155 (1971).

terpreting the electronic structures of all three molecules.

The ground state of ScO was calculated to be $^2\Delta$ using a ligand-field model.[4] More recent SCF–LCAO calculations[5] predict a $^2\Sigma^+$ ground state with a low-lying $^2\Delta$ state as the first excited state. Because of its large electronic degeneracy, a $^2\Delta$ state could make a significant contribution to the partition function if its excitation energy is comparable with kT. This uncertainty in excitation energy makes the application of the third-law method to ScO uncertain, and by analogy to YO and LaO.

Although no experimental information on a $^2\Delta$ state in either ScO or YO has been reported, a $^2\Delta$ state, called $A'^2\Delta$, has been rotationally analyzed for LaO.[3]

It is the purpose of this paper to present evidence that the low-lying electronic states of ScO, YO, and LaO can be interpreted using a model. Quantitative predictions of the excitation energies of the unobserved $^2\Delta$ states of ScO and YO are made.

Electronic Structure Model

The rotational analysis of the LaO $C^2\Pi \rightarrow A'^2\Delta$ transition[3] gave the first experimental information on a $^2\Delta$ state in the diatomic III A oxides. Revision[6] of the previous LaO "$C^2\Pi \rightarrow X^4\Sigma^+$" analysis[7] established the fact that the $C^2\Pi$ state is common to the observed $C \rightarrow X$ and $C \rightarrow A'$ transitions. The excitation energy of the $A'^2\Delta$ state could then be determined. Table I summarizes information on the term energies, T_0, and spin-orbit coupling coefficients, A, for all LaO electronic states known from rotational analyses. Data for the $A^2\Pi$ and $B^2\Sigma^+$ states were taken from Åkerlind[8] and for the $F^2\Sigma^+$ and $D^2\Sigma^+$ states from Carette and Houdart.[9] The data for ScO[10] and YO[11] are also included. Figure 1 shows the energy of each rotationally analyzed LaO electronic state with the analyzed transitions indicated by vertical arrows.

Table I: Energies and Spin-Orbit Coupling Coefficients of Rotationally Analyzed Electronic States of LaO, YO, and ScO

State	LaO T_0 (A)	YO T_0 (A)	ScO T_0 (A)
$F^2\Sigma^+$	28,049.2		
$D^2\Sigma^+$	26,960.0		
$C^2\Pi_{3/2}$	22,839.6		
	(221.4)		
$C^2\Pi_{1/2}$	22,618.9		
$B^2\Sigma^+$	17,837.8	20,741.9	20,571.2
$A^2\Pi_{3/2}$	13,497.6	16,722.8	16,554.8
	(862.7)	(428.0)	(115.2)
$A^2\Pi_{1/2}$	12,635.7	16,294.7	16,440.6
$A'^2\Delta_{5/2}$	8,168.4		
	(350.5)		
$A'^2\Delta_{3/2}$	7,468.9		
$X^2\Sigma^+$	0.0	0.0	0.0

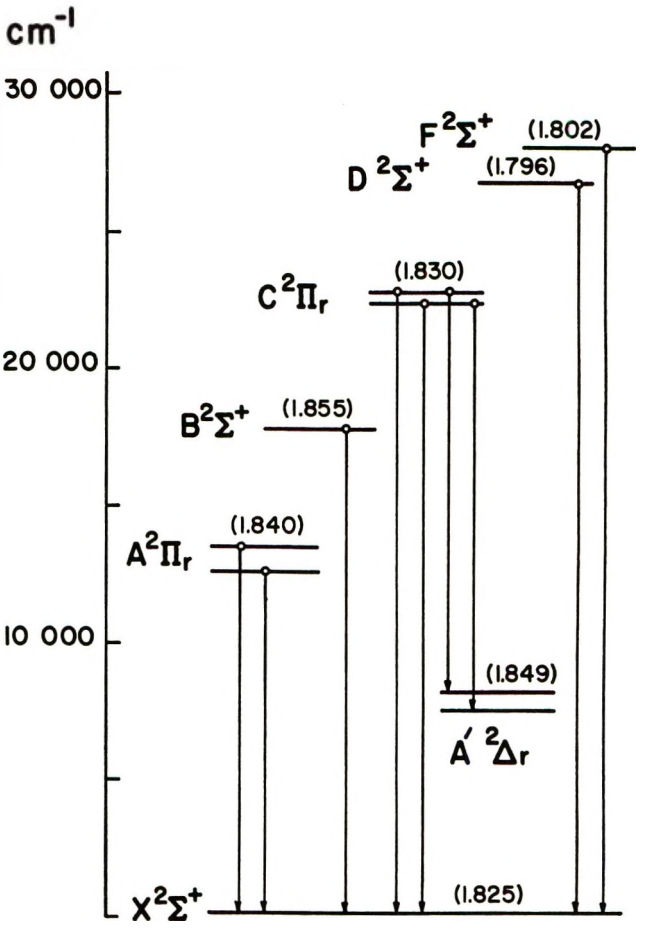

Figure 1. The electronic energies of rotationally analyzed states of the LaO molecule. Transitions which have been studied are indicated by vertical arrows. The equilibrium internuclear distance in Å for each state is in parentheses.

The proposed model for the electronic structures of ScO, YO, and LaO is based on the accumulated theoretical and experimental evidence that the unpaired electron of the low-lying electronic states is in a molecular orbital which is very atomic-like.

The SCF–LCAO calculations on ScO[5] show that the ground state, $X^2\Sigma^+$, is from a molecular orbital configuration involving a series of closed shells and a single unpaired electron in the 9σ orbital. The dominant coefficient in the linear combination for the wave function of this orbital is that of the 4s atomic orbital centered on the Sc atom. Similarly, the observed $A^2\Pi$ state is

(4) R. A. Berg and O. Sinanoglu, *J. Chem. Phys.*, **32**, 1082 (1960).
(5) K. D. Carlson, E. Ludeña, and C. Moser, *ibid.*, **43**, 2408 (1965).
(6) D. W. Green, *Can. J. Phys.*, in press.
(7) P. Carette and J. Blondeau, *C. R. Acad. Sci., Paris, Ser. B*, **268**, 1743 (1969); P. Carette, Thesis, Univ. de Lille, Lille, France, 1969.
(8) L. Åkerlind, *Ark. Fys.*, **22**, 65 (1962).
(9) P. Carette and R. Houdart, *C. R. Acad. Sci., Paris, Ser. B*, **272**, 595 (1971).
(10) L. Åkerlind, *Ark. Fys.*, **22**, 41 (1962).
(11) U. Uhler and L. Åkerlind, *ibid.*, **19**, 1 (1961).

from a configuration involving an unpaired electron in the 4π mo which is approximately a $4p_{Sc}$ orbital. The unobserved $A'^2\Delta$ state[12] is derived from an unpaired electron in an orbital which is largely $3d\delta_{Sc}$.

The near equality of the spin-splitting coefficient, γ, of the ScO $B^2\Sigma^+$ state and the Λ-doubling coefficient of the $A^2\Pi$ state has been interpreted[13] in terms of pure precession.[14] That is, the $B^2\Sigma^+$ and $A^2\Pi$ states are in large part derived from mo configurations in which the unpaired electron is in the orbitals $4p\sigma_{Sc}$ and $4p\pi_{Sc}$, respectively. A similar matching of the $B^2\Sigma^+$ spin-splitting and the $A^2\Pi$ Λ-doubling coefficients exists for YO[11] and LaO.[8]

The $^4\Sigma^+$ ground-state assignments of ScO and LaO have been reassigned as $^2\Sigma^+$ with hyperfine splitting.[6,13,15] The $X^2\Sigma^+$ states of these two molecules are examples of nearly pure case $b_{\beta S}$ coupling.[16] The strength of the coupling and therefore the magnitude of the hyperfine splitting is dependent on $|\Psi(0)|^2$, the electron density at the metal nucleus. The large hyperfine splittings observed for ScO and LaO are strong evidence that the unpaired electron in each case is principally in a metal-centered s-type orbital. Recent analysis of the LaS spectrum has shown a hyperfine splitting in the $X^2\Sigma^+$ state which is almost identical with that of the LaO $X^2\Sigma^+$ state.[17]

If we approximate the wave functions of the molecular orbitals, σ, π, and δ, corresponding to the $X^2\Sigma^+$, $A^2\Pi$, and $A'^2\Delta$ states, as metal-centered ns, np, and $(n-1)$d atomic orbitals, the molecular orbital energies, ϵ, reduce to atomic orbital energies. It is convenient to take mo energies relative to value of ϵ_σ. Taking ϵ_σ as zero, the values of ϵ_π and ϵ_δ are identical with the atomic excitation energies $\epsilon_p - \epsilon_s$ and $\epsilon_d - \epsilon_s$. Using the known[18] energies of the ^2D atomic states from the metal configurations s^2d, sd^2, and sdp, the values of $\epsilon_p - \epsilon_s$ and $\epsilon_d - \epsilon_s$ can be approximated.[19] These approximations furnish a method for making quantitative calculations of the excitation energies of the ScO, YO, and LaO $A^2\Pi$ and $A'^2\Delta$ electronic states. The excitation energies of the unobserved $A'^2\Delta$ states of ScO and YO are of principal interest.

Results and Discussion

If $\epsilon_\delta = \epsilon_d - \epsilon_s$, then the excitation energies of the $A'^2\Delta$ states would be equal to the corresponding $\epsilon_d - \epsilon_s$ value. Some refinement of this approximation may be obtained by employing the following relationship which makes use of the known $A^2\Pi$ excitation energies

$$T_0(A'^2\Delta) = \epsilon_\delta = (\epsilon_d - \epsilon_s) \times \epsilon_\pi/(\epsilon_p - \epsilon_s)$$

Table II summarizes the data used in this relationship and the results. The near agreement $\epsilon_p - \epsilon_s$ and ϵ_π in each case gives more quantitative support to the validity of the approximations used in the model.

It is difficult to estimate the accuracy of the calculated $A'^2\Delta$ excitation energies of ScO and YO. The determination of $\epsilon_p - \epsilon_s$ and $\epsilon_d - \epsilon_s$ from atomic spectroscopy data is subject to some error due to mixing of the large number of observed states. The assumption that ^2D energy differences may be used for obtaining the $\epsilon_p - \epsilon_s$ and $\epsilon_d - \epsilon_s$ values seems reasonable, but others are possible.[20] The basis of the model seems well justified by the experimental data on all three molecules and the SCF–LCAO calculations on ScO. The agreement of the calculated and observed values of $T_0(A'^2\Delta)$ for LaO also supports the validity of the model.

Table II: Atomic Excitation Energies in cm^{-1} of an Electron from an s Orbital to a p Orbital, $\epsilon_p - \epsilon_s$, to a d Orbital, $\epsilon_d - \epsilon_s$, together with the Analogous Observed and Calculated Quantities for the Diatomic Oxides

Atom	Obsd $\epsilon_p - \epsilon_s$	Obsd ϵ_π	Obsd $\epsilon_d - \epsilon_s$	Calcd $T_0(A'^2\Delta)$	Obsd $T_0(A'^2\Delta)$
La	14,263	13,067	8,257	7,600	7,819
Y	15,780	16,509	15,775	16,500	
Sc	15,951	16,498	16,917	17,500	

Conclusions

The contribution of the $A'^2\Delta$ state of LaO to the partition function can be determined. The calculated values of the excitation energies of the corresponding $A'^2\Delta$ states of ScO and YO indicate that they make no appreciable contributions to the partition functions. Even large errors in the calculated values of Table II do not alter this conclusion.

Spectroscopic transitions between the $A'^2\Delta$ and $A^2\Pi$ states of ScO and YO would be far in the infrared. Other transitions involving the $A'^2\Delta$ states would be

(12) The designation A′ will be used for the unobserved ScO and YO $^2\Delta$ states by analogy with the $A'^2\Delta$ state of LaO.

(13) A. Adams, W. Klemperer, and T. M. Dunn, *Can. J. Phys.*, **46**, 2213 (1968).

(14) J. H. Van Vleck, *Phys. Rev.*, **33**, 467 (1929); R. S. Mulliken, *Rev. Mod. Phys.*, **3**, 129 (1931).

(15) W. Weltner, D. McLeod, and P. H. Kasai, *J. Chem. Phys.*, **46**, 3172 (1967).

(16) R. A. Frosch and H. M. Foley, *Phys. Rev.*, **88**, 1337 (1952); C. H. Townes and A. L. Schawlow, "Microwave Spectroscopy," McGraw-Hill, New York, N. Y., 1955.

(17) M. Marcano and R. F. Barrow, *Proc. Phys. Soc. London (At. Mol. Phys.)*, **3**, L121 (1970).

(18) C. E. Moore, "Atomic Energy Levels," Vol. I, II, and III, National Bureau of Standards Circular 467, U. S. Government Printing Office, Washington, D. C., 1949, 1952, 1958.

(19) The lower energy one of the two ^2D states of the sdp configuration was used.

(20) The choice of the ^2D atomic state energy for comparison was made primarily because it is the only state which occurs in all three configurations, s^2d, sd^2, and sdp. A "center of gravity" for each configuration (neglecting the unobserved ^2S state of sd^2 configuration for Sc, Y, and La; see ref 18) gives values in Table II which do not alter the conclusions. The use of the doublet states for which the orbital angular momentum, L, equals the sum of the orbital angular momenta, l, of the individual electrons gives values which are very close to those of Table II. Other alternative approximations to the values $\epsilon_p - \epsilon_s$ and $\epsilon_d - \epsilon_s$ are possible, but the qualitative conclusions should not be changed.

from highly excited states for which no experimental information is available.[21] It is concluded that electronic transitions involving the $A'^2\Delta$ states of ScO and YO are unlikely to be observed from the usual thermal, flame, and arc sources. It may be possible to experimentally determine the electronic energies of these $A^{2\prime}\Delta$ states by analysis of their interactions (perturbations) with the $A^2\Pi$ states.

Acknowledgment. This work was supported in part by a grant from the National Science Foundation, GP-27138, and in part by the Office of Naval Research, Physics Branch, under Contract No. N00014-67-A-0285-0001.

(21) See, for example, A. Gatterer, J. Junkes, E. W. Salpeter, and B. Rosen, "Molecular Spectra of Metallic Oxides," Specola Vaticana, Vatican City, 1957.

The Monoisotopic Mass Spectra of the Boranes[1]

by Eileen McLaughlin, Ting Eng Ong, and R. W. Rozett*

Chemistry Department, Fordham University, New York, New York 10458 *(Received May 12, 1971)*

Publication costs assisted by the Petroleum Research Fund

The monoisotopic positive ion mass spectra for B_2H_6, B_4H_{10}, B_5H_9, B_5H_{11}, B_6H_{10}, B_6H_{12}, B_7H_{11}, B_7H_{13}, B_8H_{12}, B_8H_{18}, B_9H_{15}, $B_{10}H_{14}$, and $B_{10}H_{16}$ are reported. Monoisotopic negative ion spectra for B_2H_6, B_4H_{10}, B_5H_9, and $B_{10}H_{14}$ are given. A new least-squares technique generated the spectra from published and unpublished polyisotopic data. The monoisotopic spectra of six of the compounds have not been reported previously. The new spectra for the compounds which have been reported previously are estimated to have, on the average, a fit twenty-five times as good as those in the literature.

Introduction

The mass spectra of the boron hydrides, B_nH_m, are unusually complex for two reasons. The naturally occurring isotopes, ^{10}B and ^{11}B, are both found in significant amounts (1:4), and borane ions easily lose some or all of their hydrogen atoms before breaking boron–boron bonds. For example, in the spectrum of decaborane-14, $B_{10}H_{14}$, in the region containing ions with ten boron atoms, 165 ions which differ at least isotopically, occur over a mass range of 25 daltons. In the same mass region (100–124), 91 ions containing nine boron atoms are found. In the monoisotopic spectrum on the other hand, 15 different ions containing ten boron atoms occur. This indicates the advantage of calculating monoisotopic spectra.

The conventional method of deriving monoisotopic spectra from polyisotopic data starts with the intensity of the peak which occurs at the highest mass.[2] This is necessarily a pure ^{11}B peak due to a single formula, $B_nH_m^+$. From statistical considerations which are discussed later, one can calculate the abundance of each ion with the same formula, but with different numbers of ^{10}B and ^{11}B atoms. These intensities are then subtracted from the experimental measurements at the appropriate mass. In this way we remove from the experimental data the effect of the presence of ions containing ^{10}B with the formula $B_nH_m^+$. The residual intensity at the second highest experimental peak is now a pure ^{11}B peak due to the single formula $B_nH_{m-1}^+$. The process may be repeated until we have generated a spectrum which consists of intensities due only to formulas containing the ^{11}B isotope.

There are several drawbacks to this conventional method. Errors introduced early in the process, whether experimental or computational, are cumulatively transmitted to lower masses. Special weight is consequently put upon measurements at higher masses. In addition, one cannot use all the information available to generate the monoisotopic abundances. There are in general more experimental measurements than monoisotopic intensities to be determined. The ordinary computation does not take advantage of the overdetermined character of the problem. Finally, negative intensities almost necessarily occur when we carry out the subtractions described above. These may be due to experimental mismeasurements, the presence of impurities, and several other situations

(1) This research was supported in part by the Petroleum Research Fund administered by the American Chemical Society (PRF 1233-G2). The instrumentation was supplied in part by the National Science Foundation (GP 8220) and by the New York State Science Foundation [NYSSF (6)-13].

(2) F. J. Norton, *J. Amer. Chem. Soc.*, **71**, 3488 (1949); I. Shapiro, C. O. Wilson, J. F. Ditter, and W. J. Lehmann, *Advan. Chem. Ser.*, **No. 32**, 127 (1961); J. F. Ditter, F. J. Gerhart, and R. E. Williams, *ibid.*, **No. 72**, 191 (1968).

Table I

```
C     MONOISOTOPIC BORANE MASS SPECTRA                                  MIBS   1
C                  R W ROZETT      CHEMISTRY DEPARTMENT                 MIBS   2
C                  FORDHAM UNIVERSITY  BRONX, N Y  10458                MIBS   3
C                                                                       MIBS   4
      DIMENSION   PKSUM(100), A(6000),IB(100),IH(100),AUTHOR(4),        MIBS   5
     1IPIV(100),AUX(200), PDLMAS(100),ONEMAS(100), PKONE(100), PK(350)  MIBS   6
      DIMENSION NAME(14)                                                MIBS   7
C                                                                       MIBS   8
      MAXNUM=6000                                                       MIBS   9
      EPS=1.0E-07                                                       MIBS  10
      FRCTBL=0.9032                                                     MIBS  11
C                                                                       MIBS  12
C     TITLE CARD...MAX AND MIN MASS IN POLY SPEC                        MIBS  13
  114 READ(1,4,END=99)ICODE,MASSMN,MASSMX,NAME,NUMBO,NUMHO,ICODE1,NZERO MIBS  14
    4 FORMAT(3I5,14A4,1X,4I2)                                           MIBS  15
      IF(MASSMX)99,99,95                                                MIBS  16
   95 NUMBMX=MASSMX/11                                                  MIBS  17
      NUMHMX=MASSMX-NUMBMX*11                                           MIBS  18
      NUMBMN=MASSMN/10                                                  MIBS  19
      NUMHMN=MASSMN-NUMBMN*10                                           MIBS  20
      NUMPOL=MASSMX-MASSMN+1                                            MIBS  21
      IF(NUMHMX.GT.NUMBMX)GO TO 20                                      MIBS  22
      NUMHMX=NUMHMX+1                                                   MIBS  23
      NUMBMX=NUMBMX-1                                                   MIBS  24
   20 ADD=0.0                                                           MIBS  25
      ICOL=0                                                            MIBS  26
      MAXROW=NUMPOL                                                     MIBS  27
   11 DO 79 I=1,MAXNUM                                                  MIBS  28
      A(I)=0.0                                                          MIBS  29
   79 CONTINUE                                                          MIBS  30
      DO 34 I=1,100                                                     MIBS  31
      ONEMAS(I)= 0.                                                     MIBS  32
      PKONE(I)=0.                                                       MIBS  33
      PKSUM(I)=0.                                                       MIBS  34
   33 CONTINUE                                                          MIBS  35
      DO 32 I=1,350                                                     MIBS  36
      PK(I)=0.0                                                         MIBS  37
   32 CONTINUE                                                          MIBS  38
C                                                                       MIBS  39
C     DATA INPUT                                                        MIBS  40
C     INTRODUCE THE INTENSITIES FROM LOW MASS TO HIGH                   MIBS  41
   98 READ(1,3)(PKSUM(I),I=1,NUMPOL)                                    MIBS  42
    2 FORMAT(16I5)                                                      MIBS  43
    3 FORMAT (12 F 6.0)                                                 MIBS  44
C                                                                       MIBS  45
C     INTRODUCE THE FORMULAS FROM LOW MASS TO HIGH MASS                 MIBS  46
  651 READ(1,2,END=99)NUMB,NUMH                                         MIBS  47
      IF (NUMB)   655, 655, 652                                         MIBS  48
  652 MASS2=NUMB*11+ NUMH                                               MIBS  49
      IF(MASS2.LT.MASSMN) GO TO 651                                     MIBS  50
      MASS1=MASS2-NUMB                                                  MIBS  51
      ICOL=ICOL+1                                                       MIBS  52
      ONEMAS(ICOL)=FLOAT(MASS2)                                         MIBS  53
      IB(ICOL)=NUMB                                                     MIBS  54
      IH(ICOL)=NUMH                                                     MIBS  55
      NUMBX=NUMB+1                                                      MIBS  56
      NUM=MASS1-MASSMN+(ICOL-1)*MAXROW                                  MIBS  57
      NUMBXX=1                                                          MIBS  58
      IF(MASS1.GE.MASSMN)GO TO 660                                      MIBS  59
      IB(ICOL)=999                                                      MIBS  60
      NUMBXX=MASSMN-MASS1+1                                             MIBS  61
      NUM=(ICOL-1)*MAXROW                                               MIBS  62
C                                                                       MIBS  63
C     MATRIX OF COEFFICIENTS OF SIMULTANEOUS EQNS                       MIBS  64
  660 DO 654 NUMBII=NUMBXX,NUMBX                                        MIBS  65
      NUM=NUM+1                                                         MIBS  66
      A(NUM)=RLABUN(NUMB,NUMBII,FRCTBL)                                 MIBS  67
  654 CONTINUE                                                          MIBS  68
      GO TO 651                                                         MIBS  69
  655 MAXCOL=ICOL                                                       MIBS  70
C                                                                       MIBS  71
      DO 78  I= 1, NUMPOL                                               MIBS  72
      PDLMAS(I)=MASSMN+ADD                                              MIBS  73
      ADD=ADD+1.                                                        MIBS  74
   78 CONTINUE                                                          MIBS  75
      N=NUMPOL+1                                                        MIBS  76
      DO 200 I=N,100                                                    MIBS  77
      PDLMAS(I)=0.                                                      MIBS  78
  200 CONTINUE                                                          MIBS  79
C                                                                       MIBS  80
      WRITE(3,34)NUMBMX,NUMHMX,FRCTBL,NUMBMN,NUMHMN,ICODE,NAME         MIBS  81
   34 FORMAT('1',T20,'MONOISOTOPIC MASS SPECTRA OF THE BORANES'///      MIBS  82
     1'     FROM B',I2,'H',I2,10X,'  FRACTION B11=  ',                 MIBS  83
     2F6.4                                                              MIBS  84
     3    //'          TO B',I2,'H',I2//                               MIBS  85
     415X,I5,16A4///)                                                   MIBS  86
      WRITE (3, 780)   MAXROW, MAXCOL                                   MIBS  87
  780 FORMAT ('0',T20,' MAXROW=',I5,     '     MAXCOL=',I5)            MIBS  88
      WRITE(3,981)                                                      MIBS  89
      WRITE(3,980)(PDLMAS(I),PKSUM(I),I=1,MAXROW)                       MIBS  90
  980 FORMAT(4(5X,F10.3,F10.3))                                         MIBS  91
  981 FORMAT('0   EXPERIMENTAL INTENSITIES AND MASSES      '//)        MIBS  92
C                                                                       MIBS  93
C     SOLN OF SIMULTANEOUS EQNS (LLSQ FROM IBM SSP)                     MIBS  94
      CALL LLSQ(A   , PKSUM, MAXROW, MAXCOL, 1,PKONE,   IPIV, EPS, IER, MIBS  95
     1 AUX)                                                             MIBS  96
C                                                                       MIBS  97
C     FIND THE FRACTION OF TOTAL PEAKS AND BASE RELATIVE INTENSITY      MIBS  98
      SUMONE= 0.                                                        MIBS  99
      ONEMAX= PKONE(1)                                                  MIBS 100
      DO 39 I=1,MAXCOL                                                  MIBS 101
      IF(PKONE(I))39,39,40                                              MIBS 102
   40 SUMONE= SUMONE + PKONE(I)                                         MIBS 103
      IF (PKONE(I)  - ONEMAX)  38, 39, 38                               MIBS 104
   39 ONEMAX=  PKONE(I)                                                 MIBS 105
   38 CONTINUE                                                          MIBS 106
      ONEMAX= 100./ONEMAX                                               MIBS 107
      SUMONE= 100./SUMONE                                               MIBS 108
      WRITE(3,35)                                                       MIBS 109
      SUMNOW=0.0                                                        MIBS 110
      DO 37 I=1,MAXCOL                                                  MIBS 111
      CLAST=  PKONE(I)*SUMONE                                           MIBS 112
      IF( CLAST   )115,116,116                                          MIBS 113
  115 SUMNOW=SUMNOW+CLAST                                               MIBS 114
  116 CONTINUE                                                          MIBS 115
C                                                                       MIBS 116
C     DATA PRINTOUT AND SOLUTION PRINTOUT                               MIBS 117
      REL=  PKONE(I)*ONEMAX                                             MIBS 118
      J=.FIX(ONEMAS(I))                                                 MIBS 119
      PK(J)=REL                                                         MIBS 120
      IF(REL.LE.0.0) PK(J)=0.0                                          MIBS 121
      WRITE(3,36) I,ONEMAS(I),PKONE(I),REL,CLAST,IB(I),IH(I)            MIBS 122
   36 FORMAT(I10,2F15.3,10X,2F15.3,10X,2I5)                             MIBS 123
   37 CONTINUE                                                          MIBS 124
   35 FORMAT('0  PEAK NO.     911 MASS          B11 INTENSITY     RELATIVEMIBS 125
     2  INTENSITY      FRACTIONAL INTENSITY'//)                         MIBS 126
      N=ELOAT(MAXROW)                                                   MIBS 127
      AUX(1)= SQRT(AUX(1)/N)                                            MIBS 128
      WRITE(3,117)IER,AUX(1),SUMNEG                                     MIBS 129
  117 FORMAT('0   IER=  ',I5,'  LST SQ RMS =  ',E15.7,'      NEGATIVMIBS 130
     1ES=  ',F16.5)                                                     MIBS 131
      WRITE(3,982)                                                      MIBS 132
  982 FORMAT('0                                  DEVIATIONS'/)         MIBS 133
      N=MAXCOL+1                                                        MIBS 134
      WRITE(3,983)          (PKSUM(I),I=N,MAXROW)                       MIBS 135
  983 FORMAT(8E15.6)                                                    MIBS 136
      GO TO 114                                                         MIBS 137
C                                                                       MIBS 138
   99 CALL EXIT                                                         MIBS 139
      END                                                               MIBS 140
C                                                                       MIBS 141
      FUNCTION RLABUN(N,K,FRCTKK)                                       MIBS 142
C     CALCULATES RELATIVE ABUNDANCES OF MIXED ISOTOPE MOLECULES         MIBS 143
      DOUBLE PRECISION FRCTK,FRCTL,W,ONOM1,ONOM2,UNUM,FRCTKK,RLABUN     MIBS 144
      FRCTK=FRCTKK                                                      MIBS 145
      FRCTL=1.-FRCTK                                                    MIBS 146
      UNUM=1.00 00                                                      MIBS 147
      ONOM1=1.00 00                                                     MIBS 148
      ONOM2=1.00 00                                                     MIBS 149
      KK=K-1                                                            MIBS 150
      IF (KK)60,60,61                                                   MIBS 151
   61 DO 62 I=1,KK                                                      MIBS 152
   62 ONOM1=ONOM1*FLOAT(I)                                              MIBS 153
   60 KKK=N-K+1                                                         MIBS 154
      IF (KKK)63,63,64                                                  MIBS 155
   64 DO 65 I=1,KKK                                                     MIBS 156
   65 ONOM2=ONOM2*FLOAT(I)                                              MIBS 157
   63 DO 66 I=1,N                                                       MIBS 158
   66 UNUM=UNUM*FLOAT(I)                                                MIBS 159
   67 W=UNUM/(ONOM1*ONOM2)                                              MIBS 160
      RLABUN=W*FRCTL**(N-K+2)/FRCTL*FRCTK**K/(FRCTK**(N+1))             MIBS 161
      RETURN                                                            MIBS 162
      END                                                               MIBS 163
```

described when we discuss the sources of error. The conventional method provides no objective procedure to be followed when such internal inconsistencies arise.

Method

To remedy the situation a computer program was written which places no special weight on any peak, uses all the available information, and performs a least-squares fit restricted to positive solutions (Table I). The procedure for calculating monoisotopic borane spectra can be formulated as follows. The measured intensity at any mass, P_i, is the sum of the abundances, p_{ij}, of the different formulas which have isotopic variants at that mass. These in turn may be expressed in terms of the intensity of the monoisotopic ^{11}B ion with the same formula, m_j as in (1).

$$P_i = \sum_j p_{ij} = \sum_j r_{ij} m_j \qquad (1)$$

The fraction of the total number of ions with a set formula due to the mixed isotope containing n ^{11}B and m ^{10}B atoms, $a(n,m)$, is a function of the number of distinguishable ways one can arrange the two isotopes (*i.e.*, a binomial coefficient, the factorials in formula 2), and the fractional abundances of the ^{10}B and ^{11}B isotope, f_{10} and f_{11}, respectively, as shown in (2).

$$a(n,m) = (n + m)!f_{11}{}^n f_{10}{}^m/n!m! \qquad (2)$$

The ratio of the fraction of the isotopically mixed to that of the isotopically pure variety of the same formula, $r(n,m)$, is expressed by (3).

$$r(n,m) = a(n,m)/a(n + m,0) = (n + m)!f_{10}{}^m/n!m!f_{11}{}^m \qquad (3)$$

Equation 1 with the r_{ij} defined by (3) can be expressed in matrix form, $RM = P$. If there are k formulas in

Table II

Mass	Monoisotopic, lit.[a]	Polyisotopic calcd, lit.[b]	Polyisotopic, experimental[c]	Polyisotopic, calcd, LSTSQ[d]	Monoisotopic, LSTSQ[e]
50		0.01	0.10	0.10	
51		0.11	0.20	0.20	
52		0.92	1.30	1.15	
53		4.21	5.40	5.27	
54		10.88	13.50	13.59	
55	9.70	16.67	20.80	20.80	12.77
56	7.70	18.52	23.10	23.08	10.06
57	12.10	21.30	26.50	26.52	15.98
58	11.00	22.03	27.40	27.38	14.15
59	13.70	19.92	24.60	24.60	18.46
60	15.70	10.62	12.90	12.89	19.69
61	0.80	2.01	2.50	2.50	1.49
62	2.10	1.49	1.70	1.70	2.32
63		1.74	2.00	2.00	0.10
64		7.45	7.80	7.80	0.19
65		20.25	20.70	20.66	
66	5.70	35.23	35.40	35.47	6.36
67	22.50	41.54	41.50	41.45	24.30
68	16.60	43.86	44.00	44.04	15.71
69	14.70	57.30	57.70	57.68	18.57
70	32.40	79.11	79.40	79.41	29.57
71	5.80	100.00	100.00	100.00	12.37
72	100.00	88.00	86.00	86.00	100.00
73	3.30	49.25	49.40	49.40	5.49
74	46.60	48.58	48.20	48.21	47.13
75	0.30	34.16	34.10	34.11	1.82
76	39.20	23.21	22.60	22.60	40.15
RMD	2.23				0.06

[a] B_5^+ to $B_6H_{10}^+$, S. G. Gibbons and I. Shapiro, *J. Chem. Phys.*, **30**, 1483 (1959). [b] Polyisotopic spectrum recalculated from *a*. [c] Experimental polyisotopic spectrum from *a* for B_6H_{10}. [d] Polyisotopic spectrum recalculated from data in last column. [e] Monoisotopic spectrum, this work, Table VI.

Table III

Formula	Intensities $B_2H_6(-)$[a]	Intensities B_2H_6[b]
B	0.00	14.98
BH	0.24	5.01
BH_2	7.33	12.63
BH_3	3.16	0.51
BH_4	20.34	0.00
B_2	0.00	2.03
B_2H	0.00	5.51
B_2H_2	13.14	65.26
B_2H_3	100.00	23.55
B_2H_4	2.96	48.41
B_2H_5	0.00	100.00
B_2H_6	0.00	2.43
RMD	0.512	0.012

[a] R. E. Enrione and R. Rosen, *Inorg. Chim. Acta*, **1**, 169 (1967). [b] F. J. Norton, *J. Amer. Chem. Soc.*, **71**, 3489 (1949).

the monoisotopic spectrum, M, and l experimental intensities in the polyisotopic spectrum, P, then R is a

Table IV

B_4H_{10}[a]

Formula	Intensities	Formula	Intensities
B	24.63	B_3H_2	24.44
BH	4.33	B_3H_3	24.17
BH_2	19.20	B_2H_4	13.51
BH_3	0.47	B_3H_5	31.98
BH_4	0.30	B_3H_6	3.50
BH_5	0.10	B_3H_7	0.00
B_2	0.82	B_3H_8	0.36
B_2H	1.89	B_3H_9	0.26
B_2H_2	6.45	B_4	7.98
B_2H_3	4.11	B_4H	15.10
B_2H_4	2.20	B_4H_2	16.72
B_2H_5	6.81	B_4H_3	27.80
B_2H_6	0.17	B_4H_4	68.66
B_2H_7	0.24	B_4H_5	20.49
B_2H_8	0.02	B_4H_6	100.00
B_3	1.99	B_4H_7	13.08
B_3H	6.38	B_4H_8	11.20
		B_4H_9	0.00
		B_4H_{10}	0.43
		RMD	0.352

$B_4H_{10}(-)$[b]

Formula	Intensities
BH_3	0.07
BH_4	0.76
B_2H	0.10
B_2H_2	0.18
B_2H_3	1.32
B_2H_4	2.87
B_2H_5	0.32
B_3H_5	10.05
B_3H_6	4.03
B_3H_7	100.00
B_4H_7	0.40
B_4H_8	0.84
B_4H_9	5.50
RMD	1.635

[a] Manufacturing Chemists Association, Serial No. 30, 1960. [b] Unpublished polyisotopic data which is the basis of the monoisotopic spectrum published, D. F. Munro, J. E. Ahnell, and W. S. Koski, *J. Phys. Chem.*, **72**, 2682 (1968).

kxl matrix of coefficients defined by (3). One cannot simply find the inverse of R since it is not a square matrix. Rather, we reduced the matrix of coefficients to upper triangular form by a Householder transformation. Then the function, F, is reduced to a minimum by an iterative method: $F = |P - RM|$. This is equivalent to minimizing $(P - RM)$.[2]

The accuracy of this technique was tested by reproducing a monoisotopic spectrum from the polyisotopic spectrum previously calculated from it. The useful-

Table V

Formula	Intensities $B_5H_9(-)$[a]	B_5H_9[b]	B_5H_{11}[c]
B	0.00	48.63	36.01
BH	0.00	7.28	10.42
BH_2	0.00	28.91	40.71
BH_3	0.00	0.00	3.60
BH_4	0.00	0.00	0.88
B_2	0.00	0.63	0.00
B_2H	0.00	2.96	0.16
B_2H_2	1.20	4.84	7.36
B_2H_3	2.81	3.09	6.21
B_2H_4	0.89	0.51	1.46
B_2H_5	1.93	2.54	13.77
B_2H_6	0.00	0.47	1.19
B_2H_7	0.00	0.52	3.06
B_2H_8	0.00	0.18	0.25
B_3	0.00	1.64	2.81
B_3H	0.39	2.96	3.59
B_3H_2	0.19	10.10	16.85
B_3H_3	3.67	7.71	17.96
B_3H_4	28.12	4.02	12.21
B_3H_5	6.95	1.06	27.90
B_3H_6	0.00	1.17	5.11
B_3H_7	0.00	0.06	0.83
B_3H_8	0.00	0.00	0.00
B_3H_9	0.00	0.00	2.37[d]
B_3H_{10}	0.00	0.00	3.67[d]
B_4	0.00	5.33	7.34
B_4H	0.00	9.34	14.79
B_4H_2	0.00	15.64	24.57
B_4H_3	48.16	18.10	33.73
B_4H_4	0.00	40.15	63.78
B_4H_5	5.43	8.48	19.65
B_4H_6	16.89	4.86	17.78
B_4H_7	0.00	0.30	1.87
B_4H_8	0.00	0.00	6.57
B_4H_9	0.00	0.00	0.63
B_4H_{10}	0.00	0.00	0.45
B_5	0.00	20.68	17.52
B_5H	0.00	15.33	11.91
B_5H_2	0.00	19.94	22.21
B_5H_3	2.34	18.60	15.96
B_5H_4	0.00	19.05	19.97
B_5H_5	0.00	100.00	79.81
B_5H_6	0.38	6.23	15.48
B_5H_7	13.72	72.61	100.00
B_5H_8	100.00	2.64	12.29
B_5H_9	23.12	75.65	32.39
B_5H_{10}			0.75
B_5H_{11}			0.69
RMD	0.651	0.120	0.512

[a] See footnote *a* of Table III. [b] American Petroleum Institute Project 44, National Bureau of Standards No. 334, Mass Spectra Data, U. S. Government Printing Office, Washington, D. C., 1949. [c] Manufacturing Chemists Association Research Project, No. 31, Mass Spectra Data, 1960. [d] Impurities suspected.

Table VI

Formula	Intensities B_6H_{10}[a]	B_6H_{12}[b]	Formula	Intensities B_6H_{10}	B_6H_{12}
BH_3	0.50	0.00	B_4H_6	0.05	23.88
B_2	0.42	1.77	B_4H_7	0.12	1.04
B_2H	1.08	3.57	B_4H_8	0.00	1.07
B_2H_2	2.76	15.40	B_4H_9	0.00	0.32
B_2H_3	1.92	10.10	B_5	12.77	24.66
B_2H_4	0.38	6.48	B_5H	10.06	18.32
B_2H_5	0.55	21.10	B_5H_2	15.98	31.78
B_2H_6	1.01	0.84	B_5H_3	14.15	24.70
B_2H_7	0.45	1.52	B_5H_4	18.46	34.10
B_2H_8	0.17	0.15	B_5H_5	19.69	75.29
B_3	0.80	2.18	B_5H_6	1.49	6.25
B_3H_7	1.63	4.26	B_5H_7	2.32	49.01
B_3H_2	4.39	17.01	B_5H_8	0.10	1.32
B_3H_3	3.10	16.83	B_5H_9	0.19	29.74
B_3H_4	1.71	16.63	B_6	6.36	4.39
B_3H_5	0.34	8.65	B_6H	24.30	20.76
B_3H_6	0.94	17.14	B_6H_2	15.71	12.87
B_3H_7	0.17	0.26	B_6H_3	18.57	14.84
B_3H_8	0.00	0.00	B_6H_4	29.57	22.41
B_3H_9	0.00	1.38	B_6H_5	12.37	7.38
B_4	2.69	6.96	B_6H_6	100.00	100.00
B_4H	3.61	12.13	B_6H_7	5.49	7.46
B_4H_2	6.56	20.70	B_6H_8	47.13	55.82
B_4H_3	7.89	31.92	B_6H_9	1.82	4.22
B_4H_4	6.54	52.93	B_6H_{10}	40.15	39.55
B_4H_5	2.75	16.80	B_6H_{11}		7.51
			B_6H_{12}		1.42
RMD	0.060	0.126			

[a] See footnote *a*, Table II. [b] C. A. Lutz, D. A. Phillips, and D. M. Ritter, *Inorg. Chem.*, 3, 1191 (1964).

Table VII

Formula	Intensities B_7H_{11}[a]	B_7H_{13}[a]
B_7	0.00	28.67
B_7H	0.00	40.08
B_7H_2	26.90	0.00
B_7H_3	7.67	51.72
B_7H_4	18.83	7.36
B_7H_5	23.03	0.00
B_7H_6	13.32	55.78
B_7H_7	100.00	53.30
B_7H_8	14.80	29.30
B_7H_9	43.44	41.07
B_7H_{10}	0.00	0.00
B_7H_{11}	48.82	100.00
B_7H_{12}	0.00	0.00
B_7H_{13}	0.00	53.14
RMD	0.935	5.1

[a] T. P. Fehlner and W. S. Koski, *J. Amer. Chem. Soc.*, **86**, 1012 (1964).

ness of the method was determined by comparing its results with the seven monoisotopic spectra of boranes in the literature which were published together with their original polyisotopic data. Judged by the criterion of the root mean square deviation, RMD, of the calculated from the observed polyisotopic spectrum,

Table VIII[a]

B_8H_{12}[a]				B_8H_{18}[b]			
Formula	Intensities	Formula	Intensities	Formula	Intensities	Formula	Intensities
B	21.11	B_6	2.25	B	37.79	B_6	0.29
BH	0.78	B_6H	7.45	BH	5.55	B_6H	3.30
BH_2	18.99	B_6H_2	7.07	BH_2	40.05	B_6H_2	3.31
		B_6H_3	7.62	BH_3	5.73	B_6H_3	3.60
B_2H	0.09	B_6H_4	9.94			B_6H_4	4.80
B_2H_2	1.23	B_6H_6	6.69	B_2H_2	12.16	B_6H_5	2.60
B_2H_3	0.62	B_6H_7	4.24	B_2H_3	11.25	B_6H_6	13.58
B_2H_4	1.43	B_6H_9	1.90	B_2H_4	9.50	B_6H_7	1.54
		B_6H_{10}	1.16	B_2H_5	37.52	B_6H_8	9.29
B_3H	0.23					B_6H_9	1.57
B_3H_2	1.25	B_7	10.78	B_3	0.08	B_6H_{10}	6.24
B_3H_3	0.86	B_7H	8.97	B_3H	1.96	B_7	1.24
B_3H_4	0.97	B_7H_2	12.71	B_3H_2	10.68	B_7H	1.03
B_3H_6	0.15	B_7H_3	16.10	B_3H_3	16.79	B_7H_2	1.65
		B_7H_4	7.43	B_3H_4	15.82	B_7H_3	0.94
B_4	0.78	B_7H_5	12.45	B_3H_5	27.46	B_7H_4	2.19
B_4H_2	4.28	B_7H_6	4.80	B_3H_6	22.25	B_7H_5	0.67
B_4H_3	4.82	B_7H_7	1.54			B_7H_6	1.87
B_4H_4	5.45	B_7H_8	1.42	B_4	4.37	B_7H_7	2.21
B_4H_5	1.26	B_7H_{10}	1.31	B_4H	6.95	B_7H_8	0.72
B_4H_7	0.17			B_4H_2	11.78	B_7H_9	1.24
B_4H_9	1.04	B_8	12.96	B_4H_3	24.56	B_8	1.40
		B_8H	14.06	B_4H_4	42.43	B_8H	0.56
B_5H	3.71	B_8H_3	24.90	B_4H_5	28.19	BlH_2	0.70
B_5H_2	5.02	B_8H_4	9.76	B_4H_6	100.00	B_8H_3	0.00
B_5H_3	5.03	B_8H_5	11.69	B_4H_7	62.18	B_8H_4	1.05
B_5H_4	4.56	B_8H_6	100.00	B_4H_8	83.08	B_8H_5	0.67
B_5H_5	2.52	B_8H_7	7.52	B_4H_9	25.62	B_8H_6	3.52
B_5H_6	0.10	B_8H_8	56.63	B_4H_{10}	0.89	B_8H_7	0.67
B_5H_7	0.40	B_8H_9	6.91	B_5	3.06	B_8H_8	2.72
B_5H_8	0.06	B_8H_{10}	49.37	B_5H	6.40	B_8H_9	0.97
		B_8H_{11}	7.34	B_5H_2	5.66	B_8H_{10}	2.67
		B_8H_{12}	45.92	B_5H_3	7.19	B_8H_{11}	0.45
				B_5H_4	11.06	B_8H_{12}	1.28
RMD	0.208			B_5H_5	20.95	B_8H_{14}	0.12
				B_5H_6	5.45	B_8H_{16}	0.02
				B_5H_7	22.20	B_8H_{18}	0.08
				B_5H_8	4.12		
				B_5H_9	12.66		
				B_5H_{10}	0.82		
				RMD	0.449		

[a] S. J. Steck, G. A. Pressley, F. E. Stafford, J. Dobson, and R. Schaeffer, *Inorg. Chem.*, **9**, 2452 (1970). [b] S. J. Steck, G. A. Pressley, F. E. Stafford, J. Dobson, and R. Schaeffer, *ibid.*, **8**, 830 (1969).

the present method provided an RMD 28 times smaller, on the average, than the monoisotopic spectra published previously. Table II compares the two methods.

Results

The 36 polyisotopic spectra of the boranes could be found in the literature and all but one were fitted with monoisotopic spectra. The spectrum for each compound with the minimum RMD is reported in the accompanying tables. Negative ion spectra are marked (−). The RMD is reported with each as a measure of the reliability or internal consistency of the spectra. If one may generalize from the spectra which could be studied, the RMD deviation of these results is on the average at least 25 times smaller than those now in the literature (Tables III–X).

Errors

The first and dominant source of error in the calculation of monoisotopic spectra is the presence of impurities in the sample. The large RMD of some of the spectra is certainly due to this. The least-squares technique minimizes but does not eliminate the problem. Hydrogen, whether present as a contaminant or as a thermolytic product, was ignored by disregarding masses below 10 daltons. In three cases polyisotopic spectra were corrected for obvious impurities, air and HBr. In the first case, the intensities at masses 28, 29, 32, and

Table IX

B_9H_{15}[a]

Formula	Intensities	Formula	Intensities
B	71.11	B_6H_2	8.83
BH	20.10	B_6H_3	8.63
BH_2	108.86[b]	B_6H_4	12.87
BH_3	10.35	B_6H_5	3.48
BH_4	1.60	B_6H_6	9.20
		B_6H_7	2.17
B_2	0.62	B_6H_8	3.38
B_2H	2.18	B_6H_9	1.73
B_2H_2	17.15	B_6H_{10}	2.08
B_2H_3	9.03		
B_2H_4	12.60	B_7	10.48
B_2H_5	27.90	B_7H	4.87
B_2H_6	5.38	B_7H_2	11.32
B_2H_7	3.56	B_7H_3	13.30
		B_7H_4	10.37
B_3	1.16	B_7H_5	5.47
B_3H	0.45	B_7H_6	8.31
B_3H_2	4.10		
B_3H_3	3.88	B_8	13.97
B_3H_4	5.23	B_8H	13.29
B_3H_5	1.52	B_8H_2	0.00
B_3H_6	4.39	B_8H_3	14.47
B_3H_7	0.64	B_8H_4	26.09
		B_8H_5	8.10
B_4	2.07	B_8H_6	44.42
B_4H	2.34	B_8H_7	5.95
B_4H_2	4.73	B_8H_8	13.75
B_4H_3	11.35	B_8H_9	12.48
B_4H_4	7.87	B_8H_{10}	6.08
B_4H_5	3.92		
B_4H_6	1.76	B_9	14.29
B_4H_7	0.05	B_9H	9.93
B_4H_8	12.91	B_9H_2	11.97
B_4H_9	11.94	B_9H_3	12.43
B_4H_{10}	2.47	B_9H_4	4.92
		B_9H_5	16.42
B_5	4.90	B_9H_6	6.45
B_5H	2.57	B_9H_7	100.00
B_5H_2	8.41	B_9H_8	6.45
B_5H_3	6.65	B_9H_9	55.95
B_5H_4	13.32	B_9H_{10}	11.04
B_5H_5	3.14	B_9H_{11}	96.28
B_5H_6	1.04	B_9H_{12}	5.51
B_5H_7	0.20	B_9H_{13}	29.77
		B_9H_{14}	0.00
B_6	1.53	B_9H_{15}	0.00
B_6H	7.45		
RMD	0.711		

[a] See footnote *b*, Table VIII. [b] Impurities suspected.

40 were set to zero.[3] In the second the best fit was obtained by subtracting 11 units from masses 80 and 82.[4] In the third case masses 27, 29, 31, 39, 40, 41, 42, and 43 were set to zero.[5] Borane contaminants or thermolytic products have no effect upon the fit of the monoisotopic spectrum.

It has been suggested that the use of incorrect formulas for the ions in the monoisotopic spectrum produces negative intensities.[6] Apart from other sources of error such as the presence of impurities (compounds containing elements other than boron and hydrogen), this is not generally so. If one assumes the presence of ions with higher molecular weights or nonexistent ions, the intensities of these formulas will be zero and have no effect upon the calculation. The exception to this rule arises when we are dealing with compounds at least as complex as B_6H_{12}. In such cases two formulas in the monoisotopic spectrum may occur at the same mass, for example B_6^+ and $B_5H_{11}^+$. Neither with the conventional method nor with the matrix technique can we solve for the intensity of both formulas simultaneously. One must be chosen. In the present work the formula providing the smallest RMD was selected.

While several authors have noted that negative intensities arise while subtracting the intensities of isotopically mixed ions from the experimental measurements, none seems to have observed that this is only the most obvious manifestation of a widespread phenomenon. First, negative intensities calculated for monoisotopic peaks are only the most visible form of intensities which are too low. Second, such solutions occur in series or groups, at alternate masses. Finally, equally serious, though not at all obvious, the intensities between the negative (or low) solutions are too high. These conclusions are clear if one goes to the trouble of calculating an exact polyisotopic spectrum and then deliberately tampering with one of the intensities. The phenomenon is independent of the method by which the monoisotopic spectrum is calculated; it seems to be a property of simultaneous equations coupled in the fashion found here. A too high (too low) solution arising for any reason forces the solution at the next lowest mass to be too low (too high) and so on. The perturbing error oscillates away from its source, damped as it moves on. The least-squares technique of the present work damps the error oscillation more rapidly than the conventional technique, and by accepting only positive solutions it limits the magnitude of the perturbation.

Another source of inconsistency in the spectra calculated by the method is the variety of mass spectrometers which collected the polyisotopic data. The variety of ionizing voltages, source temperatures, detector systems, and gross geometry behind the data prevents the monoisotopic data from being completely comparable. Until some one laboratory has the time and resources to generate a complete set of comparable spectra, this is the best we are able to do. Since we believe that we have calculated monoisotopic spectra from all the polyisotopic borane spectra published before

(3) A. Quayle, *J. Appl. Chem.*, **9**, 395 (1959).

(4) J. F. Ditter, J. R. Spielman, and R. E. Williams, *Inorg. Chem.*, **5**, 118 (1966).

(5) S. J. Steck, G. A. Pressley, F. E. Stafford, J. Dobson, and R. Schaeffer, *ibid.*, **9**, 2452 (1970).

(6) J. F. Ditter, F. J. Gerhart, and R. E. Williams, *Advan. Chem. Ser.*, **No. 72**, 191 (1968).

Table X

Formula	Intensities $B_{10}H_{14}(-)$[a]	Intensities $B_{10}H_{14}$[b]	Intensities $B_{10}H_{16}$[c]
B		3.47	4.80
BH		0.34	0.89
BH_2		6.31	2.89
BH_3		1.28	8.30
BH_4		0.00	33.13
BH_5		0.00	38.74
BH_6		0.00	29.18
BH_7		0.00	1.23[d]
BH_8		0.00	1.62[d]
B_2		0.00	0.00
B_2H		0.10	0.00
B_2H_2		0.39	0.66
B_2H_3		0.60	3.08
B_2H_4		0.14	0.00
B_2H_5		1.44	0.00
B_2H_6		0.00	0.00
B_2H_7		0.00	2.48[d]
B_2H_8		0.00	3.54[d]
B_3		0.00	0.00
B_3H		0.22	1.03
B_3H_2		0.56	1.19
B_3H_3		0.58	0.87
B_3H_4		0.40	2.29
B_3H_5		0.24	0.00
B_3H_6		0.16	0.00
B_3H_7		0.00	8.78
B_3H_8		0.00	0.00
B_3H_9		0.00	11.24[d]
B_3H_{10}		0.00	35.74[d]
B_4		0.00	0.00
B_4H		0.18	0.00
B_4H_2		0.98	3.14
B_4H_3		1.00	3.51
B_4H_4		0.70	8.66
B_4H_5		0.42	1.10
B_4H_6		0.37	0.00
B_4H_7		0.58	0.00
B_4H_8		2.18	0.00
B_5H		4.74	0.34
B_5H_2		10.98	43.07
B_5H_3		7.59	19.59
B_5H_4		10.92	40.59
B_5H_5		1.21	44.12
B_5H_6		0.19	8.84
B_5H_7		0.00	24.74
B_5H_8		0.00	1.12
B_5H_9		0.00	20.40
B_6		0.32	0.00
B_6H		1.82	12.05
B_6H_2		1.38	12.51
B_6H_3		2.89	0.00
B_6H_4		1.06	30.69
B_6H_5		0.83	18.50
B_6H_6		0.00	11.38
B_7		2.68	4.79
B_7H		1.60	0.62
B_7H_2		2.84	9.76
B_7H_3		3.93	17.71
B_7H_4	0.48	0.76	0.00
B_7H_5	0.38	1.80	9.63
B_7H_6	0.84	0.00	0.00
B_7H_7	1.96	0.00	11.81
B_7H_8	0.00	0.00	3.37
B_8	0.00	6.17	13.05
B_8H	0.00	3.75	6.32
B_8H_2	0.00	5.96	9.68
B_8H_3	0.00	6.61	16.31
B_8H_4	0.00	7.34	8.01
B_8H_5	0.00	0.73	19.44
B_8H_6	2.01	1.44	0.00
B_8H_7	9.09	0.00	10.01
B_8H_8	80.97	0.00	1.98
B_9	0.00	11.27	15.66
B_9H	0.00	3.13	2.88
B_9H_2	0.00	15.17	15.47
B_9H_3	0.00	12.97	14.50
B_9H_4	0.00	11.45	11.33
B_9H_5	0.00	8.13	13.69
B_9H_6	3.97	4.01	9.39
B_9H_7	0.41	4.79	29.34
B_9H_8	24.50	1.39	9.23
B_9H_9	35.11	1.35	5.01
B_9H_{10}	5.62	0.00	0.00
B_9H_{11}	10.10	0.00	25.88
B_{10}	0.00	9.92	0.00
$B_{10}H$	0.00	11.55	0.00
$B_{10}H_2$	0.00	5.34	0.00
$B_{10}H_3$	0.00	9.36	13.99
$B_{10}H_4$	0.00	10.98	7.51
$B_{10}H_5$	0.00	17.98	0.00
$B_{10}H_6$	0.00	45.04	35.55
$B_{10}H_7$	0.00	7.97	0.00
$B_{10}H_8$	36.02	100.00	100.00
$B_{10}H_9$	69.69	0.00	5.71
$B_{10}H_{10}$	67.05	72.79	39.75
$B_{10}H_{11}$	33.30	0.00	3.06
$B_{10}H_{12}$	100.00	92.68	45.64
$B_{10}H_{13}$	55.03	3.00	0.00
$B_{10}H_{14}$	58.02	13.21	22.59
$B_{10}H_{15}$			0.00
$B_{10}H_{16}$			2.39
RMD	0.188	0.137	1.765

[a] See footnote *a* in Table III. [b] A. Quayle, *J. Appl. Chem.*, **9**, 395 (1959). [c] L. H. Hall and W. S. Koski, *J. Amer. Chem. Soc.*, **84**, 4205 (1962). [d] Impurities suspected.

1971, we will gladly send the results for any published data which a reader may think preferable to those reported in this article.

A variety of other sources of error are present. The neglect of double charged and metastable peaks is one. Rounding errors in the polyisotopic and monoisotopic

spectra is another. The assumption that there is no kinetic isotope effect is implicit in the statistics used to calculate the relative abundances. In fact the RMD reported for each spectrum is rather a measure of internal consistency than of the accuracy of the experimental data. Finally, the choice of the natural abundance of the isotopes and the assumption that it is constant is a final error source. In the calculations we assumed that the ^{11}B isotope was 0.8039 of the boron present. This agrees with the 0.804 used by Lipscomb in his nmr studies[7] and is the best estimate from nuclear measurements.[8] An attempt was made to improve the fit of large groups of spectra by adjusting the ^{11}B abundance, but the results were inconclusive.

Conclusion

From the tables of results (Tables III–X) it is clear that the negative ion mass spectra of many of the boranes have not been run. Many of the positive ion spectra are fragmentary. The spectra with a RMD greater than 1.0 should be repeated. The monoisotopic spectrum of $B_{20}H_{26}$ could not be calculated, probably because of the presence of impurities.[9]

(7) G. R. Eaton and W. N. Lipscomb, "NMR of Boron Hydrides and Related Compounds," W. A. Benjamin, New York, N. Y., 1969.

(8) G. Friedlander, J. W. Kennedy, and J. M. Miller, "Nuclear and Radiochemistry," Wiley, New York, N. Y., 1964.

(9) L. H. Hall and W. S. Koski, *J. Amer. Chem. Soc.*, **84**, 4205 (1962).

Viscosity of Liquid Mixtures

by Victor A. Bloomfield*[1] and R. K. Dewan

Department of Biochemistry, College of Biological Sciences, University of Minnesota, St. Paul, Minnesota 55101
(Received March 2, 1971)

Publication costs assisted by The National Institutes of Health

We have examined expressions connecting the viscosities of binary liquid mixtures with their thermodynamic properties, using the concepts of the absolute rate and free volume theories of flow. Explicit expressions for the thermodynamic mixing functions were obtained from the solution theory recently developed by Flory and coworkers. This theory lays particular stress on equation of state contributions to the excess mixing functions, which are of central importance in determining the free volume of the solution. Detailed numerical comparison of calculated contributions to the mixture viscosities—from an ideal mixture (linear superposition) viscosity expression and from enthalpic, entropic, and free volume corrections to ideal behavior—indicates that the data are well explained by either a free volume theory or an absolute rate theory approach. A combination of the two, as has been sometimes proposed, is markedly less satisfactory. Expressions were also obtained connecting intrinsic viscosities with thermodynamic properties. While the linear superposition theory is incapable of predicting negative (or positive) intrinsic viscosities for both components in a binary mixture, it was demonstrated that activation and free volume theories can predict these phenomena and are of reasonable quantitative accuracy.

I. Introduction

The prediction of the viscosity of liquid mixtures is a goal of long standing, with both theoretical and practical import. A truly fundamental theory would predict the viscosity, along with other thermodynamic and transport properties, from knowledge of the intermolecular forces and radial distribution function alone. Such a program has had appreciable success in application to pure, simple liquids such as the liquefied rare gases.[2] For solutions, however, although the general theory has been formulated,[3] it has not yet been reduced successfully to numerical results.

One is thus forced to approximate approaches, of which two general types may be distinguished. The first is that of continuum hydrodynamics, whose application to molecular problems is identified with the names of Einstein and Stokes. This approach, in which the discrete, molecular nature of the solvent is neglected, has been remarkably successful in explaining the viscosity of dilute solutions of high polymers. Its application to solutions in which both components are of comparable size is less appropriate.

The second general approach is to correlate the vis-

(1) Alfred P. Sloan Foundation Fellow.

(2) S. A. Rice and P. Gray, "The Statistical Mechanics of Simple Liquids," Interscience, New York, N. Y., 1965.

(3) (a) R. J. Bearman and J. G. Kirkwood, *J. Chem. Phys.*, **28**, 136 (1958); (b) R. J. Bearman, *J. Phys. Chem.*, **65**, 1961 (1961).

cosity of the mixture with the properties of the pure components and with thermodynamic parameters characteristic of the interaction between components. In simplest form, the interactions may be neglected and simple additive relations assumed. One such relation commonly used is

$$\ln \eta = X_1 \ln \eta_1 + X_2 \ln \eta_2 \quad (1)$$

where η is the viscosity of the solution, and X_1, X_2, η_1, and η_2 are the mole fractions and viscosities of the two components in a binary mixture. However, it will be noted that this equation, and other similar ones, predict monotonic increases or decreases of viscosity with composition. Such monotonicity is often not observed in practice. It is therefore generally necessary to take explicit account of interactions.

There are two major semiempirical theories of liquid viscosity. The first is the absolute reaction rate theory of Eyring and coworkers.[4] This relates the viscosity to the free energy needed for a molecule to overcome the attractive force field of its neighbors, so that it can jump (flow) to a new equilibrium position. Thus the deviation of the mixture viscosity from eq 1 should be related to the free energy—more precisely, the excess free energy—of mixing.[5,6] The second semiempirical theory is the free volume theory,[7-9] which relates the viscosity to the probability of occurrence of an empty neighboring site into which a molecule can jump. This probability is exponentially related to the free volume of the liquid, so deviations from eq 1 can be attributed to variations in the free volume of the solution.

Macedo and Litovitz[10] have argued that neither of these theories is entirely adequate in its own right, and that better results for pure liquids are obtained by combining them. Thus the probability for viscous flow is taken as the product of the probabilities of acquiring sufficient activation energy and of the occurrence of an empty site. It has been shown[11] that the assumption that these two probabilities are independent, and may therefore be multiplied, is incorrect for a one-dimensional liquid. While this conclusion also presumably holds in three dimensions, it will be of interest to investigate the consequences of the assumption of independent probabilities for viscosities of liquid mixtures in the treatment that follows.

The free energy and free volume data required in these viscosity theories may occasionally be available directly from experiment. This is often not the case, however, particularly for the free volume, whose operational definition is in any event somewhat ambiguous.[10] We have therefore preferred to obtain the thermodynamic parameters from a statistical thermodynamic theory of liquid mixtures proposed by Flory and coworkers.[12-14] This theory, which bears some similarities to the corresponding states theory of Prigogine and colleagues,[15] treats the properties of mixtures in terms of reduced properties of the pure components and a single interaction parameter. It thus has a minimum of adjustable parameters. The theory is applicable to mixtures of molecules of different sizes and lays particular stress on equation of state contributions to the thermodynamic excess functions, which are of central importance in determining the free volume of the solution.

Use of theoretical expressions for the thermodynamic properties of mixtures has the further advantage that an equation for the intrinsic viscosity, or the rate of change of viscosity with concentration at infinite dilution of one component, can be explicitly formulated by expanding the thermodynamic functions in a power series in concentration and keeping only the first nontrivial terms.

In this paper we shall first write down an equation for the viscosity of a liquid mixture in terms of the quantities which might contribute to it: the viscosities of the pure components and the changes in enthalpy, entropy, and free volume upon mixing. We then use the Flory[13] theory to obtain explicit expressions for these contributions in terms of properties of the pure components and an interaction parameter. The results are numerically compared with experimental data on the viscosities of several binary liquid mixtures over the whole range of relative composition. We then derive an equation for the intrinsic viscosity and apply it to these mixtures.

In the following paper we compare the "thermodynamic" intrinsic viscosity theory developed here with a continuum hydrodynamic treatment of the intrinsic viscosity of chain molecules, in calculating the intrinsic viscosities of a homologous series of n-alkanes.

II. Theory of Mixture Viscosity

Combining the absolute rate and free volume theories of viscosity, one obtains[4,9,10] for the viscosity of the solution

$$\eta = A \exp[\Delta G^{\ddagger}/RT + \gamma v^*/v_f] \quad (2)$$

$\Delta G^{\ddagger}$ is the activation free energy per mole of solution, R is the gas constant, and T is the absolute temperature. v^* is the empty volume which must be available for a molecular segment jumping to its new site, v_f is the free

(4) S. Glasstone, K. J. Laidler, and H. Eyring, "The Theory of Rate Processes," McGraw-Hill, New York, N. Y., 1941, Chapter 9.

(5) W. E. Roseveare, R. E. Powell, and H. Eyring, *J. Appl. Phys.*, **12**, 669 (1941).

(6) M. R. V. Krishnan and G. S. Laddha, *Ind. Eng. Chem., Fundam.*, **7**, 324 (1968).

(7) A. K. Doolittle, *J. Appl. Phys.*, **22**, 1471 (1951); **23**, 236 (1952).

(8) M. L. Williams, R. F. Landel, and J. D. Ferry, *J. Amer. Chem. Soc.*, **77**, 3701 (1955).

(9) M. H. Cohen and D. Turnbull, *J. Chem. Phys.*, **31**, 1164 (1959).

(10) P. B. Macedo and T. A. Litovitz, *ibid.*, **42**, 245 (1965).

(11) V. A. Bloomfield, *ibid.*, **52**, 2781 (1970).

(12) P. J. Flory, R. A. Orwoll, and A. Vrij, *J. Amer. Chem. Soc.*, **86**, 3507, 3515 (1964).

(13) P. J. Flory, *ibid.*, **87**, 1833 (1965).

(14) A. Abe and P. J. Flory, *ibid.*, **87**, 1838 (1965).

(15) I. Prigogine, "The Molecular Theory of Solutions," North-Holland Publishing Co., Amsterdam, 1957.

volume per segment in the solution, and γ is a factor of order unity. As will be seen below, v^* is also identified with the hard-core volume of a segment, and it is therefore implicitly assumed in eq 2 that viscous flow occurs by segmental motion rather than by motion of whole molecules. An equation of the same form holds for the pure components

$$\eta_i = A \exp[\Delta G_i^{\ddagger}/RT + \gamma v^*/v_{fi}] \qquad (i = 1, 2) \quad (3)$$

where the subscript labels the property of pure component i. (It should be noted that Macedo and Litovitz[10] write $\Delta E^{\ddagger}$, the energy of activation, for $\Delta G^{\ddagger}$ in these equations. Use of $\Delta G^{\ddagger}$ seems more consistent with the fundamental assumptions of absolute rate theory.)

Following Roseveare, *et al.*,[5] we now assume

$$\Delta G^{\ddagger} = X_1 \Delta G_1^{\ddagger} + X_2 \Delta G_2^{\ddagger} - \alpha \Delta G^{R} \qquad (4)$$

where ΔG^{R}, the residual free energy,[13] is closely related to the excess free energy of mixing as discussed below. α is a constant of order unity. In the absence of independent knowledge of the values or significance of α and γ, we shall henceforth set them both equal to unity.

Substitution of eq 4 in eq 2, taking logarithms of the resulting equation and of eq 3, and simple manipulation then yields

$$\ln \eta = X_1 \ln \eta_1 + X_2 \ln \eta_2 - \frac{\Delta G^{R}}{RT} + v^*\left(\frac{1}{v_f} - \frac{X_1}{v_{f1}} - \frac{X_2}{v_{f2}}\right) \quad (5)$$

The residual free energy of mixing can, in turn, be broken down into enthalpy and entropy contributions

$$\Delta G^{R} = \Delta H_M - T\Delta S^{R} \qquad (6)$$

ΔH_M is the enthalpy of mixing per mole of solution. ΔS^{R} is the residual entropy per mole;[13] that is, the entropy of mixing minus the combinatorial entropy. The residual entropy differs from the conventionally defined excess entropy of mixing in that the combinatorial entropy is not necessarily computed according to the ideal mixing law for molecules of the same size.

The free volume per segment is defined as the difference between the total volume per segment and the hard-core volume

$$v_f = v - v^* \qquad (7)$$

Further, we define a reduced volume

$$\tilde{v} = v/v^* \qquad (8)$$

Upon substitution of eq 6–8 into eq 5, we obtain

$$\ln \eta = X_1 \ln \eta_1 + X_2 \ln \eta_2 - \frac{\Delta H_M}{RT} + \frac{\Delta S^{R}}{R} + \left(\frac{1}{\tilde{v} - 1} - \frac{X_1}{\tilde{v}_1 - 1} - \frac{X_2}{\tilde{v}_2 - 1}\right) \quad (9)$$

$$= \ln \eta_{id} + \ln \eta_H + \ln \eta_S + \ln \eta_V$$

This equation displays explicitly the various contributions to the mixture viscosity: the ideal mixture viscosity computed from eq 1, the enthalpy and residual entropy of mixing, and the difference in free volume between solution and pure components.

III. Expressions for the Thermodynamic Functions

In this section we transcribe from the work of Flory, *et al.*,[12–14] the pertinent expressions for the thermodynamic quantities needed in eq 9. The reader is referred to the original papers for derivations and detailed discussion.

A molecule of type i may be characterized by the number of segments, r_i, it contains, and by the number of contact sites, S_i, per segment. (The definition of a segment is left somewhat vague, since in the final expressions all segment properties occur as ratios. The ratio of the number of segments of two molecules is taken as the ratio of their hard-core molar volumes V_i^*: $r_1/r_2 = V_1^*/V_2^*$.)

Then the segment fractions are

$$\phi_1 = \frac{r_1 X_1}{r_1 X_1 + r_2 X_2} \qquad (10)$$

and the site fraction of component 2 is

$$\theta_2 = \frac{r_2 S_2 X_2}{r_1 S_1 X_1 + r_2 S_2 X_2} \qquad (11)$$

One defines characteristic pressures P_1^* and P_2^* and characteristic temperatures T_1^* and T_2^* of the pure components. The method for determining P_i^*, T_i^*, and v^* from the specific volume, thermal expansion coefficient, and isothermal compressibility or thermal pressure coefficient has been presented by Flory, *et al.*,[12–14] who tabulate values of these for a number of liquids.

The reduced temperature of pure component i is

$$\tilde{T}_i = T/T_i^* \qquad (12)$$

while the reduced temperature of the mixture is

$$\tilde{T} = \frac{\phi_1 P_1^* \tilde{T}_1 + \phi_2 P_2^* \tilde{T}_2}{\phi_1 P_1^* + \phi_2 P_2^* - \phi_1 \theta_2 X_{12}} \qquad (13)$$

X_{12} is an interaction parameter with units of pressure, determined from the experimental ΔH_M at equimolar concentrations of components 1 and 2, and tabulated for numerous mixtures by Abe and Flory.[14]

The reduced volume of the mixture is the sum of the reduced volumes of the pure components and the reduced excess volumes

$$\tilde{v} = \tilde{v}^{\circ} + \tilde{v}^{E} \qquad (14)$$

where

$$\tilde{v}^{\circ} = \phi_1 \tilde{v}_1 + \phi_2 \tilde{v}_2 \qquad (15)$$

and $\tilde{v}^{E}$ can be written to adequate approximation as

$$\tilde{v}^E = (\tilde{v}^\circ)^{7/3}[4/3 - (\tilde{v}^\circ)^{1/3}](\tilde{T} - \tilde{T}^\circ) \quad (16)$$

$$\tilde{T}^\circ = [(\tilde{v}^\circ)^{1/3} - 1](\tilde{v}^\circ)^{-4/3} \quad (17)$$

The enthalpy of mixing is

$$\Delta H_M = X_1 P_1^* V_1^* \left(\frac{1}{\tilde{v}_1} - \frac{1}{\tilde{v}}\right) + X_2 P_2^* V_2^* \left(\frac{1}{\tilde{v}_2} - \frac{1}{\tilde{v}}\right) + \frac{X_1 V_1^* \theta_2}{\tilde{v}} X_{12} \quad (18)$$

We may define[15] a parameter C_i by

$$C_i = P_i^* V_i^* / R T_i^* \quad (19)$$

$3C_i$ is the effective number of external degrees of freedom per molecule of i. Then eq 18 becomes

$$\frac{\Delta H_M}{RT} = \frac{X_1 C_1}{\tilde{T}_1}\left(\frac{1}{\tilde{v}_1} - \frac{1}{\tilde{v}}\right) + \frac{X_2 C_2}{\tilde{T}_2}\left(\frac{1}{\tilde{v}_2} - \frac{1}{\tilde{v}}\right) + \frac{X_1 C_1 \theta_2 X_{12}}{\tilde{v}\tilde{T}_1 P_1^*} \quad (20)$$

The residual entropy is

$$\Delta S^R = -\frac{3X_1 P_1^* V_1^* \tilde{T}_1}{T} \ln \frac{\tilde{v}_1^{1/3} - 1}{\tilde{v}^{1/3} - 1} - \frac{3X_2 P_2^* V_2^* \tilde{T}_2}{T} \ln \frac{\tilde{v}_2^{1/3} - 1}{\tilde{v}^{1/3} - 1} \quad (21)$$

Introduction of eq 19 allows this to be rewritten as

$$\frac{\Delta S^R}{R} = 3X_1 C_1 \ln \frac{\tilde{v}_1^{1/3} - 1}{\tilde{v}^{1/3} - 1} - 3X_2 C_2 \ln \frac{\tilde{v}_2^{1/3} - 1}{\tilde{v}^{1/3} - 1} \quad (22)$$

Equations 14, 20, and 22, along with the tabulated properties of the pure components and the single interaction parameter X_{12}, enable calculation of the various contributions to the mixture viscosity according to eq 9.

IV. Comparison with Experimental Results

Table I summarizes the results of these calculations for four binary liquid mixtures as a function of X_2, the mole fraction of component 2. Experimental values of the mixture viscosities of CCl_4–C_6H_{12}, C_6H_6–C_6H_{12}, and C_6H_6–CCl_4 were determined by Grunberg;[16] those for the CCl_4–$C(CH_3)_4$ system by Thomaes and Van Itterbeek.[17] Necessary values of the thermodynamic properties of the pure components, and of the interaction parameter X_{12}, were obtained from the compilation by Abe and Flory.[14] The number of systems for which a comparison of calculated and experimental viscosities may be made, using the theory presented in this paper, is at present rather limited, because of the lack of suitable thermodynamic and viscosity data obtained under comparable conditions.

Columns 2–5 of Table I list the various terms in the viscosity expression defined in eq 9, while column 6 gives values of the free energy contribution, defined by $\eta_G = \eta_H\eta_S$. It is not clear *a priori* whether all of the contributions to the mixture viscosity in eq 9 are equally important and should be considered together in computing η. We have therefore tabulated in columns 7–12 various combinations of the calculated contributions to η, combining them multiplicatively in accord with the additive logarithmic relation in eq 9. The viscosity theories mentioned in the Introduction correspond to some of these combinations: the absolute rate theory to $\eta_{id}\eta_G$, the free volume theory to $\eta_{id}\eta_V$, and the Macedo–Litovitz[10] theory to $\eta_{id}\eta_V\eta_H$. The last column in Table I lists the experimental mixture viscosities.

The terms η_H, η_S, and η_V act as multiplicative corrective factors to the ideal mixture viscosity η_{id}. In the systems considered here, the enthalpy of mixing is positive. Thus $\Delta H^{\pm}$, the enthalpy of activation, is smaller for the mixtures than it is for the pure components, so that the work needed to form the activated complex for flow is lowered, and the viscosity of the mixture is smaller than predicted by η_{id}. The entropies of mixing in these systems are also uniformly positive. Therefore $\Delta S^{\pm}$ is either less positive or more negative for the real mixture than for the ideal one, in either case resulting in an increase in η over η_{id}. The free volumes of the mixtures are greater than those of the pure components, leading to increased fluidity or decreased viscosity according to the free volume theory.

Inspection of Table I reveals that the experimental viscosities are best reproduced by either $\eta_{id}\eta_G$ or $\eta_{id}\eta_V$, for which agreement within theory and experiment is generally within a couple of per cent. The worst case is probably the system benzene–cyclohexane, for which Abe and Flory[14] have observed that disparities between observed and calculated values of the thermodynamic properties are also rather large. It should be emphasized that the calculations employ no adjustable parameters, being dependent only on the properties of the pure components and a single interaction parameter determined from thermodynamic measurements at a single solution composition, $X_1 = X_2 = 1/2$.

The other calculated viscosity functions are less satisfactory, particularly for the rather nonideal systems CCl_4–C_6H_{12} and C_6H_6–C_6H_{12}. η_{id} is too large and, as remarked above, is a monotonic function of X_2 in contradiction to experiment. $\eta_{id}\eta_S$ is larger still. $\eta_{id}\eta_H$ is uniformly too low, and $\eta_{id}\eta_H\eta_V$ is even lower, since both the enthalpy and volume effects tend to increase the fluidity of the solution. Finally, the complete product $\eta_{id}\eta_H\eta_S\eta_V$ is roughly equal to $\eta_{id}\eta_H$, since the entropy and volume effects tend to cancel each other.

The slight discrepancies in Table I between calculated and experimental viscosities for the pure components are due to the fact that η was calculated from the various terms in eq 9, with $\tilde{v}$ not being set equal to $\tilde{v}_1$ or $\tilde{v}_2$ but instead being calculated from eq 14–17. There is

(16) L. Grunberg, *Trans. Faraday Soc.*, **50**, 1293 (1954).

(17) G. Thomaes and J. Van Itterbeek, *J. Mol. Phys.*, **2**, 372 (1959).

Table I: Calculated and Experimental Viscosities of Liquid Mixtures

X_2	η_{id}	η_H	η_S	η_V	η_G	$\eta_{id}\eta_H$	$\eta_{id}\eta_S$	$\eta_{id}\eta_G$	$\eta_{id}\eta_V$	$\eta_{id}\eta_H\eta_V$	$\eta_{id}\eta_H\eta_S\eta_V$	η_{exptl}
					1 = CCl_4, 2 = C_6H_{12}, 25°							
0.0	0.903	0.997	1.003	0.997	1.0	0.900	0.906	0.903	0.900	0.897	0.900	0.903[a]
0.230	0.899	0.955	1.105	0.984	0.969	0.859	0.912	0.871	0.885	0.845	0.858	0.867
0.471	0.895	0.940	1.019	0.980	0.958	0.841	0.912	0.857	0.877	0.824	0.840	0.857
0.728	0.891	0.952	1.016	0.983	0.967	0.848	0.904	0.861	0.876	0.834	0.847	0.858
1.0	0.886	0.997	1.003	0.996	1.00	0.883	0.889	0.886	0.883	0.880	0.883	0.886
					1 = C_6H_6, 2 = C_6H_{12}, 25°							
0.0	0.6	0.997	1.003	0.997	1.0	0.598	0.602	0.600	0.598	0.596	0.598	0.600[a]
0.215	0.652	0.792	1.067	0.931	0.845	0.517	0.696	0.551	0.608	0.482	0.513	0.574
0.451	0.715	0.719	1.095	0.906	0.787	0.514	0.783	0.563	0.648	0.466	0.510	0.601
0.756	0.806	0.789	1.068	0.931	0.842	0.635	0.860	0.679	0.750	0.592	0.632	0.712
1.0	0.886	0.997	1.003	0.996	1.00	0.883	0.889	0.886	0.883	0.880	0.883	0.886
					1 = C_6H_6, 2 = CCl_4, 25°							
0.0	0.600	0.997	1.003	0.997	1.00	0.598	0.602	0.600	0.598	0.596	0.598	0.600[a]
0.235	0.661	0.965	1.012	0.987	0.977	0.638	0.668	0.645	0.652	0.629	0.637	0.665
0.483	0.731	0.954	1.015	0.983	0.968	0.697	0.742	0.708	0.719	0.686	0.696	0.735
0.777	0.824	0.967	1.011	0.987	0.978	0.797	0.834	0.806	0.814	0.787	0.796	0.829
1.00	0.902	0.997	1.003	0.997	1.00	0.900	0.906	0.903	0.900	0.897	0.900	0.902
					1 = CCl_4, 2 = $C(CH_3)_4$, 0°							
0.0	1.351	0.996	1.003	0.996	1.00	1.346	1.356	1.351	1.345	1.340	1.345	1.351[b]
0.168	1.084	0.919	1.005	0.980	0.924	0.996	1.090	1.001	1.062	0.976	0.981	1.065
0.377	0.824	0.873	1.006	0.970	0.878	0.719	0.829	0.723	0.800	0.698	0.702	0.808
0.482	0.718	0.867	1.006	0.969	0.872	0.622	0.722	0.626	0.696	0.603	0.607	0.704
0.747	0.507	0.899	1.005	0.976	0.904	0.456	0.510	0.458	0.495	0.445	0.448	0.500
1.00	0.364	0.997	1.003	0.997	1.00	0.363	0.365	0.364	0.363	0.362	0.363	0.364

[a] Reference 16. [b] Reference 17.

a small difference between $\tilde{T}^\circ$ computed from eq 17 and the reduced temperature tabulated[14] for the pure component, which is used to compute $\tilde{T}$, eq 13. Thus the excess volume, $\tilde{v}^E$, does not quite vanish according to eq 16, leading to a small difference between $\tilde{v}$ and $\tilde{v}^\circ$ according to eq 14.

V. Intrinsic Viscosity

The intrinsic viscosity of solute (component 2), $[\eta]_2$, is defined as

$$[\eta]_2 = \lim_{C_2 \to 0} \frac{\eta - \eta_1}{\eta_1 C_2} \tag{23}$$

where C_2 is the solute concentration in grams per cubic centimeter. An equivalent definition is

$$[\eta]_2 = \lim_{C_2 \to 0} \frac{\ln (\eta/\eta_1)}{C_2} \tag{24}$$

If the molecular weight of solute is M_2, and the molar volume of solvent is V_1, the mole fraction of solute is, in the limit of vanishing C_2, $X_2 = n_2/(n_1 + n_2) \approx n_2/n_1 = C_2V_1/M_2$, so eq 24 may be rewritten

$$[\eta]_2 = \frac{V_1}{M_2} \lim_{X_2 \to 0} \frac{\ln (\eta/\eta_1)}{X_2} \tag{25}$$

Combination of eq 25 and 9 then leads to

$$[\eta]_2 = \frac{V_1}{M_2}\left[\ln \frac{\eta_2}{\eta_1} - \lim_{X_2 \to 0} \frac{\Delta H_M}{X_2 RT} + \lim_{X_2 \to 0} \frac{\Delta S^R}{X_2 R} + \left(\frac{1}{\tilde{v}_1 - 1} - \frac{1}{\tilde{v}_2 - 1}\right) + \lim_{X_2 \to 0} \frac{1}{X_2}\left(\frac{1}{\tilde{v} - 1} - \frac{1}{\tilde{v}_1 - 1}\right)\right] \tag{26}$$

It is evident that, according to this formulation, the intrinsic viscosity is a sum of contributions from the relative viscosities of the pure components, and changes in enthalpy, entropy, and volume upon mixing. We can thus write eq 26 in the form

$$[\eta]_2 = [\eta]_\eta + [\eta]_H + [\eta]_S + [\eta]_V \tag{27}$$

where

$$[\eta]_\eta = \frac{V_1}{M_2} \ln \frac{\eta_1}{\eta_2} \tag{28a}$$

$$[\eta]_H = \frac{V_1}{M_2} \lim_{X_2 \to 0} \frac{\Delta H_M}{X_2 RT} \tag{28b}$$

$$[\eta]_S = \frac{V_1}{M_2} \lim_{X_2 \to 0} \frac{\Delta S^R}{X_2 R} \tag{28c}$$

$$[\eta]_V = \frac{V_1}{M_2}\left[\left(\frac{1}{\tilde{v}_1 - 1} - \frac{1}{\tilde{v}_2 - 1}\right) + \lim_{X_2 \to 0} \frac{1}{X_2}\left(\frac{1}{\tilde{v} - 1} - \frac{1}{\tilde{v}_1 - 1}\right)\right] \quad (28d)$$

To evaluate these contributions, we expand the thermodynamic functions given above, in power series in X_2, and retain only first-order terms. The results are as follows. For the segment and site fractions

$$\phi_1 = 1 - \rho X_2 \quad (29)$$

$$\phi_2 = \rho X_2$$

where $\rho = r_2/r_1$

$$\theta_2 = \sigma\rho X_2 \quad (30)$$

where $\sigma = S_2/S_1$. For the reduced temperature and volume

$$\tilde{T} = \tilde{T}_1\left\{1 + \left[\frac{P_2^*}{P_1^*}\left(\frac{\tilde{T}_2}{\tilde{T}_1} - 1\right) + \frac{\sigma X_{12}}{P_1^*}\right]\rho X_2\right\} \quad (31)$$

$$\tilde{v}^\circ = \tilde{v}_1\left[1 + \left(\frac{\tilde{v}_2}{\tilde{v}_1} - 1\right)\rho X_2\right] \quad (32)$$

$$\tilde{T}^\circ = \tilde{T}_1\left\{1 + {}^1/_3\left(\frac{\tilde{v}_2}{\tilde{v}_1} - 1\right)\left[\frac{\tilde{v}_1^{1/3}}{\tilde{v}_1^{1/3} - 1} - 4\right]\rho X_2\right\} \quad (33)$$

$$\tilde{v}_E = (\tilde{v}_1)^{7/3}({}^4/_3 - \tilde{v}_1^{1/3})^{-1} T_1\left[\frac{P_2^*}{P_1^*}\left(\frac{\tilde{T}_2}{\tilde{T}_1} - 1\right) + \sigma\frac{X_{12}}{P_1^*} - {}^1/_3\left(\frac{\tilde{v}_2}{\tilde{v}_1} - 1\right)\left(\frac{\tilde{v}_1^{1/3}}{\tilde{v}_1^{1/3} - 1} - 4\right)\right]\rho X_2 \quad (34)$$

leading finally to

$$\tilde{v} = \tilde{v}_1(1 + \delta\rho X_2) \quad (35)$$

where

$$\delta = \frac{\tilde{v}_2}{\tilde{v}_1} - 1 + \left(\frac{\tilde{v}_1^{4/3}\tilde{T}_1}{{}^4/_3\tilde{v}_1^{1/3}}\right)\left[\frac{P_2^*}{P_1^*}\left(\frac{\tilde{T}_2}{\tilde{T}_1} - 1\right) + \frac{\sigma X_{12}}{P_1^*} - {}^1/_3\left(\frac{\tilde{v}_2}{\tilde{v}_1} - 1\right)\left(\frac{\tilde{v}_1^{1/3}}{\tilde{v}_1^{1/3} - 1} - 4\right)\right] \quad (36)$$

The molar enthalpy of mixing and residual entropy at infinite dilution are

$$\lim_{X_2 \to 0} \frac{\Delta H_M}{X_2 RT} = \frac{C_1\rho}{\tilde{v}_1\tilde{T}_1}\left[\delta + \frac{P_2^*}{P_1^*}\left(\frac{\tilde{v}_1}{\tilde{v}_2} - 1\right) + \frac{\sigma X_{12}}{P_1^*}\right] \quad (37)$$

and

$$\lim_{X_2 \to 0} \frac{\Delta S^R}{X_2 R} = -3C_1\rho\left[-{}^1/_3\frac{\tilde{v}_1^{1/3}\delta}{\tilde{v}_1^{1/3} - 1} + \frac{P_2^*}{P_1^*}\frac{T_1^*}{T_2^*}\ln\frac{\tilde{v}_2^{1/3} - 1}{\tilde{v}_1^{1/3} - 1}\right] \quad (38)$$

while

$$\lim_{X_2 \to 0} \frac{1}{X_2}\left(\frac{1}{\tilde{v} - 1} - \frac{1}{\tilde{v}_1 - 1}\right) = -\frac{\tilde{v}_1\delta\rho}{(\tilde{v}_1 - 1)^2} \quad (39)$$

Table II: Calculated and Experimental Intrinsic Viscosities (cc/g)

Solvent–solute	T, °C	$[\eta]_\eta$	$[\eta]_H$	$[\eta]_S$	$[\eta]_V$	$[\eta]_G$	$[\eta]_\eta + [\eta]_H$	$[\eta]_\eta + [\eta]_S$	$[\eta]_\eta + [\eta]_G$	$[\eta]_\eta + [\eta]_V$	$[\eta]_\eta + [\eta]_H + [\eta]_V$	$[\eta]_\eta + [\eta]_G + [\eta]_V$	$[\eta]_{expt}$
CCl_4–C_6H_{12}	25	−0.022	−0.282	0.075	−0.084	−0.207	−0.304	0.053	−0.229	−0.106	−0.388	−0.313	−0.274
C_6H_{12}–CCl_4	25	0.013	−0.161	0.043	−0.046	−0.118	−0.148	0.056	−0.105	−0.033	−0.194	−0.151	−0.123
C_6H_6–CCl_4	25	0.237	−0.106	0.028	−0.032	−0.078	0.131	0.265	0.159	0.205	0.100	0.127	0.244
CCl_4–C_6H_6	25	−0.507	−0.214	0.057	−0.065	−0.157	−0.721	−0.450	−0.664	−0.572	−0.786	−0.729	−0.445
C_6H_6–C_6H_{12}	25	0.414	−1.493	0.440	−0.446	−1.053	−1.079	0.854	−0.639	−0.032	−1.525	−1.085	−0.430
C_6H_{12}–C_6H_6	25	−0.542	−1.715	0.457	−0.499	−1.258	−2.257	−0.085	−1.800	−1.041	−2.757	−2.299	−1.562
CCl_4–$C(CH_3)_4$	0	−1.713	−0.770	0.014	−0.158	−0.756	−2.483	−1.699	−2.469	−1.871	−3.009	−2.627	−1.900
$C(CH_3)_4$–CCl_4	0	1.007	−0.401	0.003	−0.083	−0.398	0.606	1.010	0.609	0.924	0.747	0.526	0.929
C_6H_6–C_6H_{14}	20	−0.750	−1.798	0.468	−0.546	−1.330	−2.548	−0.282	−2.080	−1.296	−3.094	−2.626	−1.67
C_6H_6–C_7H_{16}	20	−0.402	−1.812	0.485	−0.549	−1.327	−2.214	0.083	−1.729	−0.951	−2.764	−2.278	−1.34
m		0.707	0.552	−0.135	0.161	0.417	1.259	0.571	1.123	0.868	1.526	1.292	1.00
b		0.238	−0.512	0.118	−0.145	−0.394	−0.275	0.356	−0.156	0.093	−0.365	−0.293	0.00
Cor coeff		0.883	0.690	−0.566	0.657	0.722	0.981	0.709	0.989	0.974	0.975	0.980	1.00

Equations 37–39, when substituted into eq 28, permit evaluation of the various contributions to the intrinsic viscosity of liquid mixtures. The results are compared with experiment in Table II. In all but the last two cases listed, experimental intrinsic viscosities were obtained from the data in Table I by fitting the viscosities at the three lowest concentration points for each system to a second-order power series in X_2 and logarithmically differentiating according to eq 25. For *n*-hexane and *n*-heptane in benzene, experimental intrinsic viscosities are those obtained by Rempp.[18]

We observe from Table II that the ideal contribution to the intrinsic viscosity, $[\eta]_\eta$, in two cases is of opposite sign from the experimental value. This, as remarked above, is a reflection of the inability of the ideal viscosity relation, eq 1, to yield other than a monotonic change of viscosity with composition. To assess the relative success of the various combinations of intrinsic viscosity terms in explaining the experimental data, we have performed a linear least-square regression analysis of the form

$$[\eta]_{\text{calcd}} = m[\eta]_{\text{exptl}} + b \qquad (40)$$

where $[\eta]_{\text{calcd}}$ represents in turn each of columns 3–13 in Table II. The resulting values of the slope m, intercept b, and correlation coefficient are given in the last three lines of the table. In confirmation of the impression gained from the mixture viscosity calculations of the previous section, we see that the absolute rate theory expression, $[\eta]_\eta + [\eta]_G$, and the free volume expression, $[\eta]_\eta + [\eta]_V$, come closest to giving the desired values $m = 1$, $b = 0$, with correlation coefficient near unity. Other combinations of viscosity terms give significantly poorer agreement with experiment.

VI. Discussion

We have developed above expressions connecting viscosities of binary mixtures with their thermodynamic properties, using the concepts of the absolute rate and free volume theories of flow. Explicit expressions for the thermodynamic mixing functions were obtained from the solution theory recently developed by Flory and coworkers,[12–14] though experimental data on the excess mixing functions could be used if available. The statistical thermodynamic theory of solutions we have used emphasizes equation of state contributions to the excess mixing functions. These contributions explain the positive excess ΔS of mixing and volume changes on mixing which are incomprehensible in terms of the familiar lattice theories of solutions. The "loosening" of the liquid structure attendant upon solution formation, associated with positive entropy and volume changes, is very important for the flow properties of the solution.

There appears to exist no explicit theory in the literature connecting intrinsic viscosities with thermodynamic properties. Since it is relatively difficult to measure thermodynamic mixing functions in the limit of vanishing concentration of one component, a theory which connects mixing functions at finite concentrations with limiting viscosity behavior seems of considerable value. The combination of Flory solution theory with the activated complex or free volume theories of viscosity as outlined here provides such a connection in relatively convenient analytical form.

The unsatisfactory nature of semiempirical theories of transport, such as that formulated here, is manifest because of the absence of a derivation from fundamental statistical-mechanical principles. However, such theories have often been useful in providing insight into the important physical processes involved and in enabling the calculation of values for transport coefficients which are often surprisingly accurate.

Taking the calculations reported above in this spirit, we note that either the absolute rate theory, or the free volume theory, taken separately, gives satisfactory qualitative and quantitative agreement with measured solution viscosities over the entire range of relative compositions. In a perhaps more stringent test, they also predict well the intrinsic viscosities, that is, the rate of change of viscosity with concentration at infinite dilution of one component. In particular, it should be noted that whereas linear superposition theory is incapable of predicting negative (or positive) intrinsic viscosities for both components in a binary mixture, activation and free volume theories do predict these correctly. It is important to observe that in applying absolute rate theory, both enthalpy and entropy corrections to the ideal viscosity behavior must be made, since considering the enthalpy alone overestimates the fluidity of the mixture.

We also observe that a combination of the absolute rate and free volume theories[10] is not adequate, since it greatly underestimates the mixture viscosity. This is consistent with the demonstration,[11] for a one-dimensional fluid, that consideration of activation and free volume effects as independent leads to a substantial overestimation of the probability of finding a hole in the fluid into which flow can occur.

In the following paper, the ideas developed here will be applied to the intrisic viscosity of *n*-alkanes, as typical very short polymers, for which it is shown that continuum hydrodynamic effects are less important than the molecular nature of solvent–solute interactions.

Acknowledgments. We are grateful to Peter Berget for invaluable assistance with computing. This research was supported by grants from the Alfred P. Sloan Foundation and the National Institutes of Health (GM 17855).

(18) P. Rempp, *J. Polym. Sci.*, **23**, 83 (1957).

Intrinsic Viscosity of Short-Chain Normal Alkanes

by R. K. Dewan, Victor A. Bloomfield,*[1] and Peter B. Berget

Department of Biochemistry, College of Biological Sciences, University of Minnesota, St. Paul, Minnesota 55101
(Received March 2, 1971)

Publication costs assisted by the National Institutes of Health

With various assumptions about chain geometry, intrinsic viscosity calculations for polymer chains have been extended to very short *n*-alkanes (5 to 28 carbons), using the theory developed by Kirkwood and Ullman. This continuum hydrodynamic approach fails to explain the negative values of intrinsic viscosity found experimentally for the shortest of these chains. The theory outlined in the preceding paper, which takes into account the statistical thermodynamics of solvent–solute interactions, has been used to evaluate the various viscosity contributions. This approach rationalizes the negative values and gives reasonable numerical agreement with experiment, indicating that a short polymer chain may be more profitably treated as a fairly typical small molecule than as a limiting case of a polymer. This is apparently because different physical mechanisms of viscous energy dissipation predominate in the long- and short-chain regions.

I. Introduction

Prediction of hydrodynamic properties of flexible polymers from their chemical structures has been a goal of long standing. For flexible long-chain polymers, intrinsic viscosity $[\eta]$, diffusion coefficient, and other hydrodynamic properties have been calculated using continuum hydrodynamic theories and gaussian chain statistics[2] and good agreement achieved with the experimental results in θ solvents and, after appropriate modification for excluded volume effects,[3,4] in good solvents.

For short-chain polymers, the assumption of gaussian subchains is no longer adequate and a more detailed account of chain structure must be taken. Diffusion measurements have been made for short-chain *n*-alkanes in various solvents by a number of authors[5,6] and the results have been analyzed by taking into account the details of the molecular configuration. Good agreement with experiment is obtained for all chain lengths.[5,7] For viscosity, modification of long-chain theory to deal with short chains is successful down to a minimum length, using either modification of normal coordinate theory[8] or Kirkwood–Ullman theory.[2a,9,10] These calculations are extended to very short chains, with various assumptions about chain geometry, in section II of this paper.

However, for the shortest *n*-alkane chains, of less than 12 carbons, $[\eta]$ is found to be negative[11,12] with benzene or carbon tetrachloride as solvent. Kuss and Stuart[13] had earlier reported negative values of $[\eta]$ for solutions of 1,3,5-trimethylbenzene and 2,6-dimethylnaphthalene in nitrobenzene. This cannot be explained on the basis of any continuum hydrodynamic theory. To understand the behavior of $[\eta]$ at low molecular weight one must take into account the detailed molecular nature of the solvent and of solvent–solute interaction.

An attempt to modify the hydrodynamic theory has been made by Peterlin and Bianchi[14,15] by considering separately the viscosity contribution of the monomer, and expressing the corrected intrinsic viscosity by the relation

$$[\eta]_{cor} = [\eta]_0 + [\eta]_n$$

where $[\eta]_0$ is the intrinsic viscosity of the smallest unit and $[\eta]_n$ is the conventional value for the necklace model. It was supposed that the former can be positive, negative, or zero depending on the interaction with solvent. The treatment proposed here also connects negative intrinsic viscosities with solvent–solute interaction, expressed in terms of the thermodynamics of the solution.

In the previous paper,[16] we obtained expressions for various contributions to $[\eta]$ in terms of the thermodynamic mixing functions and the viscosities of the pure

(1) Alfred P. Sloan Foundation Fellow.

(2) (a) J. G. Kirkwood and J. Riseman, *J. Chem. Phys.*, **16**, 565 (1948); J. Riseman and J. G. Kirkwood, *ibid.*, **18**, 512 (1950); (b) B. H. Zimm, *ibid.*, **24**, 269 (1956).

(3) M. Kurata and W. Stockmayer, *Fort. Hochpolym. Forsch.*, **3**, 196 (1964).

(4) N. Tschoegl, *J. Chem. Phys.*, **40**, 473 (1964).

(5) R. K. Dewan and K. E. Van Holde, *ibid.*, **39**, 1820 (1963).

(6) C. Rossi and E. Bianchi, *Nature*, **189**, 822 (1961).

(7) E. Paul and R. Mazo, *J. Chem. Phys.*, **48**, 1405 (1968).

(8) J. E. Hearst, *ibid.*, **37**, 2547 (1962); V. A. Bloomfield and P. A. Sharp, *Macromolecules*, **1**, 380 (1968).

(9) R. Ullman, *J. Chem. Phys.*, **40**, 2193 (1964).

(10) A. Perico and C. Rossi, *ibid.*, **53**, 1217, 1223 (1970).

(11) P. Rempp, *J. Polym. Sci.*, **23**, 83 (1957).

(12) D. V. S. Jain, R. K. Dewan, and K. K. Tewari, *Indian J. Chem.*, **6**, 584 (1968).

(13) E. Kuss and H. A. Stuart, *Z. Naturforsch.*, **39**, 204 (1948).

(14) A. Peterlin, *Polym. Preprints*, **9**, 323 (1968).

(15) U. Bianchi and A. Peterlin, *J. Polym. Sci. A2*, **6**, 1759 (1968).

(16) V. A. Bloomfield and R. K. Dewan, *ibid.*, **75**, 3113 (1971).

components. In section III of this paper we apply that theory to calculate $[\eta]$ of n-alkanes in benzene and show that it rationalizes the negative intrinsic viscosities of short chains.

II. Continuum Hydrodynamic Calculations of $[\eta]$ for Short Chains

The intrinsic viscosity of a chain molecule of n segments is given by

$$[\eta] = -(N_0/100M\eta_0\dot{\epsilon})\sum_{l=1}^{n}\langle(\mathbf{R}_{0l}\cdot\mathbf{e}_y)(\mathbf{F}_l\cdot\mathbf{e}_x)\rangle \quad (1)$$

where

$$\langle(\mathbf{R}_{0m}\cdot\mathbf{e}_y)(\mathbf{F}_l\cdot\mathbf{e}_x)\rangle = -\left(\frac{\zeta\dot{\epsilon}}{6}\right)\langle\mathbf{R}_{0m}\cdot\mathbf{R}_{0l}\rangle - \left(\frac{\zeta}{6\pi\eta_0}\right)\sum_{\substack{s=1\\ s\neq l}}^{n}\langle(\mathbf{R}_{0m}\cdot\mathbf{e}_y)(\mathbf{F}_s\cdot\mathbf{e}_x)\rangle\langle R_{ls}^{-1}\rangle \quad (2)$$

N_0 is Avogadro's number, M is the molecular weight of the chain molecule, η_0 is the viscosity coefficient of the solvent, and $\dot{\epsilon}$ is the velocity gradient. $\mathbf{R}_{0l}$ is the vector connecting the center of mass of the molecule with the lth chain segment and $\mathbf{F}_l$ is the force exerted on the solvent by the lth segment. In eq 2, ζ is the friction constant per chain segment and R_{ls} represents the absolute value of the vector connecting the lth to the sth chain segment. The mean distance $\langle\mathbf{R}_{0m}\cdot\mathbf{R}_{0l}\rangle$ may be computed through the identity[9]

$$\langle\mathbf{R}_{0m}\cdot\mathbf{R}_{0l}\rangle = (2n)^{-1}\left(\sum_{l=1}^{n}\langle R_{lm}^2\rangle + \sum_{m=1}^{n}\langle R_{lm}^2\rangle\right) - (^1/_2\langle R_{ls}^2\rangle) - \langle R_G^2\rangle \quad (3)$$

$\langle R_G^2\rangle$ is the mean-square radius of the molecule. The angular brackets denote averages over all conformations of the chain. The quantities $\langle(\mathbf{R}_{0m}\cdot\mathbf{e}_y)(\mathbf{F}_l\cdot\mathbf{e}_x)\rangle$ are obtained from the simultaneous solutions of the n eq 2, each equation corresponding to a different value of l. By setting m equal to l and substituting in eq 1, the intrinsic viscosity may be calculated. Since eq 2 and 3 involve statistical averages dependent on molecular conformation, three types of models were considered for alkanes.

The first such model is a self-avoiding random walk on a tetrahedral lattice, which gives a useful first approximation to the excluded volume effect in polymer chains. Domb[17] has determined, by exhaustive enumeration, the mean-square end-to-end distances $\langle R_n^2\rangle$ for self-avoiding walks of up to 14 steps (corresponding to the alkane n-$C_{15}H_{32}$) on such a lattice. For higher members of the homologous series, he gives the asymptotic relationship

$$\langle R_n^2\rangle = A_1 n^{6/5} + A_2 \quad (4)$$

where $A_1 = 1.2875$ and $A_2 = -0.2705$ for the tetrahedral lattice with unit step length. We have used these values in eq 3 by assuming that the mean-square distance between segments depends only on the number of steps between them, *i.e.*, that $\langle R_n^2\rangle = \langle R_{ls}^2\rangle$ if $|l - s| = n$.

It is more difficult to get the mean reciprocal distances $\langle R_{ls}^{-1}\rangle$ required in eq 2. For segments close to one another along the chain backbone, we have assumed that excluded volume effects are negligible and have used the values of $\langle R_n^{-1}\rangle$ tabulated by Varoqui[18] for $|l - s| \leq 12$. In the limit of very long chains with excluded volume, it has been shown[19] that the Domb–Gillis–Wilmers[20] distribution function yields

$$\langle R_n^{-1}\rangle = \langle R_n^2\rangle^{-1/2}\{\Gamma[(5 - 3\epsilon)/2]\}^{1/2}\{\Gamma[(3 - \epsilon)/2]\}^{-1/2}$$

where $\Gamma(x)$ is the gamma function and ϵ is the excluded volume exponent. According to eq 4, $\epsilon = {}^1/_5$, so we have in the asymptotic limit $\langle R_n^{-1}\rangle = 1.25596\langle R_n^2\rangle^{-1/2} = 1.1069n^{-3/5}$. Values of $\langle R_{ls}^{-1}\rangle$ for $|l - s| > 12$ were obtained by calculating the function

$$\nu_n = n^{3/5}\langle R_n^{-1}\rangle_v - 1.1069$$

where $\langle R_n^{-1}\rangle_v$ is the value obtained by Varoqui,[18] for $2 < n < 12$, and extrapolating a log–log plot of ν_n *vs.* n to values of n greater than 12. Values of ν_n obtained thereby were used in the equation

$$\langle R_n^{-1}\rangle = 1.1069n^{-3/5} + \nu_n \quad (n > 12) \quad (5)$$

The second model neglects excluded volume but includes a probably more important factor: the statistical weights of the various rotational isomeric states. Flory and Jernigan[21] have carried out calculations of $\langle R_n^2\rangle$ for n-alkane homologs assuming a threefold rotational potential about the C–C bonds and taking account explicitly of first-neighbor interdependence of the potentials. These values were used in eq 3 to evaluate the desired parameters for this model while the function $\langle R_n^{-1}\rangle$ was calculated using the relation

$$\langle R_n^{-1}\rangle = C(n)\langle R_n^2\rangle^{-1/2}$$

The function $C(n)$ was computed for each value of $|l - s|$ from the expression

$$\frac{C(n) - 1}{\left(\frac{6}{\pi}\right)^{1/2} - 1} = \frac{C'(n) - 1}{\frac{5}{3} - 1} \quad (6)$$

where $C'(n)$ is the ratio of the fourth moment to the square of the second moment of the end-to-end distance. That is, it is assumed that the fractional deviation of $\langle R^{-1}\rangle\langle R^2\rangle^{1/2}$ from its asymptotic value of $\sqrt{6/\pi}$

(17) C. Domb, *J. Chem. Phys.*, **38**, 2957 (1963).

(18) R. Varoqui, *C. R. Acad. Sci.*, **259**, 2633 (1964).

(19) P. A. Sharp and V. A. Bloomfield, *J. Chem. Phys.*, **49**, 4564 (1968).

(20) C. Domb, J. Gillis, and G. Wilmers, *Proc. Phys. Soc.* (*London*), **85**, 625 (1965).

(21) P. J. Flory and R. L. Jernigan, *J. Chem. Phys.*, **42**, 3509 (1965); R. L. Jernigan, Ph.D. Thesis, Stanford University, 1967.

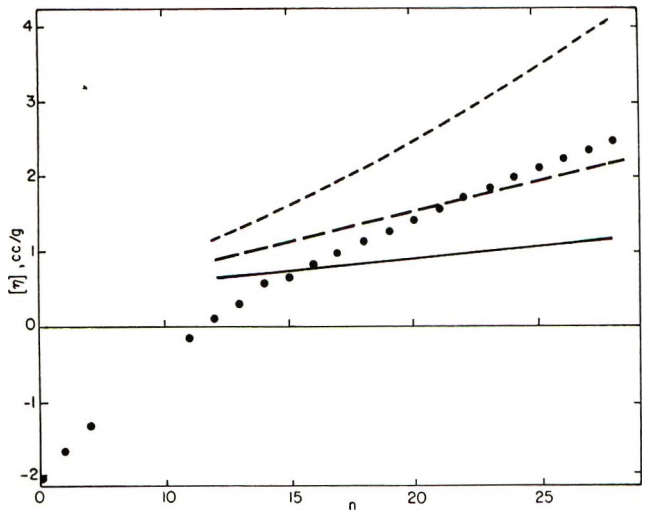

Figure 1. Intrinsic viscosity $[\eta]$ of short-chain n-alkanes as a function of n, the number of carbon atoms, calculated according to the continuum hydrodynamic eq 1. Average chain dimensions computed for self-avoiding random walks on a tetrahedral lattice (——), rotational isomeric state approximation (– – –), and all-trans conformation (---). Experimental results in benzene at 20° denoted by dots.

is the same as the fractional deviation of $\langle R^4\rangle\langle R^2\rangle^{-2}$ from its asymptotic value of $^5/_3$.

The third model is a rigid, all-trans model for which there is only one conformation for every value of n. For this model, the values of the required dimensional averages were simply calculated from the bond length and angle.

In Figure 1 we compare the values of $[\eta]$ calculated according to these three models, with the experimental values obtained for n-alkanes in benzene at 20°. The values calculated for the rotational isomeric state model agree very closely with those obtained by Perico and Rossi[10] for alkanes with hindered rotation and the hydrodynamic parameter $\lambda = \zeta/6\pi\eta_0 b_0 = 0.5$. In all of the calculations described above, we also took $\lambda = 0.5$. b_0 is the distance between nearest-neighbor segments (the C–C bond length = 1.54 Å). We observe that for n greater than 20, the combination of rotational isomeric chain statistics with the Kirkwood–Ullman viscosity treatment leads to relatively good agreement with experiment. The all-trans model gives viscosities which are too high, and the unweighted self-avoiding walk model gives viscosities which are too low, reflecting over- and underweighting, respectively, of the highly extended trans conformation.

On the other hand, for chains of less than 15 carbons, all these models fail rapidly, and it is clear that none of them will yield the negative intrinsic viscosities found experimentally with $C_{11}H_{24}$ and shorter n-alkanes. These negative values reflect the breakdown of the continuum hydrodynamic approximation implicit in eq 1 and 2, and the need to take details of solvent–solute interactions into account. This breakdown is not surprising when one observes from Figure 2 that the rms radius $\langle R_G^2\rangle^{1/2}$ of C_5H_{12} is 1.73 Å, and that of $C_{11}H_{24}$ is 3.42 Å, according to rotational isometric state calculations.[21] This is to be compared with the distance of about 2.4 Å from the center of the benzene hexagon to one of its hydrogen atoms. For $C_{20}H_{42}$ and $C_{28}H_{58}$, on the other hand, the rms radii are 5.55 and 7.14 Å, respectively.

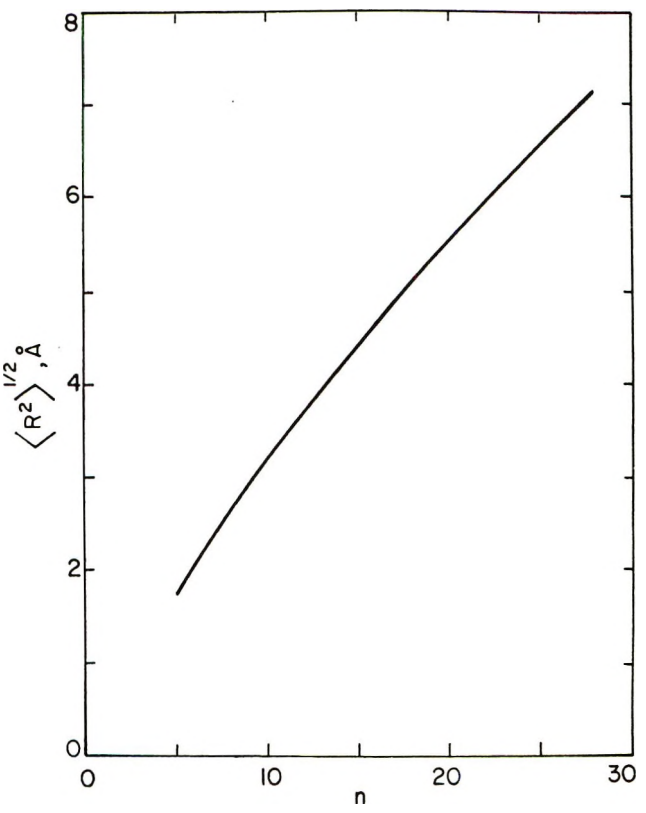

Figure 2. Root-mean-square radius $\langle R_G^2\rangle^{1/2}$, calculated by the rotational isomeric state approximation, as a function of n, the number of carbon atoms.

III. Calculation of $[\eta]$ from Thermodynamic Mixing Functions

In the preceding paper[12] we have investigated the representation of the intrinsic viscosity as a sum of contributions from the viscosities of the pure components and changes in enthalpy, entropy, and volume upon mixing. We write

$$[\eta] = [\eta]_\eta + [\eta]_H + [\eta]_S + [\eta]_V = \frac{V_1}{M_2}\left[\ln\frac{\eta_1}{\eta_2} - \lim_{X_2\to 0}\frac{\Delta H_M}{X_2 RT} + \lim_{X_2\to 0}\frac{\Delta S^R}{X_2 R} + \left(\frac{1}{\tilde{v}_1 - 1} - \frac{1}{\tilde{v}_2 - 1}\right) + \lim_{X_2\to 0}\frac{1}{X_2}\left(\frac{1}{\tilde{v} - 1} - \frac{1}{\tilde{v}_1 - 1}\right)\right] = [\eta]_\eta + [\eta]_G + [\eta]_V \quad (7)$$

For the explanation of the various symbols and the evaluation of the thermodynamic functions, the reader

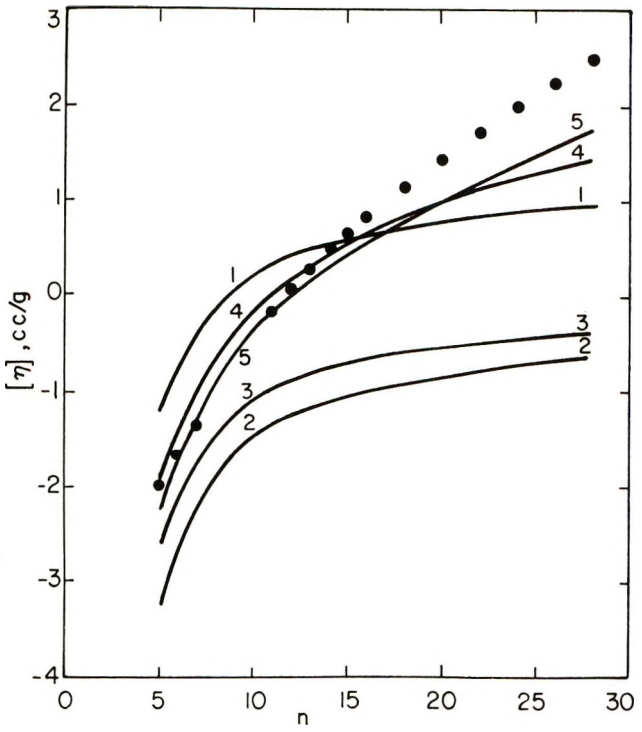

Figure 3. Intrinsic viscosity $[\eta]$ as a function of chain length n, calculated using various of the correction terms to ideal behavior in eq 7: 1, $[\eta]_\eta$; 2, $[\eta]_\eta + [\eta]_R$; 3, $[\eta]_\eta + [\eta]_G$; 4, $[\eta]_\eta + [\eta]_V$; 5, $[\eta]_I + [\eta]_G + [\eta]_C$ (where $[\eta]_C$ is given by long-dashed line in Figure 1). Dots are experimental points for n-alkanes in benzene at 20°.

is referred to the previous paper.[16] It was found that either $[\eta] = [\eta]_\eta + [\eta]_G$ or $[\eta] = [\eta]_\eta + [\eta]_V$ gave good representation of experimental data on the intrinsic viscosity of liquid mixtures.

To calculate the various thermodynamic functions in eq 7 with the help of expressions cited in the earlier paper, one needs the values of certain parameters for the various C_nH_{2n+2}–C_6H_6 systems. Those relating to properties of the benzene solvent have been tabulated by Flory, *et al.*,[22] at 0 and 25° and were interpolated to obtain values at 20°. M_2 can be expressed as $M_{C_nH_{2n+2}} = 14.026n + 2.016$, while a semilogarithmic relation of the form $\log \eta_{2n} = -0.972 + 0.0935n$ was found to hold good for $n > 10$ at 20°.[23] Flory, *et al.*,[22] have found that the reciprocal of the characteristic temperature, $1/T^*$, is approximately linear in x, the number of segments, where $x = n + 1$. At 20°, we have used

$$\frac{10^4}{T_2^*} = 1.413\left(1 + \frac{4.17}{n+1}\right) \tag{8}$$

It also appears from the data of Flory, *et al.*,[22] that for larger n ($12 < n < 18$), the reduced volume $\tilde{v}$ varies roughly linearly linearly with $1/n$. A least-squares fit gives

$$\tilde{v} = 1.1517 + 0.9879/n \tag{9}$$

For the characteristic pressure p_2^*, Flory, *et al.*,[22] give

$$p^* = 120\left(1 - \frac{1.5}{n+1}\right) \text{ cal/cc} \tag{10}$$

The ratio of the number of segments in solute and solvent, $\rho = r_2/r_1$, has been expressed as $(r_2/r_1) = (r_{2,ref}/r_1)(r_2/r_{2,ref})$ where $r_{2,ref}$ is the number of segments in a reference hydrocarbon such as C_6 or C_7. Since $r = x = n + 1$, we have $r_2/r_{2,ref} = (n+1)/(n_{ref}+1)$. Using the system C_6H_6–C_6H_{14} as a reference,[22] we thus find

$$r_2/r_1 = \frac{1}{0.695}\left(\frac{n+1}{7}\right) \tag{11}$$

The ratio of molecular contact areas per segment, $\sigma = s_2/s_1$, and the segmental interaction parameter X_{12}, should be essentially constant in a homologous series of hydrocarbons. Thus the values $\sigma = 1.05$ and $X_{12} = 9.5$ cal/cc for the C_6H_6–C_6H_{14} system[22] were chosen to represent all the hydrocarbons.

We have used the above equations for the various parameters of the homologous series to calculate the thermodynamic mixing functions required in eq 7, in the way described in the preceding paper.[16] The results are plotted in Figure 3. It is evident that good quantitative agreement is obtained up to $n = 16$ if $[\eta]$ is expressed as $[\eta]_\eta + [\eta]_V$. Other combinations of thermodynamic contributions to the intrinsic viscosity are notably less satisfactory. We have also plotted in Figure 3 the function $[\eta] = [\eta]_\eta + [\eta]_G + [\eta]_C$, where $[\eta]_C$ represents the continuum hydrodynamic viscosity calculated using eq 1 with rotational isomeric state chain statistics (long-dashed curve in Figure 1). Here, again, agreement with experiment is excellent up to $n = 16$.

IV. Discussion

We have found in the above work that we get good agreement between theoretical and experimental intrinsic viscosities if we treat short n-alkane chains as ordinary small molecules, accounting for solvent–solute interactions but neglecting continuum hydrodynamic contributions. This is rendered more plausible since $\langle R_G^2 \rangle^{1/2}$ for n-alkanes with $n < 18$ is $\leq 2R_{solv}$ as shown in Figure 2. It is qualitatively as well as quantitatively inadequate to extrapolate long-chain behavior into the very short-chain region, since the predominant mechanism of additional viscous energy dissipation due to the presence of solute changes entirely.

In the preceding paper[16] we saw that both the absolute theory expression, $[\eta]_\eta + [\eta]_G$, and the free volume expression $[\eta]_\eta + [\eta]_V$ gave reasonable agreement with experimental values of intrinsic viscosities of

(22) P. J. Flory, R. A. Orwoll, and A. Vrij, *J. Amer. Chem. Soc.*, **86**, 3507, 3515 (1964).

(23) "Handbook of Chemistry and Physics," 49th ed, Chemical Rubber Co., Cleveland, Ohio, 1968, p F-37.

mixtures of simple molecules. If only thermodynamic contributions are considered for analyzing the data on n-alkanes, it appears that $[\eta]_V$ works better than $[\eta]_G$. The reason for this is not clear.

For longer chains ($n > 25$–30), continuum hydrodynamics is quite adequate, if dimensions are calculated according to the rotational isomeric states theory, as shown in Figure 1, and continued incorporation of thermodynamic contributions leads to the underestimation of $[\eta]$. One is thus led to believe that after a certain value of n, the thermodynamic contributions decrease rapidly in significance and can be effectively neglected. This may be explained by solvent entrapment in the polymer domain so that solvent–solute contacts are no longer important in viscous energy dissipation.

Acknowledgments. This work was supported by grants from the National Institutes of Health and the Alfred P. Sloan Foundation.

Theory of the Onsager Transport Coefficients l_{ij} and R_{ij} for Electrolyte Solutions

by Michael J. Pikal

Department of Chemistry, University of Tennessee, Knoxville, Tennessee 37916 *(Received April 12, 1971)*

Publication costs borne completely by The Journal of Physical Chemistry

A simple limiting-law expression for the l_{ij} in multicomponent electrolyte systems is presented. An extended theory of the l_{ij} and R_{ij} coefficients is developed for symmetrical binary electrolytes. A term representing the effect of ion-pair formation appears in the extended theory as a natural consequence of the electrostatic interactions. The mobility of an ion pair is not an adjustable parameter but is determined by the theory. The theory includes terms of order $c^{1/2}$, $c \log c$, c, and $c^{3/2}$. The extended theory is in good agreement with experiment. The physical interpretation of the l_{ij} and R_{ij} coefficients in multicomponent and binary systems is discussed in terms of electrolyte theory. Certain aspects of the current "intuitive" interpretations given l_{ij} and R_{ij} are found to be inconsistent with electrolyte theory.

I. Introduction

The phenomenological theory of irreversible thermodynamics may be applied to transport phenomena in electrolytes, resulting in a general description of ionic transport in terms of the Onsager "conductivity" coefficients l_{ij}.[1-3] An alternate, but equivalent, description in terms of the "friction" coefficients, R_{ij}, may also be used. Ratios of the form l_{ij}/c (c = concentration) are mobilities,[2] and products of the form c_jR_{ij} have been interpreted as friction coefficients.[4] From the point of view of irreversible thermodynamics the l_{ij} or R_{ij} are more fundamental than the conventional transport properties, such as equivalent conductance, transference number, and diffusion coefficient.[2] Therefore, systematic studies of the l_{ij} or R_{ij} should lead to new insights into the nature of transport phenomena in electrolytes.[2]

In this paper, we consider several extensions of earlier theoretical studies[5-9] on the concentration dependence of the l_{ij} and R_{ij} coefficients. Before proceeding with a discussion of specific objectives, it is useful to present the phenomenological relations of irreversible thermodynamics which define the l_{ij} and R_{ij} coefficients.

The irreversible thermodynamic description of the isothermal vector transport properties of an electrolyte solution may be given in the most general linear (one dimensional) form as[1-3]

$$J_i = \sum_{k=1}^{n} l_{ik}X_k \qquad (i, k = 1, 2 \ldots, n) \qquad (1)$$

(1) D. G. Miller, *J. Phys. Chem.*, **64**, 1598 (1960).
(2) D. G. Miller, *ibid.*, **70**, 2639 (1966).
(3) D. G. Miller, *ibid.*, **71**, 616 (1967).
(4) H. S. Dunsmore, S. K. Jalota, and R. Paterson, *J. Chem. Soc., A*, 1061 (1969).
(5) L. Onsager and R. M. Fuoss, *J. Phys. Chem.*, **36**, 2689 (1932).
(6) L. Onsager, *Ann. N. Y. Acad. Sci.*, **46**, 241 (1945).
(7) L. Onsager and S. K. Kim, *J. Phys. Chem.*, **61**, 215 (1957).
(8) J. Rastas, *Acta Polytech. Scand., Chem. Met. Ser.*, **No. 50**, 37 (1966).
(9) H. Schönert, *J. Phys. Chem.*, **73**, 62 (1969).

$$J_i = \bar{c}_i V_i^\circ \tag{2}$$

$$X_k = -\frac{d\mu_k'}{dy} = -\frac{d\mu_k^C}{dy} + Z_k F\frac{d\phi}{dy} \tag{3}$$

The numerical subscripts refer to ionic components 1, 2, ..., n. The ionic conductivity coefficients l_{ik} are defined by eq 1 in terms of linear relations between *solvent-fixed* flows J_i and thermodynamic forces X_k in mole units. Equation 2 expresses the *solvent-fixed* flows in terms of the concentration of component i (in moles per cubic centimeter), denoted by $\bar{c}_i$, and the velocity of ion component i (in centimeters per second) relative to the solvent, denoted by V_i°. The thermodynamic force X_k is given by the negative of the gradient of the electrochemical potential of ion k, denoted by μ_k'. In eq 3, X_k is related to the chemical part of the electrochemical potential, μ_k^C, and the electrical potential, ϕ, in volts. The symbol F denotes the Faraday constant in coulombs per equivalent, Z_i is the signed valence of ionic component i, and y is the distance in centimeters.

For this choice of forces and flows, it is expected from statistical mechanical and other considerations[10] that the Onsager reciprocal relations will hold.

$$l_{ij} = l_{ji} \tag{4}$$

The R_{ij} ($i, j = 1, 2, \ldots, n$) or "friction coefficients" are defined by[2]

$$X_i = \sum_{k=1}^{n} R_{ik} J_k \qquad (i, k = 1, \ldots, n) \tag{5}$$

Since the matrix of the l_{ij} coefficients is nonsingular, the R_{ij} matrix ($i, j = 1, 2, \ldots, n$) is simply the inverse of the l_{ij} matrix. The R_{ij} coefficients also satisfy the Onsager reciprocal relations, $R_{ij} = R_{ji}$.

It is conventional[2] to define additional "friction coefficients" R_{oo} and R_{io} ($i = 1, 2, \ldots, n$) by the relation

$$\sum_{k=0}^{n} \bar{c}_k R_{ik} = 0 \tag{6}$$

where the subscript o refers to the solvent.

We now summarize the "intuitive" interpretations of l_{ij} and R_{ij}. The quantity $l_{ii}/\bar{c}_i$ is the "intrinsic mobility" of ion i while $l_{ij}/\bar{c}_i$ ($i \neq j$) is an "interaction mobility," that is, a measure of the degree of coupling between the motions of component i and j.[2,11] There is disagreement concerning the interpretation of the R_{ij} coefficients.[2,4,9,12] The notion that R_{ij} represents the "friction" of component i with component j was criticized by Miller.[2] Some of Miller's objections have been circumvented by Dunsmore, *et al.*[4] In the latter work,[4] the quantity $\bar{c}_i R_{ii}$ is interpreted as the sum of all friction coefficients between component i and other components in the system, while $-\bar{c}_i R_{ij}$ ($i \neq j$) is interpreted as a friction coefficient representing the frictional interaction between components i and j.

The general purpose of this paper is to present some theoretical guidelines for the interpretation of l_{ij} and R_{ij} in electrolyte systems.

We have three main objectives: (1) to present a simple limiting-law expression for the l_{ij} in multicomponent systems; (2) to extend the Onsager–Fuoss[5] limiting-law theory to include terms of higher order in concentration; and (3) to point out certain aspects of the "intuitive" interpretations of l_{ij} and R_{ij} which are not consistent with electrolyte theory.

II. Onsager-Fuoss Limiting Laws

A. Friction Coefficients. The theoretical description of ionic transport phenomena is usually given in terms of three effects: (1) the interaction of the moving ion with the surrounding solvent, which is assumed to be independent of concentration and therefore is related to the limiting ionic equivalent conductance; (2) long-range hydrodynamic interactions between the ions, termed the electrophoretic effect; and (3) long-range electrostatic interactions between a given ion and its asymmetric ion atmosphere, called the relaxation effect. Theoretical expressions for the relaxation effect and the electrophoretic effect are given in the classic 1932 paper of Onsager and Fuoss.[5] These results are given for ionic motion in a general (multicomponent) electrolyte solution to order $c^{1/2}$, where c is the concentration, and thus are "limiting laws." The limiting-law equations are discussed further by Onsager and Kim.[7]

Some of the results contained in these studies[5,7] reveal certain deficiencies in the "intuitive" interpretations of the friction coefficients and thus deserve emphasis. Denoting the friction coefficient in "microscopic" units[13] by r_{ij}, the limiting-law equations may be written in the form

$$\sqrt{n_i n_i} r_{ji} = \rho_j \delta_{ji} + \sqrt{n_j n_i} r_{ji}' + \sqrt{n_j n_i} r_{ji}'' \qquad (i, j = 1, 2, 3, \ldots, n) \tag{7}$$

where n_i and n_j refer to the concentration of i- and j-type ions in (number of ions) per cubic centimeter, and $\delta_{ij} = 0$, $i \neq j$; $\delta_{ii} = 1$). The friction coefficient for the interaction of ion j with the solvent ρ_j is given in terms of the absolute ion mobility ω_j or the limiting ionic equivalent conductance λ_j° by

$$1/\rho_j = \omega_j = \frac{\lambda_j^\circ C \times 10^{-8}}{F\epsilon|Z_j|} \tag{8}$$

In eq 8, C is the speed of light in centimeters per second, F is Faraday's constant in colulombs per equivalent, ϵ

(10) See footnote 18 of ref 2 for further comments and references.

(11) M. J. Pikal and D. G. Miller, *J. Phys. Chem.*, in press.

(12) R. W. Laity, *J. Chem. Phys.*, **30**, 682 (1959).

(13) The term "microscopic units" refers to the units resulting from the use of units of (number of ions) cm^{-2} sec^{-1} for flow and units of ergs per ion for the force.

is the electronic charge in electrostatic units, and Z_j is the signed valence of the j-type ion.

The second and third terms in eq 7 are the result of long-range coulombic interactions, and both are proportional to the square root of the total ionic strength. The single prime denotes the electrophoretic effect, while the double prime denotes the relaxation effect.

Onsager and Kim[7] show that r_{ii}'' is always positive while r_{ij}'' $(i \neq j)$ is always negative, *regardless of the* sign of Z_i and Z_j. Thus r_{ij} $(i \neq j)$ may not be interpreted simply as an interaction coefficient reflecting pairwise i–j coulombic interactions.

Another interesting result may be expressed in the form[7]

$$\sum_{j=1}^{n} n_j r_{ij}'' = 0$$

If the above equation is combined with eq 6, the result $R_{io} = 0$ is obtained. Thus, at least to the limiting-law approximation, the ion–solvent friction coefficients, R_{io} $(i = 1, 2, \ldots, n)$, do not depend on the relaxation effect. However, it is easily shown that the electrophoretic contribution, R_{io}', is zero *only* in the special case of equal ionic mobilities.

B. Conductivity Coefficients. General Limiting Law. The limiting-law expressions for the conductivity coefficients, l_{ij}, have been given explicitly only for the binary case.[8] Limiting-law expressions for l_{ij} in the general multicomponent case may be obtained by a straightforward combination of several theoretical equations given by Onsager and coworkers.[5,7] Denoting the conductivity coefficients in "microscopic" units[13] by ℓ_{ij}, we find

$$\frac{\ell_{ii}}{\sqrt{n_i n_j}} = \omega_i \delta_{ij} + \frac{\ell_{ij}'}{\sqrt{n_i n_j}} + \frac{\ell_{ij}''}{\sqrt{n_i n_j}} \tag{9}$$

where the single prime represents the electrophoretic effect

$$\frac{\ell_{ij}'}{\sqrt{n_i n_j}} = -\frac{e_j e_i}{|e_j e_i|} \frac{\sqrt{\mu_i \mu_j}}{6\pi\eta} \kappa \tag{10}$$

and the double prime represents the relaxation effect

$$\frac{\ell_{ij}''}{\sqrt{n_i n_j}} = -\frac{\omega_i \omega_j}{\bar{\omega}} \frac{|e_i e_j|}{3DkT} \sqrt{\mu_i \mu_j} Q_{ij} \kappa \tag{11}$$

In eq 10 and 11, $1/\kappa$ is the familiar radius of the ion atmosphere, μ_i is the ionic strength fraction of ionic component i

$$\mu_i = \frac{n_i e_i^2}{\sum_{i=1}^{n} n_i e_i^2} \tag{12}$$

and $\bar{\omega}$ is an average ionic mobility defined by

$$\bar{\omega} = \sum_{i=1}^{n} \mu_i \omega_i \tag{13}$$

The term Q_{ij} is our notation for a unitless complex function of ionic mobility and ionic strength fractions, which in the Onsager and Kim notation[7] may be written in the form

$$Q_{ij} = \sum_{p=2}^{n} (1 - \sqrt{q_p}) \chi_j^p \chi_i^p \tag{14}$$

The original paper[7] should be consulted for a definition of the terms in eq 14. In practice, Q_{ij} must be evaluated by numerical methods[7] for each multicomponent electrolyte system considered.

By a straightforward extension of the arguments made in establishing the sign of r_{ij}'', it may be shown that ℓ_{ii}'' is always negative and ℓ_{ij}'' $(i \neq j)$ is always positive, regardless of the sign of Z_i and Z_j. However, as shown in eq 10, the electrophoretic term ℓ_{ij}' is negative if ions i and j have charges of like sign, and ℓ_{ij}' is positive if ions i and j have charges of opposite sign. Thus, l_{ij} $(i \neq j)$ may not be interpreted simply in terms of pairwise i–j coulombic interactions.[2,3]

Simplified Limiting Law. Since the function Q_{ij} cannot, in general, be expressed in simple form, the dependence of l_{ij} on ionic strength fraction and mobility is not obvious from the form of eq 11. It would be useful to obtain a simple (approximate) expression for l_{ij} which would correctly represent the gross features of the l_{ij} for dilute multicomponent systems. Our numerical calculations show that although l_{ij} is a sensitive function of ionic mobilities ω_i and ω_j, Q_{ij} is a rather insensitive function of the ionic mobilities. We note that, for equal ion mobilities, the function Q_{ij} may be expressed in simple form[14]

$$Q_{ij} = (1 - 1/\sqrt{2})(\delta_{ij}/\mu_j - 1) \tag{15}$$

Thus, if the equal ion mobility approximation, eq 15, is used to evaluate Q_{ij}, and the result substituted into eq 11, one might expect to obtain a good approximation for the relaxation effect ℓ_{ij}''.

Combining eq 9–11 with Q_{ij} given by eq 15, and converting into "macroscopic" units to obtain l_{ij}, we find

$$10^{12} l_{ii}/c_i = 0.10740 \frac{\lambda_i^\circ}{|Z_i|} - 0.10740 \left[\frac{\lambda_i^{\circ 2}/Z_i^2}{\sum_i \mu_i \lambda_i^\circ/|Z_i|} (1 - \mu_i) A_{ii} + \frac{B_0}{2} Z_i^2 \mu_i \right] I^{1/2} \tag{16}$$

$$10^{12} l_{ij}/\sqrt{c_i c_j} = 0.10740 \sqrt{\mu_i \mu_j} \times \left[\frac{(\lambda_i^\circ/|Z_i|)(\lambda_j^\circ/|Z_i|)}{\sum_i \mu_i \lambda_i^\circ/|Z_i|} A_{ij} - \frac{B_0}{2} Z_i Z_j \right] I^{1/2} \quad (i \neq j) \tag{17}$$

(14) This result (eq 15) follows directly from theoretical equations presented in ref 5 and 7.

The terms involving A_{ij} are due to the relaxation effect, with A_{ij} given by

$$A_{ij} = \frac{\epsilon^2|Z_iZ_j|}{DkT}\frac{1}{3(2+\sqrt{2})}\frac{\kappa}{I^{1/2}} \qquad (18)$$

where I is the total ionic strength, D is the dielectric constant of the solvent, k is Boltzmann's constant, and T is the absolute temperature. The electrophoretic effect is given by the terms involving B_0, where

$$B_0 = \frac{F\epsilon}{C \times 10^{-8}}\frac{\kappa}{I^{1/2}}\frac{1}{3\pi\eta} \qquad (19)$$

Equations 16 and 17 are valid *approximations* for the limiting laws in any electrolyte mixture and, of course, include binary systems as a special case. Our numerical calculations indicate that eq 16 and 17 are surprisingly good approximations for the complete (*i.e., exact*) limiting laws even when the ionic mobilities differ considerably. For example, in the binary $LaCl_3$–H_2O system, where the ionic mobilities differ by more than a factor of 3, the approximate relaxation effects given in eq 16 and 17 are in error by about 20%. In the $CaCl_2$–H_2O system, the errors in the relaxation terms are only about 10%. The electrophoretic terms are identical in both the approximate and complete equations.

In Table I, the approximate and complete limiting laws are compared for the ternary system H_2O–LiCl(0.25 *M*)–KCl(0.2 *M*). The subscripts 1, 2, and 3 refer to Li^+, K^+, and Cl^-, respectively. Experimental l_{ij} values[3] are also included for comparison. Although the ionic mobilities of Li^+ and Cl^- differ by about a factor of 2, the approximate limiting law is found to be an excellent approximation for the complete limiting law. The total ionic strength (0.45) is much too high to expect quantitative agreement between experiment and a limiting-law theory. However, it is significant to note that the limiting laws are in qualitative agreement with experiment. In particular, l_{22}/c_3 and l_{33}/c_3 are correctly predicted by the limiting laws to be nearly equal and about twice the value of l_{11}/c_1. Also, the limiting laws correctly predict the signs and relative magnitudes of the l_{ij} ($i \neq j$) coefficients. Since the charges on ions 1 and 2 are of like sign, the electrophoretic effect for l_{12} is negative. The negative sign and small magnitude of l_{12} is simply the result of the negative electrophoretic effect being slightly larger than the positive relaxation effect.

C. Experimental Tests of the Limiting Laws. The general limiting laws include binary systems as a special case. The validity of the limiting laws for the more common transport coefficients, such as equivalent conductance, has ample experimental support in binary systems.[15] Since the common transport coefficients are combinations of the l_{ij},[2] the limiting laws for l_{ij} should also be valid, at least in binary systems. This conclusion is supported by the work of Lorenz,[16] where

Table I: Ternary l_{ij}: Comparison of Limiting-Law Theories for H_2O–LiCl–KCl

1 = Li^+; 2 = K^+; 3 = Cl^-

		H_2O–LiCl (0.25 *M*)–KCl (0.2 *M*)		
	$I \rightarrow 0$ (theory)	Complete L.L.	Approximate L.L.	Experiment
$10^{12}l_{11}/c_1$	4.154	3.25	3.28	3.60
$10^{12}l_{22}/c_2$	7.895	6.33	6.35	7.29
$10^{12}l_{33}/c_3$	8.200	6.35	6.38	7.17
$10^{12}l_{12}/\sqrt{c_1c_2}$	0.0	−0.34	−0.36	−0.20
$10^{12}l_{13}/\sqrt{c_1c_3}$	0.0	1.12	1.09	0.52
$10^{12}l_{23}/\sqrt{c_2c_3}$	0.0	1.17	1.20	0.69

dilute binary l_{ij} data are compared with predictions of the limiting laws. Surprisingly, the l_{12} data for 1–1 salts[1] remain in good agreement with the limiting law up to fairly high concentrations ($c \approx 0.05$).[16] As expected, unsymmetrical electrolytes show the greatest deviations from the limiting laws.[16] Our own l_{ij} and R_{ij} calculations on additional binary systems[2] support the generality of Lorenz's observations and indicate, as expected, that the limiting laws for R_{ij} are also valid.

The limiting law for diffusion of a tracer ion in a binary matrix solution is another special case of the general limiting laws. In tracer diffusion, the electrophoretic effect vanishes, and the concentration dependence of the intrinsic mobility of the tracer ion $(l_{ii}/c_i)^*$[17] depends on concentration of the matrix solution through the relaxation effect.[6] Experimental evidence[18] indicates the limiting laws for tracer diffusion are valid.

A quantitative test of the limiting laws for general multicomponent systems is not possible due to lack of suitable data. However, since the limiting laws are apparently valid for the special cases of tracer diffusion and binary l_{ij}, it may be inferred that the general limiting laws are also valid.

III. Extended Theory of l_{ij} and R_{ij} for Symmetrical Electrolytes

The limiting laws offer only a first-order approximation for the concentration dependence of l_{ij} and R_{ij}, and in general, agreement with experiment is expected only at high dilutions. It is of interest to extend the

(15) See, for example, H. S. Harned and B. B. Owen, "The Physical Chemistry of Electrolytic Solutions," 3rd ed, Reinhold Publishing Corp., New York, N. Y., 1958.

(16) P. B. Lorenz, *J. Phys. Chem.*, **65**, 704 (1961).

(17) The intrinsic mobility of the tracer ion $(l_{ii}/c_i)^*$ in Miller's units[2] is related to the tracer diffusion coefficient D_i^* in cm^2/sec by[3]

$$\frac{D_i^*}{RT} = 10^3\,(l_{ii}/c_i)^*$$

(18) R. Mills and E. W. Godbole, *J. Amer. Chem. Soc.*, **82**, 2395 (1960).

theory for l_{ij} and R_{ij} to higher concentrations by evaluating the contribution of higher order terms in the relaxation and electrophoretic effects. In particular, the contribution of ion-pair formation to the l_{ij} is of interest since this information is of interest in establishing a detailed physical interpretation of the l_{ij} and R_{ij}. We now consider the development of an extended theory of l_{ij} and R_{ij} for binary *symmetrical electrolytes.*

It has been shown[1,2,8] that values of l_{ij} in binary electrolytes (*i.e.*, l_{11}, l_{12}, and l_{22}) may be calculated from a knowledge of equivalent conductance Λ, transference numbers t_i, and thermodynamic diffusion coefficient L according to the relationship

$$\frac{l_{ij}}{c} = \frac{(-1)^{i+j}t_i t_j \Lambda}{|Z|10^3F^2} + L/c \qquad (20)$$

Therefore, theoretical expressions for l_{ij} may be derived by combining theories of equivalent conductance, transference, and diffusion. This procedure is satisfactory provided the theories for Λ, t_i, and L employ the same physical model and are mutually consistent in their mathematical approximations.

To develop theoretical equations for l_{ij}, existing mutually consistent "extended" theories for conductance[19] and diffusion[20] are combined using eq 20. The model common to both "extended" theories is the usual charged sphere in a continuum approximation which results in the "ion-atmosphere" description of electrolytes.[5] Both the "extended" conductance theory[19] and the "extended" diffusion theory[20] are developed retaining the full exponential of the Boltzmann equation. As a result, the effect of electrostatic ion-pair formation appears as a natural consequence of coulombic interactions. Both extended theories result in Bjerrum[21] ion-pair formation.[20]

The recovery of the l_{ij} equations from the conductance and diffusion theories is complex algebraically, but is straightforward. The procedure may be summarized as follows. The theoretical equations for the transference number and the equivalent conductance are evaluated from the Kremp–Kraeft–Ebeling (KKE) conductance theory.[19] In the KKE theory all terms of higher order than c in concentration are dropped. Thus, when the theoretical product $t_i t_j \Lambda$ is formed, all product terms of higher order than c are dropped.

Next a slight modification of the KKE theory is made. The function denoted by $Q^{\mathrm{Rel}}(b)$ in the KKE theory[19] is written in the form

$$Q^{\mathrm{Rel}}(b) = 1.9341 + \frac{1}{2}\frac{T(b)}{T(b) - 1} - 6Q(b)$$

where $Q(b)$ is the Bjerrum function[21] (defined by eq 23) and $T(b)$ is defined in the Appendix, eq A6.

Since $Q(b)$ is directly proportional to the Bjerrum equilibrium constant for ion-pair formation,[21] K_A, the term in the conductance equation proportional to $Q(b)$ represents the effect of ion-pair formation. Since $Q(b)$ is negative when $b < 2$, this interpretation of the $Q(b)$ term can be valid only when $b > 2$. If the degree of association is small, the association term in a conductance theory is directly proportional to $K_A cf$,[2] where f is the mean ionic activity coefficient. If terms of higher order than c are dropped, as in the KKE theory, f becomes unity. We thus "extend" the KKE theory to include some terms of order $c^{3/2}$ by replacing $Q(b)$ in the KKE equations by $f^2Q(b)$. Since this substitution is valid only when b is large, we adopt the convention $f = 1$ when b is small (*i.e.*, $b \sim 2$).

The diffusion theory defined by eq 51 and 53 of ref 20 is employed in the l_{ij} calculations. The negative exponential integral function $Ei(2\kappa a)$ which appears in the diffusion theory is approximated by

$$Ei(2\kappa a) \cong -0.5772 - \ln 2\kappa a$$

Finally, the theoretical expressions for $t_i t_j \Lambda$ and L/c are combined according to eq 20.

A. The Theoretical Equations. The l_{ij} Coefficients. The resulting theoretical equations for the intrinsic mobilities l_{ii}/c may be written in the form

$$10^{12}l_{ii}/c = \frac{0.10740}{|Z|}\left\{\lambda_i^\circ - \left(\frac{\lambda_i^{\circ 2}}{\Lambda^\circ}\alpha + \frac{\beta_0}{4}\right)c^{1/2} + \left[E_1'\frac{\lambda_i^{\circ 2}}{\Lambda^\circ} - E_2'\left(1 + \frac{\lambda_1^\circ\lambda_2^\circ}{\Lambda^{\circ 2}}\right)\right]c \ln c + \left[\frac{\lambda_i^{\circ 2}}{\Lambda^\circ}j_R(b) + j_E(b,\Lambda^\circ)\right]c - 12\left[\frac{\lambda_i^{\circ 2}}{\Lambda^\circ}E_1'Q(b) - \frac{2}{3}E_2'\frac{\lambda_1^\circ\lambda_2^\circ}{\Lambda^{\circ 2}}I(b)\right]f^2c\right\} \qquad (21)$$

where b is the Bjerrum parameter, and a is the usual "effective ionic diameter" with

$$b = \frac{\epsilon^2Z^2}{DkT}\frac{1}{a} \equiv \beta/a \qquad (22)$$

The functions $Q(b)$ and $I(b)$[22] are complex integral functions[20-22] whose asymptotic expansions for large b are given by

$$Q(b) \approx \frac{e^b}{b^4}(1 + 4/b + \ldots) \quad (b \gg 1) \qquad (23)$$

$$I(b) \approx \frac{e^b}{b^3}(1 + 3/b + \ldots) \quad (b \gg 1) \qquad (24)$$

When b is small (*i.e.*, $b \sim 2$, as in aqueous 1–1 electrolytes) we take $f = 1$. When b is large, f denotes the

(19) D. Kremp, W. D. Kraeft, and W. Ebeling, *Ann. Phys. (Leipzig)*, **18**, 246 (1966).

(20) M. J. Pikal, *J. Phys. Chem.*, **75**, 663 (1971).

(21) (a) N. Bjerrum, *Kgl. Danske Videnskab. Selskab.*, **7**, No. 9 (1926); (b) see also R. M. Fuoss and F. Accascina, "Electrolytic Conductance," Interscience Publishers, New York, N. Y., 1959.

(22) This function is defined in the Appendix, eq A11.

limiting-law approximation for the mean ionic activity coefficient

$$f^2 = e^{-\beta\kappa} \quad (25)$$

The symbols α and E_1' represent "constants" arising from the relaxation effect, while β_0 and E_2' represent "constants" arising from the electrophoretic effect. The function $j_R(b)$ arises from the relaxation effect, while $j_E(b,\Lambda^\circ)$ is a function coming from the electrophoretic effect. The notation used here is precisely defined in the Appendix.

The theoretical result for the interaction mobility l_{12}/c may be written in the form

$$10^{12}l_{12}/c = \frac{0.10740}{|Z|}\left\{\left(\frac{\lambda_1^\circ\lambda_2^\circ}{\Lambda^\circ}\alpha + \frac{\beta_0}{4}\right)c^{1/2} - \left[E_1'\frac{\lambda_1^\circ\lambda_2^\circ}{\Lambda^\circ} + \frac{E_2'}{2}\left(1 + 2\frac{\lambda_1^\circ\lambda_2^\circ}{\Lambda^{\circ 2}}\right)\right]c\ln c + \left[J_E(b,\Lambda^\circ) - \frac{\lambda_1^\circ\lambda_2^\circ}{\Lambda^\circ}j_R(b)\right]c + 12\left[E_1'\frac{\lambda_1^\circ\lambda_2^\circ}{\Lambda^\circ}Q(b) + \frac{2}{3}E_2'\frac{\lambda_1^\circ\lambda_2^\circ}{\Lambda^{\circ 2}}I(b)\right]f^2c\right\} \quad (26)$$

where $J_E(b,\Lambda^\circ)$ is an "electrophoretic" function defined in the Appendix (eq A12).

The R_{ij} Coefficients. The theoretical expressions for the R_{11}, R_{12}, and R_{22} coefficients are obtained by inversion of the l_{ij} matrix.[2] The various terms in cR_{ij} $(i,j = 1,2)$ are grouped according to their concentration dependence to give equations similar in form to eq 21 and 26. Terms of order $c^{1/2}$, $c\ln c$, c, and cf^2 are retained. All higher order terms are dropped. Using the theoretical expressions for R_{11}, R_{12}, and R_{22} and eq 6, theoretical expressions for the "solvent friction coefficients" R_{i0} $(i = 0,1,2)$ are derived. Since the "friction" coefficients R_{12}, R_{10}, and R_{20} are normally preferred for interpretation of data,[4] explicit equations will be presented only for these coefficients.

The theoretical equations for R_{12} and R_{i0} $(i = 1, 2)$ may be written in the form

$$-10^{-12}cR_{12} = \frac{|Z|}{0.10740}\left\{\left(\frac{\alpha}{\Lambda^\circ} + \frac{\beta_0}{4\lambda_1^\circ\lambda_2^\circ}\right)c^{1/2} - \left[E_1'/\Lambda^\circ + \frac{E_2'}{2\lambda_1^\circ\lambda_2^\circ}\left(1 + \frac{2\lambda_1^\circ\lambda_2^\circ}{\Lambda^{\circ 2}}\right)\right]c\ln c + \gamma_{12}(b,\Lambda^\circ)c + 12\left[\frac{E_1'}{\Lambda^\circ}Q(b) + \frac{2E_2'}{3}\frac{I(b)}{\Lambda^{\circ 2}}\right]f^2c\right\} \quad (27)$$

$$-10^{-12}c_oR_{i0} = \frac{|Z|}{0.10740}\left\{1/\lambda_1^\circ + \frac{\beta_0}{4}(1/\lambda_1^{\circ 2} - 1/\lambda_1^\circ\lambda_2^\circ)c^{1/2} + E_2'\left[(1/\lambda_i^{\circ 2})\left(1 + \frac{\lambda_1^\circ\lambda_2^\circ}{\Lambda^{\circ 2}}\right) + \frac{1}{2\lambda_1^\circ\lambda_2^\circ}\left(1 + \frac{2\lambda_1^\circ\lambda_2^\circ}{\Lambda^{\circ 2}}\right)\right]c\ln c + \gamma_{i0}(b,\Lambda^\circ)c - \frac{8E_2'}{\Lambda^\circ\lambda_i^\circ}I(b)f^2c\right\} \quad (28)$$

The functions $\lambda_{12}(b,\Lambda^\circ)$ an $\lambda_{i0}(b,\Lambda^\circ)$ are rather complex and are defined in the Appendix (eq A13 and A14).

In the theoretical equations for l_{ij} and R_{ij}, the terms involving α and E_1' are due to the relaxation effect (*i.e.*, asymmetry of the ion atmosphere), while the terms involving β_0 and E_2' are due to electrophoretic effect (*i.e.*, hydrodynamic interactions due to the presence of an ion atmosphere). Although the terms proportional to cf^2 originate in the relaxation and electrophoretic calculations, it will be shown later that these terms may be interpreted in terms of ion-pair formation if b is large.

It should be noted that while *both* the relaxation effect and the electrophoretic effect make significant contributions to all the concentration-dependent terms for l_{ij}/c and cR_{12}, the relaxation effect does *not* affect R_{i0} measurably. The only terms in R_{i0} involving the relaxation effect is a very small relaxation-electrophoretic product term in γ_{i0}, which depends on $\alpha\beta_0\cdot(\lambda_1^\circ - \lambda_2^\circ)$. This result is expected. As Miller shows,[2] R_{i0} may be expressed in terms of the transference number and the thermodynamic diffusion coefficient. Diffusion in a binary system is independent of the relaxation effect.[5,20] The transference number, as calculated from the KKE theory, shows only a slight dependence on the relaxation effect through the product $\alpha\beta_0(\lambda_1^\circ - \lambda_2^\circ)$.

The theoretical expressions for $10^{-12}cR_{ii}$ and $10^{-12}(c_o^2/c)R_{oo}$ are similar to eq 28. The limiting values for $10^{-12}cR_{ii}$ and $-10^{-12}c_oR_{i0}$ are identical. However, $10^{-12}cR_{ii}$ depends on both the relaxation effect and the electrophoretic effect. The quantity $10^{-12}(c_o^2/c)R_{oo}$ depends only on the electrophoretic effect, and its limiting value involves both λ_1° and λ_2°.

The Fuoss–Onsager–Skinner (FOS) conductance theory[23] is also developed using the full exponential of the Boltzmann equation. Theoretical expressions for l_{ij} and R_{ij} based upon the FOS conductance theory are similar to the results given in eq 21–28. The limiting-law terms are identical. The small differences between "$c\ln c$ terms" are not experimentally detectable. Although differing in detail, the "c terms" are of similar form and magnitude. We note that the R_{i0} coefficients are completely independent of the relaxation effect using the FOS theory. The most significant differences occur in the terms proportional to cf^2, basically because the KKE theory predicts Bjerrum ion-pair formation[19] while the FOS theory leads to "contact" ion-pair formation.[23] The KKE theory and the extended diffusion theory[20] are consistent in that both theories lead to Bjerrum ion-pair formation.[20] Thus, only the results based upon the KEE theory are explictly given here. However, most of our conclusions based upon eq 21–28 also follow from the corresponding equations based upon the FOS conductance theory.

(23) R. M. Fuoss, L. Onsager, and J. F. Skinner, *J. Phys. Chem.*, **69**, 2581 (1965).

Schönert[9] recently suggested that the concentration dependence of the l_{ij} or R_{ij} coefficients may be expressed in terms of power series expansions involving concentrations of the components in the solution. Our results are in partial agreement with Schönert's suggestions. Terms of order $c^{1/2}$ and $(c^{1/2})^2$ are present. However, terms of order c ln c are also present. A power series representation of the c ln c terms converges slowly when $c < 1$. Thus, the concentration dependence of l_{ij} and R_{ij} in dilute electrolytes is best described with a series composed of terms of order $c^{n/2}$ ($n = 1, 2, 3, \ldots$) and $c^{n/2}$ ln c ($n = 2, 3, \ldots$).

Because of mathematical and physical approximations made during the development of the KKE conductance theory[19] and the extended diffusion theory,[20] eq 21, 26, 27, and 28 are limited to dilute solutions, *i.e.*, systems for which $\kappa a \ll 1$. Of course, even in dilute solutions, the theoretical l_{ij} and R_{ij} equations are not exact. For example, neither the recently proposed modification of the c ln c term in conductance[24,25] theory nor the Onsager–Provencher "chemical kinetic effect"[26] is included in the $l_{ij}(R_{ij})$ theory. Since neither of these effects is given to order c in concentration, they may not be incorporated into the $l_{ij}(R_{ij})$ equations in a consistent manner. In general, both effects are small, although in some cases the "chemical kinetic effect" is significant.[26]

For most electrolyte systems, one expects eq 21, 26, 27, and 28 to be good approximations below concentrations corresponding to $\kappa a \sim 0.2$. Although the extended diffusion theory has been experimentally checked,[20] the KKE theory has not been experimentally tested. Thus, to verify the essential validity of the theoretical l_{ij} and R_{ij} equations, we now examine the correspondence between theory and experiment.

B. Experimental Test of the Extended Theory. Aqueous 1–1 Electrolytes at 25°. For aqueous 1–1 electrolytes at 25° the Bjerrum parameter b is small (*i.e.*, $b = 1.8$ when $\mathring{a} = 4$ Å), and as discussed earlier, we take $f = 1$ in eq 21, 26, 27, and 28. Given the limiting ionic conductances λ_1° and λ_2°, the contributions of the various terms in the theoretical l_{ij} and R_{ij} equations are evaluated using the equations in the Appendix, existing tabulations of $Q(b)$[15] and $I(b)$,[20] and numerical values for the fundamental constants.[21b] For the usual aqueous 1–1 electrolyte (*i.e.*, $\mathring{a} \sim 4$ Å), the term in l_{12}/c of order c ln c partially cancels the term of order c. Thus, deviations from the limiting law at finite (but dilute) concentrations are small. The same comment is valid for cR_{12}.

Numerical calculations show that the electrophoretic effect in l_{ij}/c for aqueous 1–1 salts depends only slightly on the limiting ionic conductances λ_i° and the a parameter. For a series of aqueous 1–1 electrolytes, specific effects in l_{ij}/c are due to the dependence of the relaxation effect on the limiting ionic conductances and the a parameter. Several general trends are worth noting.

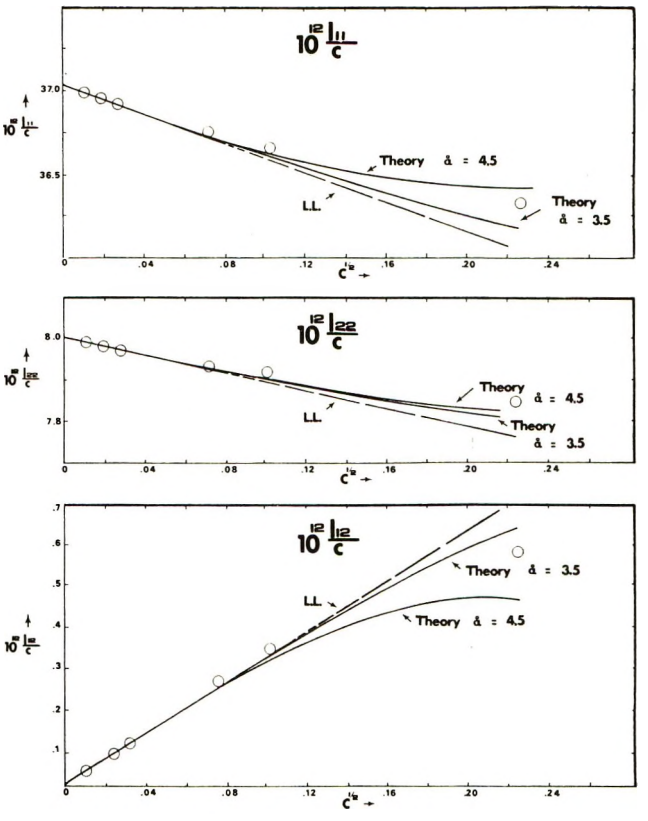

Figure 1. l_{ij}/c for HCl–H_2O at 25°. Comparison of theory with experiment: O, experimental.

First, as a is decreased for a given salt (*i.e.*, constant λ_2° and λ_1°), the magnitude of the relaxation effect increases. Since the contribution of the relaxation effect to the intrinsic mobility l_{ii}/c is negative, the value of l_{ii}/c decreases as a decreases. The contribution of the relaxation effect to l_{12}/c is positive. Thus, as a decreases, l_{12}/c increases.

Second, for a given value of a, the value of l_{ii}/c decreases as $\lambda_i^{\circ 2}/\Lambda^\circ$ increases, while l_{12}/c increases as $\lambda_1^\circ\lambda_2^\circ/\Lambda^\circ$ increases.

A numerical comparison of the extended l_{ij} theory with data for aqueous HCl, LiCl, NaCl, and KCl[2] shows the theory to be quantitative below about 0.01 M. The results are not particularly sensitive to the choice of the a parameter at concentrations where the theory is expected to be valid, *i.e.*, $\kappa a < 0.2$. As several examples of these comparisons, the extended theory, the limiting-law, and the experimental data are compared in Figure 1 for HCl and in Figure 2 for LiCl. The broken line represents the limiting law (labeled "L.L."), *i.e.*, only the $c^{1/2}$ term. The subscript 1 refers to the cat-

(24) P. C. Carman, *J. Phys. Chem.*, **74**, 1653 (1970).

(25) L. Onsager and M. S. Chen, *Proc. Nat. Acad. Sci. U. S.*, **63**, 2281 (1969).

(26) L. Onsager and S. W. Provencher, *J. Amer. Chem. Soc.*, **90**, 3134 (1968).

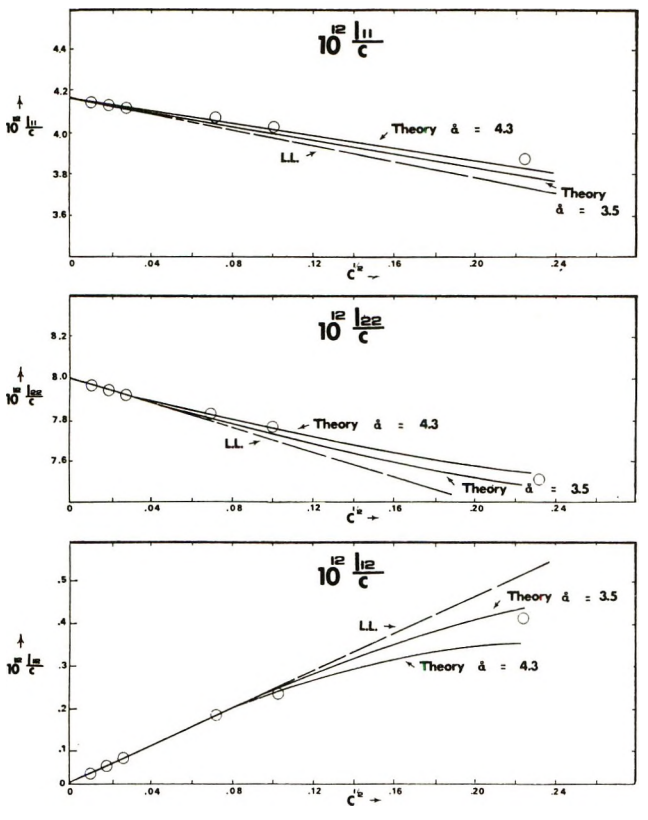

Figure 2. l_{ij}/c for LiCl–H_2O at 25°. Comparison of theory with experiment: O, experimental.

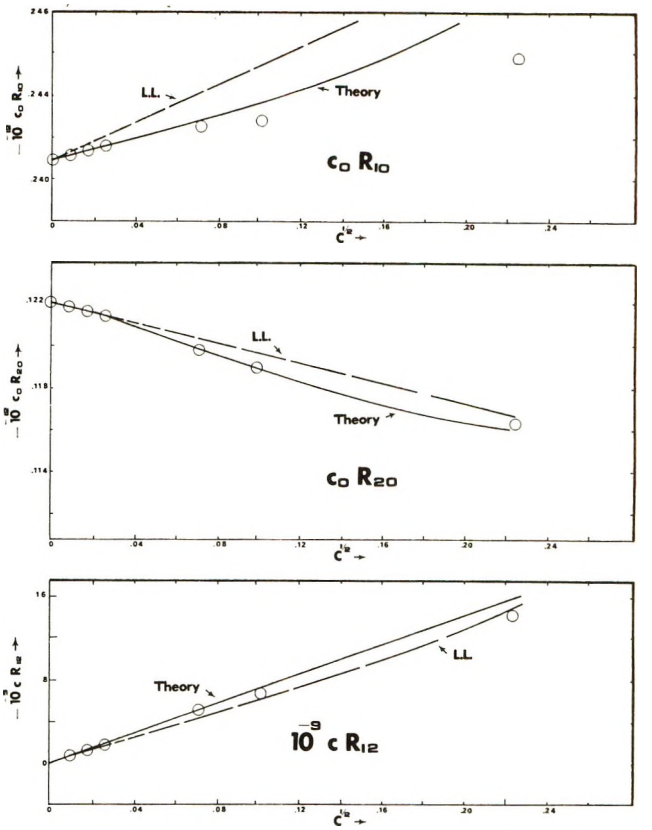

Figure 3. $c_j R_{ij}$ ($i \neq j$) for LiCl–H_2O at 25°. Comparison of theory with experiment: å = 3.5; O, experimental.

ion while the subscript 2 denotes the anion, in these cases Cl^-. The extended theory, denoted by a solid curve (labeled "theory"), is given for two values of the a parameter. The higher a values are those given by Robinson and Stokes,[27] which are based on a Debye–Hückel activity coefficient theory including hydration. The a value of 3.5 Å was arbitrarily selected to illustrate the variation of the theoretical l_{ij} with a.

As illustrated in Figures 1 and 2, the limiting laws are in good agreement with the data at low concentrations and in fair agreement even at $c = 0.05$. These observations are in accord with previous studies.[16] The extended theory and the limiting laws do not differ greatly at low concentrations. Deviations of the data from the limiting laws are positive for the intrinsic mobilities l_{ii}/c and negative for the interaction mobilities l_{12}/c. These deviations are qualitatively predicted by the extended theory for both choices of the a parameter. It may be noticed that the use of $a = 4.0$ Å in the extended theory for both HCl and LiCl would result in surprisingly good agreement between theory and experiment up to 0.05 M (*i.e.*, $\kappa a \sim 0.3$).

Comparing the concentration dependence of the intrinsic mobilities plotted in Figures 1 and 2, it is observed that the intrinsic mobility of the hydrogen ion (*i.e.*, l_{11}/c for HCl) decreases quite rapidly with increasing concentration. This strong concentration dependence is due to the dependence of the relaxation effect on the ratio $\lambda_1^{\circ 2}/\Lambda^\circ$, which is large for HCl. Also, comparing Figures 1 and 2, it is observed that l_{12}/c for HCl is significantly larger than l_{12}/c for LiCl. This difference in l_{12}/c values arises from the dependence of the relaxation effect on $\lambda_1^\circ\lambda_2^\circ/\Lambda^\circ$.

Since the extended theory for l_{ij} is in satisfactory agreement with experiment, one may infer that the extended theory for R_{ij} also compares favorably with experiment. The validity of the preceding statement is illustrated in Figure 3 where c_oR_{10}, c_oR_{20}, and cR_{12}, calculated from theory (eq 27 and 28) for LiCl are compared with the corresponding data. The broken line represents the limiting law, while the solid curve represents the extended theory with $a = 3.5$ Å. For R_{10} and R_{20}, the extended theory is clearly a better approximation than the limiting law. For R_{12}, the extended theory differs but slightly from the limiting law. However, we note that the maximum observed in a plot of $c^{1/2}R_{12}$ *vs.* $c^{1/2}$ is obviously not predicted by the limiting law but *is* predicted by the extended theory.

From Figure 3, it is obvious that the R_{12} theory is in excellent agreement with experiment below about 0.01 M. Thus, contrary to earlier skepticism,[9] $-R_{12}$ does indeed become infinite as the concentration decreases toward zero.

(27) R. A. Robinson and R. H. Stokes, "Electrolyte Solutions," 2nd ed, Academic Press, New York, N. Y., 1959.

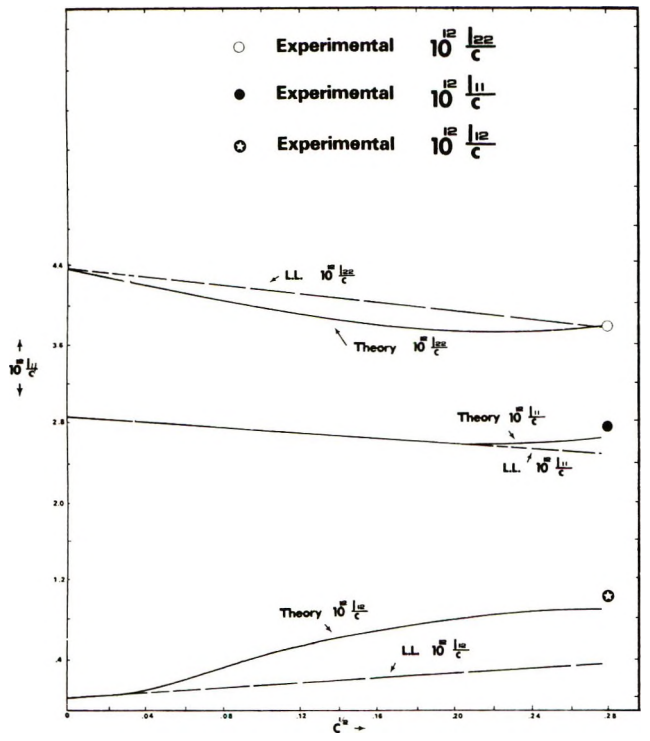

Figure 4. $10^{12}l_{ij}/c$ for $ZnSO_4$–H_2O at 25°. Comparison of theory with experiment: $\mathring{a}$ = 3.9.

Aqueous $ZnSO_4$ at 25°. It is desirable to test the extended theory for $l_{ij}(R_{ij})$ for electrolytes where the Bjerrum parameter b is large, *i.e.*, for aqueous 2–2 electrolytes. Unfortunately, no suitable l_{ij} data exist in the literature. However, a survey of the literature does provide suitable transport data[28,29] from which l_{ij} are calculated (using eq 20) for 0.005 M aqueous zinc sulfate at 25°. The following data are calculated: $10^{12}l_{11}/c = 2.69_1$; $10^{12}l_{22}/c = 3.75_8$; $10^{12}l_{12}/c = 0.945$, where the subscripts 1 and 2 denote the cation and anion, respectively.

Theoretical values of l_{ij} for aqueous $ZnSO_4$ are computed from eq 21 and 26 using limiting conductance data from the literature[15,27] and using a = 3.9 Å. This choice of a was prompted by Guggenheim's theoretical analysis[30] of activity coefficient data, in which the full Boltzmann exponential was retained. Guggenheim found good agreement between theory and experiment for aqueous 2–2 electrolytes when, $3.5 < a < 4.0$. For $ZnSO_4$, a value slightly less than 4.0 Å is indicated. We note that when b is large (*i.e.*,here $b \sim 7$ for $a \sim 4$ Å), $Q(b)$ and $I(b)$ are large and change rapidly as b changes. Thus, the calculated values of l_{ij} for $ZnSO_4$ are quite sensitive to the choice of a.

In Figure 4, the limiting-law, the extended theory, and the experimental data are compared for aqueous $ZnSO_4$. The limiting law is represented by the broken line (denoted "L.L."); the extended theory is represented by the solid curve (denoted "theory"); and the experimental points are given as circles. Although the experimental data are at a rather high concentration ($\kappa a \sim 0.2$), the agreement between the extended theory and the data is quite satisfactory. It should be noted that the limiting law is an exceedingly bad approximation in the case of the interaction mobility l_{12}/c. Significant differences between the extended theory for l_{12} and the limiting law occur at very low concentrations.

In spite of the limited quantity of experimental data, the comparison presented in Figure 4 does establish the essential validity of the extended theory for l_{ij} under conditions of large b.

C. The Effect of Ion-Pair Formation. Intuitively, one expects ion-pair formation to increase the interaction mobility l_{12}/c. The *net* effect of ion-pair formation on an intrinsic mobility l_{ii}/c is not obvious. However, intuitively, one expects the effect to depend on the difference between the mobility of the free i-type ion and the mobility of the ion pair. It will now be demonstrated that when b is large the terms in the extended theory proportional to cf^2 represent the effects of ion-pair formation.[31]

Using the approximation $\Lambda^\circ/2 \approx \sqrt{\lambda_1^\circ\lambda_2^\circ}$, converting ionic conductances λ_i° into absolute mobilities ω_i by means of eq 8, and using the asymptotic expansions for $Q(b)$ an $I(b)$ given by eq 23 and 24, the terms proportional to cf^2 in eq 21 and 26 which we denote by $(10^{12}l_{ii}/c)_{IP}$ and $(10^{12}l_{12}/c)_{IP}$ become

$$\left(10^{12}\frac{l_{ii}}{c}\right)_{IP} = 0.10740\frac{F\epsilon}{C \times 10^{-8}}(\omega_m - \omega_i)K_A f^2 c \quad (29)$$

$$\left(10^{12}\frac{l_{12}}{c}\right)_{IP} = 0.10740\frac{F\epsilon}{C \times 10^{-8}}\omega_m K_A f^2 c \quad (30)$$

where for large b, ω_m is given by

$$\omega_m = \frac{1}{2}\left[\sqrt{\omega_1\omega_2} + \frac{1}{6\pi\eta a}\right] \quad (31)$$

As shown recently,[20] the quantity ω_m is the theoretical value for the mobility of the ion pair. The quantity K_A is the Bjerrum[21] association constant for large b

(28) For 0.005 M aqueous zinc sulfate at 25°, the following experimental values for equivalent conductance Λ, transference number t_1, and thermodynamic diffusion coefficient L were obtained: Λ = 84.9_1, from existing tabulations;[15] t_1 = 0.382_9, from Dye, Farber, and Karl;[29] $10^{12}L/c = 2.02_0$, from the smoothed $ZnSO_4$ data given in Figure 2 in ref 20.

(29) J. L. Dye, M. P. Farber, and D. J. Karl, *J. Amer. Chem. Soc.*, **82**, 314 (1960).

(30) E. A. Guggenheim, *Trans. Faraday Soc.*, **56**, 1152 (1960); see also ref 20.

(31) The Onsager–Provencher "chemical kinetic" effect,[26] which is not included in our theory for l_{ij}, *may* be significant in systems where significant ion-pair formation is present. As Onsager and Provencher show,[26] the kinetics of dissociation and recombination involved in the equilibrium between free ions and ion pairs provides an additional mechanism for relaxing the asymmetric ion atmosphere surrounding a moving "free" ion. Thus this "chemical kinetic" effect decreases the magnitude of the relaxation effect. Since the relaxation effect increase l_{12}/c, the "chemical kinetic effect" decreases l_{12}/c from the value calculated by eq 26. Also, since the relaxation effect decreases l_{ii}/c, the chemical kinetic effect increases l_{ii}/c from the value calculated by eq 21.

$$K_A = \frac{4\pi N_0 a^3}{1000}\frac{e^b}{b} \qquad (32)$$

where N_0 is Avogadro's number.

The effect of ion-pair formation on the interaction mobility l_{12}/c is directly proportional to the mobility of the ion pair and the effect on the intrinsic mobility l_{ii}/c is directly proportional to the difference $\omega_m - \omega_i$.

The results presented here are based on the "large b limit" of the KKE conductance theory and the extended diffusion theory. However, equations of the same *general form* as eq 29 and 30 may be derived using alternate assumptions. Assuming that the ions may be distinctly classified as either "free ions" or ions in ion pairs, Harned and Hudson's general theory of ion-pair formation for diffusion[32] is combined, using eq 20, with the Arrhenius expression, $\lambda_i = \lambda_i^\circ\alpha$, where $1 - \alpha$ is fraction of ion pairs. If the fraction of paired ions is small, $1 - \alpha \approx cf^2K_A$, and equations of the same general form as eq 29 and 30 are obtained. However, in the Harned–Hudson–Arrhenius equations, K_A and ω_m are present as adjustable parameters. In the extended l_{ij} theory presented here, K_A and ω_m are determined by the theory.

It should be noted that, in general, $\omega_i \neq \omega_m$ and the intrinsic mobility l_{ii}/c does depend on ion-pair formation. Ion-pair formation always increases l_{12}/c. In principle, the intrinsic mobility may be either increased or decreased. For aqueous $ZnSO_4$ at 25° eq 31 gives the order: $\omega_1 \approx \omega_m < \omega_2$. Thus, for aqueous $ZnSO_4$, ion-pair formation decreases the intrinsic mobility of the anion SO_4^{2-} but has little effect on the intrinsic mobility of the cation Zn^{2+}.

Using the same development that leads to eq 29–32, the effect of ion-pair formation on R_{ij} is calculated. Denoting the terms proportional to cf^2 in eq 27 and 28 by $(-10^{-12}cR_{12})_{IP}$ and $(-10^{-12}c_oR_{io})_{IP}$, respectively, we find

$$(-10^{-12}cR_{12})_{IP} = \frac{C \times 10^{-8}}{0.10740F\epsilon}\frac{\omega_m}{\omega_1\omega_2}K_Af^2c \qquad (33)$$

$$(-10^{-12}c_oR_{io})_{IP} = -\frac{C \times 10^{-8}}{0.10740F\epsilon}\frac{1}{\omega_i}\left[\frac{2\omega_m}{\sqrt{\omega_1\omega_2}} - 1\right]K_Af^2c \qquad (34)$$

Comparing eq 34 and 31, it will be noticed that the right-hand side of eq 34 is always negative. Thus, ion-pair formation always (in this theory) decreases the "ion-solvent friction coefficient," $-c_oR_{io}$.

IV. Some General Conclusions

Since the R_{ij} coefficients become infinite as the concentration approaches zero, it does not seem reasonable to interpret R_{ij} in terms of friction between components.[2] Rather, the interpretation of c_jR_{ij} as friction coefficients[4,33] is preferable. However, the utility of the friction concept in interpreting the long-range electrostatic and hydrodynamic interactions in electrolytes is open to question. For example, cR_{12} reflects ion–solvent interactions through the appearance of λ_i° in the concentration-dependent terms. Thus, cR_{12} cannot be interpreted strictly in terms of friction between anion and cation.

Miller[2] interprets the intrinsic mobility l_{ii}/c as the mobility ion i would have in the absence of interactions with the ion of opposite charge. Since l_{ii}/c does depend on ion-pair formation, this interpretation of l_{ii}/c cannot be wholly correct.

The numerical value of the interaction mobility l_{12}/c *does* depend, to some extent, on the ion–solvent interactions since the magnitude of the relaxation effect depends upon λ_i°. Therefore, difference in ion–solvent interactions must be considered when l_{12}/c data for various electrolytes are being compared.

Both the relaxation effect and the electrophoretic effect make significant contributions to *all* the concentration-dependent terms in the intrinsic mobility l_{ii}/c. As Onsager points out,[6] the electrophoretic effect does not appear in the theoretical description of self-diffusion. Therefore, it may be concluded that there exists no exact phenomenological relationship between the self-diffusion coefficient of component i and l_{ii}/c for binary electrolytes. Similar arguments, based on the limiting-law theories, have led other workers[8,9] to the same conclusion. The results of this research show that higher order terms in the l_{ii}/c theory lead to the same conclusion.

Although the theoretical equations presented in this research are quantitative only in dilute electrolyte solutions, it seems likely that the qualitative general conclusions discussed above have some validity in any electrolyte system. For example, the practice[33,34] of employing self-diffusion data to evaluate friction coefficients in membranes is likely an approximation which ignores long-range hydrodynamic interactions (electrophoretic effect).

Acknowledgments. The author wishes to thank Dr. D. G. Miller for many informative discussions regarding the application of irreversible thermodynamics to electrolytes.

Appendix

Definition of Terms in Extended Theory for l_{ij} and R_{ij}. The relaxation constant α is defined by

$$\alpha = \frac{\kappa\beta}{c^{1/2}}\frac{1}{3(2 + \sqrt{2})} \qquad (A1)$$

and the electrophoretic constant β_0 is

(32) H. S. Harned and R. M. Hudson, *J. Amer. Chem. Soc.*, **73**, 3781 (1951).

(33) K. S. Spiegler, *Trans. Faraday Soc.*, **54**, 1408 (1958).

(34) P. Meares, D. G. Dawson, A. H. Sutton, and J. F. Thain, *Ber. Bunsenges. Phys. Chem.*, **71**, 765 (1967).

$$\beta_0 = \frac{F\epsilon|Z|}{3\pi\eta C \times 10^{-8}} \frac{\kappa}{c^{1/2}} \quad \text{(A2)}$$

where η is the coefficient of viscosity of the solvent. The relaxation term E_1' is

$$E_1' = \frac{1}{24}\left(\frac{\beta\kappa}{c^{1/2}}\right)^2 \quad \text{(A3)}$$

and the electrophoretic constant E_2' is given by

$$E_2' = \frac{1}{16}\beta_0\frac{\beta\kappa}{c^{1/2}} \quad \text{(A4)}$$

The relaxation function $j_R(b)$ is defined by

$$j_R(b) = E_1'\left[\frac{T(b)}{T(b) - 1} + 3.8682 + \ln 24E_1'\right] \quad \text{(A5)}$$

where

$$T(b) = \exp(-b)[1 + b + b^2/2] \quad \text{(A6)}$$

The electrophoretic function $j_E(b,\Lambda^\circ)$ is given by

$$j_E(b,\Lambda^\circ) = E_2'\left\{\frac{4p^2}{b} - 1.1544 - \ln 96E_1' + 2\ln b + \frac{4\lambda_1^\circ\lambda_2^\circ}{\Lambda^{\circ 2}}\left[2W\cdot I(-b) + \frac{Q^{EL}(b)}{2} - \frac{1}{4}\ln 24E_1'\right]\right\} \quad \text{(A7)}$$

where

$$p^2 = \left(\frac{\lambda_1^\circ - \lambda_2^\circ}{\Lambda^\circ}\right)^2 \quad \text{(A8)}$$

$$W = \frac{1}{2}\left[\frac{\lambda_2^\circ}{\lambda_1^\circ} + \frac{\lambda_1^\circ}{\lambda_2^\circ}\right] \quad \text{(A9)}$$

The function $Q^{EL}(b)$ is a complex electrophoretic function[19] which may be represented by the simpler empirical function

$$Q^{EL}(b) \approx -2.151 - 5.069e^{-b} - 0.390\ln b + 10.860/b \quad (1 < b < 10) \quad \text{(A10)}$$

The integral function $I(x)$ is defined by

$$I(x) = \int_0^x \left(\frac{e^u - 1 - u - u^2/2}{u^3}\right) du \quad \text{(A11)}$$

The function $J_E(b,\Lambda^\circ)$ is the electrophoretic function

$$J_E(b,\Lambda^\circ) = j_E(b,\Lambda^\circ) + E_2'[1/2\ln 24E_1' - Q^{E1}(b)] \quad \text{(A12)}$$

The coefficients of the "c" terms in eq 27 and 28 may be written as

$$\gamma_{12}(b,\Lambda^\circ) = \frac{j_E(b,\Lambda^\circ)}{\lambda_1^\circ\lambda_2^\circ} + \frac{E_2'}{\lambda_1^\circ\lambda_2^\circ}[1/2\ln 24E_1' - Q^{E1}(b)] - \frac{j_R(b)}{\Lambda^\circ} + \frac{\Lambda^\circ}{(\lambda_1^\circ\lambda_2^\circ)^2}\left[\frac{\lambda_1^\circ\lambda_2^\circ}{\Lambda^\circ}\alpha + \beta_0/4\right]^2 \quad \text{(A13)}$$

$$-\gamma_{i0}(b,\Lambda^\circ) = \frac{1}{\lambda_i^{\circ 2}} + \frac{1}{\lambda_1^\circ\lambda_2^\circ}j_E(b,\Lambda^\circ) + \frac{E_2'}{\lambda_1^\circ\lambda_2^\circ}[1/2\ln 24E_1' - Q^{E1}(b)] + \frac{(\lambda_i^\circ - \lambda_j^\circ)}{2\lambda_1^\circ\lambda_2^\circ\Lambda^\circ}\alpha\beta_0 + \frac{(\lambda_i^\circ - \lambda_j^\circ)\Lambda^\circ}{16(\lambda_1^\circ\lambda_2^\circ)^2\lambda_i^\circ}\beta_0^2 \quad \text{(A14)}$$

Interactions of Aqueous Poly(*N*-vinylpyrrolidone) with Sodium Dodecyl Sulfate. I. Equilibrium Dialysis Measurements[1a,b]

by M. L. Fishman* and F. R. Eirich

Department of Chemistry, Polytechnic Institute of Brooklyn, Brooklyn, New York 11201 *(Received October 26, 1970)*

Publication costs borne completely by The Journal of Physical Chemistry

The interactions of sodium dodecyl sulfate (SDS) and aqueous poly(*N*-vinylpyrrolidone) (PVP) were studied by means of equilibrium dialysis at 25 and 30° and at several polymer concentrations. The analytic concentrations of SDS were measured by conductivity. In order to interpret the dialysis data, it was necessary to consider the Donnan equation for the distribution of unbound SDS across the semipermeable membrane in concentrations above its cmc. The data indicate that the addition of PVP to aqueous SDS solution produces an association polyelectrolyte. At constant polymer concentration and varying SDS concentration, three regions of behavior can be distinguished. At very low ratios of detergent to polymer (S/P) minimal interaction occurs. At intermediate (S/P) ratios, clusters, or submicelles, are formed. At high (S/P) ratios, these submicelles are converted to mixed regular micelles at a cmc lower than that of pure SDS, which have a constant surface charge density and are in equilibrium with a fixed concentration of detergent ions. In region three, the fixed detergent ion concentration decreases with increasing polymer concentration while the fraction of bound sodium counterions decreases. Thus, PVP acts as a nucleating agent for detergent micelles and stabilizes detergent clusters larger than dimers but smaller than observable in the absence of polymer.

It has been shown that water soluble polymers become "association polyelectrolytes" in the presence of large, ionizable molecules such as ionic detergents, many dyes, etc.[2-11] Below, we present an investigation of the state of aggregation of a detergent ion, dodecyl sulfate, and its counterion, Na, in the presence of the macromolecule in pure or complexed form. The results, we believe, are of importance for the understanding of the effects of cosolutes on the state of solution of polymers, for the formation of coacervates, mixed precipitates, and of protein–lipid complexes.

In pure aqueous detergent solution, emf measurements have been used by Botre, Mele, and Crescenzi[12] to measure counterion binding to detergent micelles. Botre, *et al.*,[10] have extended this method to polymer–detergent solutions, but in doing so had to make an assumption concerning the value of the detergent cmc[13] in the presence of the polymer–detergent complex. In our studies, the approach of Botre, Mele, and Crescenzi has been changed by employing conductimetry and by introducing the equilibrium dialysis technique.

The chief advantage of our method is that it permits one to eliminate *a priori* assumptions of the value at which the cmc occurs in the presence of the macromolecule. Previous investigators[9-11] have assumed that the monomeric detergent concentration in equilibrium with micelles and polymer–detergent complex is the same as obtained in the absence of polymer. The data to be presented in these studies show that this assumption is not correct. Further, our data show that while this assumption may be acceptable at low polymer concentration, it becomes increasingly poorer with increasing polymer concentration.

Experimental Materials. Poly(*N*-vinylpyrrolidone) (PVP) was synthesized from 1-vinyl-2-pyrrolidone obtained from General Aniline and Film Corp. The monomer was freed of stabilizer (0.1% NaOH), by vacuum distillation immediately prior to the bulk poly-

* To whom correspondence should be addressed at Richard B. Russell Agricultural Research Center, Athens, Ga. 30604.

(1) (a) Presented in part at the 158th National Meeting of the American Chemical Society, New York, N. Y., Sept 7–12, 1969; (b) this material is taken from a doctoral dissertation by M. L. Fishman presented to the Polytechnic Institute of Brooklyn in partial fulfillment of requirements for the Ph.D. in Chemistry. The financial assistance which made this study possible by the National Institute of Health, the National Institute of Dental Research, is gratefully acknowledged.

(2) S. Barkin, H. P. Frank, and F. R. Eirich, *Ric. Sci. Sez. A*, **25**, 844 (1955).

(3) W. Scholtan, *Makromol. Chem.*, **11**, 131 (1954).

(4) S. Barkin, H. P. Frank, and F. R. Eirich, *J. Phys. Chem.*, **61**, 1357 (1957).

(5) S. Saito, *Kolloid Z.*, **154**, 19 (1957).

(6) S. Saito, *ibid.*, **158**, 120 (1958).

(7) I. Maruta, *J. Chem. Soc., Jap.*, **83**, 782 (1962).

(8) M. Nakagaki and Y. Ninomiya, *Bull. Chem. Soc.*, **37**, 817 (1964).

(9) M. N. Jones, *J. Colloid Sci.*, **23**, 36 (1967).

(10) C. Botre, F. De Martiis, and M. Solinas, *J. Phys. Chem.*, **68**, 3624 (1964).

(11) S. Gravsholt, L.T.D. Thesis, Fysisk-Kemisk Institut, Technical University of Denmark, Feb 1969.

(12) C. Botre, V. L. Crescenzi, and A. Mele, *J. Phys. Chem.*, **63**, 650 (1959).

(13) In our context we define the cmc as the fixed concentration of monomeric detergent ion in equilibrium with micellized detergent.

merization which was carried out in sealed tubes containing the azobisisobutyronitrile initiator. The PVP thus obtained was freed of monomer and low molecular weight polymers by twice dissolving it in $CHCl_3$ and precipitated into anhydrous ether, drying the polymer, dialyzing it against deionized water, and freeze drying it. By utilizing viscometry constants determined by Frank and Levy,[14] the molecular weight measured in water was found to be 420,000 and 400,000 in methanol.

Sodium dodecyl sulfate (SDS) was synthesized from lauryl alcohol (>99% pure as determined by vapor phase chromatography) obtained from the Givaudan Chemical Co. The SDS, after recrystallization from ethanol, isopropyl alcohol, and a 50:50 mixture, was extracted with hexane for several days. The cmc, taken as the value of the intersection of two straight lines in a plot of specific conductivity against concentration, was found to be 8.24 m*M*.

Deionized, singly distilled (Corning Model Ag-2 still) water was used in all experiments. The average conductivity measured 1.5 μmhos per centimeter.

Equilibrium Dialysis Apparatus. Figure 1 shows a schematic diagram of the Plexiglas equilibrium dialysis cell. The basic design was suggested by Molyneux.[15] Circular cellulose acetate membranes (80 μ thick) purchased from Carl Schleicher and Schuell Co. were used in all dialysis experiments. Each chamber of the dialysis cell contained a small Teflon ball to aid mixing. In addition, during a dialysis run, the entire cell was contained in a thermostated (±0.2°) shaker bath.

Procedure. In a typical dialysis experiment the cells were thoroughly rinsed with a soap solution and distilled water before assembling and installing the membrane. The cells were then filled with distilled water which was changed daily until the conductivity remained constant. Immediately prior to use they were drained and filled with the solutions to be equilibrated.

After seven or more days on the shaker, the solutions were withdrawn by syringe from each chamber, the liquid volume in each chamber measured, and the SDS concentration found by conductivity.

Seven days was chosen as the minimum time of a dialysis experiment as a result of a series of experiments which were run in the absence of polymer. Initially, 10 m*M* SDS was placed in one chamber of the dialysis cell and an equal volume of 26 m*M* solution in the other. Both of these concentrations were chosen to exceed the cmc of SDS because of earlier literature reports[15b-f] that equilibrium was slow, or could not be reached, when both sides of a dialysis cell contained initially unequal concentrations of detergent which both exceeded the cmc.[15g] At regular intervals, the solutions were removed from each chamber and the concentrations analyzed. Corrections were made for slight volume losses which occurred in transferring the solutions from the dialysis cell to the conductivity cell. At the end of 176 hr, the solutions were found to be 98% equilibrated, as shown by concentrations on each side which differed by only 4%. Continuing these experiments for 62 hr beyond 7 days, there was only a very slight further change in concentration (0.1%). Even so, in many of the experiments with PVP the SDS concentrations were set initially equal in both chambers to accelerate the approach to equilibrium.

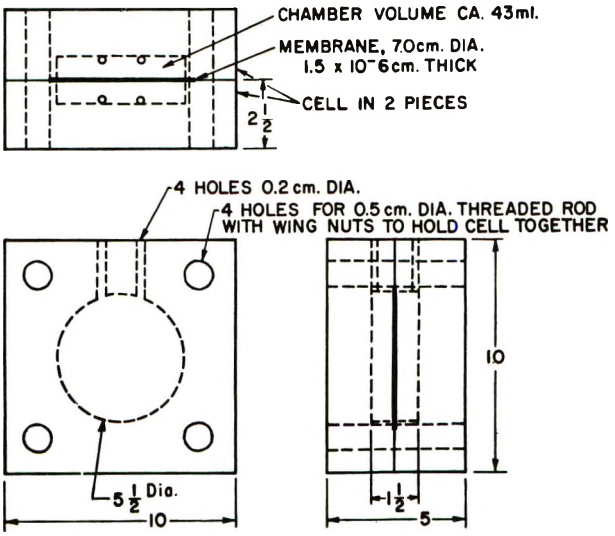

Figure 1. Dialysis cell. (All dimensions are given in centimeters.)

Under these circumstances, only small concentration changes in the two compartments were observed (<10%) and in general SDS transport occurred from outside to the inside of the cell. In several instances, the initial concentrations were set so that material had to flow from the polymer to the outside chamber. In a few other cases, initial concentrations were set much further from equilibrium, so that larger changes (5–10 m*M*) occurred. The cells were also left in the shaker bath for various lengths of time in excess of 7 days. None of these variations caused more scatter in the data of Figure 2 than in experiments where SDS transport was minimal and no more than 7 days passed between filling and measuring the contents of the dialysis cells. The raw dialysis data, from which Figure 2

(14) H. P. Frank and G. B. Levy, *J. Polym. Sci.*, **10**, 371 (1953).

(15) (a) P. Molyneux, School of Pharmacy, Chelsea College of Science and Technology, London, S. W. 3, private communication; (b) J. T. Yang and J. F. Foster, *J. Phys. Chem.*, **57**, 628 (1953); (c) B. S. Harrop and I. J. O'Donnell, *ibid.*, **58**, 1097 (1954); (d) H. B. Klevens and C. W. Carr, *ibid.*, **60**, 1245 (1956); (e) K. J. Mysels, P. Mukerjee, and M. Abu-Hamdiyyah, *ibid.*, **67**, 1943 (1963); (f) M. Abu-Hamdiyyah and K. J. Mysels, *ibid.*, **71**, 418 (1967); (g) Suggested by referee. Upon suggestion of referee, references 15b–f were included in addition to pH measurements in the Appendix. The authors were aware of the problem of slow equilibration as indicated by ref 15f which was referred to in M. L. Fishman, Ph.D. Thesis, Polytechnic Institute of Brooklyn, 1969. A copy of this is obtainable from University Microfilms, 313 First Street, Ann Arbor, Mich., Order No. 69-17,790; (h) J. Wadman, Ph.D. Thesis, Polytechnic Institute of Brooklyn, 1966.

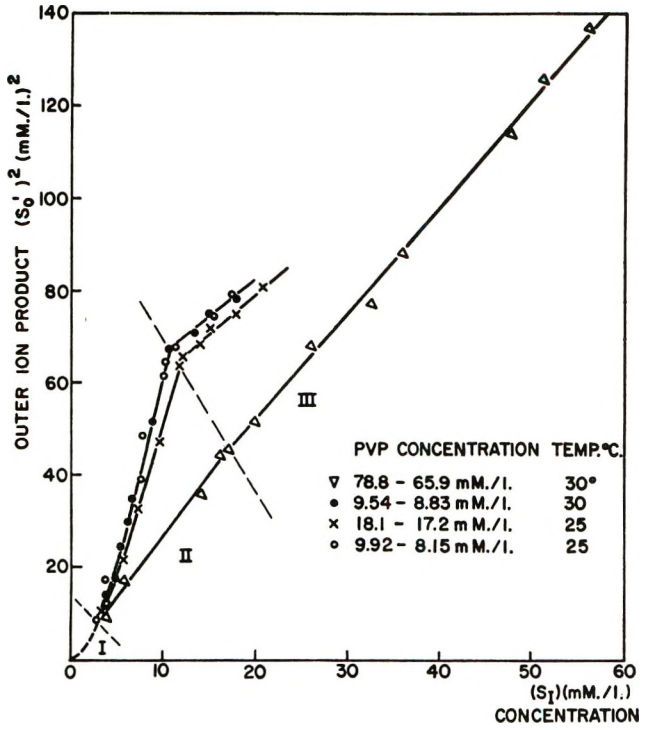

Figure 2. Dependence of outer ion product on total inside detergent concentration.

was obtained, as well as the standard errors for the slopes and intercepts of those figures, can be found elsewhere.[15g]

In addition to the precaution of predialyzing all PVP, an experiment was conducted to verify the impermeability of the dialysis membrane to PVP. Two identical blank experiments were run with a base monomer concentration in polymer of 90 mM on one side of the membrane, and pure water on the other. After 26 days, both sides were analyzed for PVP. In both experiments no PVP could be measured in the aqueous chamber, while the PVP concentration on the other side was found to be unchanged. The analysis of PVP was based on the formation of the PVP–I_3 complex which exhibits an absorption peak at 420 nm (15h). This experiment also provided evidence that PVP was not adsorbed by the container or the membrane. Analysis of the SDS gave material balances to within 5% of the original amounts present, in better than 95% of all dialysis experiments conducted.

Analysis of SDS by Conductivity. An Industrial Instruments conductivity bridge, Model RC-18, and a Klett bridge modified for use with an oscilloscope, gave the same results within 0.1% precision, for the solution conductivities. Even more important, it was found that the total specific conductance of the solutions was the linear sum of the contributions due to water (1.52) μmhos/cm polymer (0.0268PVP) μmhos/cm, and SDS (65.86C + 5.26) μmhos/cm. This was true to within an error of 1% SDS concentration, in the sub 3.5 mM range of SDS solution, as well as for the polymer concentrations employed. In the above, PVP stands for the millimolar concentrations of polymer (monomeric residues) and C for that of SDS.

At the end of a dialysis run, both chambers of the dialysis cell were diluted separately to 2–3.5 mM range in SDS concentration, and C was determined quantitatively by conductivity. This procedure enabled material balances to be determined at the end of each dialysis experiment.

Results and Discussion

The reaction model used for calculating the binding rests upon the assumption that the amount of total univalent ions present in a solution containing a polyelectrolyte, can be approximated as arising from two states only, *i.e.*, the presence of bound and free ions. The ions which are bound to the polyelectrolyte are assumed to make no contribution to the ionic activities.

The mean activity (A_i) of the free SDS on the inside, or polymer containing, chamber is given as

$$A_i^2 = \gamma_i^2[(DS_f) + \alpha[(S_I) - (DS_f)]]_{(DS_f)} \quad (1)$$

where γ_i = mean activity coefficient of free ions, (DS_f) = concentration of free or unbound detergent ions, (S_I) = total detergent concentration inside the cell, and α = degree of dissociation of sodium ions, acting as counterions to the complex. On the outside, *i.e.*, in the polymer free chamber, two cases may be distinguished. Below the cmc of SDS, the outside mean activity (A_0) is given by

$$A_0^2 = \gamma_0^2(S_0)^2 \quad (2)$$

where (S_0) = total analytic detergent concentration outside. Above the cmc, A_0 is given by

$$A_0^2 = \gamma_0^2(\text{cmc})[(\text{cmc}) + \alpha_m[(S_0) - (\text{cmc})]] \quad (3)$$

where α_m = degree of dissociation of micellar (sodium) counterions. Following Botre,[12] eq 3 assumes that in pure micellar solutions addition of detergent above the cmc merely increases the number, but not the nature, of the micelles. In other words, the concentration of monomeric detergent and the number of detergent ions per micelle are assumed to remain constant.

In eq 2 and 3, the right side, excluding γ_0^2, represents the outside ion product. If one denotes this product by (S_0'), then (4) will suffice to describe the equilibrium concentration of detergent ion on the inside, regardless of whether or not the outside detergent concentration exceeds the cmc. Of course $(S_0')^2$ must be calculated in accordance with (2) below the cmc, and in accordance with (3) above

$$(S_0')^2\gamma_0^2 = \gamma_i^2(DS_f)[(DS_f) + \alpha[(S_I) - (DS_f)]] \quad (4)$$

If one assumes that

$$\gamma_0 \cong \gamma_i \quad (5)$$

(4) can be rearranged to

$$(S_0')^2 = (DS_f)^2(1 - \alpha) + \alpha(DS_f)(S_I) \quad (6)$$

Before proceeding one should note that, when the outside detergent is below the cmc and α is unity, eq 6 becomes

$$(S_0)^2 = (DS_f)(S_I) \quad (7)$$

which is merely a form of Donnan's equation[16] for the distribution of a uni-univalent salt across a semipermeable membrane with a polyelectrolyte on one side.

Determination of the Cmc, and of Counterion Binding above the Cmc. Figure 2 shows the relationship of $(S_0')^2$ with (S_I) at three different polymer concentrations and two temperatures. Among other things, it shows that a 5-degree shift of temperature at the lowest polymer concentration does not produce a noticeable change in the data.

According to the simplified model of micelle formation assumed above, if micelles were to form in the polymer–detergent solution, α and (DS_f) would be invariant with (S_I) and $(S_0')^2$. Consequently, the data plotted in Figure 2 should be linear over the concentration range of micelle formation. Moreover, the intercept and slope of these lines would permit a calculation of α and (DS_f) by the simultaneous solution of eq 8 and 9.

$$\text{intercept} = (DS_f)^2(1 - \alpha) \quad (8)$$

$$\text{slope} = \alpha(DS_f) \quad (9)$$

The linear portion of Figure 2 (*i.e.*, for the polymer concentrations at the higher detergent concentrations) yielded the values of α and (DS_f) which appear in Table I. Also included in Table I for comparison are the values of the cmc and of α[17] for pure aqueous, SDS.

Table I shows an orderly decrease in the value of the cmc together with an increase of α as the polymer concentration increases.

Table I

PVP concn, m*M*/L.[a]	*T*, °C	Cmc	α
0	25	8.24[b]	0.18
9.92–8.65	25	7.88	0.208
9.54–8.83	30	7.89	0.209
18.1–17.2	25	7.47	0.248
78.8–65.9	30	4.06	0.556

[a] The ranges of polymer concentrations of this table and in Figure 2 were caused by water transport in the dialysis cells. [b] By conductivity measurement in this study.

Figure 2 shows that at constant polymer concentration, the linear portion of the (S_0') *vs.* (S_I) plot extends over a large range of polymer detergent ratios. This suggests a polymer participation in the micelle formation, *e.g.*, the formation of a mixed polymer–detergent micelle.

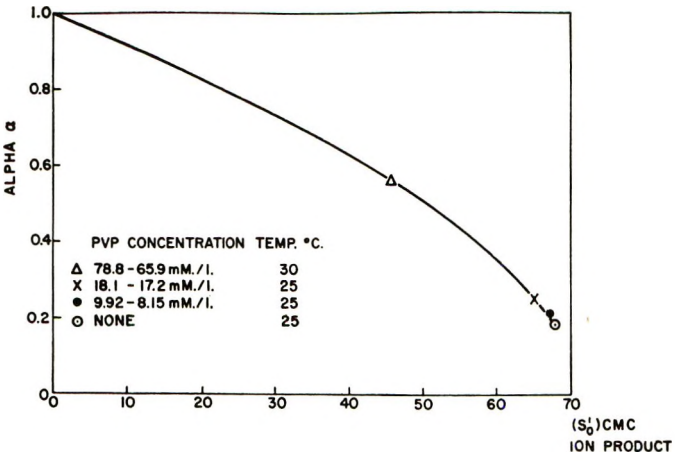

Figure 3. Dependence of α on outside ion product at the cmc.

Determination of the Unbound Detergent Ion Concentration and of Counterion Binding, below the Cmc. In view of the curvature of the lines in Figure 2 at lower polymer and detergent concentrations, the assumption of a constant (DS_f), or α, is not warranted. The line for the highest polymer concentration at the low detergent concentrations appears linear, but calculations of (DS_f) and α according to eq 7 and 8 yield a value of α which is greater than unity. Therefore, α and (DS_f) cannot be assumed to be constant either.

Nevertheless, it is possible to estimate reasonable values of α by the following empirical method based on general considerations of ion binding to polyelectrolytes. At constant polymer concentration, α, must be a decreasing function of (S_I) and, in the same way, of the outside ion product, $(S_0')^2$. Moreover, α should approach unity as $(S_0')^2$ approaches zero. Figure 3 shows α at the cmc plotted against $(S_0')^2$ at the cmc for the various polymer concentrations under the assumption that α is 1 when $(S_0')^2$ equals zero. The concentration of the pure solution at cmc is shown as a point. Since the trend of α with $(S_0')^2$ is similar to that expected at constant polymer concentration we are led to make a further assumption of correspondency, namely that solutions of the same $(S_0')^2$ have identical values of α, regardless of polymer concentration. Utilizing this assumption, eq 6 can be solved with the aid of Figure 3, by the quadratic formula for (DS_f) at all the values of (S_I) below the cmc. The difference between (S_I) and (DS_f) represents the bound sulfate. In other words, we have replaced the inadequate assumption of a constant α for bound SDS below the cmc by an estimate of α which is in accord with known similar behavior of polyelectrolytes.

Figure 4 contains the binding data thus obtained for several polymer concentrations where, r is the molar

(16) C. Tanford, "Physical Chemistry of Macromolecules," Wiley, New York, N. Y., 1961, p 225.

(17) R. J. Williams, J. N. Phillips, and K. J. Mysels, *Trans. Faraday Soc.*, **51**, 728 (1955).

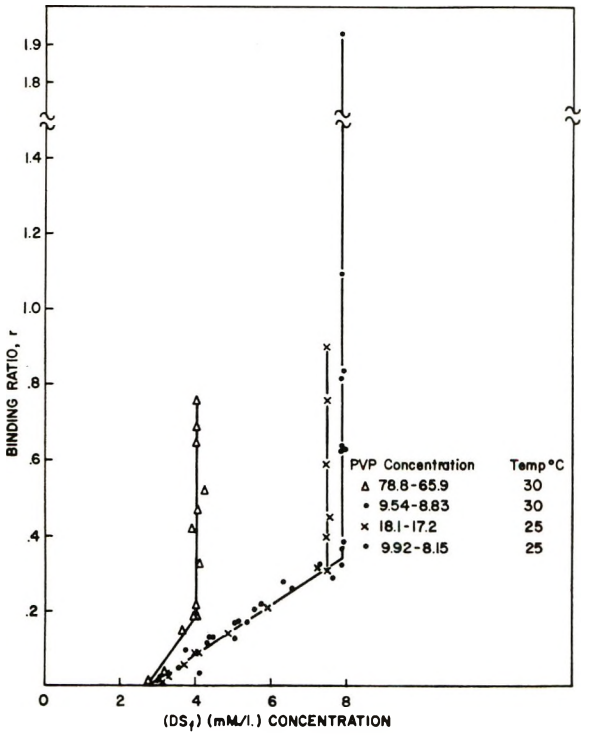

Figure 4. Binding dependence on free detergent ion concentration.

ratio of bound sulfate to total monomer units in the polymer.

The binding isotherms indicate clearly three regions of binding. The first is the low concentration region where little or no binding occurs (no points in Figures 2 and 4). In the second, there is a linear uptake of detergent ion with free SDS concentration, and the third region is marked by a fixed concentration of free DS, a steep increase in binding and/or micelle formation, and therefore by a quantitative deactivation of sulfate. Three regions of behavior have been reported for several polymer–detergent–water systems.[7-9] A mixed micellization was thought to occur in region 2, and a true micellization in region 3. Our Figure 4 indicates a relatively rapid uptake of detergent ion in region 2, particularly at the highest polymer concentration. Nevertheless, cluster or complex formation between PVP and SDS rather than true micellization may be a more accurate description of what occurs in this region, since neither the free detergent ion concentration nor the surface charge density in region 2 appears to remain constant, as should be true for regular micellization.

Binding in region 1, as indicated by Figure 4, is not perceptible under our conditions. Increasing the polymer concentration, however, causes region 2 to begin at lower values of (DS$_f$). Thus, one might identify region 1 with the binding of single detergent ions to individual sections of polymer, whereas the marked rise in detergent ion deactivation in region 2 should be attributable to a cooperative action of bound detergent ions and polymer chain sections, so as to form nuclei or micelles of low order (clusters or complexes) which eventually turn into true mixed micelles at the start of region 3. Region 2 would appear then to be a transitional region between the binding of isolated detergent ions and region 3 of true micelle formation either on the PVP or independently.

Figure 4 shows binding isotherms which are dependent on polymer concentration. Their form precludes the use of Klotz-type isotherms, or modifications thereof, as a representation of the more common types of binding.[18] Tanford[18] attributes the kind of behavior observed here to complexes involving more than one polymer molecule. In this case the molecular weight of the complex should be dependent upon polymer concentration, which our viscosity data (to be published) indicate. Accepting this premise, it would follow also that different sections of the same chain may become bridged by a detergent cluster, or micelle. This would lead to a decrease of η_{red} with increasing S/P ratio, which some viscosity data indicate. A corresponding observation has been found in the case of iodine–iodate binding to PVP.[2]

A second possibility, also likely to cause a polymer concentration dependence, is a molecular weight dependent binding in the presence of broad polymer distributions leading to a kind of fractional binding. This case could be distinguished from the first in that binding studies on narrow molecular weight fractions would fail to show a concentration dependence. Corresponding studies are in progress.

In conclusion, our results permit a quantitative description of surfactant binding to a water soluble polymer and how this affects the cmc. Moreover, the data indicate that polymers can permit the occurrence of otherwise unstable premicellar complexes and that the polymer is involved in the premature micelle formation.

Appendix

It has been suggested[15g,f] that even highly purified SDS could undergo appreciable hydrolysis if allowed to stand for 7 days or more in aqueous media and, further, by a reviewer, that an "interaction between a 'basic' polymer and an anionic surfactant doubtless depends strongly on pH," particularly in our binding regions 2 and 3. To check on these possibilities, polymer detergent solutions were made up to include one sample in region 2, and one in region 3, for the three polymer concentrations studied by us. Also, control solutions of pure aqueous polymer and detergent were made up at these concentrations. The pH values of all solutions were measured immediately upon temperature equilibration, and then 8 days later. During the interim, the solutions were kept in tightly stoppered bottles at

(18) See ref 16, p 528.

25°. All pH measurements were taken on a radiometer PHM4C meter fitted with a Thomas No. 4858-Li5 combination electrode.

The results of these measurements are given in Tables II and III and indicate that our samples of PVP were either neutral or slightly acidic and that SDS was also slightly acidic. The acidity of PVP has been observed before[19] and is likely due to a small amount of COOH end groups. The acidity of SDS may be explained either by a slight hydrolysis in the solid state, unlikely in view of the absence of hydrolysis in aqueous solution, or by the presence of traces of unneutralized dodecylsulfuric acid. In any case the SDS contained less than 0.5% acid impurity.

Table II[a]

	Concn of SDS[b]			
PVP	0	9.00	15.00	25.00
0	5.27	4.51	4.24	4.22
9.92	4.93	4.51	4.34	
18.1	5.27	4.60	4.53	
78.8	3.90	4.07		4.17

[a] pH at 25° immediately upon preparation. [b] pH values in the same row have the same concentration of PVP as indicated by the value which is given in the first column of that row. pH values in the same column have the same concentration of SDS as indicated by the value which is given in the first row of that column. All concentrations are millimolar.

Table III[a]

	Concn of SDS[b]			
PVP	0	9.00	15.00	25.00
0	5.29	4.34	4.25	4.24
9.92	5.42	4.62	4.69	
18.1	5.55	4.60	4.65	
78.8	3.96	4.10		4.21

[a] pH at 25° 8 days after preparation. [b] pH values in the same row have the same concentration of PVP as indicated by the value which is given in the first column of that row. pH values in the same column have the same concentration of SDS as indicated by the value which is given in the first row of that column. All concentrations are millimolar.

Since the pH of all polymer–detergent solutions, except one, fell between 4.1 and 5.1, with no apparent trend, it is most unlikely that a change in pH plays a significant role in our PVP–SDS interaction, particularly in view of the quantities of DS^- deactivated which were more than 10 to 100 times as great as the change in pH over these same concentration ranges. Barkin, Frank, and Eirich[4] also found that pH plays no role in the interaction of PVP with the anionic sulfonate dyes Orange II and Benzopurpurine.

(19) P. G. Assarsson, Ph.D. Thesis, Polytechnic Institute of Brooklyn, 1966.

Solute–Solvent Interactions. VI. Specific Interactions of Tetraphenylarsonium, Tetraphenylphosphonium, and Tetraphenylborate Ions with Water and Other Solvents[1]

by J. F. Coetzee* and W. R. Sharpe[2]

Department of Chemistry, University of Pittsburgh, Pittsburgh, Pennsylvania 15213 *(Received March 5, 1971)*

Publication costs assisted by the National Science Foundation

Compounds such as tetraphenylarsonium tetraphenylborate have been used extensively as reference electrolytes to split the enthalpies or free energies of transfer of electrolytes from one solvent to another into the ionic components. From the results of a proton magnetic resonance study and a consideration of information already in the literature we conclude that these reference ions undergo a variety of specific solvation effects. For this reason it is necessary to exercise caution in the interpretation of transfer energies based on the assumed ideality of such reference ions.

Introduction

A potentially rewarding approach in the study of ion–solvent interactions involves the estimation of the free-energy and related thermodynamic quantities for the transfer of individual ions from one solvent to another. However, this approach requires extrathermodynamic assumptions and constitutes a controversial subject, which has been discussed recently by several authors.[1,3-6] The most widely used assumption has been that the experimentally determined free energy or enthalpy of transfer of a "model" or "reference" electrolyte, such as tetraphenylarsonium or tetraphenylphosphonium tetraphenylborate (Ph_4AsPh_4B or Ph_4PPh_4B), consists of equal contributions by the cation and anion. The general validity of this assumption would require the absence of significant specific interactions of either ion with all solvents considered.

In this paper we report the results of a proton magnetic resonance and infrared study which show that specific interactions of Ph_4As^+, Ph_4P^+, and Ph_4B^- with a variety of solvents do occur, and that differences in the energetics of these interactions may be significant.

Nuclear magnetic resonance spectroscopy is a powerful tool for the investigation of ion–solvent and ion–ion interactions, and it has been used for such purposes with increasing frequency during the past few years. Representative of recent studies is the work of Popov,[7] Kuntz,[8] Fratiello,[9] and Strehlow and Schneider.[10] Three reviews have appeared recently.[10-12] The classical kinetic studies by Grunwald, Luz, Meiboom, and others, are not considered here. In some instances infrared[7,13,14] and charge-transfer-to-solvent[15] spectroscopy supplied valuable complementary information. The present work is concerned with the interactions of benzene and Ph_4As^+, Ph_4P^+, and Ph_4B^- ions with water, methanol, ethanol, acetonitrile, sulfolane, and dimethyl sulfoxide, studied by pmr spectroscopy and supplemented in some cases by ir data.

Experimental Section

Materials. The following solvents were purified as described before: Matheson Coleman and Bell practical grade acetonitrile,[16] Shell technical grade sulfolane,[1] J. T. Baker purified methanol,[17] Fisher Certified dimethyl sulfoxide,[18] and Fisher Certified Spec-

(1) Preceding paper in series: J. F. Coetzee, J. M. Simon, and R. J. Bertozzi, *Anal. Chem.*, **41**, 766 (1969).

(2) From the Ph.D. thesis of this author, University of Pittsburgh, 1971 (present address: Clarion State College, Clarion, Pa. 16214).

(3) O. Popovych, *Crit. Rev. Anal. Chem.*, **1**, 73 (1970).

(4) A. J. Parker, *Chem. Rev.*, **69**, 1 (1969).

(5) R. G. Bates in "Solute–Solvent Interactions," J. F. Coetzee and C. D. Ritchie, Ed., Marcel Dekker, New York, N. Y., 1969.

(6) H. Strehlow in "Chemistry of Nonaqueous Solvents," Vol. 1, J. J. Lagowski, Ed., Academic Press, New York, N. Y., 1966.

(7) M. K. Wong, W. J. McKinney, and A. I. Popov, *J. Phys. Chem.*, **75**, 56 (1971).

(8) R. P. Taylor and I. D. Kuntz, Jr., *J. Amer. Chem. Soc.*, **92**, 4813 (1970).

(9) A. Fratiello, R. E. Lee, and R. E. Schuster, *Inorg. Chem.*, **9**, 82 (1970).

(10) H. Schneider in "Solute–Solvent Interactions," J. F. Coetzee and C. D. Ritchie, Ed., Marcel Dekker, New York, N. Y., 1969.

(11) J. Burgess and M. C. R. Symons, *Quart. Rev.*, **22**, 276 (1968).

(12) J. Hinton and E. S. Amis, *Chem. Rev.*, **67**, 367 (1967).

(13) A. Allerhand and P. von R. Schleyer, *J. Amer. Chem. Soc.*, **85**, 1233 (1963).

(14) J. Buffalini and K. H. Stern, *ibid.*, **83**, 4362 (1961).

(15) M. J. Blandamer and M. F. Fox, *Chem. Rev.*, **70**, 59 (1970).

(16) J. F. Coetzee, *Pure Appl. Chem.*, **13**, 427 (1967).

(17) J. M. Simon, "Polarography and Medium Effects in Sulfolane," Ph.D. Thesis, University of Pittsburgh, 1969.

(18) C. D. Ritchie, G. A. Skinner, and V. G. Badding, *J. Amer. Chem. Soc.*, **89**, 2063 (1967).

tranalyzed chloroform.[19] The sources of other chemicals are indicated as follows: Alfa Inorganics, A; J. T. Baker Analyzed, B; Eastman White Label, EWL; Fisher Certified grade, F; Fisher Certified Spectranalyzed, FS; U. S. Industrial, USI. Tetraphenylphosphonium chloride (B), tetraphenylarsonium chloride (B), tetraphenylstibonium bromide (A), and sodium tetraphenylborate (B) were dried *in vacuo* at 50°. Sodium perchlorate (F) was recrystallized from water and dried *in vacuo* at 100°. Tetraethylammonium chloride (EWL) was recrystallized first from absolute ethanol and then from ethyl acetate and was dried *in vacuo* at 100°. Tetraethylammonium perchlorate was prepared as described elsewhere.[20] Benzene, *n*-hexane, cyclohexane (all FS), and absolute ethanol (USI) were used without further purification.

Measurements. Infrared spectra were recorded using double beam operation with a Beckman IR-12 spectrophotometer at room temperature (near 25°). A 0.1-mm sodium chloride liquid cell was used with a variable path length sodium chloride cell as reference. The bands reported were sharp, and frequency values had a precision of ± 1 cm^{-1}.

Proton magnetic resonance measurements were carried out on a stabilized and carefully calibrated Varian Associates A-60 spectrometer equipped with a V-6040 variable temperature controller. Solutions in sulfolane were studied at 30° ± 0.5°, and all others at 25 ± 0.5°, with the probe temperature established by a standard methanol calibration.[21] An internal standard at a concentration of 0.2% (v/v) was used: tetramethylsilane (TMS) in all but the aqueous systems, for which either *tert*-butyl alcohol[22] or acetonitrile[23] was employed. There has been some discussion concerning the general suitability of TMS as an internal standard.[24,25] To minimize any interactions that may occur between TMS and other components of the solutions studied, its concentration was kept as low as possible. In addition, we carried out double-internal-referencing experiments on selected solutions in acetonitrile using cyclohexane as the second internal reference.[24,26] The results[2] showed only a very slight and constant deviation in the chemical shift separation of the two standards in various solutions as compared to their separation in the reference solvent, carbon tetrachloride. Another check on the relative inertness of TMS was obtained by comparing the chemical shift separations of acetonitrile and water in mixtures of the two solvents with and without addition of TMS; the results were identical, as they were with *tert*-butyl alcohol instead of TMS as internal standard.[2] The calibration of the spectrometer was checked before and periodically during each measurement period. Each reported molar chemical shift value is the mean from at least two series of measurements of a minimum of five scannings each at each of several concentrations, carried out a few days apart. In addition, selected solutions were reprepared and remeasured after intervals of weeks or months. In general the precision was ±0.3 Hz or better.

Results and Discussion

Molar chemical shifts of the proton resonance of several solvents produced by a number of solutes are listed in Tables I and II.

Table I: Proton Magnetic Resonance Chemical Shifts Caused by Tetraphenylarsonium, Tetraphenylphosphonium, and Tetraphenylborate Ions and Benzene in Dipolar Aprotic Solvents

	Molar chemical shift of solvent protons, Hz[a]			
Solute	Acetonitrile[b]	Sulfolane, α-H[c]	Sulfolane, β-H[c]	Dimethyl sulfoxide[b]
Ph_4AsCl	+7.0	+2	+1	+5.0
Ph_4PCl	+5.0	+4.0	+2.0	+5.0
$NaPh_4B$	−18	−11	−16	−12
Et_4NCl	+7.4	+3.4	+1.0	+3.4
Et_4NClO_4	+2.0	+0.6	+1.0	+0.5
$NaClO_4$	+3.0	+3.7	+1.2	+1.0
C_6H_6[d]	−11	−4.6	−7.3	−1.2
Ph_4As^+[e]	−0.4	−1	0	+1.6
Ph_4As^+[f]	+1.6	0	+1	+2.1
Ph_4P^+[e]	−2.4	+0.6	+1.0	+1.6
Ph_4P^+[f]	−0.4	+1.2	+2.0	+2.1
Ph_4B^-[g]	−21	−15	−17	−13

[a] All shifts are relative to the pure solvent measured against internal TMS (see text). Negative value corresponds to high-field shift. Molar shifts calculated from data obtained over a concentration range of 0.1–0.6 *M* in acetonitrile and 0.1–0.4 *M* in sulfolane and dimethyl sulfoxide; no significant concentration dependence of molar shifts was observed. [b] Temp, 25°. [c] Temp, 30°. [d] Concentration normalized to correspond to that of phenyl groups in Ph_4B^-, Ph_4As^+, and Ph_4P^+; *e.g.*, 0.4 *M* C_6H_6 compared with 0.1 *M* $NaPh_4B$. [e] Assumption: $\Delta\nu(Et_4N^+) = 0$, $\Delta\nu(Ph_4As^+) = \Delta\nu(Ph_4AsCl) - \Delta\nu(Et_4NCl)$, with analogous relationship for Ph_4P^+; see text. [f] Alternate assumption: $\Delta\nu(ClO_4^-) = 0$, $\Delta\nu(Ph_4As^+) = \Delta\nu(Ph_4AsCl) - \Delta\nu(Et_4NCl) + \Delta\nu(Et_4NClO_4)$, with analogous relationship for Ph_4P^+; see text. [g] Assumption: $\Delta\nu(ClO_4^-) = 0$, $\Delta\nu(Ph_4B^-) = \Delta\nu(NaPh_4B) - \Delta\nu(NaClO_4)$; see text.

The chemical shift of solvent protons is generally altered by the addition of ionic solutes. Among factors known to contribute to such changes are polariza-

(19) N. Oi and J. F. Coetzee, *J. Amer. Chem. Soc.*, **91**, 2473 (1969).

(20) I. M. Kolthoff and J. F. Coetzee, *ibid.*, **79**, 870 (1957).

(21) Varian Associates, Technical Bulletin No. 87-100-110.

(22) H. Schneider and H. Strehlow, *Z. Phys. Chem.* (*Frankfurt am Main*), **49**, 44 (1966).

(23) J. E. Gordon and R. L. Thorne, *J. Phys. Chem.*, **73**, 3643 (1969).

(24) P. Laszlo in "Progress in Nuclear Magnetic Resonance Spectroscopy," Vol. 3, J. W. Emsley, J. Feeney, and L. H. Sutcliffe, Ed., Pergamon Press, Oxford, 1967.

(25) C. Franconi and F. Conti in "Nuclear Magnetic Resonance in Chemistry," B. Pesce, Ed., Academic Press, New York, N. Y., 1965.

(26) J. W. Emsley, J. Feeney, and L. H. Sutcliffe, "High Resolution Nuclear Magnetic Resonance Spectroscopy," Vol. 1, Pergamon Press, Oxford, 1965.

Table II: Proton Magnetic Resonance Chemical Shifts Caused by Tetraphenylarsonium, Tetraphenylphosphonium, and Tetraphenylborate Ions in Hydroxylic Solvents

Solute	Molar chemical shift of solvent hydroxyl proton, Hz[a] Ethanol[b]	Methanol	Water
Ph_4AsCl	−1.5	−3.5	+14[d,e]
Ph_4PCl	−1.7	−2.3	+13
$NaPh_4B$	−39[d,f]	−24[d,g]	−17
Et_4NCl	−8.7	−10	−3.0
NaCl	*h*	*h*	−5.3
Ph_4As^+ [c]	+7.2	+6.5	+17[d]
Ph_4P^+ [c]	+7.0	+7.7	+16
Ph_4B^- [c]	>−39[d,i]	>−24[d,i]	−15

[a] All shifts are relative to the pure solvent measured at 25° against internal TMS for ethanol and methanol and against methyl signal of internal *t*-BuOH for water (see text). Negative value corresponds to high-field shift. Molar shifts calculated from data obtained over a concentration range of 0.1–0.6 *M* in water and 0.1–0.4 *M* in ethanol and methanol; no significant concentration dependence of molar shifts was observed except where noted. [b] Ethanol signal is a singlet when $NaPh_4B$ is present; otherwise a triplet, and shifts refer to center peak. [c] Assumption: $\Delta\nu(Et_4N^+) = 0$, $\Delta\nu(Ph_4B^-) = \Delta\nu(NaPh_4B) - \Delta\nu(NaCl) + \Delta\nu(Et_4NCl)$, $\Delta\nu(Ph_4As^+) = \Delta\nu(Ph_4AsCl) - \Delta\nu(Et_4NCl)$, with analogous relationship for Ph_4P^+. [d] Value at 0.1 *M*; varies with concentration. [e] Values are +13, +11, and +9 at 0.3, 0.4, and 0.6 *M*, respectively. [f] Value is −45 at 0.4 *M*. [g] Values are −32 and −36 at 0.2 and 0.4 *M*, respectively. [h] Inadequate solubility. [i] Probably somewhat more negative than value for $NaPh_4B$; see text.

tion of solvent molecules by the ions and modifications in the solvent structure produced by the ions (and by nonionic solutes as well). The polarization effect usually leads to deshielding of the solvent protons and hence to a low-field shift, unless magnetic anisotropy effects are present, which may cause a high-field shift. The structural effect results in a low-field shift if the solute is a net structure maker, and a high-field shift if it is a net structure breaker. In a solvent such as acetonitrile, which probably has no hydrogen-bonded structure (although it may have significant *order* as a result of dipole association), the polarization effect is expected to be dominant, but in the alcohols and particularly in water both effects must be significant and it is no simple matter to resolve their contributions to the experimentally observed overall effect.

It is also not a straightforward matter to split the observed total effect of an electrolyte into the individual ionic contributions and to assess the reliability of such attempts. Assumptions made before concerning the molar shifts of reference ions in water include the following: $\delta(ClO_4^-) = -0.85$,[27] $\delta(K^+) = \delta(Cl^-)$,[28] $\delta(Cl^-) = 0$,[29] and $\delta(NH_4^+) = 0$.[30] We have preferred to assume that in water $\delta(Et_4N^+) = 0$ because its polarization effect should be small and, furthermore, there is considerable evidence[31] that it has neither pronounced structure-making tendencies (as the larger quaternary ammonium ions have) nor structure-breaking tendencies (as Me_4N^+ has). The same assumption was used for the remaining solvents as well. However, for the dipolar aprotic solvents listed in Table I an alternate assumption: $\delta(ClO_4^-) = 0$, also was used. We believe on the basis of infrared and other evidence that this ion interacts only very weakly with dipolar aprotic solvents; of course, in strongly structured solvents, such as water, it is known to be a powerful structure breaker and it should cause large high-field shifts. For the dipolar aprotic solvents the use of both a cation (Et_4N^+) and an anion (ClO_4^-) as reference ion has the advantage that it allows a reasonable estimate of the limits within which the shifts of individual ions must fall. It seems likely that both reference ions actually will produce small low-field shifts as a result of weak net polarization effects. Consequently, if $\Delta\nu(Et_4N^+)$ and $\Delta\nu(ClO_4^-)$ in Table I actually are small positive numbers, the shifts for Ph_4As^+ and Ph_4P^+ will be somewhat more positive than those based on Et_4N^+ and somewhat more negative than those based on ClO_4^- as reference ion. The shifts for Ph_4B^- should be somewhat more positive than those given in Table I.

In view of the uncertainties inherent in all assumptions such as these, differences of a few tenths of a Hertz in the shifts listed for ions of *opposite* charge could not be regarded as significant, even if allowance could be made for the difference in interaction sites and types of interaction of cations and anions. Similar differences between ions of like charge are not tainted by the assumptions used and therefore are more meaningful.

With few exceptions the experimentally observed shifts of the salts listed in Tables I and II vary reasonably linearly with concentration, indicating that serious complications from ion association reactions or other causes do not occur. Conductivity data exist for most of the salts in the solvents listed in Tables I and II.[2] Such data typically have been obtained over a concentration range of 10^{-4} to 10^{-2} *M*, and treatment by the Fuoss–Onsager equation yielded ion-pair formation constants smaller than 10 in most cases. Only a rough estimate can be made of the degree of ion association expected at the much higher concentrations necessary for nmr measurements. A typical example is sodium perchlorate in acetonitrile for which an ion-pair formation constant of 10 has been reported.[32] Assuming that at our higher concentrations only the

(27) J. N. Shoolery and B. J. Alder, *J. Chem. Phys.*, **23**, 805 (1955).
(28) H. G. Hertz and W. Spalthoff, *Z. Elektrochem.*, **63**, 1096 (1959).
(29) B. P. Fabricand and S. Goldberg, *J. Chem. Phys.*, **34**, 1624 (1961).
(30) J. C. Hindman, *ibid.*, **36**, 1000 (1962).
(31) C. V. Krishnan and H. L. Friedman, *J. Phys. Chem.*, **73**, 3934 (1969).
(32) R. L. Kay, B. J. Hales, and G. P. Cunningham, *ibid.*, **71**, 3925 (1967).

same type of ion association process still occurs (no higher aggregate formation, etc.), and also assuming that the above limiting value of the formation constant can be adjusted to concentration constant values by means of the Debye–Hückel equation (a very rough approximation indeed), it is found that at a concentration of 0.1 *M* some 10% of the salt is associated, with a not very different value at 0.6 *M*. From this one would conclude that, particularly since it is to be expected that the interaction of ion pairs with the solvent will be weaker than that of the free ions, corrections for ion association probably are not unduly significant and are not warranted in view of the uncertainties involved.

To interpret the pmr data for acetonitrile, it is necessary to identify its interaction site for anions. Approximate molecular orbital calculations[33] gave the charge distribution shown in Figure 1 for the acetonitrile molecule in 10^{-3} electron unit. Possible interaction sites for anions are the protons and the nitrile carbon atom. However, our infrared data for salts containing a variety of anions[34] show no change in the C–C or C≡N stretch frequencies on changing the anion, but the C–H frequency does change (also see below), indicating that all anions tested interact directly with the protons. In comparing the proton resonance shifts produced by anions with those by cations, it therefore should be kept in mind that for energetically similar interactions anions will produce much larger shifts than cations are able to transmit through their interaction at the remote nitrogen atom. Analogous considerations apply to the other solvents studied.

Our principal interest is to determine whether Ph_4B^-, Ph_4As^+, and Ph_4P^+ undergo significant interactions with the solvents studied, and, if so, whether the interactions are different for the three ions and for the six solvents tested.

I. Solvent Shifts. 1. One of the main features of the results listed in Tables I and II is that in all solvents studied Ph_4B^- causes a large high-field shift in the solvent proton resonance. The only likely interaction that can account for this, particularly in a solvent which has little hydrogen-bonded structure, is a preferential orientation of solvent molecules with their protons above and below the plane of the phenyl rings so that the protons become shielded through a magnetic anisotropy effect. The interaction of benzene with the dipolar aprotic solvents is of a similar kind, but it is impossible to judge from the pmr data alone which solute interacts more strongly, because of geometric effects.[8] There may be some steric hindrance to solvation of the phenyl groups of Ph_4B^-, and our normalization of the shifts caused by benzene does not allow for that. In addition, orientation of solvent molecules at benzene and at the phenyl groups of Ph_4B^- may not be exactly alike, even though the solvent protons undergo anisotropic shielding in both cases. Similar results

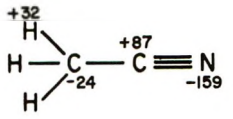

Figure 1.

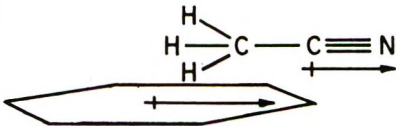

Figure 2.

were obtained by Nicholls and Szwarc for benzene and tetraphenylborate salts in various ethers.[35] In a particularly relevant study Schneider[36] observed similar magnetic anisotropy shifts for polar solutes, including acetonitrile, in benzene as solvent, and attributed these to dipole–induced dipole interactions with their magnitude determined by the ratio of the dipole moment to the molar volume of the solute. For acetonitrile the interaction shown in Figure 2 was proposed. Furthermore, a high degree of specificity in these interactions was observed, for example, marked differences between the CH_3 and CH_2 groups of propionitrile and between the two CH_3 groups of *N*,*N*-dimethylformamide. Finally, the interaction of chloroform with benzene appeared to have a different origin from that of other polar solutes. We can speculate that a similar difference may exist in the "neutral" component of the interaction of Ph_4B^- with dipolar aprotic solvents, on the one hand, and hydrogen-bonding solvents, such as water, on the other. In connection with the data for the hydroxylic solvents in Table II, a small low-field shift for sodium ion is to be expected in ethanol and perhaps methanol as well, which would make the shifts for Ph_4B^- even more high-field than the values for $NaPh_4B$. It is tempting to interpret the smaller high-field shift in water in terms of a structure-making influence of this ion, but the pmr evidence is inconclusive because the O–H concentration is higher in water than in either alcohol, and again geometric factors may be important. It is probably safer to speculate about Ph_4As^+ and Ph_4P^+: the larger low-field shifts produced by these ions in water appear to be consistent with structure making.

2. We have supplemented our pmr data for Ph_4B^- and benzene with ir measurements. It was reported before that anions produce a new absorption band at a slightly lower frequency for both the symmetric and the asymmetric stretching vibrations of the H–C bond

(33) J. A. Pople and M. Gordon, *J. Amer. Chem. Soc.*, **89**, 4253 (1967).

(34) J. F. Coetzee and W. R. Sharpe, to be published.

(35) D. Nicholls and M. Szwarc, *J. Phys. Chem.*, **71**, 2727 (1967).

(36) W. G. Schneider, *ibid.*, **66**, 2653 (1962).

of acetonitrile.[37] We obtained the following $\Delta\nu$ (sym) values: $NaPh_4B$, 7; NaSCN, 6; and benzene, 3–4 cm^{-1}. These data are consistent with a stronger overall interaction of acetonitrile with Ph_4B^- than with benzene, one that is comparable to that of SCN^- which is a highly polarizable ion and therefore probably undergoes a significant dispersion interaction with acetonitrile.

3. The solvent shifts caused by Ph_4As^+ and Ph_4P^+ in the dipolar aprotic solvents listed in Table I are small and in most cases low-field, consistent with an ion–dipole interaction leading to a preferential orientation of the solvent molecules with their protons directed away from the ion. As pointed out before, small shifts have little significance because of the uncertainties in the assumptions made in deriving single ion values. Nevertheless, the high-field shifts derived for Ph_4P^+ in acetonitrile on the basis of both assumptions appear to be out of line and may be indicative of some ion association in Ph_4PCl which would reduce the low-field shifts of this salt. It should be noted that for the shifts of Ph_4P^+ to be high field, interaction between the phenyl groups of this ion and the acetonitrile protons will have to be strong enough to overcome the "normal" electrostatic ion–dipole interaction (which amounts to several kilocalories), and consequently the resulting shifts will have to be much larger than observed. In comparing the shifts produced by Ph_4P^+ or Ph_4As^+ with those by Ph_4B^- in the same solvent, it should be borne in mind that the Ph_4B^- shifts are magnified, not only because the interaction site is directly at the solvent protons, but also because magnetic anisotropy effects by their very nature cause larger shifts than ordinary electrostatic effects can produce.[8]

4. The data for sulfolane exhibit steric influences. In particular, the shifts produced by Ph_4B^- and especially by benzene are somewhat larger for the β than for the α protons. This indicates that the phenyl rings avoid the vicinity of the α protons even though these are the more acidic, probably because of repulsion between the aromatic electrons and the oxygen atoms of sulfolane. The same explanation was given by Nicholls and Szwarc for analogous observations in certain ethers as solvents.[35]

II. Solute Spectra. The solvent shifts discussed above showed that the orientation of solvent molecules by Ph_4B^- is different from that by Ph_4As^+ or Ph_4P^+. In addition, the pmr spectra of the solutes themselves show certain marked differences. In all solvents studied the Ph_4B^- signal was found to be a complex multiplet centered at $\tau = 2.9$, in agreement with a recent report on the 100-MHz spectrum.[38] In all solvents the signal of Ph_4B^- is high field from those of Ph_4Sb^+, Ph_4As^+, and Ph_4P^+, which occur progressively more low field in the order given. The results are summarized in Table III. The three cations must have some charge delocalization, as was pointed out by Grunwald, *et al.*, for the case of Ph_4P^+ when they first proposed the use of Ph_4PPh_4B as a reference electrolyte.[39] The electronegativity increases in the order Sb, As, and P, while the vacant orbitals available to accept charge from the phenyl groups become smaller but also less diffuse in the same order. The pmr data are consistent with a net increasing charge delocalization from Ph_4Sb^+ to Ph_4As^+ to Ph_4P^+.

Table III: Chemical Shifts of Protons in Phenyl Groups

Solvent	Salt[a] Ph_4PCl	Ph_4AsCl	Ph_4SbBr
Acetonitrile	458.0, 463.5, 469.0[b]	465.6	461.3
Dimethyl sulfoxide	462.3, 467.4, 473.0[b]	469.5	464.2
Ethanol	462.0, 467.0, 472.8[b]		466.8
Water	382.0, 387.5, 396.2[b]	391.6	390.8

[a] Concentration 1.0×10^{-2} *M* in all cases. Shifts (in Hz) are low field from methyl signal of *tert*-BuOH for water, and low field from TMS for other solvents. [b] Main peak.

In all solvents the Ph_4Sb^+ signal (at a concentration of 10^{-2} *M*, limited by the solubility of Ph_4SbBr) was a fairly sharp singlet. In all solvents except water the Ph_4As^+ signal was a slightly broadened singlet (there may be some As^{75} coupling), but in water it was a multiplet (particularly marked at the higher concentrations studied, 0.3 to 0.6 *M*), which may indicate nonequivalence of either different protons in a phenyl group, or, more likely, of different phenyl groups. Such specific interaction of Ph_4As^+ with water was also indicated in a recent laser–Raman study, which showed that while this ion is tetracoordinate in methanol, the possibility exists that it is pentacoordinate in aqueous solution, with water entering the fifth coordination site.[40] In all solvents the Ph_4P^+ signal was a complex multiplet. Factors contributing to the complexity of the spectrum are P^{31} coupling and also charge delocalization, estimated by Grunwald, *et al.*,[39] to amount to 0.18 electron unit per phenyl group. We plan to study these interactions further through the H^1 and P^{31} high resolution spectra.

III. Nonideality of Reference Solutes Containing Phenyl Groups. In connection with the widespread use of compounds containing phenyl groups as reference solutes, the main implications of the results discussed above can be summarized and supplemented as follows.

1. Although it is difficult to translate nmr chemical

(37) I. S. Perelygin, *Opt. Spectrosc.*, 13, 198 (1962).

(38) R. R. Schrock and J. A. Osborn, *Inorg. Chem.*, 9, 2339 (1970).

(39) E. Grunwald, G. Baughman, and G. Kohnstam, *J. Amer. Chem. Soc.*, 82, 5801 (1960).

(40) J. B. Orenberg, M. D. Morris, and T. V. Long, *Inorg. Chem.*, 10, 933 (1971).

shift displacements into the energetics of the interactions, it is clear that all solvents tested discriminate among the three solutes: Ph_4As^+ (or Ph_4P^+), benzene, and Ph_4B^-.

2. Ph_4As^+ may undergo a specific interaction with water. For Ph_4P^+ in particular, nonequivalence of protons is likely to lead to specific solvation effects.

3. The "neutral" component of the interaction of Ph_4B^- may include a dipole–induced dipole contribution in dipolar aprotic solvents but a kind of hydrogen bonding in protic solvents. This ion possesses considerable reactivity. For example, it forms stable complexes in which one of its phenyl groups is π bonded to rhodium(I) or iridium(I).[38] The same type of interaction may be responsible for the anomalous behavior of silver tetraphenylborate reported by Parker.[4]

4. All of the phenyl-substituted ions under consideration have a fairly open structure. Extravagant claims have been made for the shielding of the central charge by the phenyl groups. Apart from any charge delocalization that may occur, screening of the central atom by the essentially flat phenyl groups is inadequate to eliminate solvation effects, which will depend on the size and shape and other specific properties of the solvent molecules.

5. The literature already contains considerable information on the peculiar properties of phenyl groups. In a classical series of studies, Friedman and coworkers have shown that phenyl groups undergo specific solvation in certain solvents and that this solvation is sensitive to what the phenyl group is bound.[31] For example, the enthalpies of transfer of Ph_4As^+ and Ph_4Sb^+ from dimethyl sulfoxide to propylene carbonate differ by 1.8 kcal mol^{-1}. Taylor and Kuntz[41] have questioned the validity of salts containing Ph_4B^- as models for testing sphere-in-continuum theory, and we agree. We have proposed for this purpose tetraalkylammonium tetraalkylborate salts instead, but even with such reference electrolytes specific perturbations arise.[42] Nevertheless, alkyl-substituted ions should be preferable to their aryl-substituted counterparts when they can be applied; unfortunately, the alkali metal tetraalkylborates are unstable in water. Fuchs, *et al.*,[43] in a thorough study have compared ionic enthalpies of transfer derived from $(C_4H_9)_4N(C_4H_9)_4B$ or $(C_5H_{11})_4N(C_5H_{11})_4B$ with those derived from Ph_4AsPh_4B as reference electrolyte and found differences of 3 and 4 kcal mol^{-1} for transfer from methanol to dimethyl sulfoxide and to dimethylformamide, respectively. It was pointed out that these differences may be the result of uncertainty in the difficult extrapolation of the enthalpy of solution of sodium tetraphenylborate as a function of concentration in methanol; a contributing factor may be specific interactions of the aryl-substituted ions. Fuchs, *et al.*, correctly advised that care should be exercised in choosing model ions for extrathermodynamic assumptions.

6. The difference between the ion–solvent quadrupole interaction terms for a cation and an anion, as treated in Buckingham's theory,[44] remains significant and solvent dependent even for otherwise ideal ions of single charge and large and equal radius. For example, for a singly charged spherical, nonpolarizable cation and anion with a radius of 4.6 Å, the difference in the enthalpy of solvation is predicted to amount to 5 kcal mol^{-1} in water, while it may vary by several kilocalories from this value in other solvents depending on the effective radius and quadrupole moment of the solvent molecules.

7. We conclude that restraint should be exercised in the interpretation of results based on the assumed ideality of reference solutes, especially those containing aryl groups. Particular caution is required in those cases where the transfer energies are small. In such instances, similar reservations apply to all other extrathermodynamic procedures that have been used to estimate transfer energies. Fortunately, in many instances the estimated solvent effects far exceed the probable uncertainties; in such cases these extrathermodynamic approaches have contributed significantly to an improved understanding of solute–solvent interactions. For particularly extensive discussions of such results the recent reviews of Popovych[3] and Parker[4] should be consulted.

Acknowledgment. We thank the National Science Foundation for support under Grant No. GP-6478X and GP-16342.

(41) R. P. Taylor and I. D. Kuntz, Jr., *J. Amer. Chem. Soc.*, **91**, 4006 (1969).

(42) C. H. Springer, J. F. Coetzee, and R. L. Kay, *J. Phys. Chem.*, **73**, 471 (1969).

(43) R. Fuchs, J. L. Bear, and R. F. Rodewald, *J. Amer. Chem. Soc.*, **91**, 5797 (1969).

(44) J. O'M. Bockris and A. K. N. Reddy, "Modern Electrochemistry," Vol. 1, Plenum Press, New York, N. Y., 1970, p 99.

Internal Hydroxyl Groups Near the Surface of Silica

by R. H. Doremus

General Electric Research and Development Center, Schenectady, New York 12301 *(Received March 8, 1971)*

Publication costs assisted by the General Electric Co.

The results of Deitz and Turner on the rate of absorption of water vapor by "96% silica glass" fibers are interpreted as resulting from the introduction of internal hydroxyl groups in the glass, rather than from adsorption or reaction at the outermost surface. The rate of introduction of these internal groups is controlled by the diffusion of water in the silica in the same way that water is introduced into fused silica at higher temperatures. The internal hydroxyl groups probably occur in pairs in a layer about 150 Å thick at the silica surface.

Hydroxyl groups on the surface of silica exist in several different forms. Isolated, terminal SiOH groups are the most stable; hydrogen-bonded hydroxyls on adjacent terminal SiOH groups start to desorb above about 200°.[1-3] Molecular water absorbs physically on the surface SiOH groups and can be rapidly pumped off at room temperature.[1-3] There is evidence for some "internal" hydroxyl groups that do not exchange with D_2O at room temperature,[2,3] but their exact nature has not been clear. The results of Deitz and Turner[4] on the rate of adsorption of water on 96% silica fibers at around 100° are interpreted in this note as resulting from the introduction of these internal hydroxyl groups. The rate of their introduction is shown to be controlled by diffusion of water in the bulk of the silica in the same way that water is introduced into fused silica at higher temperatures.[5-8] These internal hydroxyl groups probably occur in pairs in a layer roughly 150 Å thick at the silica surface.

Deitz and Turner measured the decrease in pressure of water vapor in a closed volume containing outgassed 96% silica fibers after the rapid introduction of different amounts of water vapor. The reaction of water with the outermost layer of silica groups should be rapid at about 100°, since these groups are all directly available to the water molecules. The exchange of OD for surface OH groups is fast at room temperature.[3] Adsorption of molecular water on surface hydroxyl groups should likewise be fast. Thus it seems likely that the slow decrease of water vapor pressure observed by Deitz and Turner should be attributed to the diffusion of water into the interior of silica, rather than to its reaction with external groups. The kinetic data bear out this interpretation.

The diffusion of a gas from a well-mixed, limited volume into a semifinite solid is governed by the equation[9]

$$p/p_0 = \exp X^2 \operatorname{erfc} X \tag{1}$$

where p is the gas pressure at time t, p_0 is the initial pressure, and

$$X = \frac{\sqrt{Dtk}A}{V} \tag{2}$$

in which D is the diffusion coefficient, A is the area of the solid, V is the volume of the gas in contact with this area, and the partition coefficient k is given by

$$k = c_s/c_g \tag{3}$$

where c_s is the concentration of diffusing substance in the solid at its surface, and c_g is its concentration in the gas as calculated from the pressure p.

Application of eq 1 to the diffusion of water in silica is complicated by the variation of water solubility with pressure. The concentration of hydroxyl groups in silica is proportional to the square root of the water vapor pressure,[5] because water reacts with silica according to the reaction

$$H_2O + \text{–Si–O–Si–} = 2\text{SiOH} \tag{4}$$

Equation 1 was derived for a partition coefficient of the form of eq 3 in which the concentration of hydroxyl groups is directly proportional to the pressure. Equation 1 is compared with the data of Deitz and Turner in Figure 1. Both the equation and the data are nearly proportional to $\sqrt{t}$ in the early stages of diffusion, and agree well. At later stages the data show more water absorption than predicted by eq 1. This results because the square root dependence of the surface concentration causes this concentration to decrease less

(1) R. S. McDonald, *J. Phys. Chem.*, **62**, 1168 (1958).

(2) G. J. Young, *J. Colloid Sci.*, **13**, 67 (1958).

(3) V. Ya. Davydov, A. V. Kiselev, and L. T. Zhuravlev, *Trans. Faraday Soc.*, **60**, 2254 (1964), and earlier articles by these authors.

(4) V. R. Deitz and N. H. Turner, *J. Phys. Chem.*, **74**, 3832 (1970).

(5) A. J. Moulson and J. P. Roberts, *Trans. Faraday Soc.*, **57**, 1208 (1961).

(6) G. J. Roberts and J. P. Roberts, *Phys. Chem. Glasses*, **5**, 26 (1964); **7**, 82 (1966).

(7) I. Burn and J. P. Roberts, *ibid.*, **11**, 106 (1970).

(8) R. H. Doremus in "Reactivity of Solids," Mitchell, DeVries, Roberts, and Cannon, Ed., Wiley, New York, N. Y., 1969, p 667.

(9) R. Haul, G. Dumbgen, and D. Just, *Z. Phys. Chem.*, **31**, 309 (1962).

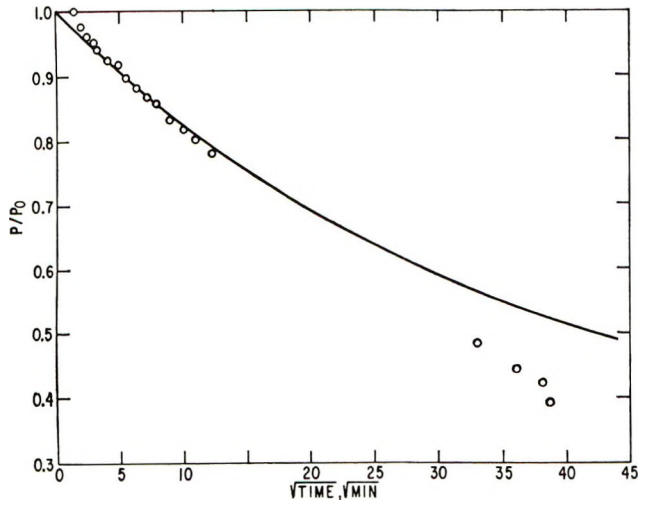

Figure 1. Absorption of water by 96% silica fibers as a function of the square root of time. Points, data of Deitz and Turner; line from eq 1.

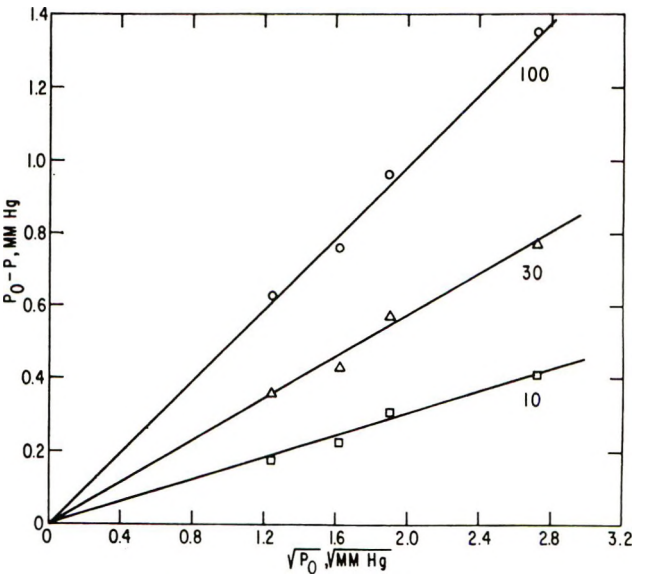

Figure 2. Absorption of water by 96% silica fibers as a function of the square root of the initial pressure of water vapor, at times in minutes shown at the lines.

than the proportionality used in eq 1, leading to more absorption than expected.

The square-root dependence of the surface concentration is confirmed by a comparison of the amount of water adsorbed with different initial pressures of water vapor. The data of Deitz and Turner are plotted in Figure 2 as amount of water absorbed as a function of square root of initial pressure, at different times of absorption. The straight lines passing through the origin confirm the square-root dependence and explain the nonzero intercept in the linear plot in Figure 2 of Deitz and Turner. Had these authors used initial pressure instead of actual pressure in their plot, their lines would have been curved.

The effective diffusion coefficient D in cm²/sec of water in fused silica found by Moulson and Roberts[5] for the temperature range from 600 to 1200° was

$$D = 10^{-6} \exp(-9210/T) \qquad (5)$$

where T is the absolute temperature. If this coefficient is extrapolated to 100°, its value is about 2×10^{-17} cm²/sec. The average distance a molecule diffuses in 1000 min with this diffusion coefficient is given by the relation $\sqrt{2Dt}$ or about 150 Å. At room temperature this value is about 6 Å. Thus at 100° in several hours water diffuses into silica an appreciable distance, but at room temperature the amount of diffusion into the bulk is quite small.

A further complication in the application of eq 1 to data on water diffusion in silica is the concentration dependence of the diffusion coefficient,[6-8] which was assumed independent of concentration in eq 1. Even with a concentration-dependent diffusion coefficient the absorption in the early stages should be proportional to the square root of time, although the proportionality constant can be different than that found from eq 1. This concentration dependence of the diffusion coefficient is connected with the mechanism of diffusion of water in silica. All the previous data[5-7] are consistent with the following model.[8] The water molecules in the gas phase dissolve in the silica and diffuse molecularly. The solubility of gases such as helium and hydrogen in fused silica, even near room temperature, is well established,[10] and water molecules should dissolve in the silica in a similar way. These dissolved molecules react with the silica by eq 4, forming pairs of hydroxyl groups in the silica. These hydroxyl groups are very immobile and are formed and removed by diffusion of molecular water. Any adsorbed water on the silica surface is at equilibrium with the vapor and with the water dissolved molecularly in the outer silica layers. Reaction 4 also goes to equilibrium on the outermost layers; deeper into the silica the amount of reacted water decreases as the amount of molecularly dissolved water drops off.

In any event the linear dependence of the amount of water absorbed by 96% silica fibers on the square root of time, as shown in Figure 1, is evidence that the rate of this absorption is controlled by the diffusion of water into the silica. The linearity of rate with the square root of initial pressure of water is further evidence for this mechanism.

(10) R. H. Doremus in "Modern Aspects of the Vitreous State," Vol. 2, Butterworths, London, 1962, p 1 ff.

Calorimetric Determination of Enthalpies of Association of Primary Aromatic Amines with Dimethyl Sulfoxide and Hexamethylphosphorotriamide[1]

by Christian Madec, Jacques Lauransan, and Pierre Saumagne*

Laboratoires de Thermodynamique Chimique et de Spectrochimie Moléculaire, Université de Bretagne Occidentale, 29N, Brest, France *(Received February 17, 1971)*

Publication costs assisted by Université de Bretagne Occidentale

The enthalpies of association of 1–1 complexes of substituted anilines, aminopyridines, and 5-aminopyrimidine with the proton acceptors DMSO and HMPT were determined at 25° by differential calorimetry. The results are compared with those reported for related hydrogen-bonded systems, and correlations between $\Delta H°$, $\Delta S°$, and $\Delta\nu$, the frequency shift of the symmetrical stretching vibration, are established.

I. Introduction

Only a few systematic studies have been made of enthalpies of association of aromatic amines with proton acceptors.[2-4] In a previous paper[5] the association constants for reactions between primary aromatic amines and the proton acceptors dimethyl sulfoxide (DMSO) and hexamethylphosphorotriamide (HMPT) were determined at room temperature by infrared spectroscopy and discussed in terms of several physicochemical parameters. The present study gives details of measurements of the heats of formation of the 1–1 complexes at 25° between substituted anilines, aminopyridines, 5-aminopyrimidine, and the proton acceptors DMSO and HMPT in dilute carbon tetrachloride solutions, as determined by a differential calorimetric method.

II. Experimental Section

1. Apparatus. A differential Technochim calorimeter was used. The contents of the calorimeter were routinely kept at 25 ± 0.1°. The temperature-sensing elements are probes with a resistance of 50 ohms. The acceptor solutions were introduced in the vessels using two syringes operated simultaneously by a Perfusor electric pump. Under these conditions, the flow rates and volumes of the two solutions are the same. Between the syringes and the reaction mixture the liquid moves through coils dipped into the thermostatic bath. The temperatures of injected solutions are then the same and are at the same temperature as the vessels. The determination of the voltages needed for the calculation of the quantity of heat emitted by the electrical simulation was made using a Hewlett-Packard Model HP 3420 B differential voltmeter ratiometer. A Sefram galvanometric amplifier Amplispot was used in order to increase the recorder sensitivity.

2. Procedure. The enthalpy of association between one donor and one proton acceptor is calculated from the heats of mixing of two solutions prepared in the same solvent. A differential method is used[6] which permits the measurement of the temperature difference which appears between two identical vessels placed in the same constant-temperature bath. The donor solution is placed in the reaction vessel and the same volume of solvent in the reference vessel. The same volume of acceptor solution is introduced simultaneously in the two vessels. A thermal unbalance due to the difference between the quantities of heat evolved in each vessel is shown by a temperature difference between the probes dipped into the two solutions. The temperature difference, ΔT is recorded as a function of time, t; the corresponding area, S, under the curve is proportional to the heat quantity, Q_c, emitted by the reaction being studied. In this differential system the energy, Q_c represents the enthalpy of association. The dilution of the acceptor solution in the solvent does not contribute to Q_c because it occurs simultaneously in the two vessels.

The dilution (10%) of the donor solution at weak concentration produces no observable temperature change under these experimental conditions. The calorimeter was calibrated electrically. When the heat quantity corresponding to the formation of C_C complex in a volume V is known, the enthalpy of formation of one mole of complex is given by

$$\Delta H°(\text{cal mol}^{-1}) = \frac{Q_c(\text{cal})}{C_C(\text{mol l.}^{-1})V(\text{l.})}$$

(1) Part of Thèse de 3ème cycle of C. Madec, Brest, 1970.

(2)(a) K. B. Whetsel and J. H. Lady, *J. Phys. Chem.*, **69**, 1596 (1965); **71**, 1421 (1967); (b) L. Abello, M. Kern, D. Caceres, and C. Pannetier, *Bull. Soc. Chim. Fr.*, 94 (1970).

(3) S. Nishimura and N. C. Li, *J. Phys. Chem.*, **72**, 2908 (1968).

(4) A. V. Iogansen, G. A. Kurkchi, and B. V. Rassadin, *Zh. Prikl. Spectrosk.*, **11**, 1054 (1969).

(5) C. Madec, J. Lauransan, and P. Saumagne, *J. Phys. Chem.*, **75**, 1157 (1971).

(6) B. Antoine, J. Lauransan, P. Saumagne, and P. Baumgartner, *Rev. Inst. Fr. Petrole Ann. Combust. Liquides*, **23**, 1389 (1968).

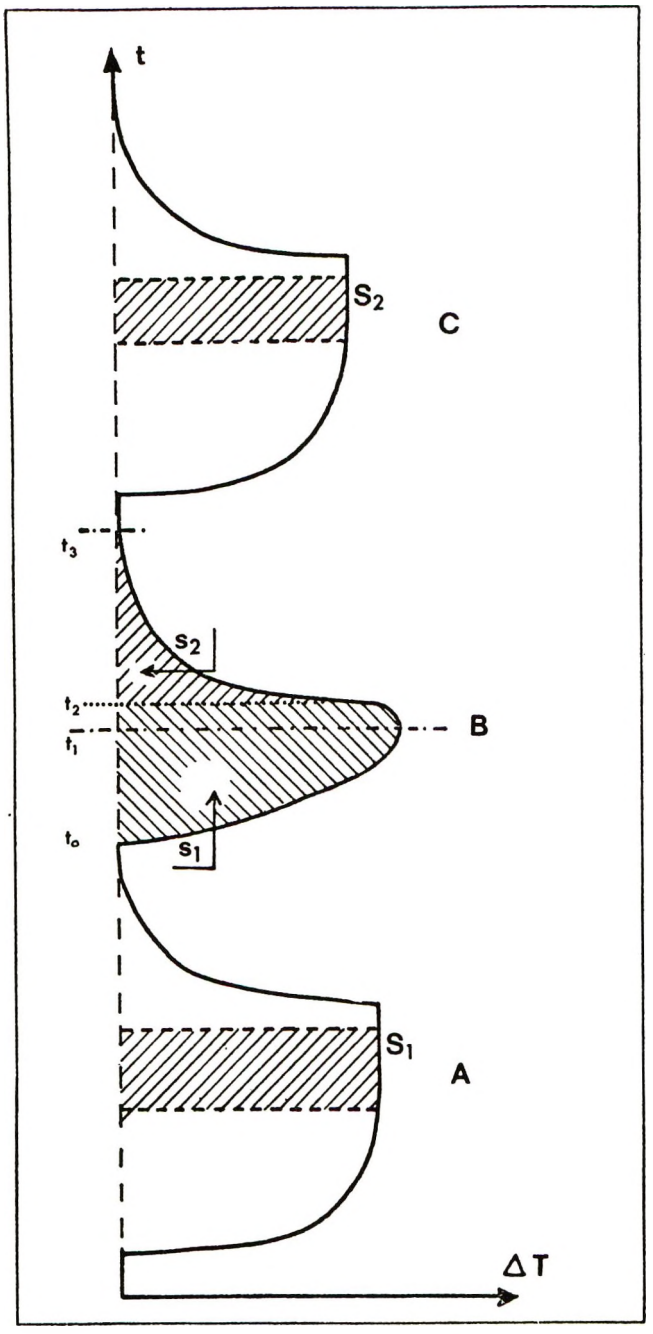

Figure 1. Recording of the curves $\Delta T = f(t)$ (see text for description).

The value of C_c is calculated from the initial concentrations of donor and acceptor when the association constant is known using the relation

$$2C_c = \left(C_D^\circ + C_A^\circ + \frac{1}{K}\right) - \sqrt{\left(C_D^\circ + C_A^\circ + \frac{1}{K}\right)^2 - 4C_D^\circ C_A^\circ}$$

Figure 1 shows the different steps in the recording of the temperature variations, ΔT, as a function of time t. The curves A, B, and C represent the quantities of heat Q_1, Q, and Q_2, respectively. The quantity Q_1 is given by the electrical simulation in the donor solution, Q_2 by the electrical simulation in the final mixture, while Q is the quantity of heat corresponding to the introduction of 10 ml of the carbon tetrachloride-acceptor solution in 100 ml of the donor solution in the same solvent.

The introduction of the acceptor solution is made in a period of 2 min (t_0–t_2). The heat of the association is not instantaneously liberated; one part of the heat serves to increase the temperature of the reaction mixture; the other part diffuses in the bath according to Newton's law: $dQ = a\Delta T\, dt$. Between t_0 and t_1, the evolved heat is larger than that diffused and the temperature of the vessel increases. Between t_1 and t_2 the evolved heat is less than that diffused and the temperature decreases. At time t_2 the reaction is complete and the measuring vessel cools according to Newton's law; hence the representative curve of (t_2–t_3) is an exponential.

In the two vessels, the volume increases from 100 to 110 ml by injection of the acceptor solution. The exchange surface between the two vessels and the bath changes, thus modifying the constant a of the cooling law. Therefore, it is necessary to utilize an electrical simulation before and after the introduction of the acceptor solution. The areas S_1 and S_2 are measured on the linear part of the curve. Under these conditions the heat given by the Joule effect is equal to that transferred to the thermostat; the resistance placed in the vessel is at constant temperature and the corresponding energy can be easily calculated.

The coefficients k_1 and k_2 are evaluated from the areas S_1 and S_2. They represent the number of calories per unit surface before and after the mixing of the solutions and are calculated using the following relations

$$Q_1 = k_1 S_1; \qquad Q_2 = k_2 S_2$$

The energy Q of the reaction is the sum of the heat quantities q_1 and q_2 which correspond, respectively, to q_1 on injection and q_2 on cooling. From t_0 to t_2, the volume changes, and the mean of the values of k_1 and is k_2 used. Then, the heat quantities are given, respectively, by

$$q_1 = \frac{k_1 + k_2}{2} s_1 \qquad \text{from } t_0 \text{ to } t_2$$

$$q_2 = k_2 s_2 \qquad \text{from } t_2 \text{ to } t_3$$

As an example, the parameters used for the determination of the association enthalpy between 2-aminopyridine and HMPT in carbon tetrachloride solution are shown in Table I.

The free enthalpy, ΔG°, and the entropy variation, ΔS°, are calculated using the classical thermodynamic relations

Table I: Values of the Parameters Used in the Determination of the Enthalpy of Association between 2-Aminopyridine and HMPT in Carbon Tetrachloride Solution at 25°

$C_{C(M)}$	s_1, cm²	s_2, cm²	k_1, cal cm⁻²	k_2, cal cm⁻²	q_1, cal	q_2, cal	Q_C, cal	$-\Delta H°$, kcal mol⁻¹
2.37×10^{-3}	3.63	1.47	0.224	0.241	0.844	0.354	1.19	4.6
	3.62	1.16	0.249	0.256	0.914	0.297	1.21	4.65

Table II: Thermodynamic Parameters for the Association of Primary Aromatic Amines with Dimethyl Sulfoxide (DMSO) and Hexamethylphosphorotriamide (HMPT) in Carbon Tetrachloride Solution at 25°

No. of compound	Compd	DMSO					HMPT				
		K, l. mol⁻¹	$\Delta\nu$,[a] cm⁻¹	$-\Delta H°$, kcal mol⁻¹	$-\Delta G°$,[b] kcal mol⁻¹	$-\Delta S°$, eu mol⁻¹	K, l. mol⁻¹	$\Delta\nu$,[a] cm⁻¹	$-\Delta H°$, kcal mol⁻¹	$-\Delta G°$,[b] kcal mol⁻¹	$-\Delta S°$, eu mol⁻¹
1	Aniline	2.5	44	3.3	1.95	4.5	7	66	4	2.55	4.85
2	2-Nitroaniline	11	76	4.7	2.8	6.4	35	112	4.7	3.5	3.1
3	3-Nitroaniline	15	67	4.1	3	3.7	65	90	4.8	3.85	3.2
4	4-Nitroaniline	22.5	76	4.4	3.2	4	85	99	4.7	4	2.3
5	4-Bromoaniline	4.5	55	3.5	2.3	4.25	14	76	4.3	2.95	4.5
6	2-Nitro-4-chloroaniline	30	81	4.4	3.4	3.4	130	116	5.1	4.25	3
7	2-Chloro-4-nitroaniline	35	87	4.5	3.5	3.5	140	114	4.9	4.3	2.6
8	2-Aminopyridine	5	61	3.8	2.3	5	18	88	4.6	3.1	5
9	3-Aminopyridine	8	54	3.8	2.6	4	27.5	76	4.8	3.35	4.8
10	4-Aminopyridine	20	65	4	3.15	2.85	65	90	4.7	3.85	2.85
11	5-Aminopyrimidine						50	88	4.9	3.7	3.95

[a] $\Delta\nu = \nu_1(NH_2) - [\nu_1(NH_2)]_{1-1}$.[5] [b] $-\Delta G°$ is calculated using K_x (see text).

$\Delta G° = -RT \ln K_x$ (K_x is the association constant when the concentrations are given in molar fraction) and

$$\Delta S° = \frac{\Delta H° - \Delta G°}{T}$$

3. Materials. The amines were commercial products of Prolabo, Aldrich, and Eastman Kodak, of highest purity commercially obtainable, and were used without further purification, except aniline which was distilled just before use. The 5-aminopyrimidine was kindly provided by Dr. P. Dizabo. DMSO obtained from Laboratories du Bois de Boulogne and HMPT from Prolabo were distilled and stored on Linde 4 Å Molecular Sieves. The purity of all these materials was checked by infrared spectroscopy. Carbon tetrachloride "RP" grade was obtained from Prolabo and used without further purification.

III. Results and Discussion

1. Presentation. Table II summaries the values of thermodynamic parameters K (determined by infrared spectroscopy), $\Delta H°$, $\Delta G°$, and $\Delta S°$ for the association between primary aromatic amines and the proton acceptors DMSO and HMPT in carbon tetrachloride solutions at 25°.

The amines are only slightly soluble in carbon tetrachloride and so the amine concentration was about 10^{-3} M and the acceptor concentration which was always larger than that of the donor was varied between 5×10^{-2} and 1×10^{-2} M. Under these conditions, the spectroscopic data show that there is no self-association of the amine, and the acceptor concentrations were chosen to avoid formation of 1–2 complexes, as confirmed by the infrared spectra.[5]

The error in $\Delta H°$ results essentially form two factors C_C and Q_C. The concentration of the complex is determined from the initial concentrations of donor $C_D°$ and acceptor $C_A°$, and from the association constant K. K is obtained by infrared spectroscopy using the Kagarise method, and because of the various overlapping band of donor and molecular complexes between 3200 and 3600 cm⁻¹, the error in K is about 10%,[5] leading to an uncertainty in C_C of 6–8%. (This can be shown by a classical treatment of the C_C relation given in the Experimental Section). The uncertainty in Q_C, which is estimated to be about 3%, results from the evaluation of the s_1 and s_2 areas. In our experimental conditions, the heat liberated in the calorimeter is very weak. We have therefore used a very sensitive scale for recording (about 0.2 cal cm⁻²) in order to obtain an area S of about 5 cm². Under these conditions, parasitic phenomena arising from dissymetry of the vessels, agitation (bath and vessels), and the injection of acceptor solutions can appear and decrease the precision. The resulting uncertainty in the value of $\Delta H°$ is about 10%.

2. Comparison with a Nondifferential Procedure.

Table III: Enthalpies of Association of Some Complexes in Carbon Tetrachloride Solutions

	Donor							
Acceptor	Methanol[a]	Ref	Phenol[a]	Ref	α-Naphthol[a]	Ref	1,1,1,3,3,3-Hexafluoro-2-propanol[b]	Ref
Pyridine	−3.88	7	−6.5	9	−5.7	12	−8.4	13
Triethylphosphine oxide	−6.34	8	−6.80	10	−7.80	8		
Dimethyl sulfoxide			−8	11			−8.7	13
Hexamethylphosphorotriamide							−9.9	13

[a] Determinated by infrared spectroscopy. [b] Determinated by calorimetry.

With a nondifferential procedure, the heat of mixing of the acceptor solution in the donor solution Q_m, the heat of dilution of the acceptor solution in carbon tetrachloride Q_a, and the heat of dilution of the donor solution in carbon tetrachloride Q_d, give the heat of complexation Q_c by the following relation $Q_c = Q_m - (Q_a + Q_d)$. In order to evaluate the relative importance of these heat quantities, the *m*-nitroaniline–DMSO system was tested at 25° with the following experimental conditions

$$C_D^\circ = 8 \times 10^{-3}\ M \qquad C_A^\circ = 5 \times 10^{-2}\ M$$

$$C_C = 3.3 \times 10^{-3}\ M$$

The heat quantities obtained are, respectively

$$Q_m = 1.32 \pm 0.04 \text{ cal}$$

$$Q_a = 2.87 \pm 0.08 \text{ cal}$$

$$Q_d = 0$$

(There is no observable temperature change under these experimental conditions.)

Then $Q_C = -1.55 \pm 0.12$ cal, and the enthalpy of association for such a system is $\Delta H^\circ = -4.3 \pm 0.4$ kcal mol^{-1}, in good agreement with the value obtained by the differential method: $\Delta H^\circ = -4.1$ kcal mol^{-1} (Table II). We note that in this case the heat of dilution of the DMSO solution (Q_a) is relatively important compared with the heat quantity arising from complexing (Q_c), so the heat of mixing Q_m is endothermic.

3. Comparison with Other Proton Donors. Table III[7-13] gives some values of the enthalpy of association of several ROH-acceptor systems in carbon tetrachloride solutions. Only a few experiments were undertaken with DMSO and HMPT, so we give the results obtained with other proton acceptors, *viz.*, pyridine and triethylphosphine oxide. The analysis of Tables II and III demonstrates that the enthalpy of formation of a hydrogen-bonded complex generally varies between −3 and −10 kcal mol^{-1}. The values of the enthalpies of association of aromatic amines with DMSO or HMPT ($3{,}5 < -\Delta H^\circ < 5$ kcal mol^{-1}) correspond to weak associations. These results are in agreement with those reported for association between aniline and other proton acceptors,[1,3] although the experimental methods and the solvent were different.

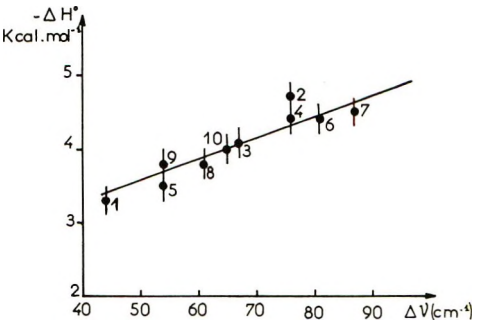

Figure 2. Plot of $-\Delta H^\circ$ *vs.* $\Delta\nu$ for amine–DMSO systems. Numbers correspond to the donors listed in Table II. The uncertainty in each value is represented by a vertical line.

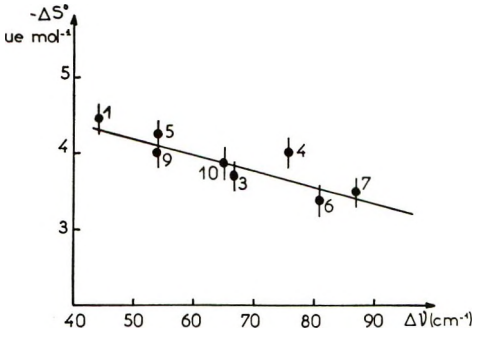

Figure 3. Plot of $-\Delta S^\circ$ *vs.* $\Delta\nu$ for amine–DMSO systems. Numbers correspond to the donors listed in Table II. The uncertainty in each value is represented by vertical line.

4. Discussion. For our results (Table II) we note that for the same donor the values of $-\Delta H^\circ$ increase with the acceptor basicity. Larger values are found for HMPT complexes than for those of DMSO. This

(7) E. D. Becker, *Spectrochim. Acta*, **17**, 436 (1961).
(8) T. Gramstad, *Acta Chem. Scand.*, **15**, 1337 (1961).
(9) S. Singh, A. S. N. Murthy, and C. N. R. Rao, *Trans. Faraday Soc.*, **62**, 1056 (1966).
(10) G. Aksnes and T. Gramstad, *Acta Chem. Scand.*, **14**, 1485 (1960).
(11) T. Gramstad, *Spectrochim. Acta*, **19**, 829 (1963).
(12) T. Gramstad, *Acta Chem. Scand.*, **16**, 807 (1962).
(13) K. F. Purcell, J. A. Stikeleather, and S. D. Brunk, *J. Amer. Chem. Soc.*, **91**, 4019 (1969).

result is in good agreement with the fact that HMPT is more basic than DMSO, as shown in a previous paper.[5] Account being taken of the uncertainty of the results, we note that for the same acceptor the values of $-\Delta H^\circ$ increase with the donor acidity.

5. Correlations between ΔH°, ΔS°, and $\Delta\nu$. Figure 2 gives a plot of $-\Delta H^\circ$ as a function of $\Delta\nu$, the frequency shift of the symmetrical stretching vibration. In Figure 3 $-\Delta S^\circ$ is shown as a function of $\Delta\nu$. Considering the precision of the results (the uncertainty in each value is represented by a vertical line in Figures 2 and 3), the correlations obtained are reasonably good. For the same acceptor, $-\Delta H^\circ$ increases with $\Delta\nu$, while $-\Delta S^\circ$ decreases when $\Delta\nu$ increases, *i.e.*, when the association is stronger.[5] We can note that similar correlations have been established for the complexing of the same donor with several proton acceptors.[14-17]

Acknowledgments. We wish to thank Dr. G. Turrell, Bordeaux, for useful corrections of the manuscript and Dr. P. Dizabo, Paris, for the gift of 5-aminopyrimidine.

(14) T. Gramstad, *Spectrochim. Acta*, **19**, 497 (1963).

(15) R. S. Drago and T. D. Epley, *J. Amer. Chem. Soc.*, **89**, 5770 (1967); **91**, 2883 (1969).

(16) M. D. Joesten and R. S. Drago, *ibid.*, **84**, 3817 (1962).

(17) T. Zeegers-Huyskens, Thesis, Louvain, 1969.

Estimation of Solute Activity Coefficients in Dilute Aqueous Mixtures of Sodium and Zinc Bromides at 25°. Comparisons with Predictions from the Guggenheim Theory of Solutions[1a]

by G. E. Boyd,* S. Lindenbaum,[1b] and R. A. Robinson[1c]

Oak Ridge National Laboratory, Oak Ridge, Tennessee 37830 *(Received May 19, 1971)*

Publication costs assisted by the Oak Ridge National Laboratory

Mean molal solute activity coefficients, $\gamma_\pm$, in dilute aqueous electrolyte mixtures were predicted with Guggenheim's theory of solutions for the system NaBr–$ZnBr_2$–H_2O. The predicted $\gamma_\pm$ were compared with values derived by applying the McKay–Perring equation to experimentally measured isopiestic concentrations for the same ternary mixture. Agreement between the theoretically predicted activity coefficients and those derived from experiment to better than 2% was found for ionic strengths below 0.45 m. The concentration dependence of $\gamma_\pm$ for NaBr (B) and $ZnBr_2$ (C) in mixtures of constant total ionic concentration, $m = m_B + 1.5m_C$, was described quantitatively by the equations $\log \gamma_B = \log \gamma_B^0 - \alpha_B m_C - \beta_B m_C^2$ and $\log \gamma_C = \log \gamma_C^0 = \alpha_C m_B - \beta_C m_B^2$, respectively. The composition-independent α_B and α_C increased strongly as m decreased; the quadratic interaction coefficients, β_B and β_C, were negative, independent of m, and surprisingly large.

A knowledge of solute activity coefficients in ternary and higher order electrolyte mixtures is required for the evaluation of the thermodynamic equilibrium constants for many reactions which take place in water solutions at room temperature. To compute standard free-energy changes in ion-exchange reactions with organic ion exchangers, for example, the mass law activity coefficient quotient, Q_γ, for the solutes in the equilibrium mixed electrolyte must be known. Frequently, investigators in the past have taken Q_γ to be unity, which holds approximately only for dilute mixtures of 1–1 type electrolytes with a common ion. Occasionally the ionic strength principle has been assumed to apply, but experimental measurements usually were conducted at concentrations too large for this approximation to be valid. Equations based on Harned's rule for electrolyte mixtures have been employed[2] to estimate activity coefficients in dilute solutions, but in this case an em-

(1) (a) Research sponsored by the U. S. Atomic Energy Commission under contract with the Union Carbide Corp.; (b) present address: Department of Pharmaceutical Chemistry, University of Kansas, Lawrence, Kan. 66044; (c) Visiting Professor of Chemistry, University of Florida, Gainesville, Fla. 32601.

(2) G. E. Boyd and G. E. Myers, *J. Phys. Chem.*, **60**, 521 (1956).

pirical extrapolation of the concentration-dependent interaction coefficients, α_B and α_C, which appear in the equations is necessary. Numerous determinations of α_B and α_C for concentrated electrolytes have been published,[3] and a theoretically justified procedure for their extrapolation to concentrations at and below 0.1 m would find use. Alternatively, a method for estimating solute activity coefficients in dilute electrolyte mixtures from data on their component binary solutions would be most valuable. Fortunately, such a method has been developed based on a semiempirical activity coefficient equation proposed independently by Guggenheim[4] and Scatchard[5] which is consistent with the Brönsted principle of specific ion interaction, which states that "ions are "specifically" influenced only by ions of opposite sign."

Comparatively few investigators[6-9] of ion-exchange equilibria have applied the Guggenheim theory of electrolyte mixtures to estimate activity coefficients, and there has been very little inquiry as to whether or not the theory is generally reliable and quantitative. The treatment as outlined by Robinson[10] has been utilized by us[9] to estimate activity coefficients in a study of the exchange equilibrium between zinc and sodium ions in aqueous 0.1 N nitrate solutions and polystyrenesulfonic acid type cation exchangers. Thus, it was assumed that the Guggenheim–Scatchard equation for the activity coefficient, γ_i, of the ith ion in a mixture applies

$$\log \gamma_i = \log \gamma^{st} + \sum_j B_{ij} m_j \qquad (1)$$

The activity coefficient, γ^{st}, is estimated on the assumption that the only interionic interaction is of the Debye–Hückel type

$$\log \gamma^{st} = -z_i^2 A I^{1/2}/(1 + 1.5 I^{1/2}) \qquad (2)$$

where z_i is the charge on the ith ion. The coefficient, B_{ij}, in eq 1 is a quantity characteristic of the interaction between an ith ion and a jth ion. In accordance with the Brönsted principle of specific ionic interaction, the summation is made over all pairs of *oppositely* charged ions. Thus, in a solution of sodium and zinc salts containing a common ion (*i.e.*, sodium bromide = B; zinc bromide = C) eq 1 gives

$$\log \gamma_B = \log \gamma^{st} + (m_B + m_C) B_B + (1/2) m_C B_C \qquad (3a)$$

$$\log \gamma_C = 2 \log \gamma^{st} + (2/3) m_B B_B + (1/3)(m_B + 4 m_C) B_C \qquad (3b)$$

The numerical evaluation of B_B and B_C may be conducted with data on dilute binary solutions as eq 1 also applies. The activity coefficients, γ_B° and γ_C°, of NaBr and $ZnBr_2$, respectively, each in its own solution in the absence of the other salt at a concentration corresponding to the ionic strength, I, of the mixture are given by

$$\log \gamma_B^\circ = \log \gamma^{st} + B_B I \qquad (4a)$$

$$\log \gamma_C^\circ = 2 \log \gamma^{st} + (4/9) B_C I \qquad (4b)$$

Eliminating B_B and B_C between eq 3 and 4 gives

$$\log \gamma_B = \log \gamma_B^\circ - F_C[(2/3) \log \gamma_B^\circ - (3/8) \log \gamma_C^\circ + (1/12) \log \gamma^{st}] \qquad (5a)$$

$$\log \gamma_C = \log \gamma_C^\circ - F_B[(1/4) \log \gamma_C^\circ - (2/3) \log \gamma_B^\circ + (1/6) \log \gamma^{st}] \qquad (5b)$$

where $F_C = I_C/I$ and $F_B = I_B/I = (1 - F_C)$ are the ionic strength fractions of electrolytes C and B in the mixture of total ionic strength, I. Thus, the activity coefficients of NaBr and $ZnBr_2$ in their mixture may be estimated from accurate measurements of their activity coefficients in their binary solutions taken at the same ionic strength as the mixture. The quantity, γ^{st}, may be computed with eq 2 with $A = 0.5071$ at 25°. In dilute solutions, the quantities within the brackets of eq 5 may be small so that precise values of γ_B° and γ_C° over the required concentration range will be necessary.

In this paper, we shall report isopiestic vapor pressure comparison measurements on dilute binary NaBr and $ZnBr_2$ solutions from which γ_B° and γ_C° may be determined. Further, isopiestic comparison measurements with aqueous sodium bromide–zinc bromide mixtures were performed from which γ_B and γ_C may be computed following an established thermodynamic procedure. These latter values will be compared with corresponding values of γ_B and γ_C obtained from eq 5a and 5b using our measured γ_B° and γ_C°. A comparison of the measured activity coefficients of *both salts* in a ternary mixture with the predictions from Guggenheim's theory does not appear to have been made. Comparisons of the measurements by Güntelberg of the activity coefficients of HCl in dilute mixtures with the alkali metal chlorides with the theory have been reported.[11] Glueckauf[12] has compared the measurements of $\gamma_\pm$(HCl) in $BaCl_2$ solutions by Harned and Geary with the predictions from eq 5a and reports excellent agreement even at ionic strengths greatly exceeding that at which eq 1 should be valid.

(3) H. S. Harned and R. A. Robinson, "Multicomponent Electrolyte Solutions," International Encyclopedia of Physical Chemistry and Chemical Physics, Vol. II, Pergamon Press, Oxford, 1968.

(4) E. A. Guggenheim, *Phil. Mag.*, **19**, 588 (1935).

(5) G. Scatchard, *Chem. Rev.*, **19**, 309 (1936).

(6) G. E. Boyd, S. Lindenbaum, and G. E. Myers, *J. Phys. Chem.*, **65**, 577 (1961).

(7) R. M. Barrer, L. V. C. Rees, and D. J. Ward, *Proc. Roy. Soc.*, **273**, 180 (1963).

(8) D. S. Flett and P. Meares, *Trans. Faraday Soc.*, **62**, 1469 (1966).

(9) G. E. Boyd, F. Vaslow, and S. Lindenbaum, *J. Phys. Chem.*, **71**, 2214 (1967).

(10) R. A. Robinson and V. E. Bower, *J. Res. Nat. Bur. Stand.*, **70A**, 313 (1966).

(11) K. S. Pitzer and L. Brewer, "Thermodynamics by G. N. Lewis and M. Randall," 2nd ed, McGraw-Hill, New York, N. Y., 1961, p 570.

(12) E. Glueckauf, *Nature*, **163**, 414 (1949).

Experimental Section

Gravimetric isopiestic vapor pressure comparison measurements at 25.00° were conducted with dilute binary aqueous solutions of NaBr and $ZnBr_2$ and with mixtures containing varying proportions of NaBr + $ZnBr_2$. Comparisons with NaCl and KCl solutions were made simultaneously to confirm that vapor pressure equilibrium had been established in each of eight sets of measurements performed with the $NaBr_2$ + $ZnBr_2$ mixtures. The binary, 1–1 electrolyte solutions of approximately 0.2 *M* concentration were prepared with dry, reagent grade, crystalline salts and triply distilled water. Quantitative analyses for halide ion were made by potentiometric titration of weighed amounts of the NaBr, NaCl, and KCl solutions with standardized 0.1000 *M* $AgNO_3$ solution. The concentrations were 0.1984 ± 0.0002, 0.1994 ± 0.0002, and 0.1992 ± 0.0001 *m*, respectively, based on duplicates.

Care was exercised in the preparation and analysis of the $ZnBr_2$ solution because of the reported[13] sensitivity of the isopiestic concentrations to small variations in the zinc to bromide ion ratio of the solution. A 5 *N* $ZnBr_2$ solution was made up with pure, freshly ignited ZnO and concentrated HBr. A precipitate formed when the solution was diluted to *ca.* 0.22 *N*; this was redissolved by the addition of very small amounts of 6 *N* NBr until a pH of 4.3 was attained. After filtering, weighed aliquots of the solution were analyzed for Zn^{2+} ion by titration with standardized $K_4Fe(CN)_6$ solution,[14] and for Br^- ion by potentiometric titration. The zinc ion normality was 0.1958 ± 0.0002. A final adjustment of the composition was made by adding a calculated volume of 8.9 *M* HBr to give zinc and bromide ion weight normalities (*i.e.*, equiv/1000 g of water) of 0.1932 and 0.1929, respectively.

The aqueous mixed electrolyte solutions with known sodium and zinc bromide concentrations were prepared by weighing-in predetermined amounts of the analyzed NaBr and $ZnBr_2$ binary solutions. The ionic fraction of zinc bromide, y_C, in the mixtures was varied in approximately equal intervals from 0.05 to 0.80.

Vapor pressure equilibrations were conducted in two series with duplicate samples of NaCl and KCl and eight solutions containing NaBr and/or $ZnBr_2$. At least 14 and sometimes as many as 28 days were taken for the attainment of equilibrium after which weighings to ±0.1 mg were made. The solutions were diluted approximately twofold by adding pure water and reequilibrated. Three dilutions were made in each of the two series. The data for the final set in series II for which an isopiestic molality of 0.02331 for NaBr was reached were rejected because of strong indications that equilibrium had not been attained. The data for the final set of mixed solutions in series I (M_{NaBr} = 0.05468) also were discarded after a statistical analysis of the data showed that large random variations in the isopiestic concentrations were present.

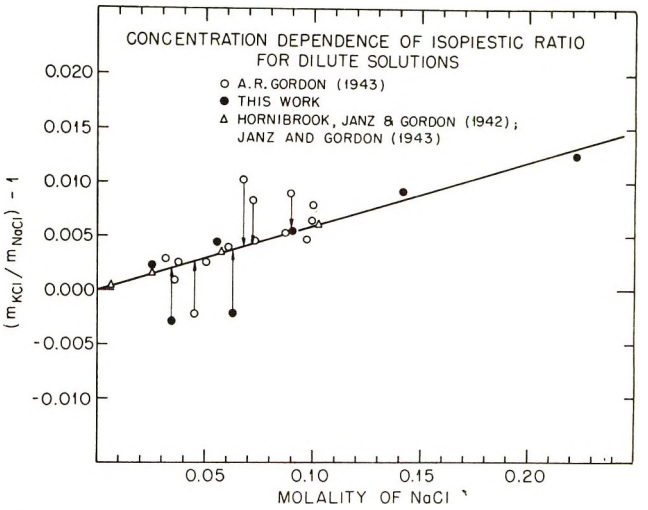

Figure 1. Concentration dependence of the isopiestic ratios for dilute NaCl and KCl aqueous solutions at 25° (comparisons of this research with Gordon, *et al.*[15–17]).

The difficulty in applying the isopiestic vapor pressure comparison method to dilute electrolyte solutions is generally recognized. A painstaking investigation of the technique with dilute NaCl and KCl solutions has been reported by Gordon.[15] The isopiestic molality ratios, M_{KCl}/M_{NaCl}, observed in our experiments are shown in Figure 1 with those computed from Gordon's data. Also shown are values calculated from osmotic coefficients derived from cell emf measurements with dilute KCl[16] and NaCl[17] solutions. The apparent concordance of the M_{KCl}/M_{NaCl} ratios for five of the seven isopiestic concentrations determined in our work with those of Gordon and coworkers leads us to infer that our measurements with the NaBr–$ZnBr_2$ ternary mixtures and the NaBr and $ZnBr_2$ binary solutions also represented equilibrium.

Experimental Results and Calculations

Isopiestic Data. The observed isopiestic concentrations are plotted in Figure 2. The function *R*, plotted as the ordinate, is defined by, $R = M_B/m$, where M_B is the molality of the binary, isopiestic sodium bromide solution, taken as the reference solution in the calculations below, and *m* is the *total ionic concentration* in the mixture, defined by, $m = m_B + 1.5m_C$, where m_B and m_C are the NaBr and $ZnBr_2$ molalities, respectively. The abscissa in Figure 2 gives the ionic fraction of $ZnBr_2$ in the mixed solution, $y_C = 1.5m_C/m$. The plots

(13) R. H. Stokes, J. M. Stokes, and R. A. Robinson, *Trans. Faraday Soc.*, **35**, 533 (1944).

(14) W. Rieman, J. D. Neuss, and B. Naiman, "Quantitative Analysis," McGraw-Hill, New York, N. Y., 1941, pp 349, 354.

(15) A. R. Gordon, *J. Amer. Chem. Soc.*, **65**, 221 (1933).

(16) W. J. Hornibrook, G. J. Janz, and A. R. Gordon, *ibid.*, **64**, 513 (1942).

(17) G. J. Janz and A. R. Gordon, *ibid.*, **65**, 218 (1943).

Table I: Values of the Parameters of Eq 6 and of the Integral in Eq 10

Series	M_B	a	S.E.	b	S.E.	c	S.E.	VARF $\times 10^6$	$M_{B\phi B}°$	J^a
I-1	0.2196	1.00082	0.00126	0.03716	0.00641	0.01810	0.00624	2.75	0.2047	0.01341
I-2	0.1401	1.00022	0.00098	0.05032	0.00500	0.01985	0.00486	1.67	0.1313	0.01001
I-3	0.08960	0.99645	0.00227	0.05117	0.01154	0.01789	0.01122	8.92	0.0845	0.00702
II-1	0.06203	1.00165	0.00092	0.07967	0.00173	...	...	2.63	0.0588	0.00510
II-2	0.03411	0.99893	0.00099	0.05422	0.00621	0.01820	0.00634	1.88	0.0326	0.00326
II-3	0.02526	0.98979	0.00471	0.05229	0.00886	...	...	69.2	0.0243	0.00223

[a] This column gives values of the integral $0.4343 \int_0^{M_{B\phi B}°} (c/M_B)\mathrm{d}(M_{B\phi B}°)$ computed with eq 12b.

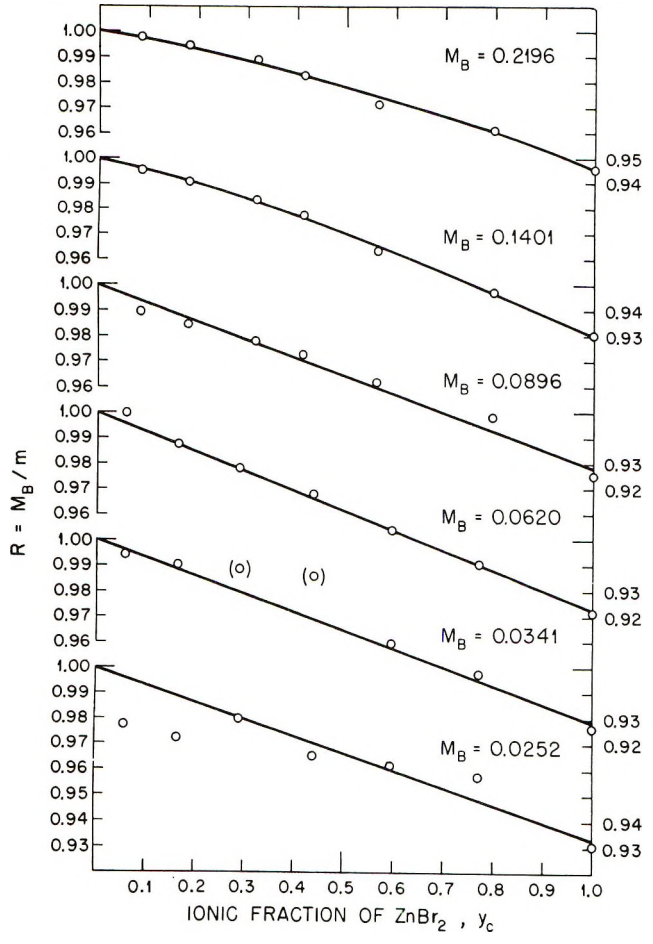

Figure 2. Composition dependence of isopiestic ratios for aqueous NaBr + $ZnBr_2$ mixtures at 25°.

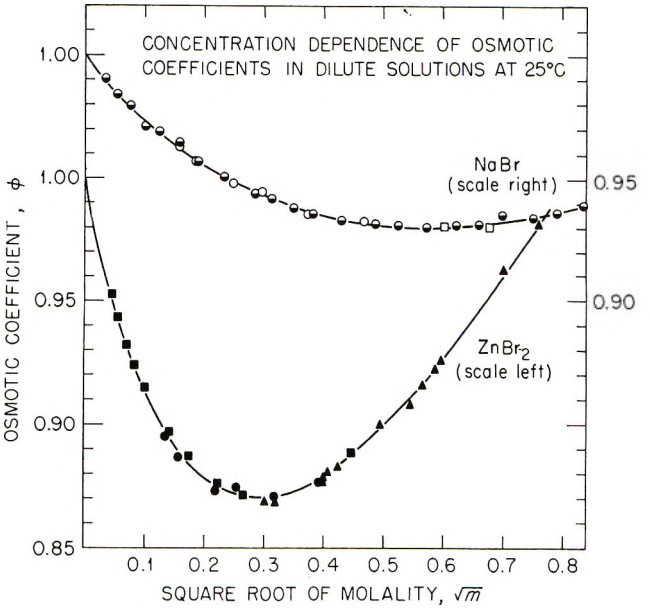

Figure 3. Concentration dependence of the osmotic coefficients of dilute aqueous NaBr and $ZnBr_2$ solutions at 25°. Upper curve: ○, this work; ◒, ref 19; □, ref 21. Lower curve: ●, this work; ■, ref 22; ▲, ref 13.

indicate that R decreased with increasing zinc ion fraction and could be described by the equation

$$R = M_B/m = a - by_C - cy_C^2 \qquad (6)$$

The parameters in eq 6 were computed with a least-squares procedure; values of a, b, and c are given in Table I together with their standard errors and the variance of the fit (VARF) to either a linear or quadratic equation in y_C.

Solute Activity Coefficients in Binary Solutions. Molal osmotic coefficients, ϕ, for the dilute, binary NaBr and $ZnBr_2$ solutions were computed from their isopiestic concentrations, M_B and M_C, respectively, with those for the KCl solutions. The necessary values of ϕ_{KCl} were interpolated with an equation obtained from a least-squares fit for the concentration dependence of the latter quantity.[18] The concentration dependence of the ϕ_{NaBr} and ϕ_{ZnBr_2} values in dilute solution is shown in Figure 3 where our values are compared with osmotic coefficients computed by us from measurements by others with these two salts, respectively.

The ϕ_{NaBr} values determined in this research (upper curve, open circles) appear to agree quite well with osmotic coefficients (half-filled circles) computed from the freezing point lowering measurements of Scatchard and Prentiss[19] corrected to 25° with the relation

(18) M. H. Lietzke and R. W. Stoughton, *J. Phys. Chem.*, **66**, 508 (1962).

(19) G. Scatchard and S. S. Prentiss, *J. Amer. Chem. Soc.*, **55**, 4355 (1933).

Table II: Parameters Describing the Concentration Dependence of the Osmotic Coefficients for Electrolytes Measured in This Research (Eq 7)

Electrolyte	A	B	C	D	VARF × 10^6	Concn range, m
NaBr	2.5298	−0.09949	0.19057	−0.08609	1.35	0.0–0.88
$ZnBr_2$	1.8532	+0.04214	0.04176	−0.01405	3.35	0.0–0.63

$$\phi_{25} - \phi_0 = 7.72 \times 10^{-5}(\phi_L - \bar{L}_2)$$

and values of the apparent molal heat content, ϕ_L, and the relative partial molal heat content, $\bar{L}_2$, taken from Harned and Owen.[20] A satisfactory agreement with the osmotic coefficients computed from isopiestic concentrations published by Robinson[21] (open squares) also may be noted. The concordance of our zinc bromide osmotic coefficients (lower curve, filled circles) with those derived from the isopiestic measurements of Stokes, Stokes, and Robinson[13] (filled triangles) and with ϕ_{ZnBr_2} values (filled squares) computed from activity coefficient measurements by Stokes and Stokes[22] with the Gibbs–Duhem equation appears to be good.

The data shown in Figure 3 were fitted by least-squares techniques to the equation

$$\phi = 1 - \frac{S}{A^3 I}[(1 + AI^{1/2}) - 2\ln(1 + AI^{1/2}) - (1 + AI^{1/2})^{-1}] + BI + CI^2 + DI^3 \quad (7)$$

where I is the ionic strength of the solution, S is the Debye–Hückel slope ($S = 1.17202$ for a 1–1 electrolyte), and A, B, C, and D are empirical constants. Numerical values for these constants are summarized in Table II.

Substitution of eq 7 into the Gibbs–Duhem relation and integrating analytically gives the mean molal activity coefficient, $\gamma_\pm$

$$\ln \gamma_\pm = -\frac{SI^{1/2}}{1 + AI^{1/2}} + 2BI + (3/2)CI^2 + (4/3)DI^3 \quad (8)$$

Activity Coefficients in Ternary Solutions. Several alternative procedures may be applied to derive solute activity coefficients from isopiestic vapor pressure measurements on NaBr + $ZnBr_2$ + H_2O mixtures. The method of longest standing is that of McKay and Perring[23] whose thermodynamic treatment for ternary systems has been shown[3] to lead to the equation

$$\log \gamma_B = \log \Gamma_B + \log R + 0.4343\int_0^{M_B\phi_B^\circ} f(m,M_B,y_C)\mathrm{d}(M_B\phi_B^\circ) \quad (9)$$

where γ_B and Γ_B are the mean molal activity coefficients of sodium bromide in the mixture and in the reference binary NaBr solution at molality, M_B, respectively, $f(m,M_B,y_C)$ is defined by eq 10 and 11, and the other symbols have the meanings defined above. In applying eq 9 and the corresponding equation for log γ_C, however, uncertainties can arise in the evaluation of the integral which appears as the third member of the RHS. An extrapolation of $f(m,M_B,y_C)$ to $M_B\phi_B^\circ = 0$ must be performed empirically. To avoid this defect in the McKay–Perring treatment, Scatchard has developed two alternative methods for computing activity coefficients from isopiestic concentrations in ternary mixtures: (a) the "neutral component"[24] and (b) the ion component[25] procedures. We have applied the "neutral component" and the McKay–Perring treatment to our data, but we shall present results only from the latter because more accurate values of γ_B and γ_C were obtained than when computations following the neutral component method were performed. The principal reason for the lower accuracy obtained with the neutral component method appeared to reside in the relatively narrow concentration range over which the measurements with mixtures were conducted.

Substituting eq 6 in 9 gives, for each M_B

$$\log \gamma_B = \log \Gamma_B + \log R + 0.4343 y_C^2 \int_0^{M_B\phi_B^\circ} (c/M_B)\mathrm{d}(M_B\phi_B^\circ) \quad (10)$$

Values of $M_B\phi_B^\circ$ and of the integral in eq 10 are listed in columns 10 and 11 of Table I. Zinc bromide activity coefficients, γ_C, were found with eq 11

$$\log \gamma_C = \log \Gamma_C + \log R' + 0.4343(1 - y_C)^2 \int_0^{M_B\phi_B^\circ} (c/M_B)\mathrm{d}(M_B\phi_B^\circ) \quad (11)$$

where $R' = (1.5M_C/M_B)R$. The values of log Γ_B and log Γ_C for M_B and M_C, respectively, were derived with eq 8 and the constants A, B, C, and D given in Table II; log R was evaluated with eq 6 and the constants in Table I, and log R' was obtained with the relation log R' = log $(1.5M_C/M_B)$ + log R.

The evaluation of the integral term in eq 10 and 11 is partially arbitrary because the nature of the func-

(20) H. S. Harned and B. B. Owen, "The Physical Chemistry of Electrolyte Solutions," 3rd ed, Reinhold Publishing Co., New York, N. Y., 1958.

(21) R. A. Robinson, *Trans. Faraday Soc.*, **35**, 1217 (1939).

(22) R. H. Stokes and J. M. Stokes, *ibid.*, **41**, 688 (1945).

(23) H. A. C. McKay and J. K. Perring, *ibid.*, **49**, 163 (1953).

(24) G. Scatchard, *J. Amer. Chem. Soc.*, **83**, 2636 (1961).

(25) G. Scatchard, R. M. Rush, and J. S. Johnson, *J. Phys. Chem.*, **74**, 3786 (1970).

tional relationship between (c/M_B) and $M_B\phi_B^\circ$ is not known. Further, there were serious uncertainties in the experimental values of (c/M_B) for the three most dilute series of mixtures investigated. The extrapolation to $M_B\phi_B^\circ = 0$ therefore was based on the values given in Table I for $M_B = 0.2196$, 0.1401, and 0.0896, respectively, which could be represented by the empirical equation

$$(c/M_B) = 0.2198 - 0.6740M_B\phi_B^\circ \qquad (12a)$$

Accordingly, the numerical values listed in column 11, Table I, were obtained with the expression

$$0.4343\int_0^{M_B\phi_B^\circ}(c/M_B)\mathrm{d}(M_B\phi_B^\circ) = 0.4343M_B\phi_B^\circ[0.2198 - 0.3370M_B\phi_B^\circ] \qquad (12b)$$

The log γ_B and log γ_C values computed with eq 10 and 11 were subtracted from log γ_B° and log γ_C° values, respectively, for NaBr in a *binary* NaBr solution at a molality equal to the total ionic concentration, m, of the mixed NaBr + $ZnBr_2$ solution, and for $ZnBr_2$ in a solution of zinc bromide only at a molality equal to $(m_B + 1.5m_C)/1.5$, and the resultant log $(\gamma_B^\circ/\gamma_B)$ and log $(\gamma_C^\circ/\gamma_C)$ were plotted against m_C and m_B, respectively. The numerical magnitudes of log γ_B° and log γ_C° were estimated with eq 8 and the constants in Table II. A linear plot was not found for any of the mixtures; hence, the data for the most concentrated sets were fitted to the equations

$$\log \gamma_B = \log \gamma_B^\circ - \alpha_B m_C - \beta_B m_C^2 \qquad (13a)$$

$$\log \gamma_C = \log \gamma_C^\circ - \alpha_C m_B - \beta_C m_B^2 \qquad (13b)$$

in which it is assumed that α_B, α_C, β_B, and β_C are functions only of m at constant temperature. The α and β coefficients in eq 13a,b are related by thermodynamics

$$3(\alpha_B + 1.5\alpha_C) = \text{constant} - 2(2\beta_B + 4.5\beta_C)m \qquad (14)$$

provided that β_B and β_C are independent of m.[26] With the mixtures thus far reported in the literature, the magnitudes of the β coefficients have been extremely small, and any variation of β_B and β_C with m was beyond experimental detection. The data for the three most concentrated mixtures measured in this research should be suitable for the estimation of β_B and β_C because the quadratic terms in eq 13a,b will be the most readily detected. A summary of the values from least-squares fits for $M_B = 0.2196$, 0.1401, and 0.0896 is presented in Table III.

The most reliable β values should be those for which $M_B = 0.2196$ and 0.1401, and it is gratifying that almost identical values of β_B and β_C were obtained with these mixtures. Notably different values for the quadratic concentration coefficients were found when $M_B = 0.0896$. In this instance, however, the quadratic terms in eq 13a,b contribute at the most (*i.e.*, for $y_C = 1.0$) only 0.00083 and 0.00161 to log γ_B and log γ_C. Therefore, it was assumed that β_B and β_C were constant and independent of m for all mixtures examined in this research. Values of α_B and α_C computed with $\beta_B = -0.200$ and $\beta_C = -0.227$ are summarized in Table IV. A plot of α_B, α_C, and the sum $(\alpha_B + 1.5\alpha_C)$ against $M_B \approx m$ is given in Figure 4; a linear dependence of $(\alpha_B + 1.5\alpha_C)$ on m with a slope close to the predicted value, $(2/3)(2\beta_B + 4.5\beta_C) = -0.95$, was observed.

Table III: Interaction Coefficients for Sodium–Zinc Bromide Aqueous Mixtures at 25°

M_B	α_B	$-\alpha_C$	β_B	β_C	$^2/_3(2\beta_B + 4.5\beta_C)$
0.2196	0.0905	+0.110	−0.198	−0.245	−1.00
0.1401	0.211	+0.238	−0.203	−0.209	−0.90
0.0896	0.438	+0.397	−1.22	0.114	−1.28

Table IV: Parameters of Eq 13a and 13b ($\beta_B = -0.20$, $\beta_C = -0.23$)

M_B	α_B	$-\alpha_C$	$(\alpha_B + 1.5\alpha_C)$	Δ^a
0.02526	1.337	0.997	−0.159	0.0007
0.03411	1.145	0.918	−0.232	0.0004
0.06203	0.629	0.571	−0.228	0.0011
0.08960	0.407	0.366	−0.142	0.0024
0.1401	0.211	0.238	−0.146	0.0002
0.2196	0.0905	0.110	−0.075	0.0006

[a] Δ is the average difference between log γ_C(obsd) and that calculated by eq 13b with $\beta_C = -0.23$ and the α_C values listed in this table.

The unusual feature revealed by the figure is that α_B and α_C increase rapidly with decreasing total ionic concentration and attain surprisingly large values. The error in the computation of these interaction coefficients is proportional to $(1/m)$. The error is not known accurately, however; consequently, it has been omitted from the figure. Recent investigations by others[27,28] with mixtures of 1–1 and 2–1 type electrolytes have indicated an increase in α_B and α_C occurs on dilution. These investigations, however, did not extend to concentrations below 0.5 m, nor did the interaction coefficients reach the large values shown in Figure 4. It is of interest to note that a formulation of the properties of ionic solutions based on cluster expansion theory by Friedman[29] indicates that α_B and α_C may approach in-

(26) R. A. Robinson and R. H. Stokes, "Electrolyte Solutions," 2nd ed, Butterworths, London, 1959, p 442.

(27) R. A. Robinson and V. E. Bower, *J. Res. Nat. Bur. Stand.*, **69A**, 19 (1965).

(28) J. N. Butler and R. Huston, *J. Phys. Chem.*, **71**, 4479 (1967).

(29) H. L. Friedman, "Ionic Solution Theory Based on Cluster Expansion Methods," Monographs in Statistical Physics and Thermodynamics, Vol. III, Interscience, New York, N. Y., 1962.

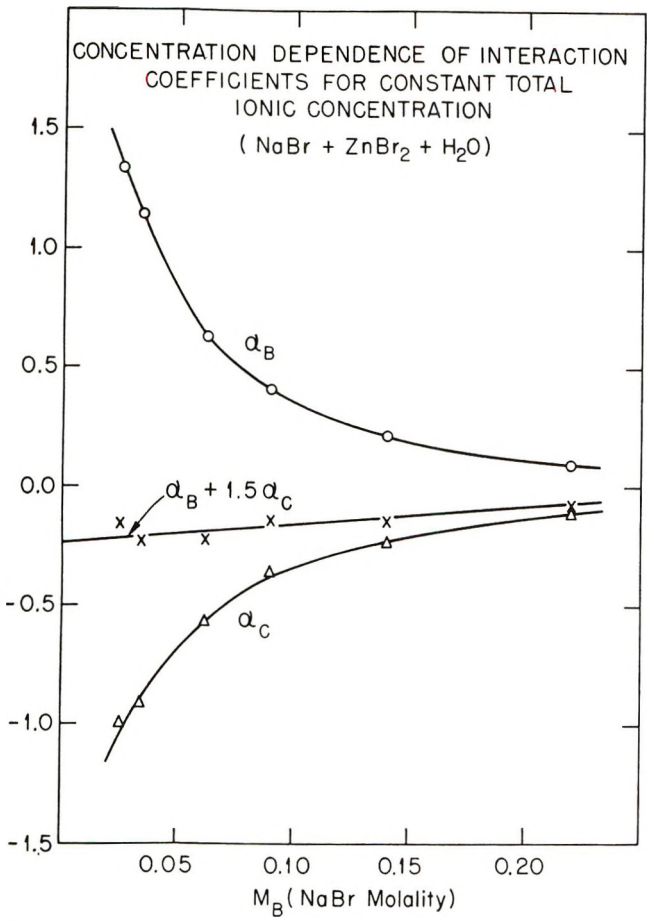

Figure 4. Concentration dependence of Harned interaction coefficients for ternary NaBr–$ZnBr_2$–H_2O mixtures at 25° and constant total ionic concentration.

definitely large values at a vanishingly small ionic strength.

Comparisons of Predicted with Observed NaBr and $ZnBr_2$ Activity Coefficients. Equation 5a and 5b were employed to estimate the activity coefficients of NaBr and $ZnBr_2$ in mixtures when each solute was, respectively, present at trace concentrations (*i.e.*, $F_C = F_B = 1$). These values, which are listed in the second column of Table V, may be compared with the activity coefficients in the third column which were computed from the experimental data with the McKay–Perring (MKP) treatment; the difference, Δ, is presented in the fourth column of the table. The mean difference between the predicted with the observed values for NaBr is approximately 1.0%, and for $ZnBr_2$ it is approximately 2.3%. The extent of the agreement appears to be satisfactory considering the difficulty and time-consuming nature of the experimental measurements with dilute mixtures and especially the uncertainty in the evaluation of the McKay–Perring integral which appears in eq 10 and 11. The choice of slightly different, but probably less justified, dependence of (c/M_B) on $M_B\phi_B°$ than that of eq 12a was found to give differences of 1.2 and 0.8% for NaBr and $ZnBr_2$, respectively.

Discussion

This research appears to be the first in which isopiestic vapor pressure comparison measurements have been made and employed to estimate both solute activity coefficients in dilute ternary electrolyte mixtures. An important conclusion is that eq 5a and 5b, which are general for 1–1 plus 2–1 electrolyte mixtures, may be used to describe sodium bromide–zinc bromide mixtures with fair accuracy. This result is of interest because this particular system is unusual by reason of the strong interaction between zinc and bromide ions in aqueous mixtures, which is known to lead to complex ion formation (*viz.*, $ZnBr_4^{2-}$). Even at the relatively small bromide ion concentrations employed in our measurements, some association may have occurred. Stokes and Stokes[22] have compared the concentration dependence of the osmotic coefficients for $ZnBr_2$ with $MgBr_2$ and suggest that it may not be permissible to regard the former solute as fully dissociated even at 0.1 *m*. Large Harned interaction coefficients, α_B and α_C, were observed with the more dilute solutions. This behavior, however, may not be unique with NaBr–$ZnBr_2$–H_2O mixtures as there are indications that a similar behavior may occur with other mixtures of 1–1 with 2–1 electrolytes. The sodium–zinc bromide system also required unusually large β_B and β_C coefficients to describe the composition dependence of the respective solute activity coefficients, and this feature has not been observed with any other electrolyte mixtures of the same type. Conceivably, these unusual β coefficients reflect the strong, specific interaction of bromide ions with zinc ion. Therefore, studies with dilute aqueous mixtures of $NaClO_4$ and $Zn(ClO_4)_2$ would be of interest.

Table V: Comparison of Predicted (G) and Observed (MKP) Solute Activity Coefficients for NaBr and $ZnBr_2$ Present at Trace Concentrations in Their Aqueous Mixtures at 25°

$I = 3m_C$	$-\log \gamma_{NaBr}^{G}$ (eq 5a)	$-\log \gamma_{NaBr}^{MKP}$ (eq 13a)	Δ
0.0543	0.0803	0.0856	−0.0053
0.0737	0.0889	0.0968	−0.0079
0.1346	0.1068	0.1128	−0.0060
0.1937	0.1176	0.1192	+0.0016
0.3011	0.1305	0.1292	+0.0013
0.4645	0.1410	0.1338	+0.0072

$I = m_B$	$-\log \gamma_{ZnBr_2}^{G}$ (eq 5b)	$-\log \gamma_{ZnBr_2}^{MKP}$ (eq 13b)	Δ
0.0253	0.1220	0.1343	−0.0123
0.0341	0.1364	0.1450	−0.0086
0.0620	0.1681	0.1757	−0.0076
0.0896	0.1892	0.1995	−0.0103
0.1401	0.2159	0.2224	−0.0065
0.2196	0.2430	0.2271	+0.0159

An Investigation of the van der Waals Effect in Nuclear Magnetic Resonance Spectroscopy by Factor Analysis and the Prediction of Diamagnetic and Paramagnetic Susceptibilities

by Paul H. Weiner[1] and Edmund R. Malinowski*

Department of Chemistry and Chemical Engineering, Stevens Institute of Technology, Hoboken, New Jersey 07030 *(Received February 8, 1971)*

Publication costs assisted by Stevens Institute of Technology

The proton shifts of nonpolar solutes in a variety of solvents are subjected to a mathematical technique called factor analysis. This technique permits the isolation of the van der Waals term from solvent anisotropy. The nature of the van der Waals effect is discussed, and the results of factor analysis are shown to be in general accord with the theory of Linder. The origin of the empirical additivity rules of Raynes, concerning methane dissolved in a number of solvents, is explained. From factor analysis of proton solvent shifts, diamagnetic susceptibilities, χ_d, of the solvents are deduced.

Introduction

The chemical shift $\delta(i,\alpha)$ of a solute i in a solvent α is generally believed to be a linear sum of contributing factors[2]

$$\delta(i,\alpha) = \delta(i,\mathrm{g}) + \sigma_\mathrm{b}(\alpha) + \sigma_\mathrm{w}(i,\alpha) + \sigma_\epsilon(i,\alpha) + \sigma_\mathrm{a}(\alpha) \quad (1)$$

where $\delta(i,\mathrm{g})$ is the gas phase chemical shift; $\sigma_\mathrm{b}(\alpha)$ is the bulk shielding effect; $\sigma_\mathrm{w}(i,\alpha)$ is the van der Waals term; $\sigma_\epsilon(i,\alpha)$ is the reaction field effect; and $\sigma_\mathrm{a}(\alpha)$ is the solvent anisotropic contribution. For nonpolar solutes the reaction field effect, $\sigma_\epsilon(i,\alpha)$, can be set equal to zero. Furthermore, if an external standard such as hexamethyldisiloxane (HMD) is employed and corrections for bulk susceptibilities are made, then eq 1 can be written as

$$\overset{\mathrm{HMD}}{\delta}(i,\alpha) = \overset{\mathrm{HMD}}{\delta}(i,\mathrm{g}) + \sigma_\mathrm{w}(i,\alpha) + \sigma_\mathrm{a}(\alpha) \quad (2)$$

where $\overset{\mathrm{HMD}}{\delta}(i,\alpha)$ is the corrected shift of solute i, relative to external HMD.

Recently, a mathematical technique called factor analysis[3] was developed and applied to the study of solvent effects in nmr spectroscopy. The chemical shift of a nonpolar solute was shown to be composed of only three fundamental factors. These factors were identified as (1) the solute gas phase shift, (2) van der Waals shift, and (3) solvent anisotropy, in accord with eq 2. When methane gas-to-solution shifts were used as an indirect measure of the van der Waals term, the anisotropic solvent shift was isolated and quantitative values for solvent anisotropy were deduced. Details of these results can be found in the original paper[3b] and will not be repeated here. The present investigation focuses attention on the van der Waals term.

Theory of van der Waals Effects

Several theoretical developments have been proposed to explain the van der Waals effect involving nonpolar solutes. Linder[4,5] and coworkers treat the solute as an oscillating dipole and the solvent as a continuum. Bernstein[6] and coworkers utilize a virial expansion of solute–solvent interactions. Both of these theories have much in common but differ in detail. Because of its relative simplicity we choose to use the continuum approach of Linder.

The shielding constant, σ_w, associated with the van der Waals effect is proportional to the square of the oscillating electric field E produced by the oscillating dipole of the solute.

$$\sigma_\mathrm{w} = \phi E^2 \quad (3)$$

The constant ϕ has been estimated to be -1×10^{-12} cm^4/esu^2 ppm. According to Linder[5]

$$E^2 = (^3/_4)hg \frac{\nu_\alpha \nu_i}{\nu_\alpha + \nu_i} \quad (4)$$

where h is Planck's constant, ν_α and ν_i are frequencies associated with the solvent and solute oscillating dipoles, respectively, and g is defined as

(1) Robert-Crooks-Stanley Fellow. Material in this paper is based on a dissertation in partial fulfillment for the Ph.D. degree at Stevens Institute of Technology.

(2) A. D. Buckingham, T. S. Schaefer, and W. G. Schneider, *J. Chem. Phys.*, **32**, 1227 (1960).

(3) (a) P. H. Weiner, E. R. Malinowski, and A. R. Levinstone, *J. Phys. Chem.*, **74**, 4537 (1970); (b) P. H. Weiner and E. R. Malinowski, *ibid.*, **75**, 1207 (1971).

(4) B. Linder, *J. Chem. Phys.*, **33**, 668 (1960).

(5) B. B. Howard, B. Linder, and M. T. Emerson, *ibid.*, **36**, 485 (1962).

(6) F. H. A. Rummens, W. T. Raynes, and H. J. Bernstein, *J. Phys. Chem.*, **72**, 2111 (1968).

$$g = \frac{2n^2 - 2}{2n^2 + 1}\frac{1}{a_i^3} \tag{5}$$

In eq 5 n is the refractive index of the solvent and a_i is the Onsager molecular radius of the solute. The oscillating frequency is related to radius r_j of the electron cloud distribution and the molecular polarizability, α, by the expression

$$\nu = \frac{2}{3}\frac{e^2}{h\alpha}\sum_j \langle r_j^2 \rangle \tag{6}$$

Furthermore we recognize that

$$V_i = {}^4/_3\pi N a_i^3 \tag{7}$$

$$\frac{4}{3}\pi N\alpha = \frac{n^2 - 1}{n^2 + 2}V \tag{8}$$

where V_i and V are the molar volumes of the solute and solvent, respectively. Placing eq 5, 6, 7, and 8 into eq 4 we find

$$E^2 = \frac{16\pi^2 N^2 e^2}{9V_i}\frac{\nu_i}{\nu_i + \nu_\alpha}\left[\frac{n^2 + 2}{2n^2 + 1}\frac{\sum\langle r_j^2\rangle}{V}\right]_{\text{solv}} \tag{9}$$

Considering quantum effects, energy absorption between solvent and solute will be greatest when $\nu_i = \nu_\alpha$. Thus eq 3 becomes

$$\sigma_w = \frac{8\pi^2 N^2 e^2 \phi}{9V_i}\left[\frac{n^2 + 2}{2n^2 + 1}\frac{\sum\langle r_j^2\rangle}{V}\right]_{\text{solv}} \tag{10}$$

Unfortunately, there is no direct way of obtaining values for $\Sigma\langle r_j^2\rangle$. Linder[5] suggested using the volume susceptibility, χ_v, as a measure of $\Sigma\langle r_j^2\rangle/V$. This approximation, however, neglects the paramagnetic contribution. This can be seen by examining the theoretical relationship[7] for the molar susceptibility, χ_M.

$$\chi_M = -\frac{Ne^2}{6mc^2}\sum\langle r_j^2\rangle + \frac{2}{3}N\sum_{l\neq k}\frac{\left|\left\langle k\left|\sum\frac{e_i}{2mc}M_j\right|l\right\rangle\right|^2}{E_l^\circ - E_k^\circ} \tag{11}$$

In this expression M_j is the total magnetic moment operator; $E_l^\circ - E_k^\circ$ is the difference between the ground state (k) and the corresponding excited state (l) of the unperturbed molecule. This equation is often written symbolically as

$$\chi_M = \chi_d + \chi_p \tag{12}$$

where χ_d, called the Langevin diamagnetism, is a function of the average dimensions of the electron cloud, and χ_p, the Van Vleck paramagnetism, is a term which depends on the symmetry of the cloud. By neglecting χ_p Linder[5] invoked an unnecessary approximation.

There are several semiempirical methods for estimating $\Sigma\langle r_j^2\rangle$. For radially symmetric systems containing k electrons, Kirkwood[8] derived the following relationship

$$\alpha = \frac{4}{9ka_0}[\sum\langle r_j^2\rangle]^2 \tag{13}$$

where a_0 is the Bohr radius. Equation 13 should apply reasonably well to quasispherical molecules such as CH_4, CCl_4, CBr_4, and CI_4 but not for mixed halogenated methanes. From additivity arguments Maslov[9] has estimated $\Sigma\langle r_j^2\rangle$ for the mixed halogens.

van der Waals Shifts by Factor Analysis

The mathematical development of factor analysis as applied to solvent effects in nmr spectroscopy has been presented previously and will not be repeated here.[3a] Factor analysis is applicable when a quantity can be expressed as a linear sum of product functions. For example, the chemical shift $\delta(i,\alpha)$ of solute i in solvent α must have the following form

$$\delta(i,\alpha) = \sum_j U_{ij}V_{j\alpha} \tag{14}$$

Here U_{ij} represents the jth solute factor of solute i, and $V_{j\alpha}$ represents the jth solvent factor of solvent α. Previous work[3b,10] indicates that this is true for nonpolar solutes. Equation 2 can be written in the form of eq 14; that is

$$\delta(i,\alpha) = \delta_{\text{gas}}\cdot 1 + \sigma_w(i)\cdot\sigma_w(\alpha) + 1\cdot\sigma_a(\alpha) \tag{15}$$

Here the van der Waals term is expressed as a product function of solute $\sigma_w(i)$ and solvent $\sigma_w(\alpha)$ parameters.[10] From eq 10 we see that

$$\sigma_w(i) = \frac{8\pi^2 N^2 e^2 \phi}{9V_i} \tag{16}$$

$$\sigma_w(\alpha) = \frac{n^2 + 2}{2n^2 + 1}\frac{\sum\langle r_j^2\rangle}{V} \tag{17}$$

In the present factor analysis scheme we have employed the same matrix of data as given in the previous work.[3b] These data consist of the chemical shifts (corrected for bulk susceptibility and referenced with respect to external HMD) of methane, ethane, neopentane, cyclohexane, cyclooctane, and TMS in a large variety of solvents such as CCl_4, CS_2, benzene, acetone, etc. When this data matrix was subjected to the factor analysis computer program, the following results were obtained. Three eigenvectors were generated; thus only three fundamental factors were needed to span the solvent space. This fact is in complete agreement with eq 2 (notice that there are three terms on the right-hand side). In the original work,[3b] discussion of

(7) Y. G. Dorfman, "Diamagnetism and the Chemical Bond," American Elsevier, New York, N. Y., 1965, p 4.

(8) Reference 7, p 31.

(9) P. G. Maslov, *J. Phys. Chem.*, **72**, 1414 (1968).

(10) E. R. Malinowski and P. H. Weiner, *J. Amer. Chem. Soc.*, **92**, 4193 (1970).

Table I: Test of the Solvent van der Waals Term $\sigma_w(\alpha)$

No.[a]	Solvent	Factor analysis	Calcd[b]	No.	Solvent	Factor analysis	Calcd
1	CH_2Cl_2	0.229	0.225	12	CH_2ClCCl_3	0.264	...
2	$CHCl_3$	0.242	0.238	13	$CHCl_2CHCl_2$	0.253	...
3	CCl_4	0.273	0.245	14	$CHCl_2CCl_3$	0.262	...
4	CH_2Br_2	0.268	0.295	15	CS_2	0.246	...
5	$CHBr_3$	0.310	0.323	16	C_6H_6	0.186	0.199[c]
6	CH_3I	0.243	0.231	17	CH_3CN	0.221	...
7	CH_2I_2	0.286	0.301	18	$(CH_3)_2CO$	0.180	0.175[c]
8	CH_2BrCl	0.245	0.263	19	$(CH_3)_2SO$	0.244	...
9	$CHBrCl_2$	0.268	0.268	20	c-C_6H_{12}	0.203	...
10	$CBrCl_3$	0.293	0.264	21	c-C_8H_{16}	0.206	...
11	CH_3CCl_3	0.254	...	22	C_6F_6	0.200	...

[a] Solvent numbers used to identify the solvents in Figure 1. [b] Calculated according to eq 17 using Maslov's additivity relation for $\Sigma\langle r_j^2\rangle$. [c] Estimated from polarizability data.

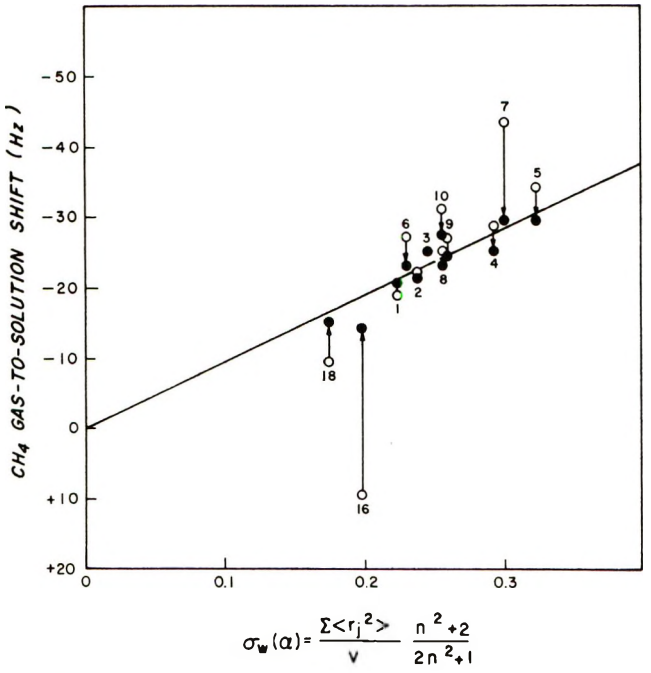

Figure 1. Methane gas-to-solution shifts *vs.* the solvent van der Waals term before and after correction for solvent anisotropy.

the theoretical nature of the van der Waals effects was side-stepped by introducing the methane gas-to-solution shift as a test factor. By this substitution it was not necessary to inject into the analysis any particular theoretical model of the van der Waals effect. The previous analysis clearly identified the following three factors: unity, methane gas-to-solution shift, and solvent anisotropy. From this scheme solvent anisotropy values were deduced for all the solvents involved. For a detailed discussion one is referred to the original paper.[3b]

In factor analysis each eigenvector can be rotated individually, and thus one can focus attention on any one fundamental factor. In the earlier work attention was focused on solvent anisotropy. In this paper we focus attention on the van der Waals term. Using the rotational scheme we can successfuly rotate an eigenvector into $\sigma_w(\alpha)$, the contribution due to the solvent (see eq 17). Values for $\sigma_w(\alpha)$ were calculated using Maslov's[9] additivity for $\Sigma\langle r_j^2\rangle$. These values, together with results of the rotation, are listed in Table I.

The three solvent test vectors (factors) were unity, $\sigma_w(\alpha)$, and $\sigma_a(\alpha)$. The simultaneous rotation of the eigenvectors into these three test vectors yielded the following equations.

$$\delta^{\mathrm{HMD}}(CH_4,\alpha) = -10.4\,(1) + 103.8\sigma_w(\alpha) + 1.10\sigma_a(\alpha)$$

$$\delta^{\mathrm{HMD}}(CH_3CH_3,\alpha) = 34.3\,(1) + 72.5\sigma_w(\alpha) + 1.07\sigma_a(\alpha)$$

$$\delta^{\mathrm{HMD}}(\text{neo-}C_5H_{12},\alpha) = 40.2\,(1) + 65.0\sigma_w(\alpha) + 1.03\sigma_a(\alpha)$$

$$\delta^{\mathrm{HMD}}(C_6H_{12},\alpha) = 74.7\,(1) + 45.5\sigma_w(\alpha) + 1.04\sigma_a(\alpha)$$

$$\delta^{\mathrm{HMD}}(C_8H_{16},\alpha) = 82.9\,(1) + 39.0\sigma_w(\alpha) + 1.06\sigma_a(\alpha)$$

$$\delta^{\mathrm{HMD}}(\mathrm{TMS},\alpha) = -14.2\,(1) + 63.5\sigma_w(\alpha) + 1.04\sigma_w(\alpha) \quad (18)$$

With these equations the shifts can be reproduced within ±1.5 Hz of the measured values. This error in reproduction is identical with the experimental error.

The validity of the analysis is confirmed by the following observations concerning the coefficients in eq 18. The coefficient of the unity vector should be the gas phase shift of the solute (see eq 15.) These coefficients compare favorably with the experimental values;[11-14] namely, methane = −8.4 Hz, ethane =

(11) In ref 12, 13, and 14 the shifts are reported with respect to methane gas. Since our reference standard is external HMD, a correction factor of −8.4 Hz must be added to each of these shifts to convert the data into external HMD basis.

Table II: Diamagnetic and Paramagnetic Susceptibilities Determined by Factor Analysis[a]

Compound	$\chi_M \times 10^6$ [b]	$\chi_d \times 10^6$	$\chi_p \times 10^6$	Compound	$\chi_M \times 10^6$ [b]	$\chi_d \times 10^6$	$\chi_p \times 10^6$
CH_2Cl_2	−46.6	−52	5	CH_2ClCCl_3	−88.0	−105	17
$CHCl_3$	−59.3	−69	10	$CHCl_2CHCl_2$	−89.8	−97	8
CCl_4	−66.8	−95	28	$CHCl_2CCl_3$	−99.1	−116	17
CH_2Br_2	−65.1	−70	5	CS_2	−41	−57	16
$CHBr_3$	−82.6	−110	27	C_6H_6	−54.8	−61	6
CH_3I	−57.2	−59	2	CH_3CN	−28.0	−40	12
CH_2I_2	−93.6	−92	−2	$(CH_3)_2CO$	−33.8	−46	12
CH_2BrCl	−55.6	−60	4	$(CH_3)_2SO$	−43.5[c]	−63	20
$CHBrCl_2$	−66.3	−81	15	C_6H_{12}	−68.1	−78	10
$CBrCl_3$	−73.1	−109	36	C_8H_{16}	−88.2[c]	−100	12

[a] χ_d and χ_p are estimated to be accurate to within $\pm 5 \times 10^{-6}$ cc. [b] Molar magnetic susceptibility from "Handbook of Chemistry and Physics," 50th ed, Chemical Rubber Co., Cleveland, Ohio, 1969–1970. [c] Determined from volume magnetic susceptibility measured in this laboratory.

36.6 Hz, neopentane = 42.1 Hz, cyclohexane = 75.6 Hz, and tetramethylsilane = −16.4 Hz. The gas phase shift of cyclooctane has not been measured; factor analysis predicts a shift of 82.9 Hz. Furthermore, according to eq 15 the coefficient of $\sigma_a(\alpha)$ should be unity. The coefficients generated from factor analysis are in excellent agreement with these criteria (see eq 18).

We can now examine the solute coefficients of $\sigma_w(\alpha)$ resulting from factor analysis. From the theoretical considerations discussed earlier this coefficient, $\sigma_w(i)$, should be inversely proportional to the Onsager molar volume (see eq 16). When $\sigma_w(i)$, generated from factor analysis, was plotted against the inverse solute molar polarization, a linear trend was observed, but the points were somewhat scattered. This scatter could be due to the neglection of a site factor to take into account the relative position of the proton in the solute molecule. A thorough discussion of site factors has been given by Rummens[15] and coworkers.[6]

The accompanying Figure 1 is a plot of methane gas-to-solution shifts *vs.* the function $(\Sigma\langle r_j^2\rangle/V)((n^2+2)/(2n+1))$. The solvents are numbered in accord with Table I. The arrows indicate the anisotropy corrections determined from factor analysis.[3b] Notice that the corrected points follow a linear relationship which passes through the origin as theoretically predicted by eq 10. We estimate the accuracy of the solvent anisotropies to be no better than ±1.5 Hz.

Solvent Additivity Rules

The empirical additivity rules observed by Raynes,[16] for methane dissolved in a number of solvents, can be understood from the previous discussion. Solvent effect additivity originates from the van der Waals contribution. The radial electron-cloud contribution $\Sigma\langle r_j^2\rangle$ is summed over all the electrons of the solvent molecule. Substituting one substituent group by another essentially amounts to replacing one set of electron terms by another set. Hence the solvent effect should be additive with respect to the substituent groups of the solvent molecule.

Fringe Benefits from Factor Analysis

These results illustrate the utility of factor analysis in testing theoretical models. When the factors have been successfully rotated into physically significant parameters, subsidiary benefits emerge. For example, diamagnetic susceptibilities, χ_d, of many of the solvents, discussed herein, have not been reported previously. However, factor analysis predicts values for $\Sigma\langle r_j^2\rangle$ from which diamagnetic susceptibilities can be calculated. Paramagnetic susceptibilities can also be estimated from measured molar susceptibilities and the diamagnetic susceptibilities obtained from factor analysis. These results are presented in Table II.

Acknowledgment. This investigation was supported in part by the U. S. Army Research Office (Durham) under Contract No. DA-31-124-ARO-D-90. The computations were carried out at the Computer Center (supported in part by a grant from the National Science Foundation) of Stevens Institute of Technology, for which we record our appreciation.

(12) W. T. Raynes and M. A. Raza, *Mol. Phys.*, **17**, 157 (1969).

(13) F. H. A. Rummens, W. T. Raynes, and H. J. Bernstein, *J. Phys. Chem.*, **72**, 2111 (1968).

(14) H. Spiesecke and W. G. Schneider, *J. Chem. Phys.*, **35**, 722 (1961).

(15) F. H. A. Rummens, *Mol. Phys.*, **19**, 423 (1970).

(16) W. T. Raynes, *J. Chem. Phys.*, **51**, 3138 (1969).

Electron Spin Relaxation in Aqueous Solutions of Gadolinium(III). Aquo, Cacodylate, and Bovine Serum Albumin Complexes

by Jacques Reuben[1]

Department of Biophysics and Physical Biochemistry, University of Pennsylvania School of Medicine, Philadelphia, Pennsylvania 19104 *(Received April 5, 1971)*

Publication costs borne completely by The Journal of Physical Chemistry

Electron spin relaxation rates of gadolinium(III) complexes in aqueous solution were obtained from epr spectra at 9.14 and 34.2 GHz. The aquo ion and the complexes with cacodylate and with bovine serum albumin were investigated at several temperatures. The results are analyzed in terms of correlation times characteristic of processes modulating the zero-field splitting of Gd(III), using the relaxation matrix given by Hudson and Lewis. Theoretically predicted features of temperature and frequency dependence of the epr line width have been recognized in the experimental results. From the relative values of the zero-field splitting constant it appears that the immediate environment of Gd(III) bound to the protein is more symmetric than that of the aquo ion. Comparison between the zero-field splitting constants, the correlation times, and their activation energies for the three complexes studied suggests that: (a) the zero-field splitting effecting electron spin relaxation is transient to a large extent; (b) for the "small" complexes the processes governing electron spin relaxation may be identified with rotational diffusion of, solvent impact upon, and inversion of the complex. A mechanism involving metal–ligand interactions coupled to slower motions of the whole polypeptide chain is suggested to account for the electron spin relaxation observed in macromolecular systems.

Introduction

Electron spin relaxation rates of paramagnetic ions (and other free radicals) are often implied as indicators of molecular dynamics in the liquid state. A theory of electron spin relaxation converging into a simple closed expression for the relaxation rate as a function of frequency and correlation time has been given by Bloembergen and Morgan.[2] Subsequently it has been found that for an exact representation the appropriate relaxation matrix has to be used and solved numerically.[3] Recently, Hudson and Lewis presented the theory of electron spin relaxation of ^8S ions, *e.g.*, gadolinium(III) in solution.[4] From the literature review given in their article[4] it appears that the available epr data on Gd(III) in solution are too limited to provide an experimental test of the theory let alone to allow any conclusions to be drawn regarding the processes leading to electron spin relaxation.

In this paper we present the results of an epr study of aquogadolinium(III) and its complexes with cacodylate (dimethylarsinate) and with bovine serum albumin (hereafter referred to as BSA). This study was carried out in conjunction with an investigation of the suitability of Gd(III) as a paramagnetic probe in proton relaxation studies of biological macromolecules, which has been published elsewhere.[5] Measurements were done at two microwave frequencies and several temperatures. The results are used to examine the theory and draw conclusions regarding the processes effecting electron spin relaxation in solutions and the symmetry of the metal ion environment in the complexes.

Experimental Section

Epr spectra at 9.14 GHz were recorded with a Varian E-3 spectrometer. Spectra at 34.2 GHz were obtained with a Varian Model V-4503 spectrometer equipped with a Model V-4561 microwave bridge. The solutions were contained in quartz capillary tubes. Temperature control was achieved by flowing precooled or preheated nitrogen using the Varian temperature control accessories. The temperature in the cavity was measured before and after each recording and was found to be constant to within $\pm 0.3°$. A modulation amplitude of 4 G at 100 kHz and microwave powers of 20–40 mW were used to record the derivative of the absorption mode. Depending on the line width, different sweep widths (scan ranges) were used. The accuracy of the line width measurements is estimated to range between ± 5 G for the narrowest lines and ± 15 G for the widest. No detailed line shape analysis was performed, but using the "moment" criterion[6] the lines were found to be Lorentzian to a good approximation. The peak-to-peak line width of the derivative of the absorption mode, ΔH, expressed in units of

(1) Career Investigator Fellow of the American Heart Association, Feb 1969–Jan 1971. To whom all correspondence should be addressed at The Weizmann Institute of Science, Rehovoth, Israel.

(2) N. Bloembergen and L. O. Morgan, *J. Chem. Phys.*, **34**, 892 (1961).

(3) A. Hudson and G. R. Luckhurst, *Chem. Rev.*, **69**, 191 (1969).

(4) A. Hudson and J. W. E. Lewis, *Trans. Faraday Soc.*, **66**, 1297 (1970).

(5) J. Reuben, *Biochemistry*, **10**, 2834 (1971).

(6) C. P. Poole, Jr., "Electron Spin Resonance," Interscience, New York, N. Y., 1967, Table 20-7, p 806.

gauss is related to the electron spin transverse relaxation time, T_{2e}, by

$$1/T_{2e} = (g\beta\pi 3^{1/2}/h)\Delta H \quad (1)$$

Crystallized bovine serum albumin, obtained from Pentex, Inc., was dissolved in 0.05 M tetramethylammonium cacodylate buffer at pH 6.3. Insoluble material was removed by centrifugation. The concentration was determined from the absorbance at 280 mμ using 0.66 as the absorbance of 1 mg/ml per cm and a molecular weight of 69,000.[7] Solutions of $GdCl_3$ were prepared from a 1 M stock solution made by reacting Gd_2O_3 (from Alfa Inorganics) with dilute hydrochloric acid. To maintain ionic strength all solutions were made 0.1 M in tetramethylammonium chloride.

Computations were done on the PDP-6 computer of the Medical School computer facility.[8] The facility kindly provided a subroutine for matrix diagonalization based on the Jacobi method.

Results

Epr measurements were performed on three solutions. Solution A was 80 mM $GdCl_3$ at pH 3. No concentration or pH dependence of the epr line width was observed in the ranges 2–80 mM $GdCl_3$ and 3–6.5 pH units. Solution B was 8 mM $GdCl_3$ in the cacodylate buffer at pH 6.3. Solution C was 0.94 mM $GdCl_3$ and 0.4 mM BSA in the cacodylate buffer at pH 6.3. A binding study by proton relaxation methods has shown that BSA has four independent and equivalent binding sites for Gd(III) with an apparent dissociation constant of 1.3×10^{-4} M at 300°K and pH 6.3.[5] Thus in solution C almost all the Gd(III) is bound to the protein.

The peak-to-peak line widths of the epr spectra are graphically presented in Figure 1 plotted against the inverse absolute temperature. The following general features are apparent. For the three systems investigated the line width at the lower frequency is larger than that at the higher frequency. At 9.14 GHz the line width decreases with increasing temperature, whereas at 34.2 GHz it increases or shows a maximum. The results obtained with $GdCl_3$ (solution A) are in good agreement with those reported by Marianelli for a 25 mM solution of $Gd(ClO_4)_3$.[9] It seems safe to assume that in both cases Gd(III) exists as the fully hydrated ion. However, in presence of cacodylate the epr line of Gd(III) is much broader. Formation of strong complexes between lanthanides and anions is well known[10] and has also been detected by nmr.[11,12] Also the proton relaxation rates due to Gd(III) in presence of cacodylate were found to be lower than those in its absence suggesting water substitution by the anion.[5] With a more than sixfold excess of cacodylate and at the relatively high pH of 6.3 it can be assumed that practically all the gadolinium is complexed and the

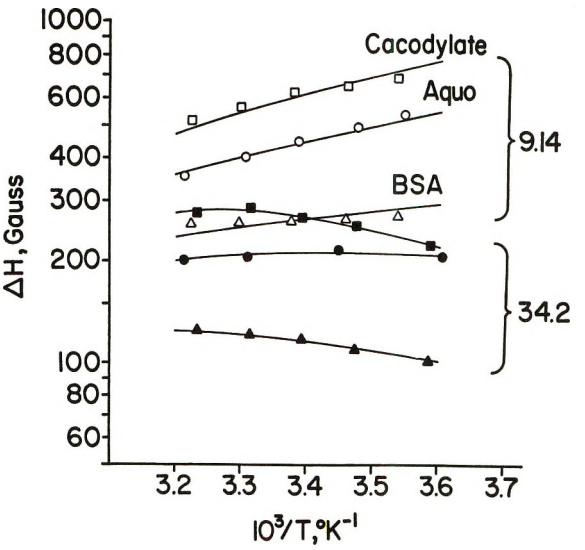

Figure 1. Peak-to-peak line widths of the epr spectra of Gd(III) as a function of inverse absolute temperature at two frequencies (in GHz): Aquo Gd(III), solution A—○, ●; Gd(III)–cacodylate, solution B—□, ■; Gd(III)–BSA, solution C—△, ▲. Curves are calculated (see text).

epr spectrum of solution B corresponds to the Gd(III)–cacodylate complex.

In order to quantitatively analyze the results, the relaxation matrix for spin $^7/_2$ systems given by Hudson and Lewis was used.[4] These authors assumed that the dominant line broadening mechanism for an ^8S ion is provided by the modulation of the zero-field splitting by a process with a characteristic time τ. The transverse relaxation rate is given by

$$1/T_{2e} = -Z\mathrm{M}(\omega,\tau) \quad (2)$$

where Z is the inner product of the zero-field splitting tensor (in rad^2 sec^{-2}) and $\mathrm{M}(\omega,\tau)$ is the relaxation matrix, ω being the electron Larmor frequency (*cf.* ref 4).

In general the epr line of Gd(III) is composed of four transitions of different intensities and line widths. A numerical solution of the relaxation matrix shows, however, that only one of these lines is significant in the observed spectrum, the others having a total contribution of, *e.g.*, less than 6% at 9.14 GHz and $\tau \leq 10^{-11}$ sec.

The relaxation matrix was diagonalized numerically for the two frequencies and for different values of τ.

(7) E. J. Cohn, W. L. Hughes, Jr., and J. H. Weare, *J. Amer. Chem. Soc.*, **69**, 1753 (1947).

(8) The computer facility of the University of Pennsylvania Medical School operates under United States Public Health Service Grant RR-15.

(9) R. Marianelli, Ph.D. Thesis, University of California, Lawrence Radiation Laboratory Report UCRL-17069, 1966.

(10) T. Moeller, D. F. Martin, L. C. Thompson, R. Ferris, G. R. Feistel, and W. J. Randall, *Chem. Rev.*, **65**, 1 (1965).

(11) J. Reuben and D. Fiat, *Chem. Commun.*, 729 (1967).

(12) E. Bock, *Can. J. Chem.*, **46**, 2418 (1968).

Table I: Constants Describing the Electron Spin Relaxation of Some Gadolinium(III) and Manganese(II) Complexes

Complex	Z, (rad/sec)^2	τ(300°K), sec	τ°, sec	E, kcal/mol
Aquo Gd(III)	$(1.1 \pm 0.1) \times 10^{20}$	5.04×10^{-12}	$(6.4 \pm 0.1) \times 10^{-14}$	2.62 ± 0.02
Gd(III)–cacodylate	$(1.35 \pm 0.01) \times 10^{20}$	6.7×10^{-12}	$(1.53 \pm 0.2) \times 10^{-14}$	3.65 ± 0.15
Gd(III)–BSA	$(0.615 \pm 0.015) \times 10^{20}$	7.65×10^{-12}	$(4.5 \pm 0.5) \times 10^{-13}$	1.7 ± 0.2
Aquo Mn(II)[a]	5.0×10^{18} [b]	2.1×10^{-12}	3.6×10^{-15}	3.9
Mn(II)–pyruvate kinase[a]	7.3×10^{18} [b]	6×10^{-12}	5.16×10^{-13}	1.5

[a] From ref 13. [b] Due to different definition the values of Z are smaller by a factor of 2 than those given in ref 13.

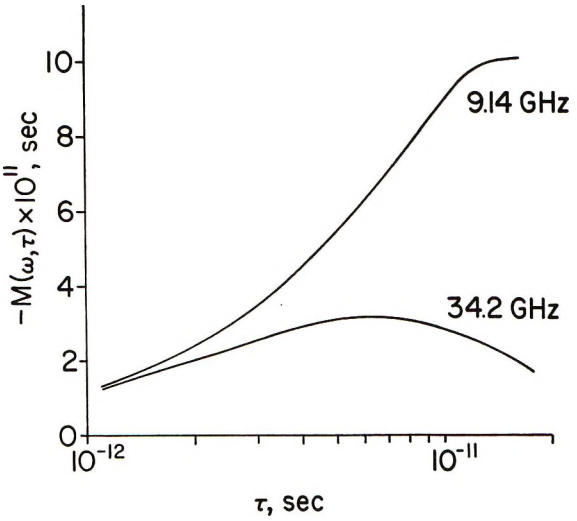

Figure 2. The calculated line width parameter $-1/ZT_{2e}$ (see text) of Gd(III) as a function of the correlation time.

The values of $-1/ZT_{2e}$ thus obtained for the most intense and narrowest transition are plotted in Figure 2 as a function of τ at two frequencies. Note the maximum occurring at $\tau \approx 1/\omega$.

The ratio, R, of the relaxation rates at two frequencies and the same temperature is independent of Z and is given by $R = M(\omega_1,\tau)/M(\omega_2,\tau)$. This function for $\omega_1/2\pi = 9.14$ GHz and $\omega_2/2\pi = 34.2$ GHz was plotted against τ and from the plot values of τ were read directly for each experimental value of R. Then a value of $-1/ZT_{2e}$ was obtained from Figure 2 and used with the experimental line width and eq 1 to calculate Z. The correlation times obtained by the above procedures could be approximately described by a simple exponential function of the form

$$\tau = \tau^\circ \exp(E/RT) \qquad (3)$$

A direct curve fitting of the experimental results was attempted. The results are shown by the curves in Figure 1. The accuracy of the curve fitting procedure was judged by the root-mean-square deviation, which in all cases was 4% or less. The range of the best fit constants was sufficiently narrow to validate making a comparison among the three complexes. The calculated values of Z, τ, τ°, and E are summarized in Table I. For comparison also included in Table I are results obtained by nmr for aquo Mn(II) and the Mn(II)–pyruvate kinase complex.[13]

Discussion

The results of the temperature and frequency dependence of electron spin relaxation rates of gadolinium(III) complexes in solution can be accommodated within the framework of the theory given by Hudson and Lewis.[4] Although measurements were done in a limited temperature range the predicted maximum in the line width as a function of temperature has experimentally been observed.

Some qualitative conclusions regarding the ligand-field symmetry of the complexes can be drawn from the values of Z related to the zero-field splitting. Replacement of water in the first coordination sphere by an anion, such as cacodylate, is expected to reduce the symmetry and indeed a higher value of Z is observed. Binding to BSA leads to a smaller zero-field splitting implying higher symmetry, *e.g.*, lower coordination number.

The identification of the correlation time for electron spin relaxation with a particular physical process seems somewhat uncertain at this time. The correlation times (at 300°K) for the three Gd(III) complexes investigated in this work are of the same order of magnitude. A similar situation is found for aquo Mn(II) and an enzyme–Mn(II) complex (*cf.* Table I).[13] A tumbling time of the order of 10^{-8} sec is estimated for BSA from Stokes law. The rotational correlation time modulating the dipolar interaction between a water proton and the unpaired electronic spin of Gd(III) for both the aquo and cacodylate complexes is 7×10^{-11} sec,[5] about an order of magnitude longer than the values of τ listed in Table I. Thus *rotational diffusion* is not the common and dominant electron relaxation mechanism for the complexes of Gd(III). Consequently the zero-field splitting effecting electron spin relaxation of Gd(III) is to a large extent transient rather than static. A transient zero-field splitting arises from symmetry fluctuations of the complex. Bloembergen and Morgan have considered the process of symmetry distortions of the complex by the impact of

(13) J. Reuben and M. Cohn, *J. Biol. Chem.*, **245**, 6539 (1970).

solvent molecules.[2] This process is likely to be effective for small complexes in solution. For ions bound to a macromolecule, however, the effectiveness of such a process is expected to be reduced since, depending upon the location of the binding site, the approach of solvent molecules will be restricted to a given geometry, *i.e.*, a relatively small solid angle of approach will be available for solvent impact. Marianelli has considered the *inversion of the complex* as a mechanism additional to rotation.[9] While this mechanism may be operative for the aquo complex it is unclear to what extent such a process may take place in "mixed" complexes and in particular in tight complexes with macromolecules. On the basis of the much higher values of τ° and the lower activation energy found for Mn(II) bound to pyruvate kinase relative to aquo Mn(II) it has been suggested that symmetry distortions of the metal–protein complex, or crystal field modulation, are brought about by *ion–ligand interactions* coupled to the slower vibrations and other motions of the whole polypeptide chain.[13] The similarity of the results obtained for Mn(II) and for Gd(III) suggests that a similar mechanism may be effective in both cases. The difficulties experienced in fitting the experimental epr data may arise from the assumption of a single correlation time obeying eq 3. The above considerations indicate, however, that two or more processes, independent or coupled, are probably effective in causing electron spin relaxation of gadolinium(III).

It should be pointed out that the current theories of electron spin relaxation are based on a specific model of a complex of a given (high) symmetry and modulation of a second-rank interaction by rotational diffusion or solvent fluctuations. The applicability of these theories to the more common complexes of low symmetry or to macromolecular complexes is still uncertain. The agreement obtained here between theory and experiment may be only apparent. It does show, however, that a more general theory should result in an expression of similar functional form to that given by Hudson and Lewis,[4] but the values of the physical parameters obtained from it may be different.

Acknowledgments. This work was carried out in the laboratory of Dr. Mildred Cohn to whom I am very much indebted for her kind hospitality and support. Thanks are also due to Dr. Takashi Yonetani, who generously made available to me his Varian V-4503 spectrometer, and to Drs. John S. Leigh, Jr. and George H. Reed for helpful discussions. This work was supported in part by United States Public Health Service Grant GM-12446.

The Nature of Deficiency in Nonstoichiometric Hydroxyapatites. I.

Catalytic Activity of Calcium and Strontium Hydroxyapatites

by S. J. Joris and C. H. Amberg*

Department of Chemistry, Carleton University, Ottawa 1, Ontario, Canada *(Received March 24, 1971)*

Publication costs assisted by the National Research Council of Canada

The catalytic activities in the dehydration of 1-butanol have been compared between two series of nonstoichiometric calcium and strontium hydroxyapatites. It is contended that incompletely coordinated cations in the lattice form stronger acid sites than the HPO_4^{2-} groups and through interaction with water molecules, further discussed in paper II, provide the necessary catalytic center for reaction. This is in contrast to previously held opinion which has assigned the role of catalytic site to HPO_4^{2-} ions.

Introduction

Causes of nonstiochiometry in hydroxyapatites are the subject of controversy in the literature. Two recent reviews[1,2] describe the different models that have been proposed to explain how calcium hydroxyapatites (CaA) depart from a calcium-to-phosphorus ratio of 1.667, typical of a stoichiometric hydroxyapatite

$$M_{10}(PO_4)_6(OH)_2 \qquad (I)$$

M = Ca, Sr, Ba, Cd, Pb

(1) W. E. Brown, "International Symposium on Structural Properties of Hydroxyapatites and Related Compounds," Gaithersburg, Md., 1968, W. A. Benjamin, New York, N. Y., in press.

(2) J. C. Elliott, *Calcif. Tissue Res.*, 3, 293 (1969).

It is uncertain whether deficiency in CaA is the result of calcium deficiencies distributed in the hydroxyapatite lattice[3-5] or whether a low Ca/P ratio is the result of formation of a mixture[6,7] of stoichiometric CaA and a phosphate having low calcium content, as for example octacalcium phosphate

$$n\mathrm{Ca_{10}(PO_4)_6(OH)_2}\cdot n'\mathrm{Ca_8(HPO_4)_2(PO_4)_4}\cdot 5\mathrm{H_2O} \quad \text{(II)}$$

The crystallographic structures of octacalcium phosphate and of CaA are similar, thus making it difficult to detect the presence of these two phases by X-ray diffraction. This is especially so for deficient apatites,[7,8] which are generally poorly crystallized. Since it is known[4] that the ir spectra of deficient CaA do not contain typical bands of octacalcium phosphate, and that the lattice constants of deficient CaA vary as a function of deficiency,[2,9] it seems reasonable to consider the deficiency in apatites as being primarily due to cationic defects distributed in the apatite lattice.

According to this model, the charge balance in the lattice would be maintained either by incorporation of a proton and loss of one hydroxyl group per missing cation (model III), or by incorporation of two protons (model IV), one of these being necessary to neutralize a hydroxyl group

$$\mathrm{Ca_{10-x}(HPO_4)_x(PO_4)_{6-x}(OH)_{2-x}} \qquad x < 1 \quad \text{(III)}$$

$$\mathrm{Ca_{10-x}(HPO_4)_x(PO_4)_{6-x}(OH)_{2-x}(H_2O)_x} \qquad x < 1 \quad \text{(IV)}$$

The purpose of this study is to compare new experimental data on deficient hydroxyapatites with models III and IV. Results on the acidity of the surface of hydroxyapatites are discussed first. In a second part of this study,[10] data on the infrared spectra of the materials will be presented.

The acid character of deficient hydroxyapatites was established[5,11] by the increase of (1) catalytic activity and (2) carbonium formation on the surface of deficient CaA as the Ca/P ratio of the materials was decreased. It was proposed[5,11] that the acid properties of the surface of deficient apatites originate from the presence of HPO_4^{2-} groups in the lattice (models III and IV). In this paper, the possibility of having acid sites other than HPO_4^{2-} groups is suggested. A discussion is given on the manner in which the strength of these acid sites is likely to vary when the cation, and therefore the lattice constants of the apatite, are changed. In order to substantiate the argument, the acid catalyzed dehydration of butanol was studied on deficient calcium and strontium apatites. Typical lattice constants are given in Table I along with data for stoichiometric materials. The existence of a complete study on the acid-catalyzed dehydration of butanol-2 on deficient CaA[11] dictated the choice of at least a similar reaction as a standard. For reasons mentioned below, we preferred the somewhat more stable butanol-1.

Table I: Lattice Constants of Stoichiometric and Deficient Calcium and Strontium Hydroxyapatites

	M/P	a_0, Å	c_0, Å	Surface of unit cell, Å²
CaA[a]	1.667	9.422	6.883	436.95
CaA	1.533	9.438	6.887	
SrA[b]	1.667	9.761	7.277	474.68
SrA	1.505	9.791	7.271	

[a] R. A. Young and J. C. Elliott, *Arch. Oral. Biol.*, **11**, 699 (1966). [b] C. Lagersen and D. Carlström, *Acta Chem. Scand.*, **11**, 545 (1957).

Experimental Section

Materials. AR grade reagents and freshly boiled deionized water were used for the synthesis of the catalysts. The CaA and SrA series were prepared by dropping 100 cc of a 1.2 *M* $(NH_4)_2HPO_4$ solution and 100 cc of a $Ca(NO_3)_2$ or $Sr(NO_3)_2$ solution into 200 cc of a 2 *M* NH_4NO_3 solution at equal rates over approximately 1 min.[4,12] The initial concentration of the solution containing the cation was varied between 1.8 and 2 mol/l. in order to obtain different degrees of deficiency in the hydroxyapatites. The reagents were mixed at 28 ± 1° in a closed system under nitrogen. The precipitates were stirred for 17 hr. The pH was kept above 8.5 throughout the reaction by use of concentrated NH_4OH. The precipitates were resuspended five times in 500 cc of CO_2-free water and centrifuged after each washing. They were subsequently dried for 24 hr (at 105° for the CaA series and 120° for the SrA series) and finally ground by mortar and pestle. About 18 g of product was recovered per synthesis.

Analysis. No phases other than hydroxyapatite were detected in the X-ray and ir spectra of the materials. The X-ray spectra indicated that the apatites were poorly crystallized; the diffraction lines were more intense for SrA than for CaA due to the larger atomic number of strontium. One calcium hydroxyapatite was put in a hydrothermal bomb for 1 week at 300° and 2000 bars. The crystallinity of the apatite was greatly

(3) L. Winand and G. Duyckaerts, *Bull. Soc. Chim. Belg.*, **71**, 142 (1962).

(4) E. E. Berry, *J. Inorg. Nucl. Chem.*, **29**, 317 (1967); **29**, 1585 (1967).

(5) J. A. S. Bett, L. G. Christner, and W. K. Hall, *J. Amer. Chem. Soc.*, **89**, 5535 (1967).

(6) D. McConnel, *Arch. Oral Biol.*, **10**, 421 (1965).

(7) W. E. Brown, J. P. Smith, J. R. Lehr, and A. W. Frazier, *Nature*, **196**, 1950 (1962).

(8) W. E. Brown, *ibid.*, **196**, 1048 (1962).

(9) O. R. Trautz, *Ann. N. Y. Acad. Sci.*, **60**, 696 (1955).

(10) S. J. Joris and C. H. Amberg, **75**, 3172 (1971).

(11) J. A. S. Bett and W. K. Hall, *J. Catal.*, **10**, 105 (1968).

(12) A. S. Posner and A. Perloff, *J. Res. Nat. Bur. Stand.*, **58**, 279 (1957).

improved by this treatment.[12,13] The X-ray pattern after hydrothermal growth did not show peaks of impurity phases that might have been hidden in the spectrum of the poorly crystallized starting material.

The precipitates were analyzed for Ca and Sr by EDTA titration and for PO_4^{3-} by a differential spectrophotometric method.[14] The average values (±1%) of triplicate determinations of Ca/P and Sr/P are given in Table II along with BET surface areas obtained from nitrogen adsorption. The surface areas were calculated from the initial weight of catalyst put in the adsorption apparatus and not on the basis of "dry" weights. The Ca/P ratio in the precipitates was always smaller than the initial ratio in solution; this was even more noticeable in the case of SrA. Similar observations have been reported in the literature.[15] Samples showing ir absorption bands typical of carbonate contamination[16] in hydroxyapatites were discarded. SrA was more easily contaminated by atmospheric CO_2 than CaA.

Table II: Analysis of Deficient Hydroxyapatites

	M/P	BET surface area, $m^2\ g^{-1}$
	CaA	
1	1.607	90.51
2	1.595	87.40
3	1.575	90.74
4	1.562	91.50
5	1.548	79.93
6	1.533	96.58
	SrA	
1	1.572	59.53
2	1.561	58.12
3	1.537	60.82
4	1.512	76.06
5	1.505	60.53
6	1.447	44.42

The lattice constants of CaA 6 and SrA 5 were determined within 0.008 Å using KCl as a standard (a_0 = 6.2931 Å at 25°) and the 002 and 300 reflections of hydroxyapatite. Values of a_0 and c_0 are presented in Table I. A comparison of the lattice constants obtained for the deficient materials with the values shown for stoichiometric apatites confirms the fact that deficient apatites show a tendency to have an increased value for a_0, while the c_0 value varies by only a small amount.[9]

Methods. The catalytic measurements were done in a steady-state flow reactor[17] operated at 350 ± 2° and 770 to 800 Torr. Constant aliquots of catalyst (200 mg) were used in order to minimize differences in heat and mass transfer in the catalyst bed. Each catalyst was activated in the reactor for 17 hr at 350° in a flow of 50 cc of helium per minute. Because of its greater thermal stability, butanol-1 was preferred to butanol-2

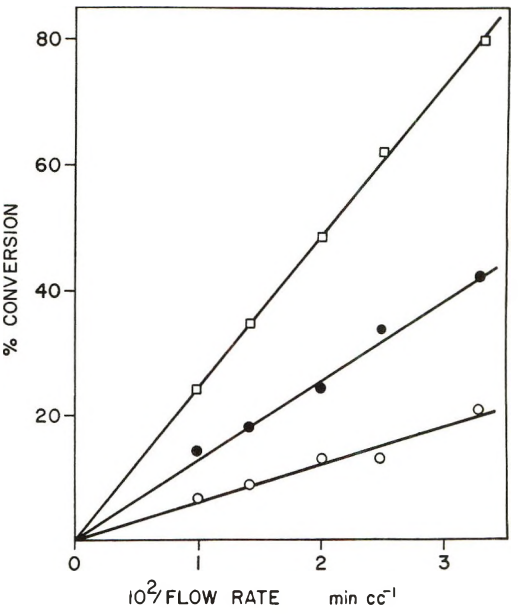

Figure 1. Influence of reciprocal flow rate on the dehydration of butanol-1 over hydroxyapatites at 350°: ○, CaA 1; ●, CaA 3; □, CaA 6 (cc at 25° and atmospheric pressure).

as a reactant. A constant partial pressure of alcohol in the carrier gas (He) was obtained by use of a gas saturator kept at 26.5 ± 1°. Resolution of unreacted butanol peaks from those of the reaction products (butene isomers, and traces of dibutyl ether and octene) was obtained by admitting 5 cc of converted gas to a Carbowax 1500–Chromosorb W analytical gc column. A Gow-Mac TRII-B detector was used for determining the percentage conversion calculated from triplicate recording of the alcohol peak in the feed and in the converted gas. The conversion percentages were corrected for differences in butanol partial pressure between the reactor and the bypass (5–10%), which resulted from differences in pressure drop between these two parts of the apparatus. This would also include a correction for thermal decomposition, negligible in the present case. Such a correction would have amounted to 25–30% in the case of butanol-2 under the conditions used. About 20 to 40 min was required to reach a constant conversion of butanol-1 over the catalyst surface. As shown in Figure 1, plots of percentage conversion (at the steady state) *vs.* the reciprocal flow rate gave straight lines from which reaction rates were calculated.

Results and Discussion

Figure 2 shows that the rate of dehydration of butanol-1 increases as the M/P ratio of the apatite is

(13) L. Winand, *Ann. Chim.* (*Paris*), **6**, 941 (1961).

(14) A. Gee and V. R. Deitz, *Anal. Chem.*, 25, 1320 (1953).

(15) E. D. Eanes, D. H. Gillessen, and A. S. Posner, *Nature*, **209**, 365 (1965).

(16) G. Montel, *Bull. Soc. Chim. Fr.*, 1694 (1968).

(17) S. Kolboe and C. H. Amberg, *Can. J. Chem.*, **44**, 2623 (1966).

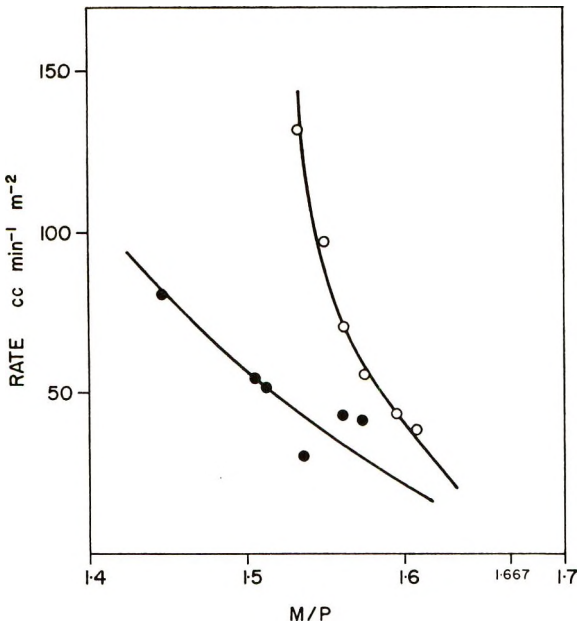

Figure 2. Rate of dehydration of butanol-1 over (O) calcium and (●) strontium hydroxyapatites at 350°.

decreased. This is consistent with the results reported on the dehydration of butanol-2 on deficient CaA.[5,11] The greater stability of primary alcohols caused the rate of dehydration of butanol-1 on CaA to be about half that of butanol-2 under present conditions.

Deficient specimens of SrA appear to be less active than the analogous calcium derivatives. As is customary, differences in surface area between the apatites are cancelled out by calculating the rate of conversion per square meter of surface rather than per gram of catalyst. However, the surface of the SrA unit cell is bigger than the surface of the CaA cell by a factor of 1.0863 (Table I). In order, therefore, to compare the catalytic activity of calcium and strontium apatites on the basis of constant number of unit cells per square meter, the rates of conversion (expressed per unit surface area) of the SrA series were multiplied by 1.086. Such a comparison is only justifiable if the average surface structure of the crystals exhibits the same features, differing only in cation size and crystal lattice dimensions. In support of this, it is interesting to note that the mean value for surface area is 89.4 m^2/g ($\pm 4.5\%$) for all samples of the CaA series as compared with 60 m^2/g ($\pm 10\%$) for the SrA series. The ratio of these values (1.49) is very close to the ratio of molecular weights of SrA and CaA (1.472), indicating thus that the surface areas per mole of SrA and CaA are comparable.

One strontium apatite (SrA 5) was dried at different temperatures (*e.g.*, 75, 100, 120, 150°). The effect of drying temperature on the reaction rate (per m^2 of catalyst surface) is shown in Figure 3. The increase of reaction rate with drying temperature may be due in part to an increase of crystallinity of the catalyst: the width of

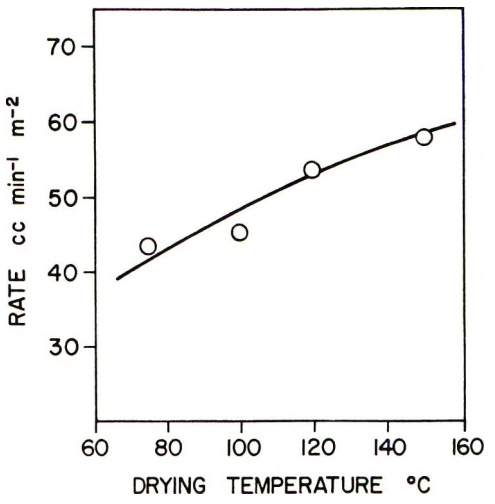

Figure 3. Influence of drying temperature of SrA 5 on the rate of dehydration of butanol-1.

the 211 reflection in the X-ray spectra decreases by 5% as the drying temperature is changed from 75 to 150°. The surface areas of these samples were found to be scattered between 60 and 70 m^2/g. It might be thought that the degree of crystallinity, and hence the reaction rate, should not be sensitive to initial drying temperature, as long as it is below the reaction temperature of 350° at which each catalyst is stabilized before reaction. However, it is known[15] that crystallinity is strongly influenced by the amount of water present in the sample, so that a "memory effect" of this type could be a reasonable explanation of the observed change. We have at present insufficient information to identify the precise reason for increased activity in poorly crystallized materials, although such effects are not unknown. However, it should be recognized that the above differences in the preparation of the catalysts alter the rate of conversion by factors that are considerably smaller than those observed when the cation or the M/P ratio of the catalysts are changed (Figure 2).

It has been proposed[5,11] that the acid properties of deficient CaA are related to the presence of a proton near the site of cation deficiency. This proton is likely to be hydrogen-bonded to oxygen atoms of the nearest phosphate tetrahedra, as the shortest distance between oxygen atoms near a calcium site is 2.48 Å.[18] The presence of HPO_4^{2-} groups in deficient CaA has been confirmed by spectroscopy[10,19] and by quantitative analysis.[4,5]

On the basis of the results presented in Figure 2 it appears to the present authors that sites other than HPO_4^{2-} groups can have acidic properties in the lattice of deficient apatites. It is implied in models III and IV that one hydroxyl group is missing per cation defect.

(18) M. I. Kay, R. A. Young, and A. S. Posner, *Nature*, **204**, 1050 (1964).

(19) N. W. Cant, J. A. S. Bett, G. R. Wilson, and W. K. Hall, private communication, 1970.

It must be remembered that in a stoichiometric apatite the oxygen atom of a free hydroxyl group is coordinated to three cations. This is repeated along the c axis at planes found at $z = 0.25$ and $z = 0.75$. Kay and Young[18] have shown that in stoichiometric CaA the oxygen atom of a free hydroxyl group is located 0.3 Å above the plane of the triangle formed by the calcium atoms to which it is coordinated. If, in order to maintain an overall charge balance in the lattice, one hydroxyl group is missing per cation defect (models III and IV), it is likely that there will be a negative charge deficiency in the vicinity of the cations remaining in the above triangle. (More than one cation is unlikely to be missing from the triangle, because only one OH group is avaliable). Such negative charge deficiencies could confer a Lewis-type of acidity to the deficient apatite. When a water molecule occupies the position of a missing hydroxyl group (model IV) a delocalization of the free electrons of the water oxygen will probably occur in order to fill the orbitals of the cations remaining in the triangles. This polarization would confer a Brønsted acidity to the protons of the water molecule. The strength of the acid sites resulting from negative charge defects in the lattice should then decrease with an increase of basicity of the cation in the apatite.

On the other hand, the acidity of the HPO_4^{2-} groups in hydroxyapatites is likely to be related to the degree of hydrogen bonding between the proton and the oxygen atoms of the phosphate group to which it is attached. An increase in lattice constants of the apatite is likely to decrease the strength of this hydrogen bonding[20] and consequently make the HPO_4^{2-} proton more active in an acid-catalyzed reaction.

An increase in cation basicity and lattice constants of a deficient apatite has therefore opposite effects on the strength of the two types of acid sites that can be present in the lattice (HPO_4^{2-} groups or negative charge defects). Since SrA contains a more basic cation and has larger lattice constants than CaA, a comparison of the catalytic activity of these two apatites should enable one to detect which of the acid sites is the more active in the dehydration reaction. If it can be assumed that the surface properties of the apatites are related to the properties of the lattice, it must be concluded from the lower activity of the SrA series (Figure 2) that at 350° the acid properties of the surface of deficient hydroxyapatites are due more to negative charge defects than to the presence of HPO_4^{2-} groups. The rate of reaction seems indeed to be influenced more by an increase of basicity of the cation in the apatite than by the effect of increased lattice constants on the acidity of HPO_4^{2-} groups. A confirmation of this conclusion is seen in the fact that it is very much more difficult to deuterate the proton of HPO_4^{2-} groups in deficient CaA than it is to deuterate the proton of the free hydroxyl group[5,10,19]. The low reactivity of the HPO_4^{2-} proton in acid-catalyzed or deuterium-exchange reactions is probably related to a high degree of hydrogen bonding and possibly less favorable access than in the case of the proton of the free hydroxyl group (or of the water molecule that can replace it in a deficient apatite).

If our proposed mechanism can be regarded as having received sufficient confirmation by our results, then at the same time the requirement of OH deficiencies in cation deficient apatites has received indirect proof. The requirement is an inherent part of this mechanism.

Further implications of our results, especially with regard to the ir spectra of deficient apatites, are discussed in the second part of this study.[10]

Acknowledgments. The authors are grateful to the National Research Council of Canada for a generous operating grant and to the Canada Council, who granted S. J. Joris a postdoctoral fellowship. The authors are also indebted to Dr. G. Chao, Geology Department, Carleton University, in whose laboratory the X-ray spectra of the apatites were taken. They also wish to thank Mr. Scott Murray for technical assistance during part of this work.

(20) W. C. Hamilton and J. A. Ibers, "Hydrogen Bonding in Solids," W. A. Benjamin, New York, N. Y., 1968, p 100.

The Nature of Deficiency in Nonstoichiometric Hydroxyapatites. II. Spectroscopic Studies of Calcium and Strontium Hydroxyapatites

by S. J. Joris and C. H. Amberg*

Department of Chemistry, Carleton University, Ottawa, Ontario, Canada, K1S 5B6 *(Received March 24, 1971)*

Publication costs assisted by the National Research Council of Canada

The assignment of a band at 870 cm^{-1} for Ca-deficient hydroxyapatite (CaA), and at 850 cm^{-1} for Sr-deficient SrA, to the ν_5 symmetrical P–O(H) stretching vibration has been confirmed by high-pressure deuterium exchange. The observed increases in band intensity of these bands are in agreement with previous studies on CaA, which have shown increasing HPO_4^{2-} concentration with decreasing Ca/P ratios, and may thus be extended to other apatite lattices. The frequency of the masked librational band, ν_L(OH), in SrA and $Ca_{7.5}Sr_{2.5}A$ has been inferred from the ν_L(OD) bands after deuteration of the materials. Unexpectedly, the intensity of ν_L(OH) bands in CaA did not decrease with increasing deficiency, although partially fluoridated and carbonated lattices showed such a decrease. An attempt is made to explain the behavior of the ν_L(OH) mode on the basis of the presence of one H_2O molecule for each missing OH^- group; the implications of this for the vibrational modes of the H_2O molecule are discussed in the light of the observed spectra. The results are consistent with the mechanisms proposed in paper I, in which the lattice H_2O molecules can participate in a catalytic dehydration reaction. The presence of octacalcium phosphate in the nonstoichiometric apatites is discussed.

Introduction

In the first part of this study[1] experimental evidence was given to support the suggestion[2,3] that hydroxyl groups are missing in the lattice of cation-deficient hydroxyapatites. Surprisingly, we have found no direct proof in the literature of this fact, even though most workers appear to have accepted the concept. What had been proven before[2,3] was that nonstoichiometric hydroxyapatites contain HPO_4^{2-} groups which contribute to maintenance of the overall charge balance in the apatite lattice.

In this paper, new spectroscopic evidence for the presence of HPO_4^{2-} groups and OH^- defects in deficient calcium and strontium hydroxyapatites (CaA and SrA) is presented. Since a complete description of the infrared spectra of stoichiometric CaA[4-6] and SrA[5,7] can be found in the literature , only bands of interest for this study are shown in Table I. Unless otherwise stated, the values in Table I are taken from ref 4 for CaA and from ref 7 for SrA. Infrared spectra of nonstoichiometric hydroxyapatites are very similar to those of stoichiometric ones. In addition to the bands found in the spectrum of stoichiometric calcium hydroxyapatite, the spectrum of deficient CaA contains a weak band at 870 cm^{-1}, and weak shoulders at 1210 and 1130 cm^{-1}.[2,3,6,8] It is known that the intensity of the 870-cm^{-1} band increases as the Ca/P ratio of the apatites is decreased.[3,8] The latter evidence was based on the study of only a limited number of deficient materials. The 870-cm^{-1} band was assigned[2] to a stretching mode of P–O(H). This assignment appeared to be uncertain as the band failed to shift by deuteration.[3,6]

In the first part of this paper, we discuss the assignment of the bands observed at 870 and 850 cm^{-1} in deficient CaA and SrA, respectively. Results of the determination of the change of intensity of these bands with deficiency are presented. In the second part of the paper, changes in intensity of bands related to the motion of the lattice OH^- groups are discussed. Finally, the suggestion[9] that layers of octacalcium phosphate are responsible for a low metal-to-phosphorus ratio in hydroxyapatites is viewed in the light of experimental results obtained in this study.

Experimental Section

Materials. Synthesis, analysis, and lattice constants of the deficient CaA and SrA series used in this study were described in another paper.[1]

A stoichiometric calcium hydroxyapatite (CaA–TS) was prepared by heating a mixture of 3 mol of $Ca_3(PO_4)_2$ and 1 mol of CaO at 900° in a stream of H_2O vapor.[10]

(1) S. J. Joris and C. H. Amberg, *J. Phys. Chem.*, **75**, 3167 (1971).

(2) E. E. Berry, *J. Inorg. Nucl. Chem.*, **29**, 317 (1967).

(3) J. A. S. Bett, L. G. Christner, and W. K. Hall, *J. Amer. Chem. Soc.*, **89**, 5535 (1967).

(4) C. B. Baddiel and E. E. Berry, *Spectrochim. Acta*, **22**, 1407 (1966).

(5) W. E. Klee and G. Engel, *J. Inorg. Nucl. Chem.*, **32**, 1837 (1970).

(6) N. W. Cant, J. A. S. Bett, G. R. Wilson, and W. K. Hall, private communication, 1970.

(7) V. M. Bhatnagar, *Experientia*, **23**, 697 (1967).

(8) L. Winand and G. Duyckaerts, *Bull. Soc. Chim. Belg.*, **71**, 142 (1962).

(9) W. E. Brown, J. R. Lehr, J. P. Smith, and A. W. Frazier, *Nature*, **196**, 1050 (1962).

(10) R. Wallayes, *Ann. Chim. (Paris)*, **7**, 808 (1952).

Table I: Typical Bands in the Infrared Spectra of Stoichiometric CaA and SrA (ν in cm^{-1})

Assignment	CaA	SrA	$\Delta\nu$
ν_S(OH)	3572[a]	3590	+18
$\nu_3'' + \nu_1$	1998	1968	−30
ν_3'	1028	1015	−13
ν_1	962	947[b]	−15
ν_L(OH)	635	548	−87
ν_4'''	603	595	−8

[a] See ref 6. [b] See ref 5.

X-Ray spectra of this apatite were much better resolved than those of deficient apatites obtained by precipitation. The width of the 002 reflection at one half the maximum height was 0.175° 2θ for Ca–TS as compared with 0.325° 2θ for deficient CaA. These values were not corrected for instrumental aberrations. Sharpening of the bands in the ir spectrum of Ca–TS is shown in Table II.

Table II: Results after Band Resolution in the 500–700 Cm^{-1} Range for CaA

	Ca/P	ν_4''' $\Delta\nu_{1/2}$, cm^{-1}	ν_L(OH) $\Delta\nu_{1/2}$, cm^{-1}	ν_L(OH) Intensity at band max (normalized)
		CaA–TS		
	1.667	4.6	9.6	0.755
		CaA		
1	1.607	6.8	13.3	0.482
2	1.595	6.9	13.6	0.473
3	1.575	6.8	14.1	0.462
4	1.562	6.5	14.8	0.462
5	1.533	6.9	14.7	0.441

An apatite containing 75% calcium and 25% strontium ($Ca_{7.5}Sr_{2.5}A$) was prepared by the same procedure used for the synthesis of single-cation apatites.[1] The X-ray spectrum of $Ca_{7.5}Sr_{2.5}A$ did not show phases other than that of hydroxyapatite, and the peaks were found at values intermediate to those of CaA and SrA. This indicates that $Ca_{7.5}Sr_{2.5}A$ is a single phase[11] and not a mixture of CaA and SrA.

Partially fluoridated hydroxyapatites (FA) were prepared by stirring 3 g of deficient CaA in 200 cc of H_2O containing 5.04×10^{-5} to 2.52×10^{-3} mol of NaF[12] overnight at room temperature. After impregnation, the materials were resuspended four times in 400 cc of water and centrifuged. They were dried for 24 hr at 105° and finally ground. The percentage fluoride in the fluoridated hydroxyapatites was determined with an Orion ion-selective electrode. No peaks due to CaF_2 were found in the X-ray spectra of the materials.

One partially carbonated calcium hydroxyapatite (CO_3A) was prepared by adding 0.03 mol of $(NH_4)_2CO_3$ to the NH_4NO_3 solution used in the synthesis.[1] The ir spectrum of CO_3A showed the bands typical of substitution of OH^- and PO_4^{3-} groups by carbonate.[13]

Attempts to precipitate a calcium-deficient deuterioxyapatite from D_2O solutions of dehydrated Ca $(NO_3)_2$, $KHPO_4$, and ND_4OD failed; they resulted in the formation of mixtures of phosphates.

Methods. Deuteration of deficient hydroxyapatites was carried out at 150° and about 20 Torr of D_2O vapor on samples that had been dehydrated overnight at 250° and 10^{-5} Torr prior to exposure. In one experiment, 200 mg of D_2O and 150 mg of CaA (Ca/P = 1.533) were placed in a gold tube which was then welded at both ends. This tube was inserted for 2 days in a hydrothermal bomb maintained at 2000 bars and 250°. A higher operating temperature, *e.g.*, 500°, resulted in a loss of structure. The sample was vacuum dried after the high pressure treatment.

Infrared spectra were recorded at 25° on a Perkin-Elmer 225 grating spectrophotometer. The instrument was calibrated by comparison with a polystyrene film. Intensity measurements were obtained from KBr pellets of the materials. Spectra in KBr and in mulls of Nujol agreed within ± 1 cm^{-1}. Spectra of deuterated materials were measured in Nujol or Fluorolube mulls with CsI optics.

Results and Discussion

HPO_4^{2-} Groups. The presence of HPO_4^{2-} groups in deficient CaA (models III and IV of ref 1 shown below) was suggested by the presence in the ir spectra of a band at 870 cm^{-1}, the intensity of which increases with deficiency.[3,8] In addition, the formation of pyrophosphate by the reaction

$$2HPO_4^{2-} \longrightarrow P_2O_7^{4-} + H_2O$$

is in quantitative agreement[2] with models III and IV and causes a decrease of the 870-cm^{-1} band, along with the appearance of a band at 715 cm^{-1}, assignable to $P_2O_7^{4-}$.[6]

$$Ca_{10-x}(HPO_4)_x(PO_4)_{6-x}(OH)_{2-x} \qquad x < 1 \quad \text{(III)}$$

$$Ca_{10-x}(HPO_4)_x(PO_4)_{6-x}(OH)_{2-x}(H_2O)_x \qquad x < 1 \quad \text{(IV)}$$

By analogy with other phosphates containing HPO_4^{2-} groups[14,15] the 870-cm^{-1} band was assigned to the $\nu_5(a_1)$ symmetrical stretching vibration of P–O(H). However, this remained somewhat uncertain, since the band

(11) R. L. Collin, *J. Amer. Chem. Soc.*, **81**, 5275 (1959).

(12) T. S. B. Narasaraju, R. P. Singh, and V. L. N. Rao, *Indian J. Chem.*, **8**, 296 (1970).

(13) G. Montel, *Bull. Soc. Chim. Fr.*, 1693 (1968).

(14) E. E. Berry and C. B. Baddiel, *Spectrochim. Acta, Part A*, **23**, 1781 (1967).

(15) A. C. Chapman, D. A. Long, and D. T. L. Jones, *ibid.*, **21**, 633 (1965).

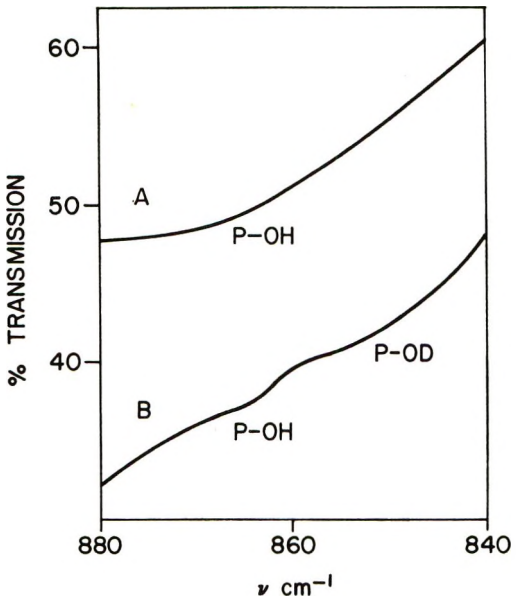

Figure 1. Deuterium exchange of HPO_4^{2-} groups in CaA: A, before exchange; B, after high-pressure exchange.

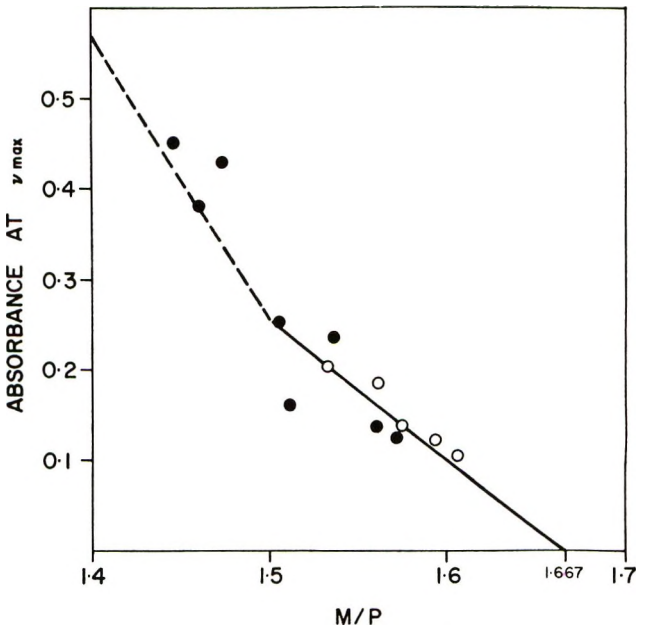

Figure 2. Influence of metal-to-phosphorus ratio on the intensity of the P–OH band in cation-deficient SrA (●) and CaA (○).

failed to shift to lower frequencies by deuteration.[3,6] From the reduced masses one can calculate the ratio of the frequencies of the P–O(D) and P–O(H) vibrations to be equal to 0.982. A shift of the ν_5 P–O(H) band by this factor was observed in octacalcium phosphate[14] and in other phosphates.[15]

Since it appeared that at 250° and 20 Torr of D_2O vapor the exchange reaction of P–O(H) to P–O(D) is too slow to be detected,[6] a deficient calcium apatite was exposed to D_2O vapor in a hydrothermal bomb kept at 2000 bars and 250°. The presence of the OD^- band (at 2634 cm^{-1}) in the spectrum of the deuterated sample indicated that the structure of the material remained stable during the hydrothermal treatment. A new band was present at 850 ± 2 cm^{-1} (Figure 1), which probably arises from the P–O(D) ν_5 mode, since the experimental ratio of P–O(D) and P–O(H) frequencies (0.977) is very close to the theoretical value (0.982). Confirmation of this assignment is also provided by comparison of the spectra of deficient calcium and strontium apatites. In the spectra of the latter, the band in question is shifted by about 20 cm^{-1} to lower frequencies. As all other bands related to P–O stretching vibrations are shifted by about the same value in the spectrum of SrA (Table I), the bands found at 870 cm^{-1} in CaA and at 850 cm^{-1} in SrA are therefore also likely to be related to the vibration of a P–O bond.

The intensity of the P–O(H) band was determined as a function of deficiency. Average values (±4%) of duplicate determinations of absorbance at maximum, normalized to the absorbance of the $\nu_3'' + \nu_1$ combination band, are shown in Figure 2 (pellets contain 8 mg of hydroxyapatite in 1 g of KBr). The results obtained for the CaA series were divided by 1.472 in order to correct for the difference of molecular weight between CaA (1005) and SrA (1480). It is confirmed by the results in Figure 2 that the intensity of the P–O(H) band increases with deficiency. It is also seen that extinction coefficients of P–O(H) in CaA and SrA are comparable. The spectroscopic results for $M/P < 1.5$ confirm the conclusion of a quantitative analysis[16,17] that, for values of $M/P < 1.5$, the amount of HPO_4^{2-} groups formed per calcium defect is twice as large (see model V or VI) as for values of $M/P > 1.5$ (see model III or IV). Indeed, it is seen in Figure 2 that the absorbance values for $M/P < 1.5$ lie close to a line (dashed) that has a slope twice as large as that of the line passing through the least-squares values of absorbance for $M/P > 1.5$. Models V and VI suggest[16] that, for reasons of stability, at least one hydroxyl group must remain in the unit cell of deficient hydroxyapatite.

$$Ca_{9-x}(HPO_4)_{1+2x}(PO_4)_{5-2x}(OH) \qquad x < 1 \quad \text{(V)}$$

$$Ca_{9-x}(HPO_4)_{1+2x}(PO_4)_{5-2x}(OH)\cdot(H_2O) \qquad x < 1 \quad \text{(VI)}$$

Hydroxyl Groups. We have proposed earlier that the catalytic activity of deficient CaA and SrA is due to hydroxyl deficiences in the lattice[1] (see models III and IV). Since the infrared spectrum of CaA contains two bands due to motions of lattice hydroxyl groups (Table I) a spectroscopic study of changes of hydroxyl concentration with deficiency was undertaken.

The 3800–3000-cm^{-1} range of the spectrum is characterized by broad absorption bands due to adsorbed water (Figure 3). Therefore, a quantitative study of the hydroxyl stretching band, ν_s(OH), can be done only

(16) E. E. Berry, *J. Inorg. Nucl. Chem.*, 29, 1585 (1967).
(17) E. E. Berry. *Bull. Soc. Chim. Fr.*, 1765 (1968).

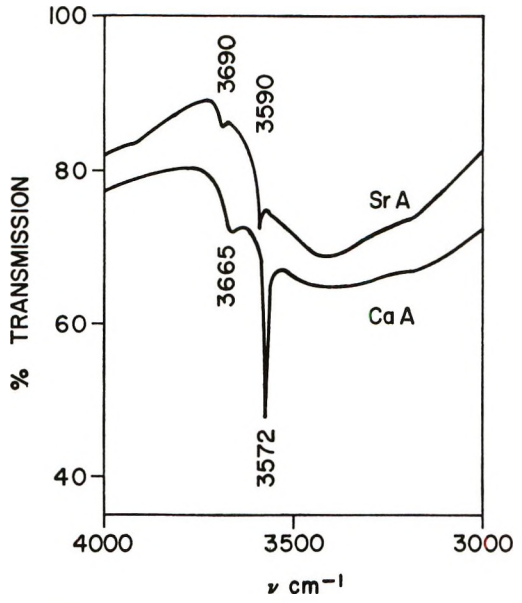

Figure 3. Hydroxyl stretching frequency region for cation-deficient CaA and SrA.

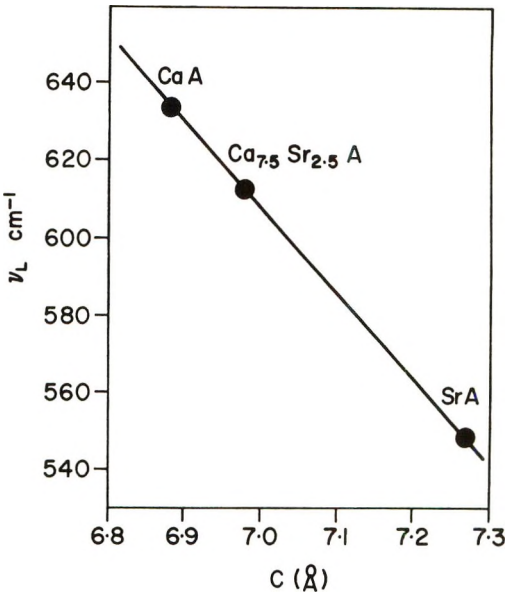

Figure 4. Influence of lattice constants on the librational band frequency.

with pressed wafers of apatite dehydrated under vacuum at 300°.[6] For reasons of experimental simplicity, the librational band of the hydroxyl groups, ν_L(OH), was selected for a quantitative study.

The librational frequency of OH^- groups in hydroxyl-containing compounds depends very much on the degree of hydrogen bonding of the OH^- proton with the surrounding anions.[14] This is illustrated in Figure 4 for hydroxyapatites. In SrA, which has larger lattice constants than CaA, the OH^- groups will librate more easily. Hydrogen bonding to oxygen atoms of surrounding phosphate tetrahedra[4] is decreased. As a result, the librational band in SrA is found at a frequency lower than that in CaA. The librational bands of SrA and $Ca_{7.5}Sr_{2.5}A$ are partially masked by the ν_4' band, found at 558 cm^{-1} in SrA. The exact frequency of the librational band of these compounds was calculated from the position of ν_L(OD) in deuterated samples, multiplied by 1.352, the value of ν_L(OH)/ν_L(OD) in CaA. Values of 612 and 548 cm^{-1} were found for ν_L(OH) in $Ca_{7.5}Sr_{2.5}A$ and SrA, respectively, (as compared with 635 cm^{-1} in CaA).

Figure 5 shows the ν_L(OH) band of CaA along with the incompletely split $\nu_4(f_2)$ P–O mode: ν_4', ν_4'', and ν_4''' at 564, 574, and 603 cm^{-1}, respectively. In order to determine the true intensity and band width of the librational band, a computer program was written to resolve the system of bands in the 500–700-cm^{-1} range in individual bands. It was assumed that the theoretical band envelope was made up of a sum of three Lorentz equations, each referring to one of the following bands: ν_L(OH), ν_4''', and ν_4'' together with ν_4' considered as a single band centered at 568 cm^{-1}. The parameters of the Lorentz equations were adjusted in a series of iterations, until the theoretical absorbance values were equal to the experimental values at the following frequencies: 564, 585, 603, 615, 635, and 645 cm^{-1}. An instance of typical agreement between experimental and calculated band envelopes is shown in Figure 5 (open circles are calculated values). Three pellets (1.5 mg of CaA in 200 mg of KBr) were prepared for each apatite studied. Average values of triplicate determinations of half-band widths (±4%) and band intensities (±3%) are presented in Table II. Intensity values were normalized to the integrated intensity (intensity times half-band width) of the 603-cm^{-1} band, which was thus used as an internal standard. In view of the errors inherent in this procedure, wing and slit width corrections were not applied.[18] At any rate, all these are minimized in considerations of intensity changes as opposed to absolute intensity values.

An increase in cation deficiency in the CaA series does not affect the band width of the phosphate ν_4''' band (Table II). However, an increase in deficiency (from Ca/P = 1.607 to Ca/P = 1.533) causes a 9% increase in the ν_L(OH) half-band width and a 10% decrease in its intensity at band maximum. The effect of Ca/P on the integrated intensity of ν_L(OH) is shown in Figure 6 and will be discussed later below. Because of its higher degree of crystallinity, Ca–TS has smaller band widths and larger intensity values than the apatites of the CaA series.

In order to test the sensitivity of the method to the detection of small changes in OH^- concentration, partially fluoridated and carbonated hydroxyapatites were synthetized. It is known that fluoride[19] and carbonate[13] ions replace OH^- groups in hydroxyapa-

(18) D. A. Ramsey, *J. Amer. Chem. Soc.*, 74, 72 (1952).
(19) R. A. Young and J. C. Elliott, *Arch. Oral Biol.*, 11, 699 (1966).

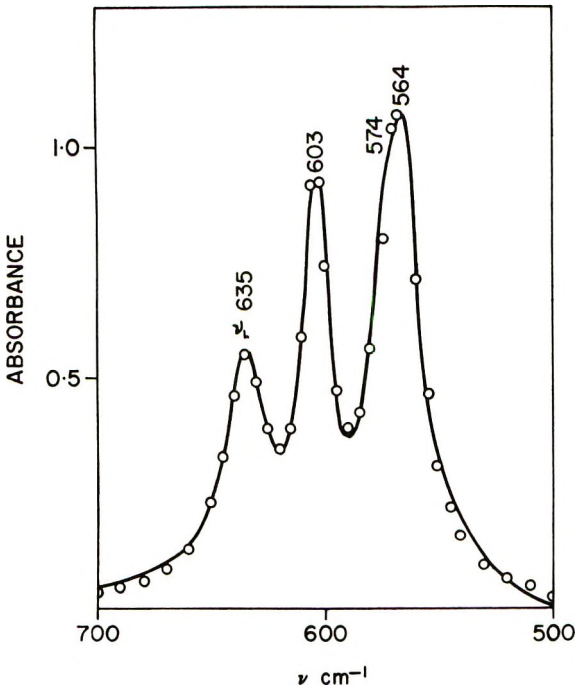

Figure 5. Band envelope in the librational frequency range for a typical cation-deficient CaA: O, calculated values.

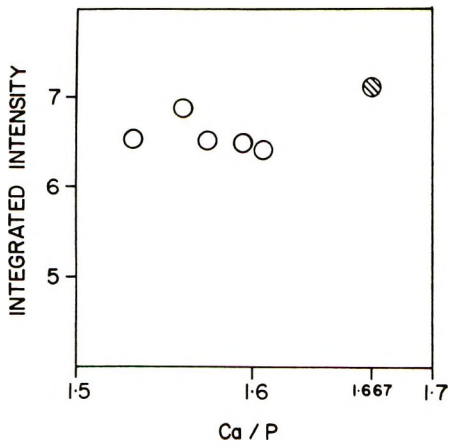

Figure 6. Influence of calcium-to-phosphorus ratio on the integrated intensity of the librational band: ⊘, stoichiometric CaA prepared by thermal synthesis; O, precipitated CaA.

tites. The results for these compounds after band resolution are shown in Table III. Partial incorporation of fluoride and carbonate increases the half-band width of the ν_4''' vibration. Similar observations are reported in the literature[20] for carbonate-containing apatites. The intensity of ν_L(OH) decreases significantly with increasing substitution by fluoride and carbonate. Changes by less than 10% of hydroxide concentration (*e.g.*, FA-1 and FA-2) can be detected by the band resolution method used. We recommend it as a useful way for monitoring changes in hydroxyl content in apatites.

On the basis of models III and IV, one would expect that for a Ca/P ratio equal to 1.5 (x = 1), the

Table III: Results after Band Resolution in the 500–700-Cm^{-1} Range for CaA with F^- or CO_3^{2-} Substitution

			ν_L(OH)		
	% FOH	ν_4''' $\Delta\nu_{1/2}$, cm^{-1}	$\Delta\nu_{1/2}$, cm^{-1}	Intensity at band max (normalized)	Integrated intensity (normalized)
			FA		
1	1.5	7.5	12.3	0.474	5.83
2	6.2	7.5	13.5	0.445	6.02
3	19.3	8.4	14.6	0.359	5.25
4	41.5	9.3	11.5	0.248	2.84
			CO_3A		
		8.7	15.8	0.303	4.77

amount of hydroxyl groups in CaA would be 50% less than in stoichiometric CaA (x = 0). It is seen however in Figure 6 that the integrated intensity of the ν_L(OH) band is almost independent of the Ca/P ratio of the apatite. This spectroscopic evidence is in apparent contradiction with (1) charge balance requirements[2,3] and (2) catalytic studies,[1] both suggesting that the lattice of deficient hydroxyapatites is deficient in hydroxyl ions.

The above contradiction may provide a partial answer to the question currently under debate[2,3,21] of the presence of a water molecule on the site of an anion deficiency (*e.g.*, models IV and VI). A possible configuration of a water molecule occupying the position of a hydroxyl group in CaA is depicted in Figure 7. The positions of the oxygen atoms in the unit cell in a direction parallel to the c axis are inscribed in the circles in ångström units. The oxygen atoms located at 2.96 Å are part of the adjoining phosphate tetrahedra. The oxygen atom at 2.02 Å belongs to the water molecule. This oxygen atom is assumed to be located 0.3 Å above a plane of calcium atoms, as is the case for the oxygen atom of an OH^- group in CaA.[19] Figure 7 shows that one proton of the water molecule can be much closer to a phosphate oxygen (2.14 Å) than the other proton (2.63 Å). The values in Figure 7 were obtained from a scale model, in which the HOH angle, bisected by the c axis, equals 109° as in the majority of inorganic hydrates.[22] Since 2.14 Å is a favorable distance for hydrogen bonding, it is likely that one proton of the water molecule will be hydrogen bonded to a phosphate oxygen at 2.14 Å, while the orher proton (at 2.63 Å from the nearest oxygen atoms) will be outside the range of hydrogen bonding. Bond lengths of 0.99 and 0.96 Å

(20) R. Z. Legeros, O. R. Trautz, J. P. Legeros, and E. Klein, *Bull. Soc. Chim. Fr.*, 1712 (1968).

(21) W. E. Brown in "International Symposium on Structural Properties of Hydroxyapatites and Related Compounds," Gaithersburg, Md., 1968, W. A. Benjamin, New York, N. Y., in press.

(22) W. C. Hamilton and J. A. Ibers in "Hydrogen Bonding in Solids," W. A. Benjamin, New York, N. Y., 1968, p 213.

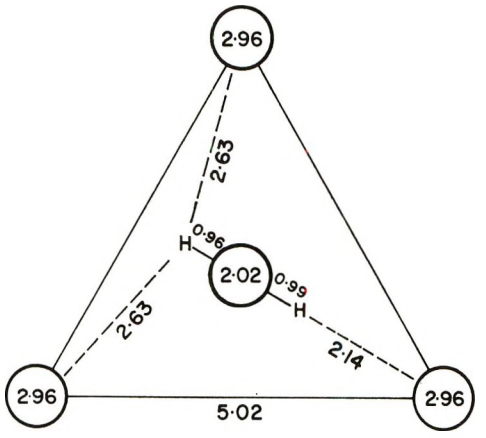

Figure 7. Interatomic distances in ångströms for a water molecule occupying the position of an OH^- group in cation-deficient CaA. The c axis is perpendicular to the plane of the paper. Circles are oxygen atoms, with location along the c axis inscribed.

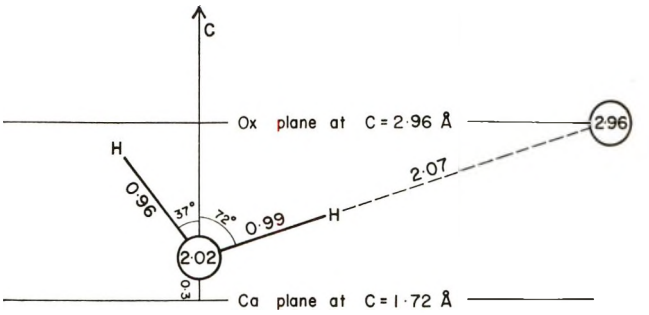

Figure 8. Interatomic distances in ångströms for a water molecule occupying the position of an OH^- group in cation-deficient CaA. The c axis is in the plane of the paper. Circles are oxygen atoms, with location along the c axis inscribed.

were chosen for the hydrogen-bonded and the nonhydrogen-bonded part of the water molecule, respectively. By comparison, when an OH^- group occupies the cage formed by the planes of calcium atoms at c = 1.72 Å, and the phosphate oxygens at c = 2.96 Å, the OH^- proton is located at 2.07 Å from the phosphate to which it is hydrogen bonded (assuming a straight hydrogen bond). The total O–H···O distance in that case equals 3.06 Å as confirmed by spectroscopic studies.[4]

The similarity of the proton-to-phosphate oxygen distance when either an OH^- group (2.07 Å) or a water molecule (2.14 Å) occupy the cage probably confers to the hydrogen-bonded part of the water molecule vibrational properties that are similar to those of the OH^- group. This would be even more pronounced if the water molecule were slightly tilted in order to accommodate a shorter hydrogen bond at one end. Such tilting is likely to occur since the other end of the water molecule is not hydrogen bonded. Consequently, the shortest proton-to-phosphate oxygen distance for a water molecule in the cage could easily equal 2.07 Å, the distance typical for the OH^- proton (Figure 8). As the frequency of the librational mode depends mainly on the degree of hydrogen bonding, as shown before, it is likely then that a water molecule in the cage will have a librational frequency very similar to, if not identical with, that of the OH^- group. Substitution of hydroxyl groups by water molecules in cation-deficient CaA may thus explain why neither the integrated intensity nor the position of the librational band change with deficiency.

For reasons described above, the stretching frequency of the hydrogen-bonded part of a water molecule in the cage could be expected to be similar to the stretching frequency of the OH^- group (*e.g.*, 3572 Å). On the other hand, the part not hydrogen bonded should have a higher stretching frequency. A band at about 3660 cm^{-1} has been reported in the spectrum of CaA.[6] On the basis of the shift by deuteration, this band was assigned to an OH^- stretching mode.[6] We postulate that the band observed at 3660 cm^{-1} in CaA and at 3590 cm^{-1} in SrA (Figure 3) is the stretching mode of the nonhydrogen-bonded part of the water molecules which are in place of the missing hydroxyl groups in cation-deficient hydroxyapatites. Confirmation of this assignment is provided by the fact that the intensity of the 3660-cm^{-1} band (relative to the 3572-cm^{-1} band intensity) is about 4.5 times larger in CaA-3 (Figure 8) than in a hydroxyapatite[6] close to stoichiometry (but having still weak P–OH absorption and catalytic activity[3]). However, a systematic investigation of changes of the 3660-cm^{-1} band intensity with deficiency has not yet been undertaken. Removal[6] of the 3660-cm^{-1} band by prolonged evacuation above 500° is another indication that our assignment may be correct. It is in accordance with the fact that the channels[13] in the hydroxyapatite structure are wide enough to enable removal of a neutral molecule. The presence of water in nonstoichiometric hydroxyapatites had been suggested before by hydrogen content measurements[3] and by the high weight losses observed by the TGA method.[17]

It should be noted that the presence of water molecules on the site of a missing OH^- ion is consistent with the conclusions of our catalytic studies.[1] On the basis of these it was proposed that incompletely coordinated cations, which seem to be the strongest source of acidity in deficient hydroxyapatites, polarize the water molecules in the cages. As a result of the delocalization of the free electrons of the oxygen by incompletely coordinated cations, the acid character of the latter would be transmitted to the protons of the water molecules.

Octacalcium Phosphate (OCP). It appears to the present authors that nonstoichiometry in the hydroxyapatites used in this study is due to ionic defects distributed in the lattice rather than to the presence of octacalcium phosphate[21] (model II of ref 1). The following arguments may be cited in support of the

above: (1) absence of OCP in the X-ray and ir spectra of the materials; (2) the proton of HPO_4^{2-} groups in OCP is easily replaceable by deuterium exchange[14] (*e.g.*, at 60° and moderate D_2O vapor pressure), while in our samples the deuterium exchange occurs only under hydrothermal conditions (Figure 1); (3) if nonstoichiometric hydroxyapatites were constituted of epitaxial intergrowths of OCP and stoichiometric apatite, there is no simple justification for the break observed at M/P = 1.5 in the relation between HPO_4^{2-} concentration and deficiency (Figure 2); (4) only the presence of water molecules replacing OH^- groups in the cages of nonstoichiometric apatites can cause the integrated intensity of the $\nu_L(OH)$ band to be independent of stoichiometry. Since pure OCP does not contain a librational band,[23] the intensity of $\nu_L(OH)$ should decrease if OCP were present in our nonstoichiometric samples.

It seems likely that, when the precipitation of hydroxyapatite is carried out by rapid mixing of the reagents, both cationic (M^{2+}) and anionic (OH^-) vacancies are present in the lattice. Experimental evidence has been given in this study that cationic and anionic vacancies are filled by interstitial protons and water molecules, respectively. This does not preclude the possibility that under different conditions of synthesis (*e.g.*, in biological systems) nonstoichiometry may result from the presence of OCP.[21]

Acknowledgments. The authors are grateful to the National Research Council of Canada for an operating grant, and to the Canada Council, who granted S. J. Joris a post-doctoral fellowship. Special thanks are due to Dr. G. Y. Chao and Dr. G. B. Skippen, Geology Department, Carleton University, in whose laboratories the X-ray spectra were determined and the high pressure deuterium-exchange experiments were performed, respectively. The authors are indebted to D. Luk and S. Murray for technical assistance.

(23) B. O. Fowler, E. C. Moreno, and W. E. Brown, *Arch. Oral Biol.*, **11**, 477 (1966).

The Gas-Phase Radiolysis of Nitrous Oxide. The Effect of the Addition of Several Hydrocarbons

by Satoshi Takao, Yoshihiko Hatano, and Shoji Shida*

Laboratory of Physical Chemistry, Tokyo Institute of Technology, Meguro-ku, Tokyo *(Received March 1, 1971)*

Publication costs borne completely by The Journal of Physical Chemistry

The effect of the addition of several paraffins and olefins on the gas-phase radiolysis of N_2O has been examined. The total G values of oxygen-containing products at 3% hydrocarbons added were around 6.8 irrespective of the nature of hydrocarbons, while $G(N_2)$ decreased by about 2.6. Consideration of possible reaction schemes both on ionic and nonionic processes leads to the conclusion that excited oxygen atoms play a major role in the nonionic processes in the gas-phase radiolysis of N_2O. On the basis of the ionic processes proposed previously and of the nonionic processes assumed here, the main features of the primary processes in the radiolysis of N_2O can be depicted as

$$N_2O \rightsquigarrow N_2O^+ + e^- \qquad G = 3.0$$
$$\searrow N_2 + O^* \text{ (excited states)} \qquad G \sim 4$$
$$\searrow N_2 + O \text{ (the ground state)} \qquad G < 0.5$$

Introduction

Nitrous oxide has been used as an electron scavenger to investigate the ionic processes in the radiolysis of hydrocarbons.[1] Since it produces nitrogen after its electron capture, many attempts[2-4] have been made to correlate the nitrogen yields and the G values of ionization, but they have failed. This is caused mainly by the fact that the mechanism of the decomposition of nitrous

(1) J. M. Warman, K.-D. Asmus, and R. H. Schuler, *Advan. Chem. Ser.*, **No. 82**, 25 (1968).

(2) S. Sato, R. Yugeta, K. Shinsaka, and T. Terao, *Bull. Chem. Soc. Jap.*, **39**, 156 (1966).

oxide in hydrocarbons as well as in itself is not yet known accurately. In connection with these problems, the accurate determination of water and other oxygen-containing products has been desired.[5-7] As to the mechanism of radiolytic decomposition of nitrous oxide itself, on the other hand, a few reports have recently been published,[8-10] which focused mainly on the ionic processes. In our previous papers,[8] an ionic mechanism in the gas-phase radiolysis of nitrous oxide was proposed, and the importance of processes other than the ionic processes was suggested. The purpose of the present study is to reveal the main features of the non-ionic processes in the radiolysis of nitrous oxide by examining the effect of the addition of hydrocarbons to nitrous oxide.

Experimental Section

Nitrous oxide was used directly from the cylinder supplied by Takachiho-Shoji Co. After several freeze–pump–thaw cycles to remove any noncondensable impurities, the obtained purity was $\gtrsim 99.995\%$. Research grade hydrocarbons also supplied by Takachiho-Shoji Co. were degassed in a vacuum system and were used without further purifications. A binary vapor mixture, about 90 cm total pressure, of N_2O and a hydrocarbon was irradiated at room temperature with ^{60}Co γ rays at a dose rate of 4.2×10^{19} eV/g hr and the highest dose used was 2.1×10^{20} eV/g. All irradiations were carried out in cylindrical vessels of about 50 cc and, prior to use, they were baked in air at 500° and then pumped at least for 0.5 hr down to 10^{-5} mm. The vessels were sealed while opened to the vacuum system. Great care was taken in the analysis of the oxygen-containing products, especially in H_2O. The noncondensable products, N_2 and CO, were collected by a Toepler pump with a gas buret and were analyzed gas chromatographically on a 5-m column of molecular sieve 5A at 60°. Quantitative analysis of water has been known to be very difficult. In this experiment, however, a good reproducibility has been attained. Water and alcohol products were analyzed gas chromatographically on a polyethylene glycol-200 column at 70° after removal of N_2O through a −120° cold trap. The products were identified by their retention times on the gas chromatographic columns by seeding with authentic samples.

Results

The results of the addition of various hydrocarbons to N_2O are shown in Figures 1–6 and summarized in Table I. The addition of small amounts of a paraffin to N_2O caused a decrease in the nitrogen yield and then made its plateau value. As shown in Figures 1–3, on the contrary, large yields of oxygen-containing products, H_2O and alcohols, were observed. In Figures 4–6 are given the effects of the addition of olefins, which have been thought to be very different from paraffins with respect to the reactivities with oxygen atoms.[11] The addition of olefins to N_2O, however, showed nearly the same effect except for observing the formation of CO instead of alcohols. These experimental results are summarized in Table I. In each case, the decrease of the nitrogen yield is about 2.6,[12] while the total yield of oxygen-containing products is around 6.8. In the case of n-C_4H_{10} the total yield of oxygen-containing products was found to be somewhat less than those in the other cases. This may be due to missing higher alcohols in the gas chromatographic analysis. In the presence of hydrocarbons, NO and O_2 were not detected and other oxygen-containing products, such as aldehydes, ketones, or epoxide, etc., were also not observed.

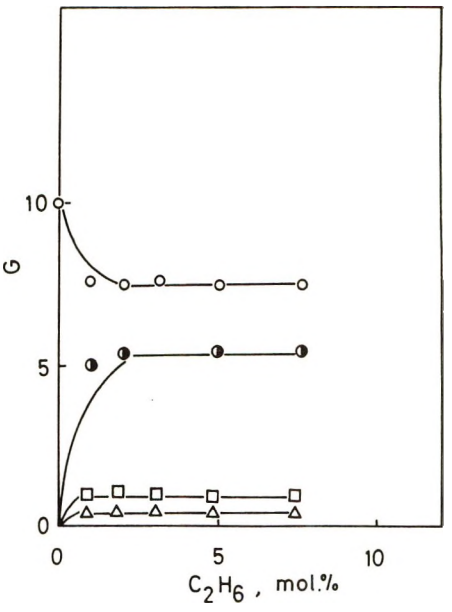

Figure 1. The effect of the addition of C_2H_6 to N_2O: ○, N_2; ◑, H_2O; □, i-C_4H_9OH; △, C_2H_5OH.

Discussion

To investigate the origin of the observed decrements of the nitrogen yields in the presence of hydrocarbons,

(3) J. M. Warman, *J. Phys. Chem.*, **71**, 4066 (1967).

(4) R. A. Holroyd, *ibid.*, **72**, 759 (1968).

(5) N. H. Sagert and A. S. Blair, *Can. J. Chem.*, **45**, 1351 (1967); K. Takeuchi, K. Shinsaka, S. Takao, Y. Hatano, and S. Shida, *Bull. Chem. Soc. Jap.*, **44**, 2004 (1971).

(6) R. O. Koch, J. P. W. Houtman, and W. A. Cramer, *J. Amer. Chem. Soc.*, **90**, 3326 (1968).

(7) A. Menger and T. Gäuman, *Helv. Chim. Acta*, **52**, 2477 (1969).

(8) S. Takao, S. Shida, Y. Hatano, and H. Yamazaki, *Bull. Chem. Soc. Jap.*, **41**, 2221 (1968); S. Takao and S. Shida, *ibid.*, **43**, 2766 (1970).

(9) J. T. Sears, *J. Phys. Chem.*, **73**, 1143 (1969).

(10) R. W. Hummel, *Chem. Commun.*, 995 (1969).

(11) (a) G. Paraskevopoulos and R. J. Cvetanović, *J. Chem. Phys.*, **50**, 590 (1969); (b) R. J. Cvetanović, "Advances in Photochemistry," Vol. 1, Interscience, New York, N. Y., 1963, p 115.

(12) According to our data reported previously,[8] the result of reaction 4, in the absence of other effects, would be to increase the yield of nitrogen by $G \sim 0.9$. The decrement observed of 2.6 corresponds, therefore, to an actual one by other reactions of ~ 3.5 G units.

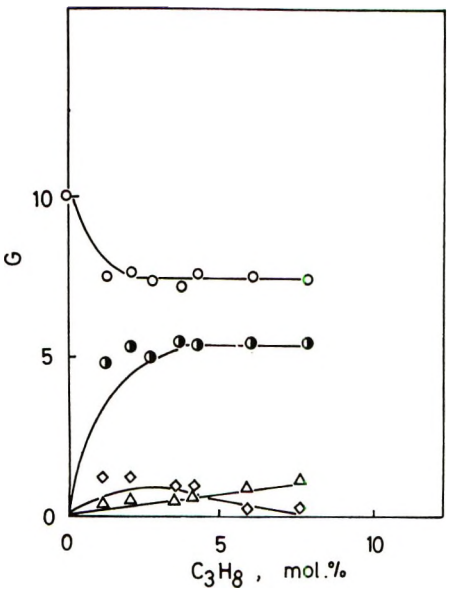

Figure 2. The effect of the addition of C_3H_8 to N_2O: ○, N_2; ◑, H_2O; ◇, n-C_3H_7OH; △, C_2H_5OH.

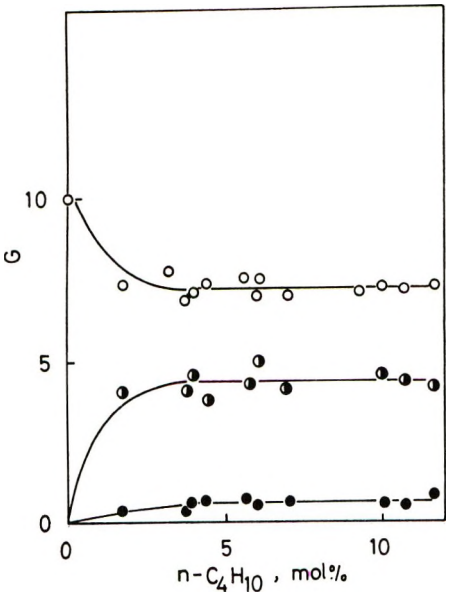

Figure 3. The effect of the addition of n-C_4H_{10} to N_2O: ○, N_2; ◑, H_2O; ●, n-C_3H_7OH.

the contribution from the ionic processes is considered, for which the following possible processes can be assumed. Electrons produced by the primary ionization of N_2O

$$N_2O \rightsquigarrow N_2O^+ + e^- \quad (1)$$

can be captured by N_2O itself prior to neutralization

$$N_2O + e^- \longrightarrow N_2O^- \quad (2)$$

Charge transfer can occur between N_2O^+ and hydrocarbon RH

$$N_2O^+ + RH \longrightarrow N_2O + RH^+ \quad (3)$$

Table I: The Effect of the Addition of Hydrocarbons to N_2O[a]

Additive[b]	$-\Delta G(N_2)$	$G(CO)$	$G(H_2O)$	G(alcohols)	G(total oxygen-containing products)
C_2H_6	2.5	0.0	5.3	1.5	6.8
C_3H_8	2.5	0.0	5.4	1.5	6.9
n-C_4H_{10}	2.7	0.0	4.8	0.7	5.5
C_2H_4	2.6	2.5	4.3	0.0	6.8
C_3H_6	2.7	0.4	6.0	0.0	6.4
cis-2-C_4H_8	2.5	0.0	7.2	0.0	7.2

[a] Total pressure, about 90 cm. [b] Concentration, 3.0%.

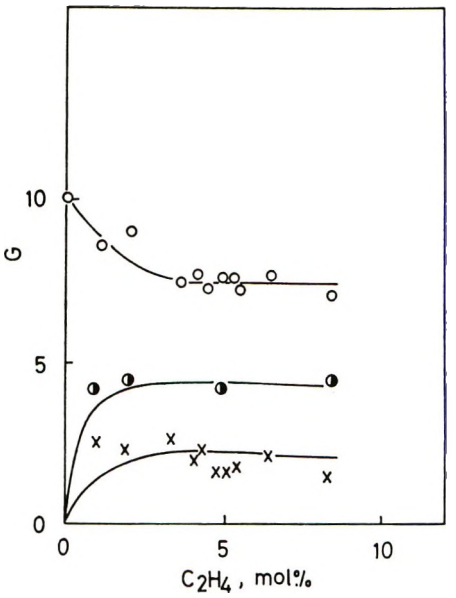

Figure 4. The effect of the addition of C_2H_4 to N_2O: ○, N_2; ◑, H_2O; ×, CO.

Neutralization of N_2O^- with RH^+ is followed by the hydrogen atom abstraction of OH

$$N_2O^- + RH^+ \longrightarrow N_2 + OH + R \quad (4)$$

$$OH + RH \longrightarrow H_2O + R \quad (5)$$

Another possibility for H_2O formation *via* ionic processes is considered

$$N_2O^- + RH \longrightarrow N_2 + OH^- + R \quad (6)$$

$$OH^- + RH^+ \longrightarrow H_2O + R \quad (7)$$

or

$$OH^- + N_2O^+ \longrightarrow OH + N_2O \quad (8)$$

Energetic considerations show all reactions except reaction 6 to be possible. The exothermicity of reaction 6 cannot be determined, because the electron affinity of N_2O is not yet known accurately.[13,14] Reac-

(13) W. J. Holtslander and G. R. Freeman, *Can. J. Chem.*, **45**, 1661 (1967).

(14) J. F. Paulson, *J. Chem. Phys.*, **52**, 959 (1970).

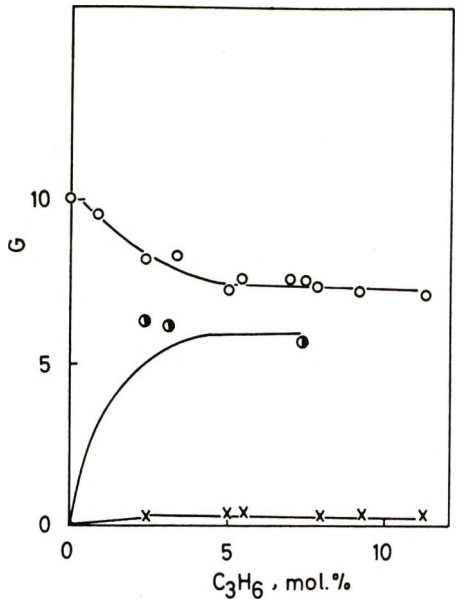

Figure 5. The effect of the addition of C_3H_6 to N_2O: ○, N_2; ◑, H_2O; ×, CO.

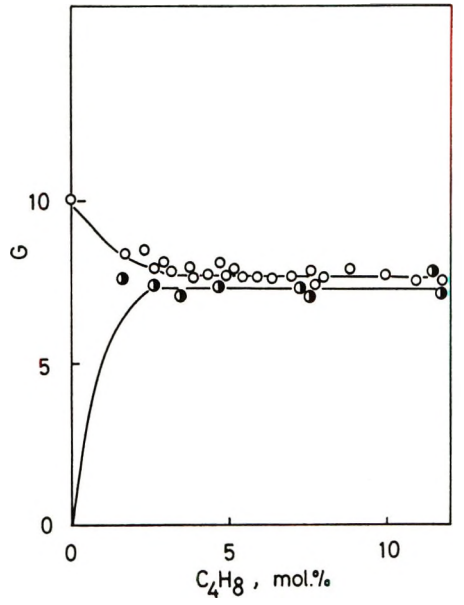

Figure 6. The effect of the addition of *cis*-2-C_4H_8 to N_2O: ○, N_2; ◑, H_2O.

tion 6 cannot occur if the electron affinity of N_2O exceeds 1.0 eV. It is likely that the electron affinity of N_2O is equal to or less than 1.0 eV.[15] At present, it seems possible that this process occurs.

According to the above scheme, however, as much nitrogen as water should be produced and the nitrogen yield should not be decreased by the addition of hydrocarbon, *i.e.*, the addition of hydrocarbon to N_2O should give rise to the formation of H_2O without decreasing the nitrogen yield. This is not the case. The observed decrease in the nitrogen yield, then, must be due to some other processes, most probably some nonionic processes. As given in Table I, the total yield of oxygen-containing products is much larger than the decrement of the nitrogen yield. Moreover, the remainder of the total yield of oxygen-containing products minus that contributed from the ionic processes assumed above is still larger than the observed decrement of the nitrogen yield. It seems that the nonionic dissociation of N_2O would be mainly as

$$N_2O \rightsquigarrow N_2 + O,\ O + N_2O \not\longrightarrow$$

with small contribution from

$$N_2O \rightsquigarrow N_2 + O^*,\ O^* + N_2O \longrightarrow N_2,\ O_2,\ \text{and NO}$$

since, according to this scheme, the addition of hydrocarbon to N_2O should result in the observation of the large yield of oxygen-containing products with small decrement of the nitrogen yield. In the above scheme, however, the small contribution of O* cannot explain the large yield of the nonionic formation of NO in the gas-phase radiolysis of pure N_2O.[8] This may arise from the reaction of O* with N_2O. It seems, then, reasonable to assume that excited oxygen atom O* plays an important role besides the ground state oxygen atom O. The former can decompose N_2O to produce N_2 but the latter cannot,[16] and both react with hydrocarbons to form oxygen-containing products.[11] In previous papers,[8] the effect of the addition of SF_6 on the gas-phase radiolysis of N_2O was examined. The following results were obtained: for the ionic processes $G(-N_2O) = 3.0 = G(e^-)$,[17] $G(N_2) = 2.1$, $G(O_2) = 0.8$, and $G(NO) = 1.8$; for the nonionic processes $G(-N_2O) = 9.6$, $G(N_2) = 8.0$, $G(O_2) = 3.0$, and $G(NO) = 3.3$. The large yield of the nonionic formation of NO certainly arises from the reaction of O* with N_2O. On the basis of the observed decrement of the nitrogen yield ($-\Delta G(N_2) = 2.6$) in the presence of hydrocarbon, combined with the above $G(NO)$ value, it may be concluded that O* plays a major role in the nonionic dissociation processes of N_2O.[18]

Then, the nonionic processes in the radiolysis of N_2O may be written as follows with the assigned G values[19-22]

(15) J. F. Paulson, *Advan. Chem. Ser.*, **No. 58**, 28 (1966).

(16) M. G. Robinson and G. R. Freeman, *J. Phys. Chem.*, **72**, 1394 (1968).

(17) G. G. Meisels, *J. Chem. Phys.*, **41**, 51 (1964).

(18) Besides the above processes, both ionic and nonionic, the possibility of the following process for N_2 formation might be considered

$$N_2O + R \longrightarrow N_2 + OR \qquad (a)$$

Since, however, N_2O has been thought to be inert with respect to reactions with free radicals,[11b] reaction a may be eliminated.

(19) The reactions of O* with N_2O to give $N_2 + O_2$ and 2NO were already reported by several authors. From a combination of the activation energy difference given by Kaufman, *et al.*,[20] and the absolute rates at 2000°K given by Barton, *et al.*,[21] an estimate of the ratio of the rate constants for the two reactions at room temperature can be obtained which is in good agreement with the ratio which has been assumed to explain the present radiolysis results. Besides, the ratio of the two reactions assumed here is not inconsistent with the conclusion of Yang and Servedio.[22]

$$N_2O \overset{\sim}{\rightarrow} N_2 + O^* \qquad \sim 4$$
$$\searrow N_2 + O \qquad < 0.5$$
$$O^* + N_2O \rightarrow N_2 + O_2 \qquad 2.6$$
$$\searrow 2NO \qquad 1.6$$

This scheme with those proposed for the ionic processes[8] can explain satisfactorily the observed product yields in the gas-phase radiolysis of pure N_2O; *e.g.*, the calculated value $G(N_2) = 9.4$ is in good agreement with the observed value $G(N_2) = 10.1$. From the considerations of photochemical studies of the reactivities of oxygen atoms,[11a,23] it may be inferred that O* and O are the excited state $O(^1D)$ and/or $O(^1S)$, and the gound state $O(^3P)$, respectively.

In this discussion, the contributions from the processes

$$N_2O^+ \longrightarrow NO^+ + N, \text{ etc.}$$

or

$$N_2O \overset{\sim}{\rightarrow} N + NO$$

and the role of N atoms were excluded. These processes, however, can be thought to be relatively small in contribution in the photochemical[23] and mass spectrometric[24] studies. Furthermore, Gordon and Ausloos[25] have already examined the effect of the addition of NO on the gas-phase radiolysis of $^{15}N^{14}NO$ and estimated the contribution of N atoms to be on the order of 1 in G unit. It is well known that HCN is formed in the reaction of N atoms with olefins.[26,27] If N atoms are produced so much as was estimated by Gordon and Ausloos in the radiolysis of N_2O, the addition of ethylene or other olefins to N_2O must result in the observation of HCN formation. The γ radiolysis of the system of N_2O with small amounts of ethylene has recently been studied, in which the formation of HCN and other N-containing products could not be observed very much.[28] It seems, then, to be assumed that the contribution of N atoms in this N_2O system is not very important.

Acknowledgment. The authors gratefully acknowledge discussions with Dr. S. Sato and Dr. H. Yamazaki of this Institute. The helpful advice and comments of the reviewers are also acknowledged.

(20) F. Kaufman, N. J. Gerri, and R. E. Bowman, *J. Chem. Phys.*, **25**, 106 (1956).

(21) S. C. Barton and J. E. Dove, *Can. J. Chem.*, **47**, 521 (1969).

(22) J. Y. Yang and F. M. Servedio, *J. Chem. Phys.*, **47**, 4817 (1967).

(23) R. A. Young, G. Black, and T. G. Slanger, *ibid.*, **49**, 4769 (1968).

(24) G. A. W. Derwish, A. Galli, A. Giardini-Guidoni, and G. G. Volpi, *ibid.*, **40**, 3450 (1964).

(25) R. Gordon, Jr., and P. Ausloos, *J. Res. Nat. Bur. Stand., Sect. A*, **69**, 79 (1965).

(26) B. Brocklehurst and K. R. Jennings, "Progress in Reaction Kinetics," Vol. 4, Pergamon Press, Oxford, 1967, p 3.

(27) T. Oka, R. Kato, S. Sato, and S. Shida, *Bull. Chem. Soc. Jap.*, **41**, 2192 (1968).

(28) T. Oka and S. Sato, unpublished results.

NOTES

Ultrasonic Relaxation of *tert*-Butyl Alcohol in Cyclohexane

by Frank Garland,* Jørgen Rassing,

Chemistry Laboratory III, University of Copenhagen, Copenhagen, Denmark

and Gordon Atkinson

Department of Chemistry, University of Maryland, College Park, Maryland 20740 *(Received August 20, 1970)*

Publication costs borne completely by The Journal of Physical Chemistry

The ultrasonic absorption technique has been applied to the investigation of the kinetics of H-bond associated alcohols dissolved in inert solvents.[1-4] It is generally concluded that the data cannot be explained by a monomer–dimer equilibrium. The fact that ultrasonic results obtained over a wide frequency range are described by one relaxation time has been used as an argument for describing the data by a single elementary reaction step of the type

$$nN \rightleftarrows N_n \qquad (1)$$

Thus $n = 4$ has been proposed for the association of *tert*-butyl alcohol in cyclohexane,[1] while $n = 3$ has

* Address correspondence to this author at the Department of Chemistry, University of Oklahoma, Norman, Okla. 73069.

(1) R. S. Musa and M. Eisner, *J. Chem. Phys.*, **30**, 227 (1959).

(2) Z. Lang and R. Zana, *Trans. Faraday Soc.*, **66**, 597 (1970).

(3) V. Solovyev, C. Montrose, M. Watkins, and T. Litovitz, *J. Chem. Phys.*, **48**, 2155 (1968).

(4) J. Rassing and B. N. Jensen, *Acta Chem. Scand.*, **24**, 855 (1970).

$$\begin{vmatrix} 4K_1[N_1] + K_n\sum_{i=2}^{n-1}[N_i] & K_n[N_1] - 2 & K_n[N_1] - 1 & K_n[N_1] - 1 & \dots \\ K_n[N_2] - 2K_1[N_1] & K_n[N_1] + 1 & -1 & 0 & \\ K_n([N_3] - [N_2]) & -K_n[N_1] & K_n[N_1] + 1 & -1 & \\ K_n([N_4] - [N_3]) & 0 & -K_n[N_1] & K_n[N_1] + 1 & \\ \cdot & & & & \\ \cdot & & & & \\ \cdot & & & & \end{vmatrix} \quad (5)$$

recently been proposed for the association of a series of alcohols dissolved in inert solvents.[2] Since a collision involving more than two molecules is very improbable, the formation of a trimer, for example, would presumably take place in two elementary reaction steps

$$\begin{aligned} 2N_1 &\rightleftharpoons N_2 \\ N_1 + N_2 &\rightleftharpoons N_3 \end{aligned} \quad (2)$$

Although the general viewpoint of alcohol association is that extensive hydrogen bonded polymerization takes place,[5-9] mechanism (2) may be a reasonable approximation in very dilute solution. However, the extent to which this approximation is fulfilled depends on the actual alcohol concentration. Since a kinetic interpretation of ultrasonic data is based on the concentration dependence of the relaxation parameters, it is presumably a much better approximation to use an association mechanism in which the number of elementary reaction steps, and thus the size of the largest polymer present, is a function of overall alcohol concentration.

We have used a mechanism of this type to explain the ultrasonic relaxation spectra which we have obtained using a pulse technique in the frequency range 10–250 MHz on solutions of *tert*-butyl alcohol dissolved in cyclohexane at 15° in the concentration range 0.04–0.31 *M*. The association mechanism considered is the following

$$\begin{aligned} 2N_1 &\underset{k_{-1}}{\overset{k_1}{\rightleftharpoons}} N_2; \quad K_1 = k_1/k_{-1} \\ N_1 + N_2 &\underset{k_{-2}}{\overset{k_2}{\rightleftharpoons}} N_3; \quad K_2 = k_2/k_{-2} \\ N_1 + N_i &\underset{k_{-i}}{\overset{k_i}{\rightleftharpoons}} N_{i+1}; \quad K_i = k_i/k_{-i} \end{aligned} \quad (3)$$

N_i denotes a polymer of i monomeric units; k_i and k_{-i} are the association and dissociation rate constants of the ith step; and K_i is the equilibrium constant of the ith step. The largest polymer formed is N_n. The mechanism is applied by assuming that the equilibrium constant for the dimerization step may be different from that of the subsequent steps, and that the latter is independent of i

$$K_1 \neq K_2 = K_3 = \dots = K_n \quad (4)$$

This assumption has been used by a number of workers to interpret alcohol self-association.[6-9]

The individual relaxation times of the mechanism can be obtained by solving the differential equations which describe the kinetics of the system when perturbed by a sound wave. It has recently been shown[4] that the relaxation times are related to the eigenvalues, λ_i, of eq 5 by the relation

$$1/\tau_i = k_{-n}|\lambda_i| \quad (6)$$

provided that

$$k_{-1} = k_{-2} = \dots = k_{-n} \quad (7)$$

and

$$k_1 \neq k_2 = k_3 = \dots = k_n \quad (8)$$

The different eigenvalues are obtained by solving the eigenvalue problem for the above matrix. The elements of the matrix can be calculated at a given overall concentration of alcohol from n, K_1, and K_n. The mechanism thus predicts several relaxation times.

The concentration dependence of n can be expressed in terms of a normalized distribution function, φ_i, giving the distribution of alcohol over the different polymeric species

$$\sum_{i=1}^{\infty}\varphi_i = \sum_{i=1}^{\infty}[N_i]/\sum_j[N_j] = 1 \quad (9)$$

A criterion for calculating the values of n to be used at given overall concentrations of alcohol can be defined by

$$\sum_{i=1}^{n}\varphi_i = \epsilon \quad (10)$$

where $\epsilon < 1$. The closer ϵ is to unity the larger n is, and the greater the fraction of alcohol chains taken into account. In this work we use $\epsilon = 0.95$. This means

(5) G. Pimentel and A. McClellan, "The Hydrogen Bond," W. H. Freeman, San Francisco, Calif., 1960.

(6) H. Dunken and H. Fritsche, *Spectrochim. Acta*, **20**, 785 (1964).

(7) N. O. Coggeshall and E. L. Saier, *J. Amer. Chem. Soc.*, **73**, 5414 (1951).

(8) R. W. Haskell, H. B. Hollinger, and H. C. Van Ness, *J. Phys. Chem.*, **72**, 4534 (1968).

(9) F. Franks and D. J. G. Ives, *Quart. Rev., Chem. Soc.*, **20**, 1 (1966).

that less than 5% of the polymer chains present are neglected. The distribution function, and hence the value of n to be used at various overall alcohol concentrations, can be calculated from the equilibrium constants of the mechanism.[10]

K_1 and K_n may be obtained from infrared data using the method of Coggeshall and Saier.[7] This method is based on the assumption that the free OH peak (observed at 3627 cm^{-1} in this work) may be taken as a measure of monomer concentration. Although nonbonded hydrogens in dimers and polymers may contribute to this absorption,[11,12] the assumption is probably reasonable in dilute solutions. The results obtained are $K_1 = 1.8\ M^{-1}$ and $K_n = 7.1\ M^{-1}$. The eigenvalues of the coefficient matrix, eq 5, may now be calculated as a function of the degree of polymerization, n. The numerically largest eigenvalue, λ_1, and the smallest, λ_{n-1}, are given in Table I, together with the size of the matrix used, n.

Table I: Two Eigenvalues and the Size of the Coefficient Matrix Used at Different Overall Alcohol Concentrations

$[A_1]$	$\lvert\lambda_1\rvert$	$\lvert\lambda_{n-1}\rvert$	n
0.0506	1.33	(0.02)	2
0.0706	1.58	(0.02)	2
0.0996	1.99	1.01	3
0.2014	2.79	0.69	5
0.3097	3.16	0.33	8

The measured sound absorption data are described by a single relaxation time

$$\alpha/\nu^2 = B + \frac{A}{1 + (2\pi\tau\nu)^2} \qquad (11)$$

α is the sound absorption coefficient measured at a frequency ν; A and τ are the relaxation strength and time, respectively, obtained by a least-squares fit of the data to eq 11 (see Table II and Figure 1); and B is the background absorption. For the mechanism given by eq 5 the expression for α/ν^2 is

$$\alpha/\nu^2 = B + \sum_{i=1}^{n-1} \frac{A_i}{1 + (2\pi\tau_i\nu)^2}$$

If, however, either

$$\tau_1 \cong \tau_2 \cong \ldots \cong \tau_i \cong \ldots \cong \tau_{n-1} \qquad (12)$$

or

$$A_j \gg A_i,\ i \neq j \qquad (13)$$

then absorption data caused by mechanism 5 will fit eq 11. Table I shows that approximation 12 is not fulfilled. According to 13, the inverse of the measured relaxation time would be proportional to that particular eigenvalue whose relaxation strength is dominant; the

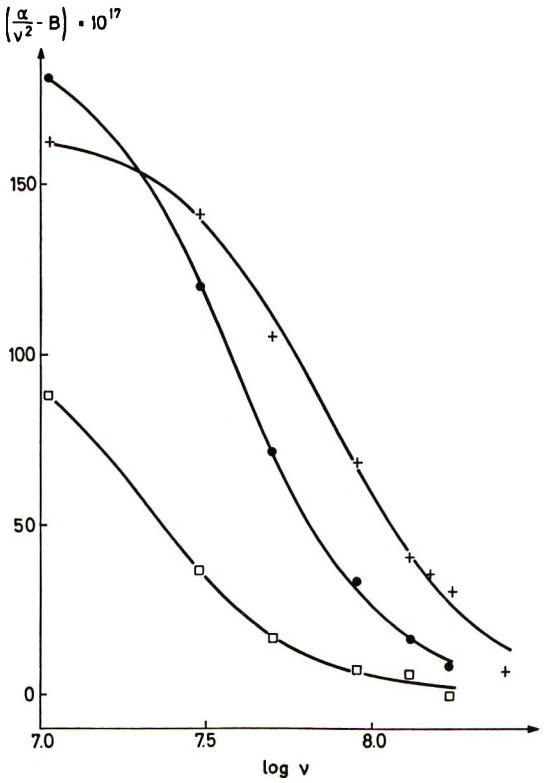

Figure 1. Ultrasonic absorption spectra of *tert*-BuOH dissolved in cyclohexane: □, 0.0467 *M*; ●, 0.1144 *M*; +, 0.3128 *M*.

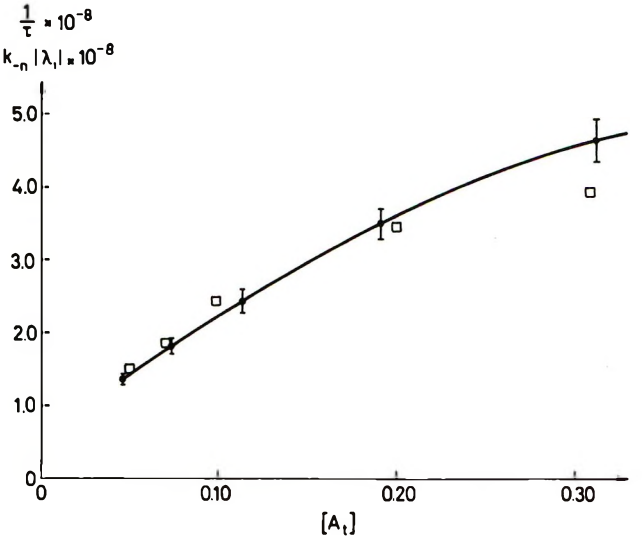

Figure 2. Reciprocal relaxation time and $k_{-n}|\lambda_1|$, indicated by squares, plotted against overall concentration of *tert*-BuOH in cyclohexane.

proportionality factor is equal to k_{-n} (see eq 6) and is independent of alcohol concentration. The eigenvalue which fulfills this criterion best is λ_1, the numeri-

(10) J. Rassing and F. Garland, *Acta Chem. Scand.*, **24**, 2419 (1970).

(11) H. C. Van Ness, J. Van Winkle, H. H. Richtol, and H. B. Hollinger, *J. Phys. Chem.*, **71**, 1483 (1967).

(12) L. J. Bellamy, R. J. Morgan, and R. J. Pace, *Spectrochim. Acta*, **22**, 525 (1960).

cally largest eigenvalue. The resulting value of k_{-n} is 1.2×10^8 sec^{-1}. Figure 2 shows that the mechanism used here describes the ultrasonic results up to about 0.2 M. The common depolymerization rate constant, k_{-n}, obtained from this mechanism is a factor of 2 larger than the value of k_{-1} which can be obtained from ultrasonic data alone by means of the extrapolation

$$\lim_{[A_t]\to 0} (1/\tau) = k_{-1}$$

Considering the approximations involved in the mechanism and the uncertainty involved in the extrapolation, we consider this to be good agreement.

Table II: Ultrasonic Relaxation Parameters Resulting from Fitting the Data to Eq 11 by Means of a Least-Squares Fitting Procedure

$[A_t]$, M	$A \times 10^{17}$, sec^2 cm^{-1}	$\tau_0 \times 10^8$, sec	$B \times 10^{17}$, sec^2 cm^{-1}
0.0467	108	0.743	184
0.0752	165	0.556	183
0.1144	195	0.415	183
0.1928	175	0.287	200
0.3128	163	0.217	190

At alcohol concentrations above 0.2 M the predicted value of $1/\tau$ is smaller than the actually measured value. Contributions from other relaxation times, polymer–polymer interactions, polymer–solvent interactions, or the breaking down of the equilibrium description itself might cause the observed deviation.

Acknowledgments. The authors are deeply indebted to Professor Thor A. Bak for his constant interest and helpful advice in connection with this work. The authors acknowledge the support of ARO (Durham) under Grant DA-AROD-31-124-G818 for the part of the work carried out at Maryland.

Excitation of Molecular Vibration on Collision. Dependence of the Rotation-Averaged Transition Probability on the Impact Parameter[1a]

by Hyung Kyu Shin

Department of Chemistry,[1b] University of Nevada, Reno, Nevada 89507 *(Received April 22, 1971)*

Publication costs assisted by the Air Force Office of Scientific Research

One of the pressing problems of vibrational energy transfer in a three-dimensional collision is the dependence of vibrational transition probabilities on the impact parameter b. Simple analyses predict that the transition probability increases with increasing collision velocity v for b less than the zero potential distance σ, while for $b > \sigma$ it decreases as v increases.[2] Furthermore, it is thought that the probability normally decreases with increasing b at a given v. However, the v and b dependences of vibrational transition probabilities are much more complicated than those predicted.[3] In this paper we study the dependence of the rotation-averaged transition probability on b at a given v by use of the sudden approximation.[4] We shall use the same terminologies and collision model presented in ref 3b; see Figure 1 of ref 3b for the collision model and definitions of the collision coordinates. For numerical discussion, we consider O_2 + Ar.

According to the sudden approximation, the probability of the $m \to n$ vibrational transition is[4,5]

$$P_{mn}(v,b,\Theta) = \langle n|\exp[2i\eta(v,b,\Theta,\xi)]|m\rangle^2 \qquad (1)$$

where the phase shift is

$$\eta(v,b,\Theta,\xi) = -\frac{1}{2\hbar}\int_{-\infty}^{\infty} V[v,b,\Theta,\xi,r(t)]\,dt \qquad (2)$$

and where ξ = vibrational coordinate, Θ = orientation angle (see Figure 1 of ref 3b), V = interaction potential energy between BC and A, r = distance between the atom and the center of mass of BC. We use the linear trajectory approximation; then we have[3b] $r^2 = b^2 + z^2$ and $z = vt$. The assumed form of the interaction potential between the collision partners is the inverse-power law

$$U(r_1,r_2) = 2D\sum_{i=1}^{2}[(\sigma/r_i)^{12} - (\sigma/r_i)^6] \qquad (3)$$

Here the atom–atom distances are

$$r_{1,2} = [r^2 \mp 2(d + \xi)S_{2,1}r\cos\Theta + (d + \xi)^2S_{2,1}^2]^{1/2}$$

where $S_{1,2} = m_{B,C}/(m_B + m_C)$ and d is the bond distance of BC. After introducing these distances, eq 3 can be expanded in a power series to obtain approximately the ξ-dependent perturbation energy as[6]

$$V[v,b,\Theta,\xi,r(t)] = 24\left(\frac{D}{\sigma}\right)\left[\left(\frac{\sigma}{r}\right)^{13} - {}^1/_2\left(\frac{\sigma}{r}\right)^7\right](S_2 - S_1)\xi\cos\Theta + 8\left(\frac{Dd}{\sigma^2}\right)\left[(42\cos^2\Theta - 3)\left(\frac{\sigma}{r}\right)^{14} - (12\cos^2\Theta - {}^3/_2)\left(\frac{\sigma}{r}\right)^8\right](S_1^2 + S_2^2)\xi \qquad (4)$$

(1) (a) This work was carried out under Grant AFOSR-68-1354 from the Air Force Office of Scientific Research; (b) Theoretical Chemistry Group Contribution No. S-1032.

(2) T. L. Cottrell and J. C. McCoubrey, "Molecular Energy Transfer in Gases," Butterworths, London, 1961, Chapter 6.

(3) (a) H. Shin, *Chem. Phys. Lett.*, 7, 436 (1970); (b) H. Shin, *J. Phys. Chem.*, 75, 923 (1971).

which, for homonuclear diatomic molecules, reduces to

$$V[v,b,\dot{\Theta},\xi,r(t)] = 4\left(\frac{D\sigma}{\sigma^2}\right)\left[(42\cos^2\Theta - 3)\left(\frac{\sigma}{r}\right)^{14} - (12\cos^2\Theta - {}^3/_2)\left(\frac{\sigma}{r}\right)^8\right]\xi \quad (5)$$

We can relate the orientation angle to the molecular rotation angle θ and its projection ϕ as

$$\cos\Theta = \frac{z\cos\theta + b\sin\theta\sin\phi}{(b^2+z^2)^{1/2}} \quad (6)$$

With eq 5 and 6, the integral in eq 2 can be readily evaluated as

$$\int_{-\infty}^{\infty} V[v,b,\theta,\phi,r(t)]\,dt = \frac{9009}{1024}\left(\frac{D\pi}{v}\right)\left(\frac{d}{\sigma}\right)\left(\frac{\sigma}{b}\right)^{13}\left(\cos^2\theta + 2\sin^2\theta\cos^2\phi - \frac{2}{13}\right)\xi - \frac{15}{16}\left(\frac{D\pi}{v}\right)\left(\frac{d}{\sigma}\right)\left(\frac{\sigma}{b}\right)^7(\cos^2\theta + 7\sin^2\theta\cos^2\phi - 1)\xi \equiv G(v,b|\theta,\phi)\xi \quad (7)$$

so that we can write the transition probability in the form

$$P_{mn} = \left\langle n\left|\exp\left[-\frac{i}{\hbar}G(v,b|\theta,\phi)\xi\right]\right|m\right\rangle^2 \quad (8)$$

We only consider the $0 \rightarrow 1$ transition here. Then with the harmonic oscillator wave functions, we obtain[7]

$$P_{01} = K^2(v,b|\theta,\phi)\exp[-K^2(v,b|\theta,\phi)] \quad (9)$$

where

$$K(v,b|\theta,\phi) = G(v,b|\theta,\phi)/(2M\hbar\omega)^{1/2}$$

For O_2 + Ar, we use the following potential parameters:[8,9] $D = 1.63 \times 10^{-13}$ erg, $\sigma = 3.42$ Å, $d = 1.207$ Å, $\omega = 3.535 \times 10^{14}$ sec^{-1}. With these values, we find

$$K(v,b|\theta,\phi) = \frac{5.5\times10^4}{v}\left[\left(\frac{\sigma}{b}\right)^{13} - 0.106\left(\frac{\sigma}{b}\right)^7\right]\cos^2\theta + \frac{1.1\times10^5}{v}\left[\left(\frac{\sigma}{b}\right)^{13} - 0.373\left(\frac{\sigma}{b}\right)^7\right]\sin^2\theta\cos^2\phi - \frac{8.6\times10^3}{v}\left[\left(\frac{\sigma}{b}\right)^{13} - 0.693\left(\frac{\sigma}{b}\right)^7\right] \quad (10)$$

The rotation-averaged probability can be expressed by

$$\bar{P}_{01} = \frac{1}{2\pi}\int_0^{2\pi}\int_0^{\pi/2} K^2(v,b|\theta,\phi)\times\exp[-K^2(v,b|\theta,\phi)]\sin\theta\,d\theta\,d\phi \quad (11)$$

The average transition probability is now a function of the collision velocity and the impact parameter. The integrand is a complicated function of the angles, but the integration can be readily carried out numerically. We performed two-dimensional integration on the XDS Sigma-7 computer by Simpson's $^1/_3$ rule by shifting the operator in the ϕ direction for each pair of strips in the θ direction. Three different spacings and Richardson's extrapolations are used to improve the results.[10]

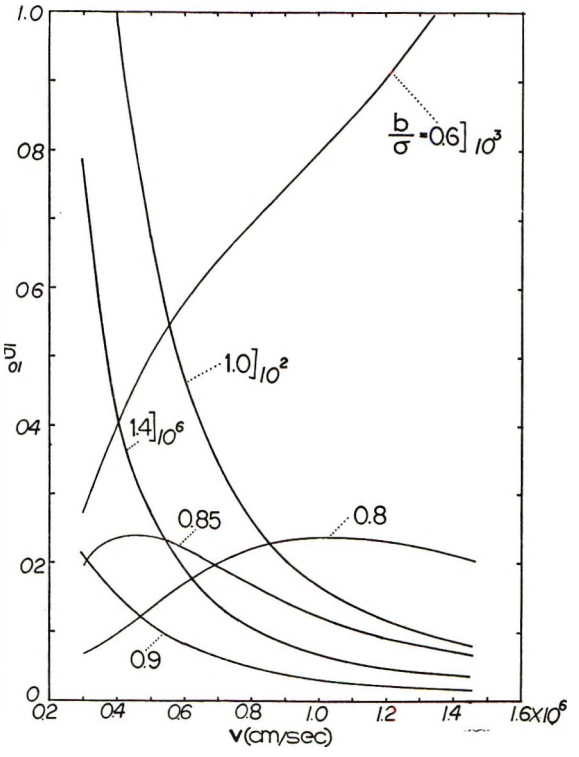

Figure 1. Dependence of the average transition probability on the collision velocity for various values of the impact parameter; the values for b/σ = 0.6, 1.0, and 1.4 are multiplied by 10^3, 10^2, and 10^6, respectively.

In Figure 1 we show the velocity dependence of the average transition probability for several different values of b. For small values of b (*e.g.*, $b/\sigma = 0.6$) the probability increases with increasing v, whereas when b is large (*e.g.*, $b/\sigma = 1.4$) it decreases with increasing v over the velocity range of 3×10^5 to 1.5×10^6 cm/sec. For intermediate values of b, the variation of $\bar{P}_{01}$ with v is anomalous. It increases to a maximum value and then decreases. As shown in Figure 1, $\bar{P}_{01}$ for b/σ = 0.8 first increases with v, but slowly falls off as v con-

(4) K. Alder and A. Winther, "Coulomb Excitation," Academic Press, New York, N. Y., 1966, pp 209–280; the original article appeared in *Kgl. Dan. Vidensk. Selsk., Mat. Fys. Medd.*, **32** (8) (1960).

(5) K. H. Kramer and R. B. Bernstein, *J. Chem. Phys.*, **40**, 200 (1964).

(6) H. Shin, *J. Phys. Chem.*, **73**, 4321 (1969).

(7) D. Rapp and T. E. Sharp, *J. Chem. Phys.*, **38**, 2641 (1963).

(8) J. O. Hirschfelder, C. F. Curtiss, and R. B. Bird, "Molecular Theory of Gases and Liquids," Wiley, New York, N. Y., 1964, pp 1110–1111.

(9) G. Herzberg, "Spectra of Diatomic Molecules," Van Nostrand, Princeton, N. J., 1950, Table 39.

(10) J. M. McCormick and M. G. Salvadori, "Numerical Methods in Fortran," Prentice-Hall, Englewood Cliffs, N. J., 1964, pp 312–317.

tinues to increase. For $b/\sigma = 0.85$, except at lower velocities, $\bar{P}_{01}$ decreases as v rises. For $b/\sigma > 0.9$, $\bar{P}_{01}$ is an increasing function of b, but after reaching a maximum value it rapidly decreases as b continues to increase. For both small and large values of the impact parameter (*e.g.*, $b/\sigma = 0.6$ and 1.4) $\bar{P}_{01}$ is very small, while for intermediate values of b it can be very large. For example, at $v = 10^6$ cm/sec, $\bar{P}_{01} = 7.94 \times 10^{-3}$, 0.239, and 1.98×10^{-7}, respectively, for $b/\sigma = 0.6$, 0.8, and 1.4.

The reason for the decrease of $\bar{P}_{01}$ with increasing b is as follows.[2,3b,11] For the present model the effective interaction potential is $U_{\text{eff}} = U + {}^1/_2\,\mu v^2(b/r)^2 \equiv U + E(b/r)^2$, μ being the reduced mass of the colliding system. For nonzero b collisions, a maximum value of the effective potential, $U_{\text{eff}}{}^m$, may show up outside of the potential minimum. If b is sufficiently large, then the potential curve is obliterated and might even become a decreasing function of r. If $E < U_{\text{eff}}{}^m$, the distance of closest approach r_0 lies in the region of the outer curve of the maximum. Therefore, when the colliding partners are approaching at large distances with $E < U_{\text{eff}}{}^m$, they will repel each other at the outer curve regardless of the nature of the potential at smaller values of r. When $b > \sigma$, an increase in E counteracts the magnitude of the potential minimum and straightens out the trajectory, thus leading to an increase in r_0. The transition probability $\bar{P}_{01}$ for $b > \sigma$ should therefore decrease with increasing v. Since the collision occurs at large distances corresponding to the outer curve, the energy transfer can be very inefficient. On the other hand, when $b < \sigma$, the potential will be mainly repulsive, and an increase in v decreases r_0. Therefore, when $b < \sigma$, $\bar{P}_{01}$ can rise with increasing v and its magnitude can be very large.

In Figure 2, the b dependence of $\bar{P}_{01}$ at $v = 5 \times 10^5$ and 1.4×10^6 cm/sec is shown on a semilogarithmic scale. At the former velocity the maximum occurs at $b/\sigma \simeq 0.85$ and at the latter it occurs at $b/\sigma \simeq 0.80$. Therefore, $\bar{P}_{01}$ increases with b at small values of b. After reaching the maximum value, it then rapidly decreases with increasing b. If the molecule is fixed on the z axis, then the zero b collision involves the collinear arrangement of BC + A; *i.e.*, $b = 0$ and $\Theta = \theta = 0$. For such a collinear collision, we can show that the vibrational transition is very efficient.[12] However, when the molecule rotates at $b = 0$, we have a linear but oriented collision ($b = 0$, $\Theta = \theta \neq 0$, $\theta' = 0$). For such an encounter, the vibrational transition becomes inefficient when Θ becomes different from 0° or 180°; in particular the vibrational transition for a homonuclear diatomic molecule is least efficient for $\Theta = 90°$. Therefore, when we take an average of the transition probability over all possible values of θ and ϕ, the resulting quantity for small b (including $b = 0$) may not be as large as that at some intermediate values of b. We must recognize that in the three-dimensional collision nonzero b encounters can also represent collinear arrangements. As long as $\Theta = \theta$, the colliding molecule and atom are collinearly oriented regardless of the value of b, but the velocity components are not directed parallel to the collinear direction of BC + A so the energy transfer cannot be efficient. In the quantum mechanical treatment it has already been shown that the partial inelastic cross section $q(E,l)$ increases to a maximum value from the s-wave result with l and then decreases as l continues to increase,[13] where l is the relative angular momentum quantum number. Although we are interested in the transition probability in the present study rather than the cross section, the appearance of the maximum in the $\bar{P}_{01}$–b plot is equivalent to that in the $q(E,l)$–l variation.

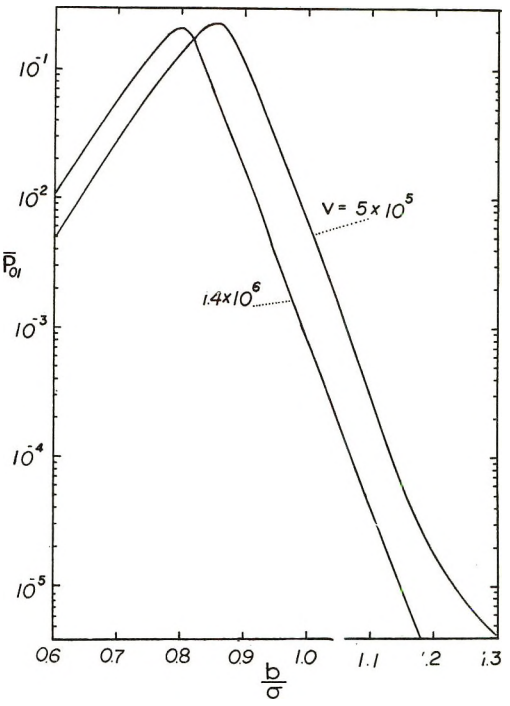

Figure 2. Dependence of the average transition probability on the impact parameter; the velocities 5×10^5 and 1.4×10^6 cm/sec are chosen.

Finally, we need to mention the validity of the sudden approximation. It can be used when the collision time is small compared with the vibrational period. For a given velocity, the approximation works better in small b collisions than in large b collisions. For $b/\sigma < 0.8$ the approximation is entirely satisfactory over the velocity range considered here. For large b, use of the approximation becomes questionable at lower v; *e.g.*, for $b/\sigma = 1.4$ the approximation can be used with confi-

(11) B. Widom and S. H. Bauer, *J. Chem. Phys.*, **21**, 1670 (1953).
(12) H. Shin, *ibid.*, **49**, 3964 (1968).
(13) H. Shin, *ibid.*, **46**, 744 (1967).

dence above 8×10^5 cm/sec. However, except for such a large value of b/σ, the questionable range of v is not wide enough to affect the result discussed above.[14]

(14) NOTE ADDED IN PROOF. For the collinear zero b collision, we need to set $b = 0$ and $\Theta = 0$ in eq 4. Comparison of the present calculation for such a collision with existing "exact" quantum mechanical and classical calculations should be interesting. However, the latter calculations are based on exponential interaction potentials which are different from the present inverse-power potential so that any quantitative comparison cannot be made; ref 3b presents a discussion on the collinear zero b collision and gives pertinent references on exact calculations.

Solvation Studies of Lithium Salts in Dimethylformamide

by Claude Lassigne and Peter Baine*

California State College at Long Beach, Long Beach, California 90801 *(Received February 17, 1971)*

Publication costs borne completely by The Journal of Physical Chemistry

Recently there have been several publications describing solvation studies of alkali metals in various nonaqueous solvents.[1-4] The interaction of lithium ions with dimethyl sulfoxide[3] is presumably due to a resonance structure of this molecule whereby the oxygen atom becomes negatively charged. We sought to test this by using an analogous system, lithium perchlorate and dimethylformamide, where resonance also makes the oxygen atom negatively charged in the latter molecule. We wish to report some results pertinent to such investigations.

Infrared Spectral Studies. The infrared spectrum of a saturated solution of lithium perchlorate dissolved in dimethylformamide (DMF) was recorded at 800–200 cm^{-1} on a Perkin-Elmer 225 spectrometer using 0.1-mm path length polyethylene cells from Barnes Engineering Co. The spectrum revealed two bands at 365 and 420 cm^{-1}, which were absent in the spectrum of pure DMF. These bands were demonstrated not to be attributable to the perchlorate ion or ion pairs by duplicating them with a solution of lithium chloride in DMF. The spectrum of DMF and a solution of lithium perchlorate are shown in Figure 1. The sharp band at 620 cm^{-1} is a perchlorate vibration. We interpret the bands at 365 and 420 cm^{-1} to be indicative of specific cation–solvent interactions. These interactions would be expected to occur through the electronegative atoms in the molecule, in this case, the nitrogen and oxygen atoms. In an attempt to determine which atom is involved, solutions of varying mole ratios of DMF and lithium perchlorate in dioxane were made. Dioxane was used as a supporting solvent since there are indications it does not interact strongly with DMF or lithium perchlorate.[5] The carbonyl band of DMF in dioxane appears at 1686 cm^{-1}, characteristic of uncomplexed DMF. As lithium perchlorate is added to the solution and the DMF–$LiClO_4$ ratio is varied, another band appears at 1670 cm^{-1}. This band increases in intensity, as the concentration of lithium perchlorate is increased. At a mole ratio of DMF:$LiClO_4$ of 2:1 most of the DMF is present in the complexed form and only a shoulder indicates the uncomplexed DMF. At the mole ratio of 4:1 two distinct bands are observed, one at 1670^{-1} due to uncomplexed DMF. For the mole ratio of 10:1 there is only one band at 1686 cm^{-1}, due to the uncomplexed ligand. An investigation of the infrared spectrum in the region 4000–625 cm^{-1} re-

Figure 1. Trace of the ir spectra of pure DMF and a solution of $LiClO_4$ in DMF. The vertical line in the spectra at 450 cm^{-1} is due to a malfunction in the machine. The dotted line more correctly represents the spectrum.

(1) W. F. Edgell, J. Lyford, R. Wright, and W. Risen, *J. Amer. Chem. Soc.*, **88**, 1815 (1966).

(2) E. Schaschel and M. C. Day, *ibid.*, **89**, 2230 (1968).

(3) B. W. Maxey and A. I. Popov, *ibid.*, **90**, 4470 (1968).

(4) J. L. Weupper and A. I. Popov, *ibid.*, **91**, 4356 (1969).

(5) L. S. Frankel, T. R. Stengle, and C. H. Langford, *Can. J. Chem.*, **46**, 3183 (1968).

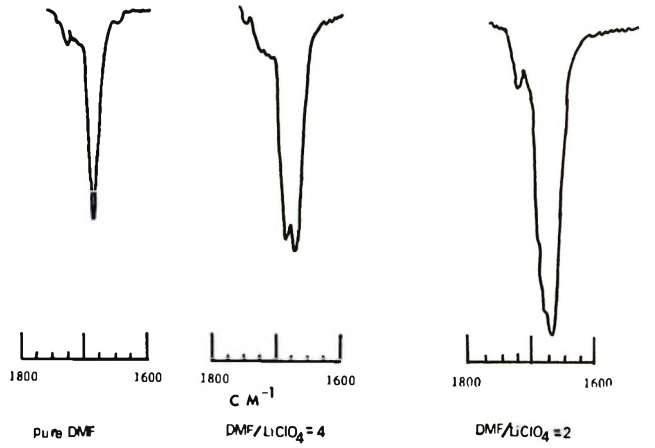

Figure 2. The splitting of the carbonyl absorption band of DMF due to interaction with lithium ions.

vealed no further new bands, however a DMF band at about 660 cm^{-1} was shifted to higher energy by about 10 cm^{-1}, as was observed in the absence of dioxane. (See Figure 1.) Analogous work in different solvent systems supports these observations.[6] It is obvious from these results that the bonding between the lithium ion and the DMF occurs through the carbonyl oxygen of the DMF. The infrared spectra are shown in Figure 2.

It is quite reasonable that the interaction of DMF with lithium ions occurs through the oxygen, since resonance in the molecule causes the oxygen to be the site of negative charge.

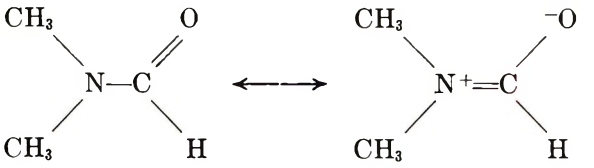

Stoichiometric Studies. In an attempt to determine the stoichiometry of the solvate, the nmr frequencies of the methyl protons were studied as a function of the mole ratio of DMF-$LiClO_4$. The methyl groups in DMF are not equivalent as might be expected from the formula because of the partial double bond character between the carbon and nitrogen atoms. The barrier to rotation as measured by Neuman and Young[7] is 18.7 kcal/mol, causing the two methyl groups to experience different environments. This causes a splitting of 8.8 Hz between the two methyl signals. Also both methyl signals are further split by long range spin–spin coupling with the aldehydic proton. The methyl protons trans to the aldehydic hydrogen are split by 0.6 Hz and cis methyl protons by 0.3 Hz. The graphs a and c in Figure 3 are plots of the DMF methyl proton resonance frequencies for various molarities of DMF in dioxane. Graph a depicts the resonance frequency of the methyl protons trans to the aldehydic hydrogen and shows no shift with concentration changes. However, the nmr signal of the methyl protons cis to the aldehydic hydrogen does vary with concentration. We interpret this as preferential solvation by dioxane around the cis methyl group due to the relative charges on the nitrogen and oxygen atoms. Plots b and d in Figure 3 illustrate the chemical shift of the methyl protons as a function of the mole ratio of DMF and lithium perchlorate. The concentration of DMF was varied to produce mole ratios from 1.0 to 8.0. The concentration of the lithium perchlorate was held constant at 0.5 *M*. A definite break is observed at a mole ratio of 3.7 for the cis methyl group and 3.8 for the trans methyl group. This indicated that the solvate has the formula $Li(DMF)_4^+$. If the system was a two component one, that is consisting of complexed and uncomplexed DMF, then the shape of the mole ratio plots would indicate small chemical shifts until all the DMF was complexed, then a trend in the direction of the

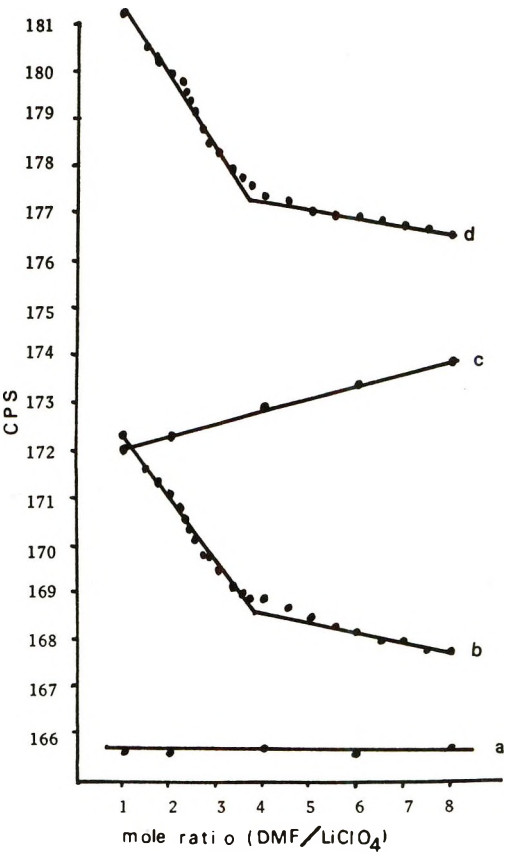

Figure 3. Curves b and d represent the chemical shift of the methyl protons as a function of the mole ratio of DMF to $LiClO_4$. The $LiClO_4$ concentration was held constant at 0.5 *M*. Dioxane was used as a supporting solvent. Curves a and c are plots of the chemical shifts for the methyl protons as a function of DMF concentrations with molarities corresponding to the DMF concentrations in graphs b and d. Thus it is 4 *M* at the 8:1 ratio marker decreasing to 0.5 *M* at the 2:1 marker.

(6) B. W. Maxey and A. I. Popov, *J. Amer. Chem. Soc.*, **91**, 20 (1969); see also W. J. McKinney and A. I. Popov, *J. Phys. Chem.*, **74**, 535 (1970).

(7) R. C. Neuman and L. B. Young, *ibid.*, **69**, 2570 (1965).

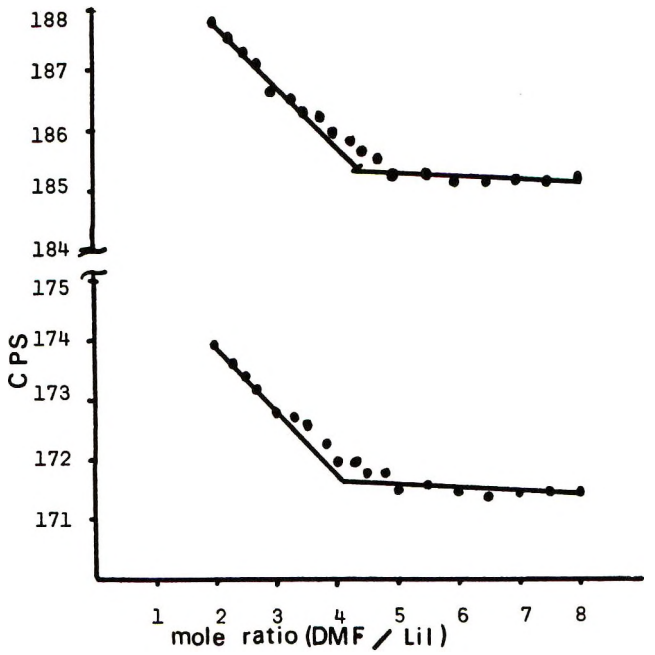

Figure 4. Curves for the chemical shifts of the methyl protons as a function of mole ratio DMF–LiI in dioxane.

DMF shift in the absence of salt. Such "two component" systems are found in the work described in ref 4 and 8. In this work the chemical shift increases rapidly after the stoichiometric ratio is reached. Obviously the methyl protons are experiencing an environment very different from the salt free environment of the DMF solution. We attribute this to the excess lithium ions competing successfully for DMF ligands already complexed to other lithium ions to form nonspecific lower solvates.

In order to assure ourselves of the validity of this result the work was repeated using lithium iodide (see Figure 4). Essentially the same results were obtained, the break being at 4.3:1. The solvation of the lithium ion in DMF is apparently independent of the anion.

The resonance of the dioxane protons was also found to vary slightly with the concentration of lithium perchlorate. At small mole ratios of DMF–$LiClO_4$, the dioxane protons underwent a shift of 2 Hz, however for larger ratios it remained constant. This may be due to the fact that dioxane competes favorably with DMF for solvation of lithium ions, particularly when the DMF is present in low concentrations. In all of this work, care was taken to ensure anhydrous conditions. Chemicals were dried by standard techniques and solutions made up on a drybox.

The nmr spectra were recorded on a JEOLCO JNM C60H instrument, using TMS as an internal standard. The frequencies were measured by the side band technique, and displayed on a Hewlett-Packard scalar. Reproducibility of measurements was to within 0.2 Hz. In order to overcome solubility problems all spectra were run at 30°.

Calculations based on conductance measurements by Paul and coworkers[9] indicate the solvation number of the lithium ion for lithium chloride in DMF to be 3.24, in rough agreement with this work. The dielectric constant of DMF is not exceptionally large[10] (D = 36.7) and ion pair formation cannot be excluded, indeed Prue and Sherrington[11] have calculated from conductivity measurements an ion pair formation constant of 35, while Criss and Held[12] calculated a value of 2×10^3 from calorimetric measurements. Butler and Synnott[13] have measured the electrode potential for the cell $Tl(s)|TlCl(s)|Li^+Cl^-(DMF)|Li(s)$. From this work, they have calculated a free energy of formation of solvated lithium ions from lithium chloride to be in −9.6 kcal/mol. These authors indicate that Li^+ in DMF may be one of the most strongly solvated cations known.

Acknowledgments. We wish to thank the Long Beach State College foundation for financial aid.

(8) M. K. Wong, W. J. McKinney, and A. I. Popov, *J. Phys. Chem.*, **75**, 56 (1971).

(9) R. C. Paul, J. P. Singla, and S. P. Marula, *ibid.*, **73**, 741 (1969).

(10) G. R. Leader and J. F. Gormley, *J. Amer. Chem. Soc.*, **73**, 5731 (1951).

(11) J. E. Prue and P. J. Sherrington, *Trans. Faraday Soc.*, **57**, 1795 (1961).

(12) R. P. Held and C. M. Criss, *J. Phys. Chem.*, **69**, 2487 (1965).

(13) J. N. Butler and J. C. Synnott, *J. Amer. Chem. Soc.*, **92**, 2602 (1970).

Proton Exchange and Nitrogen Inversion of α-Phenylethylbenzylmethylamine Using Nuclear Magnetic Resonance Spectroscopy

by Donald E. Leyden* and W. R. Morgan

Department of Chemistry, University of Georgia, Athens, Georgia 30601 *(Received March 11, 1971)*

Publication costs borne completely by The Journal of Physical Chemistry

The use of nuclear magnetic resonance spectroscopy in the study of fast reactions in solution is well documented.[1-5] Recent studies[1,3] indicate that the rate equation for proton exchange of tertiary amines in aqueous acid can be expressed as

(1) E. Grunwald and E. K. Ralph, III, *J. Amer. Chem. Soc.*, **89**, 4405 (1967).

(2) E. Grunwald, R. L. Lipnick, and E. K. Ralph, III, *ibid.*, **91**, 4333 (1969).

(3) D. E. Leyden and W. R. Morgan, *J. Phys. Chem.*, **73**, 2924 (1969).

(4) W. R. Morgan and D. E. Leyden, *J. Amer. Chem. Soc.*, **92**, 4527 (1970).

(5) W. R. Morgan, Ph.D. Dissertation, University of Georgia, 1970.

$$1/\tau = \left(\frac{k_H k_a}{k_H + k_{-a}[H^+]}\right) + \left(\frac{k_2 K_a[BH^+]}{[H^+]}\right) \quad (1)$$

where the rate parameters are as given in previous examples.[1,3,5] The parameter k_2 represents the second-order rate constant for the transfer from the protonated amine to the unprotonated amine through a solvent bridge. A more recent study indicates that the mechanism for nitrogen inversion involves the kinetically controlled formation of a nonhydrated species R_3N which is capable of inversion.[4,5] This can be expressed as

$$R_3NH^+\cdots HOH + HOH \underset{k_{-a}}{\overset{k_a}{\rightleftharpoons}} R_3N\cdots HOH + H_3O^+ \quad (2)$$

$$R_3N\cdots HOH \underset{k_{-H}}{\overset{k_H}{\rightleftharpoons}} R_3N + H_2O$$

$$R_3N\cdots HOH \xrightarrow{k_i} R_3N^*$$

where R_3N^* indicates an inverted species of R_3N. In some cases, inversion may be further promoted through a mechanism involving two amine molecules in a concerted proton exchange involving a "well aligned, hydrogen-bonded hydrate" species as represented by the second term in eq 1.

Using a steady-state approximation on the concentration of R_3N in eq 2, an expression for the rate of inversion of the nitrogen atom as a function of hydrogen ion concentration may be represented by eq 3. The

$$1/\tau = \frac{k_H k_a f}{k_H f + k_{-a}[H^+]} + \frac{k_2 K_a[BH^+]}{[H^+]} \quad (3)$$

quantity f is $k_i/(k_i + k_{-H})$.[6] The second term in eq 3 is introduced as a generality as a mechanism second order in amine has been observed for similar compounds.[4]

Of particular interest here are the values k_H and k_i which are the rate constants for the rupture of the $R_3N\cdots HOH$ hydrogen bond leading to exchange and the rate constant for uninhibited nitrogen inversion, respectively.

The relationship between k_H and the ability of the water molecule hydrogen bonded to the amine nitrogen to participate in hydrogen bonding to the benzene π-electron cloud has been discussed.[3] The value of k_H found here is in agreement with previous predictions. Studies by Grunwald, *et al.*,[2] in different solvent systems also indicate that the strength of dispersion force interactions between the water molecule and the amine substituents is a definite factor in the rate of rupture of the $R_2N\cdots HOH$ bond. Previous studies on a series of substituted α-phenylethylbenzylmethylamines indicated that the rate constants of inversion, k_i, for these compounds are in the range 10^4–10^6 sec^{-1}.[7] However this study and previous investigations[4,5,8] indicate that the rate constant for nitrogen inversion of *tert*-benzylamines is of the order of 10^8–10^9 sec^{-1} at room temperature.

Experimental Section

Spectra were obtained on a Hitachi-Perkin-Elmer R-20 nmr spectrometer operated under slow passage conditions. Data were obtained at 50° to eliminate a slight viscosity dependence upon the line width at the higher concentrations used. Temperature regulation was obtained to within ±1° using a variable temperature probe available with the instrument.

Solutions from which the experimental data were obtained were prepared using standard dilution techniques. Amine concentrations ranged from 1.0 to 0.25 M, while excess acid, HCl, was present in concentrations from 0.01 to 4.0 M. Specific rates were obtained by use of equations given for first-order interaction.[3,5] τ values were adjusted to yield a minimum standard deviation between computed and experimental spectra. T_2 values were assumed to be controlled by the inhomogeneity of the magnetic field and were found to be approximately 0.3 sec from measurement of $N\text{–}CH_3$ proton line widths under conditions where no exchange broadening occurs. The spectral changes associated with the increased rates of proton exchange and nitrogen inversion have been discussed in some detail[5,6] and will not be presented here. However, it should be mentioned that an asymmetric carbon center adjacent to an asymmetric nitrogen allows the observation of the two diastereomers under conditions of slow nitrogen inversion. Integration of the two signals shows that one diastereomer is more favorable (1.3:1) than the other. However, the rate of exchange and inversion measured from the methyl resonance of the two isomers is the same.

α-Phenylethylbenzylmethylamine (I) was obtained by refluxing acetophenone and benzylamine in benzene forming a Schiff base.[9] Reaction was deemed complete when the calculated amount of water was collected in a Dean–Stark tube. Reaction time for 0.5 mol of reactants was approximately 8 hr. The Schiff base was reduced to the secondary amine and then converted into the desired tertiary amine by methylation with methyl iodide in ethanol. Identification was obtained from nmr and infrared spectra.

The acid dissociation constant, K_a, for the amine salt

(6) R. B. Martin has drawn to our attention that the f term in the denominator of eq 3 was missing from our eq 10 in ref 4. Fortunately, this did not affect any conclusions in the earlier work as the f terms cancel in the low acidity region and the product $k_H f$ is negligible in the denominator in the high acidity region.

(7) A. Ehrenberg, B. G. Malmstron, and T. Vanngard, Ed., "Magnetic Resonance in Biological Systems," Pergamon Press, New York, N. Y., 1966, p 94.

(8) C. H. Bushweller and J. W. O'Neal, *J. Amer. Chem. Soc.*, **92**, 2159 (1970).

(9) S. I. Kegam and S. Yamada, *Chem. Pharm. Bull.*, **14**, 1389 (1966).

was obtained at 50° in a mixed solvent system using a differential potentiometric method.[10] The solvent system water–*tert*-butyl alcohol was used due to the insolubility of I in water. Apparent pK_a values were obtained for a series of solutions of varying volume per cent *tert*-butyl alcohol and extrapolated to 0%. This value was found to be 7.45 and was used in the treatment of the rate data.

Results and Discussion

A plot of $1/\tau$ *vs.* $1/a_{H^+}$ for N–H proton exchange for I is linear with no amine concentration dependence. The linearity permits the assumptions $k_H \ll k_{-a}[H^+]$ and $k_a \gg k_2K_a[BH^+]/[H^+]$. These assumptions yield eq 4 which describes the rate of exchange in terms of

$$1/\tau = \frac{k_H k_a}{k_{-a}[H^+]} = \frac{k_H K_a}{[H^+]} \qquad (4)$$

k_H and the acid dissociation constant K_a. This allows only the evaluation of the parameter k_H which was found to be 1.3×10^9 sec^{-1}. Values of k_a and k_{-a} cannot be determined separately from the data. Comparison of the value of k_H with those previously obtained can be made only if the value of k_H for I is corrected to 25°. An activation energy for exchange was not determined for this compound, but an estimate may be made on the limits of activation energies using the range of values previously determined for similar compounds.[3] Assuming that the value of the activation energy falls between 8 and 16 kcal/mol, one may calculate a range of k_H at 25° of 1.4×10^8 to 4.2×10^8 sec^{-1}. Space-filling models indicate that there is much steric hindrance to rotation about the nitrogen atom and the substituent phenylethyl–carbon bond. This reduction in the movement of the substituent groups would allow the interaction between the $R_3N\cdots HOH$ water molecule and the π-electron cloud of either benzene ring to be favorable. Therefore, a k_H value of the order of that for dibenzylmethylamine would be expected for I. The results given above may be compared with a value of 2.8×10^8 sec^{-1} for dibenzylmethylamine.[3]

Interpretation of the results for inversion was complicated by a chemical shift change between the N–CH_3 protons in the two diasteromers as a function of the concentration of amine. The same effect was observed for the methylene protons in dibenzylmethylamine. These variations in chemical shift may lead to false kinetic results unless corrections are made. However, unlike dibenzylmethylamine the chemical shift between the methylene protons of the benzyl group in I did not appear to be concentration dependent. This would indicate that the factor producing change was localized about the nitrogen atom. Grunwald suggested that in the high salt concentrations being used the possibility of a "well aligned, hydrogen-bonded hydrate, $B\cdot H_2O\cdot HB^+$" exists.[11] If such a species were favorable, this

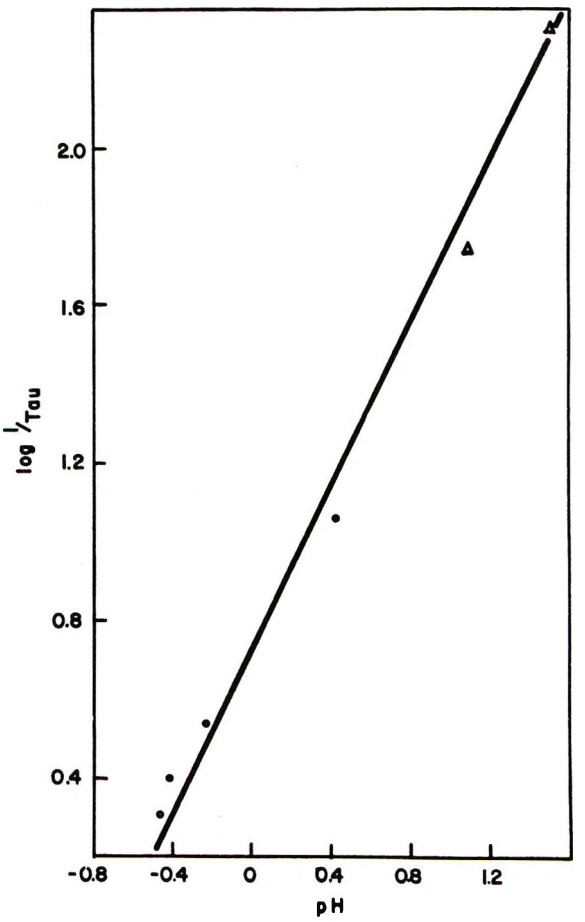

Figure 1. Log $1/\tau$ *vs.* pH for the inversion of α-phenylethylbenzylmethylamine: △, data obtained from *N*-methyl protons; ○, data obtained from phenylethyl protons.

may account for the abnormal chemical shift changes observed. Previous investigators have observed internal chemical shift changes with variation in the dielectric constant of the solvent.[12,13] Whatever the cause, it does not appear to affect all compounds or all groups in a given compound equally. Thus careful evaluation of the spectral parameters must be made in studies of this type.

Figure 1 shows a plot of log $1/\tau$ *vs.* pH for inversion of the nitrogen atom in I. Figure 1 includes data from analysis of the spectra arising from both the N–CH_3 and phenylethyl protons. There was no amine dependence observed, thus eliminating the second-order term of eq 3. From the linearity of Figure 1 it is also assumed that $k_H f \ll k_{-a}[H^+]$ thus yielding eq 5. Substituting the values of 1.3×10^9 sec^{-1} for k_H and

(10) A. L. Bacarella, E. Grunwald, H. P. Marshall, and E. L. Purlee, *J. Org. Chem.*, **20**, 747 (1955).

(11) E. Grunwald, personal communication.

(12) E. L. Griffith and J. Roberts, *J. Amer. Chem. Soc.*, **87**, 4089 (1965).

(13) S. Brownstein, E. C. Horswill, and K. V. Ingold, *ibid.*, **92**, 7217 (1970).

3.54×10^{-8} for K_a into eq 5 yields a value of 0.15 for the term $(k_i/k_t + k_{-H})$. This is in agreement with previous values for other similar compounds.[4] An

$$1/\tau = \left(\frac{k_H k_a}{k_{-a}[H^+]}\right)\left(\frac{k_t}{k_i + k_{-H}}\right) \quad (5)$$

additional point of interest is the fact that essentially identical results obtained from the N–CH_3 and phenylethyl protons preclude any concern as to whether inversion or C–N bond rotation is being observed, as is the concern with low temperature studies of the free amine.[8,13]

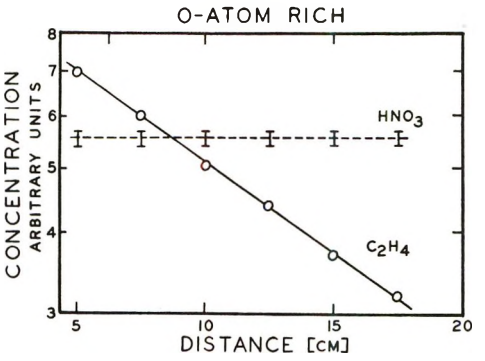

Figure 1. Plot of the concentration of HNO_3 and C_2H_4 against reaction distance under O-atom rich conditions.

Mass Spectrometric Study of the Reactions of Nitric Acid with O Atoms and H Atoms

by E. D. Morris, Jr.,* and H. Niki

Scientific Research Staff, Ford Motor Company, Dearborn, Michigan 48121 *(Received May 12, 1971)*

Publication costs assisted by Ford Motor Company

Nitric acid has been reported as a product in smog chamber experiments[1] and in the upper atmosphere.[2] Therefore, it is of considerable interest to obtain information on the chemical fate of HNO_3 in these systems. The reaction $O + HNO_3 \rightarrow OH + NO_3$ has been suggested as being extremely fast in two recent studies of photochemical reactions of HNO_3 in the presence of NO_2 at wavelengths above 3300 Å.[3,4] On the basis of postulated mechanisms, Jaffe and Ford[3] obtain a bimolecular rate constant on the order of magnitude of 10^{-11} cc/molecule-sec, while Berces and Forgeteg[4] suggest 10^{-10} cc/molecule-sec. The reactions of HNO_3 with H atoms have been studied by Berces, Forgeteg, and Marta.[5] From the photolysis of HNO_3 in the presence of H_2 and CO, they have assigned a rate constant of 1×10^{-12} cc/molecule-sec to the reaction $H + HNO_3 \rightarrow OH + HNO_2$. In the present paper, we have attempted to measure the rate of reaction of HNO_3 with O atoms and with H atoms directly using a mass spectrometer coupled to a discharge-flow system.

The flow reactor and the mass spectrometric detection technique have been described in detail elsewhere.[6] Oxygen atoms were generated by passing O_2 diluted in helium through a microwave discharge. The total pressure in the flow reactor was typically 1 Torr with a linear flow velocity of 10 m/sec. The HNO_3 sample, obtained from the vapor above a solution of concentrated nitric acid in sulfuric acid, was introduced into the reactor through a movable inlet so that the reaction time could be varied. Nitric acid has a weak parent peak but a strong fragment at m/e 46.[7] At high concentration, the parent peak is easily observed. At the low concentrations used in the kinetic runs, nitric acid was determined from the m/e 46 peak. Nitrogen dioxide, which is often an impurity in HNO_3, presents a possible interference at m/e 46. To verify the m/e 46 peak was a good measure of HNO_3 concentration, a small amount of NH_3 was added. The m/e 46 peak dropped rapidly to zero. On this time scale, NO_2 does not react with NH_3. These preliminary results indicate a very fast heterogeneous reaction between NH_3 and HNO_3 producing NH_4NO_3 as a product.[8]

When a small amount of HNO_3 (10^{12} molecules/cc) was added to a large excess of O atoms (10^{14} molecules/cc), little or no decay of m/e 46 was observed, contrary to the predictions of the reported rate constants. In order to set an upper limit on the $O + HNO_3$ rate constant, two compounds with known, relatively slow O-atom rates were used as references. Ethylene or acetylene was added through the movable inlet and a plot made of the hydrocarbon concentration as a function of slider distance. Then using the same flow conditions and O-atom concentration, HNO_3 was added through the movable inlet. Several experiments were also performed where the hydrocarbon reactant and HNO_3 were added simultaneously. Figure 1 shows the first-order decay of the parent peak of ethylene together with the behavior of the m/e 46 peak. In all experiments a decay of the 46 peak could not be detected beyond the limits of experimental scatter. If the nitric acid did contain some NO_2, this would increase the rate of m/e 46 decay since $k_{O+NO_2} = 5.4 \times 10^{-12}$ cc/mole-

(1) For example, see the review by A. P. Altshuller and J. J. Bufalini, *Environ. Sci. Technol.*, 5, 39 (1971).

(2) D. G. Murcray, T. G. Kyle, F. H. Murcray, and W. J. Williams, *J. Opt. Soc. Amer.*, 59, 1131 (1969).

(3) S. Jaffe and H. W. Ford, *J. Phys. Chem.*, 71, 1832 (1967).

(4) T. Berces and S. Forgeteg, *Trans. Faraday Soc.*, 66, 640 (1970).

(5) T. Berces, S. Forgeteg, and F. Marta, *ibid.*, 66, 648 (1970).

(6) H. Niki, E. E. Daby, and B. Weinstock, *Symp. (Int.) Combust. [Proc.] 12th*, 277 (1969).

(7) R. A. Friedel and J. L. Shultz, *Anal. Chem.*, 31, 1128 (1959).

(8) This reaction may account for the NH_4NO_3 found in the Los Angeles atmosphere. For example, see D. A. Lundgren, *J. Air Pollut. Contr. Assoc.*, 20, 603 (1970).

cule-sec,[9] although under the conditions used here any NO_2 would be consumed if the first 5 cm allowed for mixing before kinetic measurements were made. If one takes the steepest possible slope through the HNO_3 data consistent with the assigned error bars, the reaction of O atoms with HNO_3 is at least 10 times slower than the reaction of O atoms with ethylene or acetylene. Since $k_{O+C_2H_4} = 5.2 \times 10^{-13}$ cc/molecule-sec[6] and $k_{O+C_2H_2} = 1.3 \times 10^{-13}$ cc/molecule-sec,[10] this corresponds to an upper limit of 2×10^{-14} cc/molecule-sec for k_{O+HNO_3}. This result differs by three or four orders of magnitude from the two previous studies. The source of discrepancy is not immediately obvious; however, an error in the postulated mechanism is a possibility. We have reported here only an upper limit since the O-atom concentration could not be further increased to detect slower reactions. It is possible that HNO_3 is regenerated by secondary reactions. However, this is unlikely since the large excess of O atoms would react with intermediates such as OH or NO_3. Preliminary results of Stuhl[11] using a pulsed uv photolysis chemiluminescent method[12] to follow small concentrations of O atom in excess HNO_3 also indicate the reaction of O atoms with HNO_3 is several orders of magnitude slower than previously suggested.

We have also used this flow discharge method to investigate the reaction of H atoms with HNO_3. Atomic hydrogen was generated from H_2 diluted in helium. The rate of m/e 46 decay was compared with the decay of *trans*-2-butene under H-atom rich (10^{14} molecules/cc) conditions. The relative rates of *trans*-2-butene and HNO_3 were determined by introducing each separately under the same conditions and H atom concentration, as well as simultaneously, as described earlier. The maximum rate of m/e 46 decay consistent with experimental scatter was at least 10 times slower than the decay of *trans*-2-butene. The rate constant for H + *trans*-2-butene is 9×10^{-13} cc/molecule-sec.[13] Thus at 1 Torr total pressure, the rate constant for the reaction of H with HNO_3 is less than 1×10^{-13} cc/molecule-sec. This is an order of magnitude slower than the value determined by Berces, Forgeteg and Marta.[5] If any NO_2 were present it would be very rapidly consumed since $k_{H+NO_2} = 4.8 \times 10^{-11}$ cc/molecule-sec.[14]

Thus, in the discharge-flow system used here, no evidence of a fast reaction of HNO_3 with O or H atoms was observed. This in in disagreement with previous photochemical studies.

(9) F. S. Klein and D. J. Herron, *J. Chem. Phys.*, **44**, 3645 (1966).
(10) K. Hoyermann, H. Gg. Wagner, and J. Wolfrum, *Z. Phys. Chem.*, **63**, 193 (1969).
(11) F. Stuhl, private communication.
(12) F. Stuhl and H. Niki, *Chem. Phys. Lett.*, **7**, 197 (1970).
(13) E. E. Daby and H. Niki, *J. Chem. Phys.*, **51**, 1255 (1969).
(14) L. F. Phillips and H. I. Schiff, *ibid.*, **37**, 1233 (1962).

what's happening on the frontiers of chemical research?

in short, critical articles that cover all areas *of chemical research.*

Whether you are a practicing chemist, professor or student, you want to keep up with the latest developments. Yet few of you have the time to read thoroughly all the journals of primary publications.

ACCOUNTS fills the gap.

Written by investigators active in the fields reviewed, ACCOUNTS' concise, brief articles place recent developments in perspective—and relate them to earlier work and their probable future significance.

Once you start relying on ACCOUNTS to keep you informed, you'll wonder how you got along without its monthly arrival.

Complete and mail back the form below. We'll prove how valuable this publication can be to you.

American Chemical Society / 1155 Sixteenth Street, N.W., Washington, D.C. 20036

Please send me ACCOUNTS OF CHEMICAL RESEARCH at the following subscription rates:

ACS members:	☐ U.S. $ 5.00	☐ Canada, PUAS $ 8.00	☐ Other Nations $ 8.50
Nonmembers:	☐ U.S. $10.00	☐ Canada, PUAS $13.00	☐ Other Nations $13.50

Name _____ Title _____

Employer _____

Address: ☐ Home ☐ Business _____

City _____ State/Country _____ Zip _____

Nature of employer's business? ☐ Manufacturing or processing ☐ Academic ☐ Government ☐ Other _____ (Please indicate)

Note: Subscriptions at ACS Member Rates are for personal use only.

☐ I am an ACS member ☐ I am not an ACS member

Payment must be made in U.S. currency, by international money order, UNESCO coupons, U.S. bank draft; or order through your book dealer.

323

need to know about...

The most advanced theory?
The latest applications?
Newest chemicals and reagents?

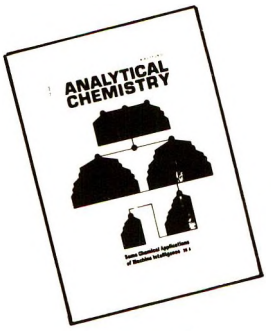

Then ANALYTICAL CHEMISTRY is designed for you.

Each month you receive information that is fresh, current and relevant to *today's needs*. Brand new ideas are introduced. One of them might be the answer to one of your problems.

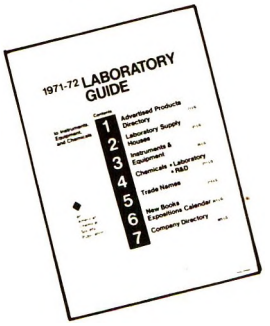

Two other good reasons for starting your ANALYTICAL CHEMISTRY subscription now are the 1971-72 *LABORATORY GUIDE* to Instruments, Equipment and Chemicals and the valuable *ANNUAL REVIEWS* issue.

The 500-page LABORATORY GUIDE gives you 20,000 separate entries with more than 1000 manufacturers selling over 600 products.

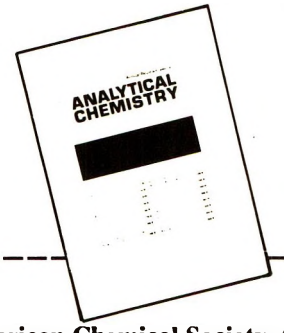

The special April ANNUAL REVIEWS issue presents authoritative researchers reviewing the latest methodology and applications of analytical science.

Be sure to benefit from AC's thorough coverage of the analytical sciences. Just complete the form below and mail it back to us today.

American Chemical Society / 1155 Sixteenth Street, N.W., Washington, D.C. 20036

Please send me ANALYTICAL CHEMISTRY at the following subscription rates:

ACS members:	☐ U.S. $5.00	☐ Canada $7.00	☐ PUAS $ 7.50	☐ Other Nations $ 8.50
Nonmembers:	☐ U.S. $7.00	☐ Canada $9.50	☐ PUAS $17.50	☐ Other Nations $18.50

Note: Subscriptions at ACS Member Rates are for personal use only.

NAME _____ POSITION _____

ADDRESS _____

CITY _____ STATE/COUNTRY _____ ZIP _____

YOUR COMPANY _____ NATURE OF COMPANY'S BUSINESS _____

☐ **I am an ACS member** ☐ **I am not an ACS member** ☐ **Bill me for $**_____

☐ Payment enclosed in the amount of $_____(payable to American Chemical Society). Payment must be made in U.S. currency by international money order, UNESCO coupons or U.S. bank draft; or order through your book dealer.

A2A